



## Characterization and Quantification of Deposit Build-up and Removal in Straw Suspension-Fired Boilers - Ph.d. thesis Muhammad Shafique Bashir

Shafique Bashir, Muhammad

*Publication date:*  
2012

*Document Version*  
Publisher's PDF, also known as Version of record

[Link back to DTU Orbit](#)

*Citation (APA):*  
Shafique Bashir, M. (2012). *Characterization and Quantification of Deposit Build-up and Removal in Straw Suspension-Fired Boilers - Ph.d. thesis Muhammad Shafique Bashir*. DTU Chemical Engineering.

---

### General rights

Copyright and moral rights for the publications made accessible in the public portal are retained by the authors and/or other copyright owners and it is a condition of accessing publications that users recognise and abide by the legal requirements associated with these rights.

- Users may download and print one copy of any publication from the public portal for the purpose of private study or research.
- You may not further distribute the material or use it for any profit-making activity or commercial gain
- You may freely distribute the URL identifying the publication in the public portal

If you believe that this document breaches copyright please contact us providing details, and we will remove access to the work immediately and investigate your claim.

---

# Characterization and Quantification of Deposit Build-up and Removal in Straw Suspension-Fired Boilers

PhD Thesis

---

Muhammad Shafique Bashir

Supervisors:

Kim Dam-Johansen  
Peter Arendt Jensen  
Flemming J. Frandsen  
Stig Wedel

CHEC Research Centre  
Department of Chemical and Biochemical Engineering  
Technical University of Denmark  
DK-2800 Lyngby, Denmark  
June 11, 2012



# Preface

This thesis is written in a partial fulfillment of the requirements to obtain the Doctor of Philosophy degree at the Technical University of Denmark (DTU). The work has been carried out at Combustion and Harmful Emission Control (CHEC) Research Centre at the Department of Chemical and Biochemical Engineering (KT), DTU, under the supervision of Prof. Kim Dam-Johansen, Asc. Prof. Peter Arendt Jensen, Asc. Prof. Flemming Frandsen, and Asc. Prof. Stig Wedel. The project was financially supported by Energinet.DK (PSO project 7217) and Vattenfall A/S. A significant part of the project was made in collaboration with Vattenfall A/S.

A number of people have in various ways contributed to this project, and their help and support is gratefully acknowledged. First and foremost, I would like to thank my supervisors for providing me the opportunity to work on an interesting and rather challenging project. I wish my gratitude to them for their vision and suggestions during the course of my research. Parts of this research work are indirect results of their advice and helpful comments. I am also thankful to them for providing me the opportunity to present this work in international scientific conferences.

I am grateful to Kim Dam-Johansen for all his inspiration and supportive criticism during the project. Sincere thanks to Peter Arendt Jensen for his continuous support and constructive criticism in dealing with the difficult and rather complicated issues encountered during the project. I am also grateful to Flemming Frandsen and Stig Wedel for careful reading of the reports and manuscripts. Excellent ash course and doctoral thesis by Flemming Frandsen helped me a lot. Help from Stig Wedel was significant in dealing with mathematical related issues of the project, which is gratefully acknowledged.

Heartfelt thanks to Johan Wadenbäck and Søren Thaaning Pedersen from Vattenfall A/S for fruitful discussions during the project workshops, and technical support during the full-scale measurements at Amager Power Station. Without their help, the difficult task of full-scale measurements would not be completed within time and to my satisfaction. I am also thankful to DONG Energy for providing access to their boiler. Thanks

## PREFACE

---

to the operational staff at the Amager Power Station and Avedøre Power Station for their technical support during the full-scale measurements.

Thanks to the technicians from the workshop at the department, especially, Thomas Wolfe for all his enormous help and support during the full-scale measurements. Berit from DTU CEN needs special thanks for her kind help in SEM-EDS analysis.

I am thankful to all colleagues and Ph.D. students at CHEC for nice discussions during and after working hours. I would like to thank Joussef Hussein Chhaban, Hao Wu, Ngoc Trung, Samira Telschow, Michael Lykke Heiredal, and Anders Rooma Nielsen.

Many thanks to my close friends, Pir Adeel Zahid Saifi, Muhammad Riaz, Muhammad Hamid Rafiq and Muhammad Waseem Arshad, for maintaining an excellent relationship for more than eleven years.

Finally, I would like to pay heartfelt thanks to my family in Pakistan and in Denmark. In Pakistan, my father being the source of tenacity, and my mother, whose love is more than I can write and describe. In Denmark, my wife, Asma, for all her love, patience and support. My son, Arham, born during the mid of the Ph.D. study, for all his presentation of love in an enjoyable and fascinating way, providing me a time full of relaxation after long working hours in the office.

Muhammad Shafique Bashir  
Lyngby, Denmark (June 11, 2012).

# Dedication

I dedicate this work to Dr. Sb, being a source of motivation and curiosity.



# Abstract

An increased use of biomass in large suspension-fired power plants can be a relatively economic and potentially also efficient way to utilize biomass for heat and power production. However, large deposit formation problems limit the electrical efficiency by limiting the maximum applicable superheater temperature, and the deposits may also cause boiler stops where different parts of the boiler have to be cleaned. This project aims at providing scientifically based knowledge on understanding of ash deposit formation and shedding in biomass suspension-fired boilers. Deposit probe measurements have been conducted in different biomass suspension-fired boilers by using advanced ash deposition probes. Two kinds of ash deposition probes have been used. A horizontal probe that has been developed further, which can register probe temperature, deposit mass uptake, heat uptake and video monitoring. First steps have also been taken for the development of a vertical probe that was employed for ash deposit formation measurements on a boiler furnace wall.

In the first series of probe measurements, the influence of straw firing technology (grate and suspension) on ash transformation, deposit formation rate and deposit characteristics has been investigated. Full-scale probe measurements were conducted at a 250 MW<sub>th</sub> suspension boiler, firing straw and wood in suspension, and the results were compared with measurements conducted at a 105 MW<sub>th</sub> straw-fired grate boiler. Bulk elemental analysis of fly ashes revealed that fly ash from suspension firing of straw has high contents of Si, K and Ca, while fly ash from straw grate firing was rich in the volatile elements, K, Cl and S. SEM-EDS analysis showed that the fly ash from straw suspension firing consists of three kinds of particles: 1) flake type Si rich particles, 2) molten or partially molten particles (> 20 μm) rich in Si, K and Ca with small amounts of Mg, P, and potassium salts on the outer surface, and 3) small particles rich in K, Cl and S (aerosols, between 0.1 and 5 μm). Ash deposition data were compared with data from previously conducted deposit probe measurements in biomass-fired grate boilers. The comparison showed an increasing trend in deposit formation rate with increase in flue gas temperature. At a flue gas temperature of 650 °C, the deposit formation rate is typically from 5 to 30 g/m<sup>2</sup>/h and at 900 °C, the deposit formation rate is typically 20 to 110 g/m<sup>2</sup>/h. At higher fuel alkali



## ABSTRACT

---

contents ( $K > 0.9$  wt.%), the increase in deposit formation rate with flue gas temperature was more significant, compared to the increase in deposit formation rate at lower fuel alkali contents ( $K \leq 0.9$  wt.%). An increased flue gas temperature probably increases the fraction of molten ash as well as provides an increased content of gas phase alkali species, and both will lead to an increased deposit formation rate. The deposit formation rates during straw suspension firing and straw grate firing were on similar levels. This was observed even though the concentration of fly ash in the flue gas was higher during straw suspension firing.

The objective of the second probe measuring series was to investigate the influence of fuel type (straw share in wood), probe exposure time, probe surface temperature (500 °C, 550 °C and 600 °C), and flue gas temperature (600–1050 °C) on the transient deposit build-up and shedding in a 350 MW<sub>th</sub> suspension boiler, firing straw and wood. Two different measures of deposit formation rate are used in the analysis of the data. The first is the integral deposit formation rate (IDF-rate) found by dividing the integral mass change over integral time intervals (of order several hours) by the time interval. The IDF-rate is then the result of both the deposit formation rate and shedding events in a given period. In this work IDF-rates were determined using 12 h intervals. The IDF-rate is similar to deposit formation rates determined from previous full-scale measuring data. A second measure, the derivative-based deposit formation rate (DDF-rate), was determined by calculating the local values of the time derivative of the deposit mass uptake, removing large negative values signifying major shedding events, and finally time smoothing the derivatives to remove excessive noise. The DDF-rate excludes the major shedding events. The overall DDF-rates were measured to be between 234 and 3105 g/m<sup>2</sup>/h. The IDF-rates were measured between 1 and 95 g/m<sup>2</sup>/h. The results showed that the DDF-rate was influenced by flue gas temperature and straw share, while changes in probe surface temperature had no significant influence. The IDF-rate, qualitatively related to the ratio between the time-integrated DDF-rate and the integration time, followed the same trends. Quantification of naturally occurring deposit shedding and deposit shedding during plant sootblowing was made via deposit mass uptake signals obtained from the deposit probe. The deposit shedding process was characterized by calculation of the amount of deposit removed at a shedding event [g/m<sup>2</sup>] and the frequency of the shedding events [h<sup>-1</sup>]. The results showed that the shedding process is stochastic and the amount of deposit removed varies even at constant local conditions. However, the deposit shedding rates showed an increasing trend with increase in flue gas temperatures and probe deposit mass loads. The deposit shedding rate was in most of the cases higher at a probe temperature of 500 °C than at a probe temperature of 600 °C. A possible reason for this is partial melting and/or sintering of the innermost deposit layer (rich in K, Cl and S) at higher probe

surface temperature. This could cause the adhesion strength of the deposit to the probe to increase at the higher probe temperature. Quantification of the necessary Peak Impact Pressure (PIP) needed to remove the deposit was also made by use of a sootblowing probe in conjunction with the deposit probe. Results of deposit removal by artificial sootblowing showed that the deposits formed on a 500 °C probe temperature and at exposure time less than 91 h can be removed with a PIP of less than 55 kPa. However, an increase in probe exposure time and/or probe surface temperature (to 600 °C) significantly increases the PIP needed to remove the deposits.

As a part of the third probe measurement series, full-scale probe measurements of deposit build-up and shedding were conducted at a 800 MW<sub>th</sub> suspension boiler, firing wood and natural gas, with the addition of coal fly ash. The results showed that the addition of coal fly ash can significantly affect the ash deposition behaviors and the deposit properties. At the location of the probe measurements with flue gas temperature of 1250–1300 °C, although the addition of coal fly ash increases the DDF-rate and the ash deposition propensity, the deposits formed during coal ash addition seem to shed frequently, suggesting that they are easily removable. On the other hand, the amount of K<sub>2</sub>SO<sub>4</sub> in the deposits was significantly reduced when coal fly ash was added, which is favorable from corrosion point of view. At the location with flue gas temperature of 750–800 °C, the deposits formed without coal ash addition were dominated by small particles rich in K, Ca, S and Cl. With the addition of coal fly, the Cl disappeared in the deposits, which were dominated by calcium-alumina-silicates rich particles, supplemented by a small amount of K<sub>2</sub>SO<sub>4</sub> particles. The ash deposition propensity was decreased when coal ash was added.

A mechanistic model of ash deposit build-up and heat uptake was used to simulate the deposit formation process. The model describes the deposit related processes as a function of the local parameters as flue gas temperature, probe surface temperature and fuel changes. Simulation results showed that the model over predicts the DDF-rate quantitatively but the qualitative behavior was in accordance with the experimental findings. The model predictions regarding probe heat uptake were satisfactory both quantitatively and qualitatively.



# Resumé

En øget anvendelse af biomasse i store suspensionsfyrede kraftværker er en relativt økonomisk og effektiv måde, at anvende biomasse til kraft-varme produktion. Sammenlignet med kulfyring giver anvendelsen af biomasse anledning til dannelse af relativt store mængder af askebelægninger i fyrrummet og på overhederne. Disse belægninger kan i nogle tilfælde forøge korrosions problemer, og ved kraftig belægningsdannelse kan det være nødvendigt at stoppe og rense kedlen manuelt. For at begrænse problemerne kan overhedertemperaturen sænkes, men det formindsker el virkningsgraden. Dette PhD projekt sigter mod tilvejebringelse af eksperimentelle data der forøger forståelsen af askebelægningsdannelse og -afkast i biomasse suspensionsfyrede kedler. Der er i projektet udført belægningsondemålinger på forskellige biomassefyrede suspensions kedler. Der er anvendt to typer af belægningssonder i projektet. Der er anvendt en horisontal sonde der er blevet videreudviklet, og som kan registrerer temperaturer, belægningsvægt og energioptag; og hvor belægningsprocessen kan videofilmes. Der er desuden taget de første skridt til udvikling af en vertikal sonde, der vil kunne anvendes til målinger af belægningsdannelse på kedelvægge i fyrrummet.

Den første fuldskala målekampagne blev udført på Amagerværkets unit 2, som er en  $250 \text{ MW}_{th}$  suspensions fyret kedel der anvender halm og træ. De opnåede sonde måle resultater blev sammenlignet med målinger udført på en  $105 \text{ MW}_{th}$  halmfyret ristededel. Elementaranalyse af flyveaske viste, at flyveaske fra suspensionsfyring af halm har et højt indhold af Si, K og Ca, mens flyveaske fra halmfyring på rist havde højt indhold af K, Cl og S. Der blev fundet belægningsdannelses rater som var nogenlunde ens for det suspensionsfyrede og det ristefyrede anlæg.

Den anden probe målekampagne blev udført på Amagerværkets  $350 \text{ MW}_{th}$  suspensionsfyrede blok et kedel, der forbrænder halm og træ. Målet med dette studie var at undersøge effekten af; brændselstype (andel af halm i træ), sondeeksponeringstid, sondeoverfladetemperatur ( $500 \text{ }^\circ\text{C}$ ,  $550 \text{ }^\circ\text{C}$  og  $600 \text{ }^\circ\text{C}$ ) samt røggastemperatur ( $600\text{--}1050 \text{ }^\circ\text{C}$ ) på transient belægningsopbygning og afkast. To forskellige mål for belægningsopbygningshastigheden blev anvendt til dataanalysen, IDF (Integral Deposit Formation) raten og

## RESUMÉ

---

DDF (Differential Deposit Formation) raten. IDF raten angiver belægningsopbygningsraten inkluderende både opbygning og afkast i et givet tidsinterval. DDF raten angiver den øjeblikkelige belægningsopbygningsrate i en periode hvor der ikke sker belægningsafkast. Generel ses betydeligt højere DDF rater end de bestemte IDF rater.

Belægningsopbygningsraten blev influeret af røggastemperatur og halm fraktion, mens ændringer i sondens overfladetemperatur ikke havde væsentlig indflydelse. Kvantificering af naturligt forekommende belægningsafkastning samt belægningsfjernelse forårsaget af værkets sodblæsning blev foretaget via masseoptags signaler fra belægningssonderne. Resultaterne viste at afkastningsprocessen er stokastisk, og at mængden af afkastet belægning varierer selv ved konstante lokale betingelser. I de fleste tilfælde var afkastningshastigheden højere ved en sonde temperatur på 500 °C end 600 °C.

Belægninger i kedler fjernes ofte ved sodblæsning, hvor en stråle af højtryksdamp rettes mod kedeloverflader belagt med askebelægninger. En sodblæser probe med trykluft blev anvendt til at undersøge det nødvendige sodblæser stråle stagnationstryk (PIP) som krævedes for at fjerne belægningerne. Forsøgene viste at de dannede belægninger ved en sonde temperatur på 500 °C og en eksponeringstid kortere end 91 timer kan fjernes med et PIP på under 55 kPa. Øget sonde eksponeringstid og/eller sonde overfladetemperatur (600 °C) øgede det nødvendige PIP for fjernelse af belægningerne.

En tredje målekampagne med den horisontale sonde blev udført på Avedøreværkets 800 MW<sub>th</sub> suspensionsfyret kedel, der anvender træ og naturgas med tilsætning af kulflyveaske. Resultaterne viste at tilsætningen af kulflyveaske kan påvirke akseaflejningsprofilen samt aflejringernes egenskaber. På trods af at tilsætningen af kulflyveaske øger belægningsdannelseshastigheden, lader belægningerne dannet ved røggastemperaturer på 1250–1300 °C og under kulaske tilsætning, til at blive afkastet med en højere frekvens, hvilket indikerer at de er lettere at fjerne.

En tidligere udviklet mekanistisk model for askeopbygning og varmeoptag er anvendt til simuleringer, og resultaterne er sammenlignet med en del af de tilvejebragte sondemåledata. Modellen beskriver de belægningsdannende processer som funktion af lokale parametre, som røggastemperatur, sonde overfladetemperatur og ændringer i flyveaske sammensætning. Simuleringerne viste at modellen giver kvalitativt overensstemmende resultater med sonde måledata, mens den kvantitative bestemmelse af belægnings rater ikke er bestemt præcist.

# Contents

<b>Preface</b>	<b>ii</b>
<b>Dedication</b>	<b>iv</b>
<b>Abstract</b>	<b>vi</b>
<b>Resumé</b>	<b>x</b>
<b>Nomenclature</b>	<b>xxvi</b>
<b>Incorporated Publications</b>	<b>xxx</b>
<b>1 Introduction</b>	<b>1</b>
1.1 Background . . . . .	1
1.2 Project Objectives . . . . .	5
1.3 Thesis Structure . . . . .	6
<b>2 Literature Review</b>	<b>9</b>
2.1 Introduction . . . . .	9
2.2 Biomass Fuel and Ash Formation . . . . .	10
2.2.1 Biomass as a CO <sub>2</sub> -neutral Fuel . . . . .	10
2.2.2 Characterization of Biomass Fuels . . . . .	12
2.2.3 Biomass Combustion Technologies . . . . .	16
2.2.4 Release of K, S and Cl during Biomass Combustion . . . . .	19
2.3 Biomass Ash Deposit Formation . . . . .	21
2.3.1 Deposit Formation Processes . . . . .	21
2.3.2 Development of Ash Deposits . . . . .	22
2.3.3 Deposit Physical and Chemical Properties . . . . .	28
2.4 Shedding of Deposits . . . . .	30
2.4.1 Mechanisms of Deposit Shedding . . . . .	30
2.4.2 Industrial Deposit Shedding Techniques . . . . .	33
2.4.3 Review of Deposit Shedding Investigations . . . . .	37
2.5 Practical Experiences of Biomass Suspension Firing . . . . .	40

2.5.1	Review of Ash Deposition during Pilot-scale Biomass Suspension Firing . . . . .	40
2.5.2	Review of Ash Deposition during Full-scale Biomass Suspension Firing . . . . .	45
2.6	Modeling of Ash Deposit Formation . . . . .	48
<b>3</b>	<b>Design and Development of Probes for Online Monitoring of Deposit Build-up and Removal</b>	<b>51</b>
3.1	Introduction . . . . .	51
3.2	Review of Deposit Probes used for Ash Deposit Build-up In- vestigations . . . . .	52
3.2.1	Types of Deposit Probes Based on Mechanical Design	53
3.2.2	Types of Deposit Probes Based on Cooling Media . .	54
3.3	Description of the Horizontal Ash Deposition Probe System .	57
3.3.1	Horizontal Ash Deposition Probe . . . . .	57
3.3.2	Description of the Port Plate . . . . .	60
3.4	Description of the Artificial Sootblowing Probe . . . . .	61
3.5	Design and Development of the the Vertical Ash Deposition Probe . . . . .	64
3.5.1	Commissioning of the Vertical Probe . . . . .	68
<b>4</b>	<b>Ash Transformation and Deposit Build-up during Biomass Suspension and Grate Firing</b>	<b>71</b>
4.1	Introduction . . . . .	71
4.2	Equipments, Materials and Methods . . . . .	73
4.2.1	Boilers . . . . .	73
4.2.2	Fuels . . . . .	76
4.2.3	Ash Deposition Probe . . . . .	76
4.2.4	Procedure of Measurements . . . . .	76
4.3	Results and Discussion . . . . .	80
4.3.1	100% Straw and Wood Firing . . . . .	80
4.3.2	Comparison of Full-scale Measurements . . . . .	82
4.3.3	Video Observations . . . . .	87
4.3.4	Chemical Compositions of Fly Ashes and Deposits . .	89
4.3.5	Fly Ash Melting . . . . .	94
4.4	Conclusions . . . . .	95
<b>5</b>	<b>Transient Deposit Build-up and Shedding during Straw and Wood Suspension Combustion</b>	<b>99</b>
5.1	Introduction . . . . .	99
5.2	Equipments, Materials and Methods . . . . .	101
5.2.1	Boiler . . . . .	101
5.2.2	Fuels . . . . .	102
5.2.3	Ash Deposition and Sootblowing Probe . . . . .	106

## CONTENTS

---

5.2.4	Procedure of Measurements . . . . .	106
5.3	Ash Deposit Build-up . . . . .	109
5.3.1	Data Treatment . . . . .	109
5.3.2	Chemical Compositions of Fuel Ash, Residual Ash and Deposits . . . . .	116
5.3.3	Comparison of IDF-rates with Previously Conducted Probe Measurements . . . . .	119
5.3.4	Influence of Local Conditions on the DDF-rate . . . . .	123
5.4	Ash Deposit Shedding . . . . .	127
5.4.1	Video Observations of Shedding Events . . . . .	127
5.4.2	Data Treatment . . . . .	128
5.4.3	Influence of Different Parameters on the Shedding Pro- cess . . . . .	131
5.4.4	Net Deposit Accumulation Rate . . . . .	138
5.4.5	Deposit Removal by using an Artificial Sootblowing Probe . . . . .	141
5.5	Probe Heat Uptake . . . . .	143
5.6	Conclusions . . . . .	144
<b>6</b>	<b>Ash Deposit Build-up and Shedding during Wood Suspen- sion Combustion with Coal Ash Addition</b>	<b>147</b>
6.1	Introduction . . . . .	147
6.2	Equipments, Materials and Methods . . . . .	148
6.2.1	Boiler . . . . .	148
6.2.2	Fuels . . . . .	148
6.2.3	Ash Deposition Probe . . . . .	149
6.2.4	Procedure of Measurements . . . . .	149
6.3	Results and Discussion . . . . .	156
6.3.1	Data Treatment . . . . .	156
6.3.2	Influence of Local Conditions on Ash Deposition Propen- sity . . . . .	163
6.3.3	Comparison of Results with Previously Conducted Probe Measurements . . . . .	166
6.3.4	Morphology and Chemical Composition of Fly Ashes and Deposits . . . . .	169
6.3.5	Discussion on Characterization of Fly Ashes and De- posits . . . . .	175
6.4	Conclusions . . . . .	178
<b>7</b>	<b>Mechanistic Modeling of Deposit Build-up during Biomass Suspension Firing</b>	<b>182</b>
7.1	Introduction . . . . .	182
7.2	Mechanistic Modeling of Deposit Formation Processes . . . . .	183
7.2.1	Heat Transfer Modeling . . . . .	187



7.2.2	Simulation Conditions . . . . .	188
7.2.3	Simulation Results . . . . .	188
7.3	Conclusions . . . . .	195
<b>8</b>	<b>Innovative Ideas for Deposit Shedding in Biomass Suspension-Fired Boilers</b>	<b>196</b>
8.1	Introduction . . . . .	196
8.2	Proposed Ideas for Deposit Shedding in Biomass Suspension-Fired Boilers . . . . .	196
8.2.1	Deposit Removal Using Ring (DRUR) . . . . .	196
8.2.2	Deposit Removal using Mechanical Hitting . . . . .	198
8.2.3	Steam Sootblower Optimization . . . . .	198
8.2.4	Fuel/Ash Mixing . . . . .	198
<b>9</b>	<b>Conclusions and Suggestions for Further Work</b>	<b>200</b>
9.1	Conclusions . . . . .	200
9.1.1	Ash Transformation and Deposition during Biomass Suspension and Grate Firing . . . . .	200
9.1.2	Transient Deposit Build-up and Shedding during Straw and Wood Suspension Combustion . . . . .	202
9.1.3	Ash Deposit Build-up and Shedding during Wood Suspension Combustion with Coal Ash Addition . . . . .	204
9.1.4	Mechanistic Modeling of Ash Deposit Build-up and during Biomass Suspension Firing . . . . .	205
9.2	Future Work . . . . .	206
	<b>References</b>	<b>208</b>
	<b>Appendices</b>	<b>217</b>
	Appendix A: Full-scale measurements at AMV2 . . . . .	218
	Appendix B: Full-scale measurements at AMV1 . . . . .	228
	Appendix C: Full-scale measurements at AVV2 . . . . .	264

# List of Figures

1.1	Share of renewable energy in the global final energy consumption, 2009 [1]. . . . .	2
2.1	Possible reduction in CO <sub>2</sub> -emissions by increasing boiler efficiency and introduction of biomass to co-fired power plants [23]. . . . .	11
2.2	Share of fuels other than coal for electricity production in Denmark (in percentage contribution of each fuel) [54]. . . . .	12
2.3	Danish energy target for 2050 [8]. . . . .	12
2.4	A Van Krevlen diagram, showing atomic O:C and H:C ratios as a function of fuel ranks [14]. . . . .	13
2.5	S, N, Cl, Na and K contents in wood chips, Danish straw and coal (fired in Denmark) based on heating value of the fuel. Modified from Sander [59]. . . . .	14
2.6	Schematic drawing of a grate-fired boiler used for biomass firing [63]. . . . .	17
2.7	Schematic drawing of a suspension-fired boiler used for biomass firing. Modified from Tobiasen et al. [5] and van Lith [63]. . . . .	18
2.8	Schematic illustration of biomass combustion and ash transformation on a grate [60]. . . . .	19
2.9	Deposit formation on a tube, a) diffusion and thermophoresis, b) inertial impaction [42]. . . . .	23
2.10	Slagging in the high temperature region [15]. . . . .	24
2.11	Graphical representation of deposit outer layer thickness impact on deposit outer surface temperature. Simulation results using a standard coal ash. . . . .	24
2.12	Ash deposition on the superheaters during straw and coal co-firing [2]. . . . .	25
2.13	Ash deposition on the screen tubes during 100% straw firing in suspension [5]. . . . .	26
2.14	Graphical representation of different types of deposit sintering [2]. . . . .	27

LIST OF FIGURES

---

2.15	Principal sketch of the wheat straw-derived deposits during pilot-scale experiments at Sandia MFC [17]. . . . .	28
2.16	Structure of mature deposits from Ensted boiler (straw grate fired boiler). The superheater steam temperature was from 389 to 470 °C and the flue gas temperature was just below 900 °C [21]. . . . .	29
2.17	Deposition rate as a function of melt fraction for two different types of salt mixtures [68]. . . . .	29
2.18	Deposit erosion mechanism, 1) initial deposits on the tube, 2) deposits after shedding though erosion [42]. . . . .	31
2.19	Relationship between the deposit viscosity and the deposit strength. Cases are ordered in the sequence of decreasing viscosity [42]. . . . .	32
2.20	Longitudinal and lateral component of a force, caused by the interaction between a sootblower jet and a deposit [36]. . . . .	33
2.21	Different sootblowers employed in solid fuel fired boilers, a) rotary, b) retractable, c) wall, d) rake [72]. . . . .	34
2.22	Mechanisms of deposit removal: brittle break-up (a) and debonding (b) [36]. . . . .	35
2.23	Pictures of the deposit probe during full-scale measurements at a straw grate-fired boiler at three different flue gas temperatures [35]. . . . .	39
2.24	Ash deposition rate reported for individual biomass fuels during pilot-scale suspension firing [28, 41, 73, 80, 82, 83]. Flue gas temperature was between 800 and 1000 °C. . . . .	43
2.25	Ash deposition rate reported for pilot-scale suspension firing of biomass mixtures and/or with addition of additives [28, 41, 73, 82, 83]. Flue gas temperature was between 800 and 1000 °C. . . . .	43
2.26	Ash deposition rate as a function of Cl-content in the biomass fuel during pilot-scale suspension firing. Flue gas temperature was around 1000 °C [28, 41, 80]. . . . .	44
2.27	Ash deposition rate as a function of Cl-content in the biomass fuel during pilot-scale suspension firing. Flue gas temperature was around 800 ±50 °C [73, 82, 83]. . . . .	44
3.1	Schematic of the deposit probe used by Madhiyanon et al. [79] to measure mass of and fouling resistance. . . . .	53
3.2	Illustration of a typical vertical probe for slagging investigations [99]. . . . .	54
3.3	Schematic drawing of the probe used for investigation of potassium salts deposition on heat transfer surfaces [17]. . . . .	55
3.4	Schematic outline of the air cooled (a) and air-water cooled (b) deposition probe [20]. . . . .	56

## LIST OF FIGURES

---

3.5	Schematic view of the horizontal probe with identified positions of probe temperature measurements, deposition area, port plate for mounting, hinge, load cell and rail for pulling out the probe. . . . .	58
3.6	Schematic illustration of the horizontal probe system. . . . .	59
3.7	Cross-sectional view perpendicular to probe axis and cross-sectional view along axis of annuli. . . . .	59
3.8	Schematic drawing of the port plate used for measurements conducted using the horizontal probe. . . . .	61
3.9	Schematic illustration of the deposition probe system used in the inspection hole at AMV1 boiler. . . . .	62
3.10	Overall sootblowing probe set up with water and air flow description. . . . .	62
3.11	Detailed drawings of the sootblowing nozzle. . . . .	63
3.12	The measured Peak Impact Pressure (PIP) as a function of applied air pressure at varying downstream distance from the nozzle exit at room temperature. . . . .	63
3.13	Proposed layout of vertical probe for heat uptake. . . . .	64
3.14	Calculated air and probe metal temperatures. . . . .	66
3.15	Detailed drawings of the vertical probe system. . . . .	67
3.16	Drawing of the vertical probe with cut and angled view. . . . .	68
3.17	Position of the thermocouples on the vertical probe, seen from boiler to the wall. . . . .	68
3.18	Temperature measurements of thermo-elements attached on the vertical probe. The values shown are for test number 3. . . . .	69
3.19	Picture of the vertical probe taken just after finishing an experiment. . . . .	70
4.1	Schematic view of the boilers. The locations of the probe measuring positions (P1, P2) at AMV2 (a) and probe position (P) at AVV2 (b) are identified. . . . .	74
4.2	Images of the probe measurement positions before and after manual cleaning during 100% straw firing at AMV2. . . . .	75
4.3	Schematic view of AMV2 boiler with identification of silos, mills, burners and deposition probe measuring positions. Modified from Tobiasen et al. [5]. . . . .	76
4.4	Percentage of applied boiler load during each measurement at AMV2 and boiler shutdown incidents. . . . .	78
4.5	Flue gas temperature, deposit mass uptake and probe heat uptake during measurements at AMV2, a) 100% straw firing, superheater region measurements (test 4, signals averaged to 1000 s), b) 100% wood firing, tube bank region measurements (test 5, signals averaged to 100 s). . . . .	81

LIST OF FIGURES

---

4.6	Impact of flue gas temperature on deposit formation rates, a) four different sets of fuel alkali contents and two types of straw firing technologies, b) different sets of probe surface temperatures and 5 different boilers. . . . .	84
4.7	Pictures of the deposit probe just after the experiments, a) ~ 20–50 cm from tip of probe (35% straw, test 1 at AMV2), b) ~ 10–30 cm from tip of probe (65% straw, test 3 at AMV2), c) ~ 10–30 cm from tip of probe (80% straw, test 2 AMV2), d) ~ 30–50 cm from tip of probe (100% straw, test 4 at AMV2), e) ~ 40–60 cm from tip of probe (100 % wood, test 5 at AMV2), f) almost complete deposition area of the probe (100% straw, test 1 at AVV2). . . . .	87
4.8	a) Flue gas temperature, deposit mass uptake and probe heat uptake during 80% straw firing at AMV2 with identified shedding events, b) picture of the deposit probe just before the first shedding event (1) at approximately 113.3 h (04:43), c) picture of the deposit probe just after the first shedding event (04:52). . . . .	88
4.9	Ash transformation during straw firing on grate and straw firing in suspension. . . . .	89
4.10	Morphology (a) and SEM-EDS analysis (b) of fly ash collected from ESP during straw firing in suspension at AMV2. . . . .	90
4.11	a) SEM image of fly ash collected from ESP during straw firing in suspension at AMV2, b) SEM image of the highlighted molten fly ash particle. . . . .	90
4.12	Particle size distribution (volume-based) of fly ash generated during straw suspension and grate firing. . . . .	91
4.13	Morphology (a) and SEM-EDS analysis (b) of outer layer of upstream deposits collected after straw firing in suspension at AMV2 (test 4 at SH). . . . .	92
4.14	Prediction of fly ash melt fraction by using the predictive model of Zhou et al. [31]. FMT: first melting temperature. . . . .	95
5.1	Drawings of AMV1 boiler with identified probe measuring position, just above the screen tubes, a) overall boiler configuration, b) schematic presentation of the boiler. Modified from Gjernes [84]. . . . .	103
5.2	Schematic drawing of the AMV1 boiler outlining the position of the plant sootblowing near the experimental set up. . . . .	104
5.3	Particle size distribution of fuel collected from two burners connected to two different mills (test 1, 22/03/2011). The particle size distribution was determined by a sieve analysis. . . . .	106
5.4	Experimental methods applied for artificial sootblowing. . . . .	108

## LIST OF FIGURES

---

5.5	Comparison of measured (suction pyrometer) and calculated flue gas temperature. . . . .	112
5.6	Raw data of flue gas temperature, deposit mass uptake, plant sootblowing events (specific number of sootblower in operation) and probe heat uptake during test 1. . . . .	114
5.7	a) Approximate manually calculated slopes of deposit mass uptake signals during 10–20 h of exposure time during test 1, b) comparison of manually calculated slopes and slopes calculated by the mathematical procedure (DDF-rate) for complete test 1. . . . .	115
5.8	Ash transformation during straw and wood (straw > 46 wt.%) suspension combustion. Comparison of fuel-, fly- and bottom ash samples from test 1 and 5. . . . .	117
5.9	Impact of molar K/Si ratio in fuel ash on the content of K, Cl and S in the fly ash during straw and wood (straw > 46 wt.%) suspension combustion. . . . .	118
5.10	Particle size distribution (volume-based) of fly ash generated during test 1. The fly ash samples were collected using a spear from the silos of the electrostatic precipitator (ESP). . . . .	118
5.11	Bulk ash analysis of deposit layers removed from the probe after it was taken out of the boiler (straw share > 46 wt.%, test 1, 5). . . . .	119
5.12	Impact of flue gas temperature on IDF-rates (12 h), a) comparison of deposit probe measurements data at different fuel alkali levels and two types of straw firing technologies, b) comparison of the some data set with marking of the probe surface temperature and boiler where the measurements were preformed. . . . .	121
5.13	Impact of fuel ash contents (a), fuel ash $\times$ K/Si molar ratio (b), and Cl-content in the fuel (c) on the IDF-rate for three different sets of flue gas temperatures (data from Figure 5.12). . . . .	122
5.14	a) Impact of flue gas temperature on the DDF-rate, data points from tests 1 to 5, b) impact of flue gas temperature on the overall DDF-rate, tests 1 to 5. . . . .	124
5.15	a) Logarithm of the DDF-rate as a function of reciprocal of absolute flue gas temperature, data points from tests 1 to 5, b) logarithm of the overall DDF-rate as a function of reciprocal of absolute flue gas temperature, tests 1 to 5. . . . .	125
5.16	Fly ash melt prediction using predictive model of Zhou et al. [31]. FMT stands for first melting temperature. . . . .	127
5.17	Data of probe mass uptake and plant sootblowing events (specific number of sootblower in operation) during test 1 with identified shedding events. . . . .	130

LIST OF FIGURES

---

5.18	Images of the ash deposition probe during test 5 on 15/04/2010 (about 4 h exposure time). . . . .	131
5.19	Impact of deposit mass load on (a) the mean amount of deposits removed naturally and (b) the mean amount of deposits removed during plant sootblowing. Data points are from tests 1 to 5. . . . .	133
5.20	Impact of flue gas temperature on (a) mean natural deposit shedding frequency and (b) mean plant sootblowing shedding frequency. Data points are from tests 1 to 5. . . . .	134
5.21	Total deposit shedding rate as a function of the DDF-rate. Data points are from tests 1 to 5. . . . .	139
5.22	Impact of flue gas temperature on the net deposit accumulation rate. Data points are from tests 1 to 5. . . . .	141
5.23	Percentage of deposits removed as a function of applied Peak Impact Pressure (PIP) at different probe exposure times and deposit mass loads, a) probe surface temperature of 500 °C, b) probe surface temperature of 600 °C. . . . .	142
5.24	Impact of temperature difference between flue gas and probe surface on probe heat uptake for different deposit mass loads (test 5). The slope is calculated by a linear fit using equation, $y = bx$ . . . . .	143
5.25	Sensitivity of heat uptake with change in temperature difference between flue gas and probe surface for different deposit mass loads. Data from all tests (1–8). . . . .	144
6.1	Schematic view of the AVV2 boiler with identified probe measuring positions. Position A: Flue gas temperature 1250–1350 °C, Position B: Flue gas temperature 750–800 °C. . . . .	152
6.2	Schematic drawing of the modified probe system (location A). . . . .	153
6.3	Outside view of the modified probe system for location A. . . . .	154
6.4	Flue gas temperature, deposit mass uptake, sootblowing events and probe heat uptake during test 3. . . . .	158
6.5	Typical example of the deposit shedding during test 6. . . . .	160
6.6	DDF-rate calculated during test 3. . . . .	161
6.7	Ash deposition propensity calculated during test 3. . . . .	161
6.8	Impact of flue gas temperature on ash deposition propensity (deposition flux/ash flux, %). The points with red color indicate tests when coal ash addition was not made. . . . .	164
6.9	a) Impact of coal ash to fuel ash ratio on ash deposition propensity, b) impact of boiler load on ash deposition propensity, c) impact of biomass load on ash deposition propensity. . . . .	165

## LIST OF FIGURES

---

6.10	Impact of flue gas temperature on deposit formation rates (IDF-rates), a) comparison of deposit probe measurements data for wood firing with and without combination of other fuels (NG (natural gas), straw, furnace oil), b) comparison of data set with marking of the probe surface temperature and the boilers where the measurements were preformed. . . . .	167
6.11	SEM-EDS analysis of the fly ash samples collected from electrostatic precipitator during measurement without coal ash addition. . . . .	170
6.12	SEM-EDS analysis of the fly ash samples collected from electrostatic precipitator during measurement with coal ash addition. . . . .	170
6.13	SEM-EDS analysis of outer-layer of upstream deposits formed during measurements without coal ash (location A, test 6). . . . .	171
6.14	SEM-EDS analysis of the downstream deposits formed during measurement without coal ash addition (location A, test 6). . . . .	172
6.15	SEM-EDS analysis of the upstream deposits formed during measurement without coal ash addition (location B, test 8). . . . .	172
6.16	SEM-EDS analysis of the downstream deposits formed during measurement without coal ash addition (location B, test 8). . . . .	173
6.17	SEM-EDS analysis of the outer-layer of upstream deposits formed during measurement with coal ash addition (location A, test 10). . . . .	173
6.18	SEM-EDS analysis of the downstream deposits formed during measurement with coal ash addition (location A, test 10). . . . .	174
6.19	SEM-EDS analysis of the upstream deposits formed during measurement with coal ash addition (location B, test 9). . . . .	175
6.20	SEM-EDS analysis of the downstream deposits formed during measurement with coal ash addition (location B, test 9). . . . .	175
6.21	A summarized picture of the deposits based on SEM-EDS analysis. . . . .	176
7.1	A schematic of the deposit layers on the horizontal ash deposition probe [31]. . . . .	184
7.2	Simulation results of deposit mass uptake for the first six hours for different sets of flue gas temperatures and probe surface temperatures. The fuel (fly ash) input is case 1 (straw > 20 wt.%) shown in Table 7.1. . . . .	191
7.3	Simulation results of the DDF-rate ( $\frac{dm_d}{dt}$ ) for the first six hours for different sets of flue gas temperatures and probe surface temperatures. The fuel (fly ash) input is case 1 (straw > 20 wt.%) shown in Table 7.1. . . . .	191



LIST OF FIGURES

---

7.4	Simulation results of deposit mass uptake for the first six hours for different sets of flue gas temperatures and probe surface temperatures. The fuel (fly ash) input is case 2 (straw < 20 wt.%) shown in Table 7.1. . . . .	192
7.5	Prediction of heat uptake for different deposit mass loads on the probe. . . . .	195
8.1	A schematic of deposit removal using a ring. . . . .	197
8.2	a) A schematic layout of the ring for deposit removal on a superheater tube, b) a potential ring that can be used with modifications. . . . .	197

# List of Tables

1.1	Qualitative comparison of biomass conversion technologies to produce electricity, heat and/or power. +++ relatively good, + relatively poor, x relatively cheap, xxxx relatively expensive. Adopted from Egsgaard et al. [6]. . . . .	2
2.1	Difference in properties of Danish straw, wood chips and coal. Adopted from Flemming [2], Sander [59], Telfer et al. [61] and Glarborg et al. [62]. . . . .	15
2.2	Fuel analysis of biomass and coal fuels. Adopted from Frandsen [2]. . . . .	16
2.3	Operating comparison of solid fuel firing technologies. Adopted from Glarborg et al. [62]. . . . .	17
2.4	Deposit shedding mechanisms [42]. . . . .	31
2.5	Review of shedding investigations in different solid-fuel fired boilers and lab-scale facilities. . . . .	38
2.6	Review of biomass suspension firing experiments reported in literature at different pilot-scale facilities. . . . .	42
2.7	Overall comparison of four additives investigated at AMV2, modified from Tobiasen et al. [5]. . . . .	46
2.8	Review of full-scale suspension firing of biomass. . . . .	47
3.1	Summary of the conducted measurements using vertical probe.	70
4.1	Brief operational data of the boilers (AMV2 and AVV2). . . .	75
4.2	Composition of the fuels fired during measurements at AMV2 and AVV2. . . . .	77
4.3	Typical size distribution of the pulverized straw dust to the burners at AMV2. . . . .	78
4.4	Overall comparison of conducted measurements at AMV2 in terms of deposit formation rate, probe heat uptake and deposit characteristics. . . . .	79
4.5	Deposit formation rates measured during the previous and current full-scale measurements. . . . .	85

LIST OF TABLES

---

4.6	Calculated values of potential components in the fuels responsible for ash deposition, B/A ratio, and potential deposition indices about the propensity of slagging and fouling [105]. . .	86
4.7	Composition of major elements in the fly ash and deposits formed during AMV2 (suspension) and AVV2 (grate) measurements. . . . .	93
5.1	Brief operational data of the AMV1 boiler. . . . .	102
5.2	Analysis of straw and wood pellets used at AMV1. . . . .	105
5.3	Experimental summary (AMV1). . . . .	107
5.4	Calculated constants for flue gas temperature prediction model with estimated confidence intervals. . . . .	111
5.5	Measured ash melting temperatures of fuel and fly ashes. . .	126
5.6	Summary of the analysis of natural deposit shedding for two different sets of flue gas temperature, probe surface temperature, straw share and deposit load. . . . .	135
5.7	Summary of the analysis of shedding during sootblower operation for two different sets of flue gas temperature, probe surface temperature, straw share and deposit load. . . . .	136
5.8	Mean DDF-rates and mean net deposit accumulation rates for two different sets of flue gas temperature, probe surface temperature, straw share and deposit load. . . . .	140
6.1	Analysis of the fuels fired and added coal fly ash. a.r.: as received, d.b.: dry basis. . . . .	149
6.2	Matrix of the tests conducted at AVV2. . . . .	155
6.3	Summary of the main results of the measurements conducted at AVV2. . . . .	162
6.4	Ash deposition data from the previous and current full-scale measurements conducted in biomass suspension-fired boilers. . . . .	168
7.1	Composition of the fuel input data and fly ash input data. . .	189
7.2	Simulation conditions . . . . .	190
7.3	Comparison of measured data and simulated data (initial 6 h). . .	193
7.4	Measured DDF-rates and DDF-rates resulted from the simulation for two different sets of flue gas temperatures, probe surface temperatures, straw shares and deposit mass loads. . .	194

# Nomenclature

## Latin Letters

---

$\dot{A}$	Constant for flue gas temperature prediction (Chapter 5)
$ash_{coal}$	The coal ash flow [ $\frac{kg}{s}$ ]
$ash\%$	Percentage of ash in the dry fuel
$A_r$	X-sectional area of the boiler at probe measuring position [ $m^2$ ]
$B$	Empirical constant for thermophoretic velocity calculations
$\dot{B}$	Constant for flue gas temperature prediction (Chapter 5)
$C$	Ash deposition through condensation [ $\frac{g}{m^2h}$ ]
$\dot{C}$	Constant for flue gas temperature prediction (Chapter 5)
$C_{ash,1}$	Concentration of aerosols in the flue gas [ $\frac{kg}{m^3}$ ]
$C_{ash,2}$	Concentration of large sized particles in the flue gas [ $\frac{kg}{m^3}$ ]
$C_{ash,3}$	Concentration of intermediate sized particles in the flue gas [ $\frac{kg}{m^3}$ ]
$C_{i,b}$	Concentration of gas specie in the bulk gas [ $\frac{kg}{m^3}$ ]
$C_{i,s}$	Concentration of gas specie at the probe surface [ $\frac{kg}{m^3}$ ]
$d$	Probe diameter [ $m$ ]
$\dot{D}$	Constant for flue gas temperature prediction (Chapter 5)
$D_{comp}$	Composition of the inner deposit layer adjacent to the probe
$Diff_{pred}$	Predicted flue gas temperature difference [ $^{\circ}C$ ]
$D_i$	Diffusion coefficient [ $\frac{m^2}{s}$ ]
$\frac{dm_d}{dt}$	Ash deposition rate [ $\frac{g}{m^2h}$ ]
$d_p$	Particle diameter [ $m$ ]
$\dot{E}$	Constant for flue gas temperature prediction (Chapter 5)
$\dot{F}$	Constant for flue gas temperature prediction (Chapter 5)
$f_{entrained}$	Fraction of residual ash entrained as fly ash
$f_m$	Melt fraction
$f_{nat,6}$	Mean natural deposit shedding frequency [ $h^{-1}$ ]
$F_r$	Time fraction of 6 h period with no sootblower operation
$f_s(T_s)$	Sticking probability of ash particles exposed on the deposit
$f_{soot,6}$	Mean plant sootblower deposit shedding frequency [ $h^{-1}$ ]

---

## Latin Letters

---

$f_{stick}$	Sticking efficiency of the fly ash (deposit)
$f(T_f)$	Sticking probability of the incoming ash particles
$I$	Ash deposition rate through inertial impaction [ $\frac{g}{m^2h}$ ]
$g$	Gravitational acceleration [ $\frac{m}{s^2}$ ]
$h_f$	Convective heat transfer coefficient in the furnace region [ $\frac{W}{m^2K}$ ]
$k_{eff}$	Effective thermal conductivity of the deposit [ $\frac{W}{m \cdot K}$ ]
$k_{C,i}$	Mass transfer coefficient [ $\frac{m}{s}$ ]
$k_m$	Metal plate thermal conductivity [ $\frac{W}{m \cdot K}$ ]
$k_s$	Thermal conductivity of the solid phase [ $\frac{W}{m \cdot K}$ ]
$L$	Total length of the probe [ $m$ ]
$L_d$	Effective deposition length (probe) [ $m$ ]
$L_h$	Effective heat transfer length (probe) [ $m$ ]
$L_1$	Distance from the hinge to the balance [ $m$ ]
$L_2$	Distance from the hinge to the mass center of the deposit [ $m$ ]
$m$	Air flow to the probe [ $\frac{kg}{s}$ ]
$M$	Molar mass of the component [ $\frac{g}{mol}$ ]
$m_d$	Deposit mass on the probe [ $g$ ]
$m_{d,f}$	Final signal of the load cell [ $g$ ]
$m_{d,i}$	Initial signal of the load cell [ $g$ ]
$m_f$	Wood fuel flow to the boiler [ $\frac{kg}{s}$ ]
$\dot{m}_{fuel}$	Inlet fuel (biomass) flow rate [ $\frac{kg}{s}$ ]
$m(t)$	Continuously monitored probe mass uptake [ $\frac{g}{m^2}$ ]
$< m'(t) >$	DDF-rate [ $\frac{g}{m^2h}$ ]
$NE_6$	Number of natural shedding events in a 6 h interval
$p$	Pressure [ $\frac{N}{m^2}$ ]
$q$	Heat flux (probe) [ $\frac{W}{m^2}$ ]
$Q$	Heat uptake by the probe [ $W$ ]
$Q_c$	Convective heat transfer [ $\frac{W}{m^2}$ ]
$Q_{in}$	Total heat transfer [ $\frac{W}{m^2}$ ]
$Q_{rad}$	Radiative heat transfer [ $\frac{W}{m^2}$ ]
$Re$	Reynolds number
$s$	Probe surface area [ $m^2$ ]
$s_d$	Effective deposit area [ $m^2$ ]
$SE_6$	Number of sootblowing shedding events in a 6 h interval
$Sh$	Sherwood number
$T$	Flue gas temperature [ $K$ ]
$t_1$	Start time [ $h$ ], (IDF-rate calculation)
$t_2$	Final time [ $h$ ], (IDF-rate calculation)
$T_{fg}$	Flue gas temperature [ $^{\circ}C$ ]
$T_{m,i}$	Metal plate inner temperature [ $^{\circ}C$ ]
$T_{m,o}$	Metal plate outer temperature [ $^{\circ}C$ ]
$T_{g,i}$	Air inlet temperature [ $^{\circ}C$ ]

## NOMENCLATURE

---

### Latin Letters

---

$T_{g,o}$	Air outlet temperature [ $^{\circ}C$ ]
$T_s$	Deposit surface temperature [ $^{\circ}C$ ]
$T_t$	Probe metal temperature [ $^{\circ}C$ ]
$TT_n$	Total time without plant sootblowing during a 6 h interval [ $h$ ]
$TT_s$	Total time with plant sootblowing during a 6 h interval [ $h$ ]
$u_{bg}$	Bulk gas velocity [ $\frac{m}{s}$ ]
$u_T$	Thermophoretic velocity [ $\frac{m}{s}$ ]
$\dot{V}_{fg}$	Volumetric flow rate of flue gas [ $\frac{m^3}{s}$ ]
$\nu_g$	Kinematic gas viscosity [ $\frac{m^2}{s}$ ]
$X_a$	Fraction of ash in dry wood fuel
$X_i$	Operational parameter for flue gas temperature prediction
$x_1$	Metal plate thickness [ $m$ ]
$x_2$	Slit thickness [ $m$ ]
$Y_{calc}$	Predicted flue gas temperature [ $^{\circ}C$ ]
$Y_{meas}$	Measured suction pyrometer flue gas temperature [ $^{\circ}C$ ]
$Y_{TC}$	Measured thermocouple flue gas temperature [ $^{\circ}C$ ]

### Abbreviations

---

AMV1	Amagerværket Unit 1
AMV2	Amagerværket Unit 2
AVV2	Avedøreværket Unit 2 (in Chapter 4 and 5, grate-fired boiler)
AVV2	Avedøreværket Unit 2 (in Chapter 6, suspension-fired boiler)
CCD	Charge-Coupled Device
DDF-rate	Derivative-based Deposit Formation Rate [ $\frac{g}{m^2h}$ ]
FMT	First Melting Temperature [ $^{\circ}C$ ]
ICP-IC	Inductively Coupled Plasma-Ion Chromatography
IDF-rate	Integral Deposit Formation Rate [ $\frac{g}{m^2h}$ ]
IFRF	International Flame Research Foundation
P	Probe location at AVV2-bio boiler
PIP	Peak Impact Pressure [ $kPa$ ]
P1	Probe location one at AMV2 boiler
P2	Probe location two AMV2 boiler
SCR	Selective Catalytic Reduction
SEM-EDS	Scanning electron microscopic-Energy dispersive X-ray spectroscopy
SH	Superheater
STP	Standard Temperature and Pressure
TB	Tube bank region (AMV2)

---

## Greek Letters

---

$\alpha$	Particle angle of impaction
$\delta$	Outer deposit thickness [ $m$ ]
$\delta_{d,i}$	Thickness of the initial deposit [ $m$ ]
$\delta_e$	Effective deposit thickness [ $m$ ]
$\epsilon_r$	Emissivity coefficient for deposit (0.8)
$\epsilon_{steel}$	Emissivity of steel
$\eta_{imp}$	Impaction efficiency
$\lambda$	Excess air ratio
$\mu_{fg}$	Flue gas viscosity [ $Pa \cdot s$ ]
$\rho_d$	Bulk density of the deposit [ $\frac{kg}{m^3}$ ]
$\rho_{fg}$	Flue gas density [ $\frac{kg}{m^3}$ ]
$\rho_p$	Particle density [ $\frac{kg}{m^3}$ ]
$\sigma$	Stephen Boltzmann Constant [ $5.6704 \times 10^{-8} \frac{J}{sm^2K}$ ]
$\theta$	Angular position
$\psi$	Molar ratio, (K+Na)/(2S+Cl)
$\nabla T$	Temperature gradient for thermophoretic velocity calculations [ $\frac{K}{m}$ ]

# Incorporated Publications

## Publications in international journals with peer review

Manuscripts published or submitted.

1. M. S. Bashir, P. A. Jensen, F. J. Frandsen, S. Wedel, K. Dam-Johansen, J. Wadenbäck, S. T. Pedersen, Ash transformation and deposit build-up during biomass suspension and grate firing: Full-scale experimental studies, *Fuel Processing Technology*, **97** (2012), 93–106.
2. M. S. Bashir, P. A. Jensen, F. J. Frandsen, S. Wedel, K. Dam-Johansen, J. Wadenbäck, S. T. Pedersen, Suspension-firing of biomass. Part 1: Full-scale measurements of ash deposit build-up, *Energy & Fuels*, **26** (2012), 2317–2330.
3. M. S. Bashir, P. A. Jensen, F. J. Frandsen, S. Wedel, K. Dam-Johansen, J. Wadenbäck, Suspension-firing of biomass. Part 2: Boiler measurements of ash deposit shedding, *Energy & Fuels*, **26** (2012), 5241–5255.

## Participation in national/international conferences/workshops

Participation includes oral or visual presentation and a full-paper or abstract.

1. M. S. Bashir, P. A. Jensen, F. J. Frandsen, S. Wedel, K. Dam-Johansen, J. Wadenbäck, S. T. Pedersen, Quantification of Ash Deposit Build-up and Removal in a Straw and Wood Suspension-Fired Boiler; Proc. *19<sup>th</sup> European Biomass Conference*, Berlin, Germany, 06–10 June, 2011. (Oral presentation and full-paper)
2. M. S. Bashir, P. A. Jensen, F. J. Frandsen, S. Wedel, K. Dam-Johansen, J. Wadenbäck, S. T. Pedersen, Ash deposition and shedding in straw and wood suspension-fired boilers; *1<sup>st</sup> Heat Nordic Solid Fuel Theme Days at Amagerværket (AMV)*, Copenhagen, Denmark, 04–05 November, 2010. (Oral presentation)
3. M. S. Bashir, P. A. Jensen, F. J. Frandsen, S. Wedel, K. Dam-



---

Johansen, J. Wadenbäck, S. T. Pedersen, Ash deposition and shedding in straw and wood suspension-fired boilers; *4<sup>th</sup> Annual Seminar: Biofuels Graduate School-2*, Copenhagen, Denmark, 26–28 September, 2010. (Oral presentation)

4. M. S. Bashir, P. A. Jensen, F. J. Frandsen, S. Wedel, K. Dam-Johansen, S. T. Pedersen, J. Wadenbäck, Ash deposit formation and removal in a straw and wood suspension-fired boiler; Proc. *Impact of Fuel Quality on Power Production and the Environment*, Lapland, Finland, 29 August–03 September, 2010. (Oral presentation)

5. M. S. Bashir, P. A. Jensen, F. J. Frandsen, S. Wedel, K. Dam-Johansen, S. T. Pedersen, J. Wadenbäck, Ash deposition and shedding in biomass suspension-fired boilers: Full-scale experimental study; Proc. *Dansk Kemingeniør Konference, DK2-2010*, Lyngby, Denmark, 16–17 June, 2010. (Visual presentation)

6. M. S. Bashir, P. A. Jensen, F. J. Frandsen, S. Wedel, K. Dam-Johansen, T. Wolfe, S. T. Pedersen, J. Wadenbäck, Characterization and quantification of deposit build-up and removal in straw suspension-fired boilers; Proc. *18<sup>th</sup> European Biomass Conference*, Lyon, France, 03–07 May, 2010. (Oral presentation and full-paper)

7. M. S. Bashir, P. A. Jensen, F. J. Frandsen, S. Wedel, K. Dam-Johansen, S. T. Pedersen, J. Wadenbäck, Full-scale measurements of ash deposition in straw suspension-fired boilers; *3<sup>rd</sup> Annual Seminar: Biofuels Graduate School-2*, Trondheim, Norway, 14–16 June, 2009. (Oral presentation)

8. R. Gani, C. Jimenez-Gonzalez, D. Constable, M. S. Bashir, Solvents in organic synthesis: Replacement and multi-step reaction systems; Proc. *AIChE Annual Meeting*, Philadelphia, PA, USA, 16–21 November, 2008. (Part of M.Sc. work)

# Chapter 1

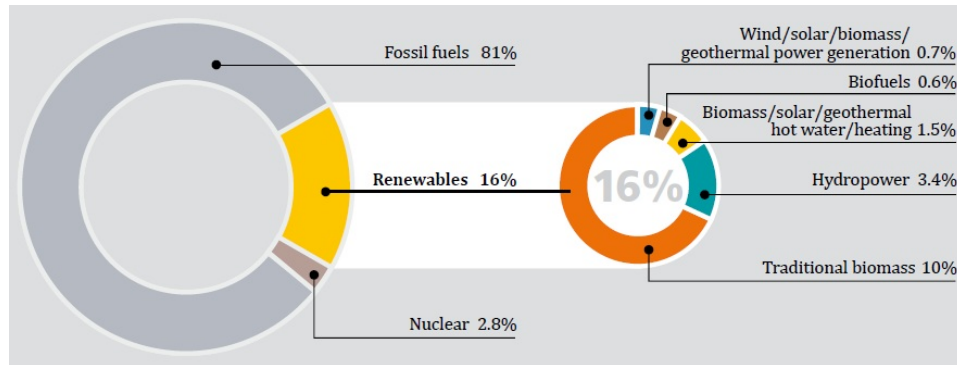
## Introduction

### 1.1 Background

Utilization of biomass for heat and power production is an attractive option to lower CO<sub>2</sub>-emissions and to make the energy supply independent of fossil fuels. In the last two decades, much attention has been paid worldwide to use biomass for heat and power production, and currently contribution of biomass for heat and power production is significant [1]. The overall contribution of biomass to the world energy supply is shown in Figure 1.1. It can be seen that the traditional biomass accounts for about 10% of the world energy supply. A significant share of biomass in simple stoves accounts for the global biomass consumption and an increased application of modern biomass boilers in developing and in developed countries can result in improved energy efficiency and reduction in harmful emissions [2]. In the regions with larger forests like Northern and Central Europe, wood can be the predominant biomass type used for energy production, while in agriculture areas, agricultural waste (straw) can be used. Overall, more than 240 Mt/year of wheat and barley straw is produced just within Europe (year 2000) [3].

Different technologies can be employed for the utilization of biomass for heat and power production, but the main process is combustion, while gasification and pyrolysis are still in the development stage. It can be seen from Table 1.1 that present deployment of gasification and pyrolysis is not available due to technological and economical barriers. In Denmark, combustion is the main process used in the thermochemical treatment of biomass.

By the end of 2009, there were 8 biomass-fired and 5 biomass co-fired power plants in Denmark [4] (8-9 grate-fired boilers, 3 suspension-fired boilers, and a single circulating fluidized bed boiler). The power plants in Denmark have been obliged to use 1.0 Mt of straw and 0.2 Mt of wood chips annually [5]. In the recent debates, new initiatives are being discussed, aim-



**Figure 1.1:** Share of renewable energy in the global final energy consumption, 2009 [1].

**Table 1.1:** Qualitative comparison of biomass conversion technologies to produce electricity, heat and/or power. +++ relatively good, + relatively poor, x relatively cheap, xxxx relatively expensive. Adopted from Egsgaard et al. [6]

	Combustion (heat)	Combustion (electricity)	Gasification	Pyrolysis
Technology	+++	++ (+)	+(+)	(+)
Environment	+++	++ (+)	+(++)	(+++)
Economics	x	xx	xxx	xxxx
Market potential	+++	+++	+++	++ (+)
Present deployment	+++	++		

ing for complete substitution of coal with biomass in the largest cities and industrial districts in Denmark [7, 8]. If this is going to be implemented in the near future, many of the Danish power plants running on coal have to be converted to use biomass. The complete substitution of coal with biomass would be possible either by commissioning of new biomass-fired boilers and/or retrofitting of existing coal-fired boilers. This process could be extremely challenging because biomass fuels differ in many ways from coal, having higher moisture contents, lower heating values and a variety of impurities, chlorine (Cl), alkali metals (K and Na), and sulfur (S) and nitrogen (N) etc. [9]. Biomass fuel ashes are compared to fossil fuel ashes often rich in elements such as chlorine (Cl), alkali metals (K and Na), silicon (Si), and calcium (Ca), and the release of some of these elements to gas phase during combustion may form alkali chlorides and ash with lower melting temperature, leading to severe ash deposition and corrosion of boiler coils [2, 5, 10–22]. Large deposit formation problems may limit the electrical efficiency by limiting the maximum applicable superheater temperatures, and the deposits may also cause many boiler stops where different parts of the boiler have to be cleaned.

In Denmark, straw is usually combusted in dedicated grate-fired boilers where the fuel is combusted in the bottom part of the furnace chamber on a moving bed. But straw is also combusted by developing coal-based suspension-fired boilers to accept some fractions of straw as fuel. The utilization of 100% straw in suspension-fired systems originally used for coal combustion, has also been considered in Denmark. In biomass suspension firing, pulverized biomass typically from pellets crushed in the coal mills is blown into the burners, where the fuel particles are burned in suspension. Combustion of straw and/or wood in suspension-fired units is an attractive option because of the often high electrical efficiency of these plants (46–48%), compared to the traditional grate-fired systems (25–30%) [2]. In this regard, Unit 2 at Avedøre Power Station (AVV2), a multi-fuel suspension-fired boiler that can apply wood, natural gas and heavy fuel oil as fuel, was commissioned a decade ago [23]. AVV2 is considered to be the world’s largest wood suspension-fired boiler [24]. Unit 2 at Amager Power Station (AMV2), previously a coal-fired drum-type boiler, was retrofitted in 2003 to use pure pulverized biomass fuel with different shares of wood and straw. Unit 1 at Amager Power Station (AMV1), commissioned in 2009, is the first dedicated biomass suspension-fired boiler that was designed to fire straw and/or wood. However, when straw is used in suspension-fired boilers, the deposit flux on the superheater tubes is expected to increase because a higher percentage (80–90%) of fly ash is entrained as fly ash during suspension firing, while only 10–30% is entrained during grate firing [17]. In addition, the vaporized critical inorganic elements, such as alkalis (K, Na) and chlorine (Cl), may result in high concentration of gaseous species in the flue gas at higher temperatures during straw suspension combustion [25, 26]. Investigations by Nordgren et al. [27] indicate that during biomass (straw and/or wood) suspension combustion, the transport of gas phase alkalis and ash to the heat transfer surfaces can be significant at higher flue gas temperatures [27]. Suspension combustion of biomass at pilot-scale have shown higher deposit formation rates during straw firing, compared to straw co-firing with woody biomass, possibly due to dilution and/or chemical interactions [27, 28]. However, to obtain better understanding of ash deposit formation during straw suspension firing, a proper description of the primary ash [29], the transport of ash species [10], the deposit formation process [30, 31], the maturing and sintering of deposits [15, 21, 32, 33], and deposit shedding process [34–36] is essential. In a broader scenario, a limited number of full-scale facilities and consequently only a few full-scale measurements can be found for 100% straw and/or wood combustion in suspension-fired boilers [27, 28, 37]. In addition, most of these studies have been based on short testing time (up to couple of hours), while more extensive full-scale measurements on straw and/or wood suspension firing are rare to find [2, 5, 38]. Therefore, more detailed and extensive full-scale studies on transient deposit formation rate

when firing straw and wood can improve our understanding of the biomass ash deposit formation processes.

To minimize deposition problems, different strategies can be employed, e.g. use of additives that can convert the vaporized inorganic species to less harmful forms [5, 26, 39], pre-treatment of fuels by leaching out alkali [40], co-firing with clean fuels [41], and use of effective deposit shedding techniques [42]. Use of additives and pre-treatment of fuels by leaching are less cost effective compared to the use of effective deposit shedding [5, 40]. The ash deposit build-up during biomass combustion is a dynamic process consisting of both the deposit formation and the deposit shedding [35]. Shedding may be initiated at the surface of the deposit, along the deposit tube interface and inside the deposit depending on the local boiler conditions and the deposit properties [42]. Deposit shedding can be caused artificially as a part of the boiler operation, e.g. by sootblowing, or naturally, without any operational or mechanical influence [2]. Mechanisms of natural shedding in combustion systems are: 1) erosion [43], 2) gravity shedding [35], and 3) thermal shock [43]. Erosion is the process of deposit shedding when non-sticky sharp edged often  $\text{SiO}_2$ -rich fly ash particles collide with non-sticky areas on a deposit surface causing deformation (ductile deposits) and a cutting action (brittle deposits) [2, 43]. Gravity shedding will occur when the gravity force on the deposit is strong enough to cause a fracture inside the deposit, or, when the gravity force exceeds the tube and deposit adhesion strength, or, through flow of a molten deposit [35]. Thermal shock induced shedding is caused by temperature changes, due to the difference in the thermal expansion coefficients of tubes and deposits. A sudden temperature gradient may cause an uneven expansion of the deposit and the tube, or, distinct, adjacent, deposit layers, leading to deposit fractures. The sudden temperature gradients can be caused by fluctuations of the flue gas or steam temperature. Artificially, ash deposits can be removed from the heat transfer surfaces by inducing mechanical or thermal stresses inside them. This can be done using the impact of the high pressure steam, air and water (sootblowing) [36, 44], or by changing the thermal load etc. Sootblowers effectively remove fouling/slagging deposits but in order to ensure maximum boiler thermal efficiency, cost effective use of sootblowers is also important, since these may consume a significant percentage of the boiler steam production [33]. In addition, a high superheater temperature ( $> 550 \text{ }^\circ\text{C}$ ) is needed due to the corresponding increased electrical efficiency, and therefore deposit shedding at elevated superheater temperatures is of significant interest.

As significant amount of biomass is utilized for heat and power production in Denmark, it is important to make the overall process efficient, and the development of innovative and optimal shedding strategies in power plant boilers is therefore essential. The ash deposition processes have been studied

for many years, but the information about the deposit shedding process is limited and the available information mainly deals with shedding of deposits in coal [34] and Kraft recovery boilers [36, 44]. While some research work has been done on biomass ash deposit shedding in recent years [33, 35], a lot of subjects are still not very well investigated. Most studies have been based on transient deposit build-up and shedding measurements in grate boilers [33, 35, 45, 46], while only limited data are available from biomass suspension firing [5, 24, 38, 48]. Also subjects like the characteristics of plant sootblowers and the influence of fuel changes on deposit build-up and shedding have not previously been studied. Most deposit probe measurements in biomass boilers have been done in the convective pass [33, 46, 49] and only a limited work have been done on boiler wall deposits [50].

The most recent full-scale straw and/or wood suspension firing investigations have been made by Tobiasen et al. [5], Peter et al. [24], Skrifvars et al. [38] and Jenkins et al. [51]. In Denmark, at the same time, the use of biomass (straw and/or wood) in suspension has gained momentum in the last decade, and thereby provides both opportunities and challenges for further investigation of deposit build-up and shedding processes. In addition to the limited full-scale experimental data, a detailed predictive model of ash deposition and shedding in a straw and wood suspension-fired boiler is also not available, and a significant effort is needed in this area.

## 1.2 Project Objectives

This project aims at providing scientifically based knowledge on the following areas:

- Understanding the deposit formation process and removal behavior of deposits in the boiler chamber and superheater region (convective pass) of biomass suspension-fired boilers.
- The influence of load, operation conditions and fuel changes (straw, wood or coal firing) on boiler deposits.
- Comparative study of the influence of different boiler types on the ash deposit formation process.
- Provide measuring data that can be used to verify a model describing the influence of fuel changes on ash deposits.
- Provide measuring data that can support activities on fuel characterization and CFD modeling.

It is important to mention that more than 90% of the project time was spent on the design and development of the probes, and performing full-scale

measurements, while rest of the time was spent on modeling and a literature study.

### 1.3 Thesis Structure

In addition to this introduction, the thesis contains nine chapters. More specifically, the thesis contains the following chapters.

**Chapter 2: Literature review.** An overview of the current knowledge about biomass as a fuel, biomass combustion technologies, release of inorganic elements from biomass, ash deposition, properties of deposits, deposit shedding mechanisms and techniques, and ash deposition modeling is presented in this chapter.

**Chapter 3: Design and development of probes for online monitoring of deposit build-up and removal.** This chapter covers an overview of the deposit probes used for ash deposit build-up and deposit characterization studies. The horizontal ash deposition probe used during the ash deposit build-up measurements and a simple artificial sootblowing probe used to remove the deposits are described in detail. The design, functionality and commissioning of a vertical ash deposition probe simulating the conditions of the boiler furnace wall is also discussed.

**Chapter 4: Ash transformation and deposit build-up during biomass suspension and grate firing.** This detailed chapter is about the comparative study of ash transformation and deposit build-up during biomass suspension and grate firing. A brief comparison was made between the data obtained from the Amager Power Station, Unit 2 (AMV2), straw suspension-fired boiler, and data obtained from measurements conducted at the Avedøre Power Station, Unit 2 (AVV2), firing straw on a grate. The influence of fuel type, probe surface temperature and flue gas temperature on ash deposit formation rate has been investigated.

**Chapter 5: Transient deposit build-up and shedding during straw and wood suspension combustion.** This chapter describes deposit probe measurements of deposit build-up and shedding in a 350 MW<sub>th</sub> suspension-fired boiler, firing straw and wood. The influence of fuel type (straw share in wood), probe exposure time, probe surface temperature (500, 550 and 600 °C), and flue gas temperature (600–1050 °C) on ash deposit formation rate and deposit shedding has been investigated. Two different measures of deposit formation rate are used in the analysis of the data. Quantification of deposit shedding as a function of experimental conditions and boiler operational parameters has been made. In addition to the changes in probe heat uptake for different deposit mass loads, ash transformation and deposit characterization during straw and wood suspension

firing is also discussed in this chapter.

**Chapter 6: Ash deposit build-up and shedding during wood suspension combustion with coal ash addition.** This chapter is summarized based on the boiler deposit measurements conducted in a wood and natural gas suspension-fired boiler with and without the addition of coal ash. Influence of coal ash to fuel ash ratio, boiler load and flue gas temperature on ash deposition has been discussed. Detailed characterization of the deposits formed with and without the addition of coal ash has been made.

**Chapter 7: Mechanistic modeling of ash deposit build-up during biomass suspension firing.** This chapter is about the development of a mechanistic model for ash deposition in a straw and wood suspension-fired boiler. Sub-model for each ash deposition process and a sub-model for heat uptake has been simulated to get better understandings of the key processes responsible for ash deposition. The model describes the deposit related processes as a function of the local parameters as flue gas velocity, flue gas temperature, probe surface temperature, and fuel changes.

**Chapter 8: Innovative ideas for deposit shedding in biomass suspension-fired boilers.** This chapter provides useful innovative ideas that can be possibly implemented for optimal ash deposit shedding in a straw and wood suspension-fired boiler.

**Chapter 9: Conclusions and suggestions for future work,** which summaries the results and outlines the suggestions for future studies.





## Chapter 2

# Literature Review

### 2.1 Introduction

The utilization of renewable energy sources seems to be essential because of the increase in CO<sub>2</sub>-emissions, increase in world energy demands and depletion of fossil fuels. Biomass is considered to be one of the most widely accepted environmental friendly renewable energy sources. The most commonly used biomass fuels include wood, short-rotation woody crops and agricultural wastes [52]. In the last two decades, much attention has been paid in the world for biomass (co)-combustion for heat and power production. Traditional biomass contributes significantly to the world's energy supply, accounting for about 10% of the world's energy supply [1]. A significant share of biomass in simple stoves accounts for the global biomass consumption and an increased application of modern biomass boilers in developing and in developed countries can result in improved energy efficiency and reduction in harmful emissions [2]. In the regions with larger forests like Northern and Central Europe, wood can be the predominant biomass type used for energy production while in agriculture areas, agricultural waste (straw) can be used.

Biomass - straw and wood - has had increasing use in Denmark since 1990 and by the end of 2009, there were 8 biomass-fired and 5 biomass co-fired plants in Denmark [4]. The power plants in Denmark have been obliged to use 1.0 Mt of straw and 0.2 Mt of wood chips annually [5]. In the recent debates, new initiatives are being discussed, aiming for complete substitution of coal with biomass in the largest cities and industrial districts in Denmark [7, 8]. The complete substitution of coal with biomass would be possible either by commissioning of new biomass-fired boilers and/or retrofitting of existing coal-fired boilers. This process could be extremely challenging because biomass fuels differ in many ways from coal, having higher moisture contents, lower heating values and a variety of impurities, chlorine (Cl),

alkali metals (K and Na), sulfur (S) and nitrogen (N) etc. [9]. Biomass fuel ashes are compared to fossil fuel ashes often rich in elements such as chlorine (Cl), alkali metals (K and Na), silicon (Si) and calcium (Ca), and the release of some of these elements to gas phase during combustion may form alkali chlorides and ash with lower melting temperature, leading to severe ash deposition and corrosion of boiler coils [2, 5, 10–22]. Large deposit formation problems may limit the electrical efficiency by limiting the maximum applicable superheater temperatures, and the deposits may also cause many boiler stops where different parts of the boiler have to be cleaned. The heat transfer through the heat exchanger can be consequently reduced, thereby reducing the efficiency of the boiler. As the growing interest in utilizing biomass in heat and power production increases, the understanding of the fundamentals of biomass combustion has considerably increased in the recent years through extensive research. However, the available full-scale experimental studies on ash deposition in biomass-fired boilers have been reported based on measurements in grate boilers. Only limited data is available from biomass suspension firing where improved knowledge on ash transformation, and transient deposit formation and shedding is wanted to optimize design and operation. In addition, predictive modeling of ash deposition and shedding in biomass suspension-fired boilers is an area demanding significant research.

An overview of the current knowledge about biomass as a fuel, biomass combustion technologies, release of inorganic elements from biomass, ash deposition, properties of deposits, deposit shedding mechanisms and techniques, and ash deposition modeling is presented in this chapter.

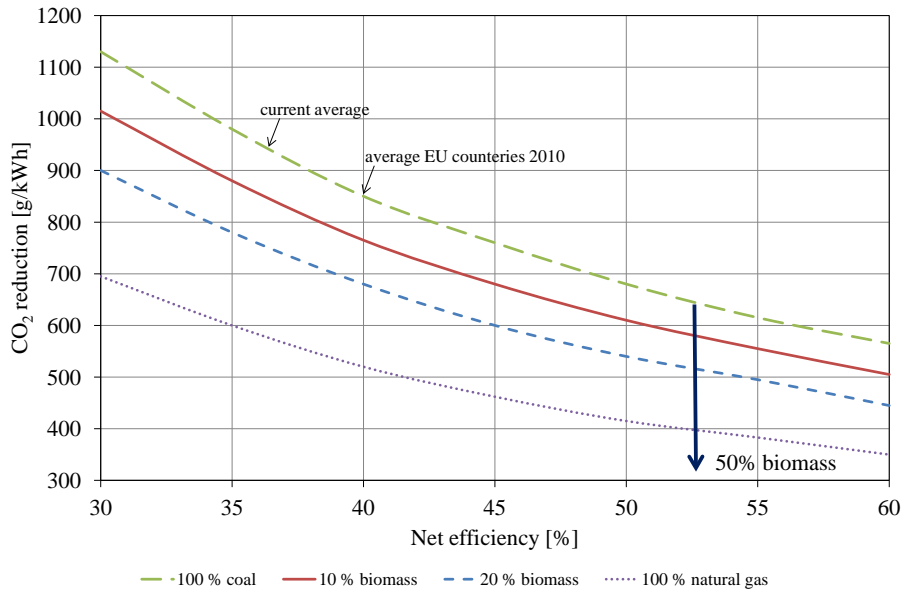
## 2.2 Biomass Fuel and Ash Formation

Biomass is typically composed of three main components (cellulose, hemicellulose and lignin) and a number of minor components (lipids, proteins, water and ash). The fraction of each class of component varies depending on species, type of plant tissue, stage of growth and growing conditions [17, 53].

### 2.2.1 Biomass as a CO<sub>2</sub>-neutral Fuel

The use of biomass as a fuel for heat and power production is an obvious solution to the societal energy demands because of the uncertainty and depletion of fossil sources. The issues related to global warming caused by CO<sub>2</sub>-emissions has put an additional focus on the so called CO<sub>2</sub>-neutral fuels - biomass. The legal binding of green house gases was established for the first time in 1997, named as the Kyoto Agreement, aiming to reduce the total emissions by 5.2% by the year 2012 [2]. Biomass was then considered all over the world a potential source to reduce the net CO<sub>2</sub>-emissions from

fossil fuels. In addition to the use of biomass only for energy production, co-firing options with coal have also been practiced in the last two decades [2]. As shown in Figure 2.1 a significant reduction in CO<sub>2</sub>-emissions is possible by increasing the boiler efficiency and utilizing larger share of biomass in coal-fired power plants.

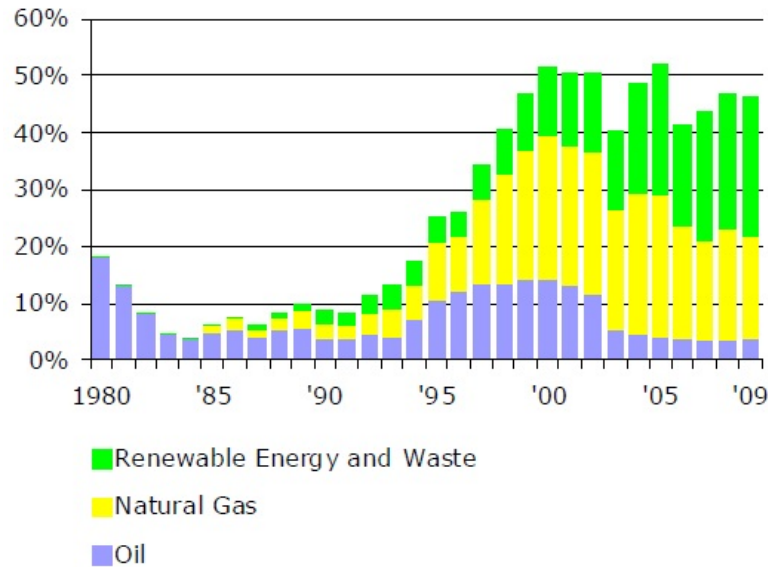


**Figure 2.1:** Possible reduction in CO<sub>2</sub>-emissions by increasing boiler efficiency and introduction of biomass to co-fired power plants [23].

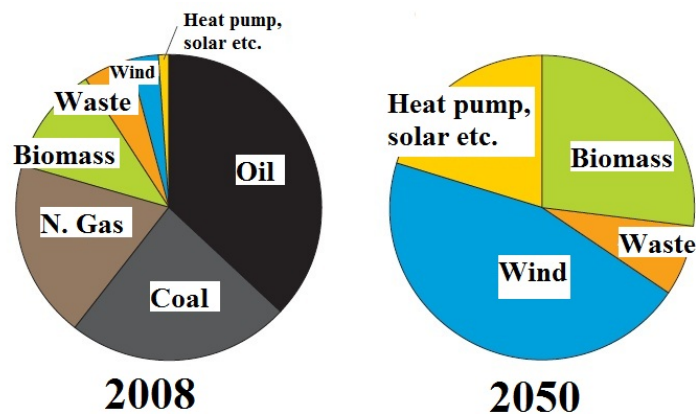
Despite the introduction of biomass, the Danish electricity production has been, and still is characterized by the utilization of coal and oil. Electricity production in Denmark in terms of percentage of fuels other than coal is shown in Figure 2.2. Significant drop in the coal share is evident from the last two decades [54]. Until the early 1990s, coal was the dominant fuel used in the production of electricity. In 2009, oil, natural gas and renewable energy together accounted for 46.3% of fuel consumption for electricity production. The share of renewable energy was the largest among the fuels other than coal. Biomass contributes about 36.1% to the renewable energy [54].

Based on the Danish energy policy in the last couple of decades, several full-scale measuring campaigns have been conducted in order to investigate the thermal conversion and utilization of biomass for heat and power production [2]. The ambitious targets for Danish energy for year 2050, demands further research on thermal conversion of biomass. To achieve a goal of fossil-fuel-free Denmark, the Danish government is ambitious to include

biomass as the second largest source of energy supply in 2050, accounting for more than 27% (Figure 2.3) [8].



**Figure 2.2:** Share of fuels other than coal for electricity production in Denmark (in percentage contribution of each fuel) [54].

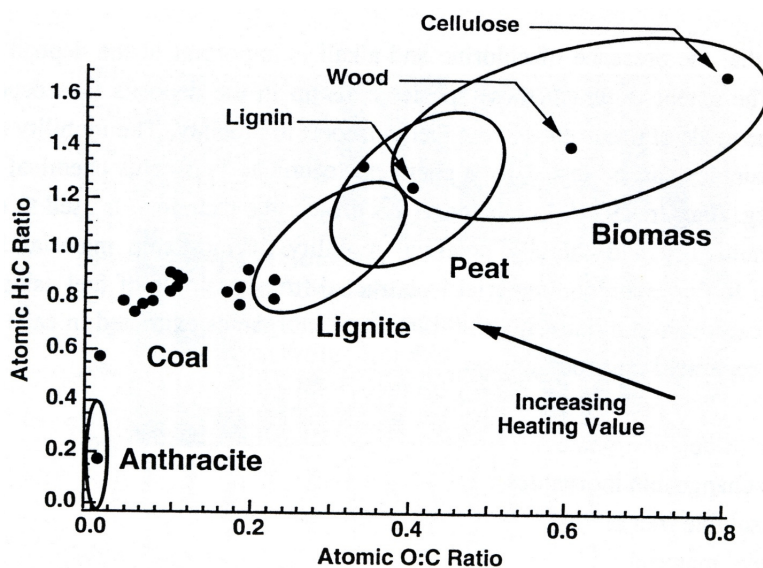


**Figure 2.3:** Danish energy target for 2050 [8].

### 2.2.2 Characterization of Biomass Fuels

Biomass fuels are different from coal in various ways. Biomass fuels are characterized by low energy density and thereby create serious issues in handling and transportation of the fuel. Differently from biomass, coal is a sedimentary organic substance originating from vegetation and formed during millions of years in the earth's crust. Coal is normally ranked based

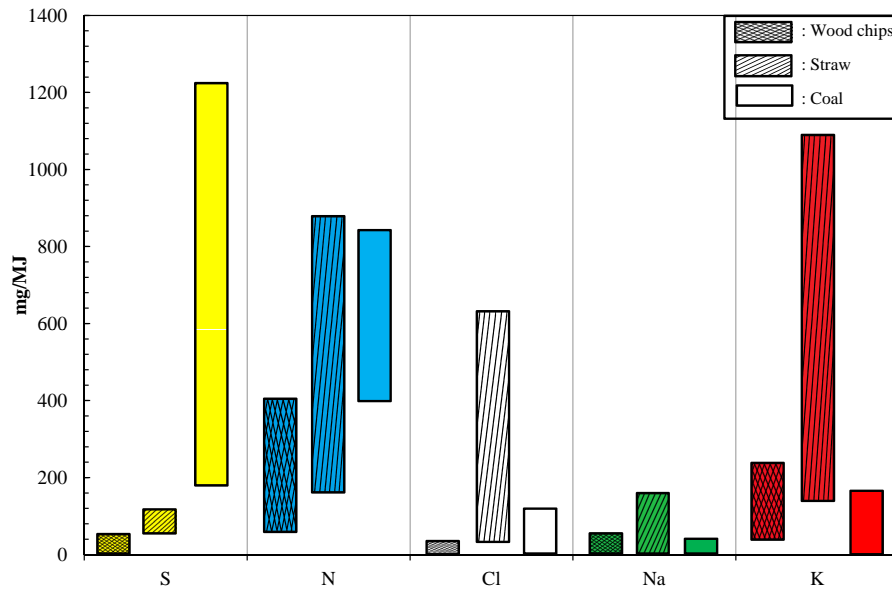
on the degree of coalification that increases with increasing maturity. High rank fuels are characterized by lower H:C and O:C ratios as shown in Figure 2.4 (Van Krevlen Diagram). Biomass fuels are characterized by higher H:C and O:C ratios, and find the least place in the upper right section of Figure 2.4. Atomic O:C ratio has significant impact on the heating values of the solid fuels. The heating values of the solid fuels normally decreases with increase in atomic O:C ratios.



**Figure 2.4:** A Van Krevlen diagram, showing atomic O:C and H:C ratios as a function of fuel ranks [14].

Nutrients needed for plant growth are the majority of the ash forming elements found in annual biomass. Furthermore, inorganic impurities can also occur as a result of contamination of the biomass with soil during harvest transport or handling. The most abundant ash forming elements in annual biomass are K, Cl, S, Ca, Mg, P, and Si [53]. In annual biomass, K and Cl are normally present in high concentrations and these will remain in ionic form and are not metabolized by the plant [53]. In wood, the presence of K and Cl is comparatively lower compared to the annual biomass fuels. S is present in annual biomass as inorganic sulfate and organically associated S of aliphatic nature such as in proteins, sulfate esters, and sulfur lipids [53]. As annual crops are characterized by high growth rates compared to wood tree, and thereby are higher production rates of proteins which require a rich S supply [53].

The inorganic material can occur as discrete minerals (soil contamination), amorphous phases, and organically associated present in the plant



**Figure 2.5:** S, N, Cl, Na and K contents in wood chips, Danish straw and coal (fired in Denmark) based on heating value of the fuel. Modified from Sander [59].

itself where it is embedded in the carbon matrix or simply salts dissolved in pore water [15]. In the organic phase, the inorganic material is often present as cations associated with oxygen-associated functional groups. According to Jenkins [14], in many biofuels the dominant fraction of the inorganic material is probably associated to oxygen containing functional groups, and more than 90% of K in clean biomass fuels appears as either water-soluble, or ion-exchangeable in ammonium acetate.

The composition of wood chips, Danish straw, and coal is shown in Figure 2.5 based on lower heating values of the fuels. It can be seen that straw contains significant amounts of Cl, K, while coal is characterized by higher S contents. A more detailed composition of Danish straw, wood chips and coal (fired in Denmark) with possible variations is shown Table 2.1. Na is found in high contents in wood, while the elements such as Al and Fe which play a significant role for ash deposition in coal-fired boilers are only present in small concentrations in straw and wood.

Differences between coal and straw are observed when comparing the chemical composition of the inorganic matter in coal and biomass as shown in Table 2.2. The elemental composition of the ash-forming matter after ashing the fuel samples according to a standard ashing procedure are pro-

vided. It is common practice to give the percentage of each of the elements analyzed as if they were present as their most common oxides [2, 9]. It is important to note that the elements very seldom are present in the ash as the oxides indicated, but normally as some more complex compounds [9]. Remarkable difference in the composition of biomass-derived ashes and coal ashes is evident in terms of K, Ca and Si.

**Table 2.1:** Difference in properties of biomass fuels and coal. Adopted from Flemming [2], Sander [59], Telfer et al. [61] and Glarborg et al. [62].

Specie	Unit	Coal		Wheat straw		Wood chips	
		Typical	Variation	Typical	Variation	Typical	Variation
Moisture	wt.%	3.0	2.1–14.0	14.0	8.0–23.0	45	20.0–60.0
LHV	$\frac{MJ}{kg}$	30.0	29.0–32.0	18.6	18.0–19.0	19.5	18.5–20.5
Ash	wt.% dry	10.0	4.0–11.0	4.5	2.0–7.0	1.0	0.3–6.0
Volatiles	wt.% dry	30.0	5.0–35.0	78.0	75.0–81.0	81.0	70.0–85.0
H	wt.% dry	5.0	3.0–6.0	5.9	5.4–6.4	5.8	5.2–6.1
C		88.0	69.0–93.0	47.5	47.0–48.0	50.0	49.0–52.0
N		1.5	1.0–1.8	0.7	0.3–1.5	0.3	0.1–0.7
S		1.0	0.9–5.0	0.15	0.1–0.2	0.05	<0.1
Cl		–	0.04–0.17	0.4	0.1–1.1	0.02	<0.1
Si		2.1	–	0.8	0.1–1.5	0.1	<1.0
Al		0.28	–	0.005	<0.03	0.015	<0.1
Fe		–	0.08–0.74	0.01	<0.03	0.015	<0.1
Ca		–	0.62–0.95	0.4	0.2–0.5	0.2	0.1–0.9
Mg		–	0.57–0.78	0.07	0.04–0.13	0.04	<0.1
Na		–	1.52–1.86	0.05	<0.3	0.015	<0.1
K		–	0.02–0.03	1.00	0.2–1.9	0.10	0.05–0.40
P		–	–	0.08	0.03–0.20	0.02	<0.1

The different fuel and ash properties of biomass in comparison with solid fossil fuels result in different combustion and deposition behavior. K rich vapors, salts and silicates with relatively low melting temperature ranges are formed during straw combustion [17]. These potassium components play a significant role in the deposit formation because they act as glue bonding the individual fly ash particles together [22]. The differences are summarized based on the combustion and deposition behavior by Yin et al. [60] as,

- Biomass fuels generally have higher volatile contents and lower heating values than coal
- Pyrolysis starts at a lower temperature for biomass fuels
- The fractional heat contribution by volatiles in biomass is of order of approx. 70% compared to approx. 36% for coal
- Biomass chars have higher oxidation reactivity, probably as a result of presence of alkalis in the char matrix
- Straw has more free alkali in ash and can aggravate fouling and slagging problems



**Table 2.2:** Fuel analysis of biomass and coal fuels. Adopted from Frandsen [2]. <sup>a</sup> wt.%, <sup>b</sup> % d.f., <sup>c</sup> % d.a.f.

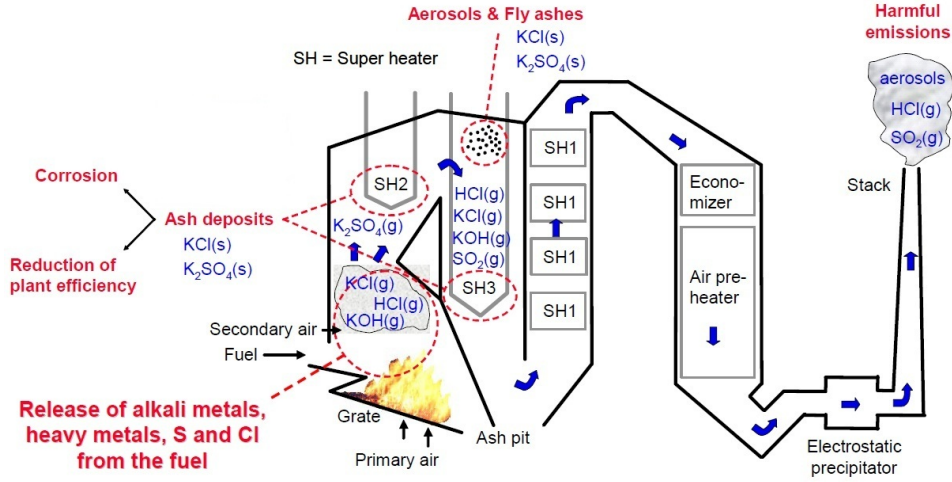
Fuel	Alfalfa	Straw (Rape)	Spruce	Bark	Illinois (6)	Upper (F)	Wyodak (A)	Beulah (Z)
Moisture <sup>a</sup>	6.90	6.40	6.10	5.40	7.97	1.13	28.09	32.24
Ash <sup>b</sup>	10.90	9.70	0.50	4.00	14.25	13.03	6.31	6.59
C <sup>c</sup>	44.60	44.70	50.90	51.60	70.46	84.39	52.52	47.77
O <sup>c</sup>	47.40	47.50	43.30	42.90	18.57	6.86	42.47	47.74
H <sup>c</sup>	5.00	5.10	5.60	5.10	4.54	4.64	3.75	3.16
S <sup>c</sup>	0.23	0.30	0.01	0.05	5.18	2.64	0.48	0.58
Na <sup>c</sup>	2.34	1.40	0.11	0.42	1.25	1.54	0.78	0.75
Cl <sup>c</sup>	0.46	0.98	0.01	0.02	0.05		0.02	0.04
<i>Ash<sup>c</sup></i>								
SiO <sub>2</sub>	11.50	7.80	21.20	25.50	42.63	44.39	36.60	18.89
Al <sub>2</sub> O <sub>3</sub>	1.10	1.60	1.30	2.80	14.95	22.38	17.71	9.83
Fe <sub>2</sub> O <sub>3</sub>	0.50	0.80	1.10	2.00	25.34	22.25	6.61	7.31
CaO	16.90	22.90	32.70	36.50	8.27	4.34	21.67	24.67
MgO	2.50	2.50	3.20	2.70	0.95	1.06	5.79	7.97
Na <sub>2</sub> O	0.60	6.80	0.20	0.30	1.17	0.32	1.89	7.75
K <sub>2</sub> O	34.80	21.60	9.40	4.70	1.59	2.54	0.47	0.44
TiO <sub>2</sub>	5.50	5.10	3.30	1.80	0.74	1.06	1.18	0.33
P <sub>2</sub> O <sub>5</sub>	16.00	3.90	21.60	13.70	0.11	0.11	0.83	0.44
SO <sub>3</sub>	5.10	12.70	1.10	1.20	4.24	1.06	7.56	22.28

### 2.2.3 Biomass Combustion Technologies

A correct evaluation of available combustion technology options for biomass conversion is important to ensure a successful and optimal biomass utilization [60]. Based on the certain type of biomass fuels, transportation cost and combustion behavior, different combustion technologies can be employed. The most commonly used systems for biomass combustion are grate-fired boilers, fluidized bed boilers and suspension-fired boilers. The choice of combustion technology is depended upon the nature and severity of the operational problems and fuel handling problems.

In grate boilers, the fuel is combusted in the bottom part of the furnace chamber on a moving bed. In biomass grate-fired boilers, two mechanisms generally generate fly ash, volatilization of inorganic elements and particle entrainment. As shown in Figure 2.6, the alkali metals, S and Cl are released from the fuels, and the formation of these flame-volatile elements resulted in the formation of aerosols when the flue gas is cooled down in the convective pass region.

Different types of grate configurations are employed based on the specific combustion requirements of a solid fuel. In a stationary sloping grate boiler, the grate does not move but the fuel burns as it slides down the slope. In a traveling grate boiler, fuel is fed in at the one side of the grate and has to be burnt before it reaches the ash dumping site of the furnace. With a vibrating grate boiler, the fuel is fed evenly over the whole grate.

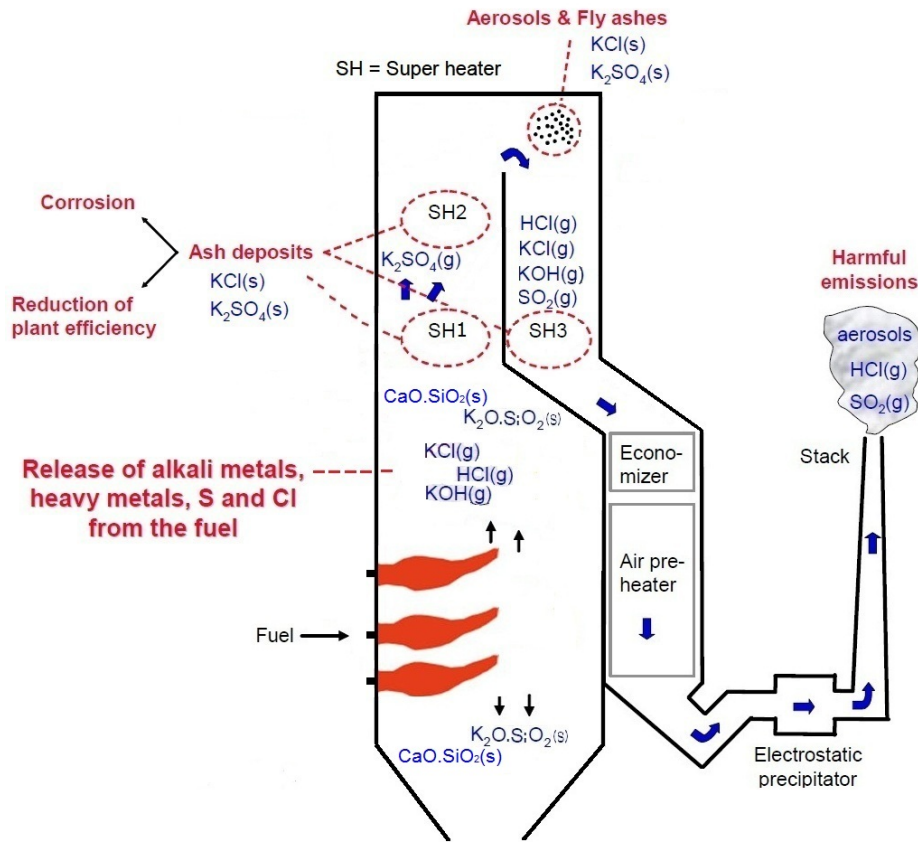


**Figure 2.6:** Schematic drawing of a grate-fired boiler used for biomass firing [63].

**Table 2.3:** Operating comparison of solid fuel firing technologies. Adopted from Glarborg et al. [62].

Technology	Combustion temp.	Gas velocity	Residence time (gas)	Residence time (solid)	Air to fuel	Ash split (fly ash/bottom ash)
	°C	m/s	s	s	ratio	%
Grate	1100–1300	4–9	1.0–3.0	1000–10000	1.3–2.5	5–30/70–95
Fluidized bed	850–900	5–8	0.5–6.0	500–1000	1.2–1.3	–
Suspension	1100–1500	5–10	1–3	1–3	1.1–1.3	80–90/10–20

Suspension firing of biomass is a fairly recent development and is practiced in relatively few installations. In biomass suspension firing, pulverized biomass typically from pellets crushed in the roller (coal) mills is blown into the burners, where the fuel particles are burned in suspension. Combustion of straw and/or wood in suspension-fired units is an attractive option because of the often high electrical efficiency of these plants (46–48%), compared to the traditional grate-fired systems (25–30%) [2]. A disadvantage of this technology is that fuel requires a comparable large amount of pre-treatment. In suspension firing, offsetting the higher efficiency results in the cost associated with drying and meeting the required fuel particle size for combustion [37]. For proper combustion in suspension fired boilers, biomass fuels are required to have a moisture content less than 15% and a fuel particle size of less than 6 mm, but this is not universal [64]. Thus, for suspension burning of fuel, the fuel handling systems require more careful design than conventional biomass firing systems [66]. The schematic drawing of a typical biomass suspension-fired boiler is shown in Figure 2.7. Suspension-fired combustion systems are generally associated with very large solid fuel boilers



**Figure 2.7:** Schematic drawing of a suspension-fired boiler used for biomass firing. Modified from Tobiasen et al. [5] and van Lith [63].

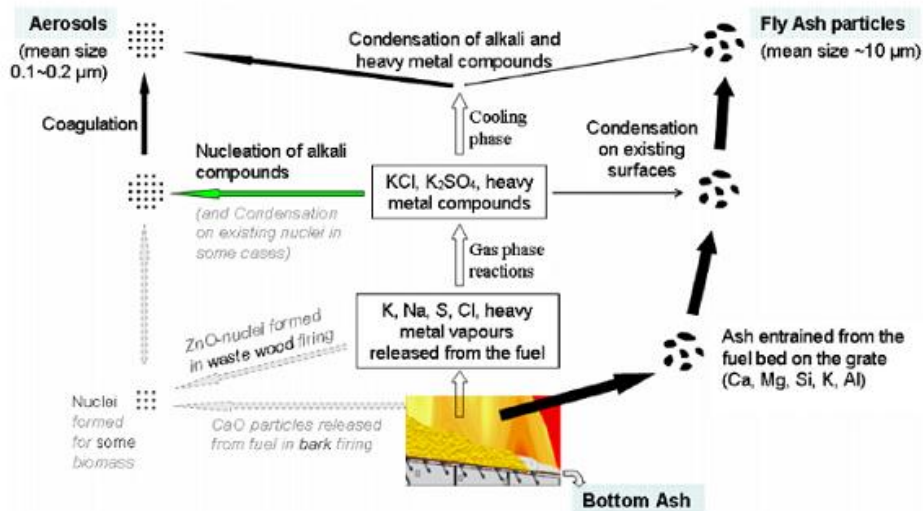
for power generation, and are not fueled with biomass alone, although there are a small number of biomass fired boilers in operation in Denmark and Sweden [5, 24, 37, 38]. Literature reports of detailed test work on pulverized fuel fired systems firing 100% biomass are relatively rare [5, 37, 38, 51]. During suspension firing, fuel particle residence time is of the order of a few seconds and peak flame temperatures are higher compared to grate firing conditions [37]. Furnace design and combustion conditions differ and the resulting fly ash and ash deposits can have different characteristics and physical appearances. A brief comparison of combustion technologies based on the common combustion variables is shown in Table 2.3.

In fluidized bed combustors, the fuel particles are suspended in a fluidizing air stream in the presence of coarse-grained bed material [65]. For fluidized bed combustors, their average combustion temperature is about

850°C, significantly lower than suspension firing systems as shown in Table 2.3. However, apart from fouling and slagging, the main issue while firing herbaceous based biofuels in fluidized bed combustors is the agglomeration of the bed material due to the presence of alkali metals in fuel ashes [65].

#### 2.2.4 Release of K, S and Cl during Biomass Combustion

The principal release of alkali metals, Cl and S for biomass combustion in a grate-fired boiler is shown in Figure 2.8. In the combustion zone, the inorganic matter, principally K, Cl and, in less amount, S, are volatilized as KCl, KOH, SO<sub>2</sub> and HCl. The nucleation begins when these volatilized elements become super saturated over solid particles containing Si and Na. K<sub>2</sub>SO<sub>4</sub>(s) is the first to become saturated (1000°C) followed by KCl(s,l) (700°C) [29, 60]. Submicron particles are mainly composed of K<sup>+</sup>, Na<sup>+</sup>, Cl<sup>-</sup> and SO<sub>4</sub><sup>-2</sup>, which together accounts for 80% of the submicron particles mass [10, 29]. Dayton and Milne [67], states that KCl was the primary gaseous alkali species released from combustion of straws and grasses with higher Cl and K contents, whereas KOH(g) was the most abundant alkali vapors released from feedstock with high alkali metal and low Cl contents. The release of Cl fits well for its presence in the fuel but combustion of a feedstock with higher K contents does not necessarily mean the high level of potassium (K) gases [53].



**Figure 2.8:** Schematic illustration of biomass combustion and ash transformation on a grate [60].

A laboratory scale reactor, meeting requirements of grate firing, was ap-

plied by Knudsen [29] to investigate the release behavior of Cl, K and S from four different types of biofuels. The results showed that between 20 and 60% of the total K is released at 900°C depending upon the fuel type. At temperatures above 900°C, the relative K-release increased almost linearly as a function of temperature until 60–90% is released at 1150°C [29]. Based on this experimental work, the conclusion was that the K-release in grate-fired boilers is significant for fuels containing high amounts of Cl and/or high amounts of K relative to Si [29]. Whereas, the K release is expected to be low for high Si fuels and low Cl-content [29]. Results showed that Cl is released in two steps, between 30–60% was released below 500°C, while the remaining Cl was released in a second step between 650 and 800°C. In the fuel samples with relatively low Cl-content, more than 80% of the fuel Cl was released in a single step below 650°C [29]. Nevertheless, at combustion above 800°C, Cl was exclusively released to the gas phase [29]. It was also concluded that, if the biofuel contains relative high amounts of Ca compared to Si, the S release was relatively low and independent of combustion temperature. In general, the occurrence of other ash forming elements such as Cl, K and P are indirectly coupled to the S release. For instance, a higher Cl-content result in a higher K-release due to formation of KCl, which will leave more Si to react with Ca and thus more S is released. The S-release was more than 30% in the temperature range investigated for all fuels. This is probably related to the occurrence of substantial amounts of volatile organic S in the biofuels. The experimental work showed that the S-release in grate-fired boilers is controlled by the availability of K and Ca to capture S in the bottom ash. The availability of K and Ca is largely determined by the relative concentration of Si [29].

Pilot-scale biomass suspension firing results of Nordgren et al. [27] showed that more than two third of K in the fly ash from straw was water soluble, out of which the contribution of KCl was more than 40%. In addition, higher level of HCl emissions were observed when pure straw was fired, compared to the HCl emissions resulted from wood and bark combustion [27]. According to Nordgren et al. [27] much higher K released to the gas phase was observed during suspension firing compared to grate firing, possibly due to high heating rates, high fuel particle temperature and limited mixing between the different fuel particles in the flame/furnace. Recent results of straw dust firing in an entrained flow reactor has showed that the aerosol rich particles were formed from the nucleation, condensation, and coagulation of the vaporized flame-volatile elements K, Cl, S, and P species [39]. The particle formation mechanism of these species during straw grate and suspension firing was believed to be similar due to similar kind of aerosols formed. Fly ash particles resulted from straw dust firing were primarily molten or partially molten spherical particles rich in K, Ca, and Si, and to some extent Si rich flakes.

## 2.3 Biomass Ash Deposit Formation

### 2.3.1 Deposit Formation Processes

When solid fuel is burned, inorganic material is being released to the flue gas in the form of gases, liquids and solid particles and the fate of the inorganics depend upon the mode of occurrence, local conditions inside the boiler, and boiler design [42]. Dry ash particles, sticky particles and gaseous ash species form deposits on the boiler surfaces. Deposits are formed due to accumulation of fly ash particles and aerosols starting by the condensation of inorganic vapors on exposed surfaces cooler than the flue gas in the boiler. Subsequent chemical reactions within the deposit and sintering will further contribute to the build-up of the deposits layers and strength [53]. Composition of the deposits can vary depending upon the position in the boiler, boiler type and fuel composition. Ash deposit formation is believed to be controlled by; diffusion followed by condensation, thermophoresis, inertial impaction and eddy impaction [28].

#### Diffusion followed by Condensation

In this process vapors are liquefied on surfaces colder than the surrounding gas. The difference in equilibrium partial pressure of the gaseous compounds caused by the temperature difference between the tube surface and the surrounding gas results in the diffusion of gas molecules toward the superheater tube. The amount of condensate in a deposit depends on the mode of occurrence of the inorganic material [10, 14]. Significant amount of K, Cl, and S is released in the gas phase during straw combustion and the condensable salts may considerably alter the deposit properties [17]. Condensed material can lower the porosity with a granular deposit, and when in contact with heat transfer surface, increase the bonding strength of the deposit leading to difficult removal of the deposits [20].

Diffusion of submicron species following the Brownian movement takes place for submicron-particles with diameters below  $0.1 \mu\text{m}$ . Normally, the amount of material deposited by small particle diffusion is less significant than that by vapor phase diffusion. Another way of ensuring a concentration gradient for Fick's diffusion is by chemical reaction around the rim of the deposit.

#### Thermophoresis

Thermophoresis is related to the movement of particles in a thermal gradient from a high temperature toward a low temperature. This phenomenon is caused by the surrounding gas molecules which continuously collide with the particles from all directions. The gas molecules on the hot fluid side of

the particle contains a higher average kinetic energy because of the higher velocity than those on cold fluid side, and this results in a net force on the particle causing them to move opposite to the temperature gradient [17]. Vapors may homogeneously nucleate to form a fume and subsequently deposit by thermophoresis on the surface and vapors may heterogeneously condense on other particles in the boundary layer and arrive at the surface through thermophoresis [10]. Deposits formed through condensation and thermophoresis covers the entire circumference of the tube (see Figure 2.9). Significant experimental work on particle deposition by thermophoresis has been carried out by Baxter and Sinquifield [55].

### **Inertial Impaction**

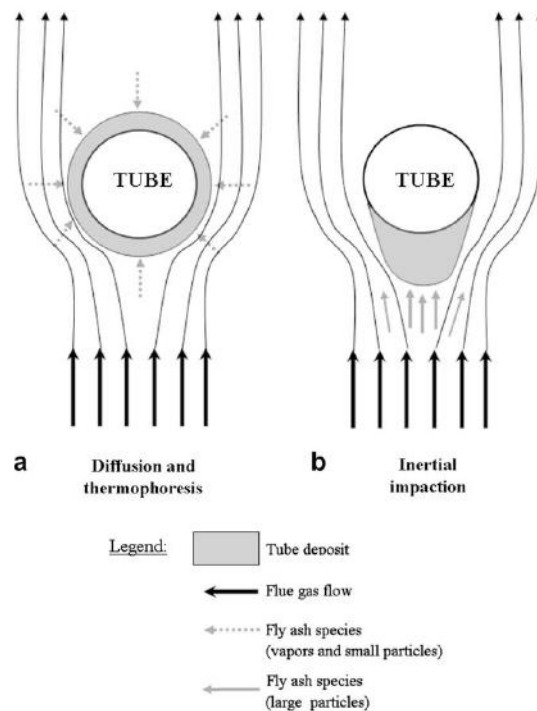
Inertial impaction takes place when large particles ( $> 10 \mu\text{m}$ ) with a large inertia do not follow the gas streamlines approaching heat transfer surface, e.g. a cylindrical tube but instead impacts on the surface. Nielsen [17] states that the capture efficiency of the particles depends upon the composition and viscosity of the melt fraction, angle of impaction, and the thermal and chemical compatibility between the particle and the deposit surface [20]. Ash particles that impact on a molten or liquid coated surface will to a higher degree stick to the surface. If the particle has too much kinetic energy in excess, it may bounce off the surface and become re-entrained in the flue gas steam [20]. The rate of inertial impaction depends upon geometry of the target, particle size, ash melting and density, and the gas flow properties [10, 14]. Deposits formed by the inertial impaction are coarse-grained and typically form an elliptically shaped deposit in the direction of the flue gases [17] (Figure 2.9). Significant experimental work has been conducted by Barnocky and Davis on deposition by inertial impaction [56].

## **2.3.2 Development of Ash Deposits**

### **Slagging**

Slagging is dominant in the area of radiant heat transfer and the initial layers of slagging comprises of primarily small, lightly sintered particles, and few larger particles that have impacted, and deformed upon impact. The composition of the initial layers for coal combustion is mostly simple metal oxides together with glassy silicate phases, but this depends a lot on the feedstock composition [20].

As the deposit grows the temperature on the outside surface increases and eventually pass the melting temperature of the deposited low melting material, at least in the outer layers (Figure 2.10 and Figure 2.11). As the



**Figure 2.9:** Deposit formation on a tube, a) diffusion and thermophoresis, b) inertial impaction [42].

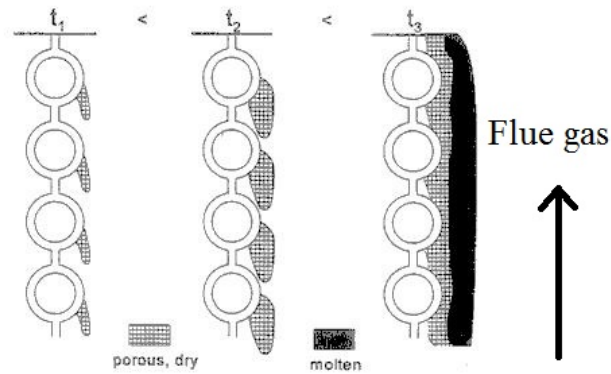
deposit surface becomes molten, most of the reaching particles tend to stick and thus the outer layer composition of slagging deposit becomes similar to the bulk fly ash chemical composition. Low excess air and inappropriate air/fuel ratio can lead to increasing slagging deposits, and reducing conditions, and excessive slagging may lead to extension of the flame into the convective section of the boiler, and possibly causing slagging there also [17, 20].

### Fouling

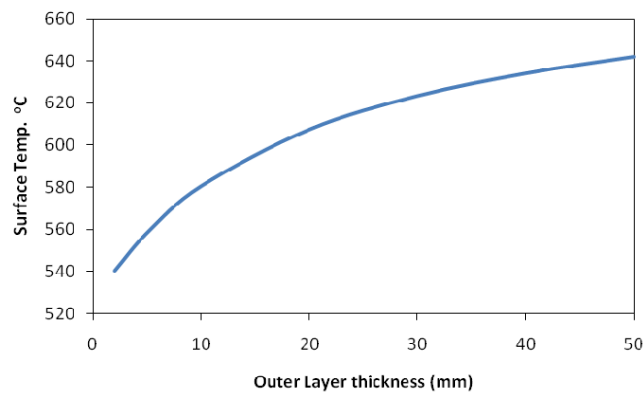
Fouling deposits form in the convective sections of the boiler and consist of fly ash particles and condensed volatile species that are more loosely bonded than the slags. Initially the outer layer of the fouling deposit is porous but later on sintering strength builds up in the deposit as a function of time and temperature [17]. In coal-fired systems, high-temperature fouling occurs in the regions where temperature exceeds the stability of the sulfate phases and consists of fly ash particles which are primarily bonded together with silicate liquids [17]. Low-temperature fouling occurs in the colder parts of the convective pass where the gas temperature is in the range of 650–975 °C and the sulfate phase dominates the bonding mechanism between the particles



[17, 57]. There are a number of common knock-on problems associated with the formation of excessive levels of ash fouling deposits in the convective sections of the boilers. These apply to all boilers fired with biomass fuels: Firstly, the generation of higher flue gas velocities in the open gas pass channels through the bank, result in increased gas-side erosion wear of the tube surfaces. Secondly, when there is excessive convective pass fouling, with blockage of a significant number of flue gas passes in the tube banks, there is tendency for the generation of high metal temperatures in tubes in the flue gas passes that remain open [17, 57]. This can result in accelerated metal wastage due to gas side corrosion.



**Figure 2.10:** Slagging in the high temperature region [15].



**Figure 2.11:** Graphical representation of deposit outer layer thickness impact on deposit outer surface temperature. Simulation results using a standard coal ash.

### Deposit Strength and Maturation

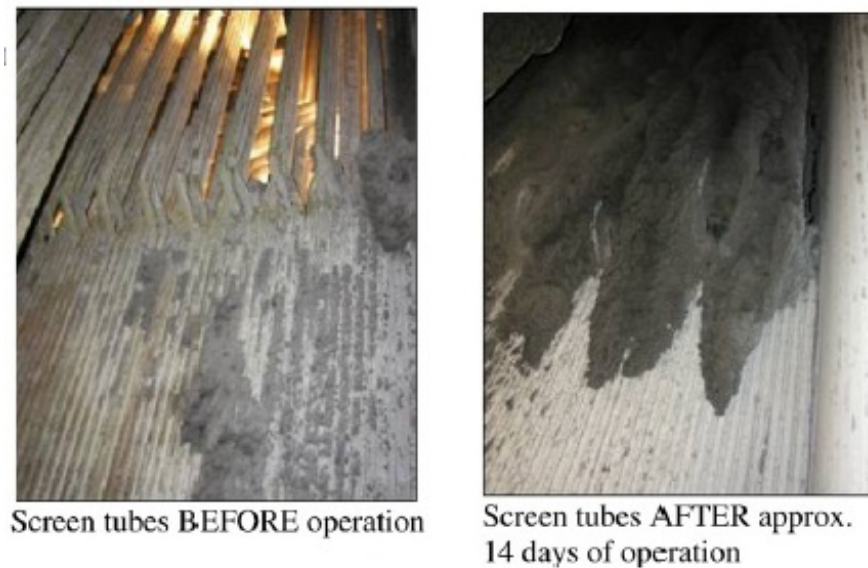
According to Nowok [58], from an engineering standpoint, a key role in achieving the performance goals in ceramics and glass ceramics is to enhance the strength of these materials. However, high deposit strengths create the basic problem of deposit removal from heat exchange surfaces. Baxter [10] states that the primary reason for strength build-up in deposits is the increase in the area of contact between particles within the deposit, which is primarily due to sintering or chemical reaction.

In addition to other reasons, with the passage of time the deposits become hard and difficult to remove as according to Jensen [46], the total deposition flux was reasonably independent of time in a straw-fired grate boiler, while the fraction of hard deposits increased with time. In addition, the fraction of hard deposit was found to be correlated with the S content in the deposits, the gas temperature and the amount of K in straw.

Severe deposits formed on the superheater tubes during straw and coal co-firing are shown in Figure 2.12, whereas mature deposits formed on the screen tubes during 100% straw firing in suspension can be seen in Figure 2.13. Ash deposits on the heat transfer surfaces cause severe problems for effective heat transfer and severe ash deposition may even cause plugging of flue gas channels as shown in Figure 2.13.



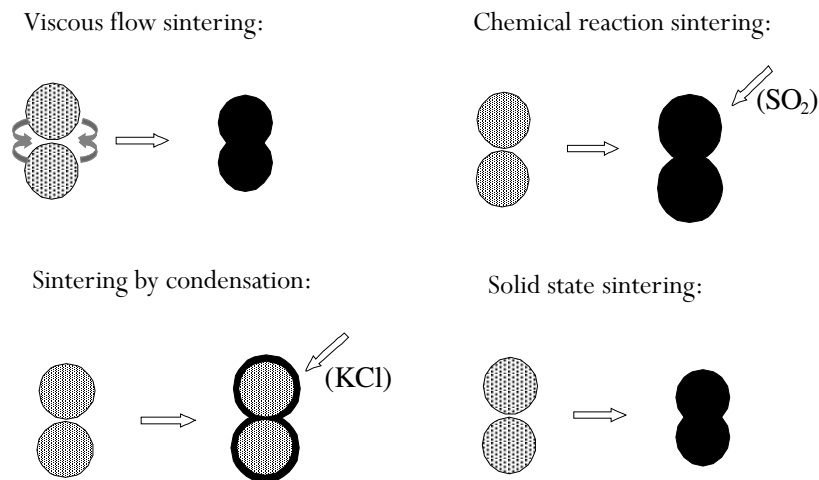
**Figure 2.12:** Ash deposition on the superheaters during straw and coal co-firing [2].



**Figure 2.13:** Ash deposition on the screen tubes during 100% straw firing in suspension [5].

### Deposit Sintering

The driving force for the sintering is the surface energy of the particles. The energy change caused by densification is connected with a decrease in surface area and a lowering of the surface energy by elimination of solid-vapor interfaces and formation of new lower energy solid-solid interfaces. Sintering may occur by several mechanisms as shown in Figure 2.14. Liquid state sintering involving a viscous liquid is typically referred to as viscous flow sintering. The rate of neck growth as a result of viscous flow sintering has been shown to be time dependent and controlled by the viscosity of the silicate liquid [20]. Chemical reaction sintering occurs when a reaction between particles leads to the formation of a third component, which forms the necks between the particles [20]. The reaction may also take place between the particles and the surrounding gas phase. Chemical reaction sintering can be important for fouling especially in the low temperature section of the flue gas channel. Solid state sintering is caused by diffusion along the particle surface, through the interior of the particles, and through the surrounding gas by vaporization and subsequent condensation. Solid state sintering is a slower sintering mechanism than the ones involving melt, but nevertheless plays an important role in the densification of low temperature fouling deposits [42]. Liquid phase or viscous phase sintering appears mainly to be the dominant mechanism.

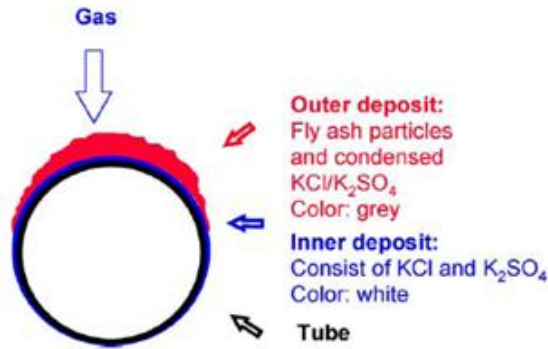


**Figure 2.14:** Graphical representation of different types of deposit sintering [2].

### Deposit Structure in Straw-fired Boilers

Principal sketch of the wheat straw-derived deposits formed on a deposition probe during tests at Sandia Multi Fuel Combustor (MFC) is shown in Figure 2.15. The deposits consist of two parts, 1) an inner layer, uniform, smooth and covering most of the surface area of the probe, and 2) the main part of the deposit located on the upstream side of the probe and consisting of individual particles. The inner layer, rich in flame-volatilized species (often alkali salts), provide a sticky surface for trapping inertial impacted particles which are non-sticky [17]. Nielsen [17] states that the deposit on the upstream side of the probe consists of impacted fly ash particles and large amounts of condensable salts, forming a matrix that glues the fly ash particles together. The fly ash particles were dominated by K and K-Ca silicates.

The structure of the mature deposits formed during straw grate firing at the Ensted boiler at a flue gas temperature just below 900 °C is shown in Figure 2.16. It can be seen that the inner deposit layer is salt rich (KCl,  $K_2SO_4$ ), intermediate deposit layer dominated by Si, Ca rich particles embedded in KCl, while the outer layer of deposits is dominated by KCl, S, and, Si and Ca rich particles [21].



**Figure 2.15:** Principal sketch of the wheat straw-derived deposits during pilot-scale experiments at Sandia MFC [17].

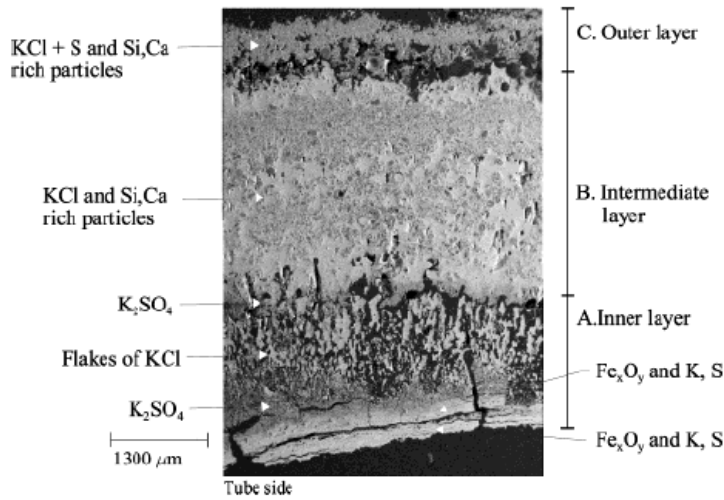
### 2.3.3 Deposit Physical and Chemical Properties

The important properties of a deposit regarding successful operation in a biofuel-fired boiler are; feasibility of removal from heat transfer areas, effective thermal conductivity and emissivity, physical strength of the deposit, elemental and chemical composition of the deposit, and morphology and melting behavior of the deposit [42], outlined below.

#### Melting Behavior

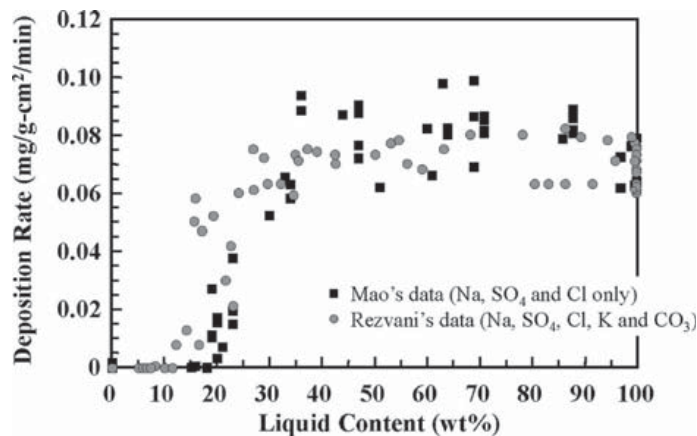
The concept of  $T_{15}$  and  $T_{70}$  is often used by researchers representing the temperatures where the deposit has 15% and 70% molten phase respectively. It is believed that significant deposit formation takes place when the melt fraction percentage is between  $T_{15}$  and  $T_{70}$  [9, 17]. This concept is normally applied for ashes containing a significant fraction of salts [9, 17]. At temperature lower than  $T_{15}$ , the deposit is almost solid, rigid and non-sticky, and in principle easy to remove, whereas for temperature above  $T_{70}$  the deposit becomes fluid like a slag [17]. The broader the temperatures gap between these two temperatures for a particular deposit material, the wider the critical area where severe thick deposits are expected to grow [17].

Deposition rate as a function of melt fraction for two different types of salt mixtures is shown in Figure 2.17. A significant difference in terms of ash deposition can be seen when the salts tested have liquid content less than 20% compared to the case when they have liquid content less than 20%. One of the conditions for the formation of a physically strong deposit is the formation of a liquid phase, which can bind solid ash particles [42]. The influence from K-contents in the deposit is critical based on its ability to drastically lower the first melting temperature of ash particles, so that deposits will contain liquid phase at lower temperatures [47].



**Figure 2.16:** Structure of mature deposits from Ensted boiler (straw grate fired boiler). The superheater steam temperature was from 389 to 470 °C and the flue gas temperature was just below 900 °C [21].

Hansen [15] studied the melting behavior of fly ashes and deposit from straw-fired boilers as a function of temperature. The fly ash and deposits were found to consist of large fraction of KCl and a smaller fraction of K, Ca, Al-silicates and quartz. The salt part melted in the range from 650 and 750 °C, whereas the silicate phase melted in the range of 1000 and 1200 °C.



**Figure 2.17:** Deposition rate as a function of melt fraction for two different types of salt mixtures [68].

## Thermal Properties

Thermal properties (thermal conductivity and emissivity) are influenced by the deposit physical structure. According to Zbogar et al. [42], the effective thermal conductivity of deposits depends upon the solid phase and gas phase thermal conductivity, the porosity, the size distribution of the pores or particles, and the degree of deposit sintering. Porous deposits have lower thermal conductivity compared to hard deposits.

## 2.4 Shedding of Deposits

To minimize deposition problems, different strategies can be employed, e.g. use of additives that can convert the vaporized inorganic species to less harmful forms [5, 26, 39], pre-treatment of fuels by leaching out alkali [40], co-firing with clean fuels [41], inhibition of sintering [2], and use of effective deposit shedding techniques [42]. Use of additives and pre-treatment of fuels by leaching are less cost effective compared to the use of effective deposit shedding [5, 40].

### 2.4.1 Mechanisms of Deposit Shedding

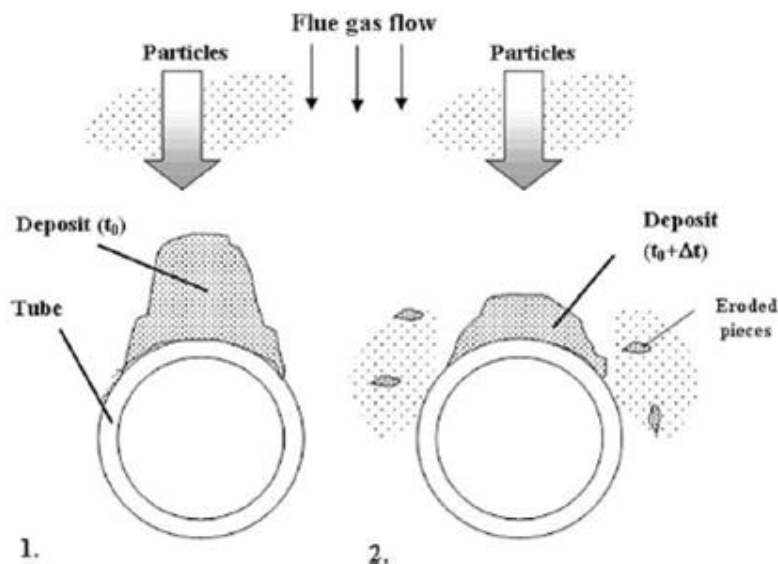
Shedding may be initiated at the surface of the deposit, along the deposit tube interface and inside the deposit depending on the local boiler conditions and the deposit properties [42]. Deposit shedding can be caused artificially as a part of the boiler operation, e.g. by sootblowing, or naturally, without any operational or mechanical influence [2, 42]. The important mechanisms of ash shedding are (Table 2.4) [42]:

- Erosion, when non-sticky, relatively large and sharp edged often  $\text{SiO}_2$ -rich fly ash particles collide with non-sticky areas on a deposit surface causing deformation (ductile deposits) and a cutting action (brittle deposits) [2, 43] (Figure 2.18).
- Gravity shedding when the gravity force exceeds the tube adhesion strength. Gravity shedding also includes deposit shedding through surface melting. Gravity shedding by surface melting is explained in Figure 2.19 and section 2.4.3.
- Through temperature changes and differences in the thermal expansion coefficients of the tube and deposit. Local temperature changes may be caused by sootblowing or by load variations/fluctuations.
- Mechanically induced tension in the deposit typically caused by vibrations or momentum transfer from sootblowing.

**Table 2.4:** Deposit shedding mechanisms [42].

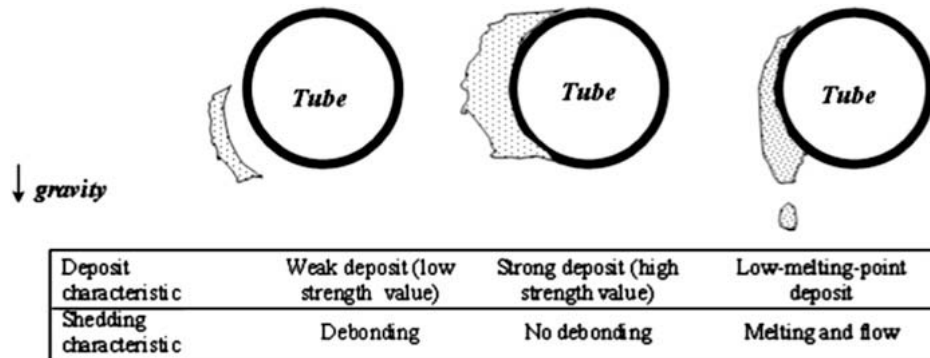
Shedding mechanism	Debonding	Within deposit	Surface removal
<b>Erosion</b>			✓
<b>Gravimetric</b>	✓	✓	
<b>Melting</b>			✓
<b>Thermal induced tension</b>			
a) Combustion fluctuations			
b) Load changes	✓	✓	
c) Sootblowing			
<b>Mechanical induced tension</b>			
a) Mechanical fluctuations	✓	✓	
b) Sootblowing			

The erosion mechanism (gravity shedding) for ash deposit on a tube is shown in Figure 2.18. According to Raask [43], the erosion rate is influenced by the shape of the incoming particles. Highly abrasive, hard and angular quartz grains cause erosion by cutting, whereas glass spheres first produce a surface deformation. Erosion wear is also influenced by the particle size of the impacting material. Smaller particles (smaller than  $5 \mu\text{m}$ ) have a small inertial momentum and they are carried around the object with the gas flow [42, 43]. The erosion rate increases as the particle size increases but obtain a constant value for larger particle ( $45 \mu\text{m}$  [42, 43]).



**Figure 2.18:** Deposit erosion mechanism, 1) initial deposits on the tube, 2) deposits after shedding through erosion [42].





**Figure 2.19:** Relationship between the deposit viscosity and the deposit strength. Cases are ordered in the sequence of decreasing viscosity [42].

Gravitational shedding is possible when the effect of gravity upon the deposit becomes larger than the attachment strength of the deposit on the tube or the internal strength of the deposit. Debonding occurs when the stresses initiated by the sootblower are greater than the tube-deposit adhesive bond at some point on the tube deposit interface.

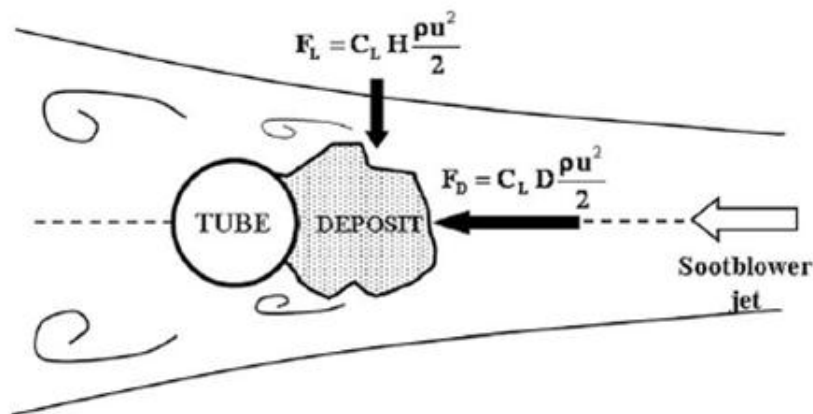
Gravity shedding is also possible by melting of the deposits especially in the furnace region. If the combustion conditions are suitable for the development of low viscosity slag deposits, molten deposits may flow down the boiler walls. The temperature gradient through such a deposit will cause the slag layers close to the wall surface to be solid, while the outer deposit layer will be molten. A relationship between the deposit viscosity and the deposit strength is shown in Figure 2.19. It can be seen that for deposit with the high liquid phase viscosity, the adhesive strength is not sufficient enough to hold the deposit in place, resulting in shedding by its own weight. Whereas, the temperature of the deposit on the right side is high enough to cause melting of the deposit, and shedding through surface melting.

Thermal shock induced shedding is caused by temperature changes, due to the difference in the thermal expansion coefficients of the tubes and deposits. A sudden temperature gradient may cause an uneven expansion of the deposit and the tube, or, distinct, adjacent, deposit layers, leading to deposit fractures. The sudden temperature gradients can be caused by fluctuations of the flue gas or steam temperature. Artificially, ash deposits can be removed from the heat transfer surfaces by inducing mechanical or thermal stresses inside them. This can be done using the impact of the high pressure steam, air and water, or by changing the thermal load etc. [36, 44].

## 2.4.2 Industrial Deposit Shedding Techniques

### Sootblowing

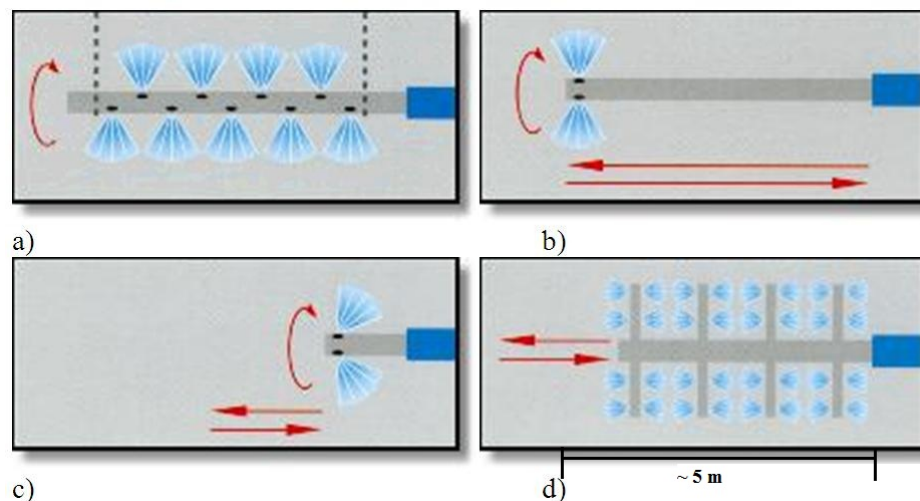
Sootblowing is currently the most common deposit shedding system used in coal, biomass and Kraft recovery boilers. Water, high pressure air or steam may be used in sootblowing systems [70]. Deposit removal occurs indirectly, due to mechanical and thermal stresses, induced in the deposit. The cleaning fluid is forced through nozzles that remove deposits from the heat transfer surfaces. The Peak Impaction Pressure (PIP) is an important parameter in sootblower design defined as the stagnation pressure (one half the fluid density times fluid velocity squared) measured along the centerline of the nozzle downstream of the nozzle outlet. PIP drops off at increasing distances from the nozzle outlet because of the fluid deceleration associated with the dispersion of the flow downstream of the nozzle exit. PIP is used to measure the effectiveness of a sootblower nozzle. In order to remove the deposit, jet must have a PIP value that induces tensions in the deposit is greater than the deposit mechanical strength, or the adhesion strength at the deposit-tube interface [70]. Longitudinal and lateral component of a force, caused by the interaction between a sootblower jet and a deposit are shown in Figure 2.20. Conventional sootblower nozzles produce an under-expanded jet, which causes a dissipative shock wave to occur outside the nozzle exit. This shock wave irreversibly converts a substantial portion of the kinetic energy of the jet into internal energy, thereby reducing the PIP available for deposit removal. If the nozzle is designed so that the jet achieves full expansion before it exits the nozzle, shock waves will be eliminated. This will increase the energy available for deposit removal [71].



**Figure 2.20:** Longitudinal and lateral component of a force, caused by the interaction between a sootblower jet and a deposit [36].

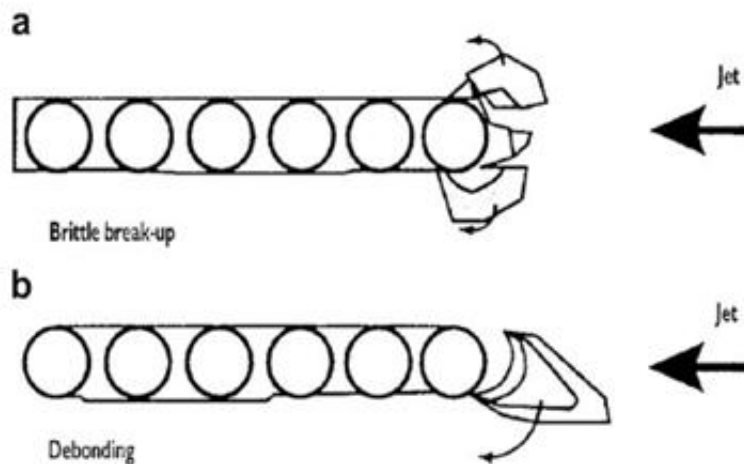
Different types of sootblowers commonly employed in the boilers are

shown in Figure 2.21. Rotary sootblowers consist of a long tube with nozzles that remains inside the system and normally placed in cool flue gas zone to avoid corrosion problems [72]. The nozzles are distributed along the tube surface and also around its circumference. The retractable sootblowers consist of a long lance with two or four nozzles in it. The nozzles are normally at the end of the lance. The retractable lance moves alongside its length and also rotates. The wall sootblowers are designed to clean the slag deposits on furnace walls. They are used in coal-fired boilers for this purpose. A nozzle in a short retractable lance tube is inserted just inside the face of the wall and rotates once to blow the fluid across the surface wall. The jet is slightly angled back toward the furnace wall. Rake blowers are designed for cleaning plane heat transfer surfaces. There are several tubes that allow the cleaning between the closely spaced fins. These blowers are usually found in the cooler parts of a boiler like the economizer and the air pre-heater.



**Figure 2.21:** Different sootblowers employed in solid fuel fired boilers, a) rotary, b) retractable, c) wall, d) rake [72].

The chemical composition and the thermal characteristics of the oxide layer, formed on the boiler tubes, influence the strength of the adhesive bond between an oxide surface and an ash deposit [70]. Non-sintered porous deposits do not possess much strength, and are easily blown away from the surface. The tube surface temperature has a significant effect on the process of deposit removal. Increasing the tube surface temperature often makes the deposit more difficult to remove. For a weak brittle deposit a sootblower jet impact can lead to a break-up of the deposit as shown in Figure 2.22. Dense, hard deposit on the other hand, can be removed by debonding from the tube surfaces (Figure 2.22).



**Figure 2.22:** Mechanisms of deposit removal: brittle break-up (a) and debonding (b) [36].

Sootblowing frequency must be balanced with the negative results of erosion because the condensate in the sootblowing can result in unnecessary corrosion [70].

### Use of Additives

In order to avoid deposition problems in biomass fired boilers, the use of different additives can be of worthwhile importance. The additives change the fly ash composition produced by favoring the formation of Cl in the gas phase (HCl), and the formation of ashes with melting temperatures greater than the sticking temperatures. Many additives have been tested both in pilot-scale and full-scale measurements in biomass-fired boilers [5, 26, 73]. The commonly used additives include Ca, S and P rich materials. Sørensen et al. [74] proposed that the addition of additives rich in Ca and P form phases rich in K-Ca-P that have higher melting temperatures. ChlorOut, a concept developed and patented by Vattenfall AB, consists of an aqueous solution of  $(\text{NH}_4)_2\text{SO}_4$  that is sprayed into the combustion zone at temperatures around 800–900°C, upstream of the superheaters [75]. It effectively converts alkali chlorides (e.g., KCl) into alkali sulphates (e.g.,  $\text{K}_2\text{SO}_4$ ). This concept has been successfully tested in a number of biomass-fired fluidized bed boilers [76]. Significant reduction in the deposition rate and Cl contents in the deposits has been reported [76]. However, the amount of  $(\text{NH}_4)_2\text{SO}_4$  and/or Ca, S and P rich additives needed to cope with K in a straw suspension-fired boiler can be beyond economical constraints.

Addition of additives in the fuel for K capture or leaching out of K from fuel is also employed to reduce the potential ash deposit formation on the

superheater tubes. Other additives may also be used to inhibit sintering of ash deposits [2, 40].

### **Addition of Coal Fly Ash**

The presence of Al and Si in coal fly ash can make it good candidate to capture K from biomass-fired boilers. Addition of coal fly ash can be economically feasible for wood-fired boilers where the amount of coal ash needed to capture K will be smaller compared to the amount of coal ash needed in straw suspension-fired boilers.

### **Shot Cleaning**

In shot cleaning, small balls are used to clean the heat transfer surfaces in a boiler. The balls are available in different geometries and materials. They are pneumatically transported to the upper section of the boiler, and then fall by gravity and impact the heat transfer surfaces. Deposits are removed and fall in the dust outlet, while the balls are collected and recycled to the next cleaning cycle [70].

### **Sound Waves**

Sound waves are used to clean the heat transfer surfaces by creating pressure fluctuations in a flowing gas stream. Normal frequencies are of 125 Hz to 250 Hz in the 140 to 150 dB range but infrasonic horns with frequencies between 15 to 20 Hz also exist [70].

### **Rapping Gears/Mechanical Fluctuations**

Rapping gears are hammers beaten on reinforced heat surface headers either mechanically or pneumatically. Because of the vibrations created by the hammers, the deposit can fall from the heat transfer surfaces [70]. Deposits that are not strongly bonded with tube can be removed using mechanical hitting (vibrations), as is done in some waste incinerators.

### **Detonation Wave Techniques**

Detonation wave technique is also used to shed ash deposits. The detonation occurs when a fuel-oxidant mixture is combusted in an ignition chamber connected to a pipe with the same or smaller diameter. Thus, the pipe has the function of transforming the flame front into a detonation wave, and bringing the wave to the desired location. A normal detonation wave has a velocity of 2200 m/s and a pressure up to 20 times the original pressure of the reactants [70]. The main mechanisms for deposit removal are pressure forces and thermal shock [70, 77].

### 2.4.3 Review of Deposit Shedding Investigations

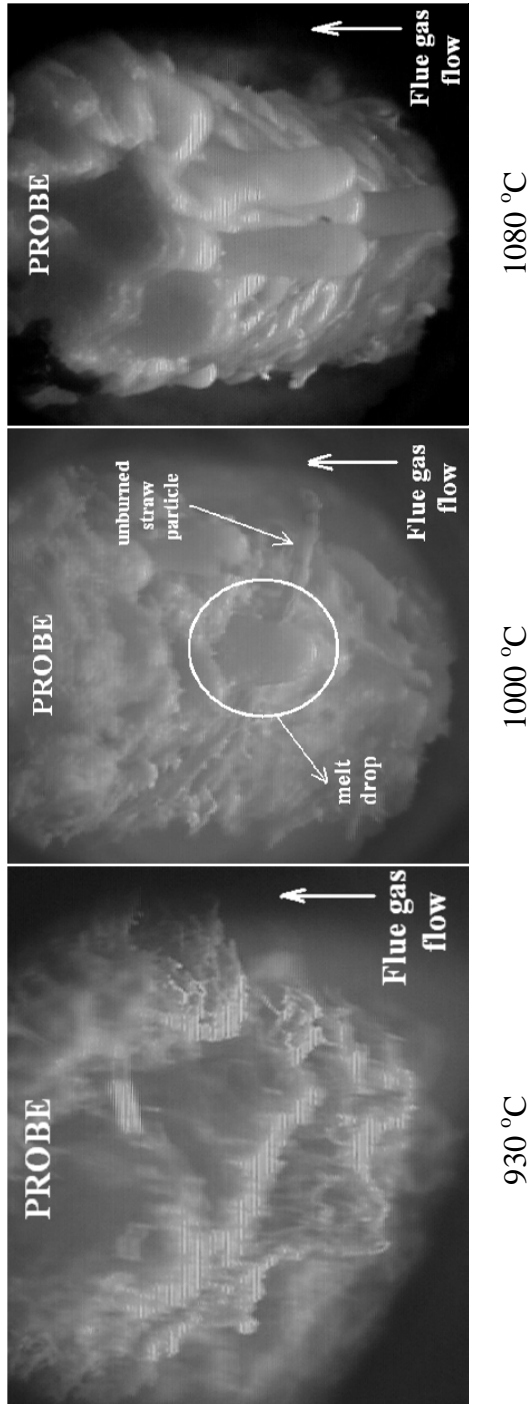
Most deposit shedding studies have been based on measurements in lab-scale equipment, grate-fired boilers and Kraft recovery boilers, while only limited data are available from biomass suspension firing. A review of shedding investigations in different solid-fuel fired boilers and lab-scale facilities is shown in Table 2.5. Ash deposit shedding through surface melting in the high temperature superheater region at the Avedøre straw grate-fired boiler was investigated by Zbogar et al. [35]. The results showed that deposit surface melting was the main mechanism of ash deposit shedding at flue gas temperatures greater than 1000 °C. The ash deposit shedding through surface melting at three different flue gas temperatures can be seen in Figure 2.23. The results showed that deposit shedding through surface melting was significant when flue gas temperature was higher than 1100 °C, the deposit surface layer was partially melted at 1000 °C, and at a temperature of 900 °C, the deposits contain mainly porous solid phase [35]. It was also found that the initial deposit formation mechanism was by condensation of salts, and then followed by upstream inertial impaction of the fly ash particles. The deposit build-up and shedding reached a steady state level after 7 days.

Deposit shedding at the Avedøre straw grate-fired boiler was investigated by Zhou et al. [33] by using an artificial sootblowing probe in a lower temperature superheater region nearer to the convective pass at flue gas temperatures between 700 and 800 °C. Investigations of Zhou et al. [33] showed that the probe surface temperature can have an influence on the Peak Impact Pressure (PIP) needed to remove the deposit. The measured PIP values were significantly lower at a probe surface temperature of 400 °C compared to a probe surface temperature of 550 °C.

Lab-scale investigations by Kaliazine et al. [36] and Sabet [78] also indicate an increase in adhesion strength of the deposit and the metal surface at higher probe surface temperatures (> 500 °C). However, after reaching a temperature value where the deposit inner layer changed to complete liquid phase, the adhesion strength was significantly reduced. Andersen [20] used temperature controlled probe for sampling of deposits during full-scale measurements in a straw and coal fired boiler. Natural deposit shedding was observed when ash deposits fall off from the probe. Shedding was believed to occur when sudden changes were seen in the probe surface temperature on the upstream side of the probe. Natural deposit shedding was observed by Madhiyanon et al. [79] during pilot-scale combustion studies of oil-palm empty-fruit-bunch (K-rich fuel). Visual observations of deposit formation and shedding on the probe showed that the deposits fall off in the form of pieces from the upstream side of the probe.

**Table 2.5:** Review of shedding investigations in different solid-fuel fired boilers and lab-scale facilities.

Location	System	Size	Flue gas temp. ( $^{\circ}\text{C}$ )	Fuels	Shedding mechanism	Ref
Avedøreværket Bio Boiler, Unit 2	Dedicated straw-fired boiler. Big bales of straw are fired on a grate.	105 MW <sub>th</sub>	900–1200	Danish straw	Shedding through surface melting.	[35]
Avedøreværket Bio Boiler, Unit 2	Dedicated straw fired boiler. Big bales of straw are fired on a grate.	105 MW <sub>th</sub>	700–900	Danish straw	Shedding through artificial sootblowing probe.	[33]
Studstrup Power Station, Unit 1	Back wall fired boiler with 12 burners.	380 MW <sub>th</sub> / 150 MW <sub>e</sub>	950–1150	Straw with Bituminous coal and American coal. Separate injection of straw up to 20% on thermal basis.	Natural shedding was observed as part of investigating ash deposition in a 2 years demonstration program.	[20]
University of Toronto	Lab-scale facility.	–	–	Wood material was considered as deposit and gypsum was used as the bonding material.	Deposit removal by debonding. Lab-scale deposit removal experiments were performed for application in Kraft recovery boilers.	[36, 78]
University of Technology Thonburi, Thailand	Grate-fired furnace.	150 kW <sub>th</sub>	790–810	Oil-palm empty-fruit-bunch	Natural shedding was observed as part of investigation of ash deposition.	[79]



**Figure 2.23:** Pictures of the deposit probe during full-scale measurements at a straw grate-fired boiler at three different flue gas temperatures [35].



## 2.5 Practical Experiences of Biomass Suspension Firing

### 2.5.1 Review of Ash Deposition during Pilot-scale Biomass Suspension Firing

Some pilot-scale biomass suspension-fired investigations on ash transformation and deposition can be found in the literature and are reviewed in Table 2.6. Lokare et al. [28] investigated the ash deposition rate for a suite of biomass fuels and biomass fuel blends (50–50 wt.%) in a 10 kW down-fired, multi-fuel flow reactor. In addition to the increase in deposition rate with fuel ash contents, higher ash deposition rates were observed for fuels with higher Cl-content. Robinson et al. [80] investigated American wheat straw, Danish wheat straw, red oak wood and switchgrass in a 30 kW Multi-fuel Combustor (MFC) at Sandia National Laboratories. Results of the ash deposition were similar to the investigations made by Lokare et al. [28] in such a fashion that the deposition rate increased linearly as a function of Cl-content in the fuel. The results showed significantly higher ash deposition rate for Danish straw, compared to switchgrass even though the ash contents of the Danish straw were lower than for switchgrass. In the same MFC reactor, the results of Nielsen [17] showed a deposit collection efficiency of 0.05–0.25 during Danish straw combustion. The deposit collection efficiency reduced to 0.01–0.04 when straw was co-fired with coal, possibly due to chemical interactions. Theis et al. [41] investigated specified mixtures of peat with bark, and peat with straw in an entrained flow reactor. Results showed a cleansing effect of peat in all mixtures with straw by reducing the ash deposition rate. The conclusion was that up to 30 wt.% bark and up to 70 wt.% straw in a mixture with peat can be burned without encountering increased deposition rates. In addition to fuel ash contents, the impact of fuel ash chemistry on ash deposit formation rates was evident. Nordgren et al. [27] investigated ash deposition behavior of straw and different woody biomasses in a 150 kW swirl powder burner. A deposition rate of 90 g/m<sup>2</sup>/h for pure straw reduced to 50 g/m<sup>2</sup>/h when straw was fired with wood at 50 wt.% share. Experimental investigations by Shenassa [81] in an entrained flow reactor also revealed increased deposit formation rates with increase in Cl-content of the feedstock.

Wu et al. [73] investigated deposition behavior of Danish straw with and without the addition of spent bleaching earth and kaolinite as additives in an entrained flow reactor. Reduced ash deposition propensity was resulted when spent bleaching earth and kaolinite were added to straw. In addition, the contents of Cl in the deposits were reduced in the presence of additives both due to dilution effects and chemical interactions. Investigation of ash deposition behavior during combustion of straw and biomass fuels was made

by Jensen et al. [82] in the same reactor, with and without the addition of Ca and P rich additives. Ash deposition rate was found to be linked with total fuel ash contents, and to some extent K contents in the fuel ash. Capablo et al. [83] investigated ash deposition and ash transformation during biomass combustion in an entrained flow reactor and a swirl burner furnace, respectively. More than 10 alternative biomass fuels with and without the addition of kaolin and limestone were investigated. The ash deposition rate was found to be linear function of ash contents of the fuels. Ash transformation results revealed two kinds of fly ash particles when biomass fuels were combusted in the swirl burner furnace. Particles with diameter less than  $1 \mu\text{m}$  were found to be rich in K, Cl, S and P, while the larger particles were rich in Si, K and Ca.

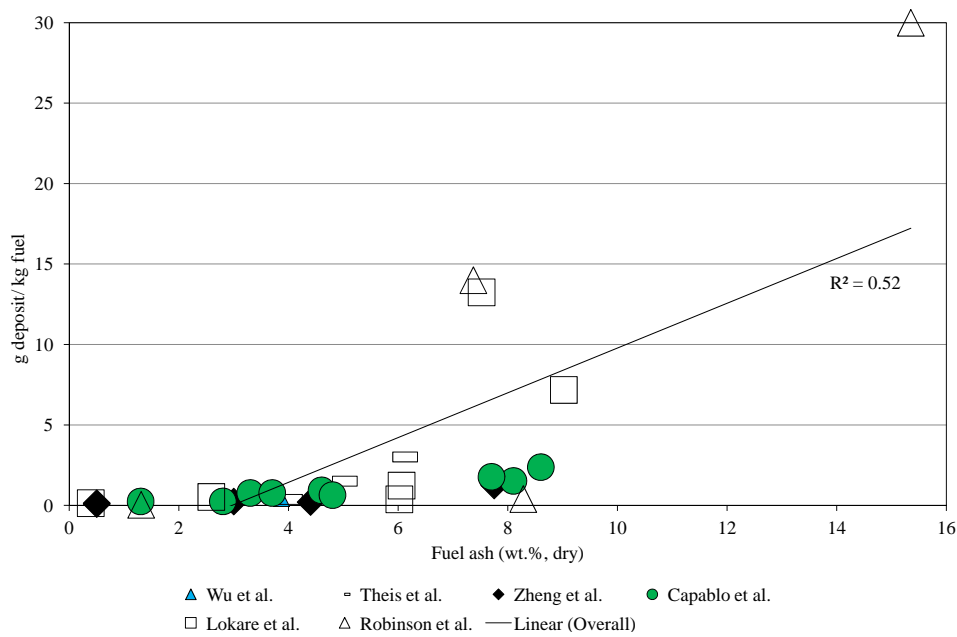
Most of the above mentioned studies revealed that the combustion of individual biomass fuels in different reactors showed a correlation between ash deposition rate and fuel ash contents as shown in Figure 2.24. However, a mixture of biomass fuels and combustion of biomass fuels in the presence of additives did not follow the similar trend of increase in ash deposition with increase in fuel ash contents as shown in Figure 2.25, where the data points with a large spread show reduced ash deposition rates compared to individual biomass combustion. The chemical interactions among the ash species could be effective in lowering the ash deposition rates.

In addition to the impact of fuel ash, and, K and Cl-content in the fuel ash, flue gas temperature may also be effective to increase the gas phase concentration of gas phase alkalis and melting behavior of the produced fly ash. K in the fuel ash can increase the fraction of molten ash as well as provide an increased content of gas phase alkali species at higher flue gas temperatures, and both will lead to an increased deposit formation rate. For the pilot-scale studies conducted at a flue gas temperatures close to  $1000^\circ\text{C}$ , the ash deposition increases linearly with increase in Cl-content in the fuels (see Figure 2.26). However, the trend cannot be seen when the flue gas temperatures close to  $800\pm 50^\circ\text{C}$  as shown in Figure 2.27. The possible explanation could be that the K-release can be significant for fuels containing high amounts of Cl and/or high amounts of K relative to Si, whereas, the K release is expected to low for high Si fuels and low Cl-content [29]. The presence of K and Cl can potentially decrease the melting temperature of the fly ash produced.

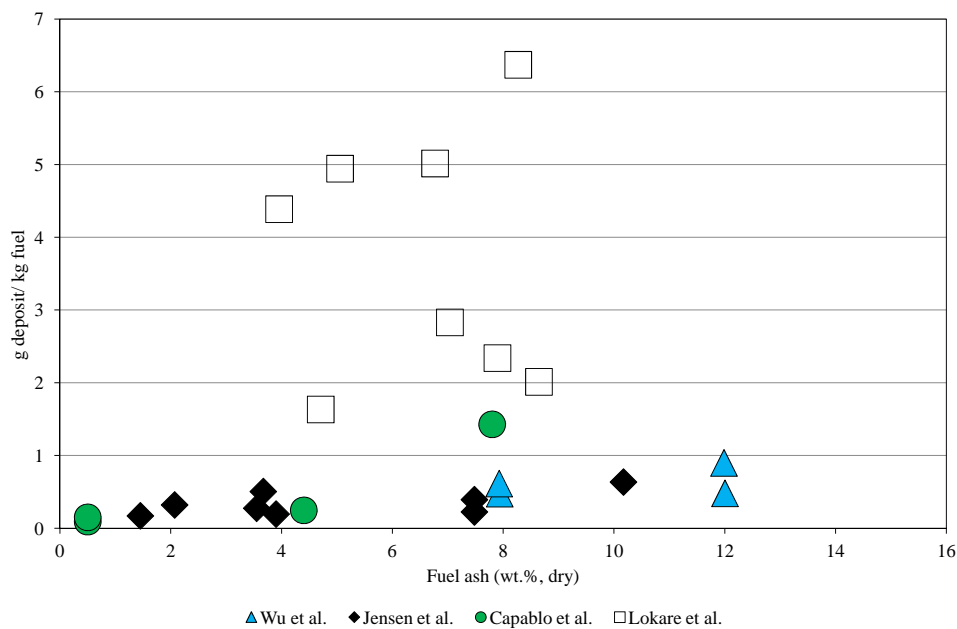
The review of above mentioned studies indicate that the true identification of the impact of the flue gas temperature and fuel ash contents on ash deposition propensity is of significant importance to quantify ash deposition in straw and wood suspension-fired power boilers.

**Table 2.6:** Review of biomass suspension firing experiments reported in literature at different pilot-scale facilities.

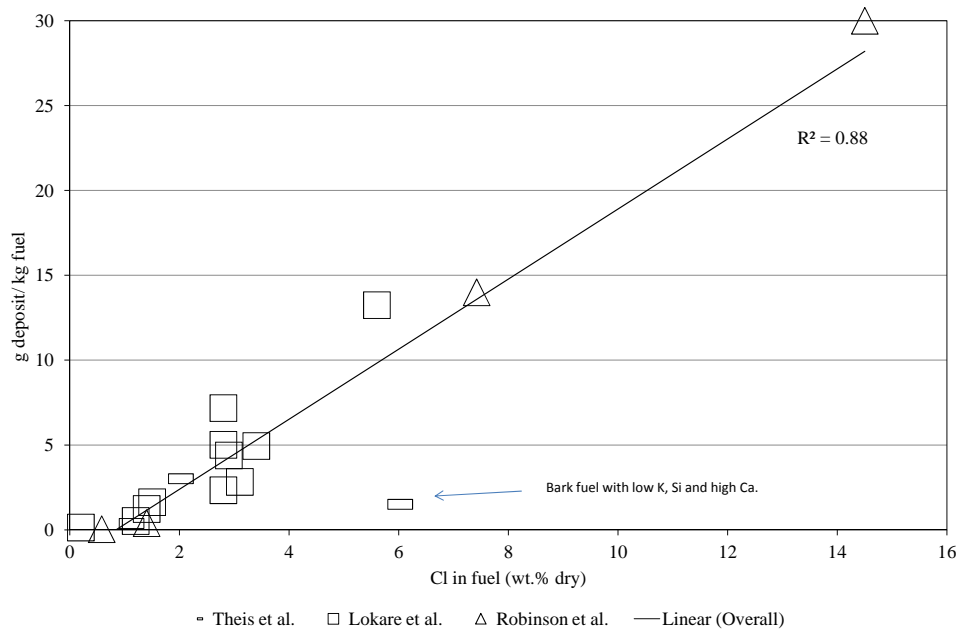
Location	System	Size	Flue gas temp. ( $^{\circ}$ C)	Probe temp. ( $^{\circ}$ C)	Fuels	Issues/Findings	Ref.
Brigham Young University	Multi-fuel, down-fired reactor with 120 mm inside diameter. Auxiliary methane was used to preheat the reactor.	10 kW	1000	500	Six pure biofuels and eight biomass fuel mixtures (50 wt.%).	Ash deposition rate was higher for fuels with higher ash and Cl-content. The deposition rate reduced for biomass mixtures due to dilution effects and chemical interactions. Ash deposition and corrosion. Higher deposition rate for fuels with higher ash and Cl-content.	[28]
Sandia National Laboratories USA	Multi-fuel, down-fired turbulent entrained flow reactor with natural gas burner. Reactor is 4.2 m high with 150 mm inside diameter. Electrical heated to control temperature of the walls.	30 kW	1000	540	Coal, straw and wood fuels. Individual fuels and fuels with different co-firing combinations.	Coal, straw and wood fuels. Individual fuels and fuels with different co-firing combinations.	[17, 80]
University of Toronto	Entrained flow reactor with natural gas addition for complete combustion. Combustion temperature adjusted by addition of air. The reactor is 6.5 m high with 180 mm furnace diameter. Swirl powder burner.	$\sim$ 5 kW	1000	550	Bark, peat and straw fuels. Individual fuels and fuels with different co-firing combinations.	Corrosion was induced by Cl in the deposits (resulted from fuel). Ash deposition and deposit characterization. High deposition rate for straw. Up to 30 wt.% bark and up to 70 wt.% straw in a mixture with peat can be burned without significant ash deposition. Ash transformation and ash deposit build-up rate (RBU). RBU for straw was higher compared to woody biomasses. Equilibrium was achieved selectively and ash matter was strongly fractioned.	[41]
Umeå/Luleå University, Vattenfall Sweden	Electrical heated entrained flow reactor having an internal diameter of 79 mm and length of about 2 m.	150 kW	800/500	550/250	Straw, bark and wood samples were fired alone and with different co-firing combinations. Thermodynamic calculations were also performed.	Straw, bark and wood samples were fired alone and with different co-firing combinations. Thermodynamic calculations were also performed.	[27]
Pilot-scale plant CHEC, DTU	Electrical heated entrained flow reactor having an internal diameter of 79 mm and length of about 2 m.	5 kW	750	470	100% straw, straw in combination with spent bleaching earth and kaolinite.	Ash chemistry and deposition behavior. Additives were effective in reducing deposition propensity and in reducing Cl and K in the deposits.	[73]
Pilot-scale plant CHEC, DTU	Electrical heated entrained flow reactor having an internal diameter of 79 mm and length of about 2 m.	5 kW	800	400-600	Combustion of biomass fuels with and without the addition of Ca and P rich additives.	Characterization and quantification of deposits. Fuels with high K content bind more Cl in the deposit. Molar ratios, P/(Na+K) (1.9-3.2) and P/Ca (0.8-0.9) resulted in high reduction efficiency of Cl in deposits.	[82]
Pilot-scale plant CHEC, DTU	Electrical heated entrained flow reactor having an internal diameter of 79 mm and length of about 2 m.	5 kW	800	550	12 alternative biomasses including, straw, wood, pectin waste etc. Biomass co-firing in combination with additives. Different alternative biomasses.	Ash chemistry and deposition behavior. High fuel ash content resulted in higher deposit formation fluxes.	[83]
Swirl burner furnace CHEC, DTU	Swirl burner furnace.	-	800-1200	-	-	Ash transformation. Two distinct kinds of particles were observed. Particles less than 1 $\mu$ m were rich in K, Cl, S and P, while larger particles were rich in K, Ca and Si.	[83]



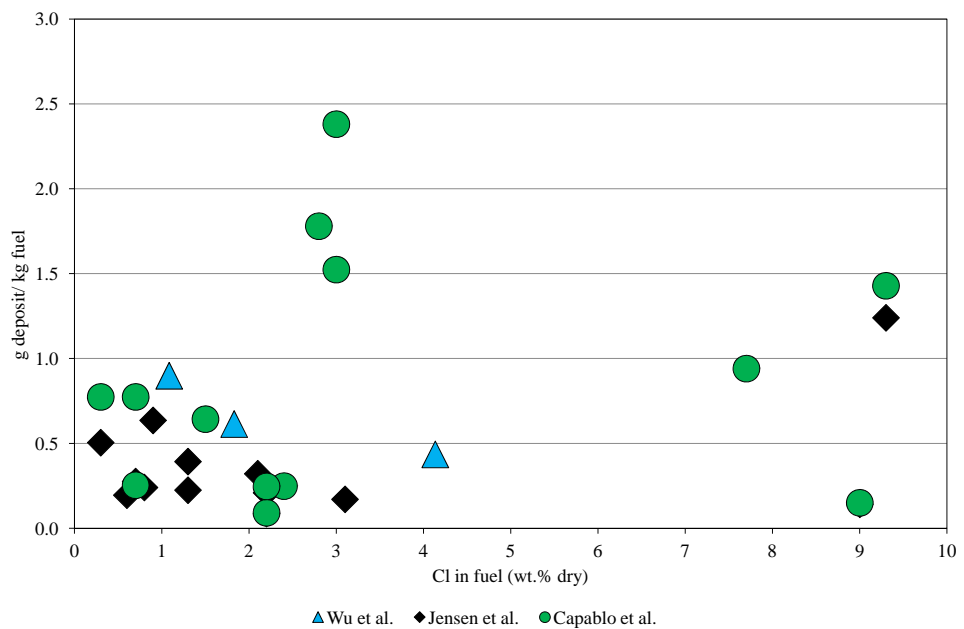
**Figure 2.24:** Ash deposition rate reported for individual biomass fuels during pilot-scale suspension firing [28, 41, 73, 80, 82, 83]. Flue gas temperature was between 800 and 1000 °C.



**Figure 2.25:** Ash deposition rate reported for pilot-scale suspension firing of biomass mixtures and/or with addition of additives [28, 41, 73, 82, 83]. Flue gas temperature was between 800 and 1000 °C.



**Figure 2.26:** Ash deposition rate as a function of Cl-content in the biomass fuel during pilot-scale suspension firing. Flue gas temperature was around 1000 °C [28, 41, 80].



**Figure 2.27:** Ash deposition rate as a function of Cl-content in the biomass fuel during pilot-scale suspension firing. Flue gas temperature was around 800 ± 50 °C [73, 82, 83].

### 2.5.2 Review of Ash Deposition during Full-scale Biomass Suspension Firing

Research on ash deposit formation during full-scale suspension firing of biomass (straw and wood) is scarce. The available full-scale investigations are by Jensen et al. [24] and Skrifvars et al. [38] on ash deposit formation during suspension firing of wood, and by Tobiasen et al. [5] and Jenkins et al. [51] on ash deposit formation during suspension firing of straw. These studies have revealed some important features about ash deposit formation during straw and wood suspension firing. However, an extensive and detailed study on the transient formation of ash deposit at different locations of the boiler is still not available in literature, and this information is needed to further promote the utilization of straw and wood in suspension firing plants.

A review of the available full-scale studies on ash deposition in biomass suspension-fired boilers is shown in Table 2.8. Tobiasen et al. [5] investigated the addition of different additives on ash deposition and overall boiler operation at Amagerværket Unit 2 (AMV2). AMV2 is a rebuilt coal boiler and the design of superheater tubes was not made accordingly that it can be used for straw firing, but it was used [5]. The factors that affect the appropriate use of additives include additive particle size distribution, reactivity, reaction temperature and time and cost [5]. The overview of results is shown in Table 2.7. Results of the full-scale measurements demonstrated that despite the use of the additives, more ash deposition resulted in the boiler for some of the additives. With chalk, the deposit flux increased significantly, and also deposits were white whereby back radiations from the slag layer on the superheater tubes were large and heat transfer was reduced. Bentonite, gave no operational problems and deposit flux was also reduced. Sand was not effective in reducing Cl-content in the fly ash and in deposits. DCP ( $\text{CaHPO}_4 \cdot 2\text{H}_2\text{O}$ ) appears to be effective in reducing Cl-content in the fly ash and the deposits, but caused problems of back radiation. Overall, sand and bentonite appeared to be attractive. Sand appeared to be cheap, but it was less reactive, and bentonite was expensive.

Unit 1 at Amager Power Station (AMV1), commissioned in 2009, is the first dedicated biomass suspension-fired boiler that was designed to fire straw and/or wood. No full-scale results have been reported regarding ash deposition from this boiler except the results presented in the present study. Moderate deposit formation rates in the range of 1 to 12  $\text{g}/\text{m}^2/\text{h}$  were measured during full-scale measuring campaign at Avedøreværket Unit 2 (AVV2), a wood suspension-fired boiler. Regarding ash deposition, no systematic tendency was observed regarding the applied fuel combinations, wood, natural gas and furnace oil. Cl contents in the deposits were low in the high flue gas temperature region, while further downstream in the flue gas channel

**Table 2.7:** Overall comparison of four additives investigated at AMV2, modified from Tobiasen et al. [5].

Evaluation of deposits	Sand	DCP	Chalk	Bentonite
Reduction in the collected amount of deposits	No	Yes	No	Yes
Reduction in Cl in the fly ash	No	Yes	No	Yes
Boiler operation	No back radiation	Back radiation	Back radiation	No back radiation

Cl-rich deposits appeared. Investigation by Skrifvars et al. [38] in a down-fired suspension boiler firing wood showed increased deposition rate (12 to 74 g/m<sup>2</sup>/h) at higher flue gas temperature (920 °C), and reduced deposition rates (3 to 13 g/m<sup>2</sup>/h) were measured at lower flue gas temperatures (750 °C). Suspension firing tests of leached straw with rice hulls at a straw suspension-fired boiler showed no significant increase in ash deposition rates, compared to the reference case of rice hulls. The Cl contents in the deposits were found to be unchanged [51].

Compared to the limited number of full-scale measurements for pure biomass suspension firing, a significant number of full-scale measurements for straw and coal co-firing can be found in literature and some of these are reviewed in Table 2.8. A more detailed investigation by Andersen [20] during co-firing straw at Studstrup Power Plant Unit 1 showed that co-combustion of straw and coal can be effective if ash 'synergy' is satisfactory. The products of combustion of biomass materials when co-fired with coal in a large utility boilers tend to have a higher level of sub-micron fume and vapor, and the fly-ash particles tend to be significantly smaller than those formed by the combustion of pulverized coal [20]. Biomass materials tend to have a relatively low ash content compared to most coals; however, the biomass ash materials tend to be relatively rich in alkali and alkaline earth metal, and these are effective fluxes for the alumino-silicate coal ashes. At low co-firing ratios, at about 10% on energy basis, recent plant experience has indicated that slagging and fouling tend to be modest [37]. However, experiences have also shown that coal quality is a very important factor when firing coal with straw due to ash deposition problems [2]. Fly ash from coal firing is often sold as filler for use in concrete mixes (among other uses), but this is not the case for fly ash from biomass firing. The reason is that the required contents of total alkali, Cl and residual carbon for the fly ash to be used in the concrete production are 5 wt.%, 0.1 wt.% and 5 wt.%, respectively. These limits were exceeded if more than 20% biomass is used on energy basis with coal [2, 20], nevertheless, this has been increased now.

Table 2.8: Review of full-scale suspension firing of biomass.

Location	System	Size	Fuels	Issues/Findings	Ref.
<b>Suspension Firing (Biomass)</b>					
Amagerværket Power Station, Unit 2 Denmark	Drum-type boiler with 12 burners. Retrofitted from oil to coal, and then coal to biomass.	250 MW <sub>th</sub>	Pulverized straw with and without the addition of additives.	Fouling and slagging. Issues of air pollution control equipments. Sand and bentonite resulted to be good additives.	[5]
Amagerværket Power Station, Unit 1 Denmark	Dedicated straw, wood and coal fired boiler with 12 burners.	350 MW <sub>th</sub>	Pulverized straw and wood with different co-firing combinations	No measurements except made in the present study.	[84]
Avedøreværket Power Station, Unit 2 Denmark	Pulverized wood-fired boiler.	800 MW <sub>th</sub>	Pulverized wood, natural gas and furnace oil.	Ash deposition, NOx and SOx emissions.	[24]
Jorbro Boiler Sweden	Down-fired.	80 MW <sub>th</sub>	Pulverized wood in combination with different shares of peat and S.	Deposition and corrosion.	[38]
California Energy Boiler	Suspension-fired.	26.5 MW <sub>e</sub>	Leached straw (20-25 wt.%) and rice hull.	Fouling and stack sampling.	[51]
<b>Suspension Firing (Straw and Coal)</b>					
Amagerværket Power Station Unit 3 Denmark	Opposed wall fired boiler with 16 burners.	250 MW <sub>th</sub>	Bituminous coal with high S in combination with different straw fuel fractions, typically 0 to 20% on thermal basis.	Fouling and slagging, emissions, performance of air pollution control equipments, and flame stability.	[85, 86]
Vestkraft Power Station, Unit 1 Denmark	Front-wall fired with 12 burners in three levels.	330 MW <sub>th</sub> /125 MW <sub>e</sub>	Bituminous coal from Russia and Columbia in combination with different straw fuel fractions, typically 10 to 25% on thermal basis. Straw was added through straw burners in the middle level. Coal-straw.	Ash deposition, corrosion, fly ash, emissions.	[87]
Kyndby Power Plant, Unit 3 Denmark	Down-fired.	180 MW <sub>th</sub>	Coal-straw.	Ash deposition.	[88]
Studstrup Power Station, Unit 1 Denmark	Back wall fired boiler with 12 burners.	380 MW <sub>th</sub> /150 MW <sub>e</sub>	Straw with Bituminous Columbian coal and American coal. Separate injection of straw up to 20% on thermal basis.	2 years demonstration program. Fouling/slagging, corrosion, fuel handling and emissions related issues were investigated.	[20]
Studstrup Power Station, Unit 4 Denmark	Opposed wall fired with 24 burners.	900 MW <sub>th</sub> /350 MW <sub>e</sub>	Straw with Bituminous Columbian coal and South African coal. Injection of straw using six modified burners. Injection of straw up to 20% on thermal basis.	Performance of air pollution control equipment (DeNOx catalyst), and ash.	[89]



## 2.6 Modeling of Ash Deposit Formation

Ash deposition modeling in biomass fired boilers is primarily based on three requirements, a) deposition flux, mass of deposit/area/time ( $\text{g}/\text{m}^2/\text{h}$ ), b) location of the deposits in the boiler, c) physical and chemical properties of the deposits and corresponding heat transfer considerations and materials related aspects [2, 31]. Generally, ash deposition models can be cataloged into three levels, i.e. the empirical indices model, the mechanistic model, and the most complicated CFD (Computational Fluid Dynamics) model.

Wang and Harb [91] summarized several existing models for ash deposition and heat transfer through the deposits and classified the total process into nine issues: (1) ash formation; (2) fluid dynamics and particle transport; (3) particle impaction; (4) particle sticking; (5) deposition growth as a function of location in the combustion chamber; (6) deposition properties and strength development; (7) heat transfer through the deposition layer; (8) the effect of deposition on operating conditions (temperatures and heat fluxes) in the combustor; (9) deposition structure and its effect on flow patterns in the combustion facility.

Traditionally, power generating facilities and some researchers have attempted to predict the severity of coal ash deposition by calculating empirical indices based upon the overall ash composition of the coal. These indices are less accurate predictors when extrapolated to other coals or operating conditions. This can be attributed to their use of overall ash compositions, while in fact deposition is initiated and propagated by individual ash particle with varying compositions and sizes.

The mechanistic models, in which the calculations of the complicated combustion process and the fluid dynamics are simplified, have been used for assessing ash deposition tendency and for predicting ash deposit behavior. Generally, a viscosity model relevant to silicate glass together with measurements of particle size and composition as well as the deposition composition is included. Detailed analysis of coal mineralogy, coal size distribution data, boiler design details, and boiler operating conditions were used as input to predict ash deposition in a pulverized coal-fired boiler and to assess boiler performance associated with the use of specified coal by Erickson et al. [92]. The simulations were in fair agreement with their tests.

The mechanistic models can provide a basement for developing comprehensive mathematical models that can simulate ash deposition and its impact on overall efficiency. A dynamic mechanistic model of ash deposit build-up and shedding through surface melting was established and demonstrated by Zhou et al. [31] in a straw grate-fired boiler. The predicted re-

sults were close to the results obtained from full-scale measurements, where a steady state was achieved between deposit build-up and shedding after 7 days.

A CFD-based deposition model was established and demonstrated by Kær [93, 94], in which the ash deposition from fly ash particles (2–250  $\mu\text{m}$ ) by inertial impaction, turbulent, and thermophoretic mechanisms, and KCl vapors-formed particles ( $\sim 0.5 \mu\text{m}$ ) by diffusion, turbulent, and thermophoretic mechanisms was considered.



## Chapter 3

# Design and Development of Probes for Online Monitoring of Deposit Build-up and Removal

### 3.1 Introduction

As described in Chapter 2, a significant amount of ash can be deposited on the boiler furnace walls and on the superheater tubes when firing KCl-containing biomass (straw) and/or co-firing high share of KCl-containing biomass with coal. To obtain accurate information on ash deposition in biomass-fired boilers, or, more precisely, to quantify ash deposition on the boiler furnace chamber and on the superheater tubes, one of the most effective ways is to use deposit probes. The deposit probes find key importance during combustion of solid fuels, and are extensively used to understand ash deposit formation and shedding processes, and to quantify and characterize the deposits. In addition, investigations of deposit pattern, composition and morphology on each side of the probe - the upstream and the downstream side - can further help to understand the mechanisms responsible for ash deposition on each side. Based on the experimental conditions, deposit probes can be air-cooled or water and air-cooled. In addition, deposit probes can be used for short time testing or for extensive full-scale measurements. Deposit probes find use either in the furnace region to investigate slagging propensity by simulating conditions of water walls or in the superheater region to investigate fouling and/or slagging by simulating conditions of typical superheater tubes. In this work, two probes are used; 1) a deposit probe used in the superheater region, termed as the horizontal probe, and 2) a deposit probe used in the boiler furnace region, termed as the vertical probe.

The ash deposition rate during simple probe measurements is normally determined by dividing the collected amount of the deposits with the probe exposure time. However, advanced probes can be more effective to truly identify online deposition and shedding processes, which are difficult to monitor using a simple deposit probe. Another advantage of the advanced online probes is that even though some information on the deposit formation process might be obtained using different simple deposit probes for different durations, there can be difficulties in guaranteeing identical boiler conditions for all probes [95]. Advanced online probes can be used to identify deposit mass uptake, deposit shedding, deposit characterization, and probe heat uptake using the temperature rise of the probe cooling fluid(s). This complete set of information finds key role to quantify transient deposit build-up and shedding, and most importantly to model ash deposit build-up and shedding processes based on the applied biomass fuel, local flue gas temperature, applied probe conditions and boiler operational conditions.

In addition to the quantification of deposit build-up, deposit shedding quantification is equally important in order to optimize the sootblowers employed in biomass-fired boilers. Steam, water and air sootblowing are the most commonly applied shedding techniques to shed deposits in the superheater region and in the boiler chamber region. Biomass-fired boilers have several water and steam sootblowers depending on the local flue gas temperature, deposit sintering characteristics and deposit quantity [2, 35]. The sootblower cleaning effectiveness depends on the sootblower location, cleaning media and Peak Impact Pressure (PIP)[44, 70, 78]. Quantification of PIP needed to remove the deposit by using artificial sootblowing probe can an effective way to optimize the design and operation of sootblowers employed in biomass suspension-fired boilers.

This chapter covers an overview of the deposit probes used for ash deposit build-up and deposit characterization studies. The horizontal ash deposition probe used during the ash deposit build-up measurements and a simple artificial sootblowing probe used to remove the deposits are described in detail. The design, functionality and commissioning of a vertical ash deposition probe simulating the conditions of the boiler furnace wall is also discussed.

### **3.2 Review of Deposit Probes used for Ash Deposit Build-up Investigations**

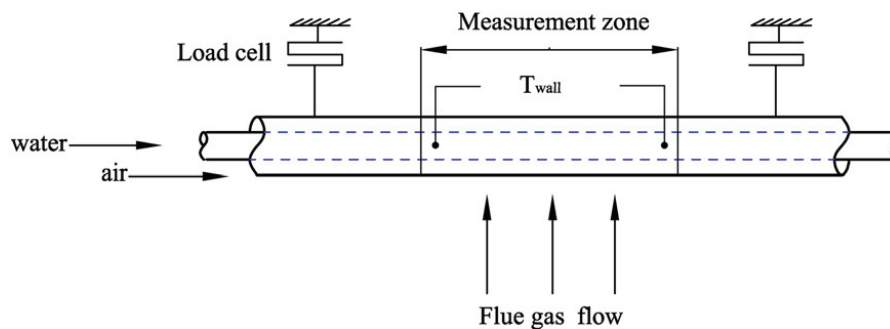
The deposit probes can find their use based on the experimental requirements i.e. deposition rate, deposit chemistry and morphology etc. Various types of deposit probes used for different experimental investigations can be found in literature.

### 3.2.1 Types of Deposit Probes Based on Mechanical Design

The deposit probes can be divided based on the mechanical design. The probes can be inserted in the furnace section to quantify and/or characterize slagging on the furnace walls (vertical probe) or can be used in superheater section to quantify and/or characterize deposits by simulating conditions of superheaters (horizontal probe).

#### Horizontal Probes

Horizontal probes are normally a long rod inserted in the superheater region of the boiler to simulate conditions of a typical plant superheater. Horizontal probe can be used for the quantification and characterization of deposits on the upstream and on the downstream side of the probe. This can be useful information to determine the ash deposition mechanisms responsible for the deposition on each side of the probe. Jensen et al. [46] investigated deposition fluxes using an air-cooled probe in the superheater region of straw-fired boilers. Vuthaluru et al. [96] used a deposition probe to study different pretreatments of coal in pulverized fuel boilers regarding deposition rates. In a recent study, Madhiyanon et al. [79] used an advanced online ash deposition probe. The probe was a double annular probe and it was possible to measure the changes in the deposit mass and fouling resistance due to ash deposition. A schematic of the deposit probe is shown in Figure 3.1. Two load cells were used to measure the amount of ash deposited, while the temperature rise of the cooling fluids was used to determine the fouling resistance caused by ash deposition.

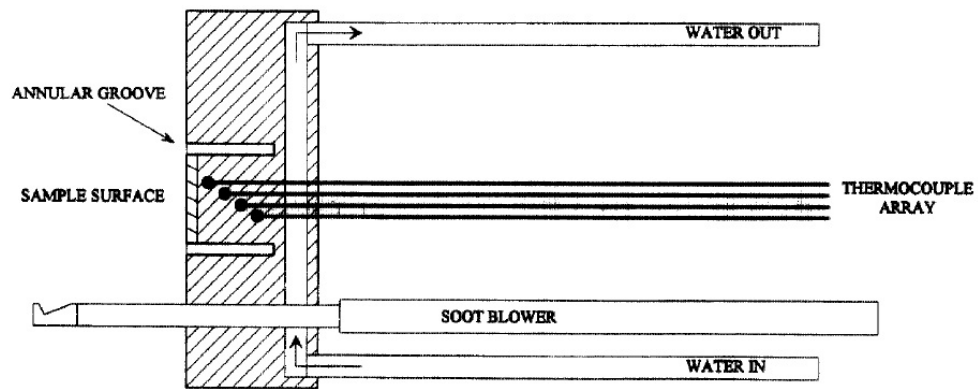


**Figure 3.1:** Schematic of the deposit probe used by Madhiyanon et al. [79] to measure mass of deposit and fouling resistance.

#### Vertical Probes

Significant amount of deposits can result on the water walls in the boiler furnace when biomass fuels with higher KCl proportions are fired in suspension-

fired boilers. In order to simulate the conditions of water walls, use of a vertical probe is a rather new concept. To investigate deposition and heat uptake in the furnace region, Gupta et al. [97] performed pilot-scale and full-scale experiments in the furnace region by using a deposition probe simulating the slagging conditions in the furnace region of a coal-fired boiler. Heinzl et al. [98] made investigations of slagging in co-combustion of biomass and coal using air-cooled probes. Illustration of a typical vertical probe used by Hanson et al. [99] for slagging investigations during pilot-scale studies is shown in Figure 3.2. A temperature array is used to measure the probe temperature. The probe is cooled by water to simulate conditions of water walls.



**Figure 3.2:** Illustration of a typical vertical probe for slagging investigations [99].

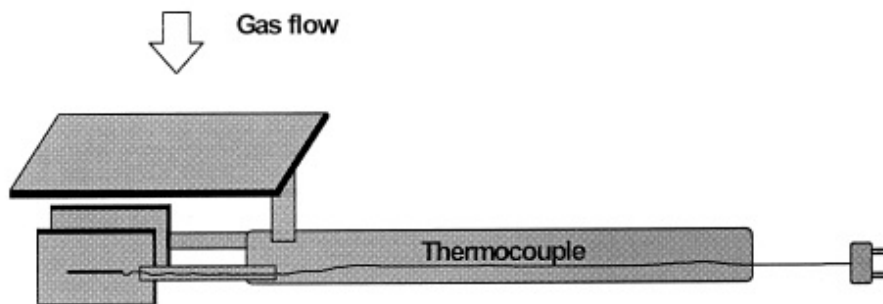
### 3.2.2 Types of Deposit Probes Based on Cooling Media

The deposit probes can be divided based on the cooling media used to keep a stable probe surface temperature during the measurements. The cooling media can be different based on the flue gas temperature and probe dimensions.

#### Air Cooled Probes

Air cooled probes are used for pilot-scale and/or full-scale investigations, primarily when the heat load to the probe is small. They can be used at higher flue gas temperatures ( $> 800\text{ }^{\circ}\text{C}$ ) during pilot-scale investigations due to a lower heat load (smaller probe surface area), compared to full-scale measurements, where higher temperature of the air coming out of the probe can be risky.

Nielsen [17] an advanced air-cooled pilot-scale probe for investigation of potassium salts on heat transfer surfaces. The probe consisted of two small (2 x 3 cm) vertical plates which were placed approximately 2 cm apart. A larger horizontal plate (6 x 9 cm<sup>2</sup>) that completely covered the underlying plates was placed 0.5 cm above the two vertical plates. This way, the horizontal plate shielded the vertical plates from the particles in the gas that came from above, allowing only vapors and submicron particles to deposit on the vertical plates. The schematic of the probe is shown in Figure 3.3. Brink et al. [95] designed and tested an air-cooled probe for on-line monitoring of deposition growth. The heat flux and corresponding thickness of the deposit was investigated for a couple of measurements in a 440 kW<sub>th</sub> grate boiler firing wood chips, bark and waste wood. The deposit probe was made of a 38 x 5 mm tube and a thermocouple was mounted at the outer surface to adjust the probe temperature close to the set point. The highest deposition rate was found during waste wood firing, whereas wood chips caused the lowest deposit build-up rate. However, it was found that the calculated thickness of the deposits was larger than the measured one, thereby demanding possible improvements in the probe design.



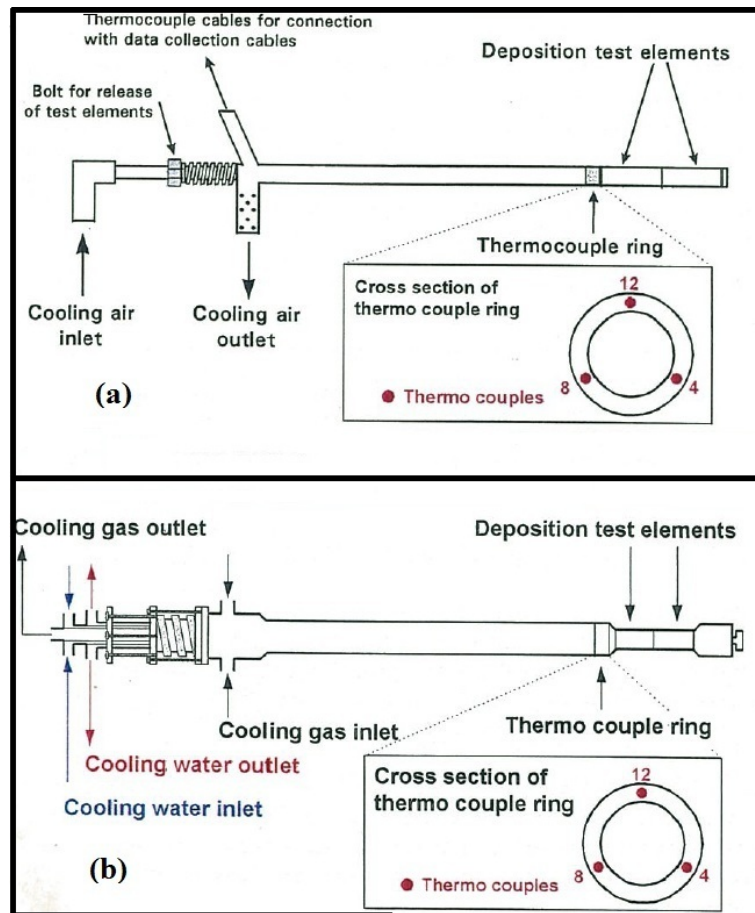
**Figure 3.3:** Schematic drawing of the probe used for investigation of potassium salts deposition on heat transfer surfaces [17].

Andersen [20] used a temperature controlled probe for deposit sampling during full-scale measurements in a straw and coal fired boiler. The probe was an advance form of the probe that was used for corrosion investigations. The probe was temperature controlled and it was possible to identify the shedding events of the deposits based on the sudden changes in the probe surface temperature. A schematic of the probe is shown in Figure 3.4 (a).

### Water and Air Cooled Probes

If the probe heat load is significant, the use of solely air cooled probe is not an appropriate solution due to difficulties in keeping the probe surface





**Figure 3.4:** Schematic outline of the air cooled (a) and air-water cooled (b) deposition probe [20].

temperature at the desired level, and a possible high air outlet temperature. Therefore, water can be used as cooling media along with air. Water and air cooled probes are in most of the cases, used during full-scale measurements when the flue gas temperature is higher ( $> 800$  °C). These probes are normally designed as double annular tubes and with air flow in the innermost and outermost tube to avoid corrosion problems and to keep the probe surface temperature close to the target temperature. The water flow is normally kept constant, while the air flow is changed based on the target probe surface temperature fluctuations. Andersen [20] used an air and water cooled probe for sampling of deposits during full-scale measurements in a straw and coal fired boiler in the high flue gas temperature region of the boiler. The probe was temperature controlled and it was possible to identify the shedding events of the deposits based on the sudden changes in the probe surface temperature. A schematic of the probe is shown in Figure

3.4 (b).

Ash deposition flux and shedding through surface melting in the high temperature superheater region (near boiler furnace) at a straw grate-fired boiler was investigated by Zbogor et al. [35] using an advanced online ash deposition/shedding probe. It was found that surface melting is the main mechanism of deposit shedding at a flue gas temperatures greater than 1000 °C. Deposit build-up and shedding at the Avedøre straw grate-fired boiler was investigated by Zhou et al. [33] by using a deposition probe and an artificial sootblowing probe in a lower temperature superheater region nearer to the convective pass at flue gas temperatures between 700 and 800 °C. The remarkable achievement of these probes was the simultaneous on-line ash deposition and shedding investigations with video monitoring.

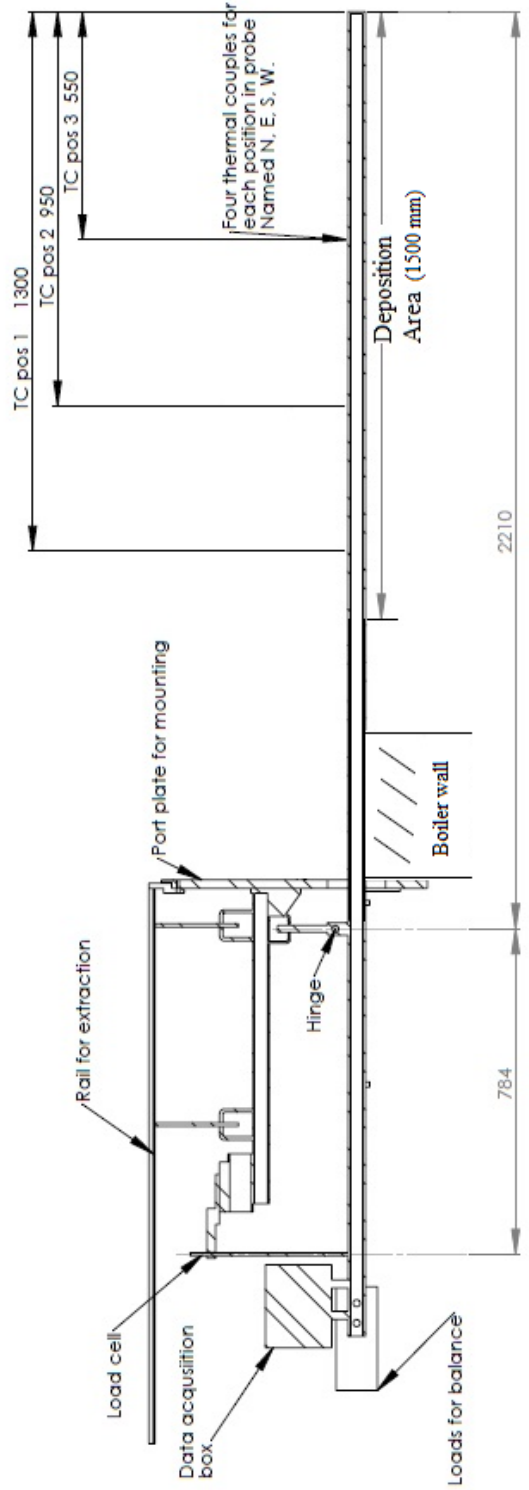
Most of the studies on ash deposition in biomass or in coal-fired power plant are short time probes because of costly extensive measurements.

### 3.3 Description of the Horizontal Ash Deposition Probe System

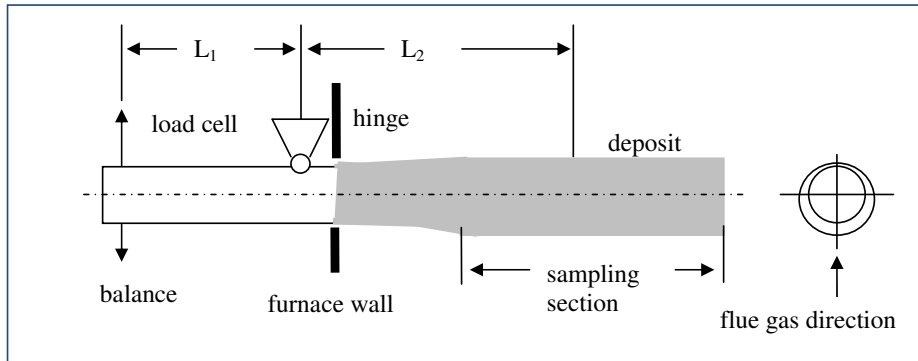
#### 3.3.1 Horizontal Ash Deposition Probe

The horizontal deposit probe used during the measurements in the present study was the same as was used by Zhou et al. [33] with minor modifications. Schematic view of the deposition probe system with identified positions of probe temperature measurements, deposition area, port plate for mounting, hinge, load cell and rail for pulling out the probe is shown in Figure 3.5, while a simplified schematic illustration of deposit probe system is shown in Figure 3.6. The probe was made of stainless steel, about 3 m long and having an outer diameter of 40.5 mm. The probe was cooled by water and air, whereby it was possible to determine heat uptake by the probe and keep a stable surface temperature. The probe hung on a hinge connected to a flange. A balance at the rear was used to oppose fluctuations in the boiler and to keep the probe aligned horizontally. A load cell was used to detect the force caused by the mass of the ash deposit on the probe.

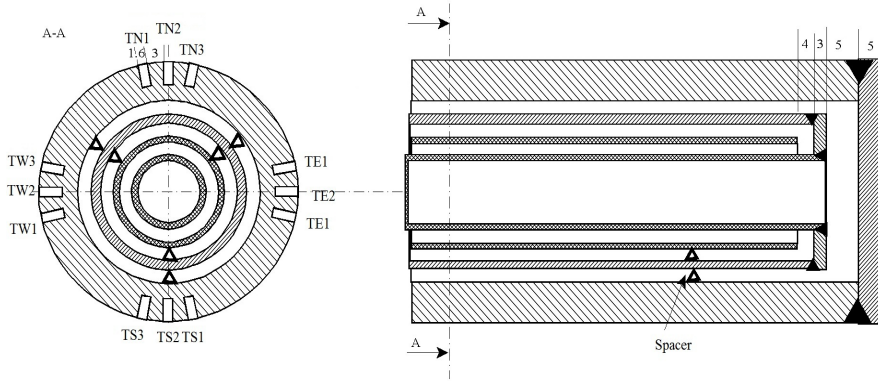
A cross-sectional view of the probe perpendicular to the probe axis and cross-sectional view along axis of annuli is shown in Figure 3.7. It can be seen that in each horizontal position of the probe (TC position 1, 2 and 3), four thermocouples provided temperatures at the N, E, S and W positions.



**Figure 3.5:** Schematic view of the horizontal probe with identified positions of probe temperature measurements, deposition area, port plate for mounting, hinge, load cell and rail for pulling out the probe.



**Figure 3.6:** Schematic illustration of the horizontal probe system.



**Figure 3.7:** Cross-sectional view perpendicular to probe axis and cross-sectional view along axis of annuli.

### Quantification of the Deposits Mass Uptake

As shown in Figure 3.5 the length of the effective ash sampling section was approximately 1500 mm, depending on the probe position relative to the boiler inner wall. The ash sampling was determined by the distribution of the deposit thickness along the probe after the probe was removed from the boiler. The thickness of the deposit was quite uniform along the sampling section of the probe. The deposit mass uptake was calculated using the following torque balance,

$$m_d \cdot g = (m_{d,i} - m_{d,f}) \cdot g \cdot \frac{L_1}{L_2} \quad (3.1)$$

where  $m_d$  is the deposit mass ( $g$ ),  $m_{d,i}$  is the initial signal of the load cell,  $m_{d,f}$  is the final signal of the load cell,  $g$  is the gravitational acceleration,

and  $L_1$  and  $L_2$  are the distances from the hinge to the balance and to the mass center of the deposit, respectively. For the used probe:  $\frac{L_1}{L_2} = \frac{785}{1460}$ , while the definitions of  $L_1$  and  $L_2$  can be seen in Figure 3.6. It is important to mention that the deposit mass is only obtainable if the probe is uniformly coated by the incoming fly ash particles.

### Quantification of the Probe Heat Uptake

The water and air flow rates are measured by flow meters at the inlets of the probe, and the temperatures of the water and air are measured by 4 thermocouples at the inlets and the outlets. The following heat balance equation was used for heat uptake calculations using steady state assumptions,

$$Q = m_w \cdot C_{p,w} \cdot (T_{w,out} - T_{w,in}) + m_a \cdot C_{p,a} \cdot (T_{a,out} - T_{a,in}) \quad (3.2)$$

where  $Q$  is the heat uptake ( $W$ ),  $m$  is the flow rate ( $\frac{kg}{s}$ ),  $C_p$  is the heat capacity ( $\frac{J}{kg \cdot K}$ ),  $T$  is the temperature ( $K$ ), and  $w$  and  $a$  represent water and air, respectively. The corresponding heat flux ( $\frac{W}{m^2}$ ) would be,

$$q = \frac{Q}{s} \quad (3.3)$$

where  $s$  is the effective probe surface area. The selected length for the effective heat transfer surface is 2 m. Here, 2 m is selected because approximately 2 m of the probe was inside the boiler.

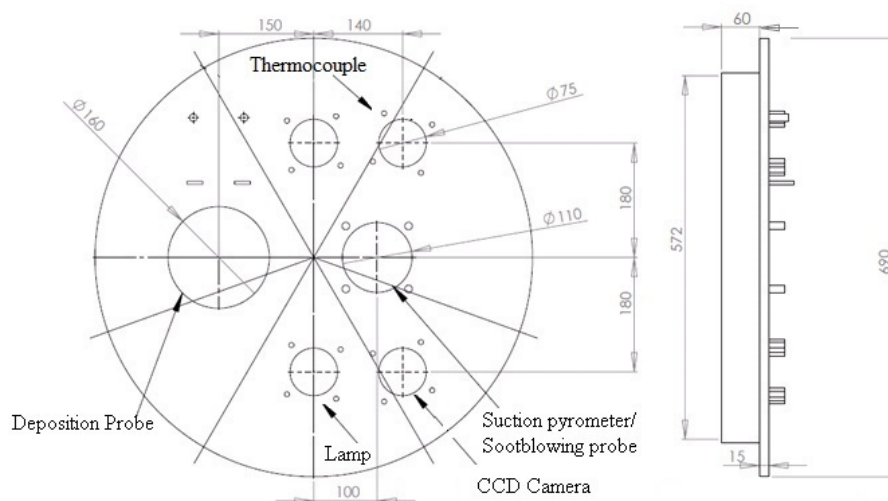
### 3.3.2 Description of the Port Plate

The kind of data needed during the full-scale measurement campaign by using the above mentioned horizontal probe is ash deposit mass uptake, heat uptake by the probe, flue gas temperature measurement by thermocouple and suction pyrometer, and video monitoring. To fulfill these requirements, a special type of port plate was prepared that could be mounted in the inspection hole of the boiler. Schematic drawing of the port plate used during the measurements is shown in Figure 3.8. In the large port, a small port for the deposit probe, a port for the thermo-element, a CCD (charge-coupled device) camera port and a port for the suction pyrometer and artificial soot-blowing probe can be seen. A significant effort was made to make each port capable of meeting the experimental results. As an example, a view of the deposition probe system used for the measurements at Amagerværket Unit 1 (AMV1) is shown in Figure 3.9. The angle of the camera was adjusted in a way that maximum area of the deposit probe could be seen. The CCD

camera registered the deposit formation and removal processes on the probe.

The flue gas temperature near the probe was continuously measured, using a simple thermocouple in a protective shell. In addition, a suction pyrometer (International Flame Research Foundation model, IFRF [100]) was also used for some periods during each test.

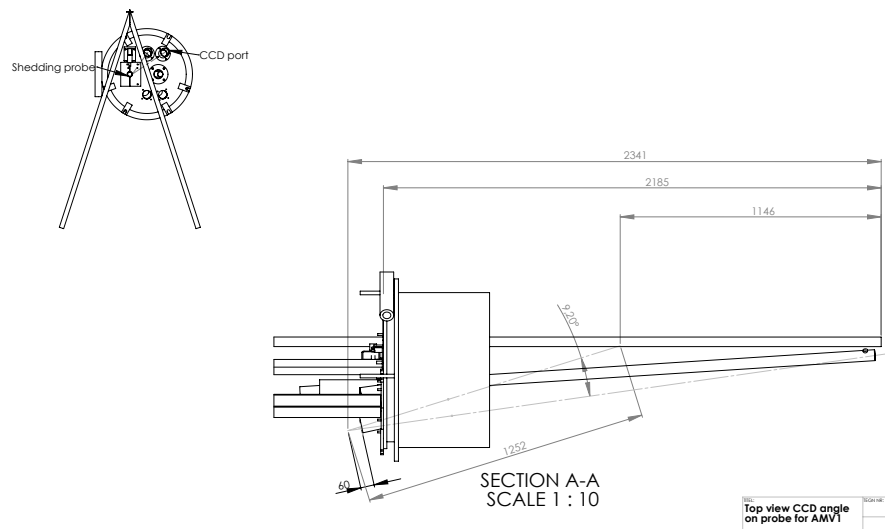
At the end of each experiment, the probe was carefully taken out of the boiler; the deposits were removed, weighed, and photographed. The pattern and characterization of the deposits were then made based on the deposits visual analysis. The deposits were scratched from the upstream and downstream side of the probe for further detailed analysis. In some of the measurements, on each side of the deposit probe, there were seen more than two deposit layers and the deposits were then characterized based on the structure and thickness of the deposit layers.



**Figure 3.8:** Schematic drawing of the port plate used for measurements conducted using the horizontal probe.

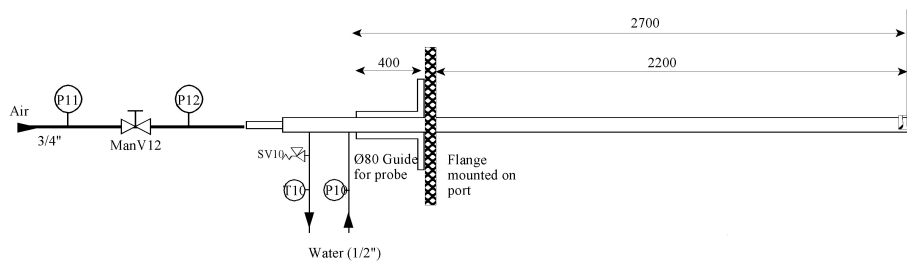
### 3.4 Description of the Artificial Sootblowing Probe

An artificial sootblowing probe with an external diameter of 42.2 mm and a length of 3 m was used for *in situ* removal of deposits. A schematic drawing of the sootblowing probe is shown in Figure 3.10 and the detailed sootblower nozzle drawing can be seen in Figure 3.11. The sootblower probe nozzle was of convergent-divergent shape, and air at a supply pressure of 6.0 bar the jet



**Figure 3.9:** Schematic illustration of the deposition probe system used in the inspection hole at AMV1 boiler.

was fully expanded. The sootblower nozzle was fixed at the end of the probe. The Peak Impact Pressure (PIP) of the nozzle was measured along the axial centerline as a function of the supplying air pressure in the laboratory at room temperature. The PIP of the jet, defined as the centerline stagnation pressure of the jet, was used to characterize the removal of deposits by the sootblowing probe. The measured values of PIP are shown in Figure 3.12 and it is important to notice that these values are measured at room temperature. In the applied range of PIP, there can be a little impact of flue gas temperature on PIP, but the measurement of PIP at temperatures close to the flue gas temperature was not possible. The measured PIP increases with the supplied air pressure, and drops off quickly with the axial distance from the nozzle exit (Figure 3.12).



**Figure 3.10:** Overall sootblowing probe set up with water and air flow description. (P10, P11 and P12 are pressure gauges for air, P10 is pressure gauge for water (to act a cooling media), while, T10 is temperature indicator.

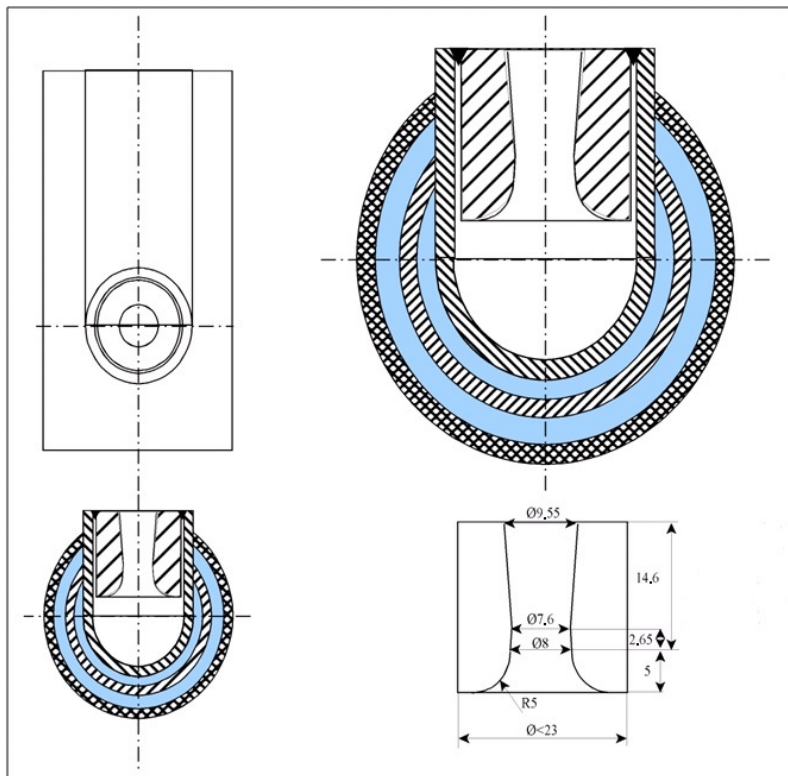


Figure 3.11: Detailed drawings of the sooblowing nozzle.

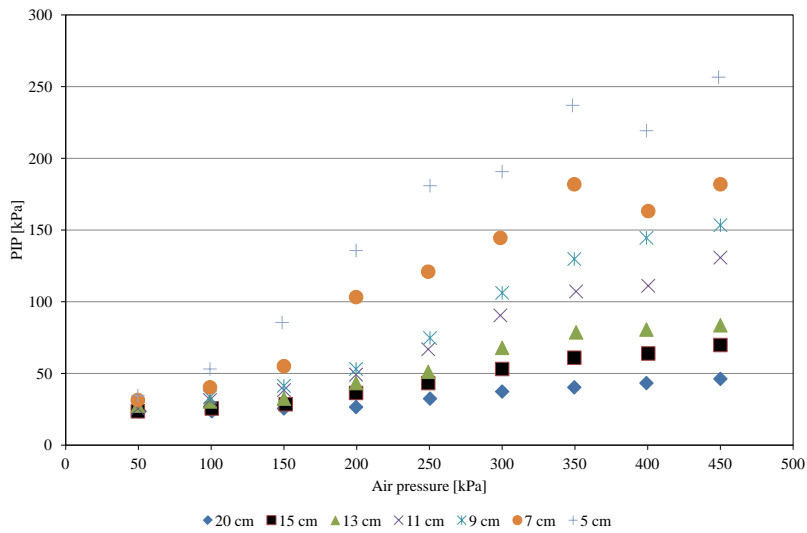


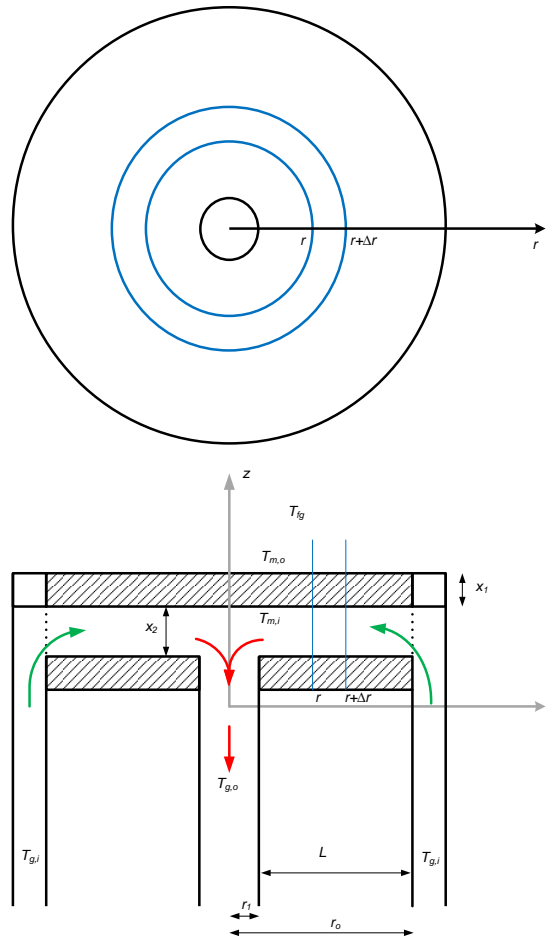
Figure 3.12: The measured Peak Impact Pressure (PIP) as a function of applied air pressure at varying downstream distance from the nozzle exit at room temperature.



### 3.5 Design and Development of the the Vertical Ash Deposition Probe

It was one of the objectives of the project to investigate ash deposit build-up in the furnace region of the boiler, and a vertical ash deposit probe was therefore designed to simulate the conditions of the boiler furnace wall. Before the start of the design of the probe, heat transfer calculations were performed to calculate the air flow needed to cool the probe, and to identify of the probe dimensions for the only available port at the boiler. The proposed layout of the vertical probe for heat uptake calculations is shown in Figure 3.13.

The overall heat balance equation can be written as,



**Figure 3.13:** Proposed layout of vertical probe for heat uptake calculations.

$$\frac{dQ_{in}}{dL} = \frac{dQ_c}{dL} + \frac{dQ_{rad}}{dL} \quad (3.4)$$

$$dQ_c(r) = h_f (T_{fg} - T_{m,0}) \cdot \pi \left( r^2 - (r + \Delta r)^2 \right) \quad (3.5)$$

$$\frac{dQ_c}{dr} = h_f (T_{fg} - T_{m,0}) \cdot \pi \cdot 2r \quad (3.6)$$

$$\frac{dQ_c}{dL} = h_f (T_{fg} - T_{m,0}) \cdot \pi \cdot 2 (r_0 - L) \quad (3.7)$$

$$\frac{dQ_{rad}}{dL} = \epsilon_{steel} \sigma (T_{fg}^4 - T_{m,0}^4) \cdot \pi \cdot 2 (r_0 - L) \quad (3.8)$$

Here,  $\epsilon_{steel}$  is the emissivity of the metal and  $\sigma$  is the Stephen Boltzmann constant.

$$\frac{dQ_{in}}{dL} = (T_{m,o} - T_{m,i}) \cdot \frac{k_m}{x_1} \cdot 2\pi (r_0 - L) \quad (3.9)$$

Here,  $x_1$  is the metal plate thickness, and  $k_m$  is the metal plate thermal conductivity.

The air outlet temperature was predicted using,

$$dT_g \cdot C_{p_{air}} \cdot \dot{m} = dL \cdot \frac{dQ_{in}}{dL} \quad (3.10)$$

$$\int_0^L dT_g = \int_0^L \frac{1}{C_{p_{air}} \cdot \dot{m}} \cdot dQ_{in} \quad (3.11)$$

The boundary conditions are,

$$\text{BC1: at } L = L, \quad r = r_0, \text{ and } T_g = T_{g,i} \quad (3.12)$$

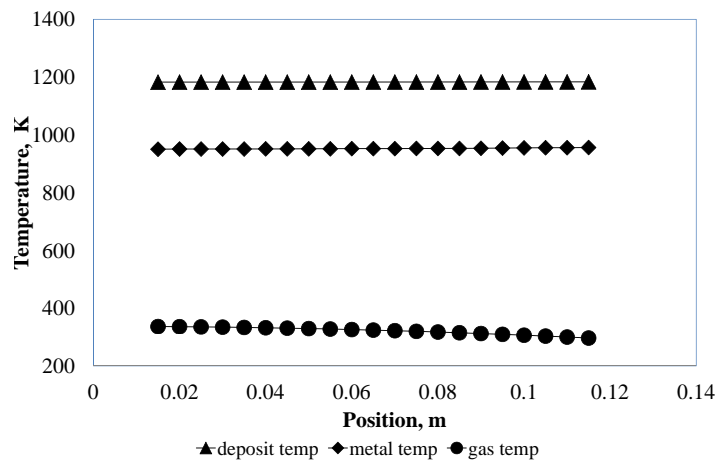
$$\text{BC2: at } L = 0, \quad r = r_0 - r_1 \quad (3.13)$$

The above mentioned set of equations was solved for different sets of inlet air temperature, air velocity and slit thickness. It was found that the deposit temperature and the metal temperature vary insignificantly and even

a significant amount of air flow was not able to cool the probe at the desired temperature range, between 400 and 650 °C. A typical example of the results of outlet air temperature, deposit temperature and metal temperature is shown in Figure 3.14. The heat transfer calculations revealed that there is need of removable metallic pins to be installed in the metal plate to enhance the heat transfer. In addition, a water chamber was prepared for heat transfer enhancement.

A complete drawing of the vertical probe is shown in Figure 3.15, while the vertical probe with cut and angled view is shown in Figure 3.16. The probe was made of stainless steel, with 130 mm diameter facing the boiler chamber. The probe was cooled by water and air, whereby it was possible to determine heat uptake by the probe and keep a stable surface temperature. The probe hung on a hinge connected to a flange using the same principle of horizontal probe. A load cell was used to detect the force caused by the mass of the ash deposit on the probe. The temperatures measurements were made at 45°, 135°, 225°, 315° position of the probe, while a thermocouple in the middle of the probe was used as the target probe surface temperature as shown in Figure 3.17.

A special type of port plate was prepared that could be mounted at a acoustic pyrometer port at Amager Unit 1 (AMV1). More details of the boiler can be found in Chapter 5. The probe measuring position was about 9 m above the upper row of the burners. In the port plate, a small port for the deposit probe and a port for the thermo-element was made as shown in Figure 3.15. A S-type thermocouple was placed just close to the deposition probe port.



**Figure 3.14:** Calculated air and probe metal temperatures.

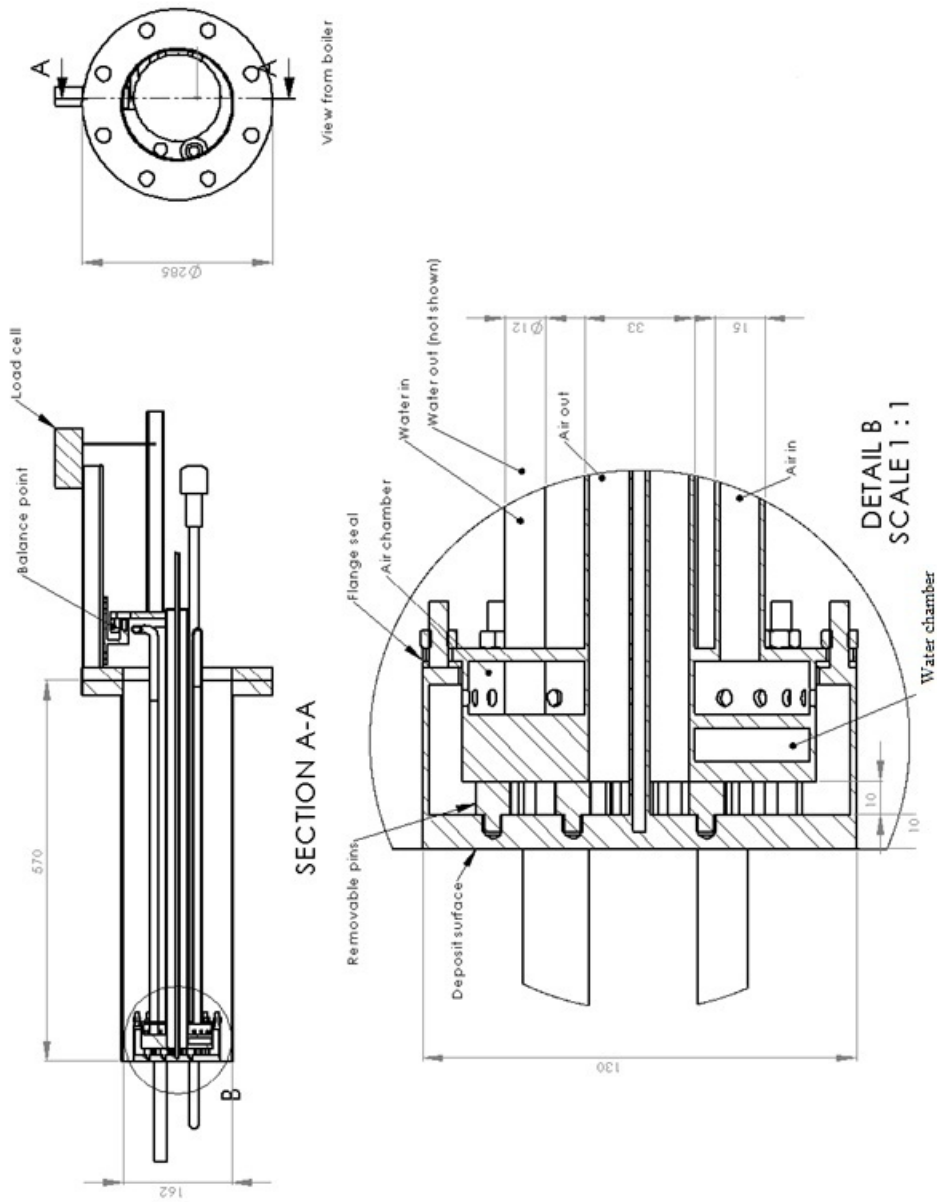
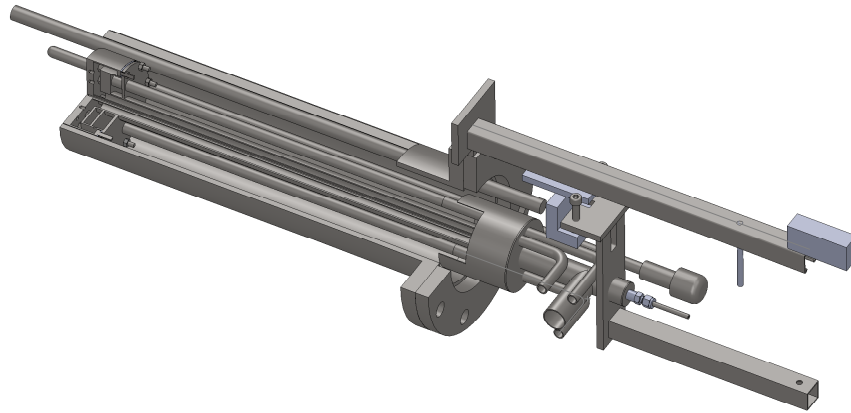
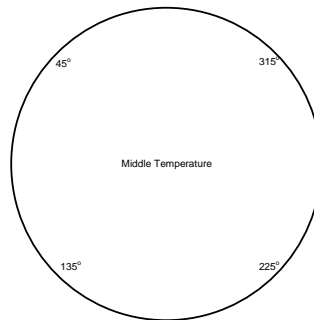


Figure 3.15: Detailed drawings of the vertical probe system.



**Figure 3.16:** Drawing of the vertical probe with cut and angled view.



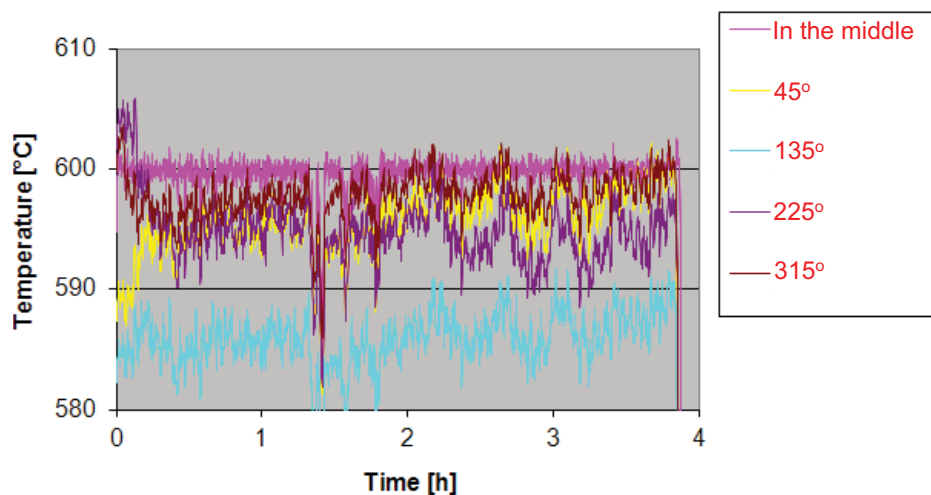
**Figure 3.17:** Position of the thermocouples on the vertical probe, seen from boiler to the wall.

The deposit mass uptake and probe heat uptake were calculated by using the same equations used for the horizontal ash deposition probe. An endoscope could potentially be used for video monitoring, but a market search revealed that none meeting the current requirements is available. An endoscope that can be used at high flue gas temperatures (1200 °C) is available, but lacking the ability to look back at the deposition probe.

### 3.5.1 Commissioning of the Vertical Probe

The vertical probe measurements were conducted at Amager Unit 1 (AMV1). The vertical probe was mounted on the balance point, and goes through a tube into the boiler. The experiments were done by inserting the probe, so that the plate was at level with the boiler wall. The parameters that could be changed were the plate surface temperature and the exposure time. At the end of each experiment, the probe was carefully taken out of the boiler; the deposits were removed, weighed, and photographed. The pattern and characterization of the deposits was then made based on the deposits visual

analysis. A summary of the conducted measurements by using vertical probe is shown in Table 3.1. As the boiler was operating at under-pressure, a pressure difference between the boiler and the outside, forced us to close the gap between the port plate and the deposit probe, in order to stop the air flow. This effectively disabled the mass-uptake measurements by the probe. As explained in the table in most of the measurements conducted the collected amount of the deposits is very small and even an increase in probe surface temperature is not effective in enhancing the deposit mass uptake. However, the set point temperature was held nicely through the commissioning period, which is satisfying, but because of the limitations that only one probe measuring position has to be used, the commissioning phase was ended with partial success. As an example, the results of probe surface temperature measured during test 3 (see Table 3.1) are shown in Figure 3.18. The results seems to be satisfactory in controlling the probe surface temperature at the required levels. The main problem however proved to be the collection of the ash deposits, which, if present, were removed because of the air inlet flow, when the probe was extracted. Covering of the complete set-up with a box could have eliminated the problem of air flow, but that was beyond the time schedule of the Ph.D. project.



**Figure 3.18:** Temperature measurements of thermo-elements attached on the vertical probe. The values shown are for test number 3.

The picture of the probe taken just after an experiment is shown in Figure 3.19. It can be seen that the amount of deposits collected is extremely low.

**Table 3.1:** Summary of the conducted measurements using vertical probe.

Experiment Number	Probe surface temp. °C	Exposure time h	Results and comments
1	450	168	Very few deposits on the probe were seen. The probe seems to be corroded. In addition, sealing tape that was used to stop air flow was broken, thereby the experiment was not successful.
2	550	48	Very few deposits on the probe were seen, even though the air inlet was completely sealed. The probe was corroded.
3	600	4	Small layer of deposits was seen on the probe. The probe seems to be corroded.
4	650	24	Some deposits were seen on the probe from the side boiler wall. However these deposits were blown away while taking the probe out of the boiler.



**Figure 3.19:** Picture of the vertical probe taken just after finishing an experiment.

## Chapter 4

# Ash Transformation and Deposit Build-up during Biomass Suspension and Grate Firing

Most of the contents of this chapter have been taken from the peer reviewed manuscript, M. S. Bashir, P. A. Jensen, F. J. Frandsen, S. Wedel, K. Dam-Johansen, J. Wadenbäck, S. T. Pedersen, Ash transformation and deposit build-up during biomass suspension and grate firing: Full-scale experimental studies, *Fuel Processing Technology*, **97** (2012), 93–106 [101].

### 4.1 Introduction

Combustion of biomass can induce large operational problems due to ash deposit formation on the superheater tubes because of the presence of substantial amounts of K and Cl in biomass-derived ashes [2, 21, 22, 45, 103]. The deposit formation process in biomass-fired boilers is influenced both by the fuel composition and boiler type [42]. In Denmark, straw is usually combusted in grate-fired boilers where the fuel is combusted in the bottom part of the furnace chamber on a moving bed. Suspension-fired systems originally used for coal combustion, have also recently been considered for biomass (straw and wood) combustion in Denmark. In biomass suspension firing, pulverized biomass typically from pellets crushed in the coal mills (roller mills) is blown into the burners, where the fuel particles are burned in suspension. Combustion of straw and/or wood in suspension-fired units is an attractive option because of the often high electrical efficiency of these plants (46–48%), compared to the traditional grate-fired systems (25–30%) [2]. However, when biomass is used in suspension-fired boilers, the



deposit flux on the superheater tubes is expected to increase. When straw is burned in stoker and grate-fired boilers, the percentage of fly ash entrained is typically 10–30%, while 80–90% is entrained during suspension firing [17]. Vattenfall A/S in Copenhagen retrofitted a suspension-fired boiler at the Amager Power Station (Amagerværket, Unit 2), from coal to straw, but experienced fouling and slagging problems in the superheater regions and furnace walls.

Some full-scale experimental studies on ash deposition in straw-fired boilers have been reported based on measurements in grate boilers [2, 33, 35, 46, 102]. Only limited data is available from biomass suspension firing where improved knowledge on ash transformation and transient deposit formation is needed to optimize design and operation [2, 27, 69]. Pilot-scale suspension-fired investigations by Nordgren et al. [27] and Theis et al. [41] indicate reduced deposit formation rate by co-firing straw with woody biomass and co-firing straw with peat, respectively. However, full-scale studies on 100% straw and wood suspension firing are rare to find except the recent investigations made by Tobiasen et al. [5] and Skrifvars et al. [38]. Therefore, further full-scale boiler deposit studies of straw suspension firing with wood will be useful to optimize the boiler operation and to improve our understanding of the ash deposit formation process.

The aim of this study was to investigate ash transformation and deposition behavior in two biomass-fired boilers, firing wheat straw and/or wood. The influence of straw firing technology (grate and suspension) on the ash transformation, deposit formation rate and deposit characteristics has been investigated. Full-scale measurements of ash deposition were made in the superheater and convective pass regions of Unit 2 at the Amager Power Station (straw and/or wood suspension-fired, AMV2) and Unit 2 at the Avedøre Power Station (straw grate-fired, AVV2). The measurements were conducted by use of an advanced on-line ash deposition probe. The composition of fuel and fly ash was analyzed and straw ash transformation in suspension and grate firing conditions was investigated. The influence of co-combustion of wood with straw on deposit formation rate, probe heat uptake and deposit characteristics was also investigated during suspension firing conditions.

Bulk elemental analysis of fly ashes revealed that fly ash from suspension-firing of straw has high contents of Si, K and Ca, while fly ash from straw-firing on grate was rich in the volatile elements K, Cl and S. SEM-EDS analysis showed that the fly ash from straw suspension firing consists of three kinds of particles: 1) flake type Si rich particles, 2) molten or partially molten particles rich in Si, K and Ca with small amounts of Mg, P, and potassium salts on the outer surface, and 3) small particles rich in K,

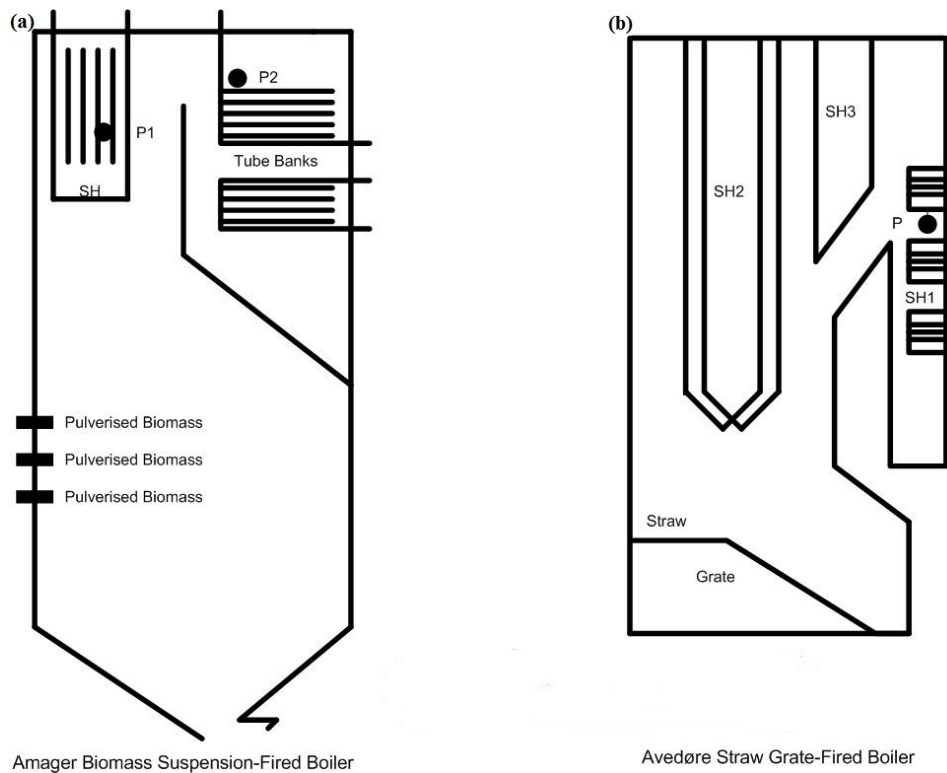
Cl and S (aerosols). Investigations of deposit formation rates revealed a deposit formation rate close to  $38 \text{ g/m}^2/\text{h}$  during straw grate firing. Data from straw suspension firing showed a deposit formation rate of  $41 \text{ g/m}^2/\text{h}$ . The deposit formation rates during straw suspension firing and straw grate firing were on similar levels. This was observed even though the concentration of fly ash in the flue gas was significantly higher during straw suspension firing. Data from 35% straw suspension firing with wood showed a deposit formation rate of  $33 \text{ g/m}^2/\text{h}$  for the first 12 h. The deposit formation rate increased to  $41 \text{ g/m}^2/\text{h}$  with 100% straw firing. The probe heat uptake reduction up to 40 h of exposure time was 3.0, 7.3, 8.4 and  $16.5 \text{ kW/m}^2$  during 35, 65, 80 and 100% straw firing, respectively.

## 4.2 Equipments, Materials and Methods

### 4.2.1 Boilers

AMV2 was previously a coal-fired suspension drum-type boiler. It was retrofitted in 2003 to use pure pulverized biomass fuel with different shares of wood and straw. AMV2 is a  $250 \text{ MW}_{th}$  front wall-fired boiler with 12 burners at three levels with a maximum overall capacity of  $57 \text{ t/h}$  biomass. The boiler capacity was reduced to  $\sim 70\%$  when it was retrofitted from pulverized coal to straw [66]. Tobiasen et al. [5] and Berg et al. [66] mentioned that certain changes in the boiler systems were made in order to make the boiler capable of firing biomass. The solid fuel grinding mills (modified coal roller mills) were re-used with modifications, and also the fuel pipes and the low-NOx coal/oil-burners were re-used [66]. In the burners, the outer part of the primary air tube with flame holder was shortened in order to obtain an earlier mixing of inert primary air/fuel and secondary combustion air in the burner opening [66].

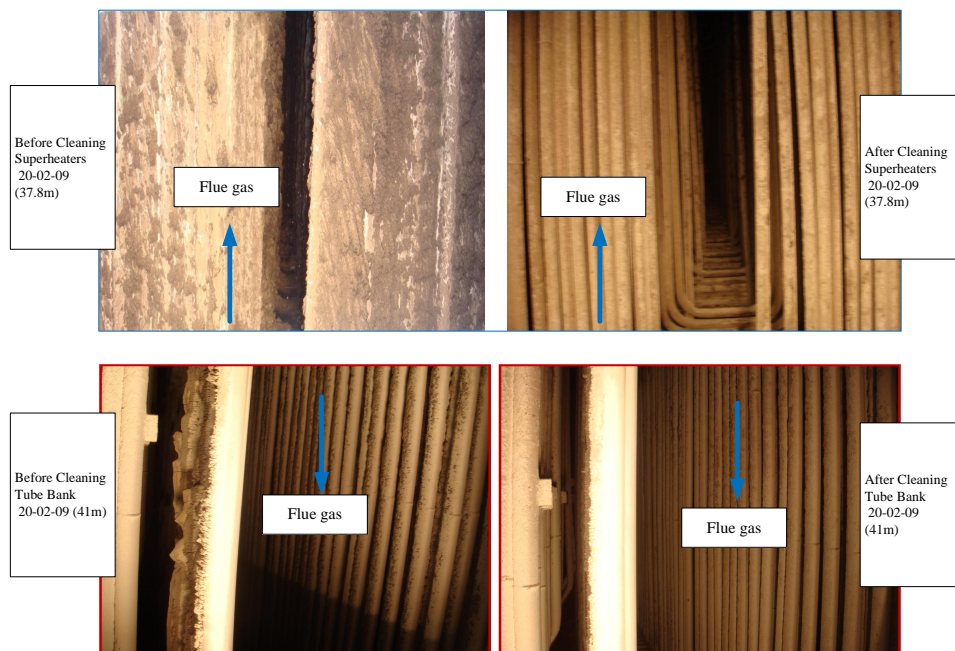
Measurements at AMV2 were conducted from February to April during the district heating season. A schematic drawing of the boiler is shown in Figure 4.1 (a). Probe measurements were conducted at position 1 in the superheater region (SH, 1<sup>st</sup> Pass) and position 2 in the tube bank region (TB, 2<sup>nd</sup> Pass). Previous experiences at AMV2 have shown that when straw is fired, significant ash deposition occurred on the superheater tubes and furnace walls, which made it necessary to manually clean the boiler at regular intervals. The maximum operation period on 100% straw was limited to approximately two weeks due to severe ash deposition on the superheaters that have insufficient distance between them (113 mm) [5, 66]. Cleaning of the boiler was only possible during complete shut-down, leading to long periods without heat/power production and significant cleaning costs [5, 66]. The probe measurement positions used are shown in Figure 4.2 before and after



**Figure 4.1:** Schematic view of the boilers. The locations of the probe measuring positions (P1, P2) at AMV2 (a) and probe position (P) at AVV2 (b) are identified. SH stands for superheater.

manual cleaning, showing significant ash deposition in the superheater region and possible obstruction of the flue gas flow. A more elaborative drawing of the boiler including the probe measuring positions is shown in Figure 4.3. During the experiments, the boiler was utilizing pulverized biomass consisting of straw from Denmark and wood from Russia. Biomass pellets were normally unloaded at the power plant and transported to conical silos. There was no fixed share of straw or wood to be combusted and fuel firing was based on the fuel available in the silo. The straw and/or wood pellets were crushed in the roller mills and then blown into the burners, where the fuel particles were burned in suspension. The flue gases after passing through superheaters and screen tubes, pass through the tube bank section and after that moves to the economizer before reaching to the electrostatic precipitator.

AVV2, also called AAV2-bio boiler, is a dedicated straw-fired vibrating grate boiler with a thermal capacity of  $105 \text{ MW}_{th}$ , corresponding to 26 t/h of straw (bales). A schematic drawing of the boiler and probe measur-

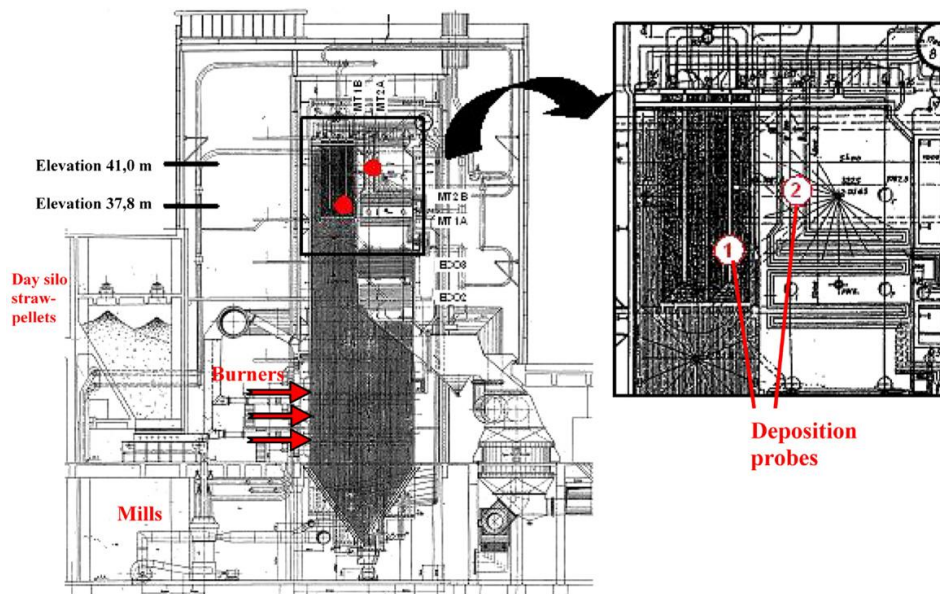


**Figure 4.2:** Images of the probe measurement positions before and after manual cleaning during 100% straw firing at AMV2. The upper image is from the superheater region (SH, 37.8m stands for probe measuring position) and the bottom image is from the tube bank region (TB, 41m stands for probe measuring position). It can be seen that severe ash deposition has clogged the superheater tubes.

ing position is shown in Figure 4.1 (b). As shown in Figure 4.1 (b), the flue gas moves up through the boiler combustion chamber to the secondary superheater (SH2) located at the top of the boiler, through the tertiary superheater (SH3) in a horizontal pass, and to the primary superheater (SH1) in the second gas pass. After passing through the economizer, air preheater, and the bag filter, the flue gas leaves the plant through the stack. The brief operational data of AMV2 boiler and AVV2 boiler are shown in Table 4.1.

**Table 4.1:** Brief operational data of the boilers (AMV2 and AVV2).

Parameter	AMV2	AVV2
Capacity (biomass)	250 MW <sub>th</sub>	105 MW <sub>th</sub>
Firing method	Suspension firing	Grate firing
Burners	12 (3 rows, 3*4)	Vibrating grate
Steam data	120 bar/480 °C	160 bar/583 °C



**Figure 4.3:** Schematic view of AMV2 boiler with identification of silos, mills, burners and deposition probe measuring positions. Modified from Tobiasen et al. [5].

#### 4.2.2 Fuels

The analysis of the fuels fired during the measurements is shown in Table 4.2. It is seen that straw fuels contain a higher amount of ash than wood. Fuel analysis also shows that the straw fuel is rich in Si, K and Cl, compared to the wood fuel. The slight difference in the fuel analysis of straw from AVV2 and straw from AMV2 is possibly due to seasonal variations (rain and time of harvesting). Typical size distribution of the pulverized straw dust to the burners at AMV2 is shown in Table 4.3. It can be seen that about 70% particles are greater than 200  $\mu\text{m}$ .

#### 4.2.3 Ash Deposition Probe

The deposit probe used during the measurements was made of stainless steel, about 3 m long and having an outer diameter of 40.5 mm. The probe was cooled by water and air, whereby it was possible to determine heat uptake by the probe and keep a stable surface temperature. More details of the deposit probe and complete probe system have been described in Chapter 3.

#### 4.2.4 Procedure of Measurements

A series of probe measurements were conducted at AMV2 in the superheater region with 35, 65, 80 and 100% straw shares mixed with wood. Each mea-

**Table 4.2:** Composition of the fuels fired during measurements at AMV2 and AVV2.

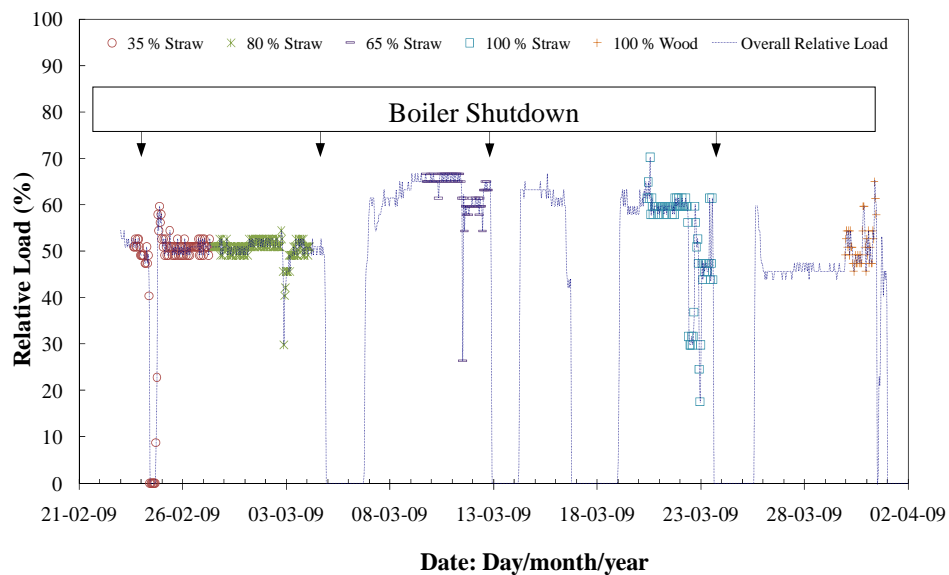
Fuel/Analysis	Straw (AMV2)	Wood (AMV2)	Straw (AVV2)
<i>Proximate analysis</i>			
Moisture (wt.%, a.r.)	7.40	9.45	10.20
Ash (wt.%, d.b.)	5.90	3.30	4.70
Volatiles (wt.%, d.b.)	75.50	79.50	76.60
MJ/kg: a.r.	16.00	16.65	–
<i>Ultimate analysis (wt.%, d.b.)</i>			
C	45.00	49.10	47.23
H	5.900	6.200	6.340
N	0.630	0.130	0.406
S	0.088	0.018	0.090
Si	1.357	0.750	1.100
Al	0.028	0.051	0.008
Ca	0.430	0.200	0.340
Fe	0.046	0.034	0.008
K	0.826	0.087	0.920
Na	0.094	0.029	0.024
Cl	0.398	0.010	0.358
Mg	0.065	0.031	0.065

surement lasted 3–5 days. At AVV2, 100% straw was fired. The probe surface temperature was fixed to 500 °C in all the measurements in order to simulate typical superheater tubes in a biomass-fired boiler [5, 35]. A single test was conducted in the tube bank region when firing wood (Figure 4.1 (a)). The influence of straw firing in suspension on the ash transformation, deposit formation rate and deposit characteristics has been investigated by comparison of results from the two boilers. A summary of the main experimental conditions is shown in Table 4.4. At AMV2, in the areas where the probe was mounted the mean flue gas temperature was in the range of 580–850 °C and the mean calculated flue gas velocity was in the range of 3.83–5.49 m/s. At AVV2, the mean flue gas temperature was in the range of 770–785 °C and the measured flue gas velocity was 7.05 m/s during test 1. Main combustion variables during the probe tests such as fuel mixture, flue gas temperature, and excess air ratio are shown in Table 4.4.

The overall boiler load during the measuring campaigns at AMV2 is shown in Figure 4.4. Full load at AMV2 corresponds to 57 t/h of straw. It can be seen that AMV2 was shut down after some days. The overall boiler load was between 85 and 95% during the measurements at AVV2. Full load at AVV2 corresponds to 26 t/h of straw.

**Table 4.3:** Typical size distribution of the pulverized straw dust to the burners at AMV2. The particle size distribution was determined by sieve analysis.

Percentage	Size specification
0.6%	> 2.0 mm
9.2%	> 1.0 mm
35.8%	> 0.5 mm
69.0%	> 0.2 mm
83.6%	> 0.09 mm



**Figure 4.4:** Percentage of applied boiler load during each measurement at AMV2 and boiler shutdown incidents.

In some of the measurements at AMV2, a CCD (charge-coupled device) camera registered the deposit formation and shedding processes on the probe. The flue gas temperature near the probe was continuously measured, using a simple thermocouple in a protective shell. Additionally, a suction pyrometer (International Flame Research Foundation model, IFRF [100]) was also used for some periods in order to confirm the accuracy of the thermocouple flue gas temperature measurements. In the superheater area of AMV2, the suction pyrometer typically registered a 150–160 °C higher flue gas temperature than the thermocouple. This temperature difference was probably due to strong radiation effects in the boiler.

**Table 4.4:** Overall comparison of conducted measurements at AMV2 in terms of deposit formation rate, probe heat uptake and deposit characteristics. The flue gas temperature for the first four tests is the thermocouple temperature plus 160 °C. SH: superheater, TB: tube bank. <sup>a</sup> measured, <sup>b</sup> 22 h, <sup>c</sup> 27 h, <sup>d</sup> 1.2 h, <sup>e</sup> 2.1 h, <sup>f</sup> 45 h, <sup>g</sup> 47.3 h, <sup>h</sup> 49 h.

Location (test no.)	SH (1)	SH (3)	SH (2)	SH (4)	TB (5)	SH (1)	SH (2)
Exposure time (h)	90	72	124	76	24	743	72
Probe metal temperature (°C)	500	500	500	500	500	500	500
Straw (% mass basis)	35	65	80	100	0	100	100
Wood (% mass basis)	65	35	20	0	100	0	0
Mean boiler load (%)	46	63	50	53	52	85-95	90-95
Mean flue gas temperature (°C)	848	820	849	837	581	770	785
Excess air ratio ( $\lambda$ )	2.20	2.19	2.19	2.26	2.20	-	-
Flue gas flow (Nm <sup>3</sup> /s)	310	395	319	337	276	-	-
Bulk gas velocity (m/s), calculated	4.30	5.49	4.43	4.67	3.83	7.05 <sup>a</sup>	-
Net plant sootblowing frequency (1/h)	0.85	-	0.92	1.10	-	-	-
Deposit formation rate, (g/m <sup>2</sup> /h), 12 h	33.0	-	33.0	41.0	1.0	36.8 <sup>b</sup>	38.0 <sup>c</sup>
(Mean flue gas temperature, °C, 12 h)	(856)	-	(863)	(848)	(586)	(760-800)	(775-809)
<i>Deposit mass uptake (g/m<sup>2</sup>)</i>							
Initial (2 h)	105	150 <sup>d</sup>	198	707	3	810 <sup>b</sup>	80 <sup>e</sup>
After 40 h	516	1274 <sup>f</sup>	280	2610	-	3390 <sup>g</sup>	1860 <sup>h</sup>
Final (2 h)	1041	1475	1520	1670	-	4050	2440
<i>Heat uptake (kW/m<sup>2</sup>)</i>							
Initial (2 h)	32.2	29.4 <sup>d</sup>	32.9	37.1	12.4	40.3 <sup>b</sup>	40.6 <sup>e</sup>
After 40 h	29.2	22.1 <sup>f</sup>	24.5	20.6	-	30.0 <sup>g</sup>	27.0 <sup>h</sup>
(Heat uptake reduction)	(3)	(7.3)	(8.4)	(16.5)	-	(10.3)	(13.6)
Final (2 h)	23.3	23.1	21.3	28.3	10.2	19	28.7
<i>Number of deposit layers</i>							
Upstream side	2	3	3	3	2	3	2
Downstream side	1	2	2	2	1	2	2
<i>Mean deposit thickness (mm)</i>							
Upstream side	~5	~20	~25	~25	~3	10-30	~6
Downstream side	~2	~3	~5	~5	~1	~6	~2

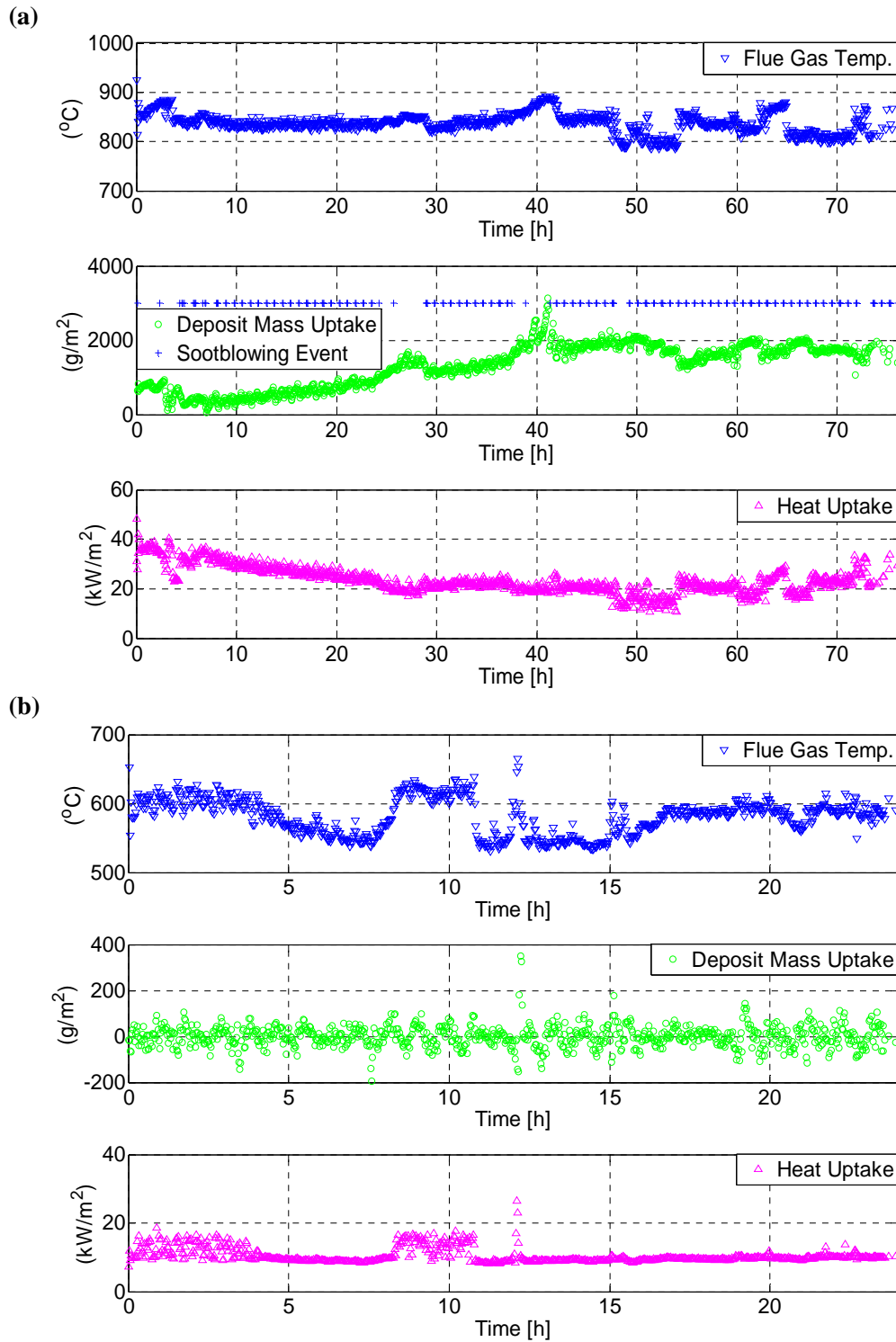


## 4.3 Results and Discussion

### 4.3.1 100% Straw and Wood Firing

Retractable steam sootblowers were used for 2–5 minutes during boiler operation; typically after regular intervals (40–45 minutes) during measurements at AMV2 (tests 1–4). Sometimes the sootblowers were completely stopped for a couple of hours. The sootblower located nearest to the probe measuring position was shut down during the measurements, while sootblowers located about 4 m below the measurement position, and in the front wall of the measurement position were still in operation. The mean sootblowing frequency during the tests at AMV2 is shown in Table 4.4. Sootblower operation caused significant fluctuations in the air flow used to keep the probe temperature constant at 500 °C and corresponding changes in the probe heat uptake signal. When plant sootblowers were in operation, some fluctuations in the deposit mass uptake signal were also prominent.

Examples of probe measuring results of 100% straw and wood firing at AMV2 are shown in Figure 4.5. The local flue gas temperature, deposit mass uptake and probe heat uptake measured during 100% straw firing are shown in Figure 4.5 (a). Some fluctuations in the deposit mass uptake and probe heat uptake signals were induced by a poor control of the probe air supply particularly when plant sootblowers were in operation. However, by showing average values over 1000 s, those short time fluctuations are leveled out. The boiler was running at a load of 53% during the test. The flue gas temperature shown in Figure 4.5 (a) is the thermocouple temperature plus 160 °C (the typical difference in temperature readings during the measurements with suction pyrometer and thermocouple). The registration of the deposit mass uptake signals showed an average amount of 707 g/m<sup>2</sup> of deposits that were collected on the probe in the initial 2 h. The deposit mass increases gradually throughout the first 40 h and during the 40–43 h period, the deposit mass increased to more than 3,200 g/m<sup>2</sup>. After a peak in the flue gas temperature, there was a steep reduction in the deposit mass due to removal of a complete deposit layer. For the rest of the measurement, the deposit mass uptake signal remained between 1,500 and 2,000 g/m<sup>2</sup>. The probe heat uptake decreases continuously to a level of 20 kW/m<sup>2</sup> during the first 28 h. The probe heat uptake stayed at that level for the next 20 h, whereafter it fluctuated around that level possibly due to flue gas temperature fluctuations. After the test was finished, the probe was removed from the boiler chamber and deposit samples from the probe surface were collected. Deposits obtained after the 100% straw firing test were sintered and adhered strongly to the probe.



**Figure 4.5:** Flue gas temperature, deposit mass uptake and probe heat uptake during measurements at AMV2, a) 100% straw firing, superheater region measurements (test 4, signals averaged to 1000 s), b) 100% wood firing, tube bank region measurements (test 5, signals averaged to 100 s).

A single measurement in the tube bank region (Position 2, Figure 4.1 (a)) was conducted with 100% wood firing. Measurement results are shown in Figure 4.5 (b). The mean flue gas temperature was 581 °C during this test. The deposit mass uptake signal fluctuates around zero, indicating only intermittent adhesion of a powdery ash deposit to the probe. The probe heat uptake during this measurement is nearly constant for long periods, where it stays just below 10 kW/m<sup>2</sup>. Detailed signals of flue gas temperature, deposit mass uptake, and probe heat uptake for each test conducted at AMV2 are presented in Appendix A.

### 4.3.2 Comparison of Full-scale Measurements

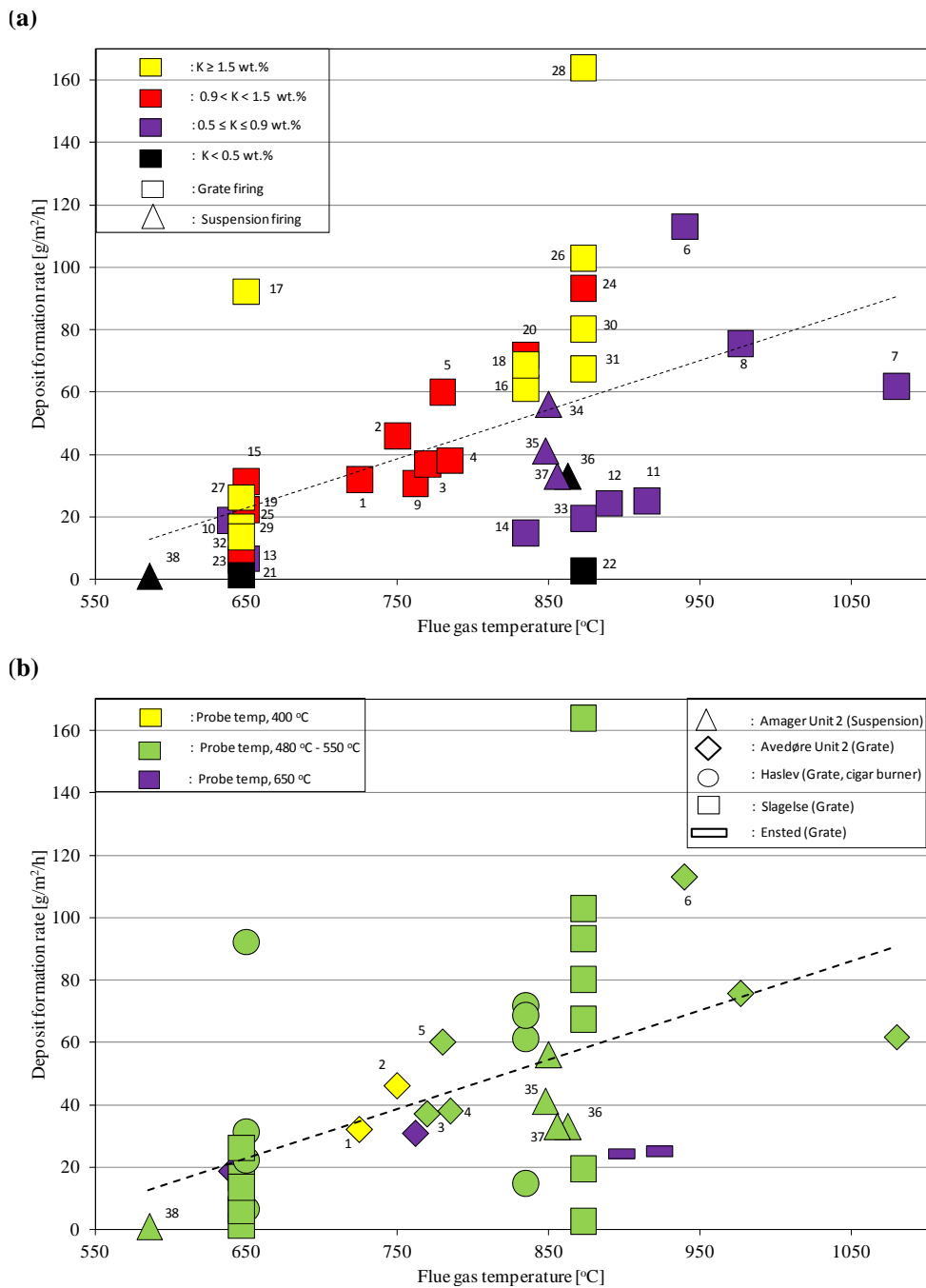
Comparison of the results regarding the probe exposure time, mean boiler load, flue gas temperature, bulk gas velocity, deposit mass uptake, probe heat uptake, and deposit characteristics is shown in Table 4.4. The first four out of five measurements at AMV2 were made in the superheater (SH) region, while the last measurement was conducted in the tube bank (TB) region. Both measurements at AVV2 were conducted in the convective pass region nearer the first superheater. During test 1 (35% straw firing) at AMV2, the deposit formation rate was 33 g/m<sup>2</sup>/h for the first 12 h. The deposit formation rate increased to 41 g/m<sup>2</sup>/h when 100% straw was fired. The deposit formation rate in the tube bank region (test 5) during 100% wood suspension firing was extremely small ( $\sim 1$  g/m<sup>2</sup>/h). It can also be seen that the deposit formation rate and primarily the initial deposit mass uptake (average for 2 h) increases when 100% straw was fired (Table 4.4). Decreased deposit formation rates have been observed by Nordgren et al. [27] and Lokare et al. [28] by introducing different biomass fuels with decreasing straw contents during pilot-scale suspension-fired investigations. This is possibly due to ash dilution effects and/or chemical interactions [27, 28]. Another possible reason could be that a larger amount of condensed KCl (from straw) can possibly increase the contact area between particles, and when in contact with the probe surface, strengthen the bonding of the deposit on the superheater tube. During both tests at AVV2, the deposit formation rate was similar and close to 38 g/m<sup>2</sup>/h in the initial 22–27 h.

The reduction in the probe heat uptake up to 40 h of exposure time at AMV2 increases with increasing straw share (see Table 4.4). The probe heat uptake reduction up to 40 h of exposure time was 3.0, 7.3, 8.4 and 16.5 kW/m<sup>2</sup> during 35, 65, 80 and 100% straw firing, respectively. The probe heat uptake reduction during straw grate firing was 10.3 and 13.6 kW/m<sup>2</sup> for test 1 and test 2 at AVV2, respectively. The data shown in Table 4.4 indicate generally a moderate increase in deposit formation rate and heat uptake reduction (up to 40 h) with increased straw share. However, the data show also some fluctuations that are possible during full-scale measurements

because of the associated difficulties to keep all parameters reasonably constant.

A comparison of previous full-scale deposit probe measurements made at different straw-fired boilers and the current measurements is shown in Table 4.5 and Figure 4.6. The boiler types, combustion variables such as fuel type and local flue gas temperature, probe surface temperature, and the measured deposit formation rates are shown in Table 4.5. The data points in Figure 4.6, even those at approximately the same conditions, have a large spread, which is a result of the difficulties of keeping all operational parameters constant during full-scale measurements. However, within the range of deposit formation rates from 1 to 160 g/m<sup>2</sup>/h, the following systematic tendencies can be observed.

- A tendency to increased deposit formation rate with an increase in flue gas temperature is observed. At a flue gas temperature of 650 °C, the deposit formation rate is typically from 5 to 30 g/m<sup>2</sup>/h and at 900 °C, the deposit formation rate is typically 20 to 110 g/m<sup>2</sup>/h. At higher fuel alkali contents ( $K > 0.9$  wt.%, yellow and red points), the increase in deposit formation rate with flue gas temperature is steeper compared to the increase in the deposit formation rate at lower fuel alkali contents ( $K \leq 0.9$  wt.%, violet and black points). Increased flue gas temperatures probably increase the fraction of molten ash as well as provide an increased content of gas phase alkali species, and both will lead to an increased deposit formation rate.
- Most of the deposit measurements were conducted with probe surface temperature in the range from 480 to 550 °C (all marked green in Figure 4.6 (b)) and a few were conducted with lower (400 °C) or higher temperatures (650 °C). It can be seen that changed probe surface temperatures in the range from 400 to 650 °C do not seem to significantly influence the deposit formation rate.
- The deposit formation rates during straw firing in suspension and grate boilers are on similar levels as indicated by the points 1–33 (grate, square symbols) and 34–38 (suspension, triangular symbols) in Figure 4.6 (a). This is observed even though the concentration of fly ash in flue gas was significantly higher during suspension firing.
- The deposit formation rate measured by the advanced *in situ* deposit probe (points 1–6 and 35–38 in Figure 4.6 (b)) and measurements obtained with the more simple deposit probes show reasonably similar results indicating that both methods can be used to determine initial deposit formation rates.



**Figure 4.6:** Impact of flue gas temperature on deposit formation rates, a) four different sets of fuel alkali contents and two types of straw firing technologies, b) different sets of probe surface temperatures and 5 different boilers. Amager Unit 2 is a straw and/or wood-fired suspension boiler. Avedøre Unit 2 is a straw-fired grate boiler. Haslev is a cigar type boiler where big bales of straw are fired directly. Slagelse and Ensted are both straw-fired grate boilers. **Graph details:** a) the color represents the range of fuel alkali in wt.%, while the point shape represents the straw firing technology, b) the color represents the probe surface temperature, while the point shape represents the boiler type.

**Table 4.5:** Deposit formation rates measured during the previous and current full-scale measurements. <sup>a</sup> Measurements with advanced *in situ* deposit probes, <sup>b</sup> Mean of three measurements, <sup>c</sup> Ash, K, Cl and Si contents were estimated by using straw share in wood.

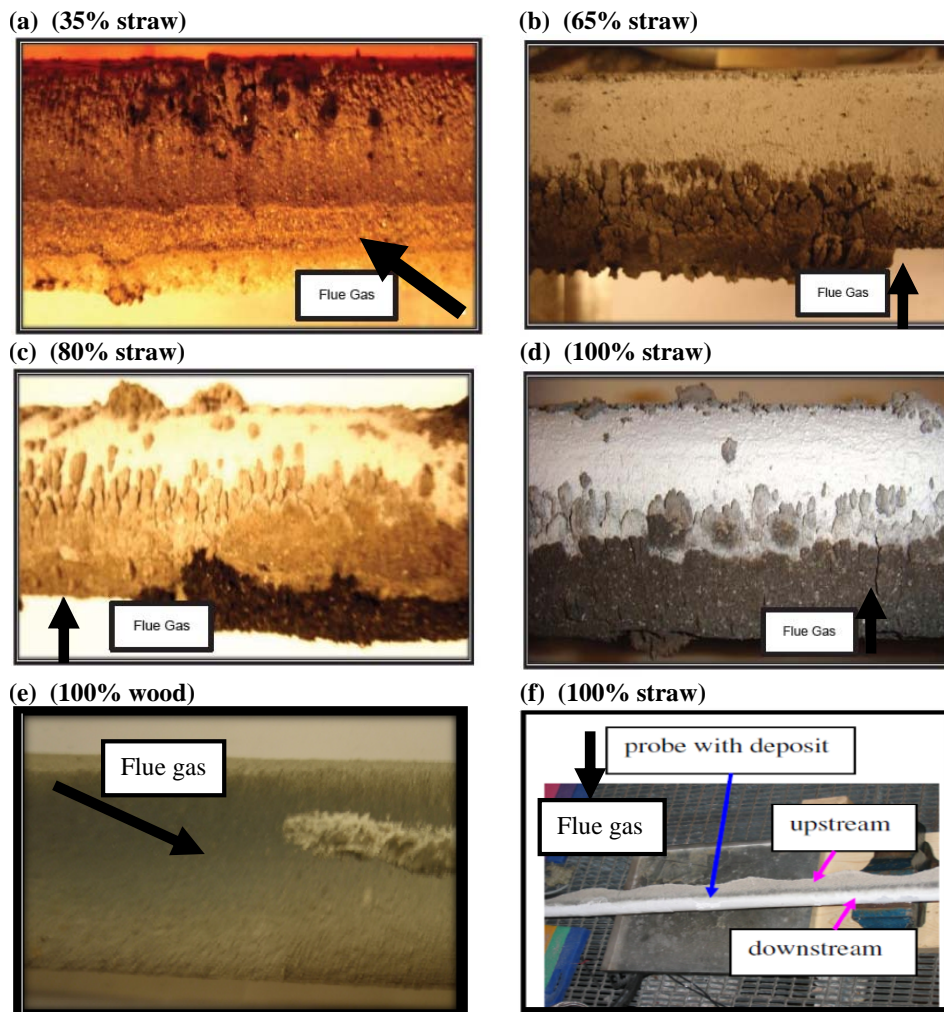
No	Boiler	Type	Capacity	Fuel	Fuel analysis	K	Cl	Si	Probe location	Probe temp. °C	Flue gas temp. °C	Exposure time h	Exposure rate g/m <sup>2</sup> /h	Ref.
1 <sup>a</sup>	Avedøre 2	Grate-fired	105 MW <sub>th</sub>	Straw	Ash	0.92	0.36	1.10	Convective Pass	400	725	24.0	32.0	[33]
2 <sup>a</sup>	Avedøre 2	Grate-fired	105 MW <sub>th</sub>	Straw	4.7	0.92	0.36	1.10	Convective Pass	400	750	24.0	46.0	[33]
3 <sup>a</sup>	Avedøre 2	Grate-fired	105 MW <sub>th</sub>	Straw	4.7	0.92	0.36	1.10	Convective Pass	500	770	22.0	36.8	[33]
4 <sup>a</sup>	Avedøre 2	Grate-fired	105 MW <sub>th</sub>	Straw	4.7	0.92	0.36	1.10	Convective Pass	500	785	27.0	38.0	[33]
5 <sup>a</sup>	Avedøre 2	Grate-fired	105 MW <sub>th</sub>	Straw	4.7	0.92	0.36	1.10	Convective Pass	550	780	24.0	60.0	[35]
6 <sup>a</sup>	Avedøre 2	Grate-fired	105 MW <sub>th</sub>	Straw	5.5	0.69	0.32	—	Furnace	500	940	24.0	113.0	[104]
7	Avedøre 2	Grate-fired	105 MW <sub>th</sub>	Straw	4.7	0.75	0.25	1.18	Furnace	500	1080	3.8	61.8	[104]
8	Avedøre 2	Grate-fired	105 MW <sub>th</sub>	Straw	4.5	0.81	0.26	1.08	Furnace	500	977	4.9	75.6	[104]
9	Avedøre 2	Grate-fired	105 MW <sub>th</sub>	Straw	4.7	0.75	0.25	1.18	Convective Pass	650	762	5.3	30.7	[104]
10	Avedøre 2	Grate-fired	105 MW <sub>th</sub>	Straw	4.5	0.81	0.26	1.08	Convective Pass	650	640	5.3	18.8	[104]
11	Ensted	Grate-fired	39 MW <sub>th</sub>	Straw	4.4	0.90	0.28	1.10	Near to Superheater	650	915	4.5	25.0	[104]
12	Ensted	Grate-fired	39 MW <sub>th</sub>	Straw	4.8	0.90	0.28	1.20	Near to Superheater	650	890	4.3	24.3	[104]
13	Haslev	Cigar-burner	23 MW <sub>th</sub>	Straw	4.1	0.71	0.29	0.96	Superheater	510	650	8.0	6.6	[46]
14	Haslev	Cigar-burner	23 MW <sub>th</sub>	Straw	4.1	0.71	0.29	0.96	Furnace Chamber	510	835	8.0	14.9	[46]
15	Haslev	Cigar-burner	23 MW <sub>th</sub>	Straw	4.9	1.29	0.52	0.89	Superheater	510	650	8.0	31.3	[46]
16	Haslev	Cigar-burner	23 MW <sub>th</sub>	Straw	4.9	1.29	0.52	0.89	Furnace Chamber	510	835	8.0	61.3	[46]
17	Haslev	Cigar-burner	23 MW <sub>th</sub>	Straw	5.0	2.05	0.56	—	Superheater	510	650	8.0	92.2	[46]
18	Haslev	Cigar-burner	23 MW <sub>th</sub>	Straw	5.0	2.05	0.56	—	Superheater	510	835	8.0	68.7	[46]
19	Haslev	Cigar-burner	23 MW <sub>th</sub>	Straw	4.3	1.15	0.44	—	Superheater	510	650	8.0	22.3	[46]
20	Haslev	Cigar-burner	23 MW <sub>th</sub>	Straw	4.3	1.15	0.44	—	Furnace Chamber	510	835	8.0	71.7	[46]
21	Slagelse	Grate-fired	31 MW <sub>th</sub>	Straw	6.0	0.41	0.06	2.03	Superheater	510	647	8.0	1.3	[46]
22	Slagelse	Grate-fired	31 MW <sub>th</sub>	Straw	6.0	0.41	0.06	2.03	Superheater	510	873	8.0	2.6	[46]
23	Slagelse	Grate-fired	31 MW <sub>th</sub>	Straw	4.5	0.97	0.20	—	Superheater	510	647	8.0	6.2	[46]
24	Slagelse	Grate-fired	31 MW <sub>th</sub>	Straw	4.5	0.97	0.20	—	Furnace Chamber	510	873	8.0	93.2	[46]
25	Slagelse	Grate-fired	31 MW <sub>th</sub>	Straw	4.5	1.83	0.32	0.56	Superheater	510	647	8.0	16.6	[46]
26	Slagelse	Grate-fired	31 MW <sub>th</sub>	Straw	4.5	1.83	0.32	0.56	Superheater	510	873	8.0	102.9	[46]
27	Slagelse	Grate-fired	31 MW <sub>th</sub>	Straw	6.5	2.60	0.95	—	Superheater	510	647	8.0	26.2	[46]
28	Slagelse	Grate-fired	31 MW <sub>th</sub>	Straw	6.5	2.60	0.95	—	Furnace Chamber	510	873	8.0	163.8	[46]
29	Slagelse	Grate-fired	31 MW <sub>th</sub>	Straw	6.0	1.86	0.51	—	Superheater	510	647	8.0	13.6	[46]
30	Slagelse	Grate-fired	31 MW <sub>th</sub>	Straw	6.0	1.86	0.51	—	Furnace Chamber	510	873	8.0	80.2	[46]
31	Slagelse	Grate-fired	31 MW <sub>th</sub>	Straw	7.3	2.07	0.86	1.73	Furnace Chamber	510	873	8.0	67.4	[46]
32	Slagelse	Grate-fired	31 MW <sub>th</sub>	Straw	4.9	0.69	0.14	1.59	Superheater	510	647	8.0	6.6	[46]
33	Slagelse	Grate-fired	31 MW <sub>th</sub>	Straw	4.9	0.69	0.14	1.59	Superheater	510	873	8.0	19.4	[46]
34 <sup>b</sup>	Amager 2	Suspension-fired	250 MW <sub>th</sub>	Straw	5.6	0.90	0.23	1.35	Superheater	480	800-900	12.0	56.0	[5]
35 <sup>a</sup>	Amager 2	Suspension-fired	250 MW <sub>th</sub>	Straw	5.9	0.83	0.40	1.36	Superheater	500	848	12.0	41.0	[5]
36 <sup>a,c</sup>	Amager 2	Suspension-fired	250 MW <sub>th</sub>	Straw/wood	4.2	0.35	0.15	0.96	Superheater	500	856	12.0	33.0	[5]
37 <sup>a,c</sup>	Amager 2	Suspension-fired	250 MW <sub>th</sub>	Straw/wood	5.4	0.68	0.32	1.24	Superheater	500	863	12.0	33.0	[5]
38 <sup>a</sup>	Amager 2	Suspension-fired	250 MW <sub>th</sub>	Wood	3.3	0.09	0.01	0.75	Tube Bank Region	500	586	12.0	~1.0	[5]

At the end of each experiment at the AMV2 boiler, the probe was carefully taken out of the boiler; the deposits were removed, weighed, and photographed. The pattern and characterization of the deposits are summarized in Table 4.4. Images of the probe after each experiment are shown in Figure 4.7. The deposits obtained after 35% straw firing at AMV2, were brownish and with an approximate thickness of 5 mm on the upstream, and 2 mm on the downstream side of the probe. The deposits were evenly distributed on the deposition sampling area of the probe (up to 1500 mm starting from the tip of the probe). During 65% straw firing, the deposits were evenly distributed with an approximate thickness of 20 mm on the upstream side and 3 mm on the downstream side. During 100% straw firing at AMV2, the deposits were sintered and formed three layers on the upstream side and two layers on the downstream side of the probe. The white layer of deposits on the downstream side of the probe indicates that potassium salts have been deposited via condensation and thermophoresis (Figure 4.7 (d)). During 100 % wood firing at AMV2 in the tube bank region, the deposits were powder-like and evenly distributed along the entire circumference of the probe and could be easily removed by sootblowing. Deposits obtained after test 1 at AVV2 were somewhat unevenly distributed, while during test 2, the deposits were rough and evenly distributed.

The calculated values of potential indices about the propensity of slagging and fouling are shown in Table 4.6. The values of the Cl contents in the fuel and fuel ash K/Si molar ratios for both straw fuels are high, while for wood fuel these values are low. The slagging index value for all the fuels is found to be less than 0.6 indicating low slagging potential [105]. However, for fuels with very low S contents the slagging index is not representative of true slagging propensity [105]. The fouling index values for the straw fuels are found to be in the high fouling tendency range, while low fouling tendency for wood fuel. All of these indices indicate that co-firing straw with wood can potentially reduce the ash deposition propensity, which has been seen in the present study.

**Table 4.6:** Calculated values of potential components in the fuels responsible for ash deposition, B/A ratio, and potential deposition indices about the propensity of slagging and fouling [105]. <sup>a</sup> ratio of basic compounds to acidic compounds,  $B/A = ((Fe_2O_3 + CaO + MgO + Na_2O + K_2O)/(SiO_2 + Al_2O_3))$ , <sup>b</sup>  $(B/A) \times S$  contents in the dry fuel, <sup>c</sup>  $(B/A) \times (Na_2O + K_2O)$ .

Fuel/Index	Straw (AMV2)	Wood (AMV2)	Straw (AVV2)
Cl in dry fuel (wt.%)	0.398	0.010	0.358
Molar: K/Si	0.44	0.08	0.60
(B/A) <sup>a</sup>	0.66	0.30	0.73
Slagging index <sup>b</sup>	0.06	0.01	0.07
Fouling index <sup>c</sup>	12.53	1.30	17.77



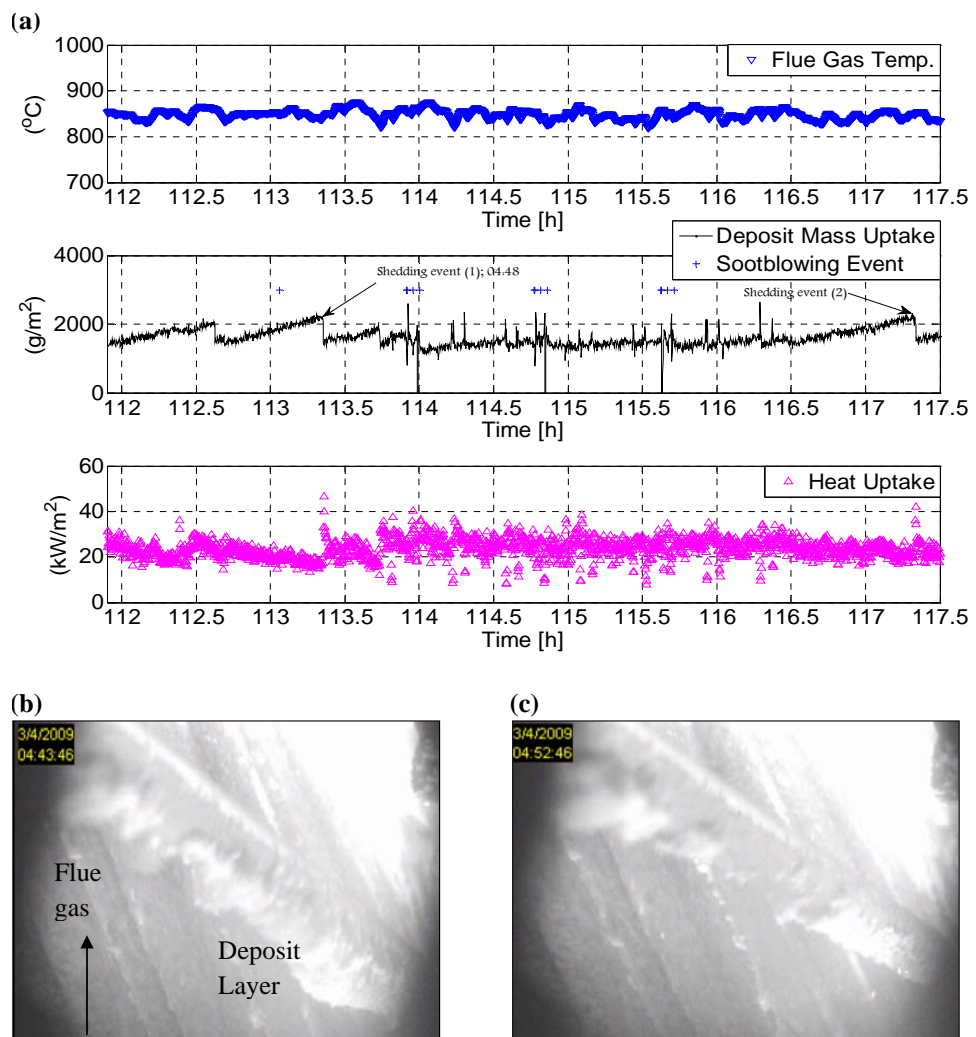
**Figure 4.7:** Pictures of the deposit probe just after the experiments, a)  $\sim 20\text{--}50$  cm from tip of probe (35% straw, test 1 at AMV2), b)  $\sim 10\text{--}30$  cm from tip of probe (65% straw, test 3 at AMV2), c)  $\sim 10\text{--}30$  cm from tip of probe (80% straw, test 2 AMV2), d)  $\sim 30\text{--}50$  cm from tip of probe (100% straw, test 4 at AMV2), e)  $\sim 40\text{--}60$  cm from tip of probe (100% wood, test 5 at AMV2), f) almost complete deposition area of the probe (100% straw, test 1 at AVV2). Black arrows show direction of flue gas flow.

### 4.3.3 Video Observations

The amount of deposit on a probe is a function of deposit build-up and shedding events. The deposit mass uptake signals were continuously monitored and deposit shedding events were confirmed by video recordings. The larger shedding events appear as sudden downward changes in the deposit mass uptake signal with concurrent sudden increases in the probe heat uptake sig-



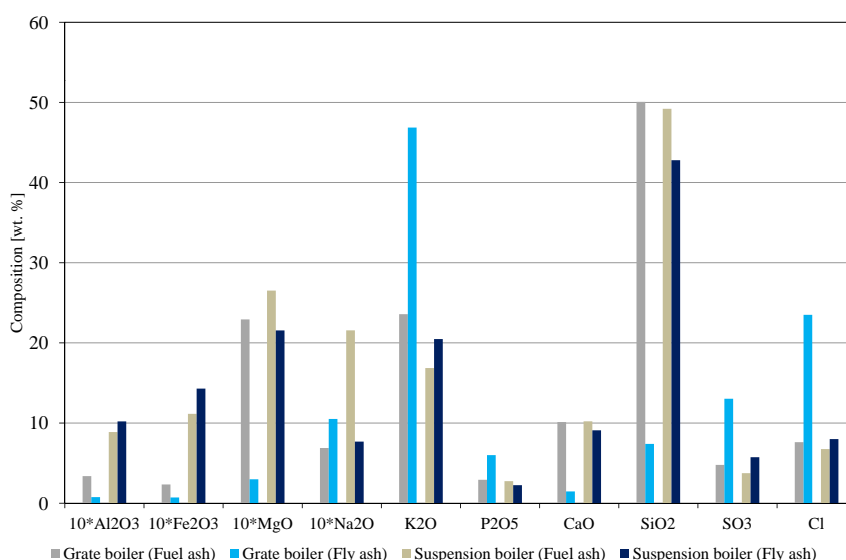
nal (Figure 4.8 (a)). For the shedding event at 113.3 h, Figure 4.8 (b) and (c) shows images of the probe before and after shedding during 80% straw firing at AMV2. For most of the shedding events during 80% straw firing at AMV2, it was found that the predominant deposit removal mechanism was debonding i.e. the phenomenon when a complete layer of deposit detaches from the superheater tube. The gravitational force exerted by the increasing amount of deposit exceeded the available adhesion strength. More images collected during test 2 are shown in Appendix A.



**Figure 4.8:** a) Flue gas temperature, deposit mass uptake and probe heat uptake during 80% straw firing at AMV2 with identified shedding events, b) picture of the deposit probe just before the first shedding event (1) at approximately 113.3 h (04:43), c) picture of the deposit probe just after the first shedding event (04:52).

#### 4.3.4 Chemical Compositions of Fly Ashes and Deposits

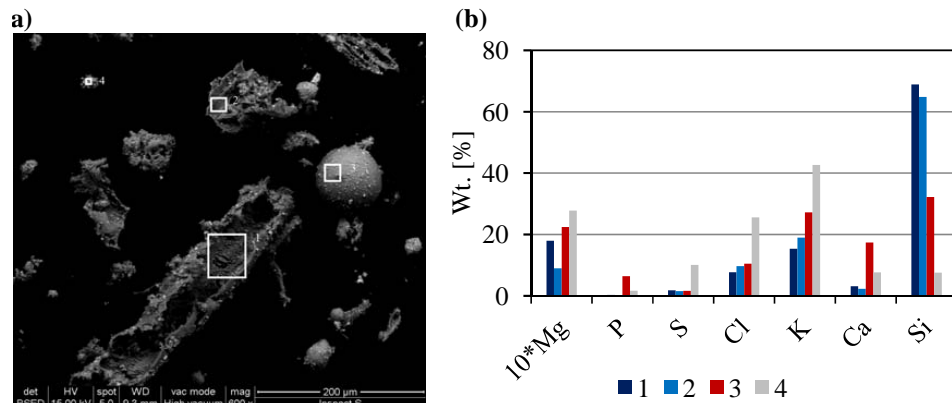
Fly ash samples were collected from the electrostatic precipitator (ESP) during measurements at AMV2 and finally an overall representative sample was selected for bulk fly ash analysis by ICP-OES. Fly ash samples were also taken from the bag house filter during the AVV2 measurements. The bulk composition of fuel and fly ash samples collected during measurements at AMV2 and AVV2 is shown in Figure 4.9. The most remarkable difference is that fly ash from straw suspension firing contains high contents of Si, K and Ca, while fly ash from straw grate firing is rich in the volatile elements K, Cl and S. The depletion in the fly ash of the non-volatile elements such as Al, Fe, Mg, Ca and Si during straw grate firing indicates that these elements are mainly transformed to bottom ash. The enrichment of the volatile elements (K, Cl and S) in the grate-fired fly ash implies that these elements after release from the combustion zone condense as aerosols or are absorbed on the larger fly ash particles.



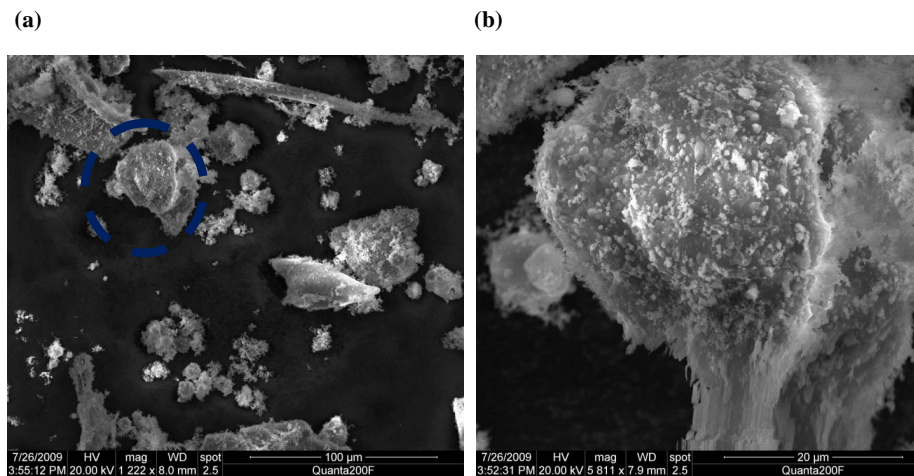
**Figure 4.9:** Ash transformation during straw firing on grate and straw firing in suspension.

SEM-EDS analysis was also made to characterize morphology and composition of fly ashes from straw suspension firing (Figure 4.10). It can be seen that the fly ash consists of three kinds of particles: 1) flake type Si rich particles (spots 1 and 2), 2) molten or partially molten particles ( $> 20 \mu\text{m}$ ) rich in Si, K and Ca with small amounts of Mg, P, and potassium salts on the outer surface (spot 3), and 3) small particles rich in K, Cl and S (aerosols, between  $0.1$  and  $5 \mu\text{m}$ ) (spot 4). The observed fly ash structure matches the data published by Knudsen [29] on biomass ash transformation.

A more elaborative SEM-EDS image of the straw suspension-fired fly ash is shown in Figure 4.11 (a). Irregular shapes of the particles are evident, smaller particles possibly rich in K, Cl and S (aerosols), particles having shape similar to the original straw ash possibly rich in Si and K, and molten particles in semi-spherical shape (K, Ca and Si) (see Figure 4.11 (b)).

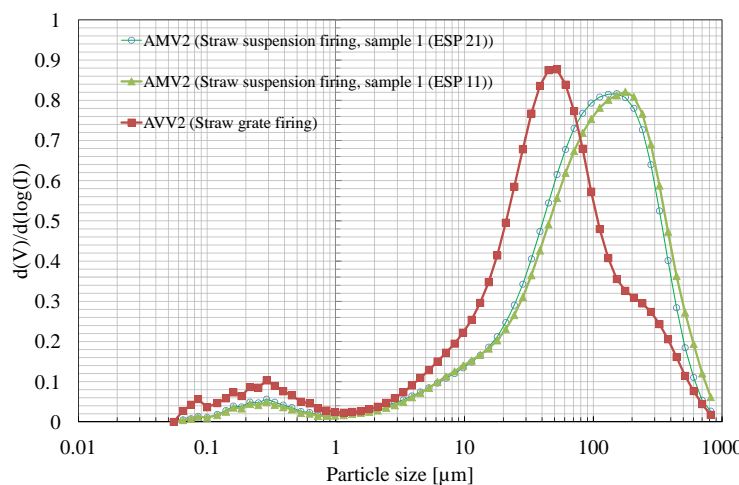


**Figure 4.10:** Morphology (a) and SEM-EDS analysis (b) of fly ash collected from ESP during straw firing in suspension at AMV2.



**Figure 4.11:** a) SEM image of fly ash collected from ESP during straw firing in suspension at AMV2, b) SEM image of the highlighted molten fly ash particle.

The particle size distribution of fly ash from straw suspension firing and straw grate firing is shown in Figure 4.12. The bi-model particle size distribution indicates that during straw suspension combustion, the fine particles are formed because of vaporized inorganic elements and the formation of coarse particles is possibly due to fragmentation during char oxidation. The



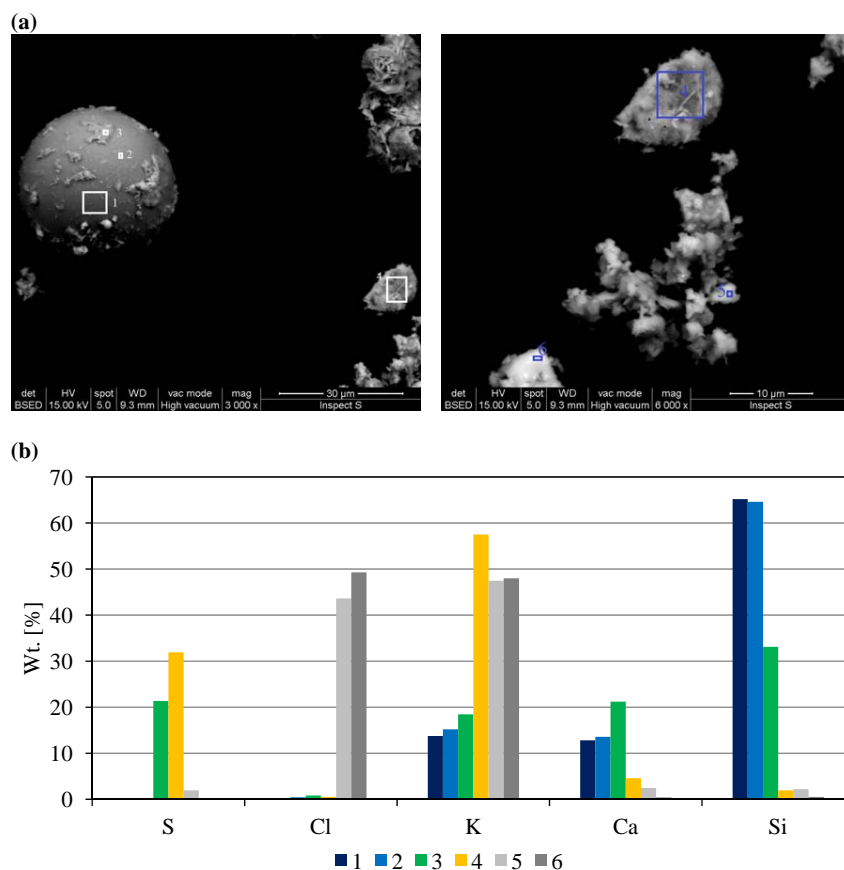
**Figure 4.12:** Particle size distribution (volume-based) of fly ash generated during straw suspension and grate firing. ESP 21: electrostatic precipitator in the second row (21), ESP 11: electrostatic precipitator in the first row (11).

fine particles appear to have a peak at around 0.15–0.30  $\mu\text{m}$  indicating that these particles are potentially formed as a result of the vaporization of the inorganic elements [25, 26]. It is also important to note that the formation of fine particles is analogous to that of straw grate firing. The previous straw grate firing investigations show that the formation of fine particles is initiated by the homogeneous nucleation of  $\text{K}_2\text{SO}_4$  from the gas phase and followed by condensation of  $\text{KCl}$  and  $\text{K}_2\text{SO}_4$  [25, 26, 29].

The inorganic matter, principally K, Cl and, in less amount, S, are volatilized as  $\text{KCl}$ ,  $\text{KOH}$ ,  $\text{SO}_2$  and  $\text{HCl}$ . However, the variation in the distribution of Cl between  $\text{KCl}$  aerosol and gas phase  $\text{HCl}$  is dependent upon the K, Cl, Si, Al, Ca and S contents in the biomass fuel. The determination of the exact distribution between  $\text{KCl}$  and  $\text{HCl}$  is possible through measurements, which was beyond the scope of the current study. However, previous investigations by Christensen et al. [25] and Zeuthen et al. [26] at straw-fired boilers have shown large amounts of  $\text{KCl}$  aerosols in the fly ash. Cl influence the deposit formation process because  $\text{KCl}$  has a relatively low melting temperature and  $\text{KCl}$  can also be present in the gas phase in the boiler chamber and thereby  $\text{KCl}$  contributes to the deposit formation process by condensation on boiler surfaces.  $\text{KCl}$  rarely appears in bottom ash, but is often seen in relatively high concentrations in straw fly ash [25, 26].

The elemental composition of the main ash forming elements in the deposits is shown in Table 4.7. It can be seen that during straw suspension firing, the outer layer of upstream deposits contain a significant amount of

Si, K and Ca, indicating that large particles impact on and stick on the upstream side of the probe [2, 73]. A difference in terms of elemental composition of the upstream outer deposits during 35% and 100% straw firing is evident from Table 4.7. The Ca and Mg contents were reduced when the straw share was increased, while the K, Cl and Si contents were increased. The possible reason is changes in the ash forming elements of fuels. Morphology and SEM-EDS analysis of the outer layer of upstream deposits collected from straw suspension firing indicate that large molten particles are rich in Si, K and Ca (spots 1 and 2 in Figure 4.13) with some S, K and Ca enriched small particles on the outer surface (spot 3). The presence of  $K_2SO_4$  particles is evident from spot 4, while spot 5 and 6 show the presence of KCl particles. Si, Ca and Mg contents in the upstream deposits are higher than those in the fly ash during straw grate firing indicating that the predominant phenomenon for ash deposition is also inertial impaction (see Table 4.7).



**Figure 4.13:** Morphology (a) and SEM-EDS analysis (b) of outer layer of upstream deposits collected after straw firing in suspension at AMV2 (test 4 at SH).

**Table 4.7:** Composition of major elements in the fly ash and deposits formed during AMV2 (suspension) and AVV2 (grate) measurements.

Boiler Sample	AMV2 Fuel ash		AMV2 Fly ash		AMV2 Fly ash ESP		AMV2 Fly ash filter		AMV2 Deposit			AMV2 Deposit			
	Straw	Wood	Fuel ash	Straw	Fly ash	ESP	Grate	Grate	Up-stream	Down-stream	Up-stream	Up-stream	Up-stream	Up-stream	Down-stream
Description	Straw	Wood	Fuel ash	Straw	Fly ash	ESP	Grate	Grate	Outer	Middle	Outer	Outer	Middle	Outer	Overall
Layer	–	–	–	–	–	–	–	–	Outer	Middle	Outer	Outer	Middle	Outer	Overall
Grate/Suspension	Suspension	Suspension	Grate	Grate	Suspension	Suspension	Suspension	Suspension	35	65	80	100	100	100	100
Straw (wt.%)	100	0	100	100	100	100	100	100	35	65	80	100	100	100	100
Al <sub>2</sub> O <sub>3</sub>	0.89	3.64	0.34	0.34	1.02	1.02	0.08	0.08	1.21	0.47	0.76	0.66	–	–	1.00
CaO	10.21	9.33	10.12	10.12	9.09	9.09	1.47	1.47	20.99	4.88	12.73	13.85	3.96	3.23	2.14
Fe <sub>2</sub> O <sub>3</sub>	1.12	1.82	0.23	0.23	1.43	1.43	0.07	0.07	2.86	0.19	0.44	0.46	–	–	–
K <sub>2</sub> O	16.86	3.41	23.58	23.58	20.48	20.48	46.86	46.86	21.68	36.32	32.52	30.12	18.59	16.48	16.13
MgO	2.65	1.73	2.29	2.29	2.16	2.16	0.30	0.30	4.48	1.16	2.65	3.15	0.91	0.99	1.04
Na <sub>2</sub> O	2.16	0.98	0.69	0.69	0.77	0.77	1.05	1.05	0.58	6.00	0.80	0.81	0.51	0.22	–
P <sub>2</sub> O <sub>5</sub>	2.75	0.76	2.93	2.93	2.25	2.25	6.00	6.00	2.75	1.11	2.75	2.52	1.83	1.40	1.47
SiO <sub>2</sub>	49.21	54.78	50.07	50.07	42.79	42.79	7.40	7.40	19.25	18.84	21.39	23.53	11.19	7.89	12.41
SO <sub>3</sub>	3.75	1.34	4.78	4.78	5.74	5.74	13.03	13.03	11.24	4.73	11.24	14.73	12.76	9.36	10.61
Cl	6.75	0.45	7.62	7.62	8.00	8.00	23.50	23.50	5.30	21.89	16.00	11.00	3.55	6.65	4.08
Molar: 2S/Cl	0.49	2.60	0.56	0.56	0.64	0.64	0.49	0.49	1.88	0.19	0.62	1.19	3.18	1.25	2.30
Molar: (K+Na)/(2S+Cl)	1.51	2.25	1.56	1.56	1.25	1.25	1.04	1.04	1.11	1.31	0.98	0.98	0.98	0.85	0.99
Molar: K/Si	0.44	0.08	0.60	0.60											

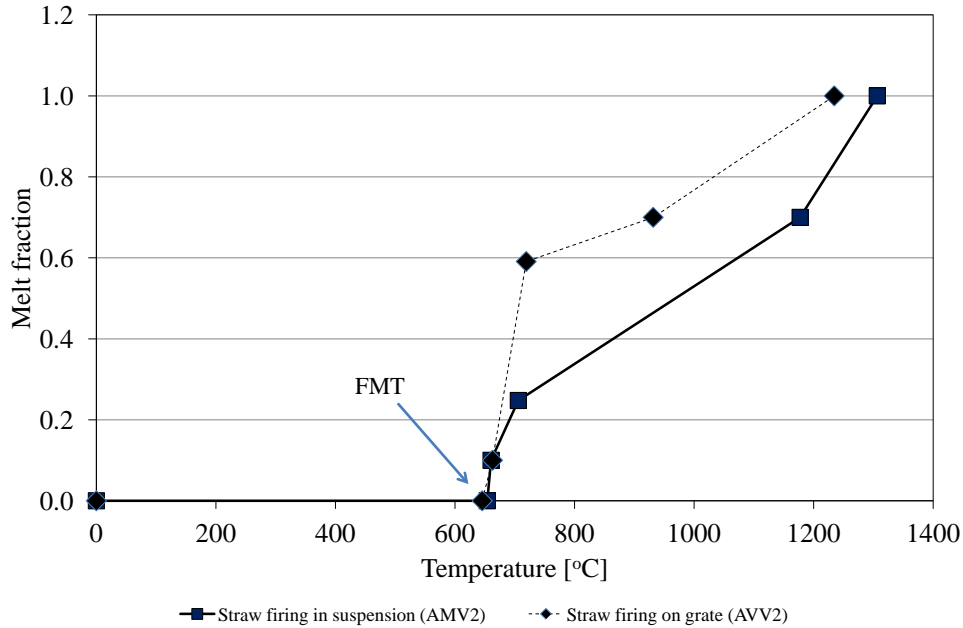
The inner deposits on the downstream side during suspension firing have high concentration of Cl and K indicating that possibly KCl has been attached via condensation and/or thermophoresis. The downstream layer formed during straw grate firing was also mainly composed of KCl (Table 4.7). The outer layer of deposits in the upstream side shows lesser amount of Cl possibly due to reduction in KCl deposition by condensation at higher deposit surface temperature caused by increase in deposit thickness on the upstream side.

The calculated molar ratios  $\psi = (K+Na)/(2S+Cl)$  of fly ashes and deposit samples (Table 4.7) indicate whether there is sufficient K available to account for all S and Cl in the form of sulfates and chlorides, because Na is available in small amount in straw and/or wood, compared to K. For ratios smaller than one, all K is probably bound as KCl and  $K_2SO_4$ , but some S and Cl must be present in other compounds. For ratios close to or greater than one, KCl and  $K_2SO_4$  probably are the predominant S and Cl containing species, while any excess K likely is found in silicates. The values of  $\psi$  for fly ash and deposits are nearly all quite close to 1, although fly ash generated by suspension-fired straw shows a slightly elevated  $\psi$  - value that may be due to K containing silicates. A different  $\psi$  - value of 1.31 for deposit from 65% straw (AMV2) is the result of unusually low S content, but is probably not much trustworthy since other species also are present in atypical amounts. However, lower 2S/Cl molar ratios of the downstream deposit layers during grate and suspension firing show significant presence of KCl, possibly deposited through condensation and/or thermophoresis in the downstream side of the probe. The presence of Cl can cause high temperature corrosion and a molar ratio of  $2S/Cl < 8.0$  significantly increases the risk of high temperature Cl corrosion [106]. In addition, a higher fuel ash K/Si molar ratio can be one of the many possible factors responsible for higher KCl contents in the AVV2 fly ash [107].

#### 4.3.5 Fly Ash Melting

A prediction of fly ash melt fraction as function of temperature based on the fly ash compositions in Table 4.7 was made by using the model proposed by Zhou et al. [31] (Figure 4.14). Both grate- and suspension-fired straw fly ashes have a first melting temperature (FMT) around 645 °C, but at higher temperatures the melt fraction of fly ash from grate firing is much higher than the melt fraction of the fly ash from suspension firing. This higher melt fraction of fly ash from grate firing leads to a much larger probability of grate-generated fly ash to stick to the probes and other surfaces. This partially explains why the deposit mass uptakes measured for straw grate- and suspension firing are comparable, even though typically only 10–30% of

the fuel ash is transferred to fly ash by stoker and grate firing, compared to a transfer of 80–90% by suspension firing [17]. So, while a higher fly ash concentration is present in suspension boilers than in grate boilers, the larger fraction molten at any temperature above the FMT lead to a greatly increased probability of the fly ash to stick to the deposit probe.



**Figure 4.14:** Prediction of fly ash melt fraction by using the predictive model of Zhou et al. [31]. FMT: first melting temperature.

## 4.4 Conclusions

A series of full-scale and long duration deposit probe measurements have been conducted in a biomass suspension boiler to investigate the deposit formation rate, probe heat uptake and ash transformation. Full-scale probe measurements were conducted at a 250 MW<sub>th</sub> suspension boiler, firing straw and wood in suspension, and the results were compared with measurements conducted at a 105 MW<sub>th</sub> straw-fired grate boiler. The probe surface temperature used for all the measurements was kept constant at a value of 500 °C. It was identified that the deposit formation rate increases moderately with straw share increase, when straw is co-fired with wood in a suspension boiler. It was found that during 35% straw fuel share on mass basis, a deposit formation rate of 33 g/m<sup>2</sup>/h (initial 12 h) was observed, while the corresponding deposit formation rate increased to 41 g/m<sup>2</sup>/h when 100% straw was fired. During straw grate firing, the measured deposit formation rate was nearly similar in two tests and approximately 38 g/m<sup>2</sup>/h.



The current full-scale measurements data were compared with data from previously conducted deposit probe measurements. The comparison showed an increasing trend in deposit formation rate with increase in flue gas temperature. At a flue gas temperature of 650 °C, the deposit formation rate is typically from 5 to 30 g/m<sup>2</sup>/h and at 900 °C, the deposit formation rate is typically 20 to 110 g/m<sup>2</sup>/h. At higher fuel alkali contents ( $K > 0.9$  wt.%), the increase in deposit formation rate with flue gas temperature was more significant, compared to the increase in the deposit formation rate at lower fuel alkali contents ( $K \leq 0.9$  wt.%). An increased flue gas temperature probably increases the fraction of molten ash as well as provides an increased content of gas phase alkali species, and both will lead to an increased deposit formation rate. It was also observed that the deposit formation rates measured in suspension and grate boilers are on similar levels. This was observed even though the concentration of fly ash in the flue gas was significantly higher in the straw suspension-fired boiler.

Shedding events registered by a CCD camera showed that the predominant phenomenon of deposit removal during 80% straw firing in suspension with wood was debonding.

The elemental composition of fly ash generated during straw suspension firing shows higher contents of Si and Ca, compared to grate firing fly ash that is rich in the volatile elements K, Cl and S. SEM-EDS analysis indicated that the fly ash generated during straw firing in suspension consists of three kinds of particles: 1) flake type Si rich particles, 2) molten or partially molten particles ( $> 20 \mu\text{m}$ ) rich in Si, K and Ca with small amounts of Mg, P and potassium salts on the outer surface, and 3) small particles rich in K, Cl and S (aerosols, between 0.1 and 5  $\mu\text{m}$ ). Chemical analysis of the outer layer of upstream deposits during 35% straw-firing and 100% straw-firing indicated that by increasing the straw share in the fuel, the K, Cl and Si contents were increased, while the Ca and Mg contents were reduced.

It was also found that 35% straw firing with wood does not create severe fouling and slagging on the heat exchanger tubes at the AMV2. The experiences of the operational staff indicates that the boiler operation period may exceed more than one month without deposit related operational problems when firing maximum 50% straw with wood on mass basis. The findings related to deposit management during straw suspension firing are:

- At higher flue gas temperatures (750–950 °C), efficient soot blowing is needed to manage the boiler tube deposits with small superheater tube spacing (113 mm, current case). An increase in superheater tube spacing probably will lead to the absence of tube clogging by ash de-

posits.

- At flue gas temperatures below 650 °C, deposit formation rate is small and deposits can be easily removed by sootblowers.



## Chapter 5

# Transient Deposit Build-up and Shedding during Straw and Wood Suspension Combustion

The results presented in this chapter have been taken from the following peer reviewed manuscripts,

1) Suspension-firing of biomass. Part 1: Full-scale measurements of ash deposit build-up (published in *Energy & Fuels*) [108].

2) Suspension-firing of biomass. Part 2: Boiler measurements of ash deposit shedding (submitted to *Energy & Fuels*) [109].

### 5.1 Introduction

Potentially, most suspension-fired boilers have a better electrical efficiency (46–48%) than traditional grate-fired systems (25–30%), but only limited ash deposition data from biomass suspension firing are available [2, 5, 27, 28, 37, 41, 38, 73, 103]. Quantification of deposit formation rates and deposit shedding in biomass suspension-fired boilers is an area where relatively limited accurate knowledge is available, and improved knowledge on the transient deposit formation and shedding is needed to optimize design and operation [5, 27, 37, 38, 41, 73]. Compared to grate-fired units the deposit flux may increase during suspension firing because a larger part of the fuel ash is transformed to fly ash [17]. In addition, fuel particle residence times are of the order of a few seconds and peak flame temperatures are higher compared to grate firing conditions [27]. Investigations by Nordgren et al. [27] indicate that during biomass (straw and/or woody biomass) dust combustion at higher temperatures significant ash deposition formation may appear. Inves-

tigations of biomass suspension combustion at both pilot- and full-scale have shown higher deposit formation rate during straw firing, compared to straw and wood co-firing, possibly due to dilution and/or chemical interactions [27, 28]. However, only few full-scale measurements are reported for 100% straw and/or wood combustion in suspension-fired boilers, and most of these studies have been based on short testing time (up to 12 hours), while more extensive full-scale measurements are rare [5, 38, 51]. Therefore, detailed and extensive full-scale studies on transient deposit formation and shedding processes when firing straw and wood will improve our understanding of ash deposit formation processes.

The aim of this study is to provide long time, full-scale data on deposit formation and shedding in a 350 MW<sub>th</sub> suspension-fired boiler, firing straw and wood. In the first part of the study, an analysis is carried out, giving quantitative information about deposit formation rates as functions of operating conditions. The influence of fuel type (straw share in wood), probe exposure time, probe surface temperature (500 °C, 550 °C and 600 °C), and flue gas temperature (600–1050 °C) on ash deposit formation rate has been investigated. Two different measures of deposit formation rate are used in the analysis of the data. The first is the integral deposit formation rate (IDF-rate) found by dividing the integral mass change over integral time intervals (of order several hours) by the time interval. The IDF-rate is similar to deposit formation rates based on total deposit mass uptake divided by probe exposure time reported in previous full-scale investigations, but it is a relatively crude measure that includes all deposit shedding in addition to actual deposit formation. In order to remove major shedding events from the determination of deposition rates a second measure, the derivative-based deposit formation rate (DDF-rate), was devised. This was determined by averaging the deposit mass uptake signals over short time intervals (of order minutes), calculating the local values of the time derivative of the mass uptake, removing large negative values signifying major shedding events, and finally time smoothing the derivatives to remove excessive noise. The DDF-rate was influenced by flue gas temperature and straw share, while changes in probe surface temperature had no significant influence. The IDF-rate, qualitatively related to the ratio between the time-integrated DDF-rate and the integration time, followed the same trends.

Apart from quantification of the deposit formation rates, ash transformation was investigated by bulk ash analysis of the fuel-, fly- and bottom ash during straw and/or wood suspension firing. Bulk ash analysis of fly ashes showed that the contents of volatile elements (K, Cl, S) were slightly greater than in the fuel ash, while Ca and Si remained either in the same proportion or were slightly reduced. It was also found that with an increase in fuel ash K/Si molar ratio the concentration of the volatile elements, K,

Cl, and, to some extent, S, increased in the fly ash. The bottom ash was dominated by Si and Ca with almost no S and Cl contents, possibly due to the high volatility of S and Cl during combustion at higher temperatures.

In the second part of the study, investigations of deposit build-up and shedding have been made by use of an advanced online deposit probe and a sootblowing probe. The influences of feedstock (i.e. straw share in wood), flue gas temperature (600–1050 °C), probe surface temperature (500 °C and 600 °C) and probe exposure time on deposit shedding have been quantified. Quantification of naturally occurring deposit shedding and deposit shedding during plant sootblowing was made via deposit mass uptake signals obtained from the deposit probe. The deposit shedding process was characterized by calculation of the amount of deposit removed at a shedding event [ $\text{g}/\text{m}^2$ ] and the frequency of the shedding events [ $\text{h}^{-1}$ ]. The results showed that the shedding process is stochastic and the amount of deposit shed varies even at constant local conditions. However, the deposit shedding rates showed an increasing trend with increase in flue gas temperatures and probe deposit mass loads. The deposit shedding rate was in most of the cases higher at a probe temperature of 500 °C than at a probe temperature of 600 °C. A possible reason for this is partial melting and/or sintering of the innermost deposit layer (rich in K, Cl and S) at higher probe surface temperature. This could cause the adhesion strength of the deposit to the probe to increase at the higher probe temperature. Quantification of the necessary Peak Impact Pressure (PIP) needed to remove the deposit was also made by use of a sootblowing probe in conjunction with the deposit probe. Results of deposit removal by artificial sootblowing showed that the deposits formed on a 500 °C probe temperature and at exposure time less than 91 h can be removed with a PIP of less than 55 kPa. However, increase in probe exposure time and/or probe surface temperature (600 °C) significantly increases the PIP needed to remove the deposits.

## 5.2 Equipments, Materials and Methods

### 5.2.1 Boiler

The probe measurements were conducted at Amager Power Station, Unit 1 (AMV1), firing biomass in suspension. The AMV1 boiler, a multi-fuel suspension-fired boiler, was commissioned in 2009 to use pulverized biomass with varying shares of straw and wood. The annual biomass consumption at AMV1 boiler is approximately 300,000 Mt of wood pellets and 100,000 Mt of straw pellets. The 350 MW<sub>th</sub> boiler is front wall-fired with 12 burners at three levels. The pulverized biomass typically from pellets crushed in the coal mills (roller mills) is blown into the burners, where the fuel particles are burned in suspension. Due to an expected increase in the corrosion rate with

respect to temperature, the final steam temperatures of the superheaters are limited to approximately 540 °C [84]. The overall boiler operational data can be found in Table 5.1, while schematic boiler drawings with identified probe measuring position are shown in Figure 5.1 and Figure 5.2. Only one position was selected and in the selected probe measuring position, significant ash deposit build-up during straw firing has been observed. The selected probe measuring position was in one of the most contaminated areas in the boiler.

**Table 5.1:** Brief operational data of the AMV1 boiler.

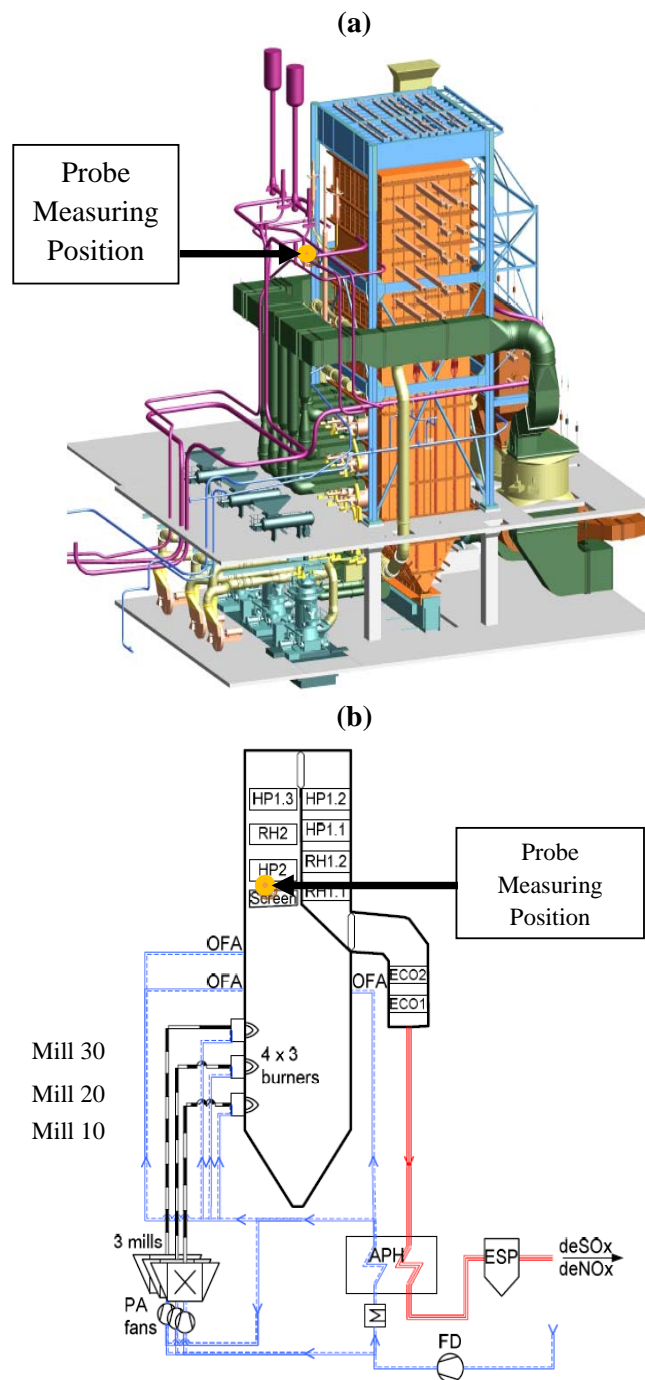
Parameter (steam)	Unit	High pressure (HP) superheater	Re-heater (RH)
Temperature	°C	540 (Biomass)	540
Pressure	bar	185	75
Flow	$\frac{kg}{s}$	138.4	123

### 5.2.2 Fuels

The compositions and analysis methods of some of the fuels fired during the full-scale measurements are shown in Table 5.2. It is seen that the straw ash has a high content of Si, K and Ca. During the experiments, the fuels were continuously sampled before the burners and then analyzed. It shall be mentioned that pure straw and wood fuel samples shown in Table 5.2 were collected from the fuel silos, while fuel sample just before the burners was collected almost each day during each test. The ash contents of the fuel from all test runs were analyzed and thereby the straw fuel fractions were determined based on the total ash contents. The detailed ash analysis was done on samples from test 1 and test 5 as shown in Table 5.2.

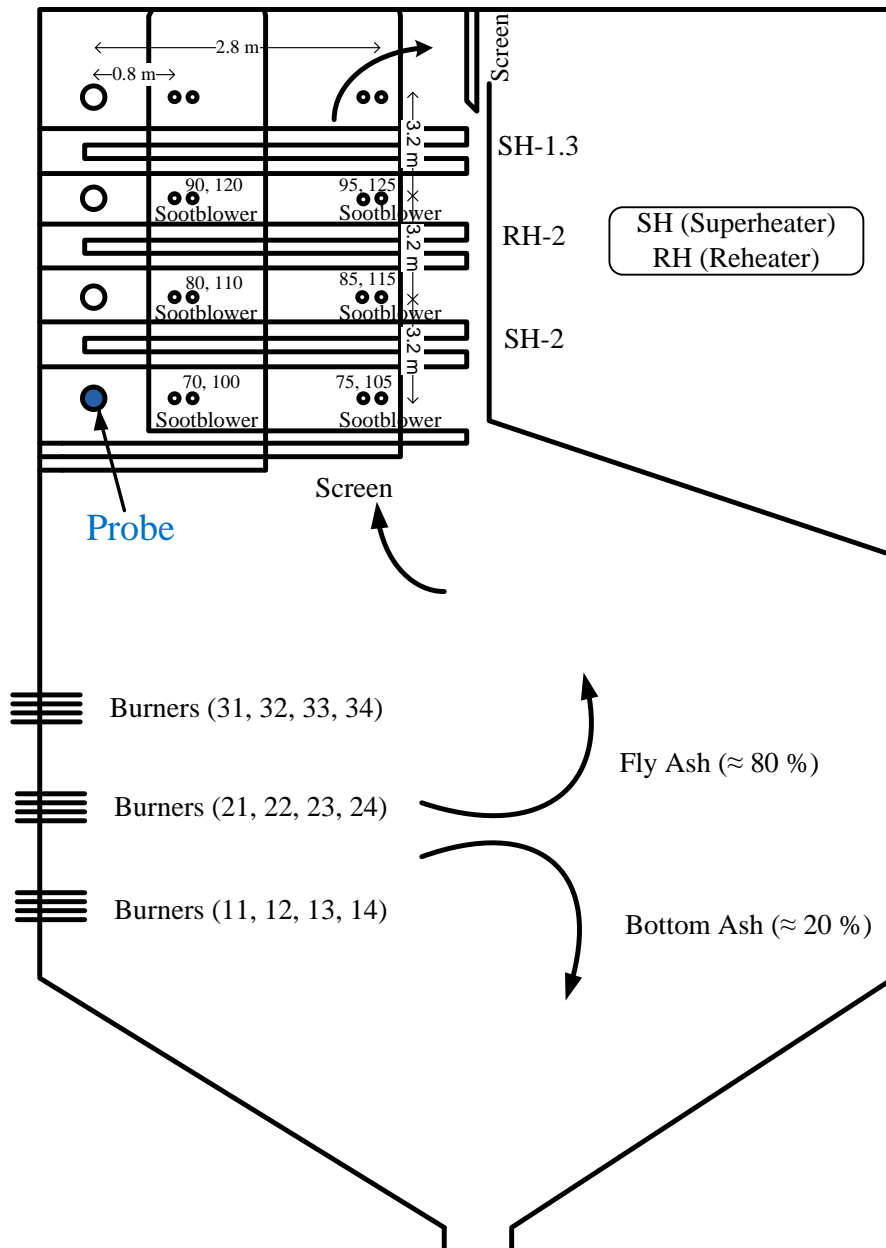
Overall, 8 test runs were carried out and the mean straw share during each test is shown in Table 5.3. In Table 5.3 mean values of each complete test are shown, while in Table 5.2 values are shown for a sample collected just before the burners. This causes a slight difference in fuel ash contents reported in Table 5.2 and Table 5.3.

The particle size distribution of the fuel particles collected just before the burners showed that close to 50% of the particles were below 500  $\mu\text{m}$  (Figure 5.3), while about 10 wt.% of the particles had a size between 1.2 and 3.1 mm.



**Figure 5.1:** Drawings of AMV1 boiler with identified probe measuring position, just above the screen tubes, a) overall boiler configuration, b) schematic presentation of the boiler. Modified from Gjernes [84]. (Top: mill 30, middle: mill 20, bottom: mill 10). HP: High Pressure, RH: Re-Heater, OFA: Over Fire Air, ECO: Economizer, APH: Air Pre-Heater.

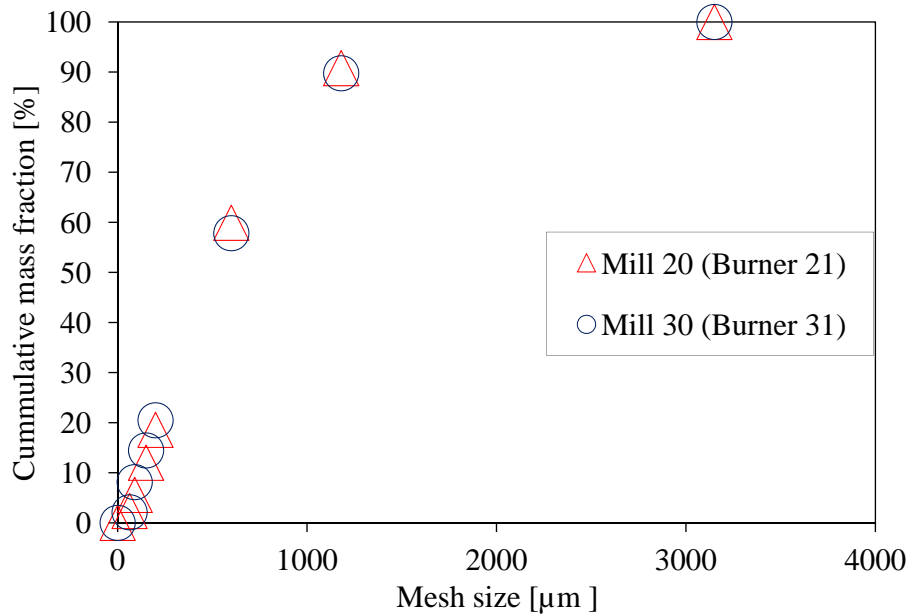




**Figure 5.2:** Schematic drawing of the AMV1 boiler outlining the position of the plant sootblowing near the experimental set up. In total, 12 sootblowers affect the deposit shedding process, 6 along the left wall of the boiler and 6 along the right wall of the boiler. The distance of each sootblower from the probe measuring position is shown. Sootblower 70 was very near to the probe measuring position (1 m to the left) and was shut down during tests 1 to 5. The first number in pair of two numbers shows the sootblowers located on the same wall where the probe is located (left wall, burner location), while the second number shows the sootblowers located on the opposite wall (right wall, burner location).

**Table 5.2:** Analysis of straw and wood pellets used at AMV1. a.r.: as received, d.b.: dry basis. <sup>a</sup> one type out of four.

Parameter	Procedure	Straw		Wood	80-85		65-70		60-65		60-65		40-45	
		Køge	Kunda <sup>a</sup>	Kunda <sup>a</sup>	% Straw	Test 1	% Straw	Test 5	% Straw	Test 5	% Straw	Test 5	% Straw	Test 5
Day/month/year		-	-	-	22/03/2010	19/04/2010	20/04/2010	20/04/2010	20/04/2010	20/04/2010	20/04/2010	20/04/2010	21/04/2010	
					(13:00)	(17:00)	(17:00)							
Ash contents (wt.%, a.r.)	EN 14775:2009	6.03	0.80	0.80	5.26	4.32	3.56	4.32	3.63	2.74				
Ash contents (wt.%, d.b.)	EN 14775:2009	6.54	0.86	0.86	5.63	4.57	3.78	4.57	3.84	2.88				
Moisture (wt.%, a.r.)	EN 14774-3:2009	7.86	6.83	6.83	6.67	5.61	5.94	5.61	5.55	5.03				
Higher heating value (MJ/kg, d.b.)	EN 14918:2010	18.71	20.47	20.47	17.62	19.68	19.39	19.68	19.35	19.87				
Volatiles (wt.%, d.a.b.)	EN 15148:2009	80.91	85.24	85.24	82.87	82.58	82.15	82.58	-	83.11				
C (wt.%, d.b.)	CEN/TS 15104:2006	50.52	55.54	55.54	51.16	52.44	52.89	52.44	52.57	53.91				
S (wt.%, d.b.)	CEN/TS 15289:2006	0.15	0.035	0.035	0.121	0.105	0.095	0.105	0.093	0.068				
N (wt.%, d.b.)	DS/EN ISO 10304-1:2009	0.59	0.73	0.73	0.80	0.62	0.63	0.62	0.68	0.75				
H (wt.%, d.b.)	EN 14918:2010 Calculated	5.79	6.15	6.15	5.85	5.92	5.97	5.92	5.96	6.02				
O (wt.%, d.b.)	EN 14918:2010 Calculated	36.11	36.68	36.68	36.43	36.19	36.45	36.19	36.67	36.28				
Cl (wt.%, d.b.)	DS/EN ISO 10304-1:2009	0.29	0.003	0.003	-	0.155	0.184	0.155	0.191	0.093				
<i>Ash analysis (wt.%, d.b.)</i>														
Al <sub>2</sub> O <sub>3</sub>	DIN 51729/ASTM3682	0.66	-	-	0.95	1.88	1.3	1.88	0.97	2.11				
CaO	DIN 51729/ASTM3682	14.56	-	-	8.30	9.97	11.05	9.97	11.8	17.69				
Fe <sub>2</sub> O <sub>3</sub>	DIN 51729/ASTM3682	0.50	-	-	0.47	6.81	1.03	6.81	0.58	1.13				
K <sub>2</sub> O	DIN 51729/ASTM3682	17.88	-	-	15.25	12.58	15.92	12.58	20.41	13.96				
MgO	DIN 51729/ASTM3682	3.39	-	-	2.25	2.11	2.29	2.11	2.54	2.90				
N <sub>2</sub> O	DIN 51729/ASTM3682	0.69	-	-	0.57	0.59	0.87	0.59	1.04	1.03				
P <sub>2</sub> O <sub>5</sub>	DIN 51729/ASTM3682	5.56	-	-	2.47	2.17	2.46	2.17	2.60	2.13				
SO <sub>3</sub>	DIN 51729/ASTM3682	2.43	-	-	2.36	2.03	2.16	2.03	1.88	2.43				
SiO <sub>2</sub>	DIN 51729/ASTM3682	44.51	-	-	52.05	44.89	49.15	44.89	46.95	36.87				
TiO <sub>2</sub>	DIN 51729/ASTM3682	0.05	-	-	0.06	0.11	0.10	0.11	0.06	0.13				



**Figure 5.3:** Particle size distribution of fuel collected from two burners connected to two different mills (test 1, 22/03/2011). The particle size distribution was determined by a sieve analysis.

### 5.2.3 Ash Deposition and Sootblowing Probe

The deposit probe used during the measurements was made of stainless steel, about 3 m long and having an outer diameter of 40.5 mm. The probe was cooled by water and air, whereby it was possible to determine heat uptake by the probe and keep a stable surface temperature. More details of the deposit probe and the complete probe system have been described in Chapter 3.

An artificial sootblowing probe with an external diameter of 42.2 mm and a length of 3 m was used for in-situ removal of deposits. More details of the sootblowing probe and the complete probe system have been described in Chapter 3.

### 5.2.4 Procedure of Measurements

#### Ash Deposition Experiments

A complete summary of all the conducted measurements is presented in Table 5.3. A series of probe measurements were conducted in the superheater region, just above the screen tubes. The influence of fuel type, probe exposure time, flue gas temperature, and probe surface temperature on deposit

formation rate was investigated. The fuel contained from 0 to 85 wt.% straw share in wood. Each measurement lasted 2–18 days. A CCD (charge-coupled device) camera registered the deposit formation and removal processes on the probe. The flue gas temperature near the probe was continuously measured, using a simple thermocouple in a protective shell. In addition, a suction pyrometer (International Flame Research Foundation model, IFRF [100]) was also used for some periods during each test. Due to strong radiation effects in the probe measuring area, a significant difference was identified between the flue gas temperature measured by the thermocouple and the suction pyrometer. The deposition probe was exposed to flue gas temperatures from 600 to 1050 °C. Probe surface temperatures were varied between 500 and 600 °C in order to investigate ash deposit formation rate at different probe surface temperatures.

Ash transformation was investigated by elemental analysis of inorganic elements in the fuel ash, residual ash and deposit samples for different straw shares in wood by ICP - IC (Inductively Coupled Plasma - Ion Chromatography) analysis. Fly ash was collected from electrostatic precipitators by using a spear to collect a representative sample. Bottom ash was collected from the water and ash pit at the bottom of the furnace.

Ash melting behavior was also investigated for the fuel ashes and fly ashes. The standard used was CEN/TS 15370-1:2006.

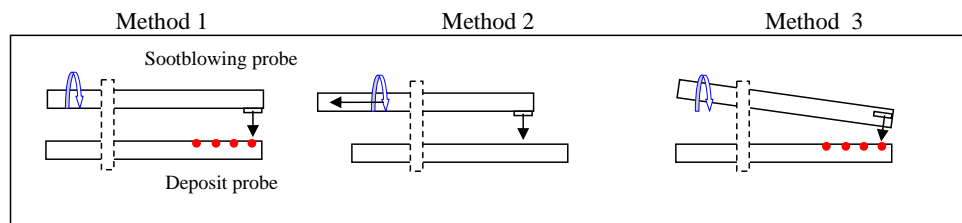
**Table 5.3:** Experimental summary (AMV1). <sup>a</sup> Plant sootblower very near to the ash deposition probe (about 1 m to the left) was shut off.

Test No	1	2	3	4	5	6	7	8
Day/month, (start-end)	22/03- 25/03	27/03- 29/03	29/03- 06/04	06/04- 09/04	15/04- 22/04	07/05- 25/05	25/05- 08/06	08/06- 18/06
Straw (wt.%)	80–85	60–65	30–35	40–50	40–50	0–10	0–10	0–10
Fuel ash content (wt.%)	~5.2	~4.0	~2.4	~3.4	~3.4	~1.0	~1.0	~1.0
Probe temperature (°C)	500	600	500	500	500 (600)	550	550	550 (600)
Exposure time (h)	56	45	185	73	168	434	335	212
Probe heat uptake investigation	✓	✓	✓	✓	✓	✓	✓	✓
Artificial sootblowing	–	✓	✓	✓	✓	–	–	–
Naturally occurring shedding events	✓	✓	✓	✓	✓	✓	✓	✓
Plant sootblowing	✓ <sup>a</sup>	✓ <sup>a</sup>	✓ <sup>a</sup>	✓ <sup>a</sup>	✓ <sup>a</sup>	✓	✓	✓

### Sootblowing Experiments

Three different methods were used to quantify the PIP needed to remove the deposits on the probe (Figure 5.4). In method 1, the sootblowing probe was placed parallel to the ash deposition probe and artificial sootblowing was started from the tip of the deposition probe with air pressure ranging from 0.5 to 4.0 bar. Method 2 is actually continuation of method 1, where the sootblowing probe was slightly pulled out (approximately 20 cm) to remove remaining layers of the deposits by using the same principle adopted in method 1. This procedure was repeated until the nozzle of the sootblowing probe reached to a distance of 1.5 m from the tip of the deposit probe. If the amount of deposits removed was not significant, method 3 was applied by reducing the distance between the nozzle and the deposition probe in the range of 5 to 20 cm, in order to achieve maximum values of PIP. During the artificial sootblowing, camera images were collected to confirm the observed changes in the deposit mass uptake signals.

In the superheater region area of the boiler retractable steam sootblowers were used for a time of 5–10 minutes (each sootblower) at regular intervals during boiler operation, typically at 8 h intervals. Six sootblowers were placed along the left wall of the boiler and six along the right wall of the boiler as shown in Figure 5.2. Information about the relative position of the plant sootblowers to the probe measuring position is also shown in the figure. The first number in pair of two numbers shows the sootblowers located on the same wall where the probe is located (left wall, burner location), while the second number shows the sootblowers located on the opposite wall (right wall, burner location). The sootblower located nearest to the probe measuring position (approximately 1 m to the left, number 70) was shut down during tests 1 to 5, while sootblowers (number 75 to 125) located further away from the probe measuring position were in operation during all the tests. A schematic description of plant sootblowing and artificial sootblowing set up near the deposition probe can be seen in Appendix B (Figure (Appendix B) 1a).



**Figure 5.4:** Experimental methods applied for artificial sootblowing.

## 5.3 Ash Deposit Build-up

### 5.3.1 Data Treatment

The results represented in this thesis are from full-scale measurements on a large operating power plant boiler. Hence, full control over all conditions influencing measurements cannot be achieved. In particular, two aspects of the measurements will be considered. One aspect is the influence of operating conditions on temperature measurements, where the primary data were thermocouple readings of the flue gas temperature. Radiation, flow fluctuations and particulates in the gas phase can all influence the readings, but in rather unpredictable ways. Hence, some suction pyrometer readings were taken and together with determinations of other operating conditions, these measurements allowed a correction of the thermocouple values. The procedure is discussed in detail in section 5.3.1.1.

The other aspect is the deposit formation rate determinations. In an ideal world, where deposited mass is monitored continuously with little or only insubstantial noise and no deposit shedding there is no doubt that the time derivative of the mass uptake signal is the true deposit formation rate. However, the measuring probe mass uptake signal, on which this paper is based, includes noise, larger shedding events and eventually some smaller (minor) shedding events, with a magnitude on the same level as the noise. The shedding events may therefore be divided into two classes: One type of event, macro-events, with so much shedding that the event times mark points across which deposit formation rate calculations cannot be done by averaging, and another type, micro-events, that are not clearly distinguishable from externally generated noise contributions, and across which it is necessary to do averaging when calculating something that is representative of the true deposit formation rate.

With this kind of measured data, it is necessary to use a terminology that clearly distinguishes between a) (true) deposition rate, b) a measure of the deposition rate found as an averaging of the time derivative over periods that do not include major shedding events, but do include some minor shedding events in addition to noise (called derivative-based deposit formation rate, DDF-rate), and finally c) the overall measure where the difference in deposit mass at two different times is divided by the time difference, and in this case with no particular concern about the presence or absence of even major shedding events (called integral deposit formation rate, IDF-rate). Each of these measures of deposition rate has its use, but it is important in the discussion of the data to distinguish between them.

The DDF-rate is determined by calculating a smoothed time deriva-

tive of the short time averaged deposit mass uptake signals. The time interval for smoothing includes minor shedding events that cannot *a priori* be distinguished from measurement noise, but excludes larger shedding events. A more detailed description of the procedure is given below in section 5.3.1.2. Since the averaging time is relatively short, and since a time smoothed derivative is the result, we settled on this measure to be called DDF-rate: derivative-based deposit formation rate. DDF-rates should represent fairly characteristic net-deposition rates, allowing its dependence on operating conditions to be determined.

The IDF-rate is a cruder measure of deposit formation rate determined as the mass deposited on the probe over large time intervals divided by the time interval length. The IDF-rate includes both minor and major shedding events of any kind and is similar to deposit formation rates determined from previous full-scale probe measurement data. More details about the procedure are given below in section 5.3.1.3.

### Corrected Flue Gas Temperature

The flue gas temperature near the probe was continuously measured, using a simple thermocouple in a protective shell, while suction pyrometer based temperature measurements were only conducted for a limited time during each experiment. The suction pyrometer measurements were conducted for 0.5 to 2 h, ranging from 1 to 3 measurements during each test. During suspension firing of biomass, the radiation effects were stronger compared to biomass grate firing [33, 35] and a typical higher flue gas temperature in the range of 50–200 °C was observed by the suction pyrometer. The presence of deposits in the experimental region may cause a difference between thermocouple and suction pyrometer measurements due to changed radiation conditions. Other possible factors responsible for a temperature difference can be the fuel flow through mills located in the top positions (Mill 30: top, Mill 20: middle, Figure 5.1) leading to a change in flame position, fuel oil loading and overall boiler load. These physical causes provided the basis for the initiation of the following empirical model relating a prediction of the gas temperature,  $Y_{calc}$ , to the actual measured thermocouple temperature,  $Y_{TC}$  :

$$Y_{calc} = Y_{TC} + Diff_{pred} \quad (5.1)$$

$$Diff_{pred} = \dot{A} + \dot{B}X_{ash} + \dot{C}X_{oilload} + \dot{D}X_{boilerload} + \dot{E}X_{mill20} + \dot{F}X_{mill30} \quad (5.2)$$

$X_i$  in the above equation (5.2) represent measured operational parameters likely to influence the difference between the suction pyrometer temperature ( $Y_{meas}$ ) and the thermocouple temperature ( $Y_{TC}$ ).  $X_{ash}$  (0.70 to

5.26 [wt.%]) represents the fuel ash content,  $X_{oilload}$  (0.0 to 160.7 [MW<sub>th</sub>]) is the fuel oil loading,  $X_{boilerload}$  (59.0 to 93.4 [%]) is the relative boiler load, and  $X_{mill}$  (0.0 to 7.2 [ $\frac{kg}{s}$ ]) denotes the fuel flow rate through the mill indicated. Parameters  $\dot{A}$  to  $\dot{F}$  are empirical constants determined through fitting of the above equations to the true temperatures,  $Y_{meas}$ , measured by the suction pyrometer. The fitting was carried out by minimizing the sum of squares ( $SS$ ). Not all of these operational parameters may have a significant influence on the correction. Hence, we used the methods outlined by Kittrell [110] and Pritchard et al. [111], based on the variance-covariance matrix, to assess which parameters were most important. The final result of the fitting procedure was that the predicted temperature difference could be described well by equation (5.3).

$$Diff_{pred} = \dot{B}X_{ash} + \dot{C}X_{oilload} + \dot{D}X_{boilerload} + \dot{E}X_{mill20} \quad (5.3)$$

with the parameters shown in Table 5.4. The plot of predicted flue gas temperature versus the measured suction pyrometer temperature is shown in Figure 5.5. It can be seen that the predicted temperature values are close to the measured temperature values.

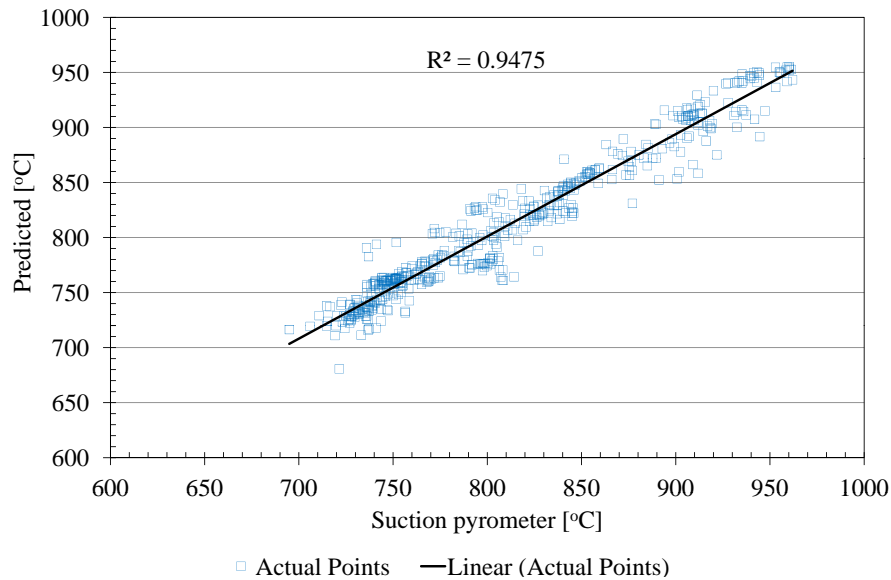
**Table 5.4:** Calculated constants for flue gas temperature prediction model with estimated confidence intervals.

Constant	Value
$\dot{B}$	$23.11 \pm 1.25$
$\dot{C}$	$0.195 \pm 0.041$
$\dot{D}$	$0.084 \pm 0.068$
$\dot{E}$	$4.78 \pm 0.48$

### Derivative-based Deposit Formation Rate (DDF-Rate)

The amount of deposit collected on the probe is a function of both the deposit formation process and shedding events. An example of raw data of flue gas temperature, deposit mass uptake and heat uptake of test 1 is shown in Figure 5.6. The measured flue gas temperatures by using thermocouple are between 500 and 800 °C. The deposit mass uptake signals show both natural and plant sootblowing shedding events (observed as a sudden deposit mass loss on the curve). The deposit mass uptake signal is influenced by several processes: large shedding events, minor shedding events, a relatively slow deposit build-up process and some noise mainly caused by boiler fluctuations. Boiler fluctuations could be mechanical vibrations or large changes in boiler flow dynamics. The most severe fluctuations are observed when the boiler





**Figure 5.5:** Comparison of measured (suction pyrometer) and calculated flue gas temperature. The predicted points are calculated from the thermo-element temperature and boiler operational data using equation 5.1, 5.2 and 5.3.

plant sootblowers were in operation. Even though the plant sootblower nearest to the probe was shutdown, the thermal and mechanical fluctuations were induced by the rest of the sootblowers, and that could cause some shedding. In order to analyze data systematically under these conditions where noise, small and large shedding events are present, a deposit mass uptake signal treatment method is developed and applied to the measuring data. The method allows us to identify shedding events and can quantify the deposit formation rate between major shedding events. The idea is to average out the noise in the deposit mass uptake signals and to identify the larger shedding events. When the plant sootblowers are used, the probe mass signal noise level increased and therefore the DDF-rate determinations were not done on mass uptake signal data obtained during sootblower operation.

The steps involved in the deposit mass signal treatment to calculate the DDF-rate are based on Matlab procedures [112, 113, 114, 115] and are:

**Step A:** The deposit mass uptake signals are filtered using a 10 point resampling method implemented in Matlab [112]. This effectively smoothes the data over 10 points, returning one resampled data point for further use.

**Step B:** Slope calculations are done using a moderately low order polynomial ( $3^{rd}$  order, current case) that is fitted to the data in a sliding window

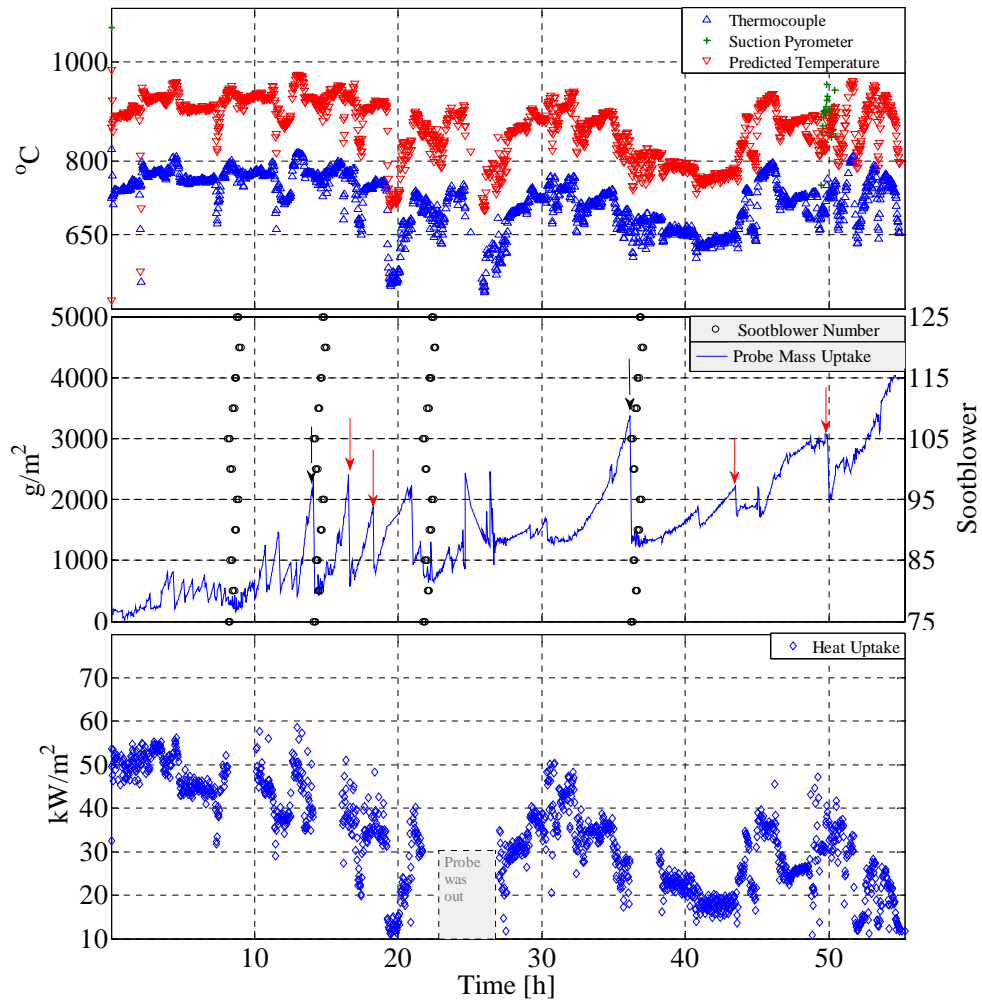
(5 data points) and finally differentiation of the model is performed [113].

**Step C:** Cut off of negative slope values is made to remove major shedding events. The cut off level is adjusted to determine the number of major shedding events accurately while still giving a satisfactory prediction of apparent deposit formation rates. A high cut off level e.g.  $-200 \text{ g/m}^2/\text{h}$  may count some noise as shedding events which results in higher deposit formation rate values. A low cut off e.g.  $-6,000 \text{ g/m}^2/\text{h}$  will include some shedding in the DDF-rate calculation and results in lower deposit formation rate values. The selected cut off level was  $-3,800 \text{ g/m}^2/\text{h}$  for all the tests. This represents a subjective judgment that strikes a balance between determining the most shedding events (a high cut off level is needed) and not removing selectively a negative noise contribution to the DDF-rate determination (a low cut off level is needed).

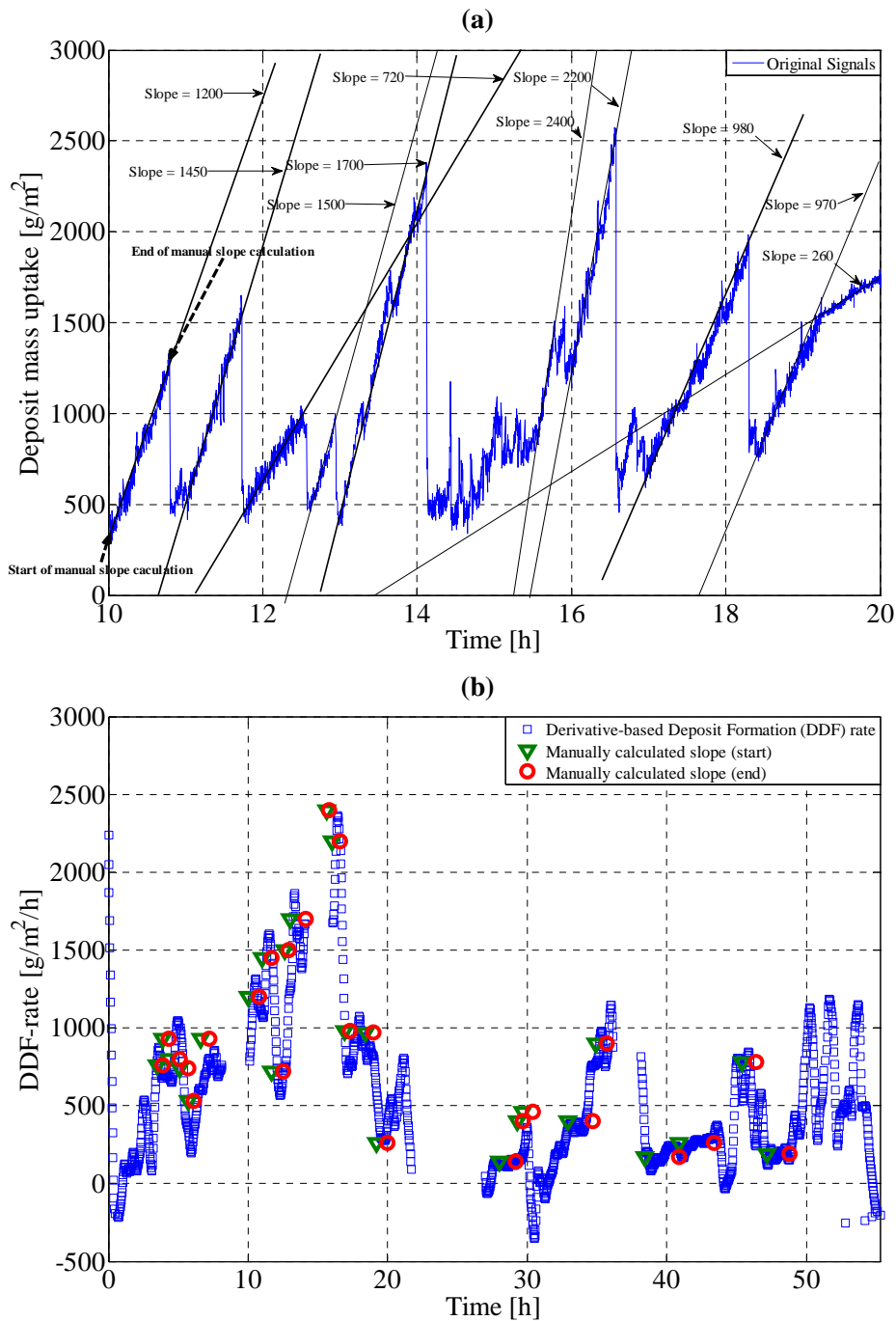
**Step D:** Smoothing of the raw slope calculations is made using a moving average filter over 31 points [114, 115]. Our choice of 15 data points on each side of the  $i$ th data point represents a subjective judgment that balances effective smoothing against undesired removal of minor, but significant variations in the deposit formation rate. The result of the smoothed data is the DDF-rate.

This complete procedure was validated. It should be kept in mind that our aim is to treat all data systematically once the subjective judgments of steps C and D have been made, thus avoiding the pitfall of seeing or not seeing trends from case to case based on incomparable criteria. To validate the above described procedure of deposit formation rate determination as DDF-rates, manual slope calculations were done on the original deposit mass uptake signals of test 1. Test 1 is appropriate for comparison because the probe mass uptake signals during this test cover three kinds of behavior: 1) with small but frequent shedding events (3–10 h), 2) with large but more frequent shedding events (10–20 h), and 3) with less frequent shedding events (28–55 h) (Figure 5.6). The approximate manually calculated slopes of the 10–20 h interval during test 1 are shown in Figure 5.7 (a) and a comparison of these slopes and the calculated DDF-rates using the procedure described above is shown in Figure 5.7 (b) for complete test 1. It is clear that the DDF-rates calculated by steps A through D are in good agreement with manually calculated average deposition rates. Since smoothing in step D is across shedding events, just excluding the most negative slopes in step C, the procedure results in a continuous change between the discrete levels determined by the manual procedure. This is an acceptable price to pay in order to get a consistent analysis of all data points and test series. The above procedure is thus adopted for the first 5 tests (Table 5.3) and the results are used to identify the influence of experimental conditions and boiler op-

erational conditions on DDF-rates. Detailed signals of flue gas temperature, deposit mass uptake, probe heat uptake, sootblowing events, DDF-rates and boiler operational conditions for the tests conducted at AMV1 can be found in Appendix B.



**Figure 5.6:** Raw data of flue gas temperature, deposit mass uptake, plant sootblowing events (specific number of sootblower in operation) and probe heat uptake during test 1. Red arrows with continuous line indicate natural deposit shedding, while black arrows with discontinuous line indicate deposit shedding through plant sootblowing. Sootblower number just represents a specific sootblower in the superheater region as seen on the secondary y-axis (middle figure).



**Figure 5.7:** a) Approximate manually calculated slopes of deposit mass uptake signals during 10–20 h of exposure time during test 1, b) comparison of manually calculated slopes and slopes calculated by the mathematical procedure (DDF-rate) for complete test 1.

### **Integral Deposit Formation Rate (IDF-Rate)**

The deposit formation rate (g/m<sup>2</sup>/h) can also be determined based on the mass increase divided by a given probe exposure time, and we have called this the integral deposit formation rate (IDF-rate). The IDF-rate is then the result of both the deposit formation rate and shedding events in a given period. In this work IDF-rates were determined using 12 h intervals. The IDF-rate is similar to deposit formation rates determined from previous full-scale measuring data [5, 101]. The latter were calculated by taking the probe out, collecting the deposits and dividing the amount of deposits with the time the probe was inside the boiler.

In mathematical terms, let  $m(t)$  be the continuously monitored probe mass uptake. If the probe signal was noise free and no shedding events of any kind occurred, the true deposit formation rate would be the derivative  $m'(t)$ . However, the signal is not noise free, and both minor and major shedding events occur, so that the derivative  $m'(t)$  represents the deposit formation rate at any time. In order to extract measures of deposition rates that are either comparable to literature values or represent mainly the deposition process, IDF- and DDF-rates corresponds to the following,

$$\text{IDF-rate} = \frac{\int_{t_1}^{t_2} m'(t) dt}{t_2 - t_1} = \frac{m(t_2) - m(t_1)}{t_2 - t_1} \quad (5.4)$$

$$\text{IDF-rate} = \langle m'(t) \rangle \quad (5.5)$$

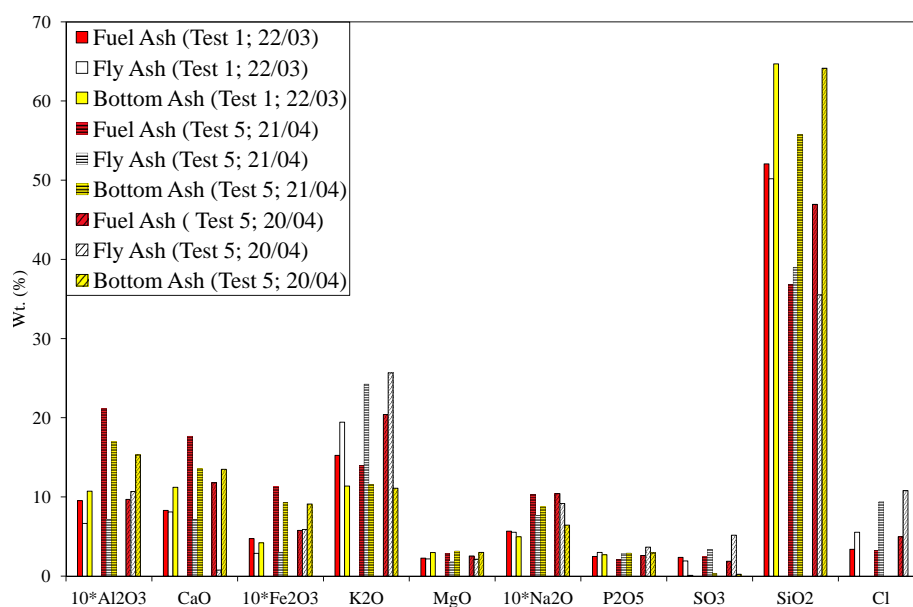
where  $\langle m'(t) \rangle$  represents a moving average over short time intervals without major shedding events. Both are rates of change of deposited mass.

### **5.3.2 Chemical Compositions of Fuel Ash, Residual Ash and Deposits**

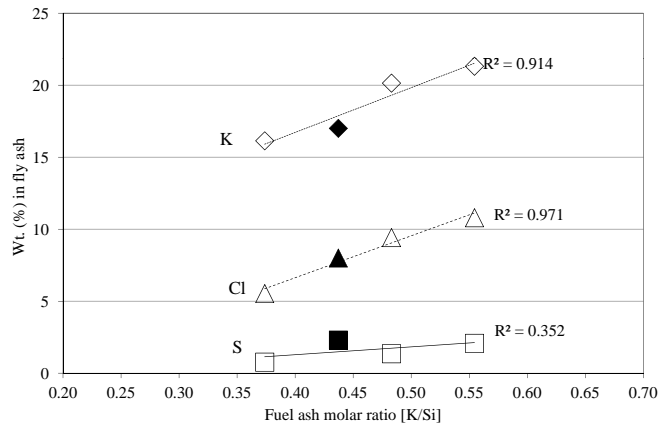
Representative samples of the fly ashes were collected from electrostatic precipitators by using a spear, while the bottom ash was collected from the water and ash pit at the bottom of the furnace. ICP - IC (Inductively Coupled Plasma - Ion Chromatography) analysis was used to determine the concentration of major elements in the fuel-, fly- and bottom ash and deposit samples. The bulk ash compositions of the fly ashes obtained from two days (22/03/2010 and 23/03/2010) during test 1 were almost identical under almost identical operating conditions, thereby supporting the reliability of the measurements. The bulk compositions of fuel-, fly- and bottom ash samples collected during test 1 and 5 are shown in Figure 5.8. It is seen that the content of the most of the volatile elements (K, Cl, S) in the fly ash (colorless bars) are greater than in the fuel ash (red bars), while Ca and Si remained either almost in the same proportion or were reduced. It can also be seen

that bottom ashes (yellow bars) are dominated by Si and Ca with almost no S and Cl, possibly caused by the high volatility of S and Cl during straw and wood combustion at higher temperatures [2, 27, 73, 107]. Compared to the fly ash from a straw grate-fired system that is rich in volatile elements, K, Cl and S, the fly ash from straw suspension firing is dominated by K, Si and Ca [33, 104]. It was seen that with an increase in fuel ash K/Si molar ratio the concentration of volatile elements, K, Cl, and, to some extent, S, increased in the fly ash (Figure 5.9). This suggests that the presence of Si tends to retain K as K-silicates in the ash and residual K can bind Cl and S in the fly ash as KCl and  $K_2SO_4$ . It has also previously been reported that the fraction of water soluble K (KCl and  $K_2SO_4$ ) in the fly ash increases with increased fuel ash K/Si molar ratio [2, 107].

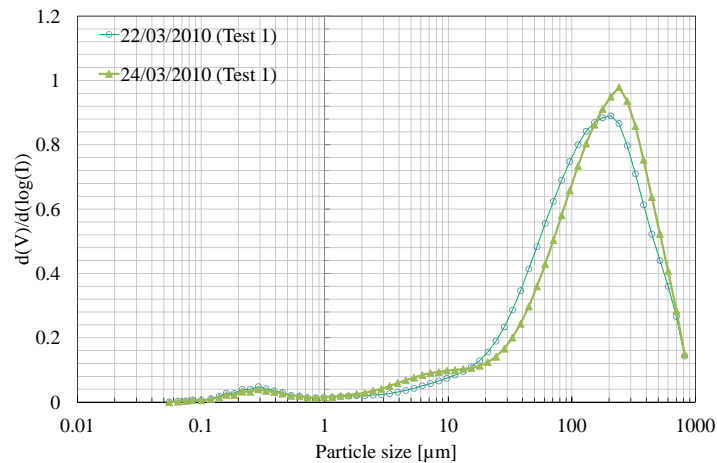
The particle size distribution of fly ash samples shown in Figure 5.10 indicates that during straw suspension combustion, the fine particles are potentially formed because of vaporized inorganic elements and the formation of coarse particles is possibly due to fragmentation during char oxidation. The fine particles appear to have a peak at around  $0.15\text{--}0.30\ \mu\text{m}$  indicating that the formation of these fine particles is analogous to the fine particle formation during straw grate firing, where the formation of fine particles is initiated by the homogeneous nucleation of  $K_2SO_4$  from the gas phase and followed by condensation of KCl and  $K_2SO_4$  [25, 26, 29].



**Figure 5.8:** Ash transformation during straw and wood (straw > 46 wt.%) suspension combustion. Comparison of fuel-, fly- and bottom ash samples from test 1 and 5.



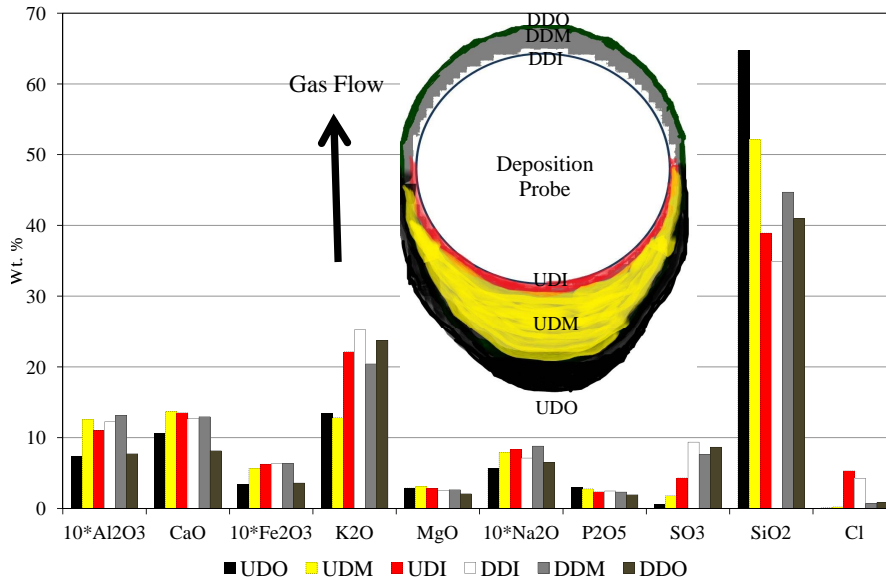
**Figure 5.9:** Impact of molar K/Si ratio in fuel ash on the content of K, Cl and S in the fly ash during straw and wood (straw > 46 wt.%) suspension combustion. The filled points show data from straw suspension-fired measurements at Amager Unit 2 (AMV2, Chapter 4) [101], while the rest of the points are from the current measurements.



**Figure 5.10:** Particle size distribution (volume-based) of fly ash generated during test 1. The fly ash samples were collected using a spear from the silos of the electrostatic precipitator (ESP).

The composition of the probe upstream and downstream deposit layers is shown in Figure 5.11. The inner layers (on the upstream and on the downstream side) were rich in K, Cl and S. K, S and Cl were found in higher proportions on the downstream side of the probe indicating that thermophoresis and/or condensation of KCl and  $K_2SO_4$  is important for the deposit formation process on the downstream side. The upstream side deposit outer layers contain large amounts of Si, K and Ca, indicating that larger particles predominantly impact on and stick to the upstream side of

the probe.



**Figure 5.11:** Bulk ash analysis of deposit layers removed from the probe after it was taken out of the boiler (straw share > 46 wt.%, test 1, 5). UDO; upstream deposits outer layer, UDM; upstream deposits middle layer, UDI; upstream deposits innermost layer, DDI; downstream deposits innermost layer, DDM; downstream deposits middle layer, DDO; downstream deposits outer layer.

### 5.3.3 Comparison of IDF-rates with Previously Conducted Probe Measurements

Probe deposit formation measurements performed on biomass-fired boilers can be found in literature (Chapter 4). The ash deposit formation rates in these measurements were determined by dividing the collected amount of the probe deposit with the probe exposure time. A comparison of these previously determined probe deposit formation rates and the IDF-rates from this study (tests 1–8) is presented in Figure 5.12. The IDF-rate in the present study was calculated from the deposit mass uptake signals after initial 12 h in order to obtain data that can be compared with previous biomass suspension-fired deposit measurements. The deposit formation rates determined in the previous full-scale measurements are also reported (termed) as IDF-rates for a better comparison. As seen in Figure 5.12 (a), there is a general tendency that an increased alkali content in the fuel (or increased straw share in wood) and an increased flue gas temperature results in an increased IDF-rate. The trend is seen both for grate firing and suspension firing. At a flue gas temperature of 650 °C, the IDF-rate is typically from

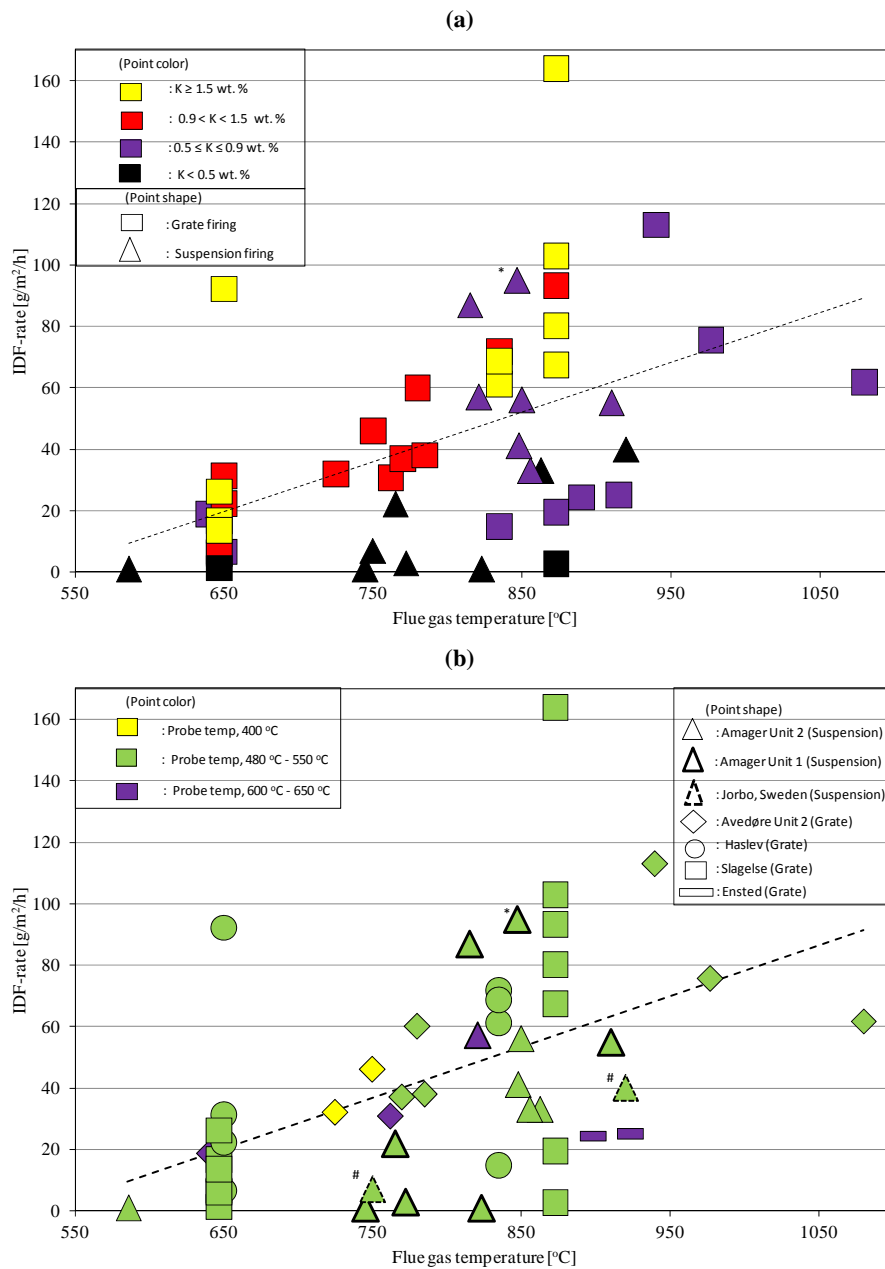


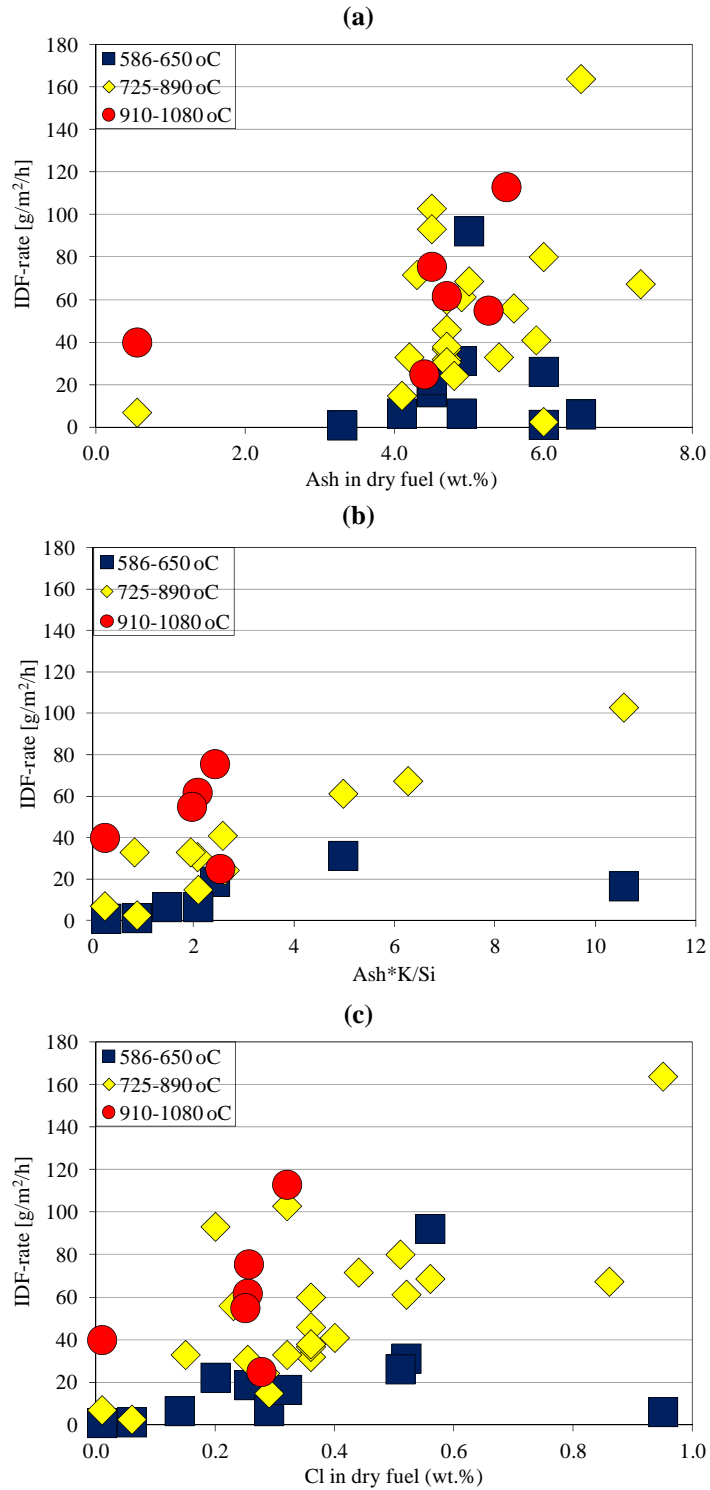
5 to 30 g/m<sup>2</sup>/h and at 900 °C, the IDF-rate is typically 20 to 110 g/m<sup>2</sup>/h. Skrifvars et al. [38] measured IDF-rate of 40 g/m<sup>2</sup>/h at 920 °C and 7 g/m<sup>2</sup>/h at 750 °C in a wood-fired pulverized fuel boiler. Bashir et al. [101] measured IDF-rate of 1 g/m<sup>2</sup>/h during wood suspension firing at a flue gas temperature of 586 °C, while IDF-rates of 41 g/m<sup>2</sup>/h and 56 g/m<sup>2</sup>/h have been measured during straw suspension firing at flue gas temperatures of about 850 °C [5, 101]. Overall, the IDF-rates during straw firing in suspension and grate boilers are on similar levels as indicated in Figure 5.12 (a). This is seen even though the percentage of fuel ash retained as fly ash can be considerably higher during suspension firing, compared to grate firing [17].

It can be seen that when firing a fuel with high alkali contents ( $K > 0.9$  wt.%, yellow and red points), the increase in IDF-rate with flue gas temperature is steeper compared to the increase in the IDF-rate with a fuel with low alkali contents ( $K \leq 0.9$  wt.%, violet and black points). Possibly the content of gas phase alkali and the fraction of molten ash increased at increased flue gas temperatures, and both will lead to an increased deposit formation rate. It is also seen that the probe surface temperature has no significant influence on the IDF-rate (Figure 5.12 (b)). The changed probe surface temperatures in the range from 400 to 650 °C seems not to cause any systematic change on the IDF-rate.

Impact of fuel ash contents, fuel ash multiplied by fuel ash K/Si molar ratio, and Cl-content in the fuel on the IDF-rate for three different sets of flue gas temperatures is shown in Figure 5.13 (there is used the same measuring data as shown in Figure 5.12). It can be seen that compared to the only fuel ash contents, the fuel ash multiplied by fuel ash K/Si molar ratios, (and the Cl-content in fuel) is more effective in predicting the IDF-rates for the applied flue gas temperature, as was also seen in the pilot-scale biomass suspension-fired studies discussed in Chapter 2 (section 2.5, [28, 41, 80]). According to Knudsen [29] the K-release can be significant for fuels containing high amounts of Cl and/or high amounts of K relative to Si, whereas, the K release is expected to low for high Si fuels and low Cl content. The presence of K relative to Si can potentially decrease the melting temperature of the fly ash particles due to the formation K and Cl rich fly ash.

The calculated overall derivative-based deposit formation (DDF) rates were between 234 to 3105 g/m<sup>2</sup>/h during tests 1–5, which are much higher than the IDF-rates. This is in agreement with expectations since IDF-rates are influenced by all shedding events during the time interval of the deposit collection. The IDF-rates provide deposit formation values that will approximately be experienced by the boiler operation personnel. However, to provide more detailed information and to test models that separate the deposit formation and shedding processes the DDF-rates data are needed.





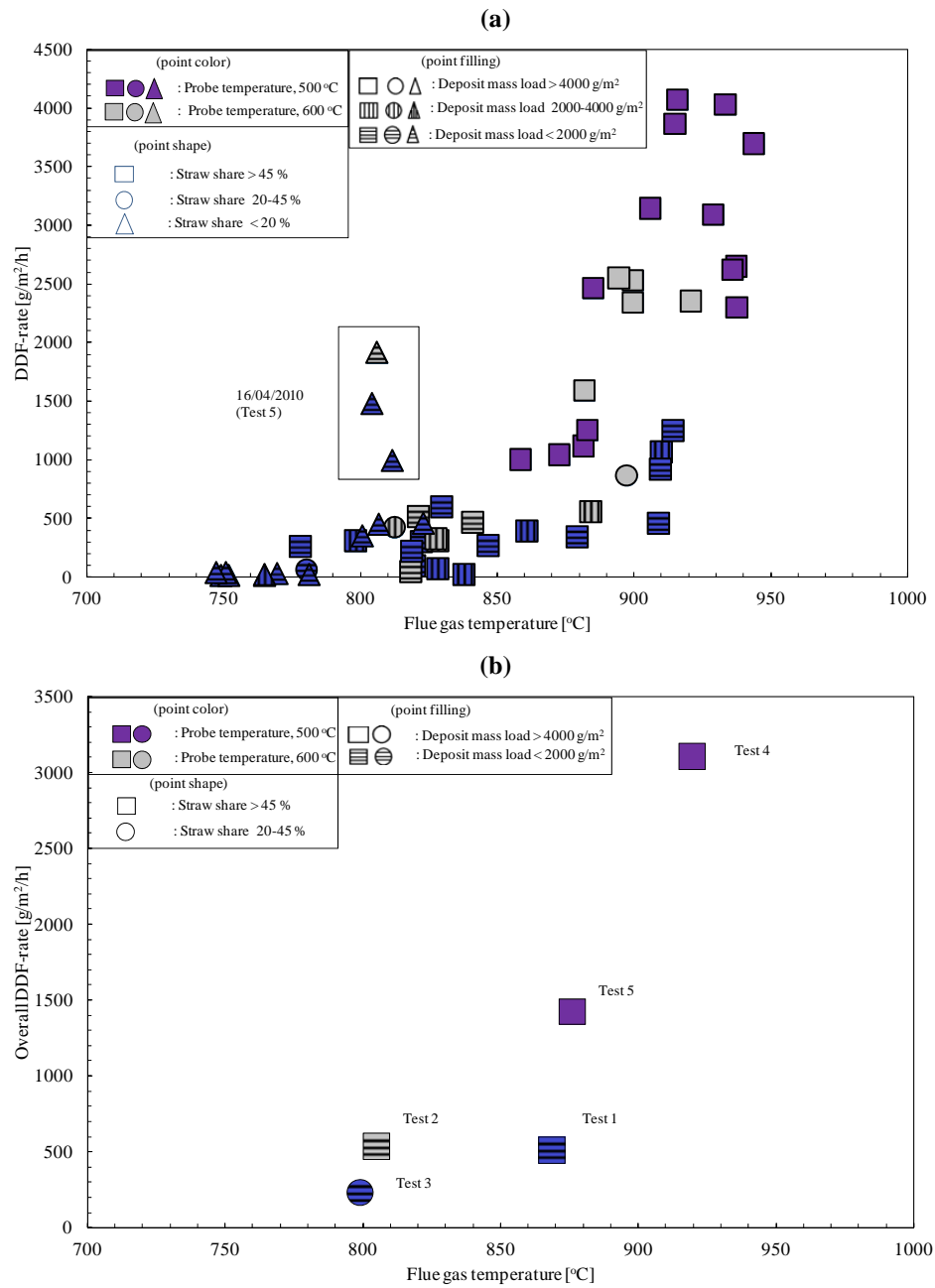
**Figure 5.13:** Impact of fuel ash contents (a), fuel ash  $\times$  K/Si molar ratio (b), and Cl-content in the fuel (c) on the IDF-rate for three different sets of flue gas temperatures (data from Figure 5.12). Limited data were available for fuel ash K/Si molar ratio.

### 5.3.4 Influence of Local Conditions on the DDF-rate

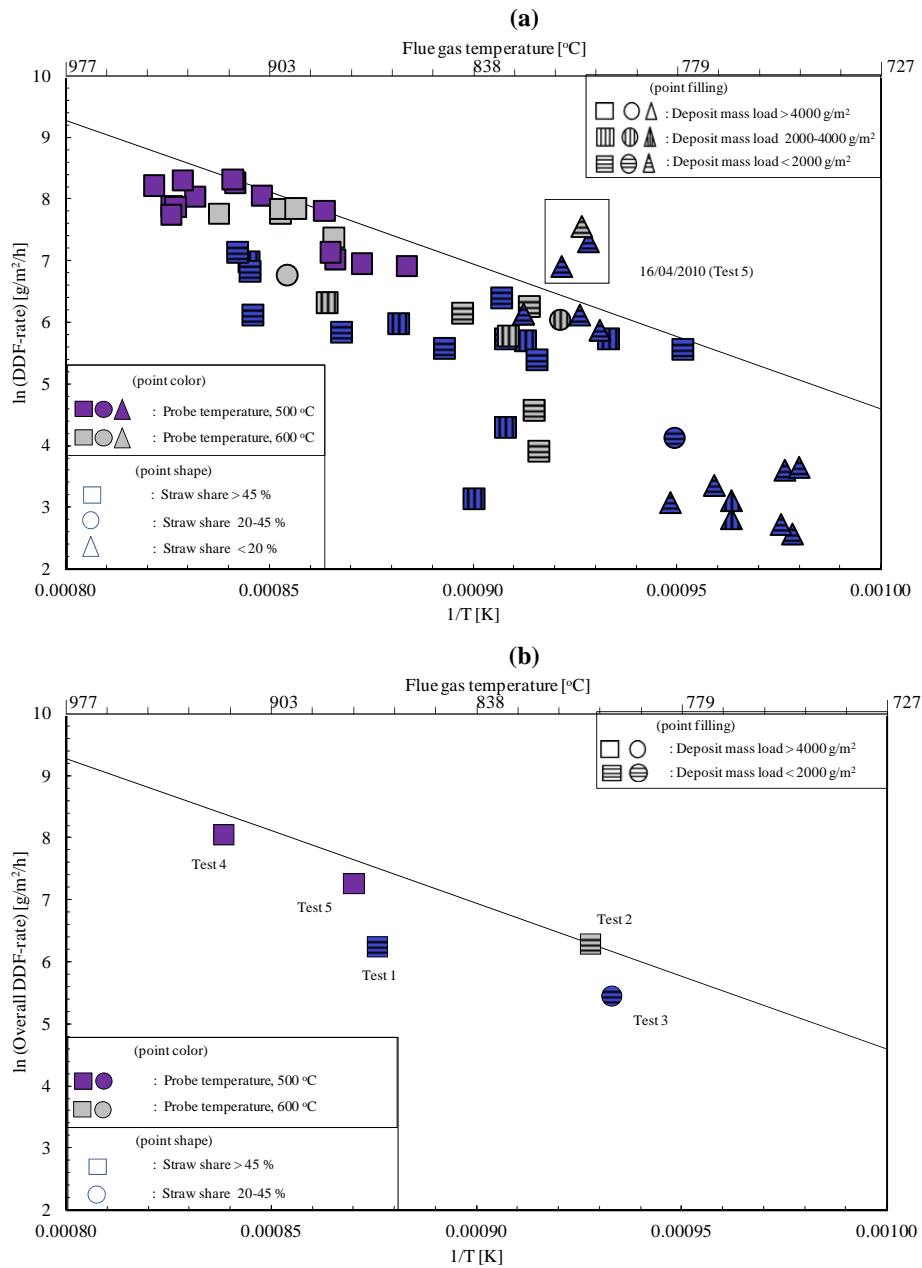
To make it possible to investigate the influence of different operational parameters on the DDF-rates, each test was divided into further sub-tests based on the number of hours (usually 6 h). A significant number of data points thus allowed us to analyze the influence of local flue gas temperature and boiler operational parameters on the DDF-rates. The DDF-rate as a function of flue gas temperature is shown in Figure 5.14 (a), where is shown additional information about the applied probe temperature, straw share in wood, and deposit mass load. No significant influence of changed probe surface temperature on the DDF-rates is seen. There is observed an increase in DDF-rates with increase in flue gas temperature. It can be seen that the DDF-rates increased strongly above a flue gas temperature of 850–880 °C. There is only one exception and that is data from the 16/04/2010 (test 5), where fuel particle grindability problem occurred in mill 20 and this probably caused the observed high DDF-rates. A possible reason for the increased DDF-rate at higher flue gas temperatures could be that the K-silicate and K-Ca-silicate particles hitting the probe to a higher degree are molten, and thereby a larger fraction of the impacted ash particles sticks to the deposit probe. A similar trend of increase in DDF-rate with increase in flue gas temperature was seen for the overall mean DDF-rate of each test as shown in Figure 5.14 (b). Increased deposit formation rate with increased flue gas temperature has also been seen in the previous full-scale measurements conducted at different straw-fired boilers [5, 33, 35, 46, 104]. The DDF-rate is lower at lower straw shares in wood and higher at high straw shares possibly due to the changed total fuel ash content level and changed melting properties of the fly ash due the changed chemical composition. Reduced ash deposit formation rates during straw co-firing with woody biomass, compared to pure straw suspension firing have been observed by Nordgren et al. [27], Bashir et al. [101] and Lokare et al. [28]. Lower ash deposit formation rates have been shown in previous full-scale measurements at straw grate-fired boilers for reduced alkali contents in straw [33, 35, 46, 104].

The very steep increases in the DDF-rates above approximately 850 °C are suggestive of an exponential, Arrhenius-like dependence on temperature. In Figure 5.15 (a), the logarithm of the DDF-rate is shown as function of the reciprocal of the absolute temperature. A straight line limit below which the majority of data lies is shown, but clearly a large spread is evident. The general trend is however followed by all points and it appears that the data points all lie in a band between two straight lines. A similar Arrhenius-like trend is seen for overall mean DDF-rate of each test as shown in Figure 5.15 (b). The equation used for straight line is,

$$\ln(\text{DDF-rate}) = \frac{-23400}{T} + 28 \quad (5.6)$$



**Figure 5.14:** a) Impact of flue gas temperature on the DDF-rate, data points from tests 1 to 5, b) impact of flue gas temperature on the overall DDF-rate, tests 1 to 5. **Graph details:** the color represents the probe surface temperature; the particular point shape represents the straw share with wood in wt.%, while the particular point filling indicates the deposit mass load.



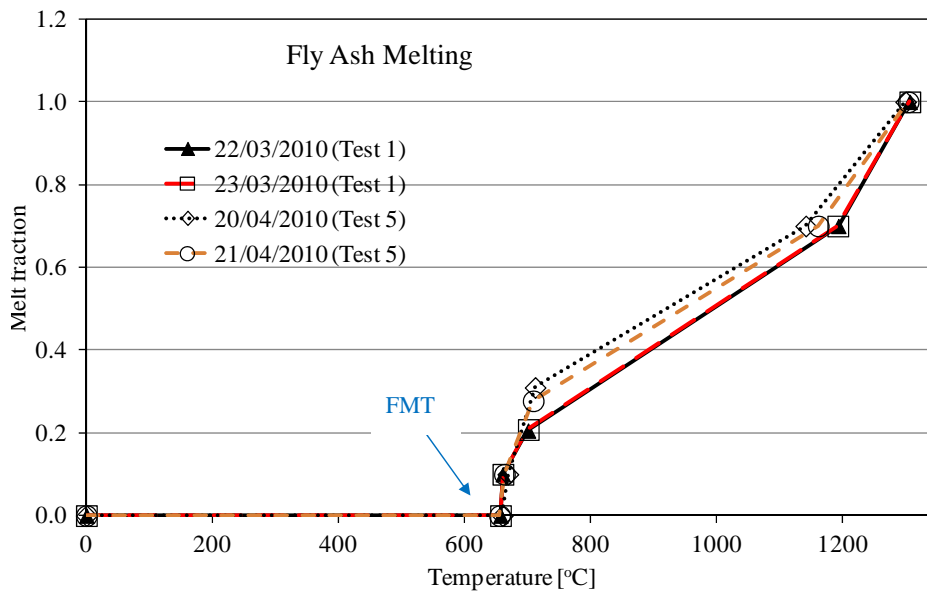
**Figure 5.15:** a) Logarithm of the DDF-rate as a function of reciprocal of absolute flue gas temperature, data points from tests 1 to 5, b) logarithm of the overall DDF-rate as a function of reciprocal of absolute flue gas temperature, tests 1 to 5. **Graph details:** the color represents the probe surface temperature; the particular point shape represents the straw share with wood in wt.%, while the particular point filling indicates the deposit mass load. The flue gas temperature in degree Celsius is shown in the secondary x-axis.

Since the full-scale measurements have been conducted in a commercial boiler, the information presented in Figure 5.14 to Figure 5.15 may be used to predict the deposit formation rate levels in the superheater region of a biomass suspension-fired boiler. The information can be used to estimate deposit formation levels as a function of surface temperature, flue gas temperature and fuel alkali content. Regarding the practical implications for the boiler operation personnel, the increase in probe surface temperature from 500 to 600 °C will not be a significant concern, but a higher fuel alkali contents in addition to higher fuel ash K/Si molar ratio and a flue gas temperature higher than 880 °C can result in significant deposit formation.

The measured ash melting temperatures of the fly ashes shown in Table 5.5 indicate that the fly ash generated from test 5 has more potential to stick to the probe surface, compared to the fly ash generated during test 1. The shrinkage temperature for the fly ash produced during test 5 was not possible to estimate due to swelling of the ash. Shrinkage and deformation temperature of the straw ash and the wood ash shows significant difference. A prediction of fly ash melt fraction as a function of temperature based on the fly ash compositions was made by using the model proposed by Zhou et al. [31] (Figure 5.16). The model seems to predict the ash melting temperature in a reasonable range if a comparison of the laboratory ash melting results and the predicted results is made (Table 5.5). The fly ashes have a first melting temperature (FMT) between 640 and 645 °C, but at higher temperatures (> 800 °C), a significant fraction of molten fly ash is seen and this could lead to a greatly increased probability of the fly ash to stick to the deposit probe. This probably induces the higher DDF-rates at higher flue gas temperatures (Figure 5.14). The higher melt fraction of fly ash from test 5 may lead to a larger probability of the generated fly ash to stick to probe, causing a higher overall DDF-rate measured for test 5 compared to test 1 (Figure 5.14 (b)). The influence of fly ash composition on the melting curves indicates that the presence of K influences the ash melt fraction [31].

**Table 5.5:** Measured ash melting temperatures of fuel and fly ashes.

Method	Fly/Fuel ash	Test 1	Test 5	Test 5	Straw	Wood
CEN/TS 15370-1:2006	Date	23/03/2010	20/04/2010	21/04/2010	–	–
Straw	(% wt.)	80–85	60–65	40–45	100	0
K in ash	(% wt.)	15.53	21.32	20.14	14.84	–
Shrinkage start temperature	°C	670	Swelling	Swelling	670	1050
Deformation temperature	°C	865	780	800	885	1210
Hemisphere temperature	°C	1110	1115	1115	1060	1225
Flow temperature	°C	1210	1260	1260	1230	1240



**Figure 5.16:** Fly ash melt prediction using predictive model of Zhou et al. [31]. FMT stands for first melting temperature.

## 5.4 Ash Deposit Shedding

### 5.4.1 Video Observations of Shedding Events

The deposit mass uptake signals were continuously monitored and deposit shedding events were confirmed by video recordings. The deposit mass uptake signals during test 1 are shown in Figure 5.17. The shedding events were divided into naturally occurring events and sootblowing initiated shedding events. Even when the nearby sootblower is turned off, the increased thermal and mechanical fluctuations induced by the rest of the sootblowers may increase the shedding rate. No artificial probe sootblowing measurements were conducted during test 1.

Confirmation of some deposit shedding events was made using the images collected at 20–30 seconds intervals. It was found that deposit shedding was primarily through debonding from the surface of the deposit probe; an example of a deposit shedding event is shown in Figure 5.18. The adhesion strength between the deposit and probe surface was not sufficient, and the deposit layer was being removed. More pictures of deposit shedding events for the tests conducted at AMV1 are shown in Appendix B. No deposit shedding through surface melting was seen in the videos collected from any of the tests, even though a flue gas temperature higher than 1000 °C, was observed during test 4 and 5. Earlier investigations of Zbogor et al. [35]



showed shedding through surface melting in a straw grate-fired boiler, at local flue gas temperatures greater than 1000 °C. Possibly the high contents of Si and Ca in the fly ash of the AMV1 boiler, and the relatively lower concentrations of the inorganic volatile elements (K, Cl and S) cause a higher melting temperature of the ash deposits generated by the suspension co-firing of straw and wood [101, 108].

Monitoring of deposit shedding from inspection holes very close to the port position revealed a small amount of deposit shedding through erosion when non-sticky, relatively large and sharp edged SiO<sub>2</sub>-rich fly ash particles collide with non-sticky area on a deposit surface causing a cutting action (brittle deposits). Significant amount of Si in the fly ash formed during straw and wood suspension firing has been reported [108]. Generally most of the deposits were removed by debonding where larger pieces detached from the tube surface.

#### 5.4.2 Data Treatment

As discussed before, during the calculation of DDF-rates, a particular negative slope cut off level was selected to determine major shedding events accurately, while still giving a satisfactory prediction of apparent DDF-rates. The selected cut off level was -3,800 g/m<sup>2</sup>/h for all the tests. This cut off level strikes a balance between including larger shedding events in the analysis and preventing deposit mass signal noise from being counted on a shedding event [108]. The selected minimum magnitude of a shedding event included in the analysis was -105 g/m<sup>2</sup> and this was calculated by equations (5.7-5.9),

$$\text{Minimum shedding event magnitude} = \text{slope cut off level} \cdot \text{sampling interval} \quad (5.7)$$

$$= -3,800 \frac{g}{m^2 h} \frac{h}{3,600s} \cdot 100s \quad (5.8)$$

$$= -105 \frac{g}{m^2} \quad (5.9)$$

The deposit probe mass uptake signals are shown in Figure 5.17 for test 1. All shedding events are marked showing both natural and plant sootblowing induced shedding events. The naturally occurring shedding was defined to occur when the plant sootblowers were not in operation and no artificial sootblowing tests were made. Sootblowing induced shedding events can occur when the plant sootblowers are in operation. Typically a plant sootblowing operation lasts for about 1–2 h. The lengths of intervals between

naturally occurring shedding incidents are very variable as seen in Figure 5.17. In the first 10–12 h, natural shedding occurs often, but with only small amounts of material. From about 12 to 21 h, the intervals between shedding events become longer, and the amounts removed in the single events are also larger compared to the previous period. Finally from 29 h to 55 h, natural shedding is infrequent, but the shedding amount is again relatively small. These changes in behavior may be related to varying boiler operation parameters, but it is worth noting that during the full 55 h, the baseline of deposited mass on the probe, increased slowly from 0 to about 2,500 g/m<sup>2</sup>. Similar behavior was observed in most of the other tests also.

Under these conditions, analysis and quantification of natural shedding during the long time test is done by averaging over shorter time intervals. These are long enough that short time random behavior does not influence results unduly, but short enough that local operating and probe conditions may be considered fairly constant. Thus, each test was divided into sections of 6 h, which were used for the data analysis to characterize the deposit shedding by means of magnitude of events [g/m<sup>2</sup>] and the incidence rate (deposit shedding frequency, h<sup>-1</sup>). With regard to natural shedding, this allow us to calculate mean incidence rates (mean natural deposit shedding frequency),  $f_{nat,6}$ , as the number of shedding events in a 6 h interval divided by the interval time. It should be noted that for each 6 h interval, the period of plant sootblowing was excluded while evaluating the natural shedding events. The mean deposit shedding frequency by natural shedding was calculated by equation (5.10),

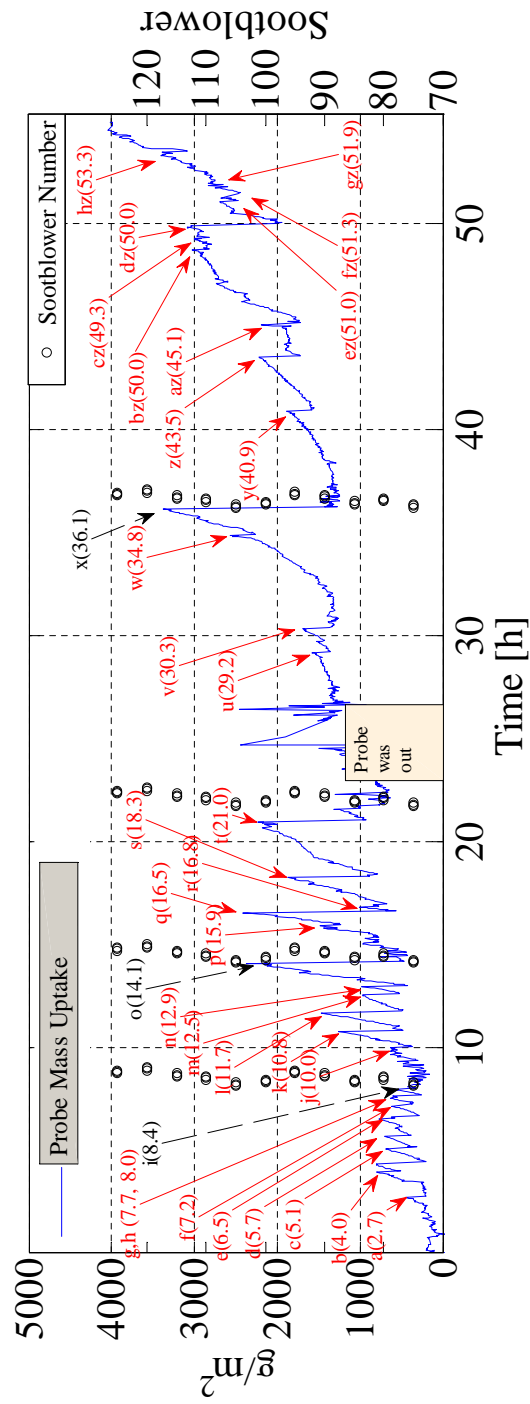
$$\text{Mean natural deposit shedding frequency} = f_{nat,6} = \frac{NE_6}{TT_n} \quad (5.10)$$

Where  $NE_6$  = Number of natural shedding events in a 6 h interval, and  $TT_n$  = Total time without plant sootblowing during a 6 h interval.

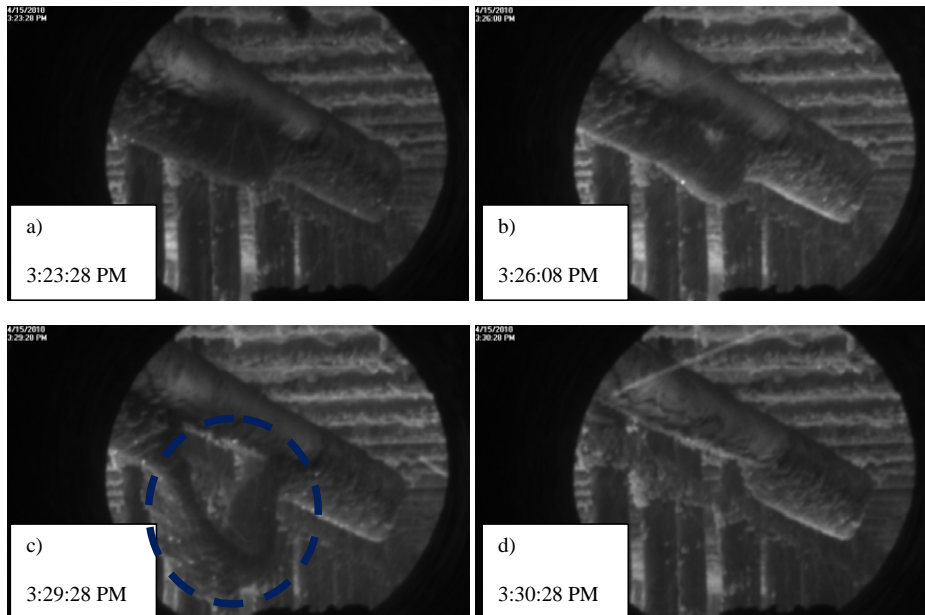
In the superheater region area of the boiler retractable steam sootblowers were used for a time of 5–10 min (each sootblower) at regular intervals during boiler operation, typically after 8 h. It was found that the 12 sootblowers influenced the shedding of the deposits from the probe surface, 6 sootblowers were placed along the left wall of the boiler and 6 along the right wall of the boiler as shown in Figure 5.2. The mean sootblower deposit shedding frequency was calculated using equation (5.11),

$$\text{Mean plant sootblowing shedding frequency} = f_{soot,6} = \frac{SE_6}{TT_s} \quad (5.11)$$

Where  $SE_6$  = Number of sootblower shedding events in a 6 h interval, and  $TT_s$  = Total time of plant sootblowing during a 6 h interval.



**Figure 5.17:** Data of probe mass uptake and plant sootblowing events (specific number of sootblower in operation as seen on the secondary y-axis) during test 1 with identified shedding events. Red arrows with continuous line show natural deposit shedding events, while black arrows with discontinuous line show deposit shedding through plant sootblowing. Sootblower number shown on the secondary y-axis represents a specific sootblower in the superheater region shown in Figure 5.2. The number attached to each event specifies the time of the shedding event.



**Figure 5.18:** Images of the ash deposition probe during test 5 on 15/04/2010 (about 4 h exposure time). From figure a to d, the process of natural deposit shedding through debonding can be clearly seen.

### 5.4.3 Influence of Different Parameters on the Shedding Process

The shedding event size ( $\text{g}/\text{m}^2$ ) and the shedding frequency ( $\text{h}^{-1}$ ), are shown in Figure 5.19 and Figure 5.20. The mean values for 6 h periods with similar conditions are presented in Table 5.6 (natural shedding) and Table 5.7 (sootblowing induced shedding). The shedding data are divided into groups to make it possible to analyze the influence of changed conditions in flue gas temperature (above or below  $850\text{ }^\circ\text{C}$ ), probe surface temperature ( $500\text{ }^\circ\text{C}$  or  $600\text{ }^\circ\text{C}$ ), straw fuel share (weight fraction of straw in the fuel above or below 20 %) and deposit mass load (above or below  $5,000\text{ g}/\text{m}^2$ ). The selected criterion of flue gas temperature is based on the results presented before (Section 5.3.4), where it was found that the deposit formation rate increases significantly when the flue gas temperature exceeds  $850\text{ }^\circ\text{C}$ . The second criterion was the probe surface temperature to investigate the influence of probe surface temperature on deposit shedding. The selected number ( $5,000\text{ g}/\text{m}^2$ ) for the deposit mass load is an arbitrary number, which was introduced to find any impact of deposit amount on the probe on deposit shedding. As seen in Table 5.6 and Table 5.7 several of the combinations of operating conditions are without data. In two cases in Table 5.6 (straw <

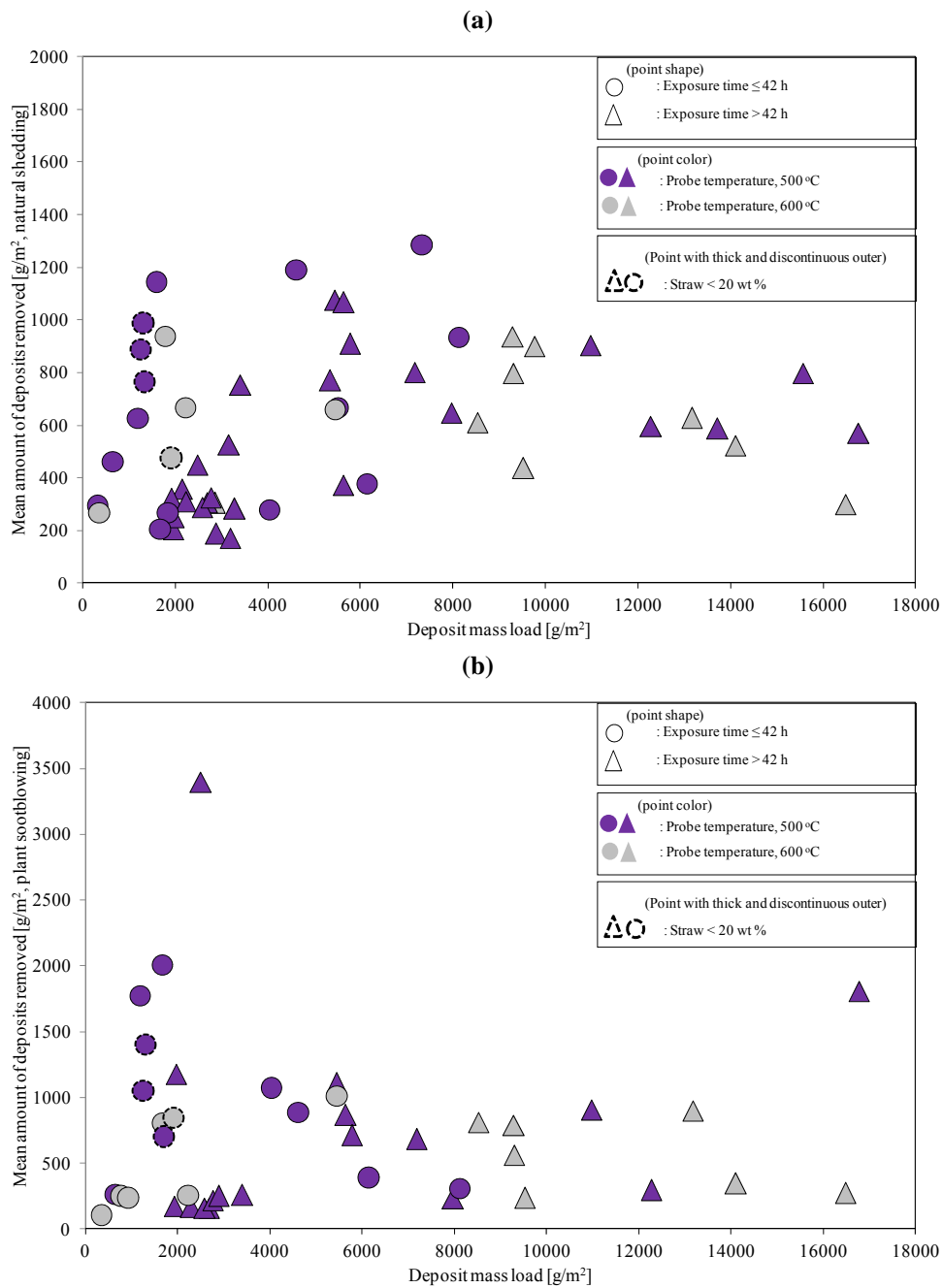
20 wt.%, deposit mass load  $< 5,000 \text{ g/m}^2$ , flue gas temperature  $< 850 \text{ }^\circ\text{C}$ , probe surface temperature  $600 \text{ }^\circ\text{C}$ ) and (straw  $> 20 \text{ wt.}\%$ , deposit mass load  $< 5,000 \text{ g/m}^2$ , flue gas temperature  $> 850 \text{ }^\circ\text{C}$ , probe surface temperature  $600 \text{ }^\circ\text{C}$ ) only one 6 h period is presented. These cases are highlighted as italic in Table 5.6 and Table 5.7 and statistically it is difficult to use these data because of the limited data points. Below the influence of local changes and changes in probe conditions on the shedding characteristics is discussed.

### Increased Deposit Load on the Probe

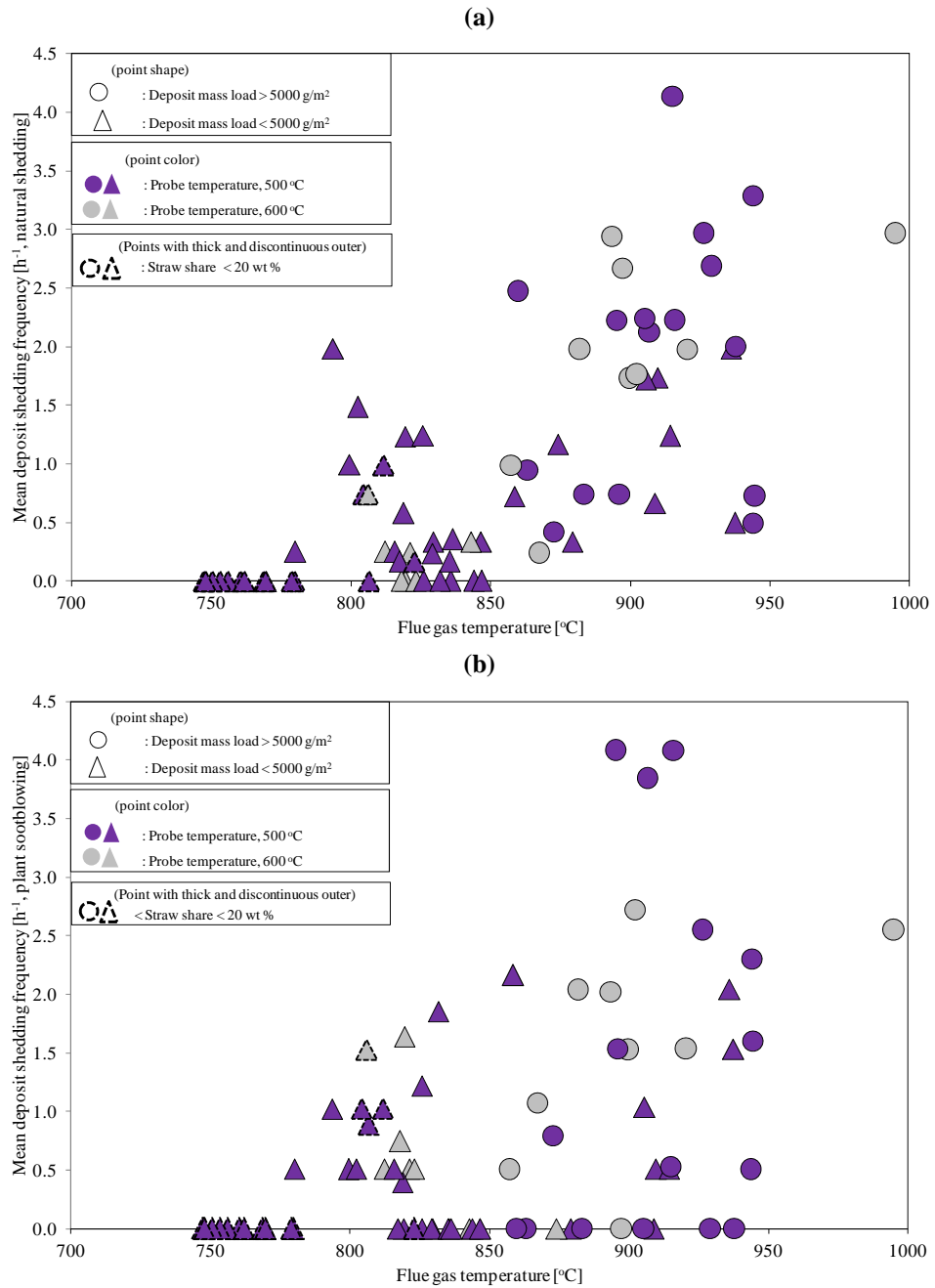
The mean amount of deposit removed at a shedding event is  $716 \text{ g/m}^2$  during natural shedding and  $805 \text{ g/m}^2$  during sootblowing initiated shedding as seen in Figure 5.19. There are seen large fluctuations in the amount of deposit removed in a single shedding event (6 h mean) from  $180$  to  $1400 \text{ g/m}^2$  during natural shedding, but there are not observed any strong influence of the total deposit mass load on the amount of deposit removed in the single event (see Figure 5.19). In most cases, the probe deposit mass increases over time and in the later stages of the experiments more than  $5,000 \text{ g/m}^2$  are collected on the probe.

Two sets of data with similar conditions except for an increase in deposit load ( $5,000 \text{ g/m}^2$ ) is only available for a flue gas temperature above  $850 \text{ }^\circ\text{C}$ , a probe temperature of  $500 \text{ }^\circ\text{C}$  and a straw fuel share above  $20 \text{ wt.}\%$  (as seen in Table 5.6 and Table 5.7). Going from a deposit mass below  $5,000 \text{ g/m}^2$  to above  $5,000 \text{ g/m}^2$  changed the mean shedding event mass from  $632$  to  $854 \text{ g/m}^2$  during natural shedding and from  $935$  to  $849 \text{ g/m}^2$  during sootblowing induced shedding. Again, this shows that even though the deposit mass level has a tendency to increase through time this does not strongly influence the amount of deposit released at a shedding event. The shedding frequency is increased from  $1.04$  to  $1.89 \text{ h}^{-1}$  during natural shedding and from  $1.29$  to  $1.56 \text{ h}^{-1}$  during sootblower induced shedding when changing from a deposit mass below  $5,000 \text{ g/m}^2$  to above  $5,000 \text{ g/m}^2$ . There is also seen a clear increase in DDF-rate when the deposit mass load is increased, and since the shedding frequency increases, the shedding rate [ $\text{g/h/m}^2$ ] increases with the increasing deposit mass.

Since the amount of deposit removed at a shedding event is approximately independent of the amount of deposits on the probe, the relative amount of deposits removed (relative to total amount on the probe) is larger at low probe deposit mass. In addition, video recordings of deposit removal by plant sootblowing indicate that for shorter probe exposure time, plant sootblowing removes deposits from the entire surface of the probe, while a complete or partial layer of deposits is removed at higher exposure times.



**Figure 5.19:** Impact of deposit mass load on (a) the mean amount of deposits removed naturally and (b) the mean amount of deposits removed during plant sootblowing. Data points are from tests 1 to 5. **Graph details:** the particular point shape represents the exposure time, the color represents the probe surface temperature, while point with thick and discontinuous outer is representative for straw share in wood.



**Figure 5.20:** Impact of flue gas temperature on (a) mean natural deposit shedding frequency and (b) mean plant sootblowing shedding frequency. Data points are from tests 1 to 5. **Graph details:** the particular point shape represents the deposit mass load, the color represents the probe surface temperature, while point with thick and discontinuous outer is representative for straw share in wood.

**Table 5.6:** Summary of the analysis of natural deposit shedding for two different sets of flue gas temperature, probe surface temperature, straw share and deposit load.

Natural deposit shedding		Flue gas temperature			
Fuel straw share	Probe deposit mass load	< 850 °C		> 850 °C	
Straw > 20 wt. %	> 5,000 g/m <sup>2</sup>	500 °C	600 °C	500 °C	600 °C
		2691	1934		
	Mean DDF-rate (g/m <sup>2</sup> /h)	16	9		
	Number of 6 h periods	134	70		
	Number of shedding events	854	730		
	Mean size of shedding event (g/m <sup>2</sup> )	10	7		
	Mean deposits removed (%)	1.89	1.92		
	Mean shedding frequency (h <sup>-1</sup> )	1612	1403		
	Mean shedding rate (g/m <sup>2</sup> /h)				
Straw > 20 wt.%	< 5,000 g/m <sup>2</sup>	234	313	1245	577
	Mean DDF-rate (g/m <sup>2</sup> /h)	19	6	8	1
	Number of 6 h periods	42	4	38	7
	Number of shedding events	343	702	632	305
	Mean size of shedding event (g/m <sup>2</sup> )	15	34	27	10
	Mean deposits removed (%)	0.47	0.15	1.04	1.17
	Mean shedding frequency (h <sup>-1</sup> )	160	107	660	356
	Mean shedding rate (g/m <sup>2</sup> /h)				
Straw < 20 wt.%	> 5,000 g/m <sup>2</sup>				
	Mean DDF-rate (g/m <sup>2</sup> /h)				
	Number of 6 h periods				
	Number of shedding events				
	Mean size of shedding event (g/m <sup>2</sup> )				
	Mean deposits removed (%)				
	Mean shedding frequency (h <sup>-1</sup> )				
	Mean shedding rate (g/m <sup>2</sup> /h)				
Straw < 20 wt.%	< 5,000 g/m <sup>2</sup>	221	1913		
	Mean DDF-rate (g/m <sup>2</sup> /h)	17	1		
	Number of 6 h periods	8	3		
	Number of shedding events	910	476		
	Mean size of shedding event (g/m <sup>2</sup> )	44	28		
	Mean deposits removed (%)	0.11	0.74		
	Mean shedding frequency (h <sup>-1</sup> )	101	353		
	Mean shedding rate (g/m <sup>2</sup> /h)				



**Table 5.7:** Summary of the analysis of shedding during sootblower operation for two different sets of flue gas temperature, probe surface temperature, straw share and deposit load.

Plant sootblowing deposit shedding		Flue gas temperature			
Fuel straw share	Probe deposit mass load	500 °C		600 °C	
Straw > 20 wt. %	> 5,000 g/m <sup>2</sup>	500 °C	600 °C	500 °C	600 °C
		2691	1934		
	Mean DDF-rate (g/m <sup>2</sup> /h)	16	9		
	Number of 6 h periods	39	30		
	Mean size of shedding event (g/m <sup>2</sup> )	849	688		
	Mean deposits removed (%)	10	9		
	Mean shedding frequency (h <sup>-1</sup> )	1.56	1.71		
	Mean shedding rate (g/m <sup>2</sup> /h)	1322	1176		
Straw > 20 wt. %	< 5,000 g/m <sup>2</sup>	234	313	1245	
	Mean DDF-rate (g/m <sup>2</sup> /h)	19	6	8	
	Number of 6 h periods	9	5	15	
	Mean size of shedding event (g/m <sup>2</sup> )	750	332	935	
	Mean deposits removed (%)	20	32	42	
	Mean shedding frequency (h <sup>-1</sup> )	0.37	0.51	1.29	
	Mean shedding rate (g/m <sup>2</sup> /h)	278	170	1208	
Straw < 20 wt. %	> 5,000 g/m <sup>2</sup>				
	Mean DDF-rate (g/m <sup>2</sup> /h)				
	Number of 6 h periods				
	Mean size of shedding event (g/m <sup>2</sup> )				
	Mean deposits removed (%)				
	Mean shedding frequency (h <sup>-1</sup> )				
	Mean shedding rate (g/m <sup>2</sup> /h)				
Straw < 20 wt. %	< 5,000 g/m <sup>2</sup>	221	1913		
	Mean DDF-rate (g/m <sup>2</sup> /h)	17	1		
	Number of 6 h periods	8	3		
	Mean size of shedding event (g/m <sup>2</sup> )	965	845		
	Mean deposits removed (%)	69	46		
	Mean shedding frequency (h <sup>-1</sup> )	0.27	1.53		
	Mean shedding rate (g/m <sup>2</sup> /h)	260	1293		

So regarding the shedding properties, an increased amount of deposits on the probe leads not to a significant change in the amount of deposit lost at a shedding event but do increase the shedding frequency and thereby the shedding rate.

### Changed Probe Surface Temperature

For two sets of data (temperature below 850 °C, deposit mass below 5,000 g/m<sup>2</sup> and a straw fuel share above 20 wt.%) and (temperature above 850 °C, deposit mass above 5,000 g/m<sup>2</sup> and a straw fuel share above 20 wt.%) in Table 5.6 and Table 5.7, the influence of a change in probe temperature from 500 to 600 °C is illustrated. However, no clear tendencies are observed, and a systematic change in amount of deposit shed in an event or the deposit frequency cannot be observed when the probe temperature is changed from 500 to 600 °C. However if one looks at the mean shedding rate, then the shedding rate is in most cases higher at a probe temperature of 500 °C than at a probe temperature of 600 °C, possibly due to partial melting and/or sintering of the innermost deposit layer (rich in K, Cl and S) at higher probe surface temperature.

### Changed Flue Gas Temperature

As seen on Figure 5.20 an increased flue gas temperature leads to an increased deposit shedding frequency, even there is seen a very large spread in the data points. Comparing the data sets with similar conditions (probe temperature 500 °C, deposit mass below 5,000 g/m<sup>2</sup> and a straw fuel share above 20 wt.%) in Table 5.6 and Table 5.7 but with different flue gas temperatures (below and above 850 °C), there is seen an increase in shedding frequency and a small increase in shedding mass is also observed when the flue gas temperature is increased.

### Increased Fraction of Straw in the Fuel

Changes in fuel straw fraction in the fuel (from above to below 20 wt.%) for the data sets with (probe temperature 500 °C, deposit mass below 5,000 g/m<sup>2</sup> and flue gas temperature below 850 °C) show an increased shedding amount with decreased straw share. However, the mean shedding rate is low at lower straw fraction.

To summarize the main observations the mean deposit shedding rate (shedding event amount times the shedding frequency) can be used as shown in Table 5.6 and Table 5.7.

- The deposit shedding rates increased at high flue gas temperatures (> 850 °C) and high probe deposit mass loads (> 5,000 g/m<sup>2</sup>) where also

high deposit formation rates are observed (DDF-rate).

- The shedding rate is in most cases higher at a probe temperature of 500 °C than that at a probe temperature of 600 °C. A possible reason could be partial melting and/or sintering of the innermost deposit layer (rich in K, Cl and S) at higher probe surface temperature. This could cause the adhesion strength of the deposit to increase at the higher probe surface temperatures.
- The deposit shedding process is a stochastic process, where the amount of deposit shed varies, even at constant conditions (Figure 5.19). The deposit shed amount is probably strongly related to the strength of the innermost salt rich deposit layer.

#### 5.4.4 Net Deposit Accumulation Rate

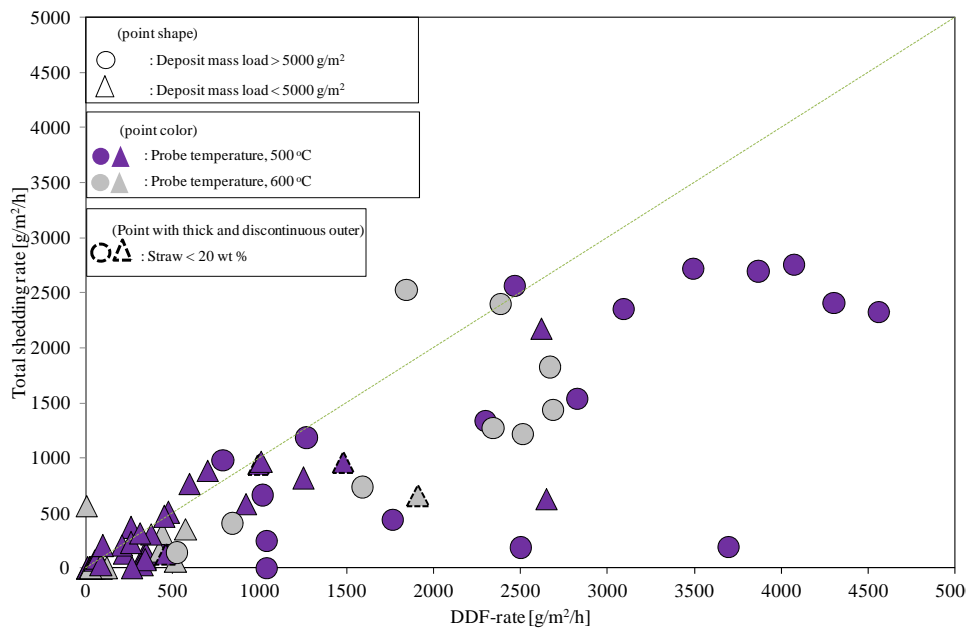
The total deposit shedding rate was calculated by using the equation (5.12)

$$\text{Total deposit shedding rate} = (\text{natural shedding rate} \cdot F_r) + (\text{sootblowing shedding rate} \cdot (1 - F_r)) \quad (5.12)$$

Here,  $F_r$  is the fraction of time of the 6 h interval when plant sootblowers were not in operation. The total deposit shedding rate as a function of the DDF-rate is shown in Figure 5.21. It can be seen that with increase in DDF-rate, the total deposit shedding rate slightly increases. It is also evident that the total deposit shedding rate is lower than the DDF-rate in most cases. This causes an accumulation of deposit mass on the probe with the passage of time. The accumulation of the deposits can be presented in the form of net deposit accumulation rate, a measure of the difference between the total shedding rate and the DDF-rate. In addition, it is of interest for the plant operators to quantify the amount of deposit finally remaining on the superheater tubes as a common result of build-up and shedding. The net deposit accumulation rate was calculated by equation (5.13),

$$\text{Net deposit accumulation rate} = (\text{DDF-rate}) - (\text{total deposit shedding rate}) \quad (5.13)$$

The calculated net deposit formation rate is shown in Table 5.8 for the changed conditions in flue gas temperature (above or below 850 °C), probe surface temperature (500 °C or 600 °C), straw fuel share (weight fraction of straw in the fuel above or below 20%) and deposit mass load (above or below 5,000 g/m<sup>2</sup>). The main observations are the following:

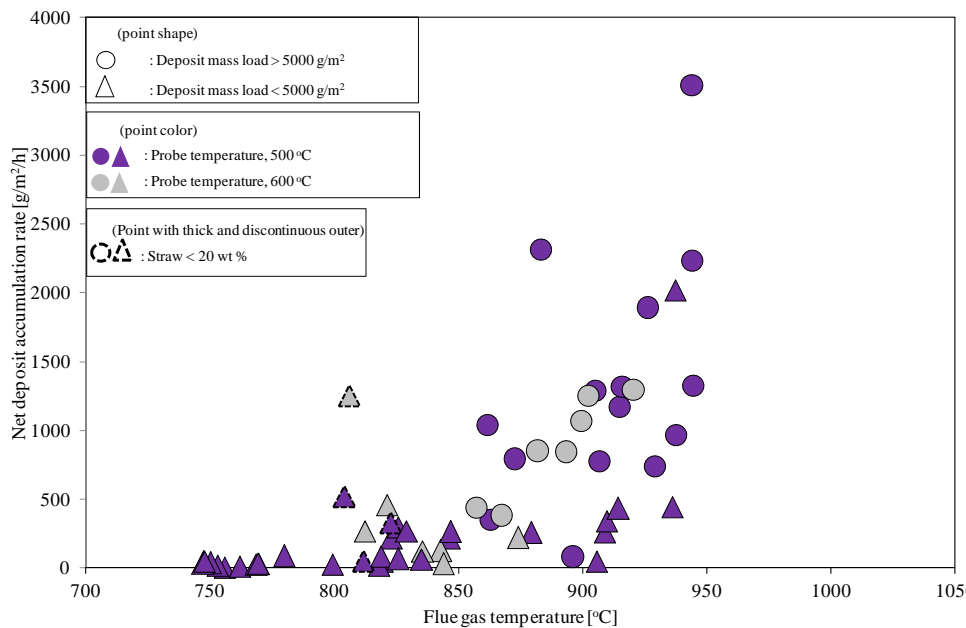


**Figure 5.21:** Total deposit shedding rate as a function of the DDF-rate. Data points are from tests 1 to 5. **Graph details:** the particular point shape represents the deposit mass load, the color represents the probe surface temperature, while point with thick and discontinuous outer is representative for straw share in wood.

- The net deposit accumulation rate increases with increase in flue gas temperature (see Figure 5.22). Increased flue gas temperatures probably increase the fraction of molten ash as well as provide an increased content of gas phase alkali species, and both will lead to an increased deposit formation rate. The increase in DDF-rate was larger than the increase in deposit shedding rate with increased flue gas temperature as shown in Table 5.8.
- The net deposit accumulation rate is low ( $452 \text{ g/m}^2/\text{h}$ ) at lower deposit mass load ( $< 5,000 \text{ g/m}^2$ ) on the probe, compared to a value of  $1155 \text{ g/m}^2/\text{h}$  for deposit mass load greater than  $5,000 \text{ g/m}^2$  (Table 5.8, probe temperature  $500 \text{ }^\circ\text{C}$ , flue gas temperature about  $900\text{--}910 \text{ }^\circ\text{C}$  and straw share more than  $20 \text{ wt.}\%$ ).
- Generally no clear tendency for the impact of probe surface temperature on net deposit accumulation rate was seen.

**Table 5.8:** Mean DDF-rates and mean net deposit accumulation rates for two different sets of flue gas temperature, probe surface temperature, straw share and deposit load. <sup>a</sup> mean value of the deposit mass load, <sup>b</sup> mean value of flue gas temperature, <sup>c</sup> mean values irrespective of probe surface temperature.

Net deposit accumulation rate		Flue gas temperature			
Fuel straw share	Probe deposit mass load	500 °C	600 °C	500 °C	600 °C
Straw > 20 wt. %	> 5,000 g/m <sup>2</sup> (9403 g/m <sup>2</sup> ) <sup>a</sup>	(909) <sup>b</sup>	(902) <sup>b</sup>	(909) <sup>b</sup>	(902) <sup>b</sup>
	Mean DDF-rate (g/m <sup>2</sup> /h)	2691	1934	2691	1934
	Number of 6 h period	16	9	16	9
	Mean total deposit shedding rate (g/m <sup>2</sup> /h)	1536	1329	1536	1329
	Mean net deposit accumulation rate (g/m <sup>2</sup> /h)	1155	605	1155	605
	Mean net deposit accumulation rate (g/m <sup>2</sup> /h) <sup>c</sup>		957		
Straw > 20 wt. %	< 5,000 g/m <sup>2</sup> (2447 g/m <sup>2</sup> ) <sup>a</sup>	(823) <sup>b</sup>	(823) <sup>b</sup>	(906) <sup>b</sup>	(874) <sup>b</sup>
	Mean DDF-rate (g/m <sup>2</sup> /h)	234	313	1245	577
	Number of 6 h period	19	6	8	1
	Mean total deposit shedding rate (g/m <sup>2</sup> /h)	185	124	793	356
	Mean net deposit accumulation rate (g/m <sup>2</sup> /h)	49	189	452	221
	Mean net deposit accumulation rate (g/m <sup>2</sup> /h) <sup>c</sup>		83		426
Straw < 20 wt. %	> 5,000 g/m <sup>2</sup>				
	Mean flue gas temperature (°C)				
	Mean DDF-rate (g/m <sup>2</sup> /h)				
	Number of 6 h period				
	Mean total deposit shedding rate (g/m <sup>2</sup> /h)				
	Mean net deposit accumulation rate (g/m <sup>2</sup> /h)				
	Mean net deposit accumulation rate (g/m <sup>2</sup> /h) <sup>c</sup>				
Straw < 20 wt. %	< 5,000 g/m <sup>2</sup> (792 g/m <sup>2</sup> ) <sup>a</sup>	(773) <sup>b</sup>	(806) <sup>b</sup>	(773) <sup>b</sup>	(806) <sup>b</sup>
	Mean DDF-rate (g/m <sup>2</sup> /h)	221	1913	221	1913
	Number of 6 h period	17	1	17	1
	Mean total deposit shedding rate (g/m <sup>2</sup> /h)	147	660	147	660
	Mean net deposit accumulation rate (g/m <sup>2</sup> /h)	73	1253	73	1253
	Mean net deposit accumulation rate (g/m <sup>2</sup> /h) <sup>c</sup>		139		

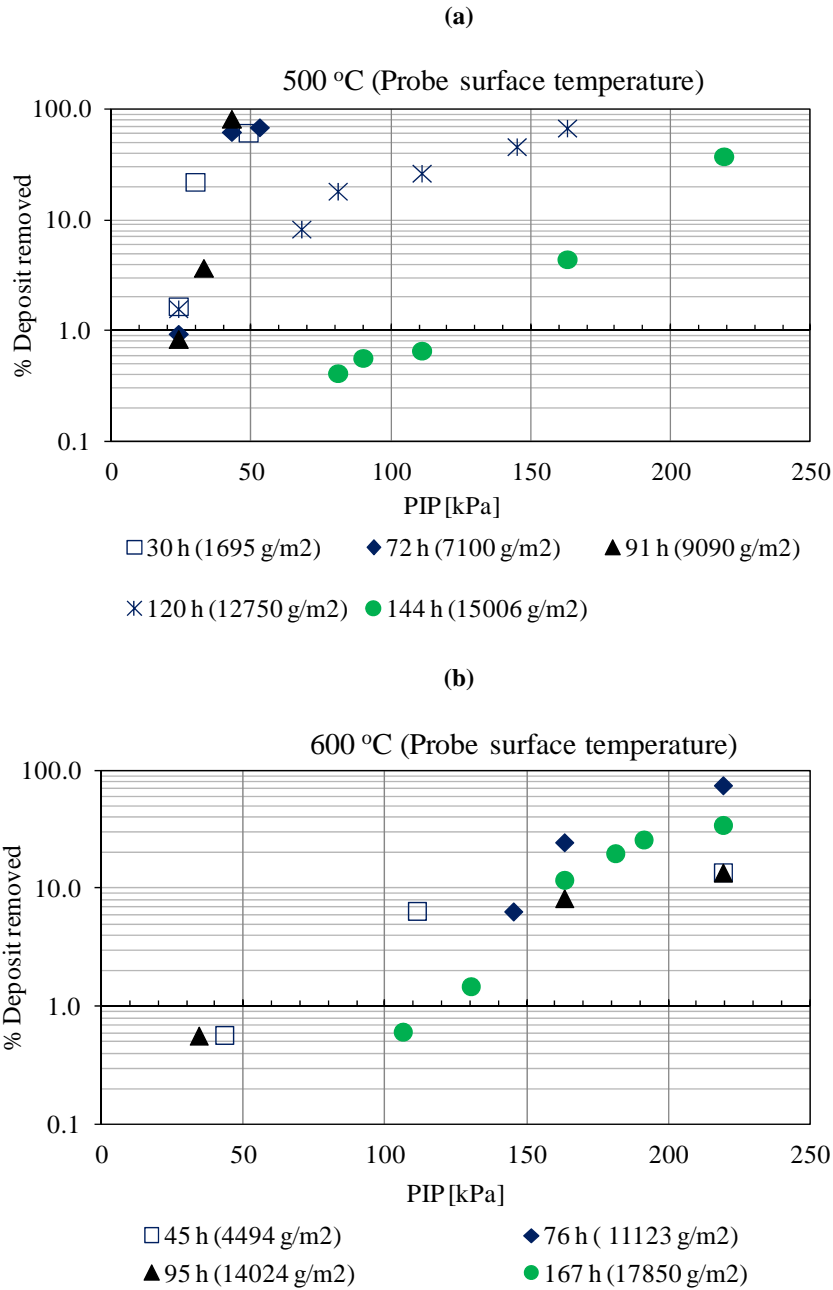


**Figure 5.22:** Impact of flue gas temperature on the net deposit accumulation rate. Data points are from tests 1 to 5. **Graph details:** the particular point shape represents the deposit mass load; the color represents the probe surface temperature, while point with thick and discontinuous outer is representative for straw share in wood.

#### 5.4.5 Deposit Removal by using an Artificial Sootblowing Probe

The PIP needed in the sootblower jet in order to remove the probe deposits at different conditions was investigated, and the results are summarized in Figure 5.23. It can be seen that increasing both probe surface temperatures and exposure times, increased the PIP necessary to remove the deposits. It is also clear that deposits formed at a 500 °C probe temperature and with exposure time less than 91 h, could be removed with a PIP of less than 55 kPa. With an increase in probe surface temperature from 500 °C to 600 °C, the PIP needed to remove the deposits significantly increased. It is also interesting to note, that the PIP seems to be independent of exposure time at the higher probe temperature. The higher probe surface temperature may cause partial melting and/or sintering of the innermost deposit layer (rich in K, Cl and S). This would enhance the adhesion between the deposit and superheater tube. At higher probe surface temperatures (> 550 °C), and longer probe exposure times, a 2–10 mm thick layer formed on the downstream probe surface. The layer grew to make contact with the thick upstream layer. This ring shaped layer will be more difficult to remove, since

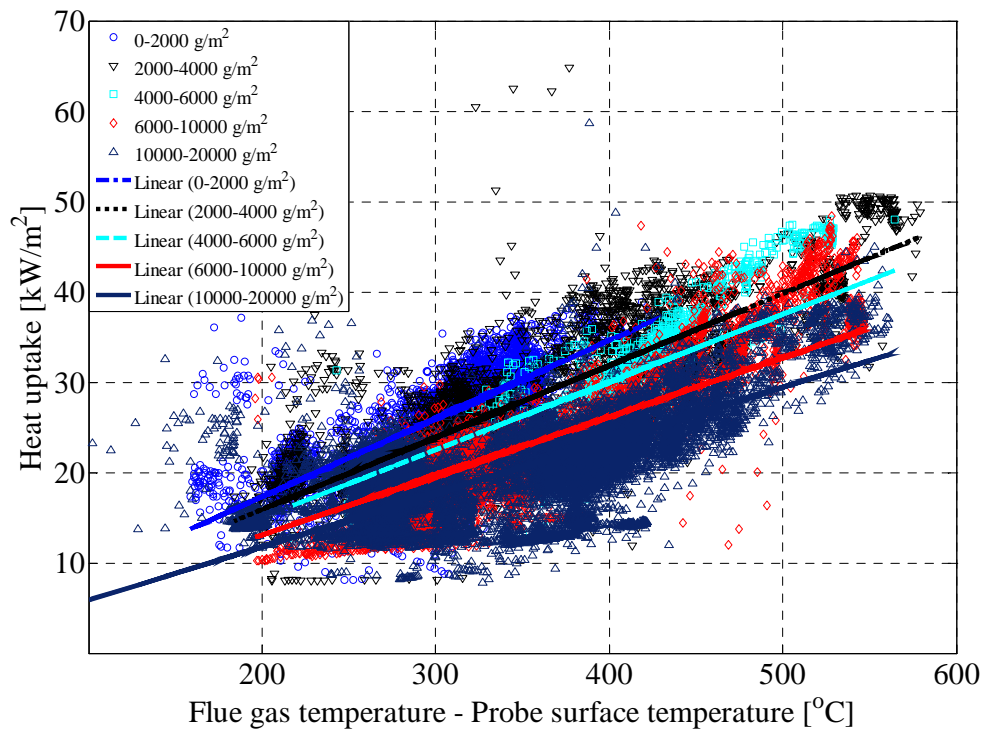
the ring must be broken by the sootblower. At lower surface temperatures (500 °C), the layer formed on the downstream side of the probe was thin, and the distinct upstream layer was easy to remove using the artificial sootblower.



**Figure 5.23:** Percentage of deposits removed as a function of applied Peak Impact Pressure (PIP) at different probe exposure times and deposit mass loads, a) probe surface temperature of 500 °C, b) probe surface temperature of 600 °C.

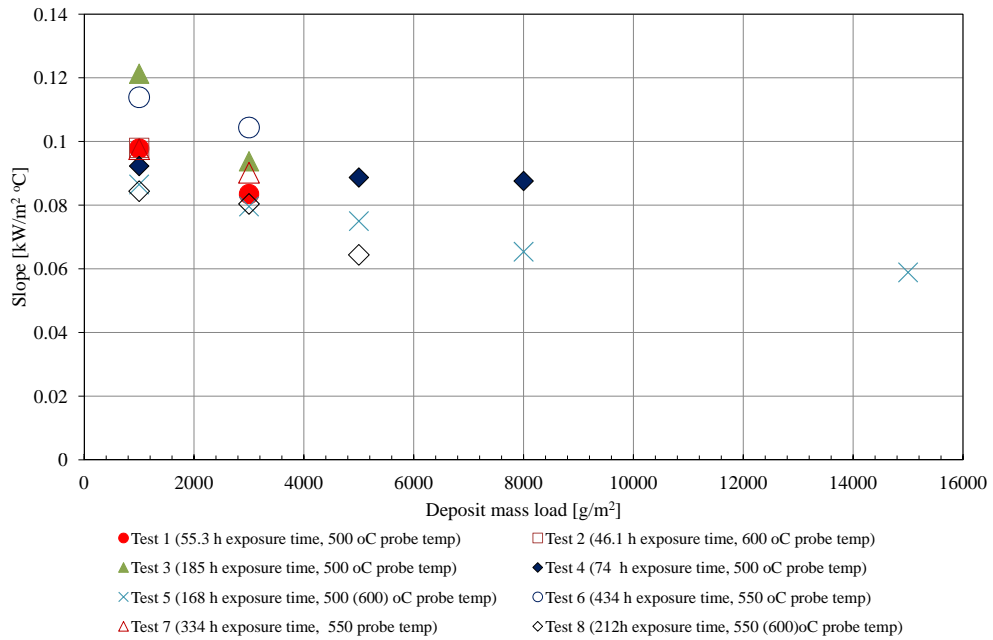
## 5.5 Probe Heat Uptake

The heat uptake in the probe, for different deposit mass loads during test 5 is shown Figure 5.24, as a function of the difference between flue gas temperature and probe surface temperature. It can be seen that when the deposit mass load is higher ( $> 5,000 \text{ g/m}^2$ ), the slope slightly decreases due to the insulation effect of the deposit layers. The slope for different deposit loads for each test was calculated and the combined slopes for all the tests for different probe mass loads are shown in Figure 5.25. A moderate reduction in the probe heat uptake was observed with increase in mass load of deposits on the probe. All the tests provided reasonably similar results. Additionally, it can be seen that up to a deposit mass load of  $5,000 \text{ g/m}^2$  the reduction in heat transfer is steeper, whereafter, the steepness of the curve is reduced. This is consistent with deposit layer being more pronounced on the upstream side, so that most of the heat uptake will occur through the downstream side.



**Figure 5.24:** Impact of temperature difference between flue gas and probe surface on probe heat uptake for different deposit mass loads (test 5). The slope is calculated by a linear fit using equation,  $y = bx$ .





**Figure 5.25:** Sensitivity of heat uptake with change in temperature difference between flue gas and probe surface for different deposit mass loads. Data from all tests (1–8).

## 5.6 Conclusions

A series of full-scale probe measurements have been conducted in a suspension-fired boiler to investigate ash deposit formation and deposit shedding when firing straw and wood. The influence of fuel type, probe exposure time, probe surface temperature, and flue gas temperature on ash deposit formation rate has been investigated. A systematic procedure to determine deposit formation rate from probe measuring deposit data was developed and termed the derivative-based deposit formation rate (DDF-rate). A comparison with previously conducted probe measurements at different straw-fired boilers was made based on another measure of deposit formation rate - integral deposit formation rate (IDF-rate). Ash transformation was investigated by bulk ash analysis of the fuel ash, residual ash and deposit layers. Quantification of naturally occurring deposit shedding, sootblowing deposit shedding and Peak Impact Pressure (PIP) needed to remove the deposits by sootblowing was made. The overall conclusions are the following:

- The bulk chemical composition of straw and wood suspension-fired fly ash shows relatively higher contents of Si, Ca, and lower contents of volatile elements (K, Cl and S), compared to grate firing conditions. However, it was also found that with an increase in fuel ash K/Si

molar ratio the concentration of volatile elements, K, Cl, and, to some extent, S, increased in the fly ash.

- The upstream side deposit outer layers on the probe contain high concentration of Si, K and Ca, indicating that larger particles impact on and stick to the probe on the upstream side. K, S and Cl were found in higher proportions on the downstream side deposit layers indicating that the downstream deposits to a greater extent are formed by thermophoresis and/or condensation of KCl and K<sub>2</sub>SO<sub>4</sub>. The innermost layers were rich in K, Cl and S.
- The Integral Deposit Formation rate (IDF-rate) increases with increased fuel K contents (straw share in wood), and with increase in flue gas temperature, but probe surface temperatures have no significant influence on the IDF-rate. The IDF-rates determined from biomass grate and suspension firing are comparable.
- The DDF-rate increases with increased straw share in wood and with increase in flue gas temperature, but probe surface temperatures have no significant influence on the measured DDF-rates.
- The overall mean DDF-rate also increases with an increase in flue gas temperature and the overall DDF-rate levels between 234 to 3105 g/m<sup>2</sup>/h were observed.
- Video recordings revealed that deposit shedding was primarily through debonding, where a deposit layer is being removed due to a break off of the deposit from the tube surface.
- It was observed that the shedding process is a stochastic process, where the shed amounts are highly variable even at constant conditions. We believe the amount of deposit shed is strongly related to the strength of the inner most salt rich deposit layer.
- The deposit shedding process was characterized by calculation of the average amount of deposit removed at a shedding event [g/m<sup>2</sup>] and the frequency of the shedding events [h<sup>-1</sup>] in 6 h periods. The average shedding event magnitude was 716 g/m<sup>2</sup> during natural deposit shedding and 805 g/m<sup>2</sup> during plant sootblower induced shedding. The shedding frequencies were 0.81 h<sup>-1</sup> and 0.89 h<sup>-1</sup> during natural deposit shedding and plant sootblower shedding events, respectively. Based on the shedding magnitude and frequency it was possible to calculate a shedding rate [g/m<sup>2</sup>/h].
- The deposit shedding rates increased at high flue gas temperatures (> 850 °C) and high probe deposit mass loads (> 5,000 g/m<sup>2</sup>) where also high deposit formation rates are observed (DDF-rate).

- The shedding rate is in most cases higher at a probe temperature of 500 °C than at a probe temperature of 600 °C.
- The net deposit accumulation rate increases with increase in flue gas temperature. Increased flue gas temperatures probably increase the fraction of molten ash particles as well as provide an increased content of gas phase alkali species, and both will lead to an increased deposit formation rate. The increase in DDF-rate was larger than the increase in deposit shedding rate with increased flue gas temperature.
- The net deposit accumulation rate is low (452 g/m<sup>2</sup>/h) at lower deposit mass load (< 5,000 g/m<sup>2</sup>) on the probe, compared to a value of 1155 g/m<sup>2</sup>/h for deposit mass load greater than 5,000 g/m<sup>2</sup> (probe temperature 500 °C, flue gas temperature about 900–910 °C and straw share more than 20 wt.%).
- Generally no clear tendency for the impact of probe surface temperature on net deposit accumulation rate was seen.
- A sootblower probe was used to investigate the needed PIP to remove the deposits. At lower temperatures (500 °C), the deposits formed at a exposure time of less than 91 h could be removed with a PIP of less than 55 kPa. At higher probe surface temperature (> 550 °C), the PIP needed to remove the probe deposits significantly increases.

## Chapter 6

# Ash Deposit Build-up and Shedding during Wood Suspension Combustion with Coal Ash Addition

### 6.1 Introduction

In the recent decades, the focus to substitute fossil fuels by wood has significantly increased the interest in efficient use of wood in large suspension-fired boilers. However, the presence of alkali metals (K) and chlorine (Cl) in wood - even in small amount - may induce operational problems due to ash deposit formation, corrosion and deactivation of SCR catalyst [2, 4, 10, 17]. However, because of the availability of limited data about wood suspension firing, an improved knowledge on the transient deposit formation and removal is essential to optimize design and operation [27, 38, 108]. Fewer full-scale pulverized wood-firing investigations are reported in the literature, and the most recent ones are by Skrifvars et al. [38], Jensen et al. [46] and Bashir et al. [101, 108]. In addition, most of these studies have been based on short testing time (up to couple of hours), while more extensive full-scale measurements are rare to find [101, 108]. Therefore, more detailed and extensive full-scale studies on transient deposit formation and shedding when firing wood with coal ash addition will improve our understanding of deposit formation and shedding processes. This chapter is about the full-scale probe measurements conducted at the Avedøreværket Unit 2, a 800 MW<sub>th</sub> suspension boiler, firing wood and natural gas. The measurements were conducted with and without the addition of coal fly ash as an additive to capture potassium (K) from wood firing. Investigations of deposit formation rate were made by use of the horizontal advanced online ash deposition probe. The influence of flue gas temperature, probe surface temperature and

boiler load on ash deposition propensity was investigated with and without the addition of coal ash. It was revealed that the addition of coal fly ash could significantly influence the ash deposition behaviors and the deposit properties.

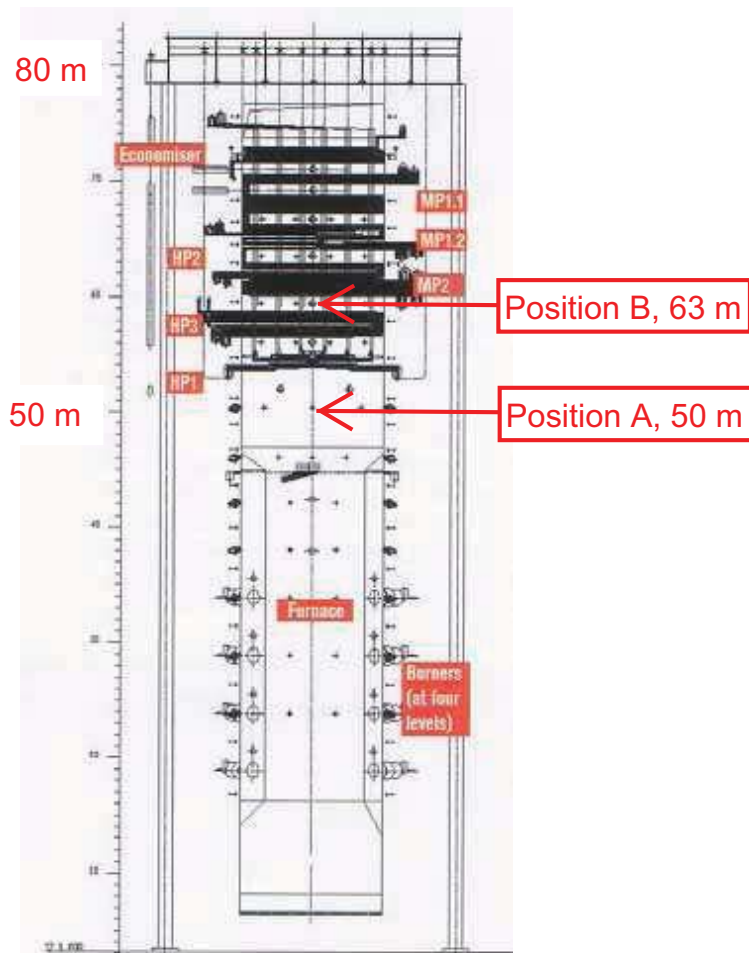
## 6.2 Equipments, Materials and Methods

### 6.2.1 Boiler

The probe measurements were conducted at the Avedøre Power Station, Unit 2 (AVV2), firing wood and natural gas in suspension. The AVV2 boiler, located in the Copenhagen area, is a multi-fuel suspension-fired boiler that can apply wood, natural gas and heavy fuel oil as fuel. The schematic drawing of the boiler is shown in Figure 6.1. The AVV2 boiler is a 80 m high Benson type boiler with a thermal capacity of 800 MW<sub>th</sub>. Overall, there are three sub-units, a straw-fired grate boiler, a suspension-fired boiler and two gas turbines [24]. In the lower part of the boiler tower is the combustion chamber, which has 16 burners in four levels (see Figure 6.1). There are three mills used to grind wood pellets, and the pulverized wood after being ground in the mills is blown into the burners, where the fuel particles are burned in suspension. Above the combustion chamber is a radiation shield, followed by the superheaters and economizers. The AVV2 boiler is being able to operate in a pure condensing mode, a pure back pressure mode or any combination. Operating in pure condensing mode, an electrical efficiency of 48% is obtainable. If operated in pure back pressure mode, using the thermal energy of the condensed steam for district heating, the total efficiency can be as high as 94% [24].

### 6.2.2 Fuels

The fuels fired during the measurements were wood-dust and natural gas. As it was not possible to obtain fuel samples, the composition of the applied fuels is adopted from previous measurements at AVV2 ([24], Table 6.1). This may introduce slight uncertainties to the results in this work. Fuel analysis shows that the wood fuel has small content of potassium (K) and chlorine (Cl), while calcium (Ca) and silicon (Si) are present in significant amounts. The coal fly ash used as an additive contains significant content of aluminum (Al) and silicon (Si), indicating possible potential of coal fly ash to capture potassium (K) formed during wood combustion. The natural gas analysis shows a large content of CH<sub>4</sub> and C<sub>2</sub>H<sub>6</sub>.



**Figure 6.1:** Schematic view of the AVV2 boiler with identified probe measuring positions. Position A: Flue gas temperature 1250–1350 °C, Position B: Flue gas temperature 750–800 °C.

### 6.2.3 Ash Deposition Probe

Details of the complete probe system used during the measurements have been described in Chapter 3. However, in the start of the current measurements, due to higher flue gas temperature ( $> 1250$  °C) at location A (Figure 6.1), it was not possible to keep the probe surface temperature between 500 and 600 °C. A possible reason was that the boiler was running with a high wood-fuel input leading to high flue gas temperatures at the probe measuring position. The problem of keeping the probe surface temperature at the desired levels was then solved by mounting the probe somewhat retracted. A special port extension pipe was installed to keep the probe only 772 mm inside the boiler. This solution believed to work satisfactory if the probe is inserted slowly in the boiler because with the formation of a small layer of

**Table 6.1:** Analysis of the fuels fired and added coal fly ash. a.r.: as received, d.b.: dry basis. Adopted from Jensen et al. [24].

Parameter	Wood	Coal ash	Parameter	Natural gas
Ash contents (wt.% a.r.)	1.0	–	–	–
Moisture (wt.% )	5.8	–	–	–
Higher heating value ( $\frac{MJ}{kg}$ d.b.)	17.0	–	Heating value ( $\frac{MJ}{kg}$ )	48.1
C (wt.% d.b.)	46.84	–	CH <sub>4</sub> (mol.%)	89.06
S (wt.% d.b.)	0.009	0.26	C <sub>2</sub> H <sub>6</sub> (mol.%)	6.08
N (wt.% d.b.)	0.094	–	C <sub>3</sub> H <sub>8</sub> (mol.%)	2.47
H (wt.% d.b.)	5.91	–	iC <sub>4</sub> H <sub>10</sub> (mol.%)	0.39
O (wt.% d.b.)	40.53	–	nC <sub>4</sub> H <sub>10</sub> (mol.%)	0.54
Cl (wt.% d.b.)	0.0043	0.0	C <sub>5</sub> H <sub>12</sub> (mol.%)	0.11
Al (wt.% d.b.)	0.014	14.0	nC <sub>5</sub> (mol.%)	0.08
Ca (wt.% d.b.)	0.14	5.2	C <sub>5+</sub> (mol.%)	0.05
Fe (wt.% d.b.)	0.013	2.3	N <sub>2</sub> (mol.%)	0.29
K (wt.% d.b.)	0.048	0.45	CO <sub>2</sub> (mol.%)	0.91
Mg (wt.% d.b.)	0.024	0.91	–	–
Na (wt.% d.b.)	0.005	0.11	–	–
P (wt.% d.b.)	0.0058	0.81	–	–
Si (wt.% d.b.)	0.17	20.0	–	–

deposits on the probe, the probe surface temperature fluctuations were considerably reduced. The drawing of the complete modified probe system used at location A is shown in Figure 6.2 and Figure 6.3. At location B (Figure 6.1), the probe system was used without significant changes and about 1400 mm probe was inside the boiler.

### 6.2.4 Procedure of Measurements

A series of deposit probe measurements were conducted in a region just below the radiation shield (location A) and in the superheater region (location B). As illustrated in Figure 6.1, the first location (location A) is situated at a level of ~50 m, which is just below the radiation shield of the boiler. This location has a very high flue gas temperature (~ 1250–1350 °C) when the boiler is close to full-load. The second location (location B) is situated at a level of ~63 m, which is in the superheater region of the boiler. The flue gas temperature at this location is about 750–800 °C for the full-load boiler.

The overall experimental summary is shown in Table 6.2. The first five tests were performed at location A in the presence of coal ash. The first three tests are at higher boiler loads, while test four is long due to the fact that the boiler was running smoothly for a longer period at lower boiler load, and test 5 is based on measurements at moderate boiler load. Test 6 and test 7 were conducted without the addition of coal ash at location A. Test 8 and test 9 were performed at location B without and with the addition of coal fly ash, respectively. Tests 10–13 were performed at location A with

the addition of of coal fly ash.

The biomass load was calculated by using wood fuel flow rate and heating value of wood. The equation used is,

$$\text{Biomass Load (\%)} = \frac{\text{Wood fuel flow rate} \times \text{Heating value of wood}}{800\text{MW}_{th}} \cdot 100 \quad (6.1)$$

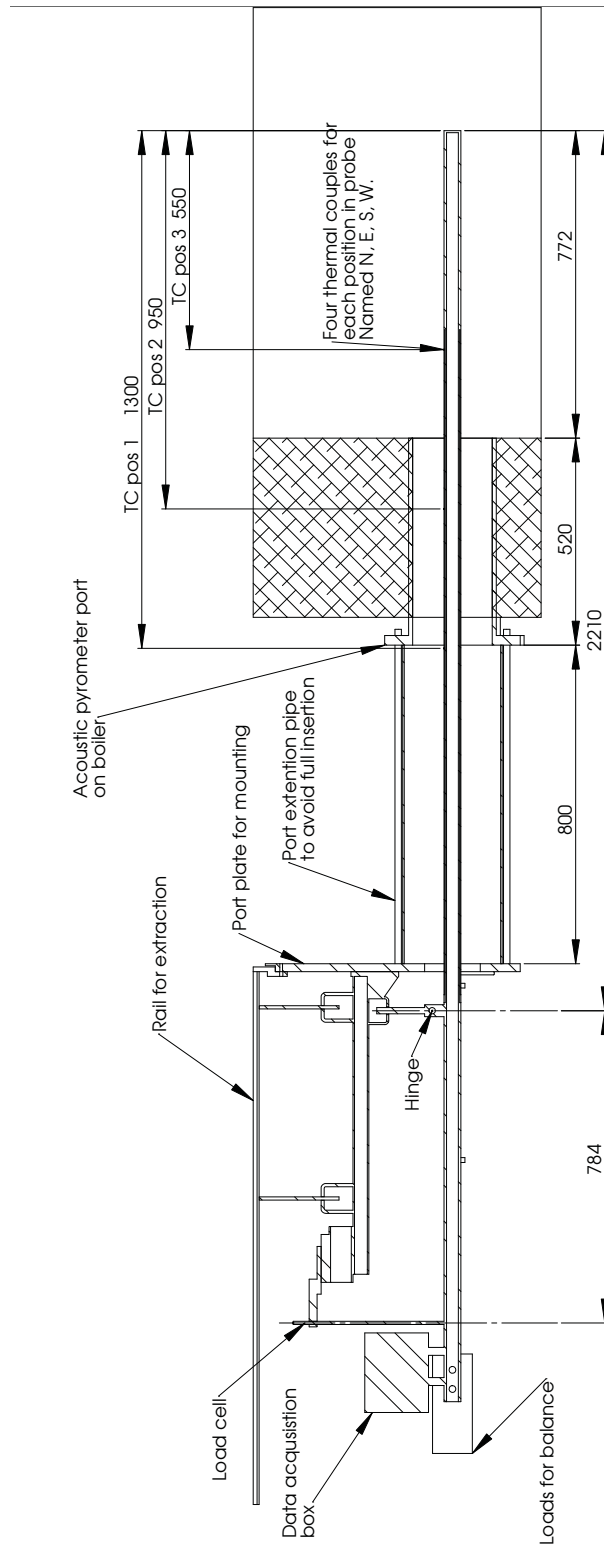
As the interpretation of full-scale measurement data can be challenging and the exact evaluation of the influence of each parameter can be difficult to obtain. In the current measurements, it was tried to investigate the influence of boiler load, probe surface temperature and flue gas temperature on ash deposition propensity with and without the addition of coal ash. The target probe surface temperatures was tried to be kept between 500 and 550 °C. However, even though only 772 mm probe was inside the boiler, due to higher flue gas temperature, slight fluctuations in the probe surface temperature were observed. The control parameters for the air flow to the probe added additional problems. However, by adjusting the air pressure to the controller and finding appropriate control parameters for the controller, the fluctuations in the probe surface temperature were considerably reduced.

The sootblowers located very near to location A (0.8 m to the right on the same wall and about 3 m to the right on the right wall) were shut down during all the tests, while sootblowers located further away from the probe measuring position were still in operation.

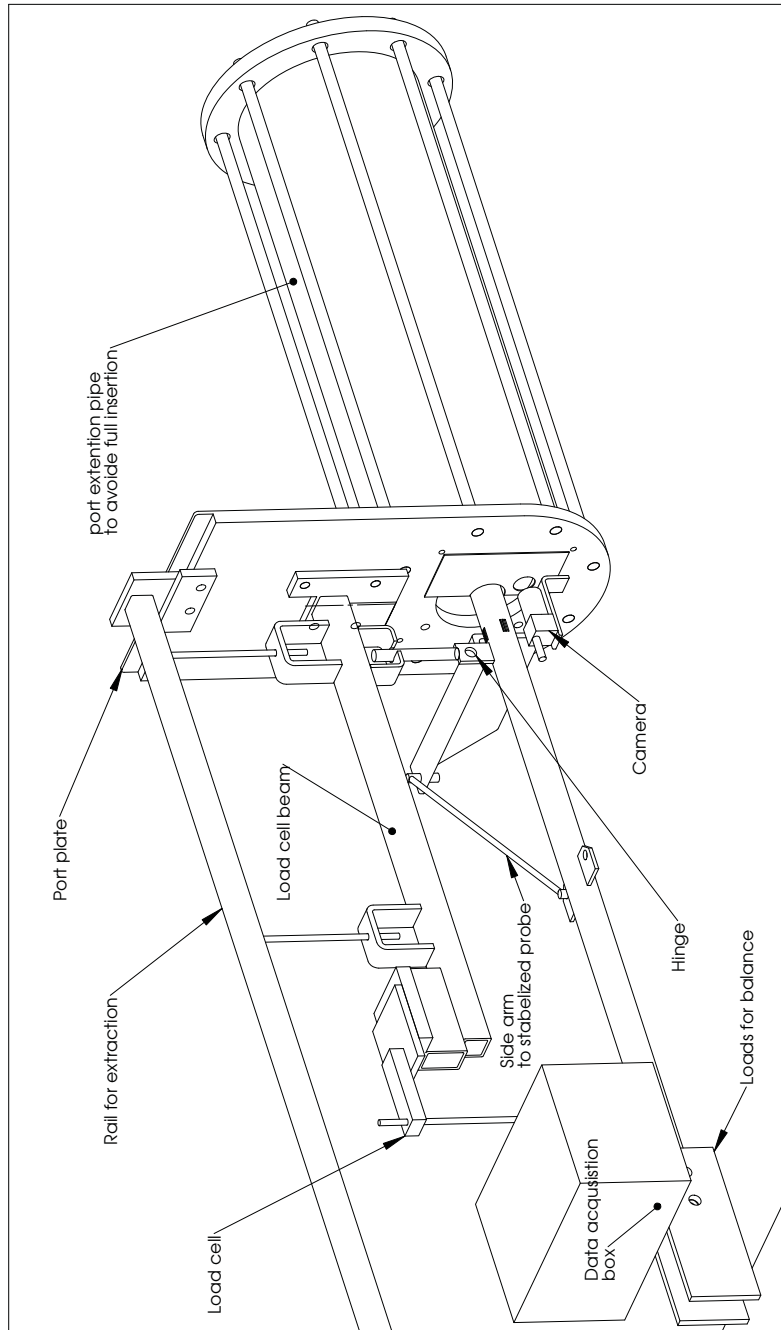
A special port for video monitoring was mounted at the right wall of the probe measuring position. The port was cooled both by water and air, and a CCD (charge-coupled device) camera was placed in the port to register the deposit formation and shedding processes on the probe. In some experiments, an additional camera was placed just below the probe (see Figure 6.3). The flue gas temperature at location A was continuously measured nearer to the probe location (at the right wall), by using a S-type thermocouple. In addition, a suction pyrometer (International Flame Research Foundation model, IFRF [100]) was also used for some periods during each test. Due to strong radiation effects in the probe measuring area at location A, the flue gas temperature measured by the thermocouple was lower than the one measured by using the suction pyrometer.

During measurements at location A (test 6, 7), deposit mass uptake signals were influenced by water condensation/evaporation in the probe due to water leakage in the probe. The probe was repaired later on.





**Figure 6.2:** Schematic drawing of the modified probe system (location A).



**Figure 6.3:** Outside view of the modified probe system for location A.

**Table 6.2:** Matrix of the tests conducted at AVV2. (✓) indicate measurements conducted with the addition of coal fly ash. (÷) indicate the measurements where no coal fly ash addition was made. <sup>a</sup> problem of water leakage from the probe was experienced.

Test no.	1	2	3	4	5	6 <sup>a</sup>	7 <sup>a</sup>	8	9	10 <sup>a</sup>	11	12 <sup>a</sup>	13
Start date (Year)	05/04 (2011)	05/04 (2011)	06/04 (2011)	08/04 (2011)	13/04 (2011)	21/11 (2011)	25/11 (2011)	30/11 (2011)	05/12 (2011)	09/12 (2011)	12/12 (2011)	13/12 (2011)	14/12 (2011)
Location	A	A	A	A	A	A	A	B	B	A	A	A	A
Exposure time (h)	26	16	28	116	52	101	66	40	24	26	18	25	20
Coal ash addition	✓	✓	✓	✓	✓	÷	÷	÷	✓	✓	✓	✓	✓
Boiler load (%)	91	98	88	41	76	92	79	81	96	93	86	83	89
Biomass load (%)	44	81	72	18	59	83	77	72	87	78	79	73	81
Probe temperature (°C) (target)	550	550	550	500	500	550	550	550	550	550	550	550	550

The probe system used at location B was slightly different. The opening to the boiler at location B has an inner diameter of 80 mm, which is much smaller than that of location A. Besides, the boiler wall at location B vibrates significantly during the measurement. In order to minimize the effect of wall vibration, a special rig was made and installed on the floor, and the probe was mounted on the rig, instead of on the vibrating boiler wall. Since the flue gas temperature was relatively low at location B, the probe was 1400 mm inside the boiler during the measurements. In order to minimize the effect of sootblowing, the two nearby soot-blowers were shut off during the measurement period. Flue gas temperature at location B was measured at the wall opposite of the deposit probe, because there was no opening available near-by. The temperature measurement was carried out by using a K-type thermocouple placed in a metallic protective shell and a suction pyrometer as mentioned above. At location B, video monitoring was not possible due to the small opening size and the availability of boiler openings.

## 6.3 Results and Discussion

### 6.3.1 Data Treatment

A large set of data was obtained from the Power Plant and the probe measurements, and a similar data treatment procedure as described in Chapter 5 was adopted for each test. As an example, the detailed signals of flue gas temperature, deposit mass uptake, events of plant sootblowing and probe heat uptake during test 3 are shown in Figure 6.4. The black lines in the deposit mass uptake signal (Figure 6.4) indicate the events when the nearby plant sootblowers were in operation. It was observed that even though the plant sootblowers located very near (0.8 m to the right on the same wall and about 3 m to the right on the right wall) were turned off, the rest of the sootblowers were to some extent effective in sometimes causing fluctuations to the deposit mass uptake signals.

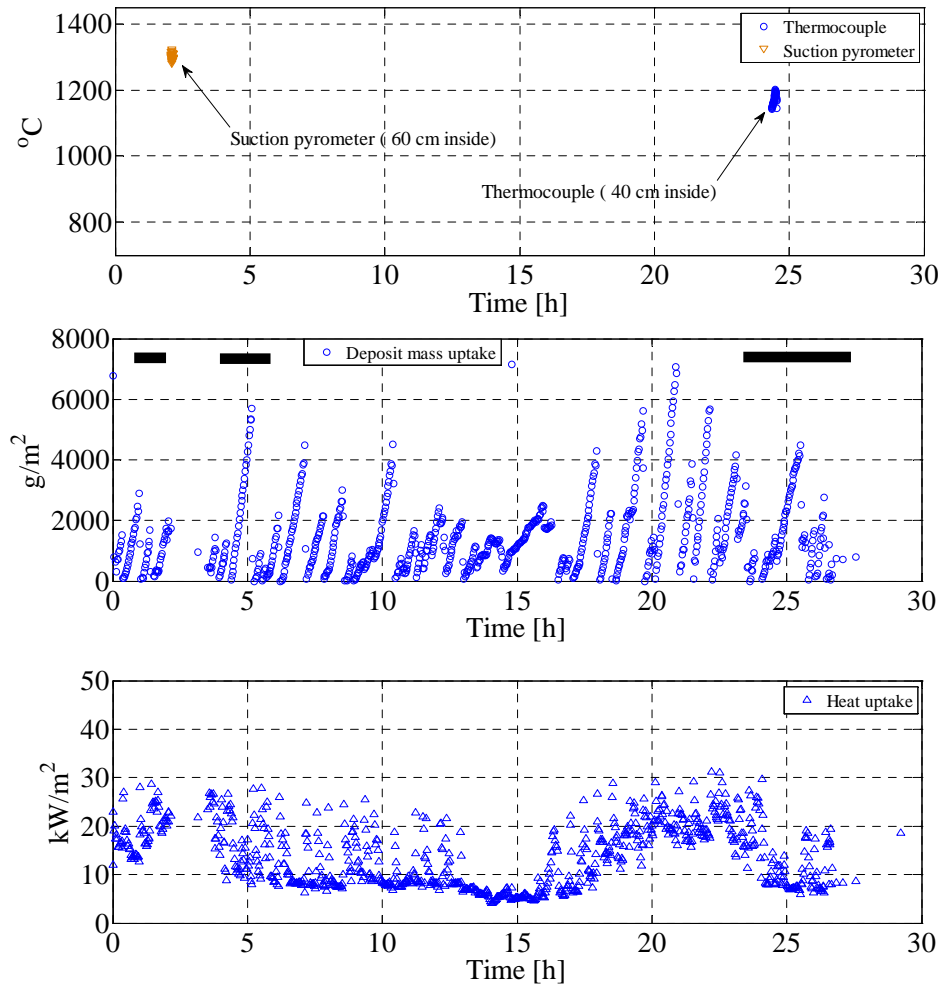
The flue gas temperature measured during test 3 was around  $1300 \pm 75$  °C based on the flue gas temperature measurements with suction pyrometer for a short period (about an hour). The flue gas temperature for the rest of the test was estimated based on the thermocouple readings and difference between temperature measured by suction pyrometer and thermocouple. The deposit mass uptake signals indicate a number of events with steep increase and then a sudden drop due to shedding of deposits (Figure 6.4). The detailed signals of flue gas temperature, deposit mass uptake, sootblowing events, heat uptake, fuel flow, boiler load, biomass load, and fly ash flow for test 3 and the rest of the tests can be found in Appendix C.

Looking at the deposit mass uptake data in the different tests the ten-

dependencies observed are the following (tests in italic format were performed without the addition of coal ash):

- Test 1. A lot of build-up and fast shedding of all the deposits up to 14 h of exposure time. About 20 events in the first 14 h can be found where all of the deposits attached to the probe are removed naturally. After 15 h the deposit level is constant at 4,000 g/m<sup>2</sup>.
- Test 2. During all the measuring time (total 15 h) there were observed fast deposit build-up to maximum 6,000 g/m<sup>2</sup> and then sudden shedding of all deposit. A lot of shedding events were observed.
- Test 3. A similar deposit build-up behavior as in test 2, but the probe was placed in the boiler for 27 h.
- Test 4. A slow deposit formation process up to 10 h and then there is observed a constant deposit build-up up to a probe residence time of 110 h. The boiler was running at lower biomass and boiler load.
- Test 5. Only small amounts of deposits are observed on the probe in most of the time (less than 200 g/m<sup>2</sup>). Several cases of fast deposit build-up and deposit shedding appear sometimes.
- *Test 6.* The test was conducted at location A without the addition of coal ash. During the measurement, problems of water leakage inside the deposit probe occurred and the deposit mass uptake signals were not accurate. The deposit shedding occurred in the form of debonding.
- *Test 7.* This test was conducted at location A without the addition of coal ash. In this test, the deposit level was reached up to a maximum value of 5,000 g/m<sup>2</sup>. The number of shedding events were less compared to the conditions when coal ash was added.
- *Test 8.* This test was conducted at location B without the addition of coal ash. The deposit level was close to 1,000 g/m<sup>2</sup>. No big shedding event was seen from the images collected.
- Test 9. This test was conducted at location B with addition of coal ash. The deposit mass uptake was lower (about 200 g/m<sup>2</sup>), compared to test 8. The addition of coal ash probably has reduced the ash deposition at this location.
- Test 10. This test was conducted at location A with addition of coal ash. In this test, again the problem of water leakage in the probe occurred, thereby except the initial 1.3 h, the deposit mass uptake signals are not reliable.

- Test 11. This test was conducted at location A with addition of coal ash. In this test the deposit level was between 400 and 500 g/m<sup>2</sup>, with smaller shedding events.
- Test 12. This test was conducted at location A with addition of coal ash. In this test, again the problem of water leakage in the probe occurred.
- Test 13. This test was conducted at location A with addition of coal ash. In this test, fast deposit build-up and shedding events were seen.



**Figure 6.4:** Flue gas temperature, deposit mass uptake, sootblowing events and probe heat uptake during test 3. The black lines in the middle figure indicate the time when the surrounding sootblowers were in operation.

### Ash Deposition Propensity

The amount of deposit collected on the probe is a function of both the deposit formation process and shedding events as shown in Figure 6.4. Typical example of the deposit shedding during test 6 is shown in Figure 6.5. Even at very high flue gas temperatures (close to 1300 °C), deposit removal through surface melting was not identified. It can also be seen that the deposits are not strongly attached to the probe and were removed through debonding.

In the presence of significant number of large shedding events, DDF-rate (see chapter 5 for details) determination can identify the momentary deposit formation rate. In addition, in the present study, the DDF-rate may be influenced by the coal ash flow rate. Therefore, ash deposition propensity provides useful information about the amount of ash actually depositing on the deposit probe. The DDF-rate represents the transient deposit build-up meaning that if the DDF-rate is equal to the total ash flux, all of the ash the probe will experience is going to stick to the deposit probe. The calculated DDF-rate can then be used to determine ash deposition propensity using,

$$\text{Ash deposition propensity} = \text{Impaction efficiency} \times \text{capture efficiency} \quad (6.2)$$

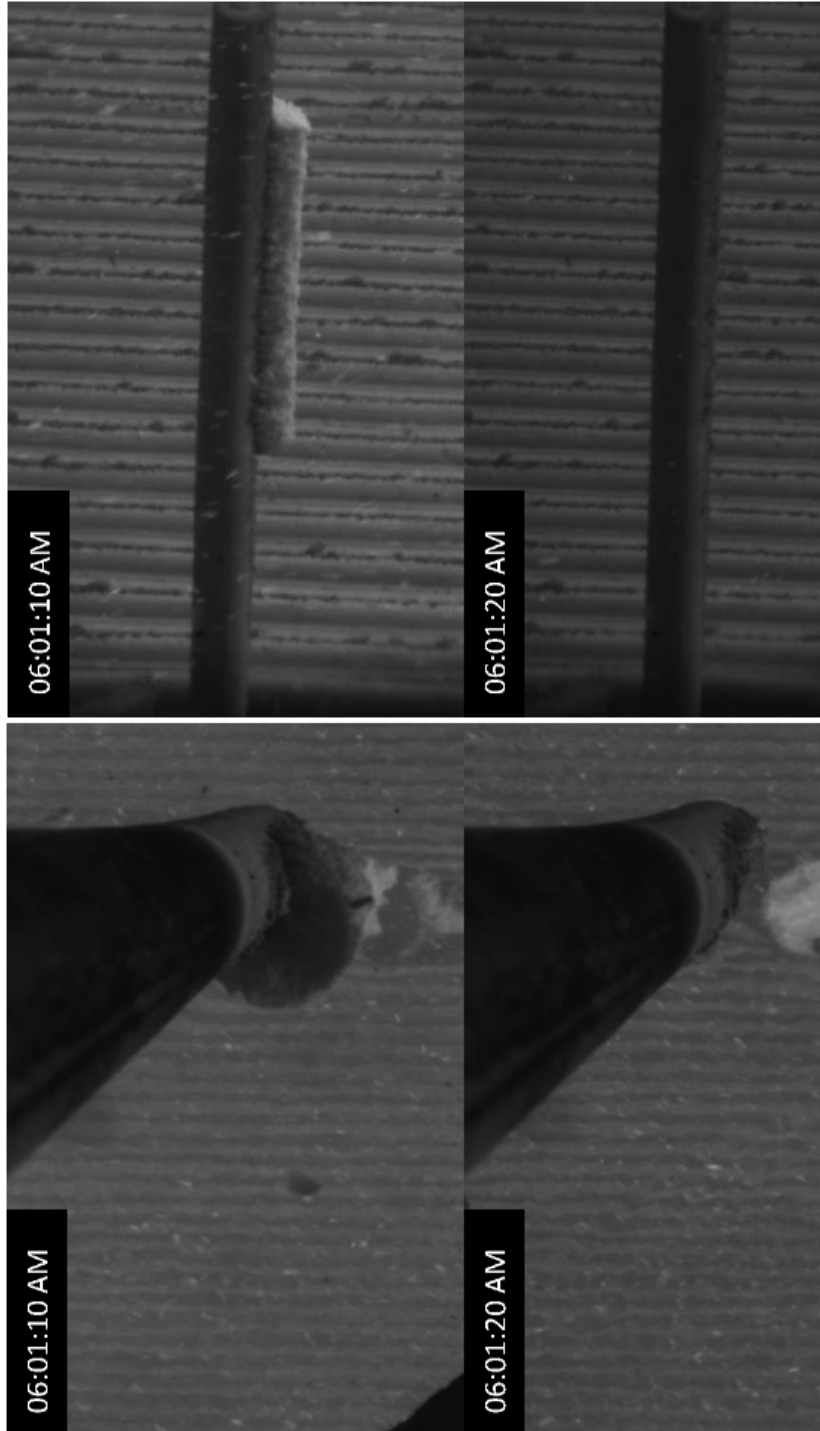
$$\text{Ash deposition propensity} = \text{Collection efficiency} \quad (6.3)$$

$$\text{Ash deposition propensity} = \frac{\text{DDF-rate}}{\text{Ash flux}} \quad (6.4)$$

$$\text{Ash flux} = \frac{m_f \cdot X_a}{A_r} + \frac{ash_{coal}}{A_r} \quad (6.5)$$

In the above equation,  $m_f$  represents the wood fuel flow to the boiler,  $X_a$  represents fraction of ash in dry wood fuel,  $ash_{coal}$  is for the coal ash flow, and  $A_r$  represents the X-sectional area of the boiler.

The calculated DDF-rate and ash deposition propensity calculated during test 3 are shown in Figure 6.6 and Figure 6.7, respectively. Both the DDF-rate and ash deposition propensity decrease at decreased biomass and boiler load (between 13 to 17 h, Appendix C). DDF-rate curve shows a big peak after the introduction of fuel through mill 10 after 17 h of exposure time, in the presence of a relatively larger natural gas flow ( $\sim 4 \frac{kg}{s}$ ). The calculated ash deposition propensity almost follows the same trend as the DDF-rate. The calculated DDF-rates and ash deposition propensities for each test can be found in Appendix C, while an overview of the conducted measurements is presented in Table 6.3.



**Figure 6.5:** Typical example of the deposit shedding during test 6. The pictures are obtained on 25/11/11 (around 91.7 h). The left pictures are from the camera placed below the probe, while the right pictures are from the camera placed on the right side of the probe.



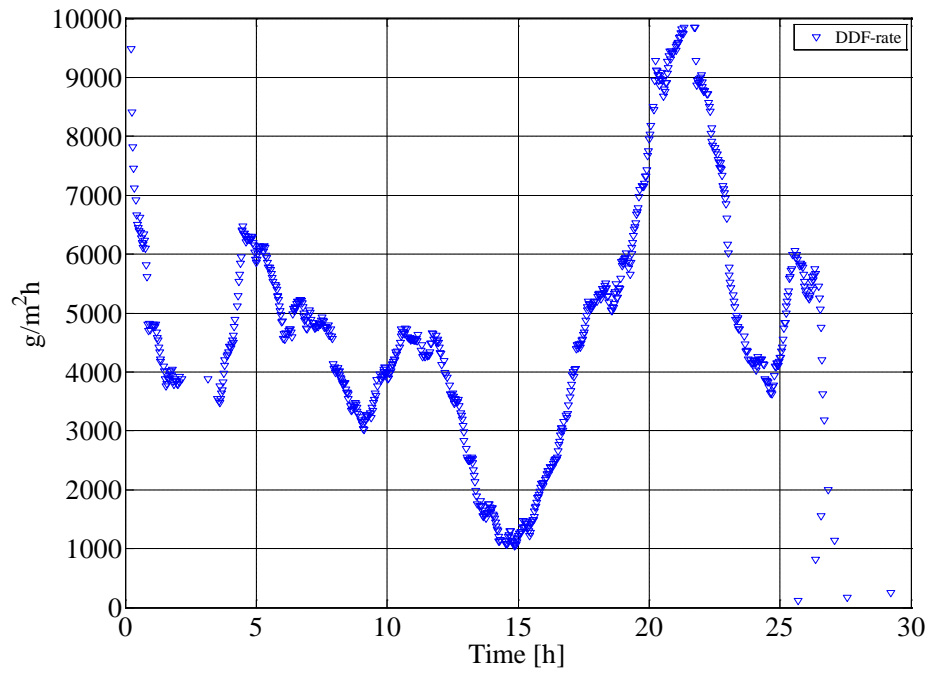


Figure 6.6: DDF-rate calculated during test 3.

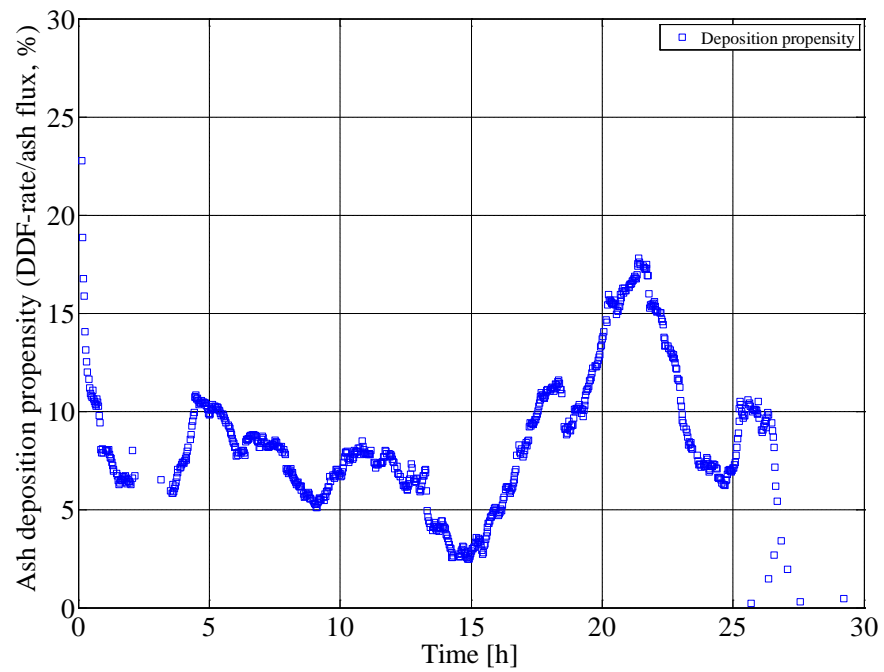


Figure 6.7: Ash deposition propensity calculated during test 3.

**Table 6.3:** Summary of the main results of the measurements conducted at AVV2. <sup>a</sup> standard deviation, <sup>b</sup> mean of overall test, <sup>c</sup> values taken where no experimental problem (water evaporation in the probe etc.) occurred.

	Unit	Test 1	Test 2	Test 3	Test 4	Test 5	Test 6 <sup>c</sup>	Test 7	Test 8 <sup>c</sup>	Test 9	Test 10 <sup>c</sup>	Test 11	Test 12 <sup>c</sup>	Test 13
Location	-	A	A	A	A	A	A	A	B	B	A	A	A	A
Exposure time	h	26	16	28	116	52	~57 <sup>c</sup>	66	0-30 <sup>c</sup>	24	0-1.3 <sup>c</sup>	18	18.8-25.1 <sup>c</sup>	20
Boiler load	%	91	98	88	41	76	94	79	84	96	90	86	83	89
Biomass load	%	44	81	72	18	59	85	77	75	87	84	79	82	81
Coal ash addition	-	✓	✓	✓	✓	✓	÷	÷	÷	✓	✓	✓	✓	✓
Natural gas flow <sup>b</sup>	$\frac{kg}{s}$	7.9	2.6	1.6	3.9	2.5	1.4	0.2	1.3	1.4	1.5	0.0	1.5	1.1
Probe surface temperature (mean of N3, E3, S3, W3)	°C	577	583	561	483	525	544	520	523	527	541	530	780	468
Coal ash to wood ash ratio	-	3.6	4.4	4.7	7.4	5.8	0.0	0.0	0.0	4.1	-	4.5	-	4.4
Ash flux	$\frac{g}{m^2/h}$	28886	58782	54931	20580	45571	11567	10422	10157	59689	59396	58600	58708	58663
Flue gas temperature	°C	1350	1250	1300	950	1075	1278	1258	776	768 <sup>b</sup>	1269 <sup>b</sup>	1260 <sup>b</sup>	-	1319
(st. dev.) <sup>a</sup>	°C	±75	±75	±75	±75	±75	-	±29	-	±7	±22	±30	-	±32
DDF-rate	$\frac{g}{m^2/h}$	4717	4501	4849	96	653	268	-	86	86	6197	543	3963	-
(st. dev.) <sup>a</sup>	$\frac{g}{m^2/h}$	±23051	±3473	±2603	±647	±1055	-	-	-	-	-	-	-	-
Ash deposition propensity	%	16.33	7.66	8.83	0.47	1.43	2.35	-	0.8	0.1	10.4	0.9	6.8	-
(st. dev.) <sup>a</sup>	%	±79.8	±5.91	±4.73	±3.14	±2.31	-	-	-	-	-	-	-	-
NOx (6% O <sub>2</sub> ) <sup>b</sup>	ppm	170	191	172	99	118	134	144	128	184	170	147	125	121
CO <sup>b</sup>	ppm	48	5	37	1	20	86	60	40	7	18	37	29	32
O <sub>2</sub> <sup>b</sup>	%	2.4	2.8	2.9	3.3	3.0	3.0	3.2	3.0	3.0	3.0	3.1	3.1	3.1
SO <sub>2</sub> <sup>b</sup>	ppm	0.33	4.82	8.23	-	4.32	-2.30	-2.40	-2.40	14.50	12.70	14.70	15.50	11.60

### 6.3.2 Influence of Local Conditions on Ash Deposition Propensity

To make it possible to investigate the influence of different operational parameters on ash deposition propensity, mean values of each test were determined. It was possible to analyze the influence of probe surface temperature, local flue gas temperature and boiler operational parameters on ash deposition propensity. However, it is important to mention that different changes in operational parameters are not independent. Table 6.3 provides an overview of the conducted measurements. It should be noted that for test 6, only the time periods that are believed not significantly influenced by water condensation/evaporation are considered. For test 8, only the time period before the moving of boiler wall ( $< 30$  h) is taken into account. For test 12, the results are shown after the cooling water shut-off problem occurred.

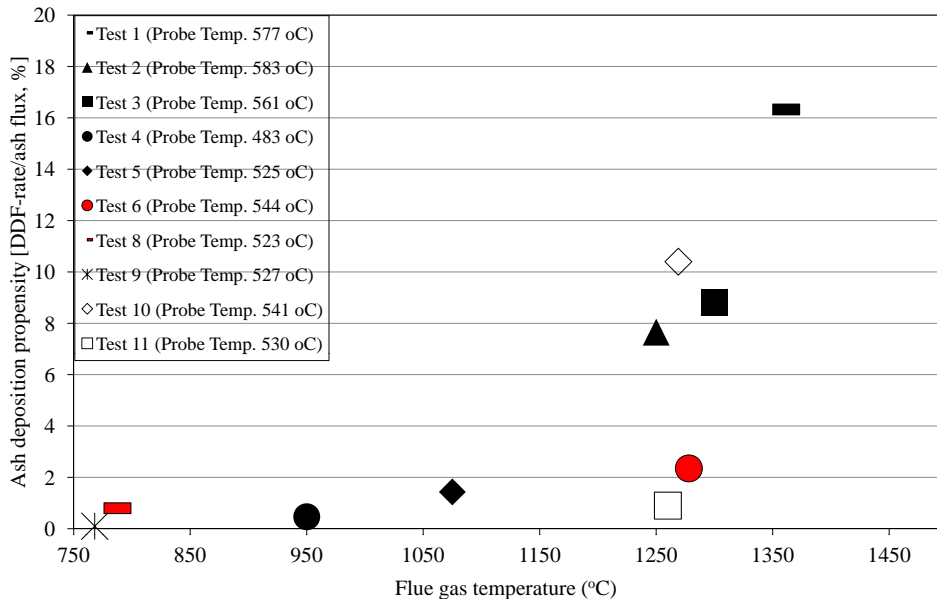
The impact of local flue gas temperature on ash deposition propensity (deposition flux/ash flux, %) is evident from Figure 6.8. It can be seen that ash deposition propensity increased with increasing flue gas temperature. The possible reason for increased ash deposition propensity at higher flue gas temperatures could be that the particles hitting the probe are partially molten, whereby a larger fraction of impacted ash particles sticks to the deposit. However, some of the parameters in Table 6.3 cannot be regarded as independent. An increase in the biomass load seems to have induced an increase flue gas temperature and decreased the coal to wood ash ratio. The impact of coal ash to fuel ash ratio on ash deposition propensity is shown in Figure 6.9 (a). It can be seen that deposition propensity increased with decrease in coal ash to fuel ash ratio. However, as shown in Figure 6.9, most of the points of high coal ash to wood ash ratio also have low biomass and boiler load. Changes in boiler load influence the flue gas temperature and the coal ash to wood ash ratio was lowest in the tests with high local flue gas temperature. For test 4, 8 and 9 (lower ash deposition propensity) the flue gas temperature was less than or equal to  $950$  °C, while for the rest of the tests (higher ash deposition propensity) the flue gas temperature was greater than  $950$  °C.

Based on the experiences from previous measurements, we believe that when high deposition flux to ash flux ratio are observed, the main cause is a high flue gas temperature.

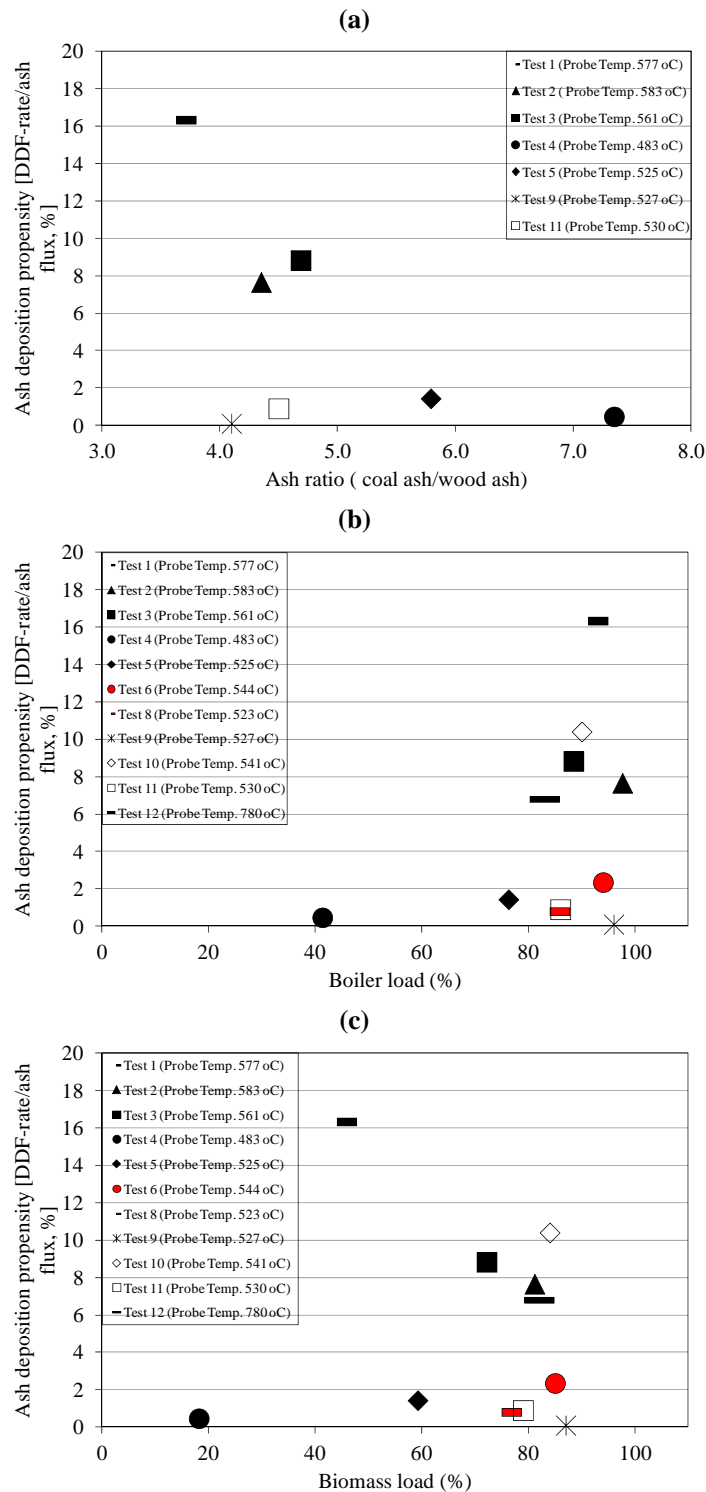
At location with high flue gas temperature of  $1250$ – $1300$  °C, the addition of coal ash increase the ash deposition propensity. With addition of coal ash, the deposit formation under this condition is characterized by a relatively fast build-up (e.g.  $\sim 1$ – $3$  h) followed by shedding of the deposit layer. Under

conditions of wood-firing without coal ash addition, the deposit formation is characterized by a long-term (e.g. 10 h) deposit build-up on the upstream side of the probe, followed by shedding of a large deposit layer. Although the addition of coal fly ash increases the DDF-rate and the ash deposition propensity, the deposits formed during coal ash addition seem to shed frequently, suggesting that they are easily removable.

At location with high flue gas temperature of 750–800 °C, under both conditions with and without coal ash addition, the deposit formation was characterized by an initial slow build-up, and after a few hours, the mass uptake of the deposit probe becomes almost constant, implying that the deposit build-up and shedding are close to equilibrium. However, the ash deposition propensity slightly reduced by injection of coal ash. In addition, the formed deposits during coal ash addition were easily removable. At lower flue gas temperature, the ash deposition was primarily due to condensation and/or thermophoresis of alkali salts. A significant fraction of alkali species was captured by coal ash, thereby the ash deposition propensity at lower flue gas temperature region was reduced. The detailed morphology and chemical composition of fly ash and deposits obtained from both locations with and without the addition of coal has been explained in section 6.3.4.



**Figure 6.8:** Impact of flue gas temperature on ash deposition propensity (deposition flux/ash flux, %). The points with red color indicate tests when coal ash addition was not made.

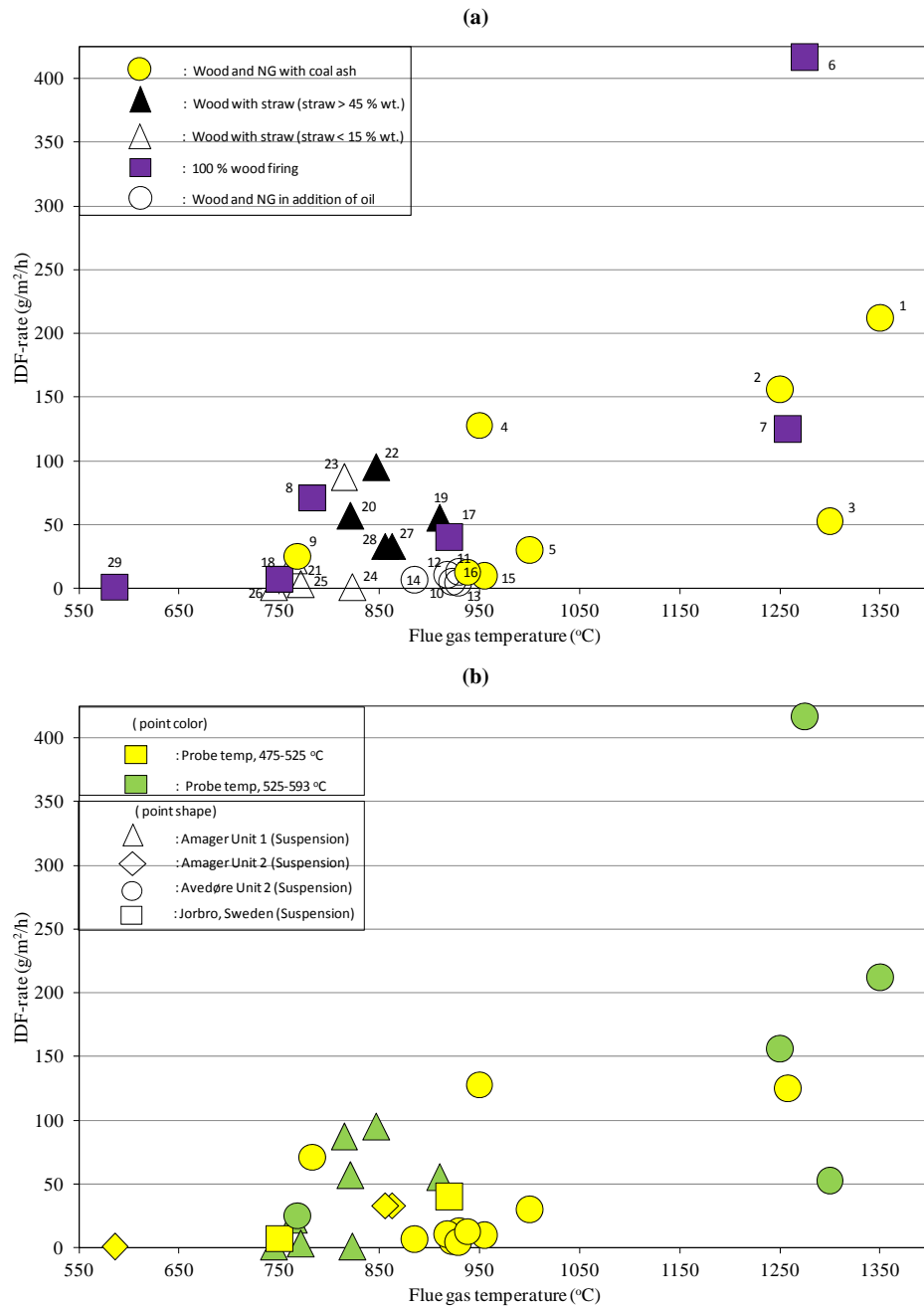


**Figure 6.9:** a) Impact of coal ash to fuel ash ratio on ash deposition propensity, b) impact of boiler load on ash deposition propensity, c) impact of biomass load on ash deposition propensity. For test 4, 8 and 9 (lower ash deposition propensity) the flue gas temperature was less than or equal to 950 °C, while for the rest of the tests (higher ash deposition propensity) the flue gas temperature was greater than 950 °C. The points with red color indicate tests when coal ash addition was not made.

### 6.3.3 Comparison of Results with Previously Conducted Probe Measurements

In previously conducted measurements at straw and/or wood-fired boilers, the deposit formation rates were calculated by inserting the probe inside the boiler for 2–12 h. In the current measurements, the deposit mass uptake signal after 12 h was measured and then divided by 12 h to get the IDF-rate. However, the IDF-rate can be influenced by shedding events during the time interval of the deposit collection. This could also happen when people report deposit formation rate when they took the probe out and divide the deposit amount collected by the probe exposure time, but the deposit mass can be significantly lower because of shedding. The values of IDF-rate calculated for the current study are therefore just representing arbitrary numbers. The deposit build-up pattern observed in tests 1–13 makes the calculated IDF-rate quite random. The deposit mass uptake at 12 h can be anywhere between 0 and 6,000 g/m<sup>2</sup>, which implies that in the case with a lot of fast shedding, IDF-rate data are not meaningful. However, apart from the fact that IDF-rate in the present measurements represents an arbitrary number, a comparison of the previous full-scale deposit probe measurements made at different wood suspension-fired boilers and the current measurements is shown in Table 6.4 and Figure 6.10. The data points, even those at approximately the same conditions, have a large spread, which is a result of the difficulties of keeping all operational parameters constant during full-scale measurements. Previous probe measurements at AVV2 Unit 2 showed values in the range of 3–13 g/m<sup>2</sup>h during wood dust and natural gas firing with oil, with and without the addition of coal ash. These measurements were performed using a simple deposit probe. The present measurements indicate increased deposit formation rates compared to previous measurements at the same boiler [24], possibly due to higher flue gas temperatures. Skrifvars et al. [38] measured deposit formation rate in the range of 12–74 g/m<sup>2</sup>h (mean 40 g/m<sup>2</sup>h of 4 measurements) at 920 °C and between 3 to 15 g/m<sup>2</sup>h (mean 7 g/m<sup>2</sup>h of four measurements) at 750 °C in a wood pulverized fuel boiler. Bashir et al. [101] measured IDF-rate of 1 g/m<sup>2</sup>/h during wood suspension firing at a flue gas temperature of 586 °C, while IDF-rates between 1 to 95 g/m<sup>2</sup>/h have been reported during wood and straw suspension firing [108]. It was observed by Bashir et al. [108] that an increased flue gas temperature and straw addition in wood (increased K contents) cause an increased deposit formation rate.

The impact of coal ash addition on IDF-rate is difficult to interpret based on the number of data points available. However, it is evident from Figure 6.10 (b) that a changed probe surface temperature seems not to cause any systematic change.



**Figure 6.10:** Impact of flue gas temperature on deposit formation rates (IDF-rates), a) comparison of deposit probe measurements data for wood firing with and without combination of other fuels (NG (natural gas), straw, furnace oil), b) comparison of data set with marking of the probe surface temperature and the boilers where the measurements were performed. **Graph details:** b) the color represents the probe surface temperature, while point shape represents the boiler type.

**Table 6.4:** Ash deposition data from the previous and current full-scale measurements conducted in biomass suspension-fired boilers. Amager Unit 2 (AMV2) and Unit 1 (AMV1) are straw and/or wood-fired suspension boilers. Jorbo, Sweden is a down-fired pulverized fuel boiler. Avedøre Unit 2 (AVV2) is a wood and natural gas fired suspension boiler.

No.	Boiler	Fuel (+ additive)	Fuel ash % wt.	Probe position	Probe surface temp. °C	Flue gas temp. °C	Exposure time h	IDF-rate g/m <sup>2</sup> h	Ref.
1	AVV2	Wood + natural gas (+ coal ash)	1.0	Just below radiation shield	577	~1350	12.0	~212.0	[24]
2	AVV2	Wood + natural gas (+ coal ash)	1.0	Just below radiation shield	583	~1250	12.0	~156.0	[24]
3	AVV2	Wood + natural gas (+ coal ash)	1.0	Just below radiation shield	561	~1300	12.0	~53.0	[24]
4	AVV2	Wood + natural gas (+ coal ash)	1.0	Just below radiation shield	483	~950	12.0	~128.0	[24]
5	AVV2	Wood + natural gas (+ coal ash)	1.0	Just below radiation shield	525	~1000	12.0	~30.0	[24]
6	AVV2	Wood + natural gas	1.0	Just below radiation shield	535	~1275	12.0	~417.0	[24]
7	AVV2	Wood + natural gas	1.0	Just below radiation shield	520	~1258	12.0	~125.0	[24]
8	AVV2	Wood + natural gas	1.0	Superheater	515	~783	12.0	~71.0	[24]
9	AVV2	Wood + natural gas (+ coal ash)	1.0	Superheater	527	~758	12.0	~25.0	[24]
10	AVV2	Wood + natural gas	0.6	Near radiation shield	500	923	~4.0	5.0	[24]
11	AVV2	Wood + natural gas	0.6	Near radiation shield	476	930	~5.0	13.0	[24]
12	AVV2	Wood + natural gas	1.2	Near radiation shield	491	918	~2.4	10.5	[24]
13	AVV2	Wood + natural gas	1.2	Near radiation shield	500	929	~4.5	4.5	[24]
14	AVV2	Wood + natural gas + oil	0.67	Near radiation shield	504	885	—	6.5	[24]
15	AVV2	Wood + oil (+coal ash)	—	Near radiation shield	503	955	~3.5	10.0	[24]
16	AVV2	Wood (+coal ash)	0.55	Near radiation shield	474	938	~2.5	12.5	[24]
17	Jorbro	Wood	0.55	Superheater	520	920	~2.0	40.0	[38]
18	Jorbro	Wood	0.55	Superheater	520	750	~2.0	7.0	[38]
19	AMV1	Straw + wood	5.1	Superheater	493	910	12.0	55.0	[108]
20	AMV1	Straw + wood	5.0	Superheater	593	821	13.5	57.0	[108]
21	AMV1	Straw + wood	1.3	Superheater	481	765	12.0	22.0	[108]
22	AMV1	Straw + wood	3.4	Superheater	479	847	6.0	95.0	[108]
23	AMV1	Straw + wood	1.6	Superheater	494	815	12.0	87.0	[108]
24	AMV1	Straw + wood	1.0	Superheater	563	823	12.0	1.0	[108]
26	AMV1	Straw + wood	0.85	Superheater	538	772	12.0	3.0	[108]
30	AMV1	Straw + wood	0.8	Superheater	539	745	12.0	1.0	[108]
27	AMV2	Straw + wood	5.4	Superheater	500	863	12.0	33.0	[101]
28	AMV2	Straw + wood	4.2	Superheater	500	856	12.0	33.0	[101]
29	AMV2	Wood	3.3	Superheater	500	586	12.0	~1.0	[101]



### 6.3.4 Morphology and Chemical Composition of Fly Ashes and Deposits

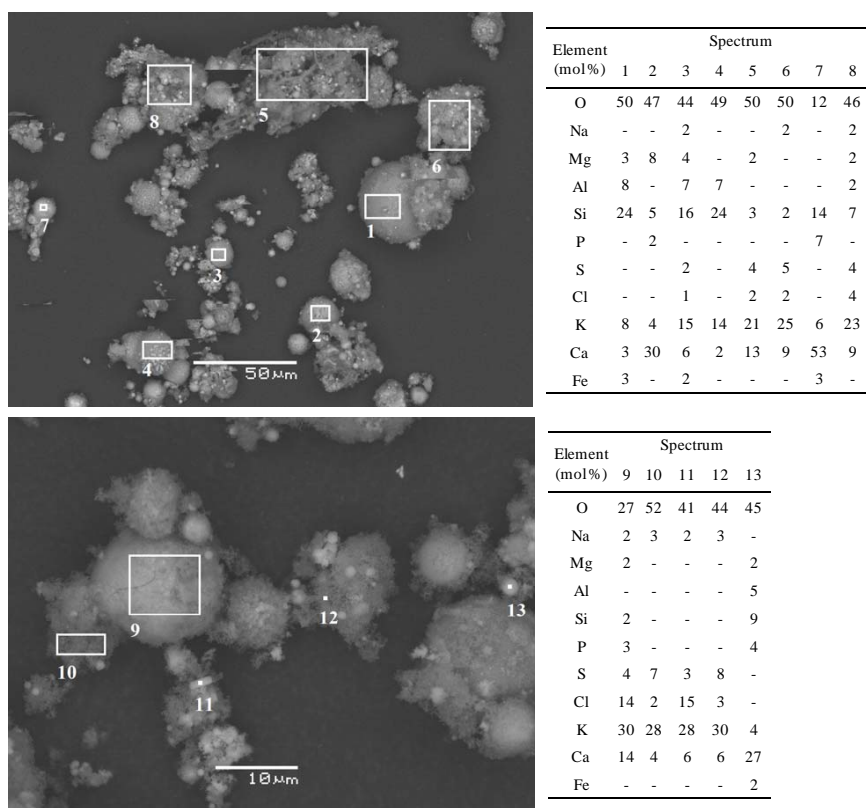
#### Fly Ash

The fly ash collected during the tests without coal ash addition are shown in Figure 6.11. SEM-EDS analysis reveals that these particles are generally dominated by Ca, Si and K. The size of the spherical particles varies significantly, from large particles with diameter around 50  $\mu\text{m}$  to small ones with a diameter of about 1  $\mu\text{m}$ . Besides the spherical particles, some extremely fine particles (much smaller than 1  $\mu\text{m}$ ) rich in K, S, and Cl are also observed. These fine particles can either attach to the surface of large particles (e.g. spectrum 9) or present as clusters themselves (e.g. spectrum 10 and 12). The morphology of these fine particles suggests that they are most likely generated from homogeneous nucleation of K, S and Cl rich species, most likely as KCl and  $\text{K}_2\text{SO}_4$ .

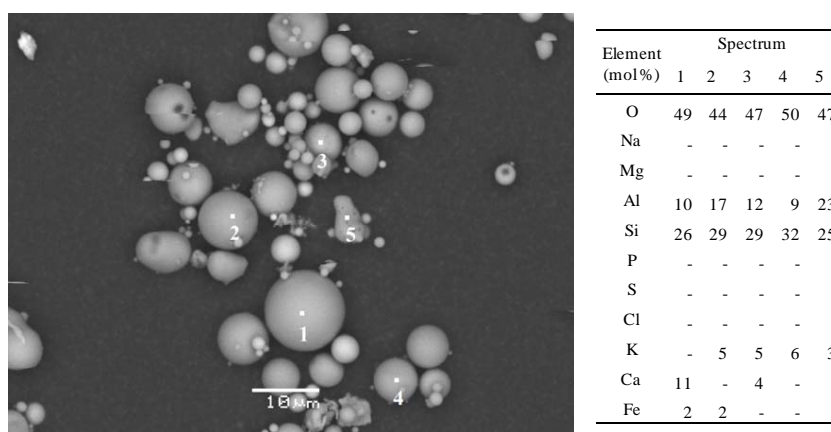
With the addition of coal fly ash, the fly ash was dominated by the added coal fly ash particles. This is evident in Figure 6.12, where a lot of spherical ash particles with large Si and Al content are seen. The presence of S and Cl is generally not observed in the fly ash collected during coal ash addition.

#### Deposits without Coal Ash Addition

At the end of the experiment, the probe was carefully taken out of the boiler; the deposits were removed, photographed and finally an overall representative sample was selected for SEM-EDS analysis to characterize morphology and composition of the deposits. Deposits from the downstream and upstream side of the probe were collected separately. An image of typical outer-layer of upstream deposits during test 6 is shown in Figure 6.13. It can be seen that the deposits are mainly comprised of ash particles with large Si, K and Ca content. The majority of these particles are relatively large spherical particles (e.g. spectrum 1, 7, 8 and 9). However, some of the particles appear to be partially melted and glued other particles together (e.g. spectrum 4, 5 and 6). Compared with the spherical particles, these partially melted particles seem to have larger Si and K content, and smaller Al content. The presence of these partially melted particles is probably important for the deposit build-up/sintering at high flue gas temperatures during suspension firing of wood. According to the SEM-EDS results, the presence of Cl is found to be negligible in the outer-layer deposits. Some S species (most likely  $\text{K}_2\text{SO}_4$ ) are detected in the outer-layer deposits, but the amount is insignificant. The upstream particles show a variety of particle types with varying particle size.



**Figure 6.11:** SEM-EDS analysis of the fly ash samples collected from electrostatic precipitator during measurement without coal ash addition.

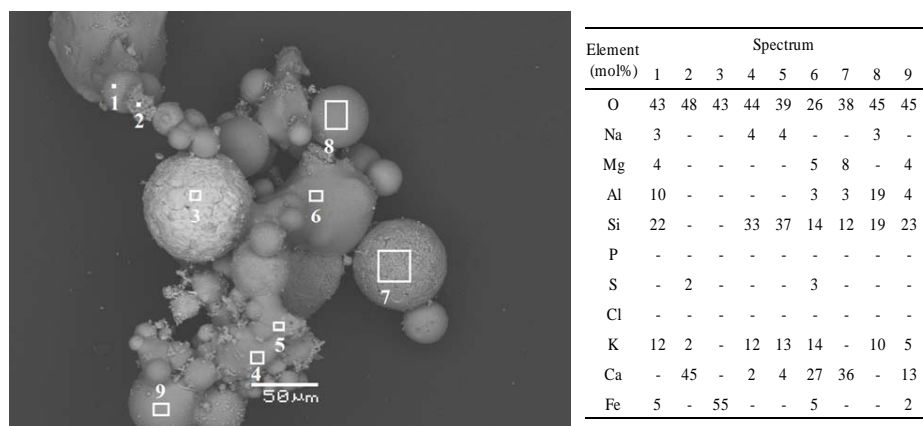


**Figure 6.12:** SEM-EDS analysis of the fly ash samples collected from electrostatic precipitator during measurement with coal ash addition.

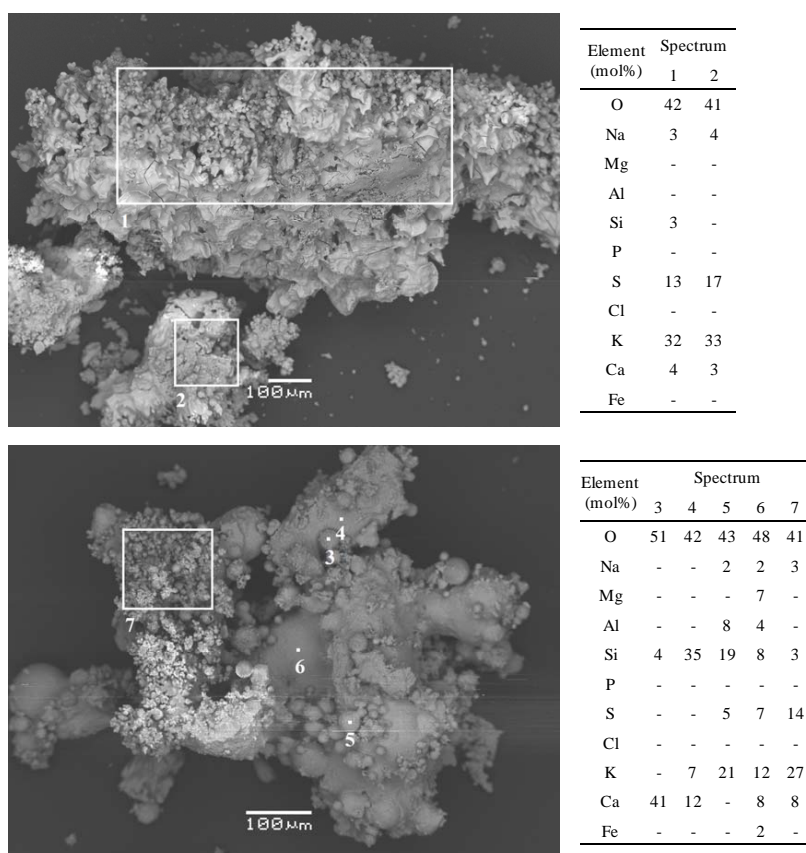
The typical SEM-EDS results of the downstream deposits collected from

test 6 are shown in Figure 6.14. It can be seen that the deposits contain a lot of S species (see spectrum 1, 2 and 7). These S species are most likely  $K_2SO_4$  since a large amount of K and S are found in both the spectrums. The morphology of these S species indicates that they are partially melted (see spectrum 1 and 2). On the other hand, some very small particles rich in K and S are also observed (see spectrum 7). Besides the S species, some K, Si and Ca rich spherical particles, and molten appearance K and Si rich particles are also seen in the downstream side deposits (see spectrum 4–6).

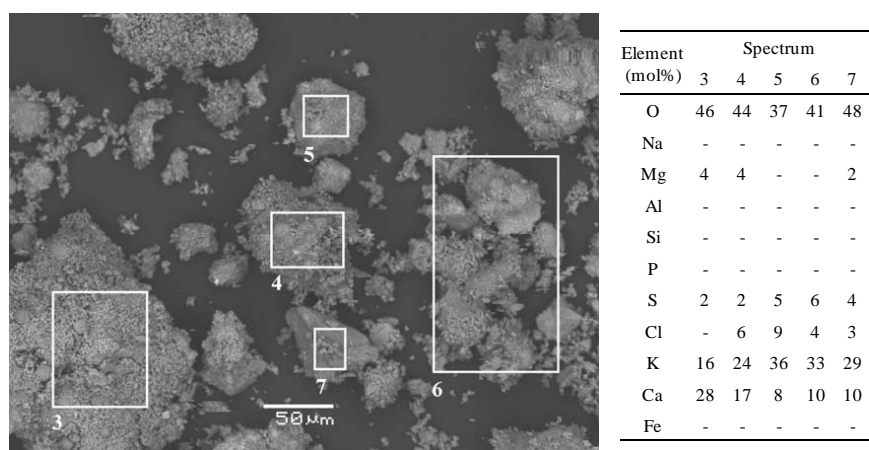
Figure 6.15 shows the typical morphologies and element compositions of the upstream deposits collected at location B during the test without coal ash addition (test 8). The general compositions of the deposits show that the upstream deposits are dominated by K, Ca, S and Cl. The morphology of the deposits indicates that they are mostly clusters of very small particles (smaller than  $5 \mu\text{m}$ ). Large fly ash particles rich in Si, Ca and K are generally not seen in the collected upstream deposits. The morphology of the downstream deposits shown in Figure 6.16 (see spectrum 6 and 7) suggests that they are dominated by clusters of very small particles rich in K, Cl, S and Ca. However, different from the upstream deposits, some relatively large ash particles (about  $10 \mu\text{m}$ ) rich in Si, Ca and K are observed in the downstream deposits (see spectrum 3 and 4).



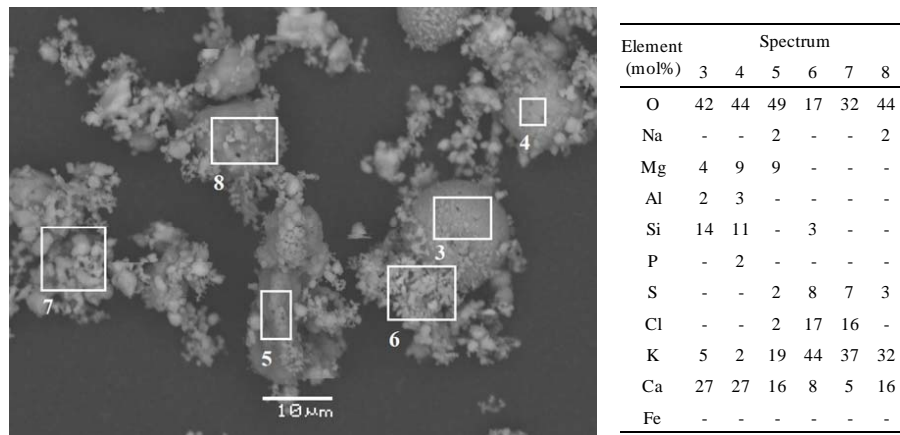
**Figure 6.13:** SEM-EDS analysis of outer-layer of upstream deposits formed during measurements without coal ash (location A, test 6).



**Figure 6.14:** SEM-EDS analysis of the downstream deposits formed during measurement without coal ash addition (location A, test 6).



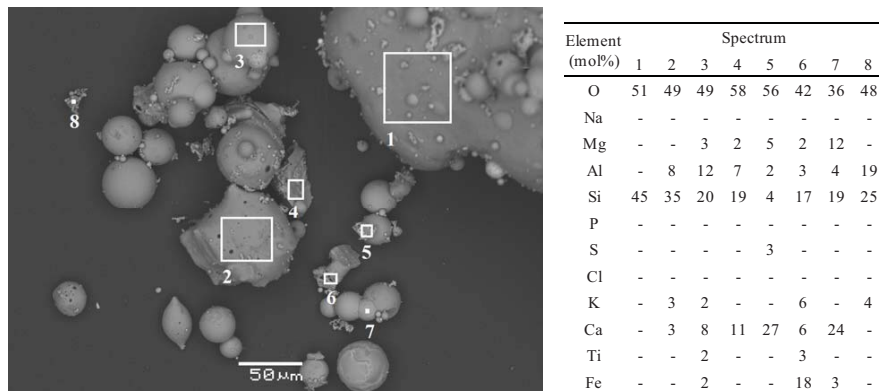
**Figure 6.15:** SEM-EDS analysis of the upstream deposits formed during measurement without coal ash addition (location B, test 8).



**Figure 6.16:** SEM-EDS analysis of the downstream deposits formed during measurement without coal ash addition (location B, test 8).

### Deposits with Coal Ash Addition

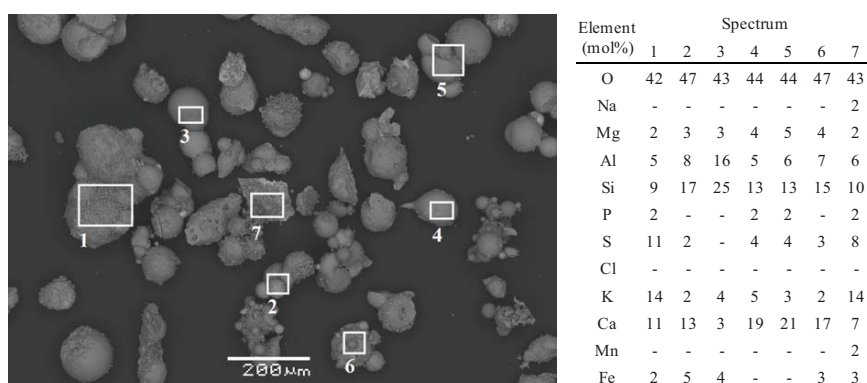
Figure 6.17 shows the morphology and elemental compositions of the outer-layer upstream deposits collected at location A during coal ash addition (test 10). It can be seen that the deposits are dominated by ash particles with large Si and Al content. The compositions of these particles are consistent with the fly ash particles obtained during coal ash addition (see Figure 6.12), suggesting that the outer-layer upstream deposits are predominantly formed by the added coal fly ash. Besides, another obvious tendency in Figure 6.17 is that S and Cl are almost not present in the outer-layer deposits.



**Figure 6.17:** SEM-EDS analysis of the outer-layer of upstream deposits formed during measurement with coal ash addition (location A, test 10).

The downstream deposits collected at location A during coal ash addition are shown in Figure 6.18. The deposits contain a large number of ash

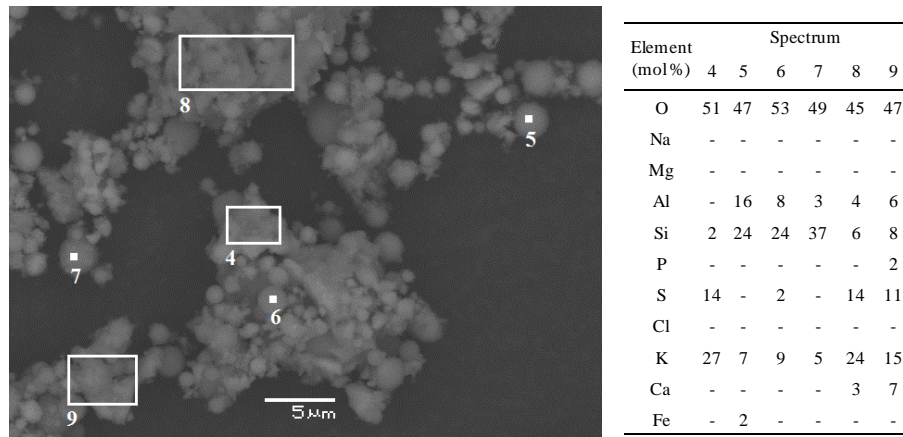
particles rich in Si, Al, K and Ca (e.g. spectrum 2–6). Majority of these ash particles have spherical appearances and are attached with other particles. A few particles with relatively large S content are observed in the deposits (e.g. spectrum 1 and 7). These particles are generally clusters of very fine particles, and are most likely  $K_2SO_4$ , but other species such as  $CaSO_4$  or K-silicates may also exist.



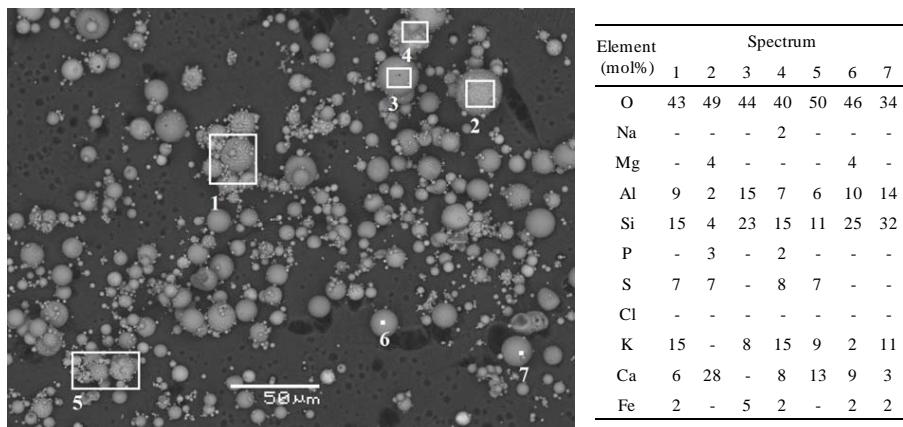
**Figure 6.18:** SEM-EDS analysis of the downstream deposits formed during measurement with coal ash addition (location A, test 10).

The upstream deposits collected at location B during the test with coal ash addition (test 9) are illustrated in Figure 6.19. The general compositions of the upstream deposits indicate that they are dominated by K, Si, S, Al and Ca. More detailed analysis suggests that the deposits are partly comprised of agglomerated small particles (smaller than  $5 \mu\text{m}$ ) with large K and S content (e.g. spectrum 4, 8 and 9). The molar ratio of K and S in spectrum 4 indicates they are most likely  $K_2SO_4$ . On the other hand, the upstream deposits also contain some spherical ash particles with large Si, Al and K content (e.g. spectrum 5–7).

Compared with the upstream deposits, the morphology and compositions of the downstream deposits formed at location B with coal ash addition are quite different. As shown in Figure 6.20, the downstream deposits from test 9 are dominated by spherical particles (between  $5$  and  $15 \mu\text{m}$ ) with large Si, Al and K content (see spectrum 2 and 3). These particles are most likely originated from the added coal fly ash. Some ash particles with relatively large K and S content are also observed in the downstream deposits, but their contribution is insignificant for the formation of downstream deposits. Similar to the upstream deposits, Cl is still not found in the downstream deposits at location B during coal ash addition.



**Figure 6.19:** SEM-EDS analysis of the upstream deposits formed during measurement with coal ash addition (location B, test 9).



**Figure 6.20:** SEM-EDS analysis of the downstream deposits formed during measurement with coal ash addition (location B, test 9).

### 6.3.5 Discussion on Characterization of Fly Ashes and Deposits

A summarized picture of the deposits formed at higher and lower flue gas temperature with and without the addition of coal fly ash is shown in Figure 6.21. It can be seen that without the addition of coal fly ash, the deposits at location A are primarily comprised of K-Ca-Si rich spherical particles, K-Si rich partially melted particles and  $K_2SO_4$  clusters. The K-Ca-Si rich and K-Si rich particles probably originate from the ash in wood pellets. During combustion, the residual ash would undergo fragmentation, melting and coalescences, and result in the formation of spherical/molten fly ash particles.

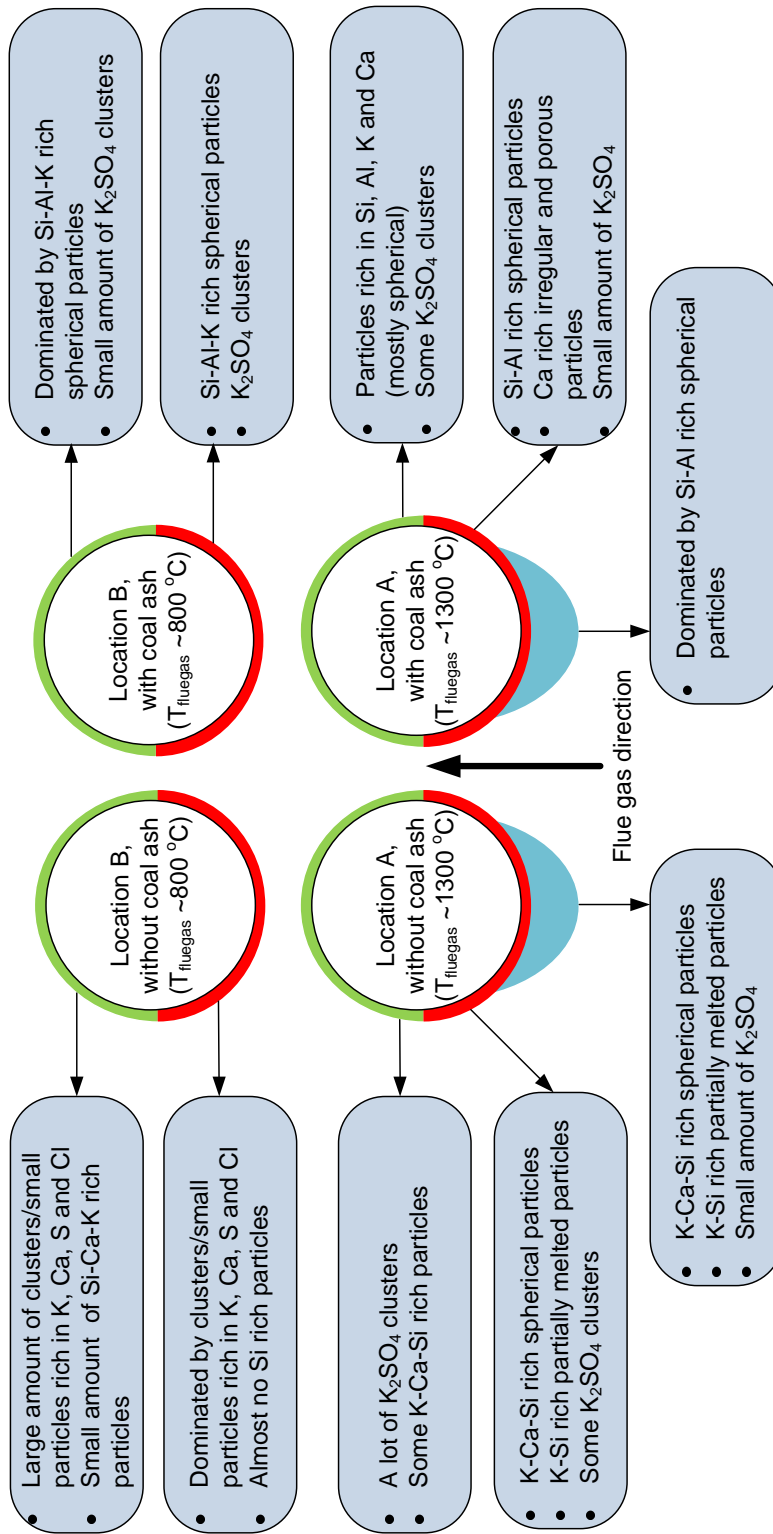


Figure 6.21: A summarized picture of the deposits based on SEM-EDS analysis.



At location A, the major deposition mechanism for these fly ash particles would be inertial impaction since the majority of these particles are found on the upstream side of the probe. Besides inertial impaction, these fly ash particles may also form deposits through thermophoresis (primarily for small ash particles), this may be an explanation to the K-Ca-Si rich particles found on the downstream of the probe. The  $K_2SO_4$  clusters found on the deposits may be formed by three different mechanisms. At Location A, the KCl and  $K_2SO_4$  (if present) in the flue gas are probably in vapor phase, due to the high flue gas temperature. Therefore, direct condensation on the surface would be an important deposition mechanism for the KCl and  $K_2SO_4$ . Besides condensation, thermophoresis could also be a mechanism for the deposition of  $K_2SO_4$ . This is mainly because the temperature difference between the probe surface and the flue gas is significant. When the gaseous  $K_2SO_4$  diffuse from bulk flue gas to the probe surface,  $K_2SO_4$  aerosols may be generated and form deposits through thermophoresis. All of the three mechanisms mentioned above are more favorable for cold surfaces. This explains why most of the  $K_2SO_4$  is found in the inner deposits collected from the downstream side of the probe.

With the addition of coal fly ash, the KCl and  $K_2SO_4$  in the flue gas would be significantly reduced. Besides, the fly ash will be dominated by the added coal fly ash as the amount of added coal fly ash greatly exceeds that of wood ash (see Table 6.3). As a result, the deposits at location A become dominated by Si-Al rich particles when coal fly ash is added. In addition, the amount of  $K_2SO_4$  in the deposits is significantly decreased, although not completely removed. The presence of  $K_2SO_4$  is probably because the added coal fly ash may not be able to totally remove the  $K_2SO_4$  and KCl in the flue gas.

Without coal ash addition, the properties of the deposits collected at location B are quite different from those collected at location A. The upstream deposits at location B are dominated by K, Ca, S and Cl species. Almost no particles containing Si are found, implying that the inertial impaction of Si-Ca-K rich particles is not an important mechanism for the formation of upstream deposits at location B. This probably related to the low flue gas temperature at this location ( $\sim 800$  °C), which would lead to a low capture efficiency of the impacted particles. Moreover, even if some Si-Ca-K rich particles are captured, the gravity of these relatively large particles may exceed the adhesion strength between the particles and the deposits/tube, thereby causing gravity shedding of these particles. The majority of the upstream deposits are found to be cluster of small particles rich in K, Ca, S and Cl. These particles are probably deposited via condensation or thermophoresis. The Cl found in the deposits is most likely KCl. Compared with the deposits at location A where most of the deposited KCl seems to

be converted to  $\text{K}_2\text{SO}_4$ , the degree of heterogeneous sulfation appears to be less significant at location B. This could be related to the relatively low flue gas temperature at this location, which may suppress the heterogeneous sulfation reaction. In addition, the  $\text{SO}_2$  concentration may be very low at this location. According to thermodynamic calculations on woody materials [63],  $\text{SO}_2$  is found to be the only stable S species at temperatures above  $1200\text{ }^\circ\text{C}$ . However, when the temperature is decreased from  $1200\text{ }^\circ\text{C}$  to  $800\text{ }^\circ\text{C}$ ,  $\text{SO}_2$  would be potentially converted to  $\text{K}_2\text{SO}_4$ . Such transformations may also happen in the boiler, and result in a very low  $\text{SO}_2$  concentration at location B. This hypothesis is supported by the extremely low  $\text{SO}_2$  concentration measured downstream of location B during the tests without coal ash addition (see Table 6.3).

Compared with the upstream deposits, the downstream deposits generally have quite similar compositions, expecting that a few more Si-Ca-K rich particles are observed. This is probably because that it is more difficult for these particles to shed through gravity once they are deposited on the downstream side of the probe.

The deposits collected at location B during coal ash addition are quite different from those obtained without coal ash addition. Almost no Cl is found in the deposits collected with coal ash addition. This could be linked to the reactions between the added coal fly ash and the KCl released from wood combustion, which can form K-aluminosilicates and gaseous HCl. In addition, the  $\text{SO}_2$  concentration in the flue gas is much higher during coal ash addition (see Table 6.3). Therefore, even if a small amount of KCl exist and form deposits, it may be converted to  $\text{K}_2\text{SO}_4$  through heterogeneous sulfation reactions. This could be an explanation to the  $\text{K}_2\text{SO}_4$  clusters found in the deposits. Besides, the  $\text{K}_2\text{SO}_4$  clusters may also be from direct deposition of  $\text{K}_2\text{SO}_4$  aerosols. The upstream deposits collected at this condition contain both small Si-Al-K rich particles and  $\text{K}_2\text{SO}_4$  clusters, whereas the downstream deposits seem to be dominated by Si-Al-K rich particles. Majority of these Si-Al-K rich particles are probably originated from the added coal fly ash. The enrichment of these particles in the downstream deposits is likely because these particles are more difficult to shed through gravity once they are deposited on the downstream side of the probe.

## 6.4 Conclusions

A series of deposit probe boiler measurements were conducted at Avedøre Unit 2 (AVV2), a wood and natural gas suspension-fired boiler. The tests were conducted both with and without coal ash addition, and at two different locations with flue gas temperatures of  $1250\text{--}1300\text{ }^\circ\text{C}$  and  $750\text{--}800\text{ }^\circ\text{C}$ ,

respectively. The conclusions are summarized in the following points:

- Changes in biomass boiler load lead to some degree to changes in boiler flue gas temperature and the used coal ash to wood ash ratio. It was therefore difficult to determine which changes that causes the observed large changes in the deposit formation rate. However, a high increase in local flue gas temperature increased the deposit formation rate in this study, and this has also been observed in other previous deposit probe measurements conducted at biomass-fired boilers.
- Video monitoring revealed that the deposits formed with coal ash addition were not sticky and could be easily removed by gravity shedding (debonding), and even at very high flue gas temperatures ( $> 1350\text{ }^{\circ}\text{C}$ ), deposit removal through surface melting was not identified. This indicates that potassium (K) has been potentially captured by coal ash to form deposits with high melting temperatures.
- At location with high flue gas temperature of  $1250\text{--}1300\text{ }^{\circ}\text{C}$ , the addition of coal ash increase the ash deposition propensity. With addition of coal ash, the deposit formation under this condition is characterized by a relatively fast build-up (e.g.  $\sim 1\text{--}3\text{ h}$ ) followed by shedding of the deposit layer. Under conditions of wood-firing without coal ash addition, the deposit formation is characterized by a long-term (e.g.  $10\text{ h}$ ) deposit build-up on the upstream side of the probe, followed by shedding of a large deposit layer. Although the addition of coal fly ash increases the DDF-rate and the ash deposition propensity, the deposits formed during coal ash addition seem to shed frequently, suggesting that they are easily removable.
- At location with high flue gas temperature of  $750\text{--}800\text{ }^{\circ}\text{C}$ , under both conditions of with and without coal ash addition, the deposit formation was characterized by an initial slow build-up, and after a few hours, the mass uptake of the deposit probe becomes almost constant, implying that the deposit build-up and shedding are close to equilibrium. However, the ash deposition propensity slightly reduced by injection of coal ash. In addition, the formed deposits during coal ash addition were easily removable.
- At the location with flue gas temperature of  $1250\text{--}1300\text{ }^{\circ}\text{C}$ , the deposits formed without coal ash addition are dominated by K-Ca-Si rich particles and  $\text{K}_2\text{SO}_4$  rich clusters. With the addition of coal fly ash, SEM-EDS analysis of the deposits shows significant presence of Ca, Al and Si, indicating that K has been captured by the coal ash to form deposits rich in calcium-alumina-silicates. Cl was not found either on the upstream side or on the downstream side of the probe, indicating that Cl has been released to the gas phase as  $\text{HCl(g)}$ .

- At the location with flue gas temperature of 750–800 °C, the deposits formed without coal fly ash addition were dominated by small particles rich in K, Ca, S and Cl. With the addition of coal fly ash, the Cl disappeared in the deposits collected at this location. The deposits were dominated by calcium-alumina-silicates rich particles, supplemented by a small amount of K<sub>2</sub>SO<sub>4</sub> particles. The ash deposition propensity is decreased when coal ash is added.



## Chapter 7

# Mechanistic Modeling of Deposit Build-up during Biomass Suspension Firing

### 7.1 Introduction

In order to predict the deposition of ash particles and heat transfer through the deposit, a mechanistic modeling technique can be potentially viable. For the assessment of the deposition tendency, mechanistic models can be used for the calculations of combustion and fluid dynamics [31]. These models provide a base for the development of a more comprehensive mathematical model for ash deposition and heat transfer [31].

This chapter is about the simulation of a mechanistic model with ash deposit build-up and heat uptake in a biomass suspension-fired boiler. The results mentioned in this chapter are based on the extension of the model proposed by Zhou et al. [31], which was developed for biomass grate firing conditions. In addition, the results are shown only for deposit build-up as deposit shedding process was not included because of time constraints. The mechanistic model is capable of quantitatively predicting ash build-up and heat uptake on a superheater tube. The model takes into account ash deposit build-up and heat uptake with changed flue gas temperature, ash composition and flow conditions. The model is intended to describe the deposit related processes as a function of the local parameters as gas velocity, ash particle size distribution, ash particle composition and gas and surface temperature.

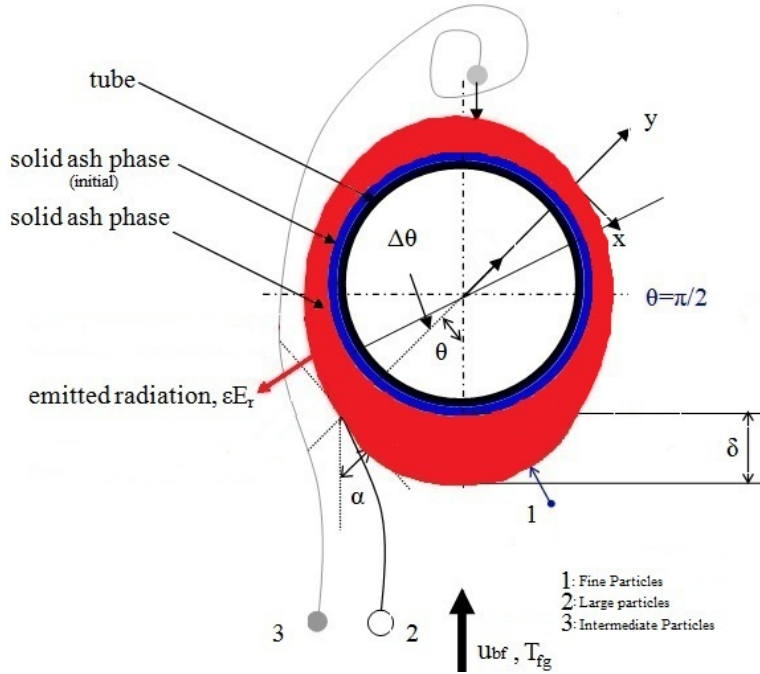
## 7.2 Mechanistic Modeling of Deposit Formation Processes

At the beginning of the deposit formation process, when the probe is perfectly clean, only vapors and fine and intermediate-sized particles (for example, deposition by condensation and by thermophoresis) which arrive at the surface in a sticky condition contribute to the initial deposit formation. Inertial impaction contributes to the ash deposit build-up after the initial deposition forms. The deposit surface temperature increases with the increase of the thickness of the deposit which results in the deposit becomes a much more efficient collector [31].

A schematic of the deposit layers on the horizontal ash deposition probe is shown in Figure 7.1. The model used is the modified version of the model used by Zhou et al. [31], which is a dynamic mechanistic model for ash deposition and shedding by surface melting in a straw grate-fired boiler. The necessary modifications in the model were made to apply the model for suspension firing conditions, without any deposit shedding considerations. For more details about the model, please refer to Zhou et al. [31].

Principal assumptions in the model are [31]:

- The incoming fly ash is uniform; and gas-particle interaction is a one-way coupling i.e. the presence of particles in the flue gas has no influence on the gas flow field.
- Particles motion and temperature follow the local gas velocity and temperature.
- The effect of ash build-up on the flow field around the probe is negligible.
- A linear temperature profile is assumed across the deposit.
- The heat transfer occurs only along the radial direction of the deposit, and the energy change caused by the phase change of the deposit is negligible.
- Heterogeneous reactions and sintering in the deposit are neglected i.e. chemical compositions of the deposits and the fly ash are the same.
- Deposit shedding is not taken into account.
- The chemical compositions and particle size of the fly ash obtained from experiments are used as input parameter in the model due to the lack of an ash transformation model.



**Figure 7.1:** A schematic of the deposit layers on the horizontal ash deposition probe [31].

The principal mechanisms by which deposits formed are; thermophoresis and diffusion and/or diffusion followed by condensation, inertial impaction on the upstream side, and eddy impaction on the downstream side. The overall deposit build-up rate can be written as,

$$\frac{dm(t, \theta)}{dt} = C(t, \theta) + TH(t, \theta) + I(t, \theta) \quad (7.1)$$

In the above equation,  $C$  counts for condensation,  $TH$  for thermophoresis and  $I$  for inertial impaction, while  $t$  is the time, and  $\theta$  is the angular position.

### Thermophoresis

Thermophoresis is a process of particle transport in a gas due to local temperature gradients [14]. Vapors may homogeneously nucleate to form a fume and subsequently deposit by thermophoresis on the surface and vapors may heterogeneously condense on other particles in the boundary layer and arrive the surface through thermophoresis [10]. The thermophoretic flux of submicron particles to the tube surface can be calculated based on the thermophoretic velocity.



$$TH(t, \theta) = \sum u_T \cdot C_{ash,i} \quad (7.2)$$

where  $u_T$  is the thermophoretic velocity and  $C_{ash,i}$  is approximated based on the aerosol concentration ( $C_{ash,1}$ ) and concentration of the intermediate sized particles ( $C_{ash,3}$ ). It was assumed that all fine particles reach the probe may stick. The mass loading of aerosol particles in the flue gas was approximated based on the correlation proposed by Zhou et al. [31]. The correlation is,  $\frac{0.00026}{\left(\frac{T_{fg}}{293.15}\right)}$ . The concentration of the intermediate sized particles ( $C_{ash,3}$ ) was estimated from the calculated concentration of large sized particles ( $C_{ash,2}$ ), which was approximated as,

$$C_{ash,2} = \frac{\dot{m}_{fuel} \cdot ash\% \cdot f_{entrained}}{\dot{V}_{fg}} \quad (7.3)$$

In this equation  $\dot{m}_{fuel}$  is the inlet fuel feeding mass flow rate,  $f_{entrained}$  is fraction of residual entrained as residual fly ash,  $ash\%$  is the percentage of ash in a dry fuel and  $\dot{V}_{fg}$  is the volumetric flow rate of flue gas. The flue gas velocity ( $u_{bg}$ ) can be estimated using,

$$u_{bg} = \frac{\dot{V}_{fg}}{A_r} \quad (7.4)$$

$A_r$  is the cross-sectional area of the boiler at the probe measurement area.

The thermophoretic velocity can be calculated based on various correlations proposed by different authors. The formula proposed by Brock [116] is,

$$u_T = -B \cdot v_g \cdot C_c \cdot \frac{\nabla T}{T_c} \quad (7.5)$$

where,  $B$  is constant and can be estimated empirically,  $v_g$  is the kinematic gas viscosity,  $T_c$  is the temperature on the surface of the tube and  $\nabla T$  ( $\frac{K}{m}$ ) is the temperature gradient.  $C_c$  is called the Cunningham slip factor and can be calculated using the method proposed by Flagan et al. [117].

### Diffusion followed by Condensation

Condensation is a mechanism by which vapors can be collected on surfaces cooler than the local gas. For the case of biomass firing, the initial deposition is governed by condensation because of the presence of alkali metals. For

simplification, the overall condensation rate controlled by mass transfer was expressed at [10],

$$C(t, \theta) = \sum k_{C,i} (C_{i,b} - C_{i,s}) \quad (7.6)$$

In this equation,  $k_{C,i}$  is mass transfer coefficient,  $C_{i,b}$  is the concentration of gas specie in the bulk gas and  $C_{i,s}$  is the concentration of gas specie at the probe surface.  $i$  represents KCl(g) and K<sub>2</sub>SO<sub>4</sub> (g) in the bulk flue gas. The mass transfer coefficient is determined by the Sherwood number (Sh),

$$Sh = \frac{k_{C,i} \cdot d}{D_i} \quad (7.7)$$

In this equation,  $d$  is the diameter of the probe and  $D_i$  is the diffusion coefficient.

### Inertial Impaction

Inertial impaction takes place when particles have too much inertial momentum to follow the gas streamlines around a heat transfer surface, and instead impacts on the surface. As mentioned by Zhou et al. [31], the influencing deposition mechanism for straw fired boilers is inertial mechanism during grate firing and will be even more important for the suspension firing of straw since the percentage of the entrained ash ranges from 80–90%. The deposition rate caused by the impaction of the particles can be written as,

$$I(t, \theta) = u_{bg} \cdot C_{ash,2} \cdot \eta_{imp} \cdot f_{stick} \quad (7.8)$$

In the above equation,  $u_{bg}$  is the bulk gas velocity,  $C_{ash,2}$  is the concentration of large sized particles,  $\eta_{imp}$  is the impaction efficiency, and  $f_{stick}$  is the sticking efficiency. For eddy impaction on the rear side of the probe, please refer to [31].

### Impaction Efficiency

Impaction efficiency of the fly ash particles hitting the probe is a function of the particles which impact on the probe, and the fraction of the particles captured once collision on the surface has occurred. The impact efficiency is dependent on the particle velocity, particle density, particle diameter, bulk gas viscosity and the probe dimensions. A dimensionless number called the Stokes number represents these parameters and is given as,

$$Stk = \frac{\rho_p \cdot d_p^2 \cdot u_{bg}}{9 \cdot \mu_{fg} \cdot d} \quad (7.9)$$

The impact efficiency can be calculated based on the Stokes number. For more details, please refer to Zhou et al. [31].

### Sticking Efficiency

The sticking efficiency of the particles depends upon the composition and viscosity of the particle and the deposit surface and the thermal and chemical compatibility between the particle and the deposit surface [20]. The combined stickiness of the deposit surface and the incoming ash particles was approximated using the following correlation [30],

$$f_{stick} = f(T_{fg}) + f_s(T_s) \cdot (1 - f(T_{fg})) \quad (7.10)$$

In the above equation,  $f(T_{fg})$  is the sticking probability for the incoming particles and  $f_s(T_s)$  is the sticking probability for the particles exposed on the surface. A prediction of ash melt fraction as function of temperature based on the ash composition was made by using the model proposed by Zhou et al. [31].

### 7.2.1 Heat Transfer Modeling

The heat transfer between the deposit and the flue gas includes contributions from radiation and convection. The overall heat balance can be approximated using,

$$\epsilon_r \sigma (T_{fg}^4 - T_s^4) + Q_c = Q_{in} \quad (7.11)$$

The convective heat transfer will be,

$$Q_c = h_f (T_{fg} - T_s) \quad (7.12)$$

In the above equations,  $\epsilon_r$  is the emissivity coefficient for deposit (ranging from 0.75–0.8 [31]),  $h_f$  is the convective heat transfer coefficient in the furnace region,  $T_s$  is the surface temperature,  $T_{fg}$  is the flue gas temperature and  $\sigma$  is the Stephen Boltzmann Constant [ $5.6704 \times 10^{-8} \frac{J}{sm^2K}$ ].

Heat transfer through the deposit layer was estimated using,

$$Q_{in} = \frac{k_{eff} (T_d - T_t)}{\delta_e} \quad (7.13)$$

In this equation,  $\delta_e$  is the effective thickness of the solid deposit,  $T_t$  is the probe metal temperature, and  $k_{eff}$  is the effective thermal conductivity of the deposit.

### 7.2.2 Simulation Conditions

Two types of fuel input data and fly ash compositions data were used as input as shown in Table 7.1. For simplification and in order to compare the results with available experimental data, only two cases of the fuels were used as input: 1) fuel (fly ash) with straw share greater than 20 wt.%, and 2) fuel (fly ash) with straw share less than 20 wt.%. The detailed simulation conditions are shown in Table 7.2. Most of the input conditions are taken from the measurement data shown in Chapter 5. The changed conditions were probe temperature (500 °C and 600 °C), flue gas temperature (770 °C, 820 °C and 900 °C) and applied fuel and fly ash input. Most of the values are kept the same as were used by Zhou et al. [31].

The deposit probe related parameters shown in Table 7.2 were approximately the same as were used by Zhou et al. [31]. The input value for the boiler cross-sectional area is different (72 m<sup>2</sup> instead of 24 m<sup>2</sup>). The fuel related input data, for example, the inlet fuel rate, the entrained ash as fly ash, and the ultimate and proximate analysis of the ash was different from the ones used by Zhou et al. [31], but the percentages of released inorganic elements are kept the same. The selected values for flue gas temperature were 770 °C, 820 °C and 900 °C. The correlations for the approximation of thermal conductivity and viscosity of the flue gas are same as were used by Zhou et al. [31]. The particle size for the fine and medium particles was kept the same, while the size of the coarse particles is different. The reason is that as shown in Chapter 4 and 5 the particle size of the coarse particles generated during suspension firing is significantly larger than the coarse particles formed during grate firing. The deposit related properties were kept the same.

### 7.2.3 Simulation Results

The simulation results of the deposit mass uptake and DDF-rate for the first six hours when straw share was more than 20 wt.% are shown in Figure 7.2 and Figure 7.3, respectively. It can be seen that there is an increase in the deposit mass uptake and DDF-rate with increase in flue gas temperature.

**Table 7.1:** Composition of the fuel input data and fly ash input data.

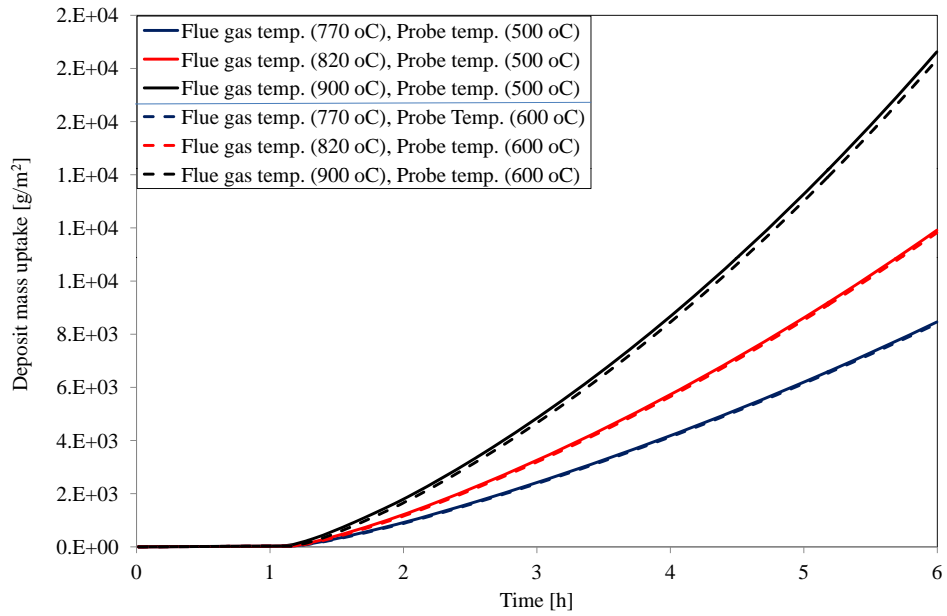
Fuel	Case 1 (straw > 20 wt.%)	Case 2 (straw < 20 wt.%)
Moisture (wt%, a.r.)	6.67	6.5
Ash (wt%, d.b.)	5.63	1.0
Volatiles (wt%, d.b.)	82.9	80.0
C	51.2	55.0
H	5.85	6.0
N	0.80	0.70
S	0.121	0.040
Cl	0.19	0.01
K	0.9	0.1
<i>Fly ash (wt%, d.b.)</i>		
Si	23.45	35.0
Al	0.35	0.50
Fe	0.20	0.20
Ca	5.78	14.0
Mg	1.31	1.0
Na	1.41	0.10
K	16.14	5.0
S	0.77	0.50
P	1.30	0.10
Cl	5.53	0.55

The qualitative behavior of the results is in accordance with the experimental findings, presented in Chapter 5. Increased flue gas temperatures probably increase the fraction of molten ash as well as provide an increased content of gas phase alkali species, and both will lead to higher amount of ash being deposited. The results of changed probe surface temperature show that the changed probe surface temperatures in the range from 500 to 600 °C do not seem to significantly influence the deposit formation rate.

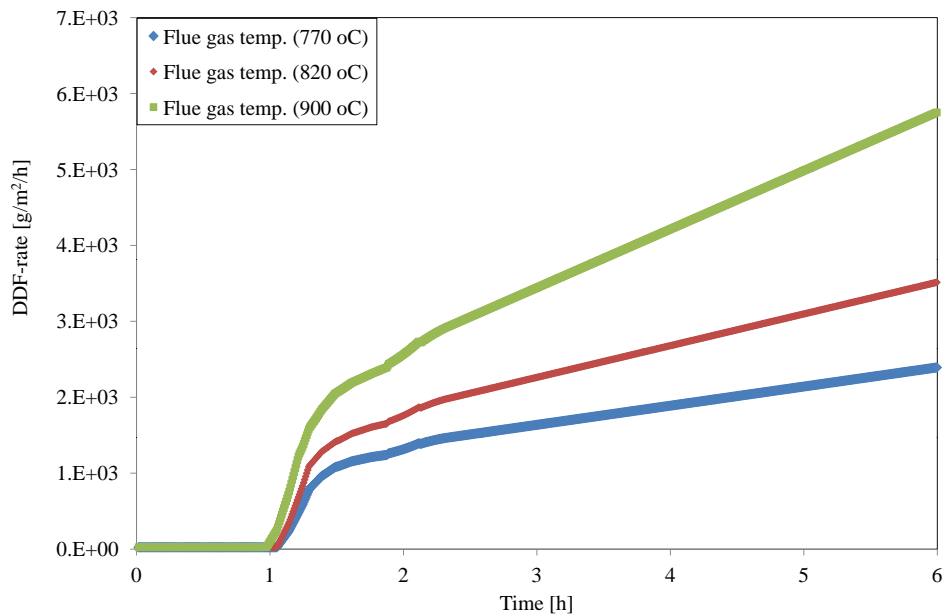
The simulation results of the deposit mass uptake for the first six hours when straw share was less than 20 wt.%, are shown in Figure 7.4. The deposit mass uptake was low possibly due to the fact that the deposit formation caused by inertial impaction is minimal because of low sticking efficiency of the fly ash and deposit. The difference between deposit mass uptake at probe temperature of 500 °C and 600 °C is possibly due to a higher deposit formation caused by condensation at lower temperature.

Table 7.2: Simulation conditions.

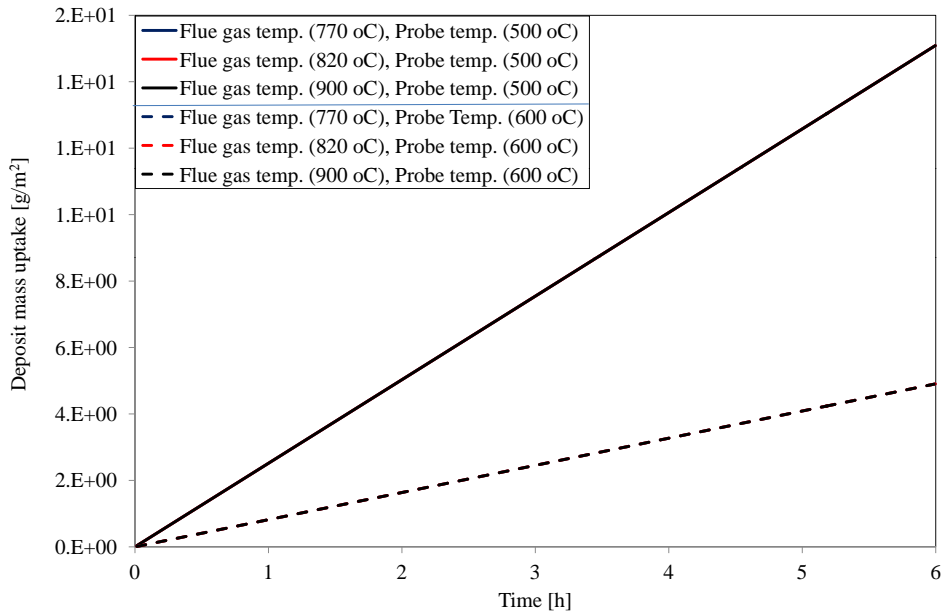
Parameter	Value
The probe	3 1.5 2.0 40.5 500/600
The boiler	72
The fuel	15.8 80 See Table 7.1 S   50 K   20 Cl   100
The gas	1.25 770/820/900 $4.8 \times 10^{-4} \cdot T_f^{0.717}$ $1.98 \times 10^{-5} \cdot (\frac{T_f}{300})^{2/3}$ 60
Fly ash	Fine particle (1) 0.27 Coarse particle (3) 110 Medium particle (2) 8 All particles 2600 See Table 7.1
Deposit	1500 0.8 6.7 5.5
Conductivity of the solid phase, $k_s, (\frac{W}{m.K})$   in the most inner layer   in other layers	
Initial deposit thickness, $\delta_{d,i}$ (m)	
Simulation time, (hour)	
Number of computation cell (semi-cylinder)	
6	
40	



**Figure 7.2:** Simulation results of deposit mass uptake for the first six hours for different sets of flue gas temperatures and probe surface temperatures. The fuel (fly ash) input is case 1 (straw > 20 wt.%) shown in Table 7.1.



**Figure 7.3:** Simulation results of DDF-rate ( $\frac{dm}{dt}$ ) for the first six hours for different sets of flue gas temperatures and probe surface temperatures. The fuel (fly ash) input is case 1 (straw > 20 wt.%) shown in Table 7.1.



**Figure 7.4:** Simulation results of deposit mass uptake for the first six hours for different sets of flue gas temperatures and probe surface temperatures. The fuel (fly ash) input is case 2 (straw < 20 wt.%) shown in Table 7.1.

A comparison of the measured DDF-rates and DDF-rates resulted from the simulation is shown in Table 7.3. High values of DDF-rates can be seen for both measured and simulated results for the case when straw share was more than 20 wt.%. For ashes produced during straw combustion, due to the presence of liquid phase, the sticking probability of the ash increases and thereby higher DDF-rates are the result. The model overestimates the DDF-rate when the straw share was more than 20 wt.% possibly due to a higher sticking efficiency of the fly ash and deposit. The melt fraction was directly taken as the sticking probability, which is rough estimation. In addition, the model only accounts for deposit build-up, and no deposit shedding mechanisms are taken into account. Experimental observations have shown that the amount of deposits on the probe can affect the rate of deposit formation rate, and for lower deposit mass loads, the DDF-rates are normally lower. The model predicted low DDF-rate for case 2 (straw < 20 wt.%) due to a lower sticking probability of the fly ash used as input. However, as shown in Table 7.3 and Figure 7.2, there is a clear relationship between measured and calculated ash deposit formation rates. Most of the data points show that even though the model does not quantitatively agree with the measured results, a qualitative agreement is seen. The results seem to be reasonable, taking into account the simplicity of the model.



**Table 7.3:** Comparison of measured data and simulated data (initial 6 h).

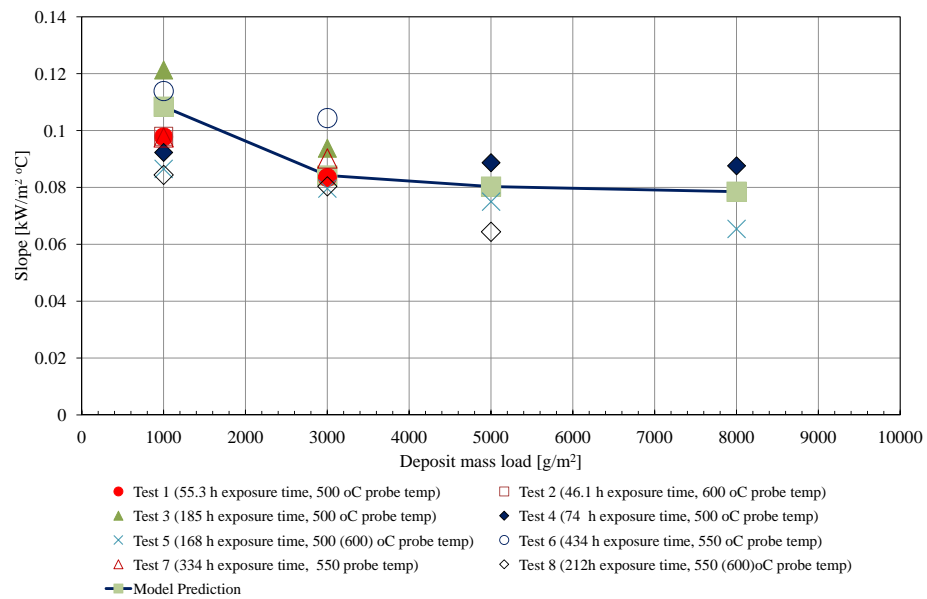
		Flue gas temp. (°C)	Probe temp. (°C)	DDF-rate (g/m <sup>2</sup> /h)	Heat Uptake (kW/m <sup>2</sup> )
Straw > 20 wt. %	Measured	909	491	457	49.7
	Simulation	900	500	3109	36.3
Straw > 20 wt. %	Measured	821	590	519	25.2
	Simulation	820	600	1975	20.2
Straw < 20 wt. %	Measured	810	525	25	33.0
	Simulation	820	500	3	32.8

The complete measured data of ash deposit formation rate (DDF-rate) are divided into groups and shown in Table 7.4 in order to make it possible to analyze the influence of changed conditions in flue gas temperature (above or below 850 °C), probe surface temperature (500 °C or 600 °C), straw fuel share (weight fraction of straw in the fuel above or below 20 %) and deposit mass load (above or below 5,000 g/m<sup>2</sup>). The details of the selection criteria have been explained in Chapter 5. The idea here is to compare the simulation results with the complete measured data to analyze the qualitative behavior of measured data and simulation data. It can be seen that simulated DDF-rate follow the measured results based on the changed conditions in flue gas temperature, probe surface temperature, straw fuel share and deposit mass load. The measured and simulated DDF-rate are low when straw share is low (below 20 wt.%), deposit mass load is low (below 5,000 g/m<sup>2</sup>) and flue gas temperature is low (below 850 °C), while change in probe surface temperature does not affect the measured and simulation results. However, in addition to the deposit build-up model, incorporation of deposit shedding model can potentially result in quantitatively more realistic deposit formation rates.

The predicted heat uptake by the model is shown in Figure 7.5 as a function of different deposit mass loads on the probe. It can be seen that the model generally predicts the probe heat uptake within the range of experimental results. The differences between the measured and simulated heat uptake can be attributed to the assumed effective thermal conductivity, which may be lower for porous deposits.

**Table 7.4:** Measured DDF-rates and DDF-rates resulted from the simulation for two different sets of flue gas temperatures, probe surface temperatures, straw shares and deposit mass loads. <sup>a</sup> mean value of flue gas temperature. <sup>b</sup> the actual value of deposit mass uptake on the probe (simulated).

Fuel straw share		Probe deposit mass load		Flue gas temperature						
				< 850 °C		500 °C		> 850 °C		
				500 °C	600 °C	600 °C	820 °C	900 °C	900 °C	900 °C
Straw > 20 wt. %	> 5,000 g/m <sup>2</sup> (~11,000 g/m <sup>2</sup> ) <sup>b</sup>	Simulation flue gas temperature								
		Mean flue gas temperature (measured, °C)							(909) <sup>a</sup>	(902) <sup>a</sup>
		Mean DDF-rate (g/m <sup>2</sup> /h) (measured)							2691	1934
		Mean DDF-rate (g/m <sup>2</sup> /h) (simulation)							4614	4594
		Mean heat uptake (kW/m <sup>2</sup> ) (measured)							34.0	18.8
		Mean heat uptake (kW/m <sup>2</sup> ) (simulation)							32.2	26.4
Straw > 20 wt. %	< 5,000 g/m <sup>2</sup> (~1,500 g/m <sup>2</sup> ) <sup>b</sup>	Simulation flue gas temperature								
		Mean flue gas temperature (measured, °C)		(823) <sup>a</sup>	(823) <sup>a</sup>				(906) <sup>a</sup>	
		Mean DDF-rate (g/m <sup>2</sup> /h) (measured)		234	313				1245	
		Mean DDF-rate (g/m <sup>2</sup> /h) (simulation)		1347	1336				1648	
		Mean heat uptake (kW/m <sup>2</sup> ) (measured)		30.6	22.3				41.6	
		Mean heat uptake (kW/m <sup>2</sup> ) (simulation)		28.6	21.8				40.4	
Straw < 20 wt. %	> 5,000 g/m <sup>2</sup>	Simulation flue gas temperature								
		Mean flue gas temperature (measured, °C)								
		Mean DDF-rate (g/m <sup>2</sup> /h) (measured)								
		Mean DDF-rate (g/m <sup>2</sup> /h) (simulation)								
		Mean heat uptake (kW/m <sup>2</sup> ) (measured)								
		Mean heat uptake (kW/m <sup>2</sup> ) (simulation)								
Straw < 20 wt. %	< 5,000 g/m <sup>2</sup> (~8 g/m <sup>2</sup> ) <sup>b</sup>	Simulation flue gas temperature								
		Mean flue gas temperature (measured, °C)		(773) <sup>a</sup>	(773) <sup>a</sup>					
		Mean DDF-rate (g/m <sup>2</sup> /h) (measured)		221						
		Mean DDF-rate (g/m <sup>2</sup> /h) (simulation)		2.5						
		Mean heat uptake (kW/m <sup>2</sup> ) (measured)		34.3						
		Mean heat uptake (kW/m <sup>2</sup> ) (simulation)		32.8						



**Figure 7.5:** Prediction of heat uptake for different deposit mass loads on the probe.

Unfortunately, because of lack of time, the shedding model was not simulated and was considered as a part of the ongoing Ph.D. project.

### 7.3 Conclusions

Modeling of the the ash deposition process and heat uptake was done to get better understandings of the key processes responsible for ash deposition. The model describes the deposit related processes as a function of the local parameters as flue gas velocity, flue gas temperature, probe surface temperature and fuel changes. Simulation results showed that when straw share was high, there is an increase in the deposit mass uptake and DDF-rate with increase in flue gas temperature. Increased flue gas temperatures probably increase the fraction of molten ash and that will lead to higher amount of ash being deposited. The results of changed probe surface temperature showed that the changed probe surface temperatures in the range from 500 to 600 °C do not seem to significantly influence the deposit formation rate. The model over predicts the ash deposition rate quantitatively but the qualitative behavior was in accordance with the experimental findings. The heat uptake model predictions were comparable with experimental findings both quantitatively and qualitatively. From a practical point of view, it was seen that the flue gas temperature and share of straw in wood are the two parameters responsible for increased deposit formation on the superheater tubes.

## Chapter 8

# Innovative Ideas for Deposit Shedding in Biomass Suspension-Fired Boilers

### 8.1 Introduction

It was one of the technical objectives of the project to provide recommendations for the optimal operation strategy of biomass suspension-fired boilers with respect to minimization of deposit related problems. Considerations regarding deposit removal techniques, optimal plant sootblowing and ash mixing to minimize deposit problems are discussed in this chapter in the form of ideas.

### 8.2 Proposed Ideas for Deposit Shedding in Biomass Suspension-Fired Boilers

#### 8.2.1 Deposit Removal Using Ring (DRUR)

Experimental findings presented in Chapter 4, 5 and 6 have showed that short exposure time ( $< 2-10$  h) deposits formed on the superheater tubes of biomass suspension-fired boilers are easy to remove. In addition, deposits removal mechanism during straw and wood suspension firing is primarily debonding. Therefore, deposit removing rings can be applied on the superheater tubes and these flexible rings may be able to remove the short exposure deposits effectively with increased deposit removal frequency compared to the natural deposit shedding frequency. A schematic of the deposit removal using a ring and a schematic layout of the are shown in Figure 8.1 and Figure 8.2, respectively. Deposit ring movement can be based on a force control set-up attached with a thin wire that can withstand at higher temperatures, or, if possible, even a complete wireless system. The concept can

be tested on the horizontal probe for small exposure time deposits. The limitations of the concept are the number of rings and the effectiveness of force controller with bigger advantage being the cost effectiveness and flexibility to be used along with other deposit removal techniques. Both erosion and operational costs imposed by the plant sootblowers can be avoided by using the rings.

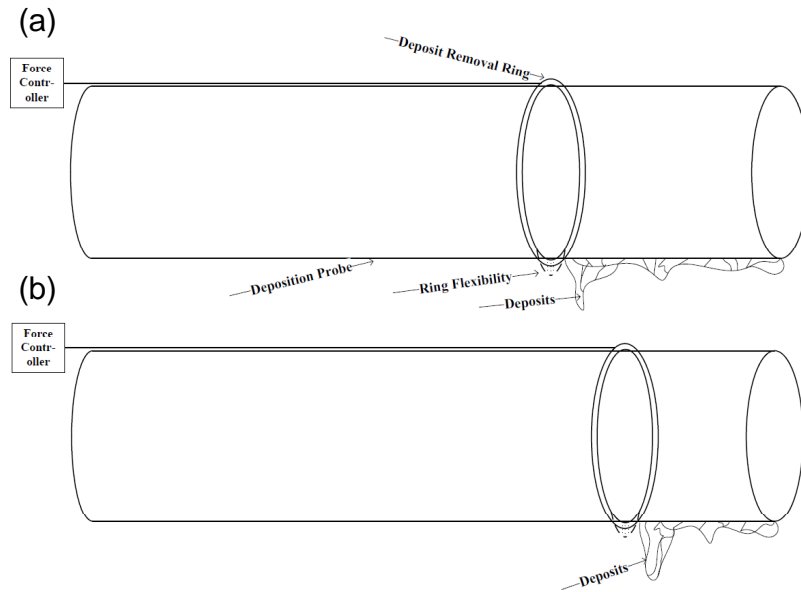


Figure 8.1: A schematic of deposit removal using a ring.

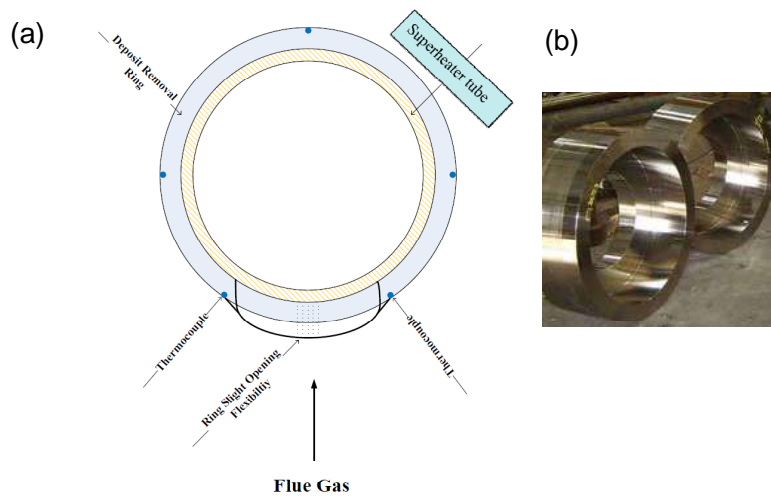


Figure 8.2: a) A schematic layout of the ring for deposit removal on a superheater tube, b) a potential ring that can be used with modifications.

### 8.2.2 Deposit Removal using Mechanical Hitting

Deposits that are not strongly bonded with the boiler tube can be removed using mechanical hitting (vibrations), as is done in some waste incinerators. Thus, the short exposure (< 2–10 h) deposits formed in biomass suspension-fired boilers can be effectively removed with increased deposit removal frequency compared to the natural deposit shedding frequency.

### 8.2.3 Steam Sootblower Optimization

Optimization of a plant sootblower can be made in terms of the frequency of the sootblowers and by controlling it by the steam temperature of the final superheaters. Experimental results presented in Chapter 5 have shown that at lower probe surface temperatures (500 °C), the deposits formed at a exposure time of less than 91 h could be removed with a PIP of less than 55 kPa. At higher probe surface temperature (> 550 °C), the PIP needed to remove the probe deposits significantly increases. Based on steam temperature of the final superheaters, the sootblowers can be optimized by reducing their excessive use, and by reducing the amount of steam used. At lower superheater temperatures (< 500 °C), the sootblower operation frequency should be lower compared to the case when superheater temperatures are higher (> 550 °C). In addition, for the shorter exposure time (< 2–10 h) deposits formed at lower superheater temperatures, the applied steam pressure to the sootblowers should be considerably lower than that is needed in the case of mature deposits and/or deposits formed at higher superheater temperatures.

### 8.2.4 Fuel/Ash Mixing

The results presented in Chapter 6 indicate that the addition of coal fly ash can significantly affect the ash deposition behaviors and the deposit properties during wood suspension combustion. The effect was evident in two measurement locations. At the location with flue gas temperature of 1250–1300 °C, although the addition of coal fly ash increases the DDF-rate and the ash deposition propensity, the deposits formed during coal ash addition seem to shed frequently, suggesting that they are easily removable. On the other hand, the amount of  $K_2SO_4$  in the deposits is significantly reduced when coal ash is added, which is favorable from a corrosion point of view. At the location with a flue gas temperature of 750–800 °C, the addition of coal fly ash reduces the ash deposition propensity and causes the formed deposits to becoming easily removable. Moreover, the Cl present in the deposits without coal ash addition disappears when coal ash is added, which is also favorable from a corrosion point of view.

## Innovative Ideas for Deposit Shedding in Biomass Suspension-Fired Boilers

Effective fuel mixing by minimizing the K/Si molar ratio in the fuel (ash) can possibly result in reducing the concentration of K and Cl in the fly ash produced as discussed in Chapter 5. During the process of pelletizing of straw, certain amount of Si and Ca can be added to the straw pellets, and this will potentially reduce the formation of K and Cl in the fly ash. A reduced percentage of Cl in the fly ash can thereby reduce the sticking efficiency of the produced fly ash.

## Chapter 9

# Conclusions and Suggestions for Further Work

### 9.1 Conclusions

This project aims at providing scientifically based knowledge on understanding of deposit formation and shedding in biomass suspension-fired boilers. In this regard, full-scale measurements were performed in different biomass suspension-fired boilers. The conclusions are thereby divided based on the full-scale measurements. In addition, a predictive model was used to quantify deposit build-up as a function of local gas temperature, probe surface temperature and fuel and fly ash chemical composition.

#### 9.1.1 Ash Transformation and Deposition during Biomass Suspension and Grate Firing

A series of full-scale and long duration deposit probe measurements have been conducted in a biomass suspension boiler to investigate the deposit formation rate, probe heat uptake and ash transformation. Full-scale probe measurements were conducted at a 250 MW<sub>th</sub> suspension boiler, firing straw and wood in suspension, and the results were compared with measurements conducted at a 105 MW<sub>th</sub> straw-fired grate boiler. The probe surface temperature used for all the measurements was kept constant at a value of 500 °C. It was identified that the deposit formation rate increases moderately with straw share increase, when straw is co-fired with wood in a suspension boiler. It was found that during 35% straw fuel share on mass basis, a deposit formation rate (Integral Deposit Formation rate, IDF-rate) of 33 g/m<sup>2</sup>/h (initial 12 h) was observed, while the corresponding deposit formation rate increased to 41 g/m<sup>2</sup>/h when 100% straw was fired. During straw grate firing, the measured deposit formation rate was nearly similar in two tests and approximately 38 g/m<sup>2</sup>/h.



The current full-scale measurements data were compared with data from previously conducted deposit probe measurements. The comparison showed an increasing trend in deposit formation rate with increase in flue gas temperature. At a flue gas temperature of 650 °C, the deposit formation rate is typically from 5 to 30 g/m<sup>2</sup>/h and at 900 °C, the deposit formation rate is typically 20 to 110 g/m<sup>2</sup>/h. At higher fuel alkali contents (K > 0.9 wt.%), the increase in deposit formation rate with flue gas temperature was more significant, compared to the increase in the deposit formation rate at lower fuel alkali contents (K ≤ 0.9 wt.%). An increased flue gas temperature probably increases the fraction of molten ash as well as provides an increased content of gas phase alkali species, and both will lead to an increased deposit formation rate. It was also observed that the deposit formation rates measured in suspension and grate boilers are on similar levels. This was observed even though the concentration of fly ash in the flue gas was significantly higher in the straw suspension-fired boiler.

The elemental composition of fly ash generated during straw suspension firing shows higher contents of Si and Ca, compared to grate firing fly ash that is rich in the volatile elements K, Cl and S. SEM-EDS analysis indicated that the fly ash generated during straw firing in suspension consists of three kinds of particles: 1) flake type Si rich particles, 2) molten or partially molten particles (> 20 μm) rich in Si, K and Ca with small amounts of Mg, P and potassium salts on the outer surface, and 3) small particles rich in K, Cl and S (aerosols, between 0.1 and 5 μm). Chemical analysis of the outer layer of upstream deposits during 35% straw-firing and 100% straw firing indicated that by increasing the straw share in the fuel, the K, Cl and Si contents were increased, while the Ca and Mg contents were reduced.

It was found that 35% straw firing with wood does not create severe fouling and slagging on the heat exchanger tubes. The experiences of the operational staff indicates that the boiler operation period may exceed more than one month without deposit related operational problems when firing maximum 50% straw with wood on mass basis. The findings related to deposit management during straw suspension firing are:

- At higher flue gas temperatures (750–950 °C), efficient soot blowing is needed to manage the boiler tube deposits with small superheater tube spacing (113 mm, current case). An increase in superheater tube spacing probably will lead to the absence of tube clogging by ash deposits.
- At flue gas temperatures below 650 °C, deposit formation rate is small and deposits can be easily removed by sootblowers.

### 9.1.2 Transient Deposit Build-up and Shedding during Straw and Wood Suspension Combustion

A series of full-scale measurements have been conducted in a suspension-fired boiler to investigate ash deposit formation and deposit shedding when firing straw and wood. The measurements were performed at Amager unit 1, a 350 MW<sub>th</sub> suspension boiler, firing straw and wood. The influence of fuel type, probe exposure time, probe surface temperature, and flue gas temperature on ash deposit formation rate has been investigated. A systematic procedure to determine deposit formation rate from probe measuring deposit data was developed and termed the derivative-based deposit formation (DDF) rate. A comparison with previously conducted probe measurements at different straw-fired boilers was made based on another measure of deposit formation rate - integral deposit formation rate (IDF-rate). Ash transformation was investigated by bulk ash analysis of the fuel ash, residual ash and deposit layers. Quantification of naturally occurring deposit shedding, sootblowing deposit shedding and Peak Impact Pressure (PIP) needed to remove the deposits by sootblowing was made. The overall conclusions are the following:

- The bulk chemical composition of straw and wood suspension-fired fly ash shows relatively higher contents of Si, Ca, and lower contents of volatile elements (K, Cl and S), compared to grate firing conditions. However, it was also found that with an increase in fuel ash K/Si molar ratio the concentration of volatile elements, K, Cl, and, to some extent, S, increased in the fly ash.
- The upstream side deposit outer layers on the probe contain high concentration of Si, K and Ca, indicating that larger particles impact on and stick to the probe on the upstream side. K, S and Cl were found in higher proportions on the downstream side deposit layers indicating that the downstream deposits to a greater extent are formed by thermophoresis and/or condensation of KCl and K<sub>2</sub>SO<sub>4</sub>. The innermost layers were rich in K, Cl and S.
- The Integral Deposit Formation rate (IDF-rate) increases with increased fuel K contents (straw share in wood), and with increase in flue gas temperature, but probe surface temperatures have no significant influence on the IDF-rate. The IDF-rates determined from biomass grate and suspension firing are comparable.
- The DDF-rate increases with increased straw share in wood and with increase in flue gas temperature, but probe surface temperatures have no significant influence on the measured DDF-rates.
- The overall mean DDF-rate also increases with an increase in flue gas temperature and the overall DDF-rate levels between 234 to 3105

$\text{g/m}^2/\text{h}$  were observed.

- Video recordings revealed that deposit shedding was primarily through debonding, where a deposit layer is being removed due to a break off of the deposit from the tube surface.
- It was observed that the shedding process is a stochastic process, where the shed amounts are highly variable even at constant conditions. We believe the amount of deposit shed is strongly related to the strength of the inner most salt rich deposit layer.
- The deposit shedding process was characterized by calculation of the average amount of deposit removed at a shedding event [ $\text{g/m}^2$ ] and the frequency of the shedding events [ $\text{h}^{-1}$ ] in 6 h periods. The average shedding event magnitude was  $716 \text{ g/m}^2$  during natural deposit shedding and  $805 \text{ g/m}^2$  during plant sootblower induced shedding. The shedding frequencies were  $0.81 \text{ h}^{-1}$  and  $0.89 \text{ h}^{-1}$  during natural deposit shedding and plant sootblower shedding events, respectively. Based on the shedding magnitude and frequency it was possible to calculate a shedding rate [ $\text{g/m}^2/\text{h}$ ].
- The deposit shedding rates increased at high flue gas temperatures ( $> 850 \text{ }^\circ\text{C}$ ) and high probe deposit mass loads ( $> 5,000 \text{ g/m}^2$ ) where also high deposit formation rates are observed (DDF-rate).
- The shedding rate is in most cases higher at a probe temperature of  $500 \text{ }^\circ\text{C}$  than at a probe temperature of  $600 \text{ }^\circ\text{C}$ .
- The net deposit accumulation rate increases with increase in flue gas temperature. Increased flue gas temperatures probably increase the fraction of molten ash particles as well as provide an increased content of gas phase alkali species, and both will lead to an increased deposit formation rate. The increase in DDF-rate was larger than the increase in deposit shedding rate with increased flue gas temperature.
- The net deposit accumulation rate is low ( $452 \text{ g/m}^2/\text{h}$ ) at lower deposit mass load ( $< 5,000 \text{ g/m}^2$ ) on the probe, compared to a value of  $1155 \text{ g/m}^2/\text{h}$  for deposit mass load greater than  $5,000 \text{ g/m}^2$  (probe temperature  $500 \text{ }^\circ\text{C}$ , flue gas temperature about  $900\text{--}910 \text{ }^\circ\text{C}$  and straw share more than 20 wt.%).
- Generally no clear tendency for the impact of probe surface temperature on net deposit accumulation rate was seen.
- A sootblower probe was used to investigate the needed PIP to remove the deposits. At lower temperatures ( $500 \text{ }^\circ\text{C}$ ), the deposits formed at a exposure time of less than 91 h could be removed with a PIP of less

than 55 kPa. At higher probe surface temperature ( $> 550$  °C), the PIP needed to remove the probe deposits significantly increases.

### 9.1.3 Ash Deposit Build-up and Shedding during Wood Suspension Combustion with Coal Ash Addition

A series of deposit probe boiler measurements were conducted at Avedøre Unit 2 wood and natural gas suspension-fired boiler, to investigate ash deposition in a wood fired boiler with coal ash addition. The probe was placed just below the radiation shield in the top of the boiler chamber. The measurements included deposit mass, heat uptake, flue gas temperature and video registration. The tests were conducted both with and without coal ash addition, and at two different locations with flue gas temperatures of 1250–1300 °C and 750–800 °C respectively. The overall conclusions are summarized in the following points:

- Changes in biomass boiler load lead to some degree to changes in boiler flue gas temperature and the used coal ash to wood ash ratio. It was therefore difficult to determine which changes that causes the observed large changes in the deposit formation rate. However, a high increase in local flue gas temperature increased the deposit formation rate in this study, and this has also been observed in other previous deposit probe measurements conducted at biomass-fired boilers.
- Video monitoring revealed that the deposits formed with coal ash addition were not sticky and could be easily removed by gravity shedding (debonding), and even at very high flue gas temperatures ( $> 1350$  °C), deposit removal through surface melting was not identified. This indicates that potassium (K) has been potentially captured by coal ash to form deposits with high melting temperatures.
- At location with high flue gas temperature of 1250–1300 °C, the addition of coal ash increase the ash deposition propensity. With addition of coal ash, the deposit formation under this condition is characterized by a relatively fast build-up (e.g.  $\sim 1$ –3 h) followed by shedding of the deposit layer. Under conditions of wood-firing without coal ash addition, the deposit formation is characterized by a long-term (e.g. 10 h) deposit build-up on the upstream side of the probe, followed by shedding of a large deposit layer. Although the addition of coal fly ash increases the DDF-rate and the ash deposition propensity, the deposits formed during coal ash addition seem to shed frequently, suggesting that they are easily removable.
- At location with high flue gas temperature of 750–800 °C, under both conditions of with and without coal ash addition, the deposit formation

was characterized by an initial slow build-up, and after a few hours, the mass uptake of the deposit probe becomes almost constant, implying that the deposit build-up and shedding are close to equilibrium. However, the ash deposition propensity slightly reduced by injection of coal ash. In addition, the formed deposits during coal ash addition were easily removable.

- At the location with flue gas temperature of 1250–1300 °C, the deposits formed without coal ash addition are dominated by K-Ca-Si rich particles and K<sub>2</sub>SO<sub>4</sub> rich clusters. With the addition of coal fly ash, SEM-EDS analysis of the deposits shows significant presence of Ca, Al and Si, indicating that K has been captured by the coal ash to form deposits rich in calcium-alumina-silicates. Cl was not found either on the upstream side or on the downstream side of the probe, indicating that Cl has been released to the gas phase as HCl(g).
- At the location with flue gas temperature of 750–800 °C, the deposits formed without coal ash addition were dominated by small particles rich in K, Ca, S and Cl. With the addition of coal fly ash, the Cl disappeared in the deposits collected at this location. The deposits were dominated by calcium-alumina-silicates rich particles, supplemented by a small amount of K<sub>2</sub>SO<sub>4</sub> particles. The ash deposition propensity is decreased when coal ash is added.

#### 9.1.4 Mechanistic Modeling of Ash Deposit Build-up and during Biomass Suspension Firing

Sub-model for each ash deposition process and a sub-model for heat uptake was simulated to get better understandings of the key processes responsible for ash deposition. The model describes the deposit related processes as a function of the local parameters as flue gas velocity, flue gas temperature, probe surface temperature and fuel changes. Simulation results showed that when straw share was more than 20 wt.%, there is an increase in the deposit mass uptake and DDF-rate with increase in flue gas temperature. Increased flue gas temperatures probably increase the fraction of molten ash as well as provide an increased content of gas phase alkali species, and both will lead to higher amount of ash being deposited. The results of changed probe surface temperature showed that the changed probe surface temperatures in the range from 500 to 600 °C do not seem to significantly influence the deposit formation rate. The model over predicts the ash deposition rate quantitatively but the qualitative behavior was in accordance with the experimental findings. The heat uptake model predictions were comparable with experimental findings both quantitatively and qualitatively. From a practical point of view, it was seen that the flue gas temperature and share

of straw in wood are the two parameters responsible for increased deposit formation on the superheater tubes.

## 9.2 Future Work

Besides the research conducted in the present study, following are the areas where more detailed investigation can further help for optimal use of straw and wood in suspension-fired boilers.

- A detailed relation between fuel ash chemistry and ash deposit formation rate.
- An accurate evaluation of binding force between deposit to probe surface.
- Implementation and testing of results from horizontal probe to vertical probe.
- Quantification of ash formation elements and processes based on single particle combustion behavior.
- A predictive model to quantify ash deposit build-up and shedding on the superheater tube and on the boiler furnace wall.



# References

- [1] REN21 (Renewable Energy Policy Network for 21<sup>st</sup> Century) Global Status Report, 2011.  
[www.ren21.net/Portals/97/documents/GSR/REN21\\_GSR2011.pdf](http://www.ren21.net/Portals/97/documents/GSR/REN21_GSR2011.pdf)
- [2] F. J. Frandsen, *Ash formation, deposition and corrosion when utilizing straw for heat and power production*, Doctoral Thesis, 2011, Technical University of Denmark, ISBN 978-87-92481-40-5.
- [3] M. P. Glazer, *Alkali metals in combustion of biomass with coal*, PhD Thesis, 2006, Technical University of Delft. Available online (19-03-2012), <http://repository.tudelft.nl/view/ir/uuid:404df03f-cbaf-49b4-9eee-5661806b8a5e/>
- [4] M. Montgomery, S. A. Jensen, U. Borg, O. Biede, T. Vilhelmsen, *Materials and Corrosion*, **62** (2011), 593–605.
- [5] L. Tobiasen, R. Skytte, L. S. Pedersen, S. T. Pedersen, M. A. Lindberg, *Fuel Processing Technology*, **88** (2007), 1108–1117.
- [6] H. Egsgaard, U. Hansen, P. A. Jensen, P. Glarborg, *Combustion and Gasification Technologies, Risø Energy Report 2*, Technical University of Denmark.  
[http://www.risoe.dk/rispubl/energy\\_report/ris-r-1430s35\\_39.pdf](http://www.risoe.dk/rispubl/energy_report/ris-r-1430s35_39.pdf)
- [7] J. M. Johansen, *Release of inorganic matter during combustion of biomass*, M.Sc. Thesis, 2011, Department of Chemical and Biochemical Engineering, Technical University of Denmark.
- [8] Green energy - towards a Danish energy without fossil fuels, Klimakommissionen (Climate Commission), 2010, Denmark. ISBN (www) 978-87-7844-878-1.
- [9] M. Hupa, *Energy & Fuels*, **26** (2012), 4–14.
- [10] L. L. Baxter, *Biomass and Bioenergy*, **4** (1993), 85–102.



- 
- [11] M. Leckner, F. Winter, A. K. Agarwal, Handbook of combustion, volume 4: solid fuels, 2010, *Wiley-VCH*, ISBN 978-3-527-32449-1.
- [12] B. Sander, N. Henriksen, O. H. Larsen, A. Skriver, C. Ramsgaard-Nielsen, J. N. Jensen, K. Stærkind, H. Livberg, M. Thellefsen, K. Dam-Johansen, F. J. Frandsen, R. van der Lans, J. Hansen, *Emissions, corrosion and alkali chemistry in straw-fired combined heat and power plants, Proceedings of 1<sup>st</sup> World Conference on Biomass for Energy and Industry*, 05–09 June, Sevilla, 2009.
- [13] L. L. Baxter, *Ash deposit formation and Deposit properties: A comprehensive summary of research conducted at Sandia's Combustion Research Facility, SAN2000-8253*, Sandia National Laboratories, Livermore, CA 94550 USA, 2000.
- [14] B. M. Jenkins, L. L. Baxter, T. R. Miles (Jr.), T. R. Miles, *Fuel Processing Technology*, **54** (1998), 17–46.
- [15] L. A. Hansen, *Melting and sintering of ashes*, PhD Thesis, 1998, Technical University of Denmark, ISBN 87-90142-31-4.
- [16] L. L. Baxter, T. R. Miles, T. R. Miles (Jr.), B. M. Jenkins, T. Milne, D. David, R. W. Bryers, L. L. Oden, *Fuel Processing Technology*, **54** (1998), 47–78.
- [17] H. P. Nielsen, *Deposition and high temperature corrosion in biomass-fired boilers*, PhD Thesis, 1998, Technical University of Denmark, ISBN 87-90142-47-0.
- [18] T. R. Miles, T. R. Miles (Jr.), L. L. Baxter, R. W. Bryers, B. M. Jenkins, L. L. Oden, *Biomass and Bioenergy*, **10** (1996), 125–138.
- [19] L. L. Baxter, *Fuel Processing Technology*, **56** (1998), 81–88.
- [20] K. H. Andersen, *Deposition formation during coal straw co-combustion in a utility pf-boiler*, PhD Thesis, 1998, Technical University of Denmark, ISBN 87-90142-47-0.
- [21] P. A. Jensen, F. J. Frandsen, J. Hansen, K. Dam-Johansen, N. Henriksen, S. Hörlyck, *Energy & Fuels*, **18** (2004), 378–384.
- [22] F. J. Frandsen, *Fuel*, **84** (2005), 1277–1294.
- [23] K. Bendixen, *USC technology in CCT boilers applying biomass cofiring, Proc. of Power-Gen Europe*, 28–30 June, Milano, 2005.
- [24] P. A. Jensen, M. Dall'ora, W. Lin, S. Clausen, J. Hansen, P. Simonson, M. Berg, A. D. Jensen *Measurements on the 800 MW<sub>th</sub> Avedøre oil*,

## REFERENCES

---

- gas and wood co-fired suspension-boiler-Analysis of emission, burnout, deposit and FTIR measurements from April 2005, PSO Project 6526, Report R0802*, CHEC Research Centre, Technical University of Denmark, 2008.
- [25] K. A. Christensen, M. Stenholm, H. Livbjerg, *J. Aerosol Sci.*, **29** (1998), 421–444.
- [26] J. H. Zeuthen, P. A. Jensen, H. Livbjerg, J. P. Jensen, *Energy & Fuels*, **21** (2007), 699–709.
- [27] D. Nordgren, H. Hedman, N. Padban, D. Boström, M. Öhman, *Fuel Processing Technology*, (2011), doi:10.1016/j.fuproc.2011.05.027.
- [28] S. S. Lokare, J. D. Dunaway, D. Moulten, D. Rogers, D. R. Tree, L. L. Baxter, *Energy & Fuels*, **20** (2006), 1008–1014.
- [29] J. N. Knudsen, *Volatilization of inorganic matter during combustion of annual biomass*, PhD Thesis, 2004, Technical University of Denmark, ISBN 87–91435–11–0.
- [30] P. M. Walsh, A. N. Sayre, D. O. Loehden, L. S. Monroe, J. M. Beer, A. F. Sarofim, *Prog Energy Combust Sci*, **4** (1990), 327–346.
- [31] H. Zhou, P. A. Jensen, F. J. Frandsen, *Fuel*, **86** (2007), 1519–1533.
- [32] M. Hupa, B-J, Skrifvars, A. Moilanen, *Fuel Processing Technology*, **62** (1989), 131–137.
- [33] H. Zhou, F. J. Frandsen, P. A. Jensen, P. Glarborg, *Ash deposit formation and removal in biomass-fired boilers, PSO Project 4106, Report R0603*, CHEC Research Centre, Technical University of Denmark, 2006.
- [34] C. L. Senior, *Energy & Fuels*, **11** (1997), 416–420.
- [35] A. Zbogar, F. J. Frandsen, P. A. Jensen P. Glarborg, P. Hansen, *Energy & Fuels*, **20** (2006), 512–519.
- [36] A. L. Kaliazine, F. Piroozmand, D. E. Cormack, H. Tran, *TAPPI Journal*, **80** (1997), 201–207.
- [37] IFRF Combustion Handbook, January 16, 2009.  
<http://www.handbook.ifrf.net/handbook/index.html>
- [38] B-J. Skrifvars, T. Lauren, M. Hupa, R. Korbee, P. Ljung, *Fuel*, **83** (2004), 1371–1379.
- [39] H. Wu, *Co-combustion of fossil fuels and waste*, PhD Thesis, 2011, Technical University of Denmark.

- 
- [40] P. A. Jensen, B. Sander, K. Dam-Johansen, *Biomass and Bioenergy*, **20** (2001), 447–457.
- [41] M. Theis, B. J. Skrifvars, M. Hupa, H. Tran, *Fuel*, **85** (2006), 1125–1130.
- [42] A. Zbogar, F. J. Frandsen, P. A. Jensen, P. Glarborg, *Prog Energy Combust Sci*, **35** (2009), 31–56.
- [43] E. Raask, *Mineral impurities in coal combustion*, Edition 41, Hemisphere Publishing Corporation, 1985.
- [44] M. I. Jameel, D. E. Cormack, H. Tran, T. E. Moskal, *Tappi Journal*, **77** (1994), 135–142.
- [45] L. A. Hansen, H. P. Nielsen, F. J. Frandsen, J. Hansen, K. Dam-Johansen, S. Hörlyck, A. Karlsson, *Fuel Processing Technology*, **64** (2000), 189–209.
- [46] P. A. Jensen, M. Stenholm, P. Hald, *Energy & Fuels*, **11** (1997), 1048–1055.
- [47] P. Isaak, H. N. Tran, D. Barham, D. W. Reeve, *Journal of pulp and paper science*, **13(5)** (1987), 154–158.
- [48] K. Wieck-Hansen, P. Overgaard, O. H. Larsen, *Biomass and Bioenergy*, **19** (2000), 395–409.
- [49] J. Sandberg, U. Sand, R. B. Fedhila, *International Journal of Green Energy*, **3** (2006), 43–61.
- [50] H. M. Brink, J. P. Smart, J. M. Vleeskens, J. Williamson. *Fuel*, **73** (1994), 1712–1717.
- [51] B. M. Jenkins, R. B. Williams, P. R. Bakker, S. Blunk, D. E. Yomogida, W. Carlson, J. Duffy, R. Bates, K. Stuci, V. Tiangco, *Combustion of leached straw for power generation, 4<sup>th</sup> Biomass Conference of the Americas*, Pergamon, Elsevier Science, Oxford, UK, 1999, pp 1357-1363.
- [52] Fundamentals in Biotechnology, Volume 7, Chapter: Biomass Feedstocks, pp. 315–324. Editor(s) H. W. Doelle and S. Rokem. ISBN 978–1–84826–258–7 (e-book).
- [53] L. Hindiyarti, *Gas phase sulfur, chlorine, and alkali metal chemistry in biomass combustion*, PhD Thesis, 2007, Technical University of Denmark, ISBN 87–91435–58–7.
- [54] Danish Energy Agency, Denmark, [www.ens.dk](http://www.ens.dk).

## REFERENCES

---

- [55] L. Baxter, G. Hatch, S. A. Sinqfield, W. J. Frederick, *An experimental study of the mechanisms of fine particle deposition in kraft recovery boilers*, 1998, International Chemical Recovery Conference Proceedings.
- [56] G. Barnocky, R. H. Davis, Elastohydrodynamic collision and rebound of spheres: Experimental verification, *Phys. Fluid*, **31** (1998), 1324–1329.
- [57] J. P. Hurley, S. A. Benson, *Energy & Fuels*, **9** (1995), 775–781.
- [58] J. W. Nowok, *Journal of Institute of Energy*, **69** (1996), 9–11.
- [59] B. Sander, *Biomass and Bioenergy*, **12(3)** (1997), 177–183.
- [60] C. Yin, L. A. Rosendahl, S. K. Kær, *Prog Energy Combust Sci*, **35** (2008), 725–754.
- [61] M. A. Telfer, D. K. Zheng, *Energy & Fuels*, **12(6)** (1998), 1135–1141.
- [62] P. Glarborg, A. D. Jensen, *Combustion and Harmful Emission Control [28244 E08]*, Course Notes, Technical University of Denmark, 2002.
- [63] S. C. van Lith, *Release of inorganic elements during wood-firing on a grate*, PhD Thesis, 2005, Technical University of Denmark, ISBN 87-91435-29-3.
- [64] Major technologies for the exploitation of renewable energy sources, May 12, 2008.  
[www.eppo.go.th/encon/encon-DC-Cogen10-Chap5.doc](http://www.eppo.go.th/encon/encon-DC-Cogen10-Chap5.doc)
- [65] S. v. Loo, J. Koppejan, The handbook of biomass combustion and co-firing, 2008, *Published by Earchscan*, ISBN 978-84407-249-1.
- [66] M. Berg, S. T. Pedersen, G. Rohde, *VGB Powertech*, **87** (2007), 93–95.
- [67] D. C. Dayton, R. J. French, T. A. Milne, *Energy & Fuels*, **9** (1995), 855–865.
- [68] H. Tran, X. Mao, D. C. S. Kuhn, R. Backman, M. Hupa, *Pulp Pap. Can.*, **130** (2002), 29–33.
- [69] P. A. Jensen, H. Zhou, F. Frandsen, J. Hansen, *Ash deposits removal in biomass power plant boilers*, 15<sup>th</sup> European Biomass Conference and Exhibition, 7-11 May, Berlin, 2007.
- [70] S. Stitt, H. Junker, L. L. Baxter, *Optimization of deposit removal in biofueled boilers: review of control systems, technologies and mechanism*, *Eltra Project no. 3144, TW 13317.00, Report 02-1036, Tech-wise*, 2002, 1–27.

- [71] M. I. Jameel, D. E. Cormack, H. Tran, T.E. Moskal, *TAPPI Journal*, **77(5)** (1994), 135–142.
- [72] Rosnik GmbH + Co, September 15, 2008.  
[http://www.rosink.com/en/Apparatebau/rb/index\\_russbl.htm](http://www.rosink.com/en/Apparatebau/rb/index_russbl.htm)
- [73] H. Wu, P. Glarborg, F. J. Frandsen, K. Dam-Johansen, P. A. Jensen, *Energy & Fuels*, **25** (2011), 2862–2873.
- [74] L. Sørensen, J. Fjellerup, U. Henriksen, International Patent Number WO 01/05911 A2, 2001.
- [75] ChlorOut, *European Patent EP 1354167*, International Patent Application: PCT/SE 02/00129, 2002.
- [76] H. Kassman, M. Berg, *Ash related problems in wood-fired boilers and effect of additives*, Workshop on ash deposition and corrosion, Glasgow, 2006.
- [77] Z. Huque, *Experimental investigation of slag removal using pulse detonation wave technique*, NIST, DOE/HBCU/OMI Annual Symposium, Miami, FL, March 16–18, 1999.
- [78] S. A. Ebrahimi-Sabet, *A Laboratory study of deposit removal by debonding and its application to fireside deposits in Kraft boilers*, PhD Thesis, 2001, Department of Chemical Engineering and Applied Chemistry, University of Toronto, ISBN 0–612–58923–4.
- [79] T. Madhiyanon, P. Sathitruangsak, S. Sungworagarn, S. Pipatmanomai, S. Tia, *Fuel Processing Technology*, **96** (2012), 250–264.
- [80] A. L. Robinson, H. Junker, L. L. Baxter, *Energy & Fuels*, **16** (2002), 343–355.
- [81] R. Shenassa, *Dynamic carryover deposition in an entrained flow reactor*, PhD Thesis, 2000, Department of Chemical Engineering and Applied Chemistry, University of Toronto, ISBN 0–612–49833–6.
- [82] P. A. Jensen, L. H. Sørensen, G. Hu, J. K. Holm, F. Frandsen, U. B. Henriksen, *Combustion experiments with biomass fuels and additives in a suspension fired entrained flow reactor - Test of Ca and P rich additives used to minimize deposition and corrosion, Report R0504*, CHEC Research Centre, Technical University of Denmark, 2005.
- [83] J. Capablo, P. A. Jensen, K. H. Pedersen, K. Hjuler, L. Nikolaisen, R. Backman, F. Frandsen, *Energy & Fuels*, **23** (2009), 1965–1976.
- [84] E. Gjernes, *Fuel flexibility at Amager unit 1 using pulverized fuels. Proc. of Power-Gen Europe*, Cologne, Germany 2006.

## REFERENCES

---

- [85] L. S. Pedersen, H. P. Nielsen, S. Kiil, L. A. Hansen, K. Dam-Johansen, F. Kildsig, J. Christensen, P. Jespersen, *Fuel*, **75** (1996), 1584–1590.
- [86] L. S. Pedersen, D. M. Morgan, W. L. van de kamp, J. Christensen, P. Jespersen, K. Dam-Johansen, *Energy & Fuels*, **11**(2) (1997), 439–446.
- [87] B. Sander, *EU project UCOR, Utilization of residues from biomass co-combustion in pulverized coal boilers, results from full-scale co-firing of coal and straw at the Vest Kraft Power Station Unit 1*, Elsam Engineering A/S, Report No. 02–443, 2002.
- [88] F. J. Frandsen, H.P. Nielsen, P. A. Jensen, L. A. Hansen, H. Libbjerg, K. Dam-Johansen, P. F. B. Hansen, K. H. Andersen, H. S. Sørensen, O. H. Larsen, B. Sander, N. Henriksen, P. Simonsen, *Impact of mineral impurities in solid fuel combustion*, edited by Gupta et al. Kluwer Academic, New York, pp 71–78, 1999.
- [89] B. Sander, K. Wieck-Hansen, *Full-scale investigations on alkali chemistry and ash utilization by co-firing of straw, 14<sup>th</sup> European Biomass Conference and Exhibition*, October, Paris, 2005.
- [90] A. Zbogor, F. J. Frandsen, P. A. Jensen, P. Glarborg, *Prog Energy Combust Sci*, **31** (2005), 1–51.
- [91] H. Wang, J. N. Harb, *Prog Energy Combust Sci*, **23** (1997), 267–282.
- [92] T. A. Erickson, S. E. Allan, D. P. McColler, J. P. Hurley, S. Srinivasachar, S. G. Klang, J. E. Baker, M. E. Morgan, S. A. Johnson, R. Borio, *Fuel Processing Technology*, **44** (1998), 155–171.
- [93] S. K. Kær, *Numerical investigation of deposit formation in straw-fired boilers*, PhD Thesis, Aalborg University, Denmark, ISBN 87–89179–39–0, 2001.
- [94] S. K. Kær, L. Rosendahl, *Extending the modeling capacity of CFD codes applied to biomass-fired boilers*, Proc. ECOS 2003, June 30 – July 2, 2003, Copenhagen, Denmark, 251–264.
- [95] A. Brink, T. Lauren, P. Yrjas, M. Hupa, J. Friesenbichler. *Fuel Processing Technology*, **88** (2007), 1129–1135.
- [96] H. B. Vuthaluru, *Fuel*, **78** (1999), 1789–1803.
- [97] S. Gupta, R. Gupta, G. Bryant, T. Wall, S. Watanabe, T. Kiga, K. Narukawa, *Energy & Fuels*, **23** (2009), 2570–2575.
- [98] T. Heinzl, V. Siegle, H. Spliethoff, K. R. G. Hein, *Fuel Processing Technology*, **54** (1998), 109–125.

- 
- [99] S. P. Hanson, M. F. Abbott, *Prog Energy Combust Sci*, **24** (1998), 503–511.
- [100] IFRF Suction Pyrometer, user information document, 2007, International Flame Research Foundation, Netherlands.
- [101] M. S. Bashir, P. A. Jensen, F. J. Frandsen, S. Wedel, K. Dam-Johansen, J. Wadenbäck, S. T. Pedersen, *Fuel Processing Technology*, **97** (2012), 93–106.
- [102] H. P. Mickelsen, F. J. Frandsen, K. Dam-Johansen, O. H. Larsen, *Fuel Processing Technology*, **54** (1998), 95–108.
- [103] K. H. Andersen, F. J. Frandsen, P. F. B. Hansen, K. Wieck-Hansen, I. Rasmussen, P. Overgaard, K. Dam-Johansen, *Energy & Fuels*, **14**(4) (2000), 765–780.
- [104] J. Hansen, P. A. Jensen, P. Glarborg, *Deposit probe measurements in the Avedøre and Ensted straw fired grate boilers, PSO Project 4792, Report R0705*, CHEC Research Centre, Technical University of Denmark, 2007.
- [105] A. A. Masiá, B. J. P. Buhre, R. P. Gupta, T. F. Wall, *Fuel Processing Technology*, **88** (2007), 1071–1081.
- [106] K. salmenoja, *Field and laboratory studies on chlorine-induced superheater corrosion in boilers fired with biofuels*, PhD Thesis, 2000, Faculty of Chemical Engineering, Åbo Akademi, Åbo/Turku, Finland.
- [107] Y. Zheng, P. A. Jensen, A. D. Jensen, B. Sander, H. Jusker, *Fuel*, **86** (2007), 1008–1020.
- [108] M. S. Bashir, P. A. Jensen, F. J. Frandsen, S. Wedel, K. Dam-Johansen, J. Wadenbäck, S. T. Pedersen, *Energy & Fuels*, **26** (2012), 2317–2330.
- [109] M. S. Bashir, P. A. Jensen, F. J. Frandsen, S. Wedel, K. Dam-Johansen, J. Wadenbäck, S. T. Pedersen, *Energy & Fuels*, **26** (2012), 5241–5255.
- [110] J. R. Kittrel *Advances in Chemical Engineering*, **8** (1970), 97–103.
- [111] D. J. Pritchard, D. W. Bacon, *Chemical Engineering Science*, **33** (1978), 1539–1543.
- [112] Matlab, signal processing toolbox, March 31, 2011.  
<http://www.mathworks.com/help/toolbox/signal/resample.html>

## REFERENCES

---

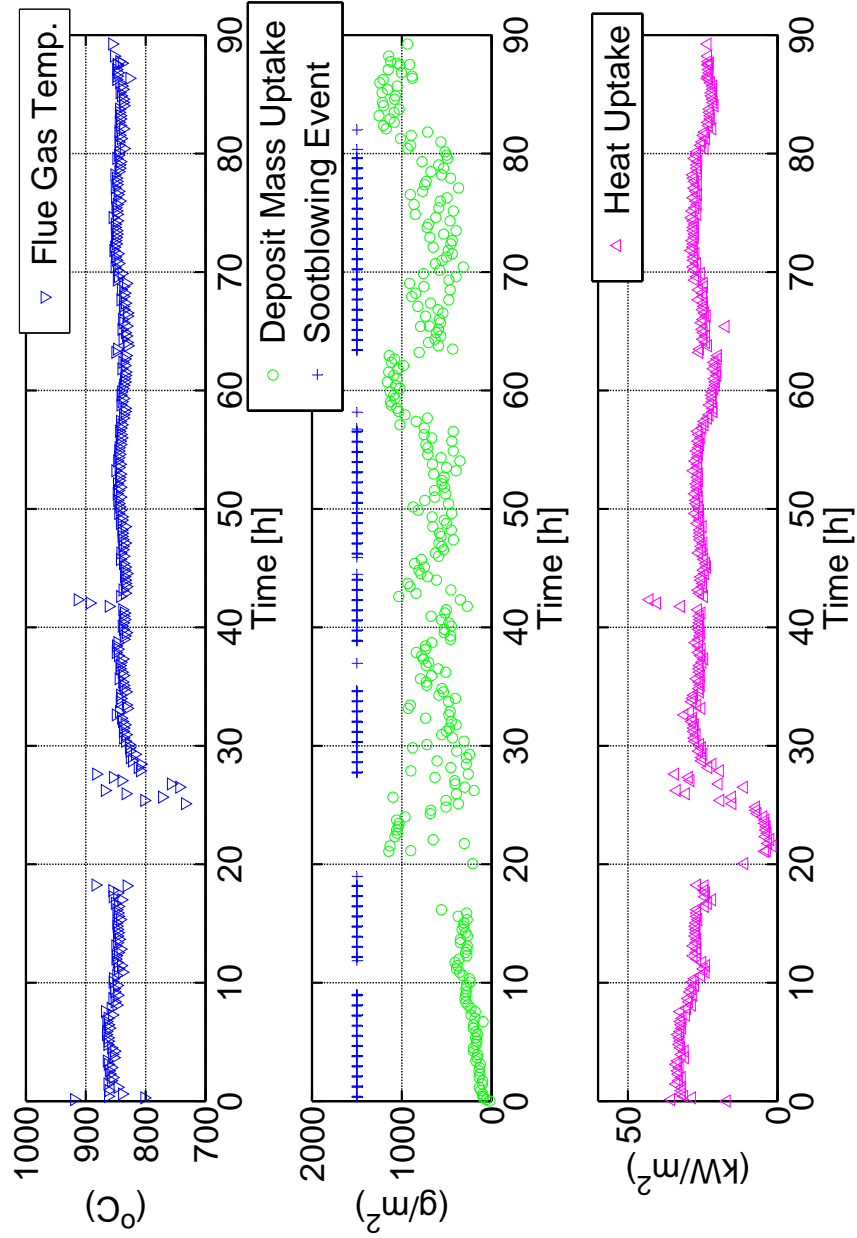
- [113] Moving slope calculation, December 16, 2010.  
<http://www.mathworks.com/matlabcentral/fileexchange/16997-movingslope>
- [114] Online book, December 31, 2010. Chapter 15, pp. 277–284  
<http://www.dspguide.com/>
- [115] Matlab, curve fitting toolbox, March 31, 2011.  
[http://www.mathworks.com/help/toolbox/curvefit/bq\\_6yqb.html](http://www.mathworks.com/help/toolbox/curvefit/bq_6yqb.html)
- [116] J. R. Brock, *J. Col. Sci.*, **17** (1962), 768–780.
- [117] R. C. Flagan, J. H. Seinfeld, Fundamentals of air pollution engineering, *Prentice-Hall Inc.*, New Jersey, (1988).
- [118] S. Vargas, *Straw and coal ash rheology*, PhD Thesis, 2001, Technical University of Denmark, ISBN 87-90142-64-0.



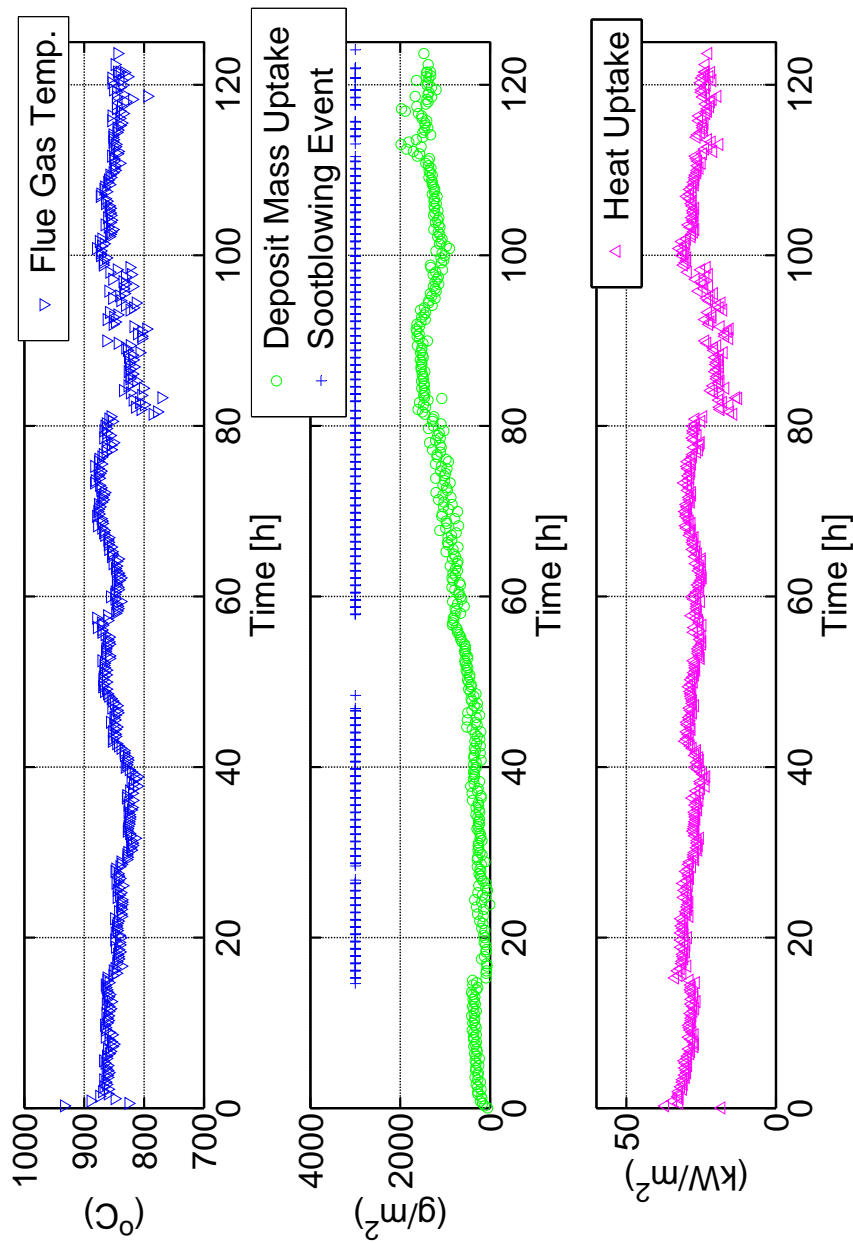
# Appendices

## **Appendix A: Full-scale measurements at AMV2**

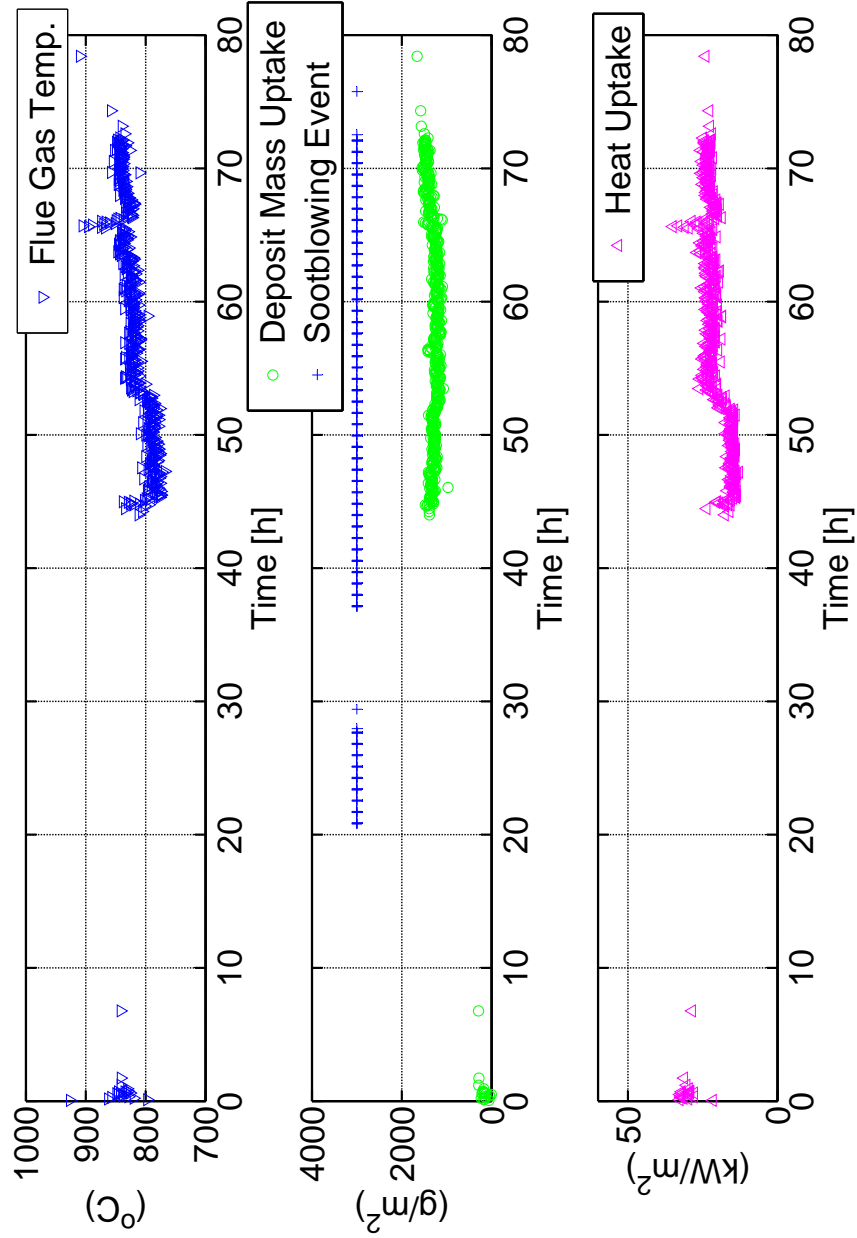
Examples of probe measuring results of the five tests conducted at AMV2 are shown in Appendix A. The local flue gas temperature, deposit mass uptake and probe heat uptake measured during test are shown, along with pictures of the deposit probe taken before and after shedding events during test 2 (80% straw firing).



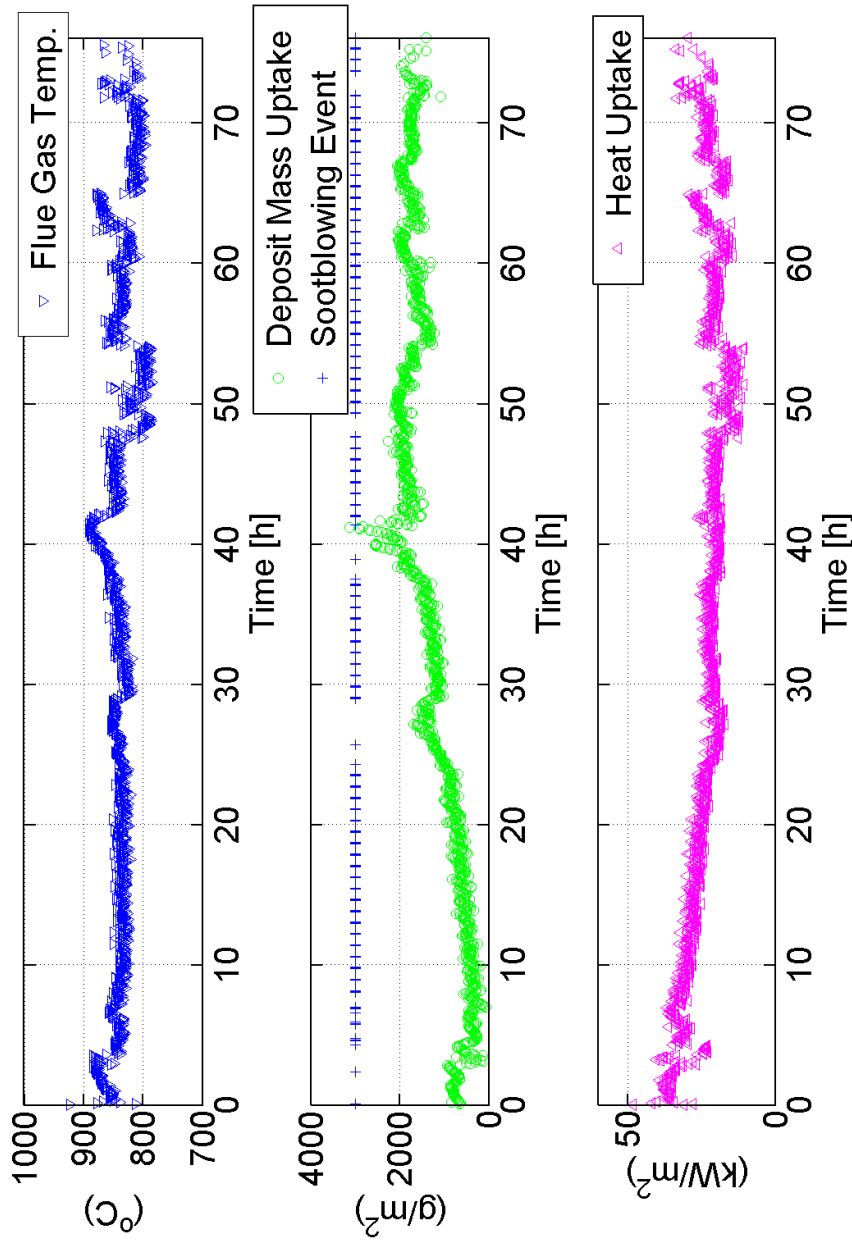
**Figure (Appendix A) 1:** Flue gas temperature, deposit mass uptake and probe heat uptake during measurements at AMV2, a) 35% straw firing, superheater region measurements (test 1, signals averaged to 1000 s).



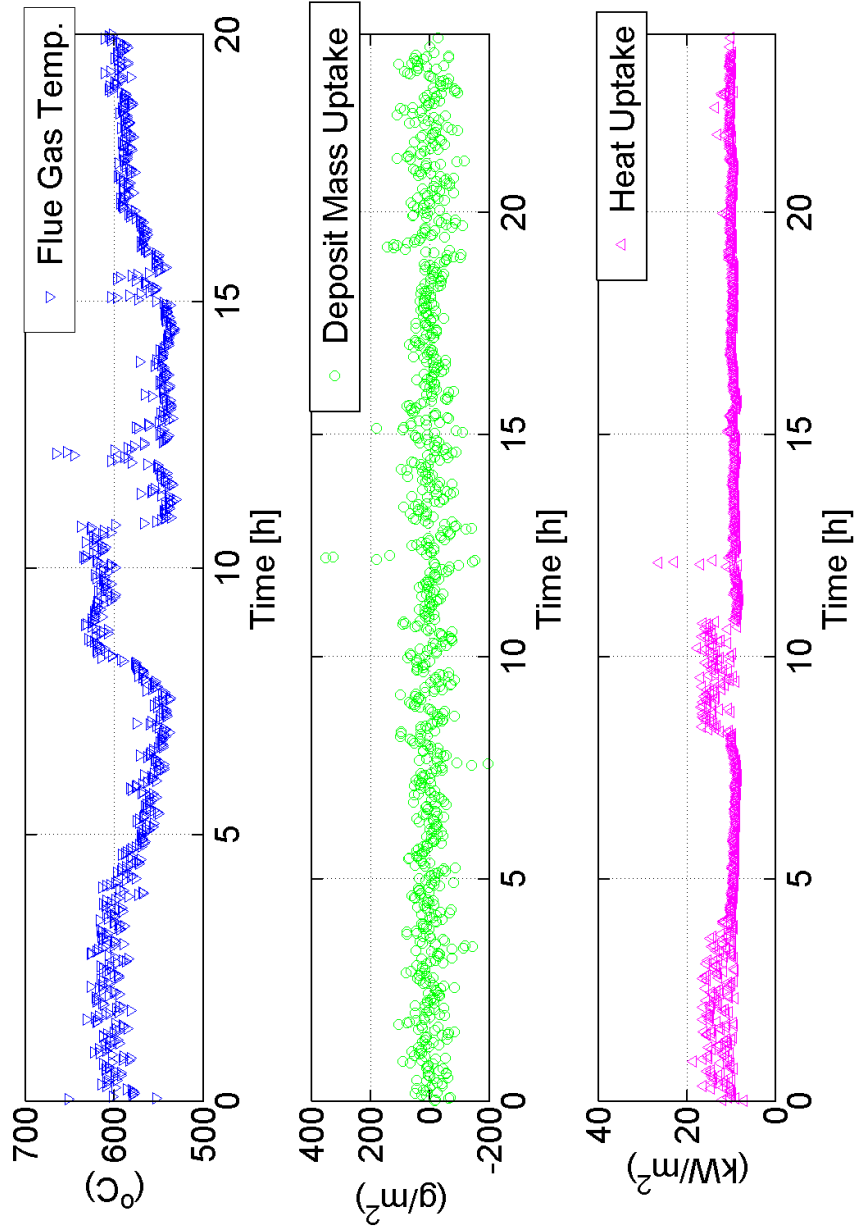
**Figure (Appendix A) 2:** Flue gas temperature, deposit mass uptake and probe heat uptake during measurements at AMV2, a) 80% straw firing, superheater region measurements (test 2, signals averaged to 1000 s).



**Figure (Appendix A) 3:** Flue gas temperature, deposit mass uptake and probe heat uptake during measurements at AMV2, a) 65% straw firing, superheater region measurements (test 3, signals averaged to 1000 s).



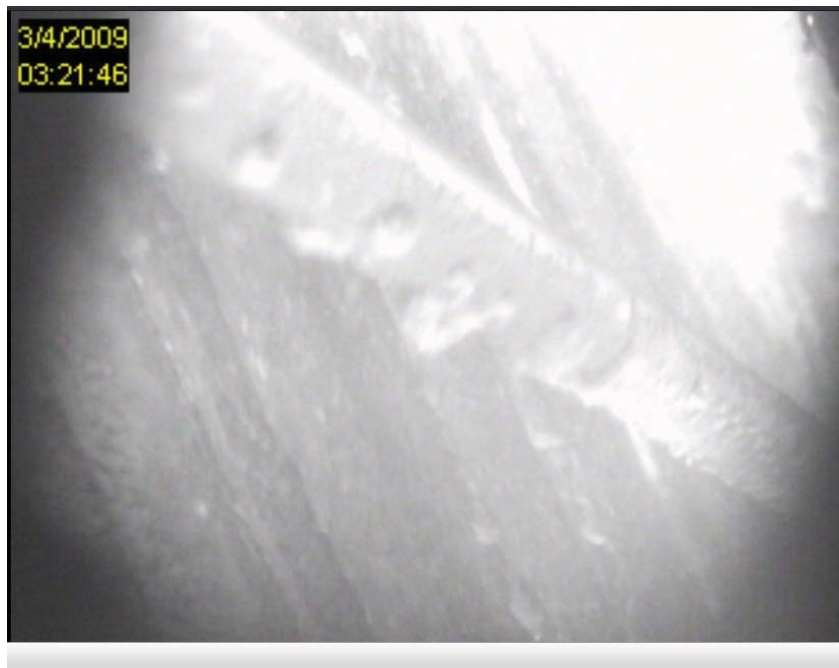
**Figure (Appendix A) 4:** Flue gas temperature, deposit mass uptake and probe heat uptake during measurements at AMV2, a) 100% straw firing, superheater region measurements (test 4, signals averaged to 1000 s).



**Figure (Appendix A) 5:** Flue gas temperature, deposit mass uptake and probe heat uptake during measurements at AMV2, a) 100% wood firing, superheater region measurements (test 5, signals averaged to 100 s).

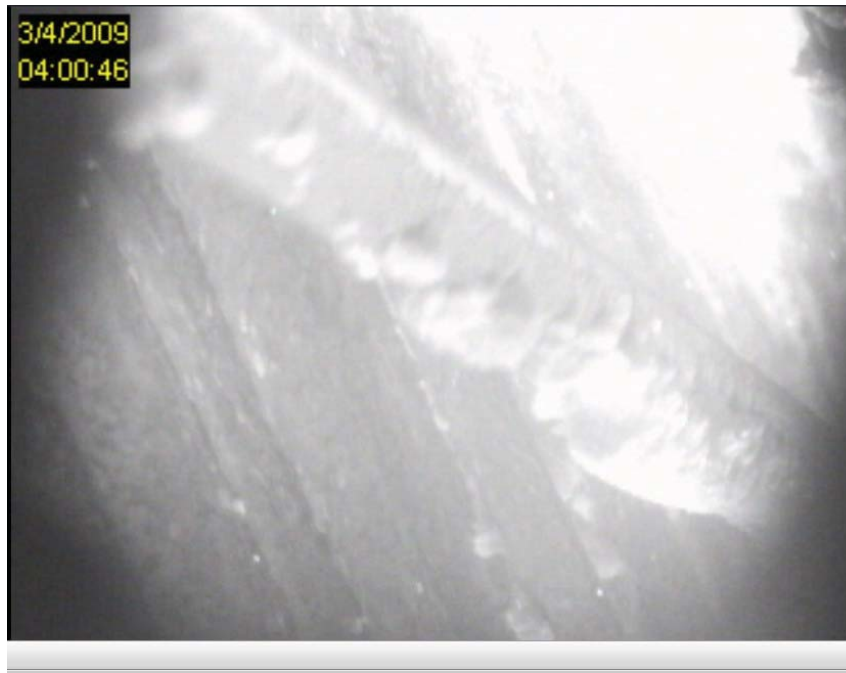


**Figure (Appendix A) 6:** Picture of the deposit probe just before shedding event during test 2 at approximately 111.8 h (03:16).



**Figure (Appendix A) 7:** Picture of the deposit probe just after shedding event during test 2 at approximately 111.9 h (03:21).

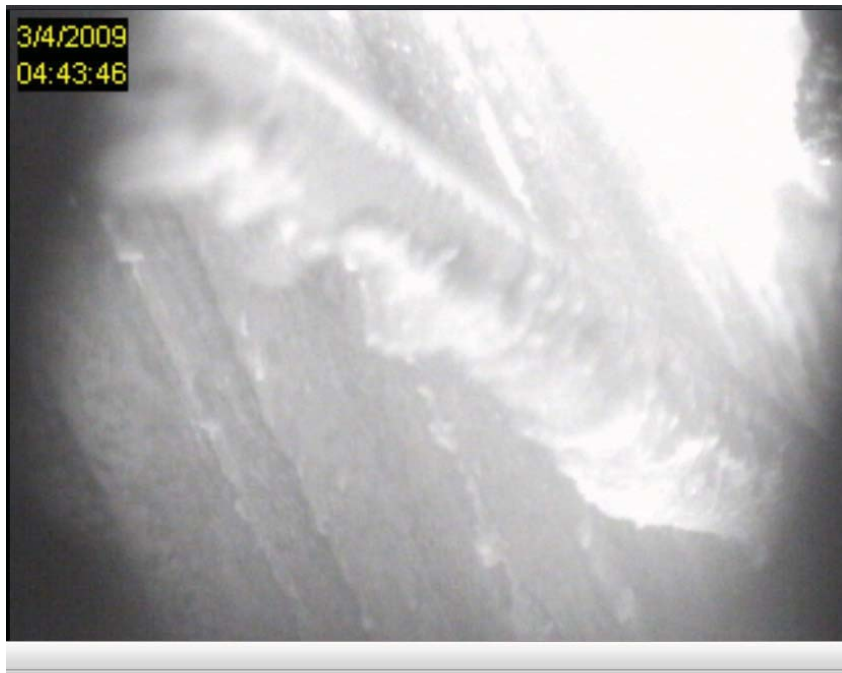




**Figure (Appendix A) 8:** Picture of the deposit probe just before shedding event during test 2 at approximately 112.6 h (04:00).



**Figure (Appendix A) 9:** Picture of the deposit probe just after shedding event during test 2 at approximately 112.6 h (04:03).



**Figure (Appendix A) 10:** Picture of the deposit probe just before shedding event during test 2 at approximately 113.3 h (04:43).



**Figure (Appendix A) 11:** Picture of the deposit probe just after shedding event during test 2 at approximately 113.4 h (04:52).



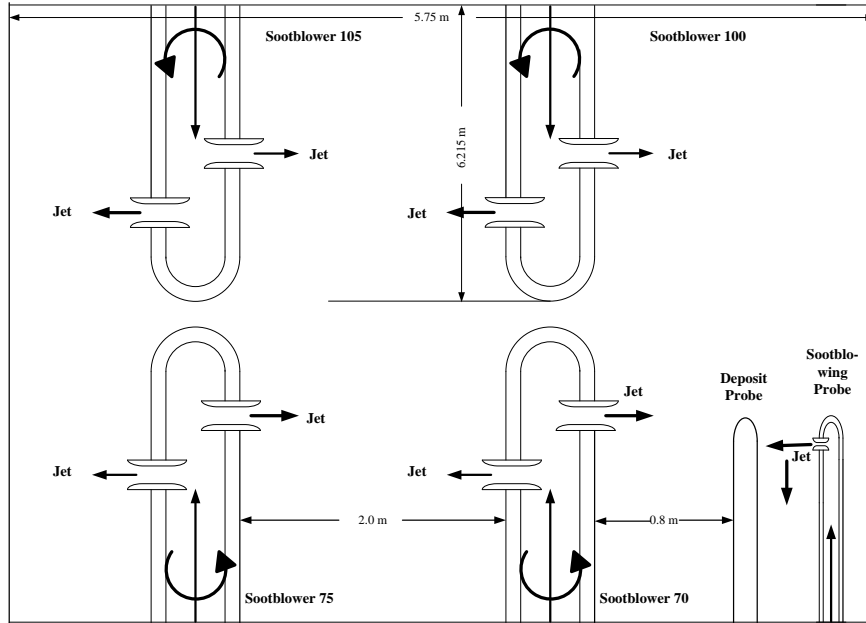
**Figure (Appendix A) 12:** Picture of the deposit probe just before shedding event during test 2 at approximately 118.2 h (08:39).



**Figure (Appendix A) 13:** Picture of the deposit probe just after shedding event during test 2 at approximately 118.6 h (09:04).

## Appendix B: Full-scale measurements at AMV1

A schematic of the plant and artificial sootblowing system near the probe measurement system is shown in Figure (Appendix B) 1a.



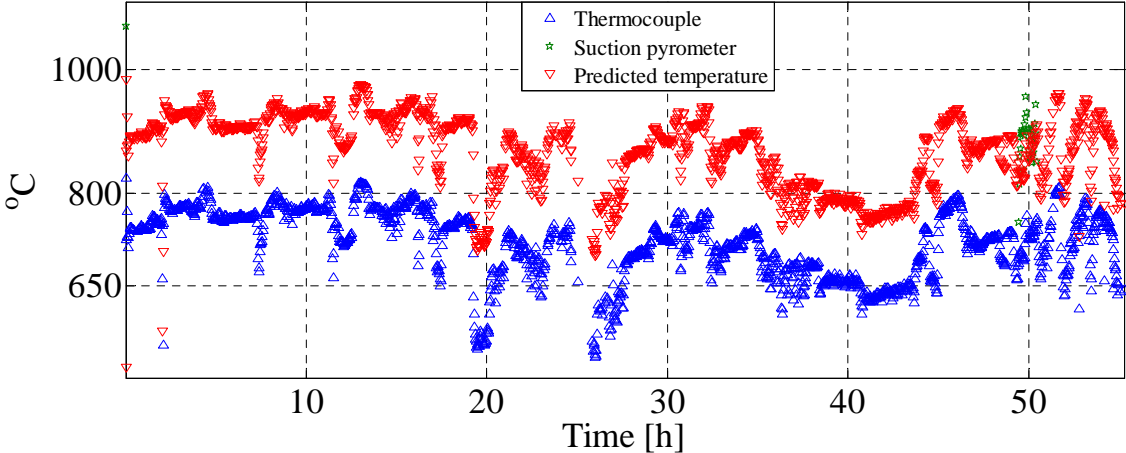
**Figure (Appendix B) 1a:** Schematic layout of plant sootblowing and artificial sootblowing near the experimental set up (seen from above).

In this Appendix, derivative-base deposit formation rate (DDF-rate) and DCS data (flue gas temperature, probe deposit mass uptake and heat uptake, air flow rate to the boiler, solid fuel flow rate through each mill, biomass load, oil load and relative boiler load) are presented for the first 5 tests conducted at AMV1. The first 5 tests are selected due to the fact that the DDF-rate calculations were made only for these tests. The plant sootblower nearest to the deposition probe was in operation during test 6, 7 and 8 and thereby the DDF-rate calculations were not made during test 6, 7 and 8.

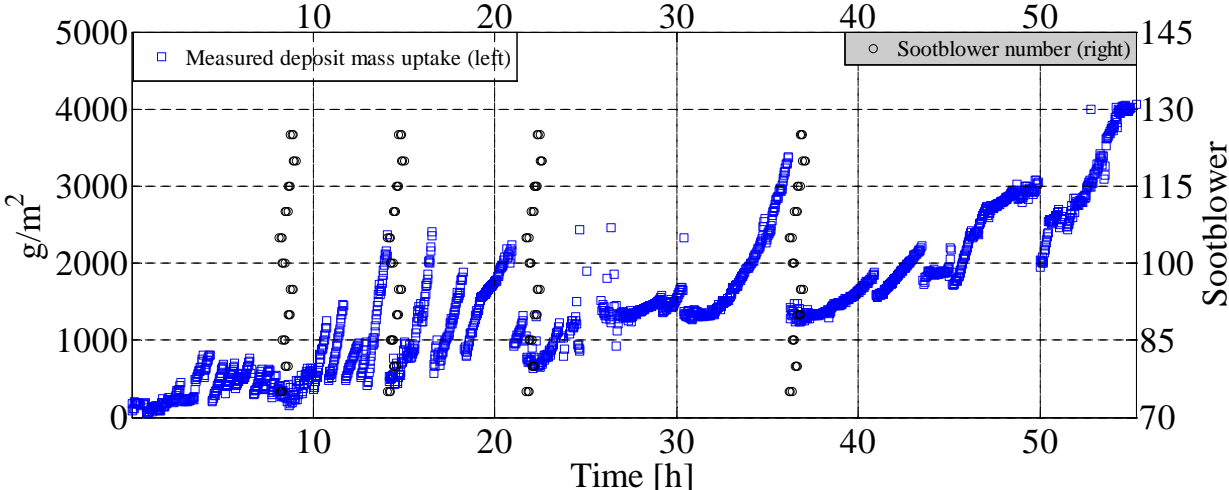
Each figure is divided into the following seven parts:

**a)** Flue gas temperature measurements during each test. The predicted flue gas temperature based on the procedure outlined in section 5.3.1.1 is also shown, **b)** deposit mass uptake signals and sootblowing events, **c)** deposit probe heat uptake, **d)** DDF-rate, **e)** Air flow rate to the boiler, **f)** Solid fuel (biomass) flow rate from each mill. The fuel from each mill is divided into four burners (Chapter 5), **g)** Biomass load, oil load and relative boiler load.

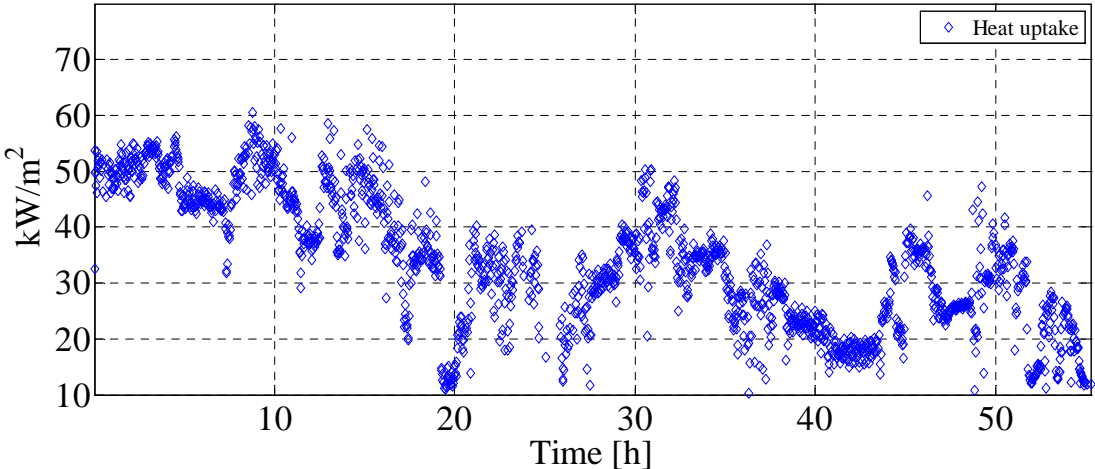
(a)



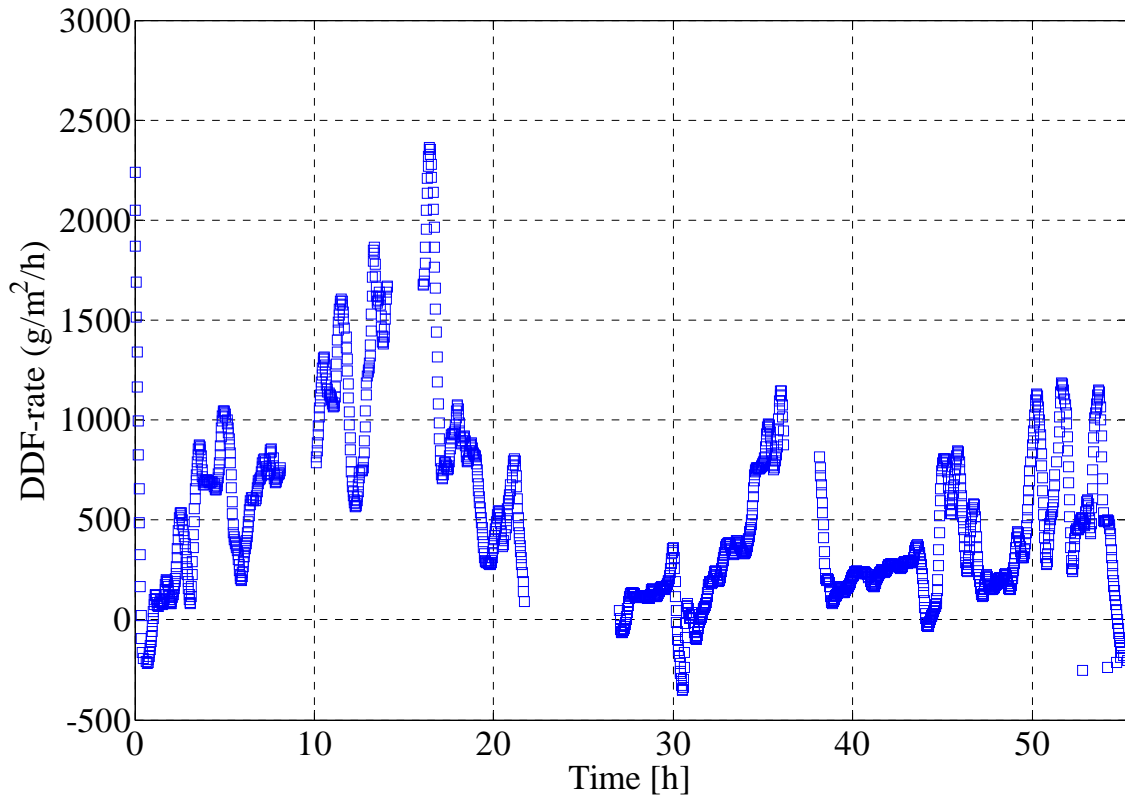
(b)



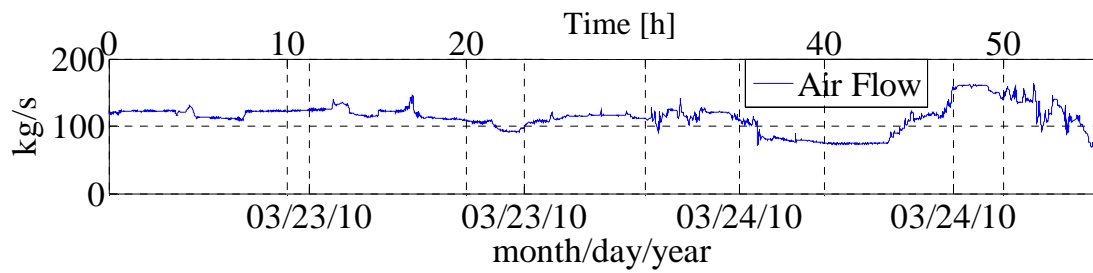
(c)



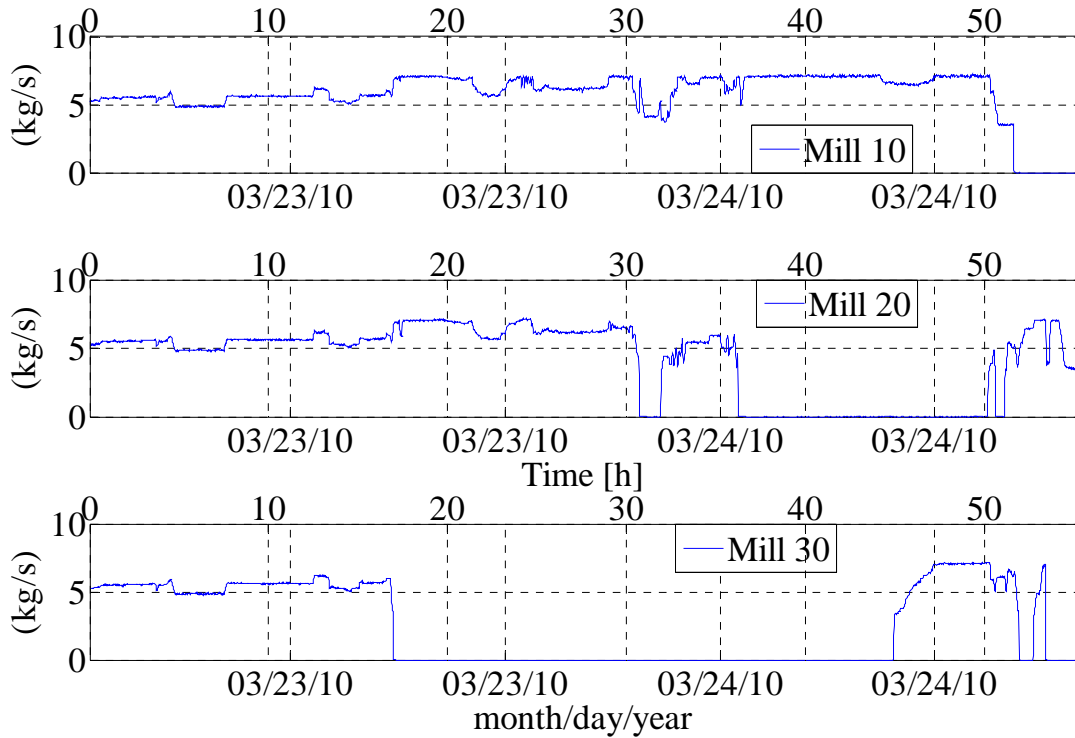
(d)



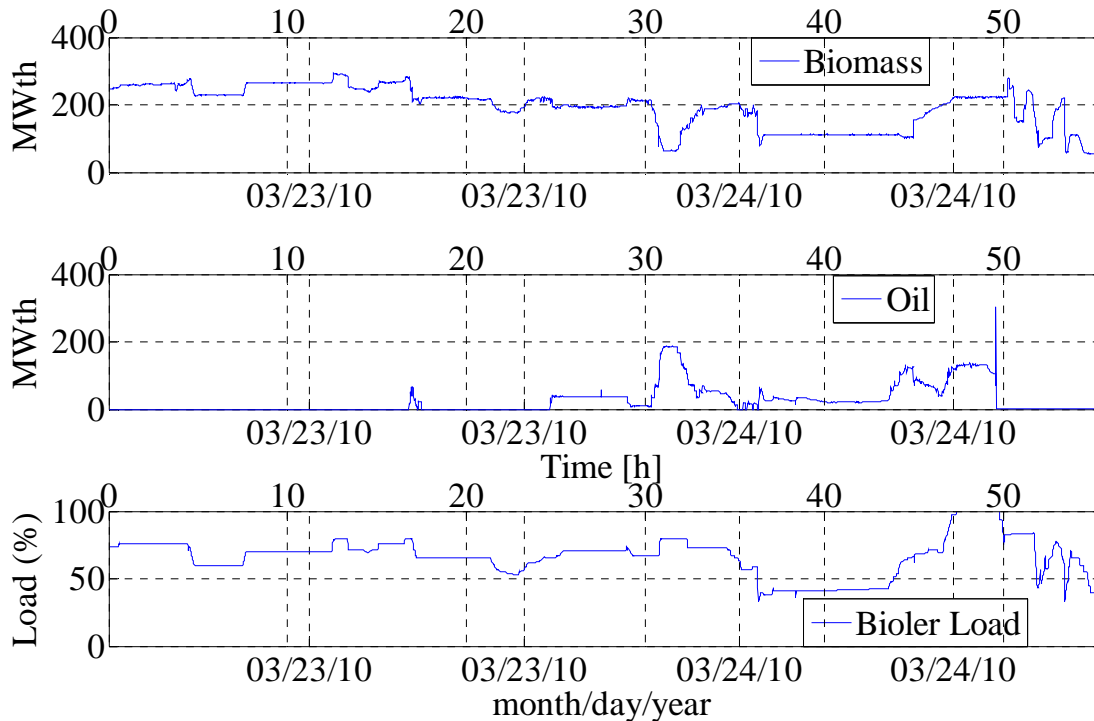
(e)



(f)



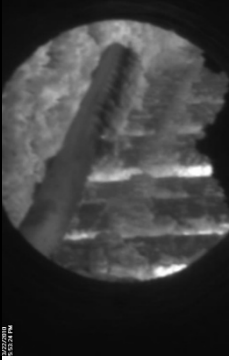
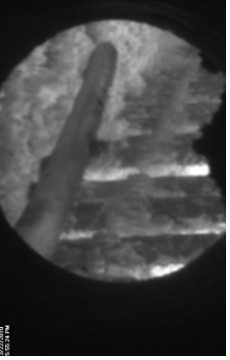
(g)



**Figure (Appendix B) 1: a) Flue gas temperature, b) probe heat uptake, c) deposit mass uptake signals, sootblowing events, d) DDF-rate, e) air flow rate to the boiler, f) solid fuel flow rate through each mill, g) biomass load, oil load and relative boiler load during test 1 (Chapter 5).**

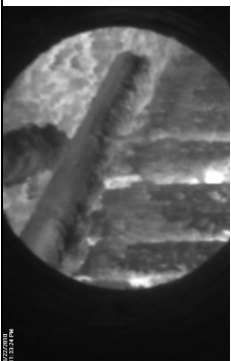
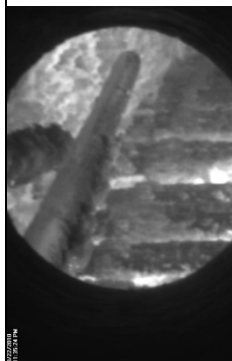
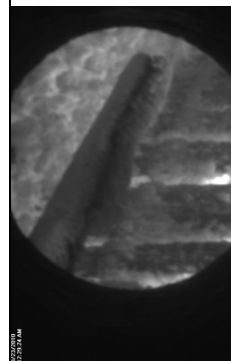
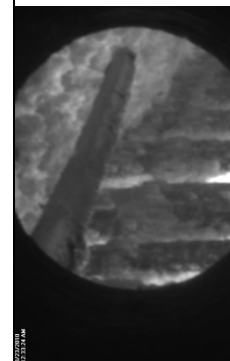
Appendix B: Full-scale measurements at AMV1

Table (Appendix B) 1: Selected shedding events during test 1 (Chapter 5).

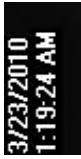
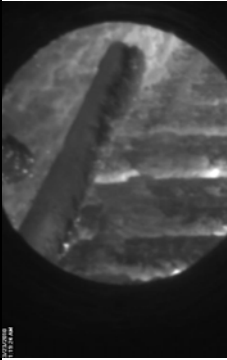

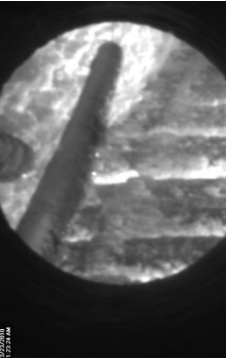
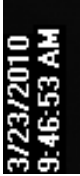
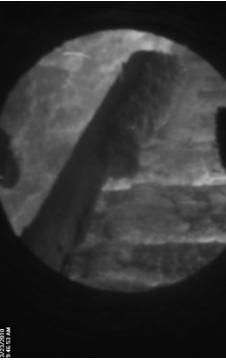
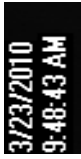
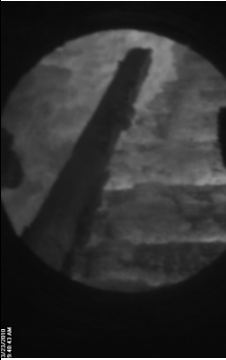
Exposure Time	Date and Time	Picture	Flue Gas Temp. (Ther.)	Flue Gas Temp. (Suc. Pyr.)	Bio-mass Load	Oil Load	Mass Uptake (2 min. avg.)	Heat Uptake (2 min. avg.)	Comments
			°C	°C	MW <sub>th</sub>	MW <sub>th</sub>	g/m <sup>2</sup>	kW/m <sup>2</sup>	
5.07-5.10	3/22/2010 5:53:24 PM		761	--	228	0	673	45.72	A complete deposit layer is formed on the upstream side of the probe.
5.13	3/22/2010 5:55:24 PM		764	--	228	0	296	47.32	The deposit layer is being removed through debonding.



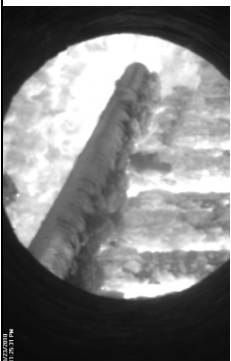
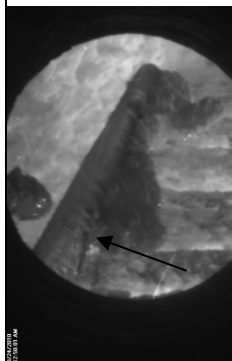
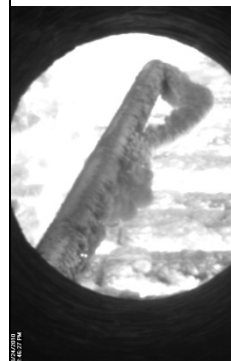
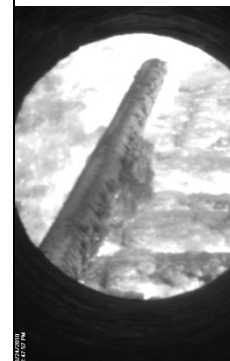
Appendix B: Full-scale measurements at AMV1

10.77		775	--	265	0	1237	42.98	A complete deposit layer is formed on the upstream side of the probe. The deposit layer is thicker nearer the tip of the probe.
10.80		775	--	265	0	817	45.89	The deposit layer is being removed through debonding. Deposits removed mainly close to the probe tip.
11.70		751	--	264	0	1502	36.73	A complete deposit layer is formed on the upstream side of the probe (1.5m from tip).
11.76		751	--	264	0	447	44.65	A deposit layer is being removed through debonding.

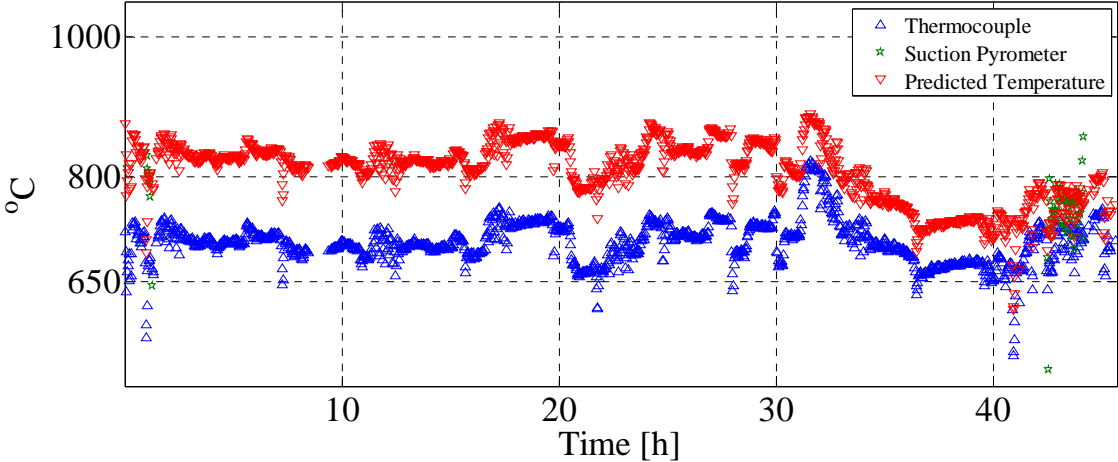
Appendix B: Full-scale measurements at AMV1

12.53			730	--	292	0	950	44.06	A complete deposit layer is formed on the upstream side of the probe.
12.60			761	--	293	0	513	51.51	The deposit layer is being removed through debonding. Deposit removal is more near the tip of the probe.
20.99			696	--	213	0	2254	29.08	A thick deposit layer is formed on the upstream side of the probe.
21.02			710	--	214	0	988	33.55	The deposit layer is being removed through debonding.

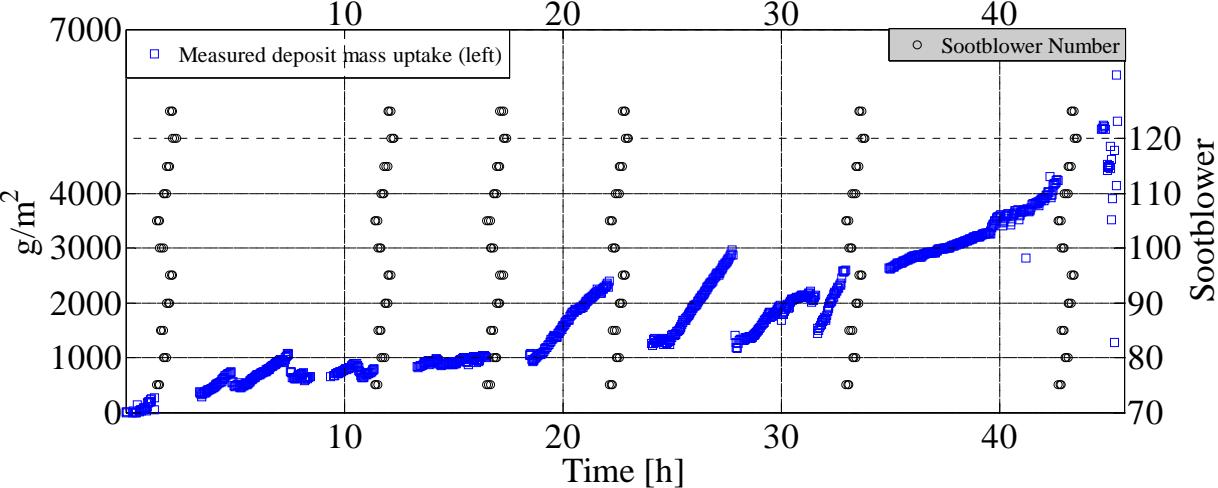
Appendix B: Full-scale measurements at AMV1

34.64		732	--	201	38	2242	35.33	This important event is shown due to reason that after some time of this event, a lot of deposits attached on the upstream side of the probe in a short time (< 1.5 h).
36.05		687	--	185	16	3274	23.88	The eposit layer is about to fall from the indicated location. Deposit removal was due to plant sootblowing. Probe metal temperature dropped when layer was removed.
49.98		749	890	222	1	2690	36.16	A deposit layer is formed on the upstream side of the probe. The deposit layer is about to fall starting from the tip of the probe. This image indicates shedding through debonding.
50.01		735	--	223	1	2072	33.85	The deposit layer is being removed through debonding.

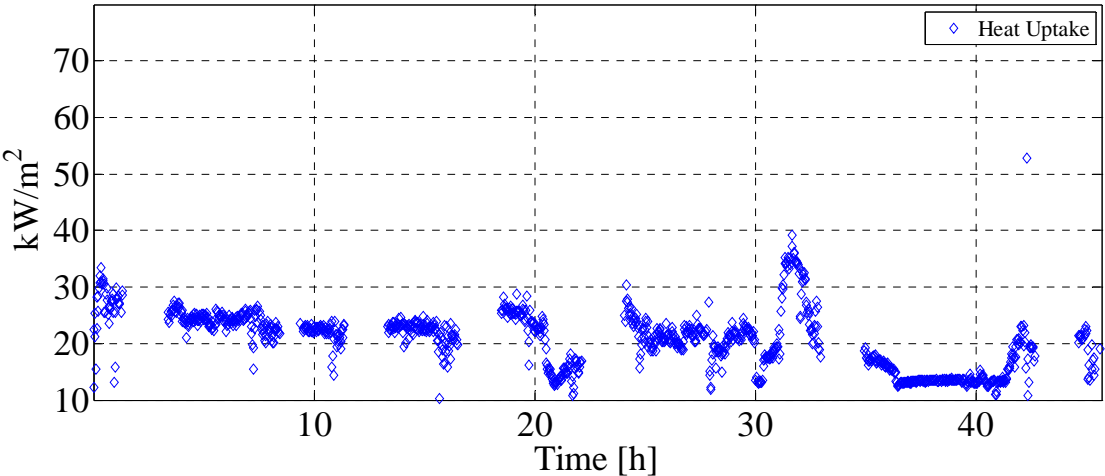
(a)



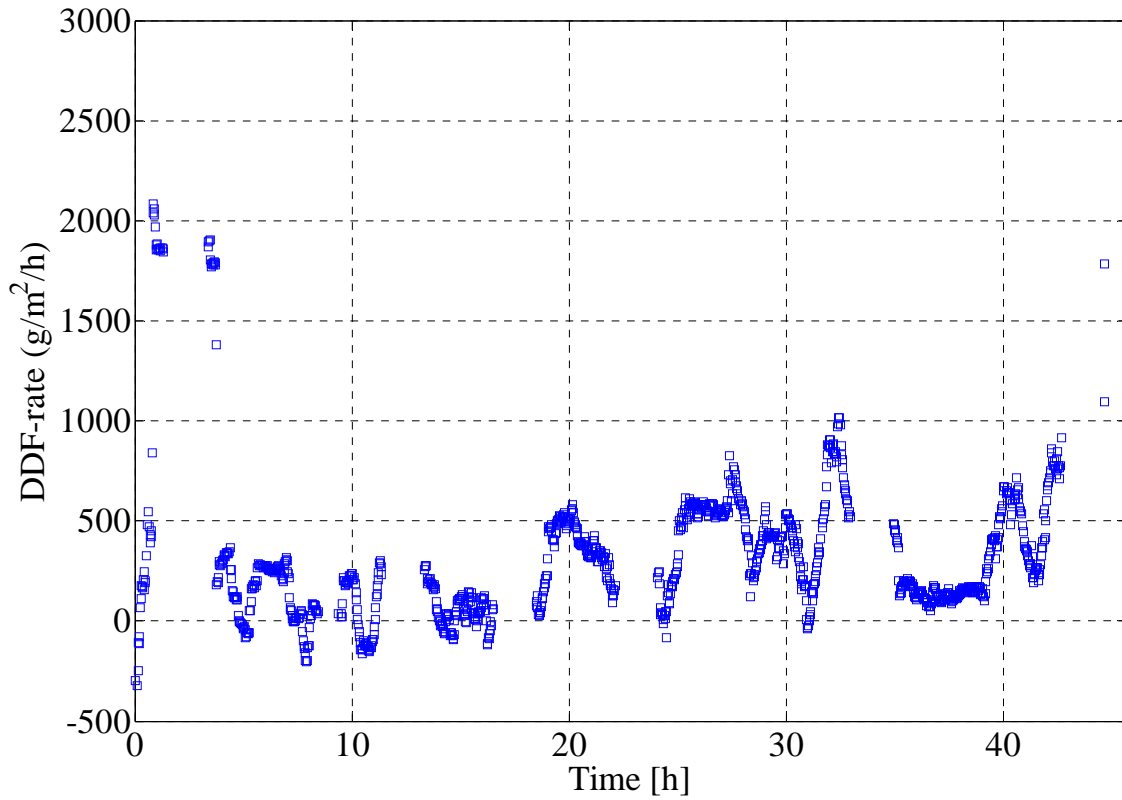
(b)



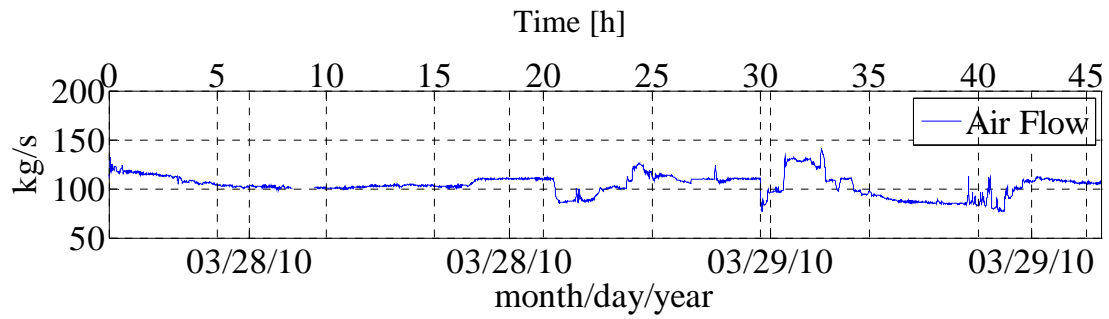
(c)



(d)



(e)



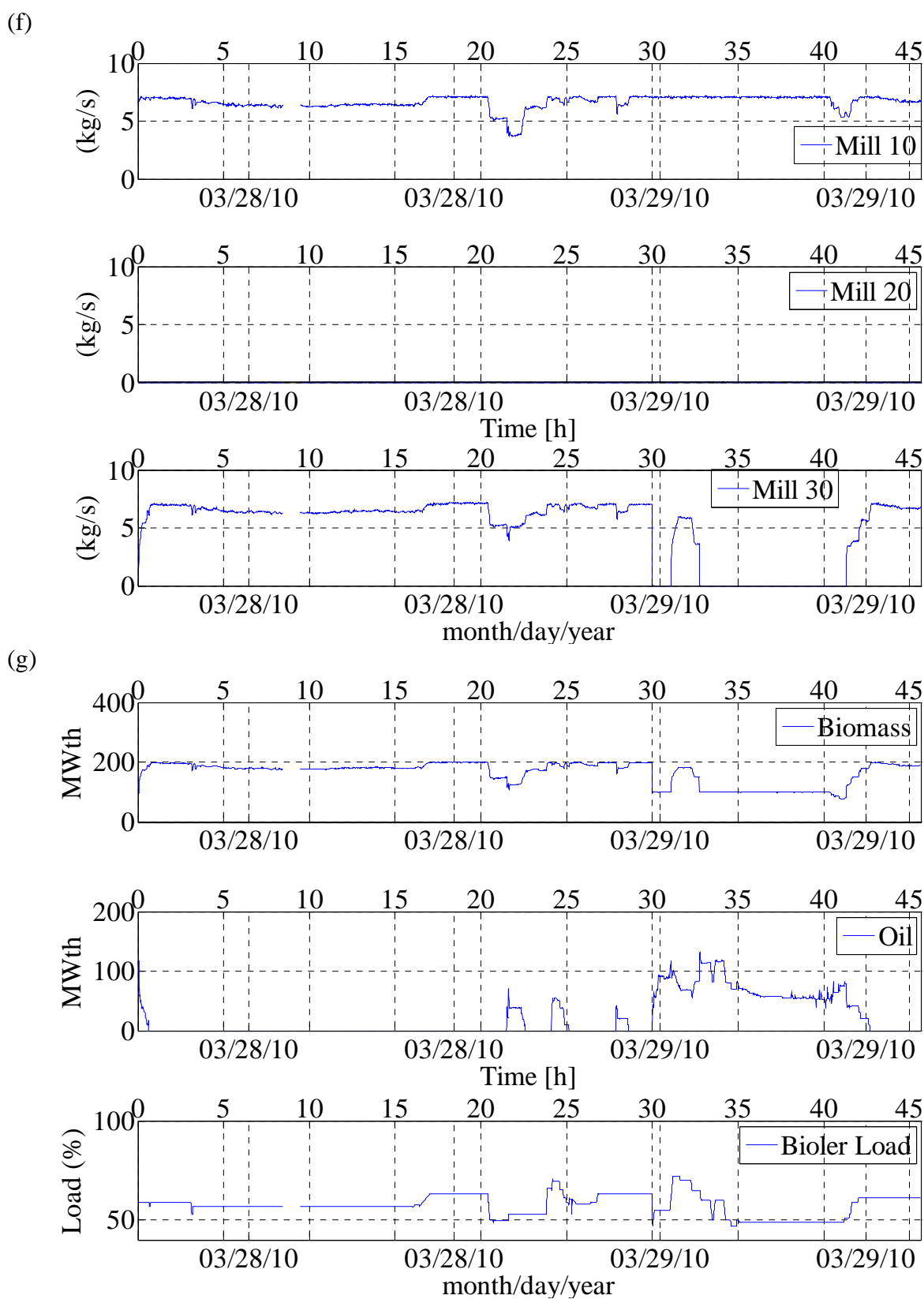
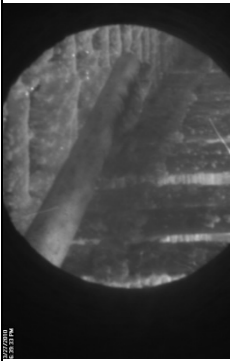
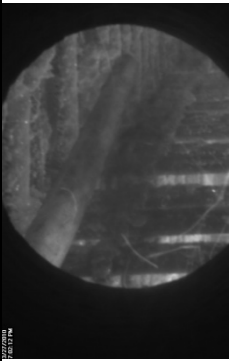


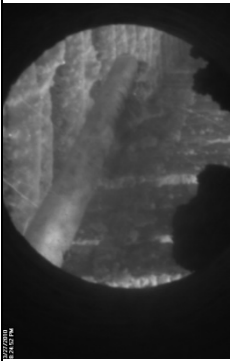
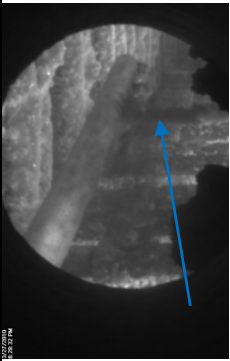
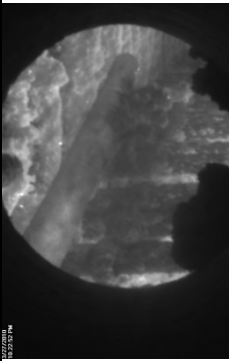
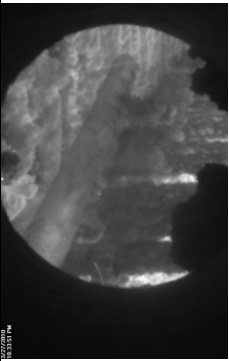
Figure (Appendix B) 2: a) Flue gas temperature, b) probe heat uptake, c) deposit mass uptake signals, sootblowing events, d) DDF-rate, e) air flow rate to the boiler, f) solid fuel flow rate through each mill, g) biomass load, oil load and relative boiler load during test 2 (Chapter 5).

Appendix B: Full-scale measurements at AMV1

Table (Appendix B) 2: Selected shedding events during test 2 (Chapter 5).


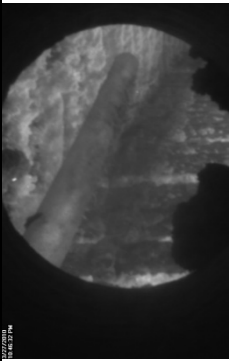
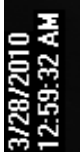
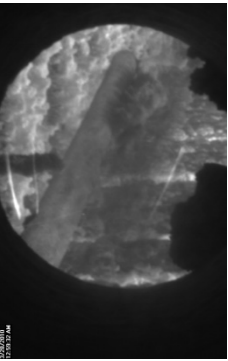
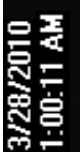
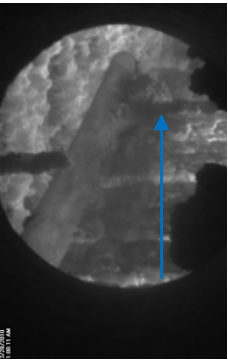

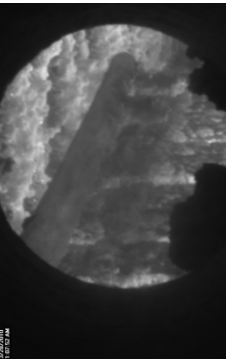
Exposure Time	Date and Time	Picture	Flue Gas Temp. (Ther.) °C	Flue Gas Temp. (Suc. Pyr.) °C	Bio-mass Load MW <sub>th</sub>	Oil Load MW <sub>th</sub>	Mass Uptake (2 min. avg.) g/m <sup>2</sup>	Heat Uptake (2 min. avg.) kW/m <sup>2</sup>	Comments
h									
1.12	3/27/2010 6:39:33 PM		679	799	198	0	202	26.35	Initial deposit layer is formed near the tip of the probe on the upstream side.
1.49	3/27/2010 7:02:12 PM		714	--	194	0	99	27.05	Complete deposit layer is being removed when plant sootblower was used.

Appendix B: Full-scale measurements at AMV1

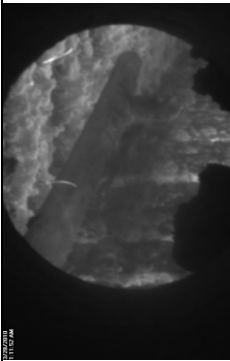
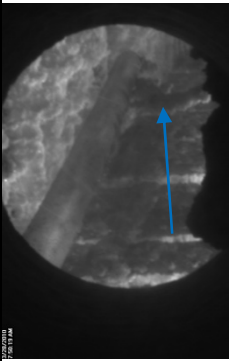
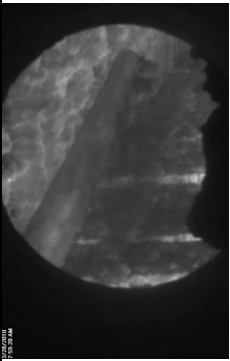
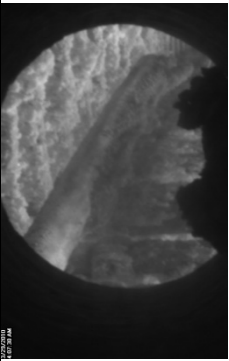
2.87		712	--	193	0	409	28.42	Ash deposit layer is formed near the tip of the probe on the upstream side of the probe.
2.93		709	--	193	0	440	27.65	A complete deposit layer is about to fall indicated by arrow.
4.84		706	--	183	0	713	25.29	Deposits formed on the upstream side of the probe are about to fall.
5.02		709	--	180	0	471	24.25	Some of the deposits have been dropped in the form of small layers.



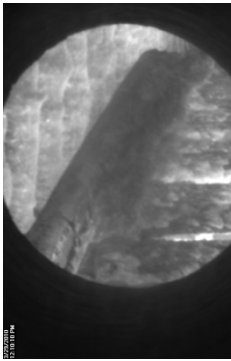
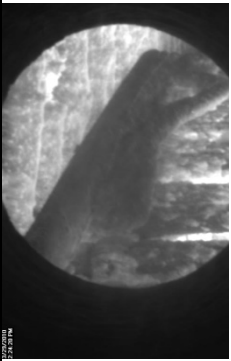
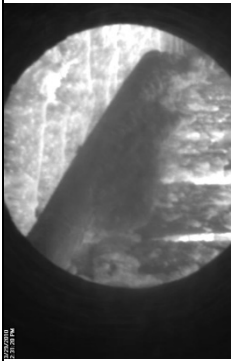
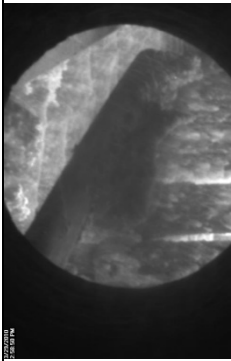
Appendix B: Full-scale measurements at AMV1

5.23			707	--	179	0	447	23.39	Almost complete deposit layer on the upstream side is removed. The whole process of deposit removal was in the form of small layers.
7.45			708	--	179	0	1067	26.12	Thick deposit layer is formed close the tip of the probe.
7.46			710	--	179	0	1060	24.48	A complete deposit layer is about to fall indicated by arrow.
7.59			705	--	178	0	750	25.35	The deposit layer has fallen.

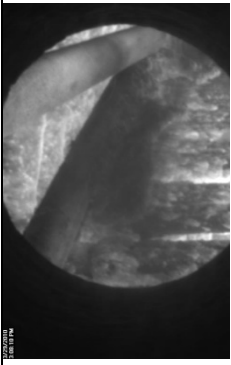
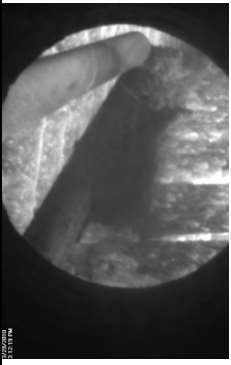
Appendix B: Full-scale measurements at AMV1

7.65		697	--	177	0	632	21.98	Another small deposit layer is being removed.
14.31		694	--	180	0	930	21.92	A small deposit layer on the upstream side of the probe is about to fall indicated by arrow.
14.45		697	--	181	0	866.74	22.75	--
34.58		705	--	98.98	79.97	2542	18.88	Very hard deposits attached on the upstream side of the probe. Deposits were difficult to remove and even oil loading has no effect on the removal of deposits.

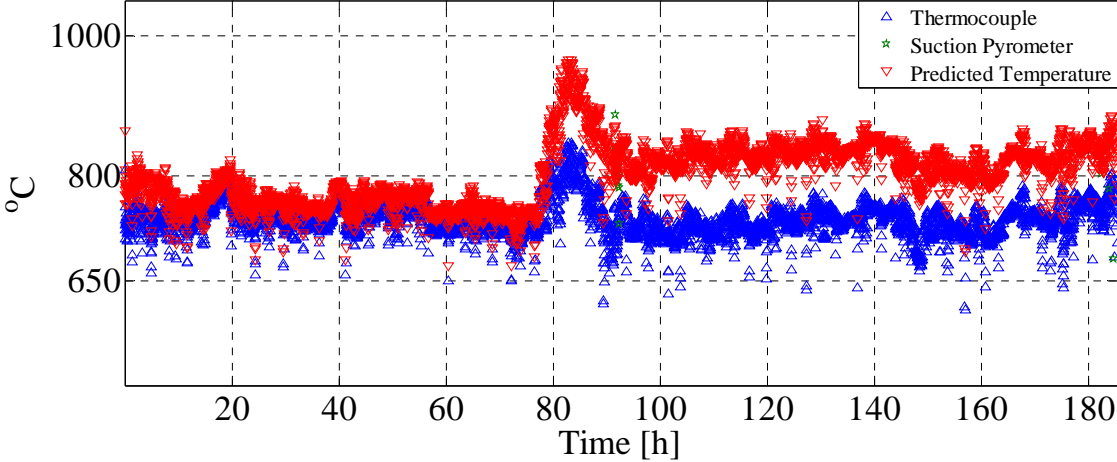
Appendix B: Full-scale measurements at AMV1

42.63		679	755.1	181.30	9.86	4221	19.18	Very hard deposits attached on the upstream side of the probe. The snapshot indicates that deposits are difficult to remove because upstream side deposit layer and a thin downstream layer formed a ring type shape.
44.86		743	--	188	0	5217	21.04	The deposit layer on the upstream side of the probe is about to fall.
44.98		748	--	188	0	4494	22.34	The deposit layer on the upstream side is being removed.
45.44		701	--	187	0	--	--	Artificial sootblowing probe is ready to remove the deposits.

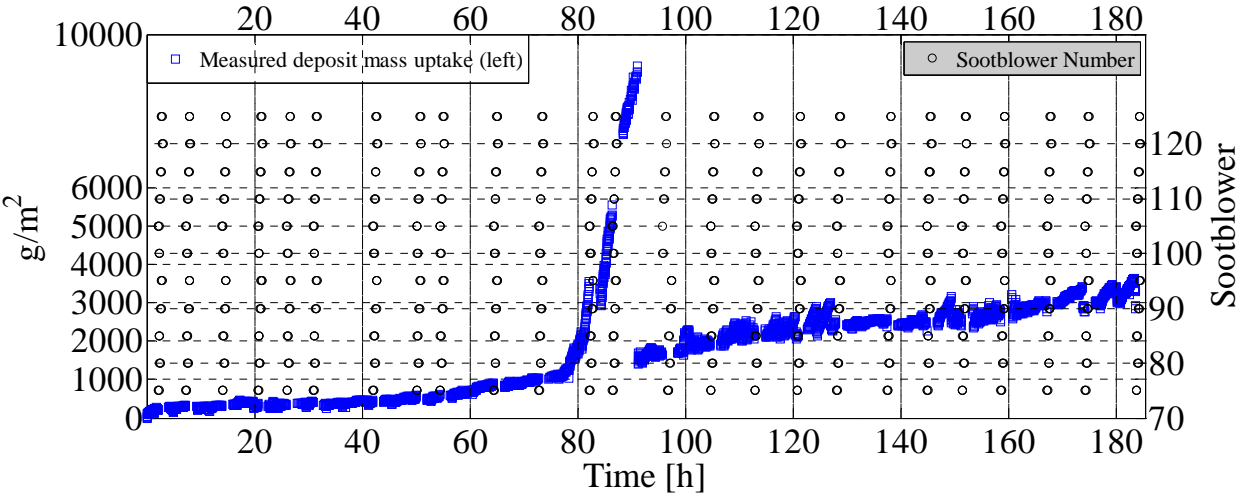
Appendix B: Full-scale measurements at AMV1

45.59		669	--	188	0	--	--	A small deposit layer on the upstream side was removed when artificial sootblowing probe was used.
45.66		691	--	188	0	3874	52.27	Another small deposit layer on the upstream side was removed when artificial sootblowing probe was used.

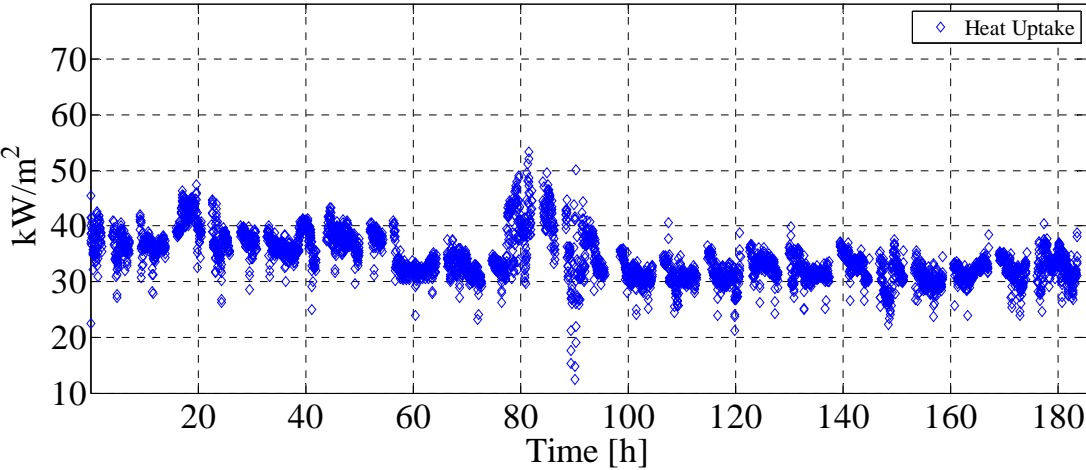
(a)



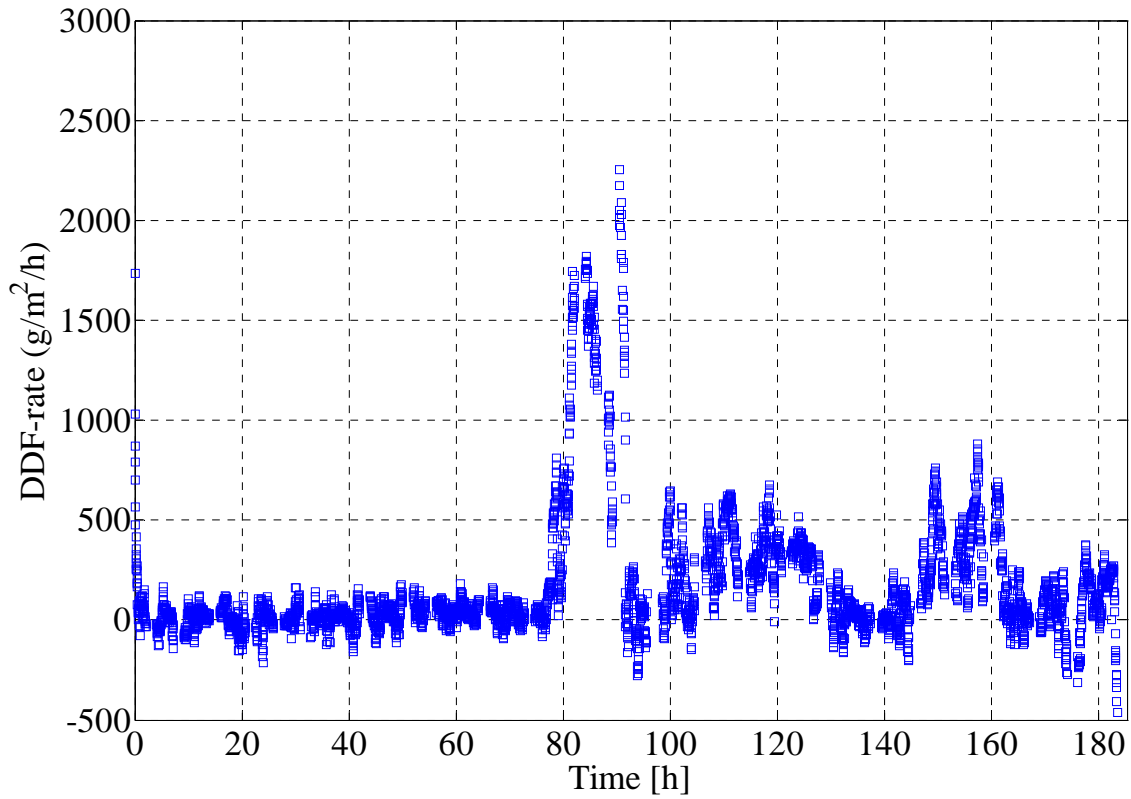
(b)



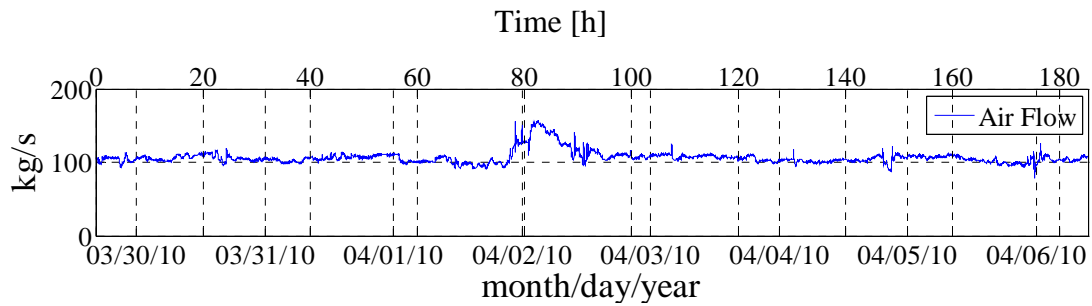
(c)



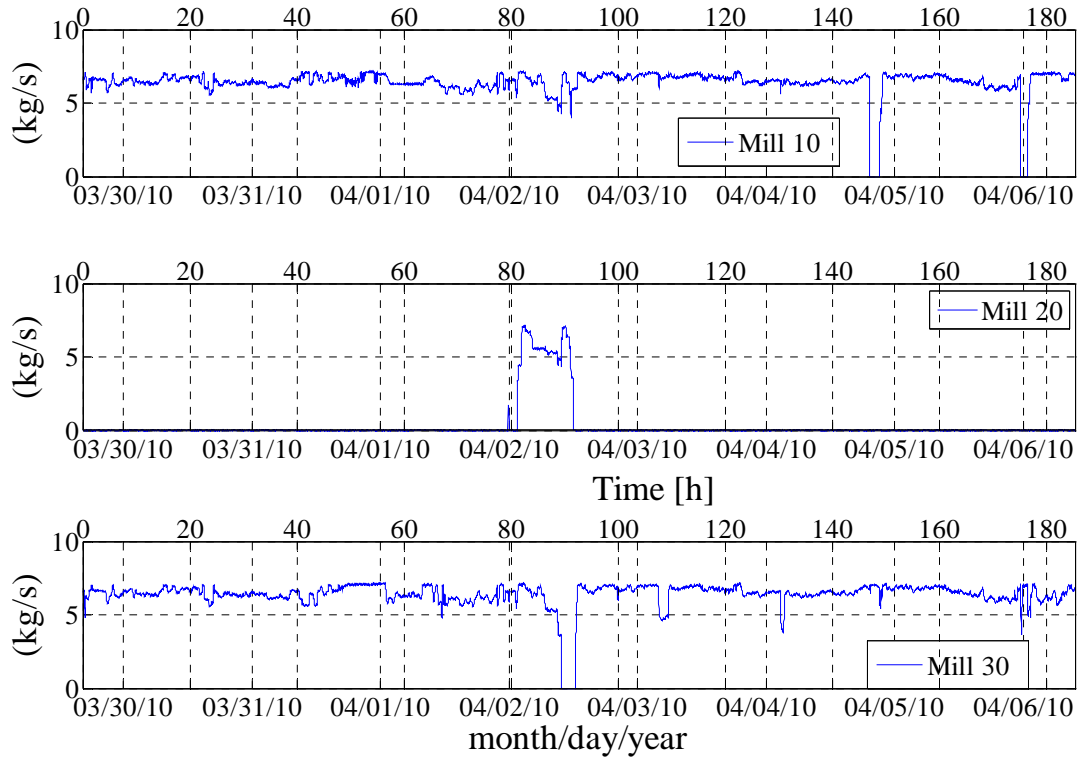
(d)



(e)



(f)



(g)

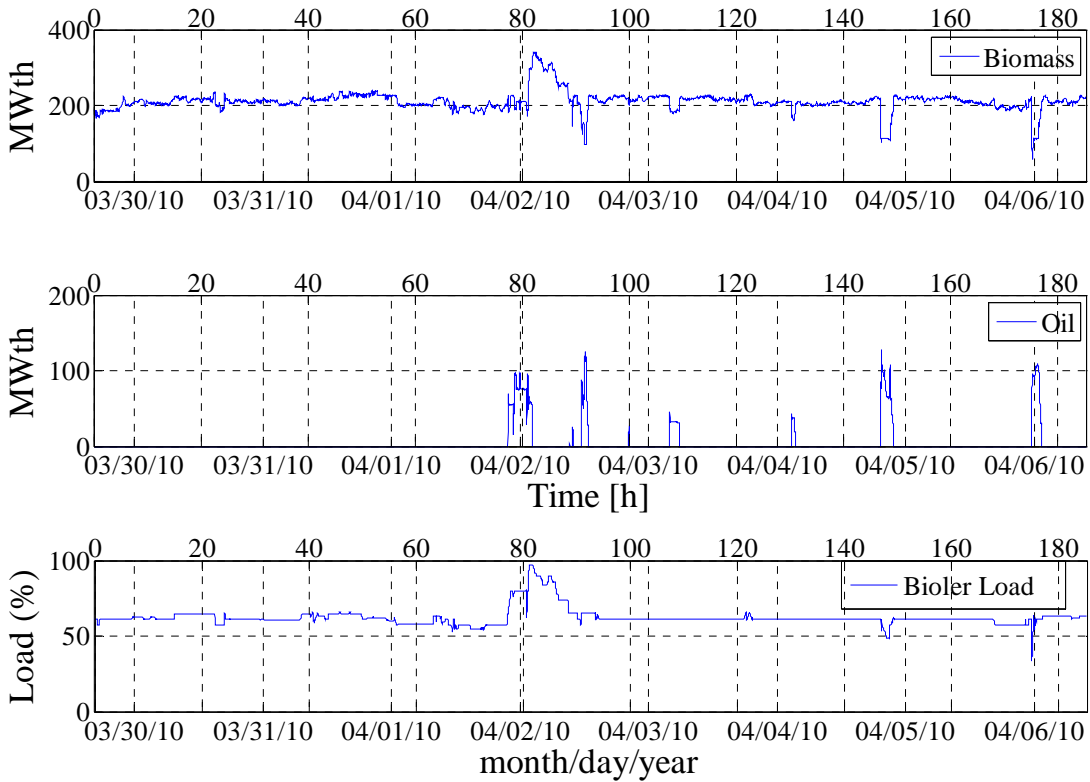
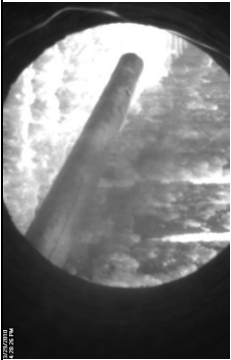
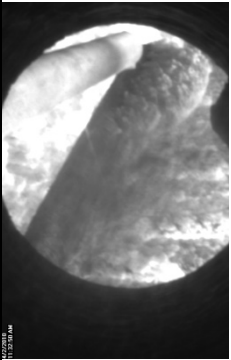


Figure (Appendix B) 3: a) Flue gas temperature, b) probe heat uptake, c) deposit mass uptake signals, sootblowing events, d) DDF-rate, e) air flow rate to the boiler, f) solid fuel flow rate through each mill, g) biomass load, oil load and relative boiler load during test 3 (Chapter 5).


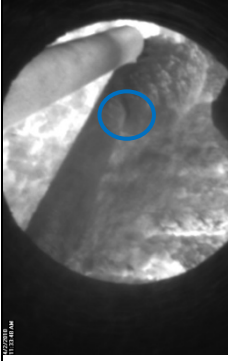
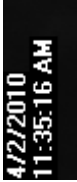
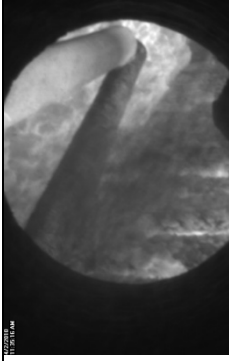

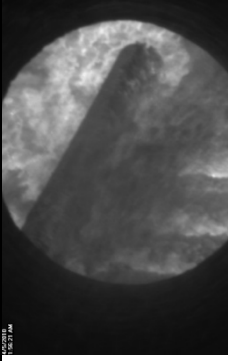

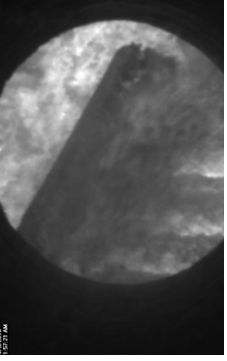
Appendix B: Full-scale measurements at AMV1

Table (Appendix B) 3: Selected shedding events during test 3 (Chapter 5).

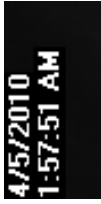
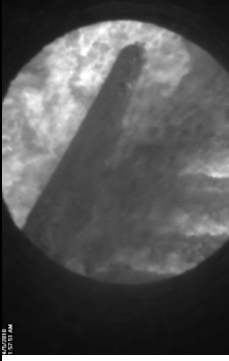
Exposure Time	Date and Time	Picture	Flue Gas Temp. (Ther.) °C	Flue Gas Temp. (Suc. Pyr.) °C	Bio-mass Load MW <sub>th</sub>	Oil Load MW <sub>th</sub>	Mass Uptake (2 min. avg.) g/m <sup>2</sup>	Heat Uptake (2 min. avg.) kW/m <sup>2</sup>	Comments
h									
0.10	3/29/2010 4:28:26 PM		735	--	185	0	70	39.91	A thin 'v' shaped layer on the upstream direction after about 6-10 min of exposure time.
91.17	4/2/2010 11:32:50 AM		742	--	125	81	9007	--	Artificial sootblowing probe was ready to remove thick layer of deposit on the upstream side of the probe.



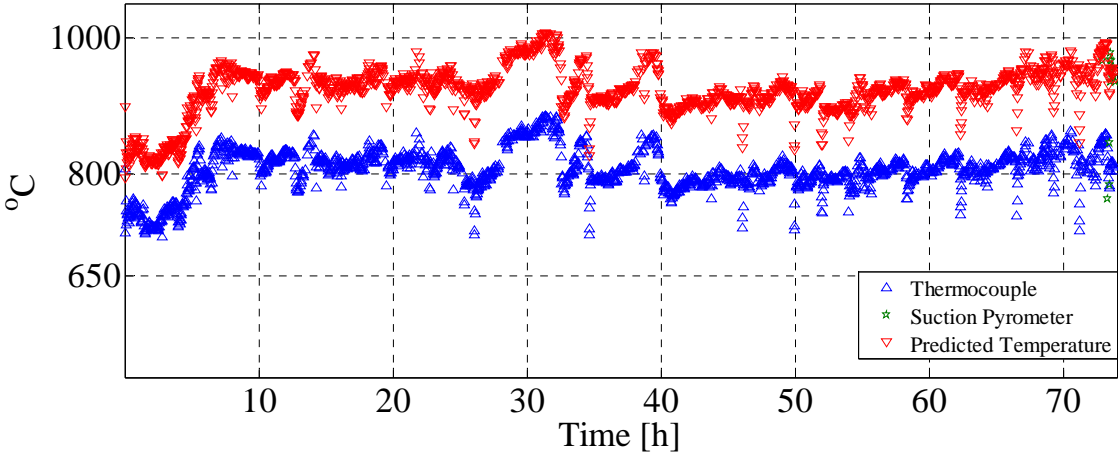
Appendix B: Full-scale measurements at AMV1

91.19			764	--	124	83	8747	--	Small amount of deposits being removed by artificial plant sootblowing (mentioned in the circle).
91.22			717	--	128	82	1584	32.05	A complete deposit layer has fallen. The PIP needed was 43 kPa.
153.56			719	--	220	0	2851	33.46	A deposit layer formed on the upstream side of the probe can be seen.
153.58			719	--	220	0	--	--	The deposit layer is about to fall on the upstream side of the probe.

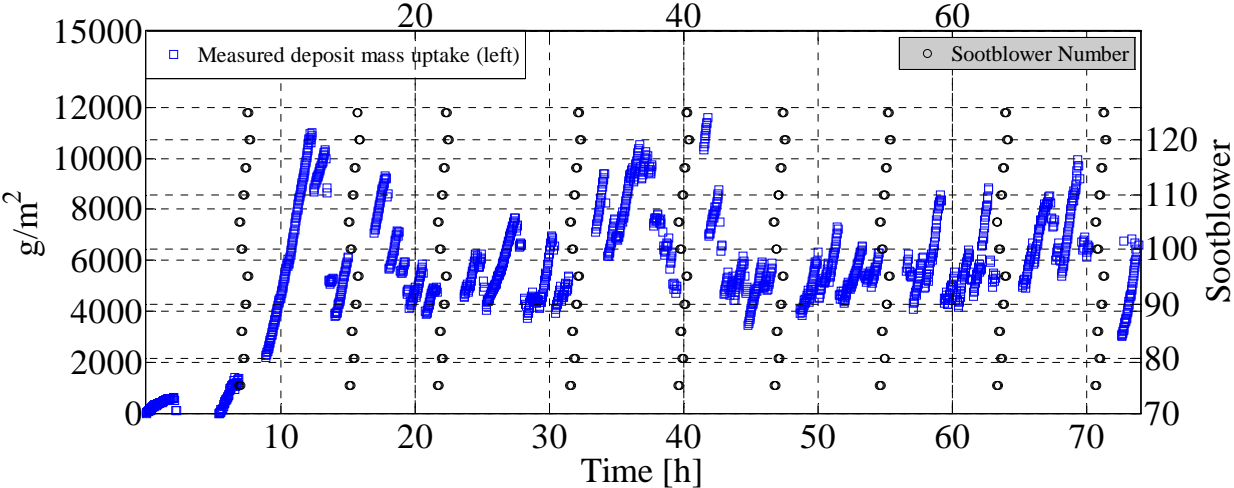
Appendix B: Full-scale measurements at AMV1

153.59			721	--	221	0	2517	34.15	A complete deposit has fallen from the upstream side of the probe.
--------	---	---	-----	----	-----	---	------	-------	--

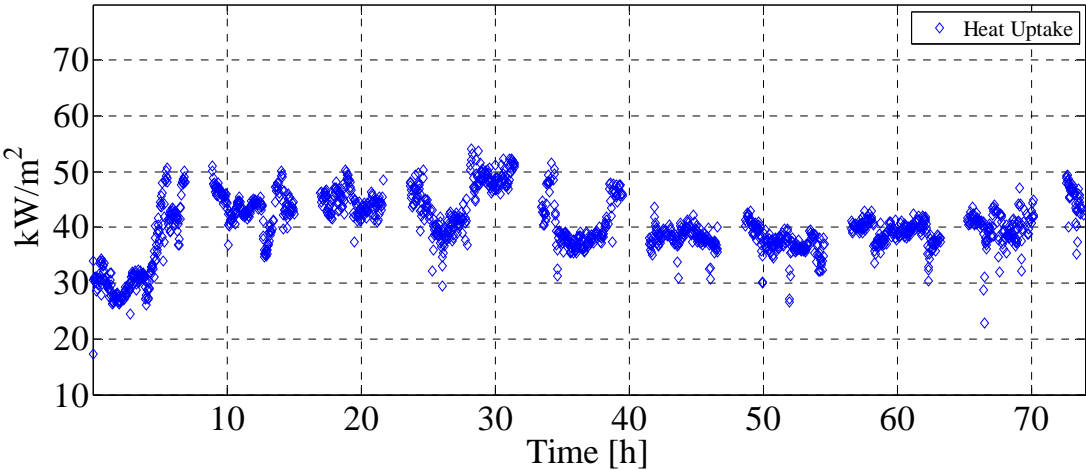
(a)



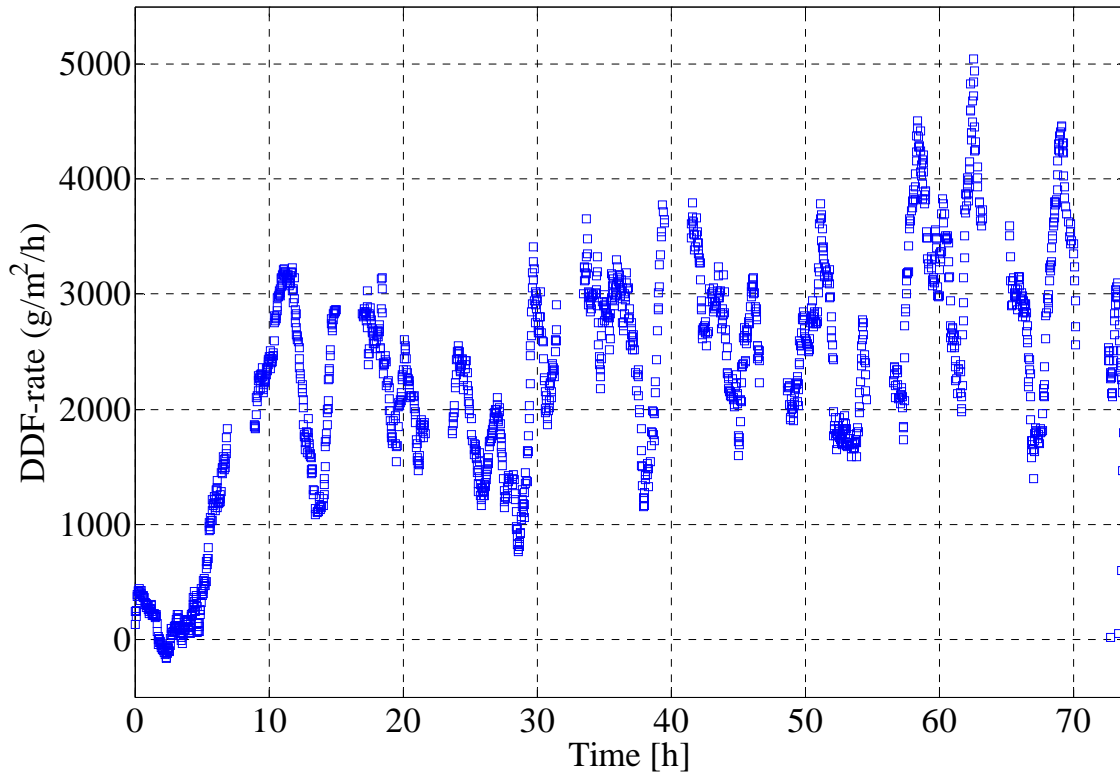
(b)



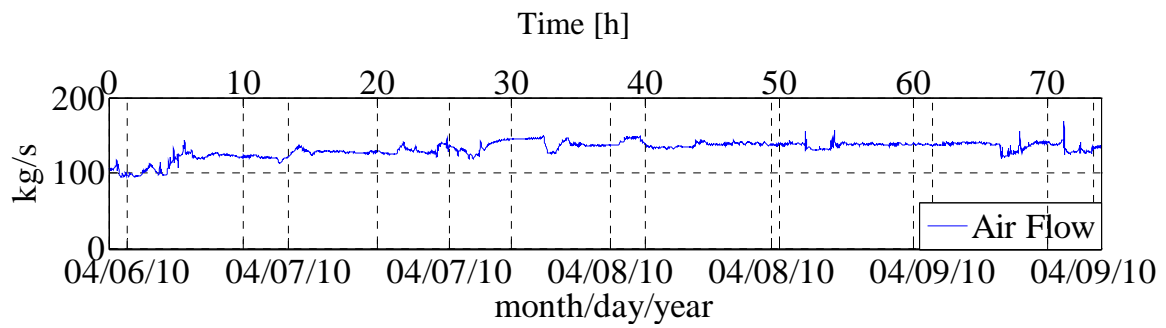
(c)



(d)



(e)



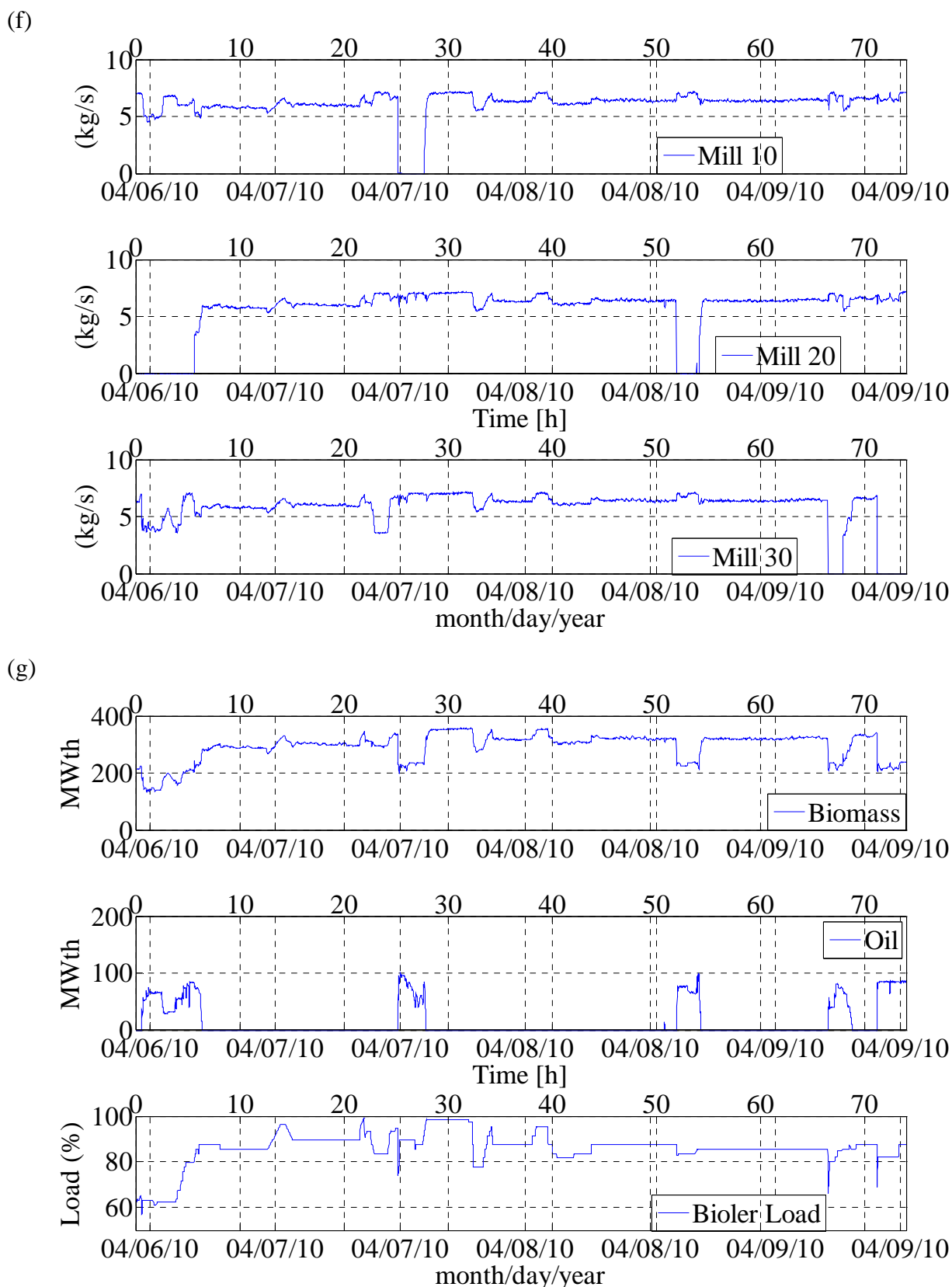
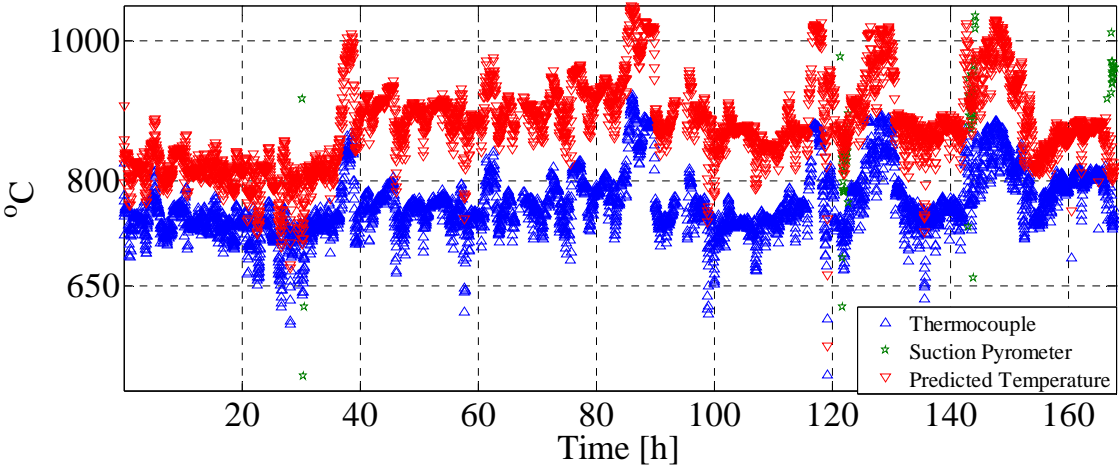
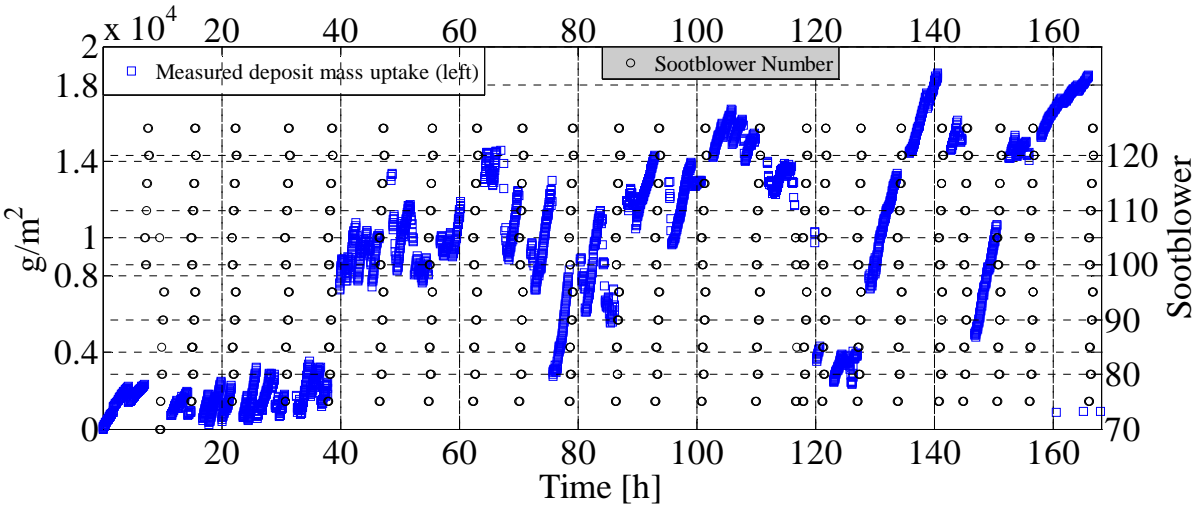


Figure (Appendix B) 4 : a) Flue gas temperature, b) probe heat uptake, c) deposit mass uptake signals, sootblowing events, d) DDF-rate, e) air flow rate to the boiler, f) solid fuel flow rate through each mill, g) biomass load, oil load and relative boiler load during test 4 (Chapter 5).

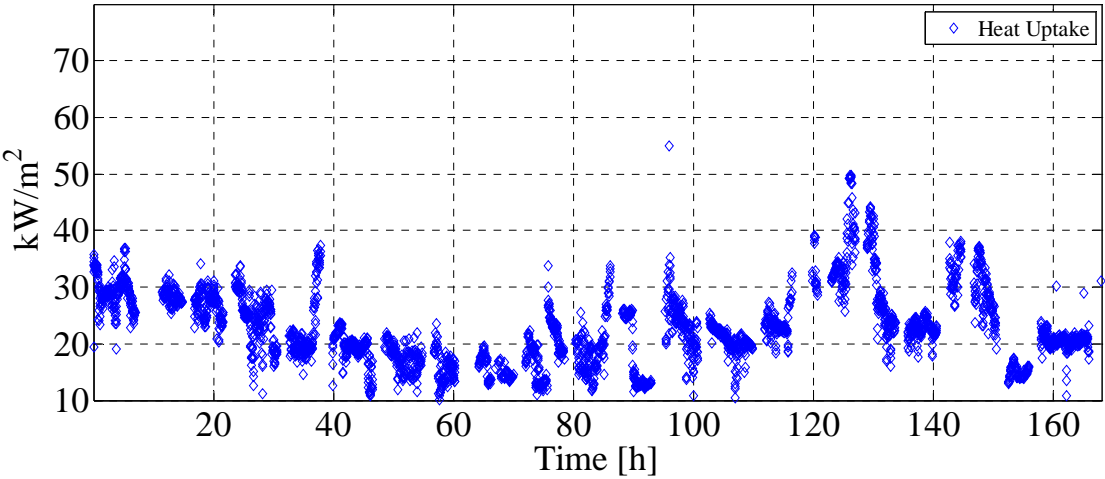
(a)



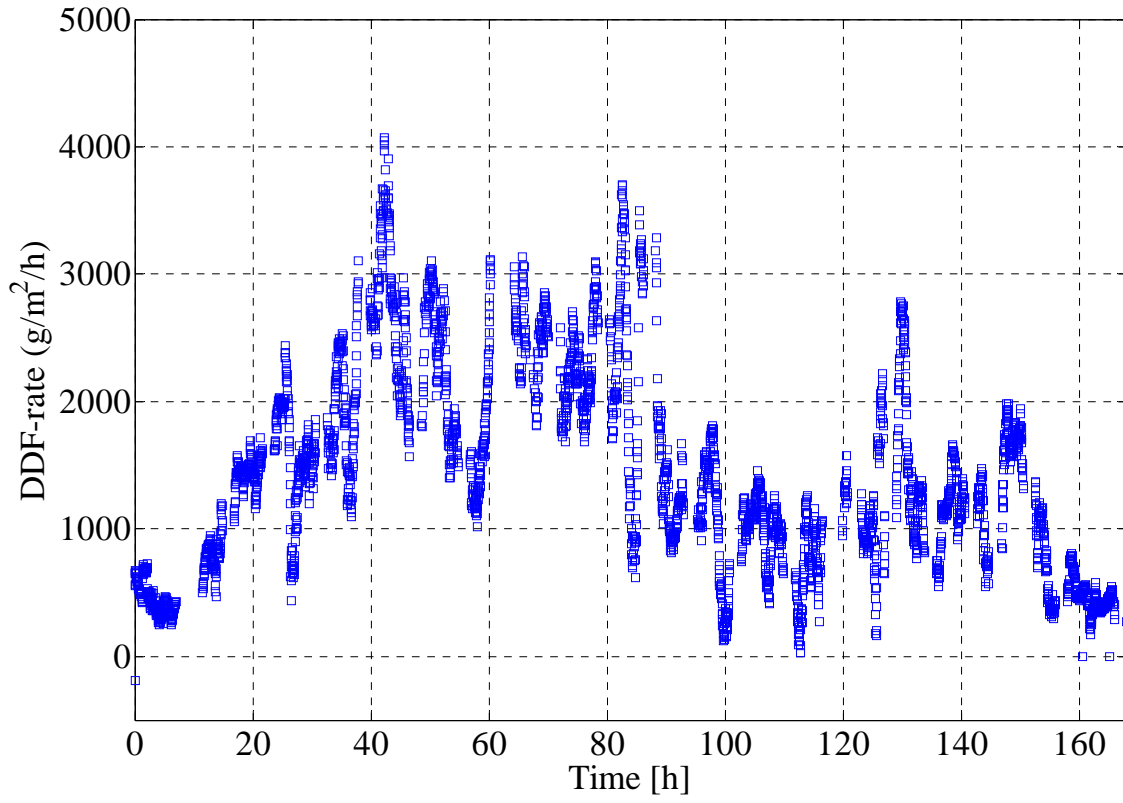
(b)



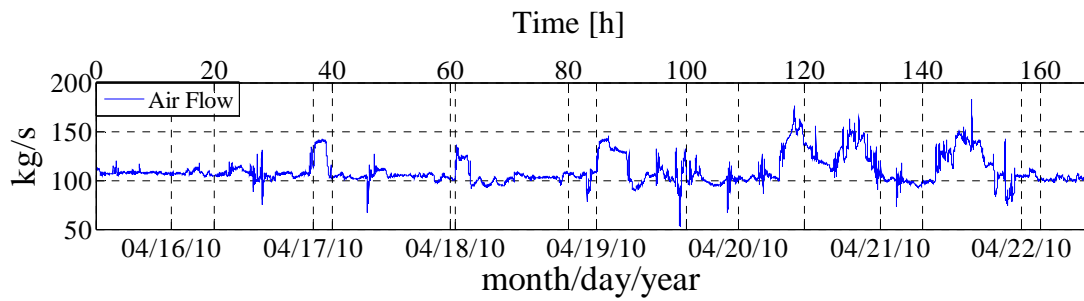
(c)

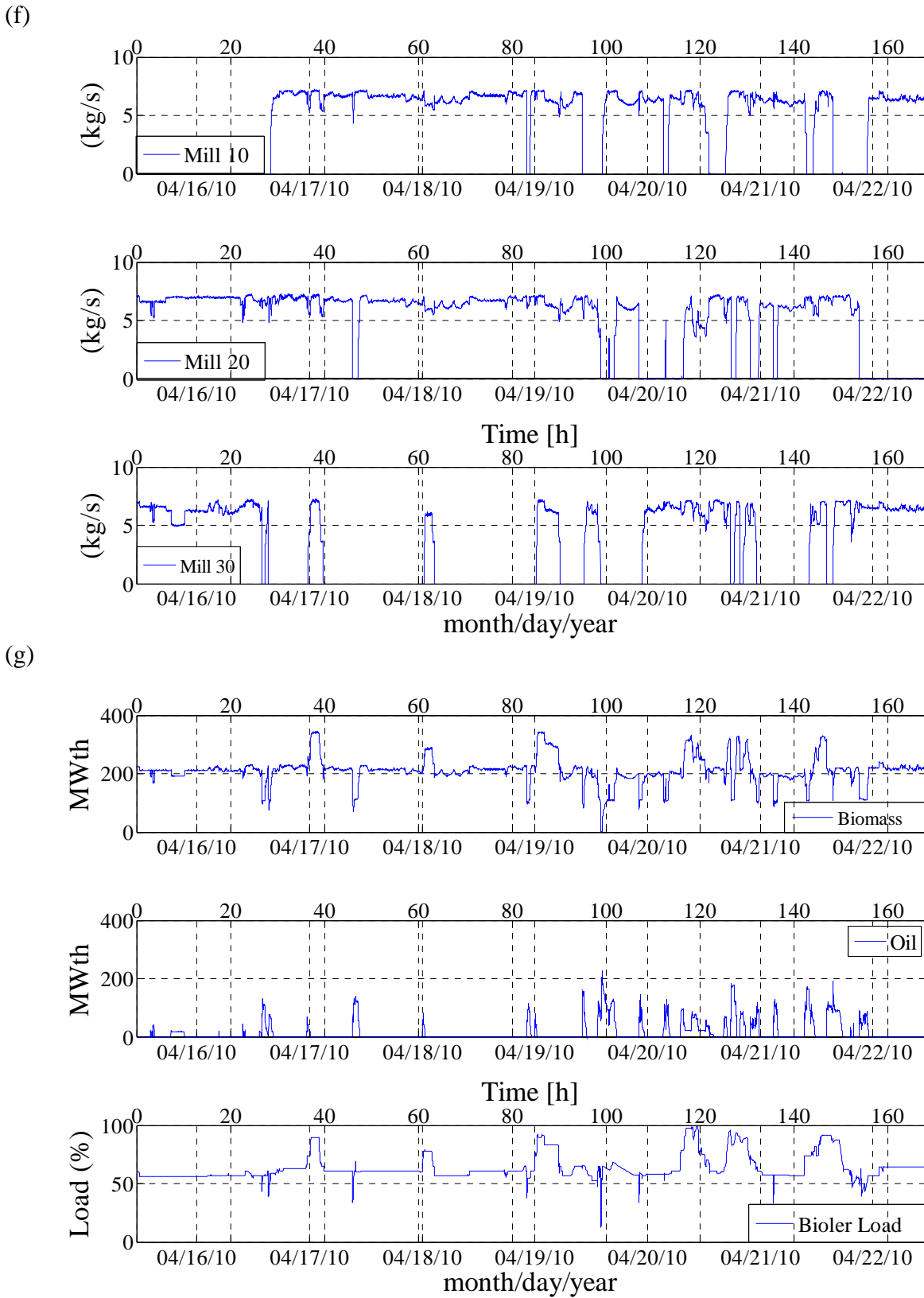


(d)



(e)

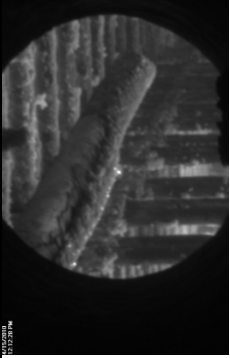
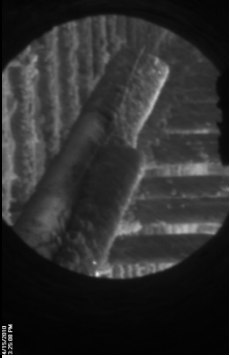





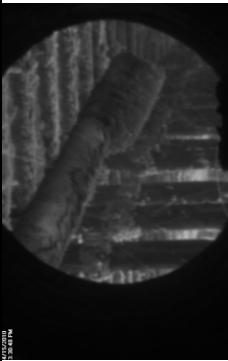




Appendix B: Full-scale measurements at AMV1

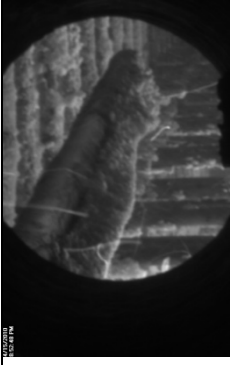
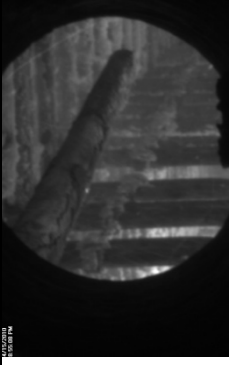
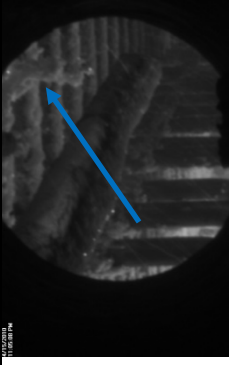
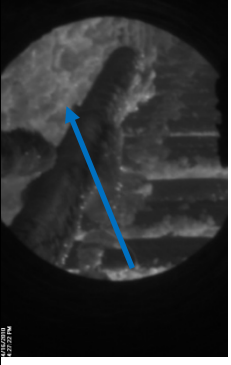
Table (Appendix B) 4: Selected shedding events during test 5.

Exposure Time	Date and Time	Picture	Flue Gas Temp. (Ther.) °C	Flue Gas Temp. (Suc. Pyr.) °C	Bio-mass Load MW <sub>th</sub>	Oil Load MW <sub>th</sub>	Mass Uptake (2 min. avg.) g/m <sup>2</sup>	Heat Uptake (2 min. avg.) kW/m <sup>2</sup>	Comments
h									
1.02	4/15/2010 12:12:28 PM		734	--	211	0	602	29.45	Deposit probe after an exposure time of about 1 hour can be seen.
4.23	4/15/2010 3:25:08 PM		748	--	212	0	2141	29.34	Deposits on the superheater tubes are being removed in the form of small pieces and sometimes complete layers.


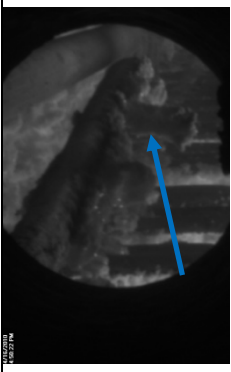

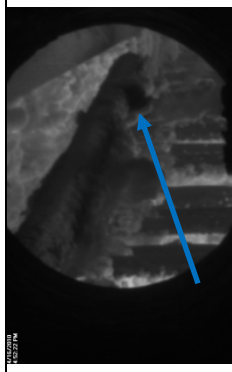

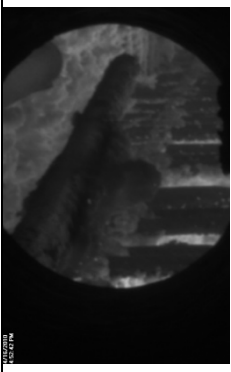

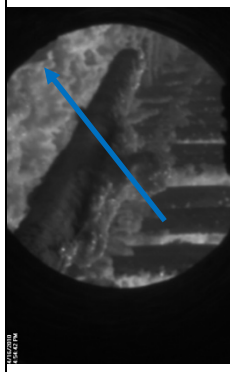
Appendix B: Full-scale measurements at AMV1

4.29		767	--	211	0	2166	28.62	A deposit layer on the upstream side of the probe is about to fall.
4.33		755	--	211	0	1401	28.74	The deposit layer has fallen.
9.32		766	--	192	19	2897	27.86	A deposit layer on the upstream side is about to fall.
9.49		763	--	192	19	2040	27.64	A deposit layer dropped near the tip of the probe.

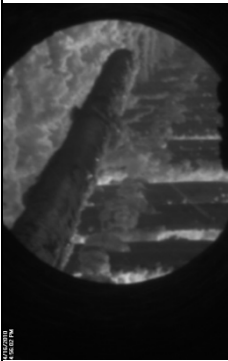
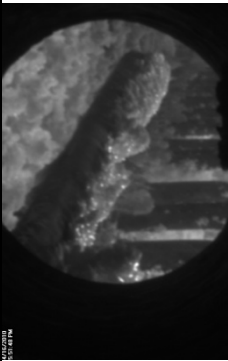
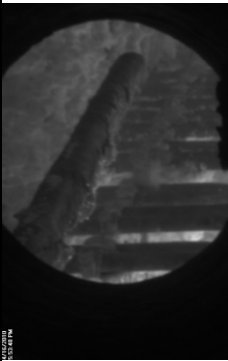
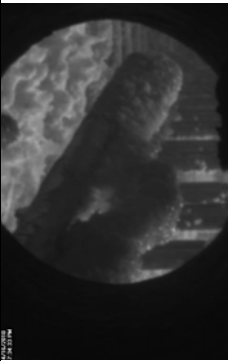
Appendix B: Full-scale measurements at AMV1

9.69		763	--	192	19	1943	27.92	A deposit layer dropped near the tip of the probe.
9.73		759	--	192	19	212	33.61	Within 30s all of the deposits were removed due to plant sootblowing. The sootblowers numbers effective were 70, 75 and 105.
11.90		732	--	210	0	969	28.33	Superheater deposit layer is about to detach because of debonding, indicated by arrow.
29.27		722	--	217	0	1118	26.47	Significant amount of deposit on the superheater tubes is indicated by arrow.

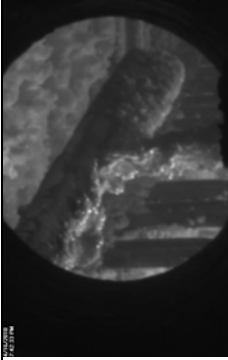
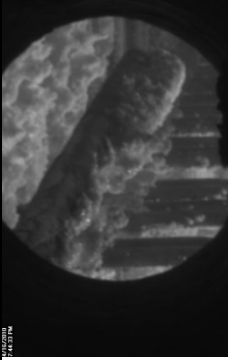
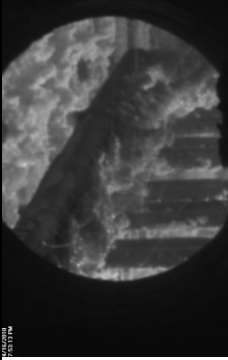
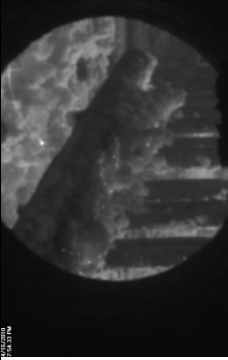
Appendix B: Full-scale measurements at AMV1

29.65			699	--	207	0	1777	23.85	A deposit layer is about to fall using artificial sootblowing probe indicated by arrow.
29.69			713	--	207	0	1323	25.08	The back spot indicated by arrow shows the point where pressurized air is hitting the probe.
29.70			713	--	207	0	1200	25.10	A deposit layer on the upstream side near the tip of the probe is removed.
29.73			--	--	--	--	--	--	Artificial sootblowing probe is ready to remove the deposits on the upstream side of the probe. The nozzle of the probe is indicated by arrow.

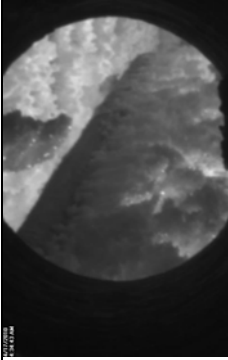
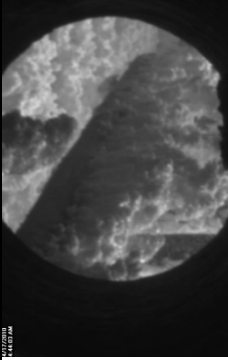
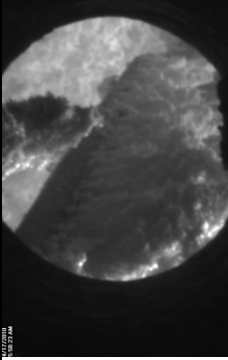
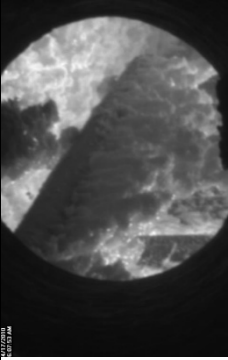
Appendix B: Full-scale measurements at AMV1

29.75		708	--	207	0	699	26.82	The deposit layer is being removed using artificial sootblowing probe. Deposit layer in the downstream side and upstream side of the probe are still present.
30.68		722	--	228	0	1826	19.89	More deposits attached on the upstream direction of the probe.
30.71		723	--	228	0	566	20.37	Most of the deposits were removed because of plant sootblowing. The sootblowers number effective were 70 and 105.
32.39		747	--	228	0	1927	22.56	A deposit layer on the upstream side of the probe is about to fall.

Appendix B: Full-scale measurements at AMV1

32.52		758	--	228	0	--	Another deposit layer is about to fall.	
32.56		753	--	228	0	1567	21.44	Picture of the deposit probe after deposit removal.
32.70		748	--	228	0	1809	21.63	A deposit layer is about to fall near the probe tip.
32.73		750	--	228	0	895	22.53	The deposit layer has fallen.

Appendix B: Full-scale measurements at AMV1

41.39		785	--	222	0	8931	23.27	Significant amount of deposits on the upstream side of the probe can be seen.
41.48		783	--	222	0	8562	21.48	Significant amount of deposits on the upstream side of the probe can potentially cause more deposits to stick to the probe.
42.79		766	--	217	0	9012	19.70	Even more deposits on the upstream side of the probe can be seen.
42.95		770	--	218	0	7845	19.94	Some deposits have fallen in the form of small layers from the upstream side of the probe.

## Appendix C: Full-scale measurements at AVV2

In Appendix C, derivative-base deposit formation rate (DDF-rate), ash deposition propensity and DCS data (flue gas temperature, probe deposit mass uptake and heat uptake, sootblowing events, solid fuel flow rate through each mill, natural gas flow, biomass load, relative boiler load, coal ash flow (kg/s), and coal ash to wood ash ratio) are presented for the 13 tests conducted at AVV2 (suspension boiler).

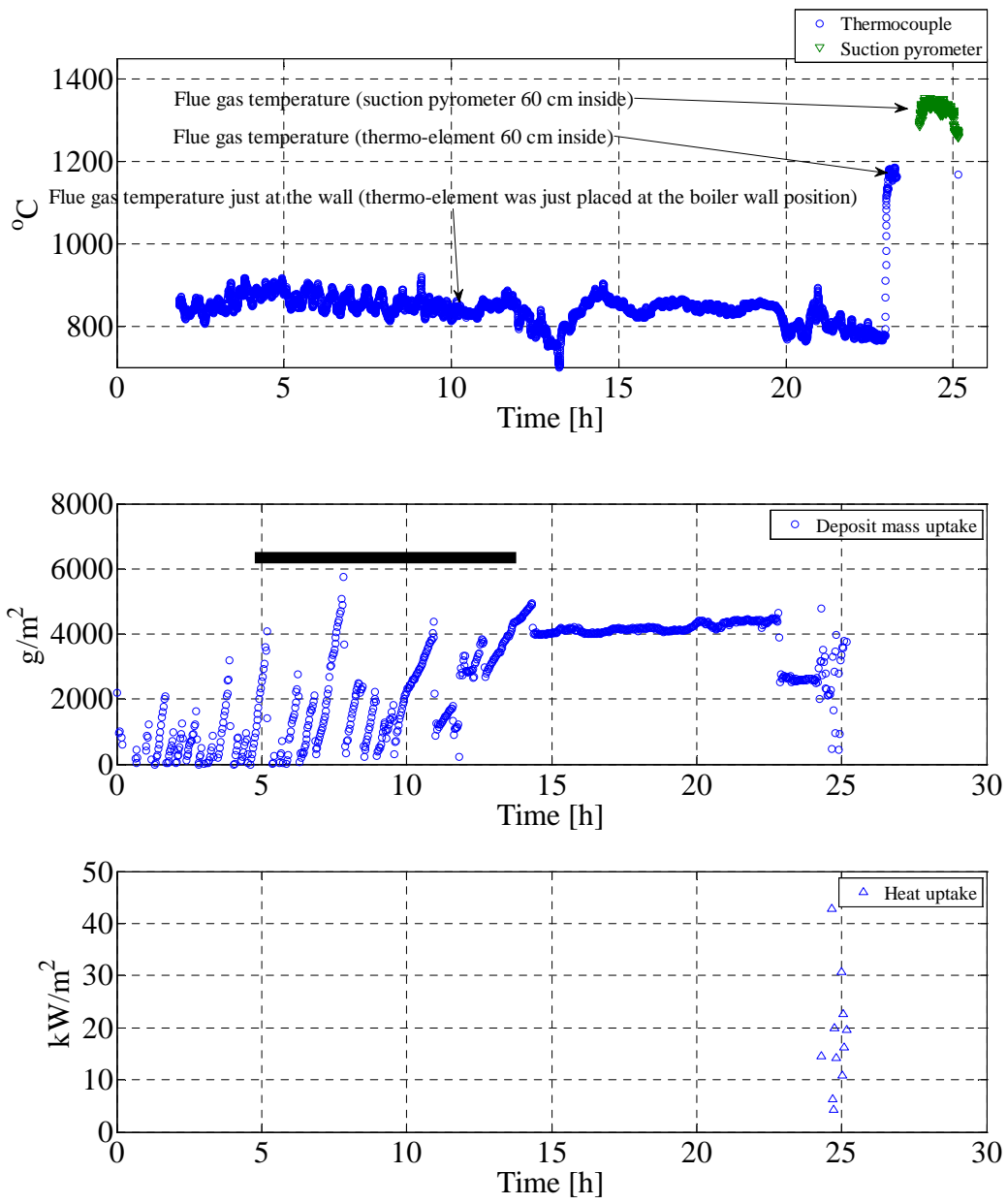
Each figure is divided into the following five parts:

**a)** Flue gas temperature measurements during each test, deposit mass uptake signals and sootblowing events, and probe heat uptake, **b)** DDF-rate, **c)** ash deposition propensity, **d)** natural gas flow rate, biomass load, boiler load, **g)** fuel flow through each mill, coal ash flow (kg/s) and coal ash to wood ash ratio.

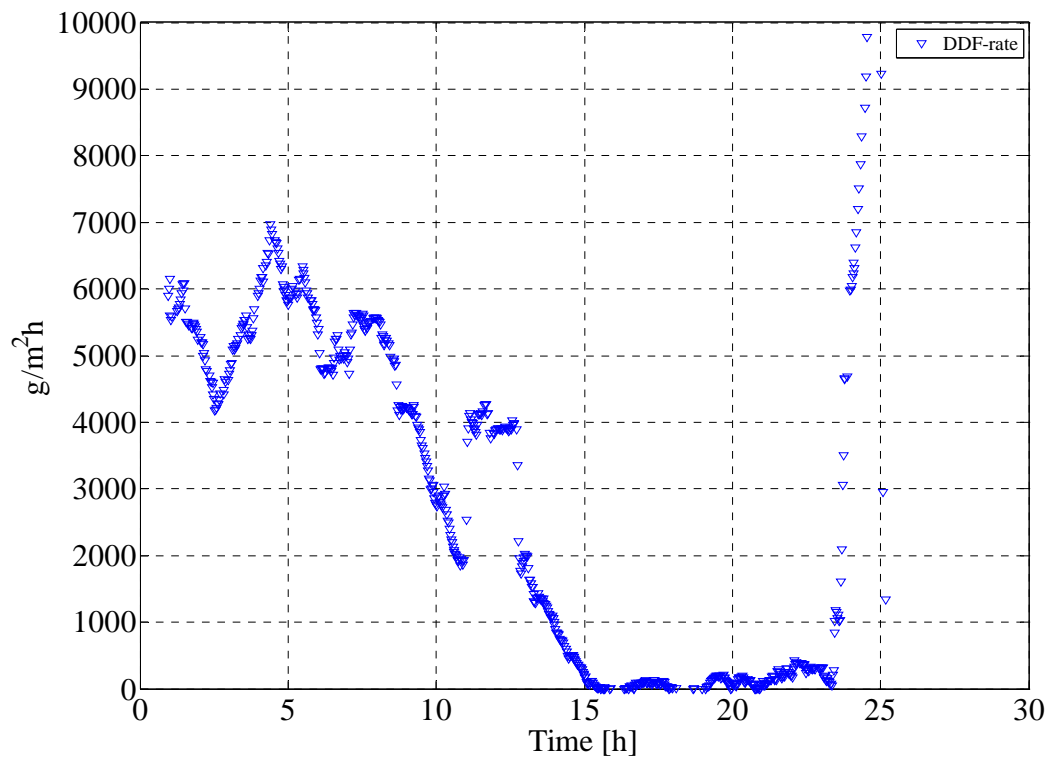


## Appendix C: Full-scale measurements at AVV2

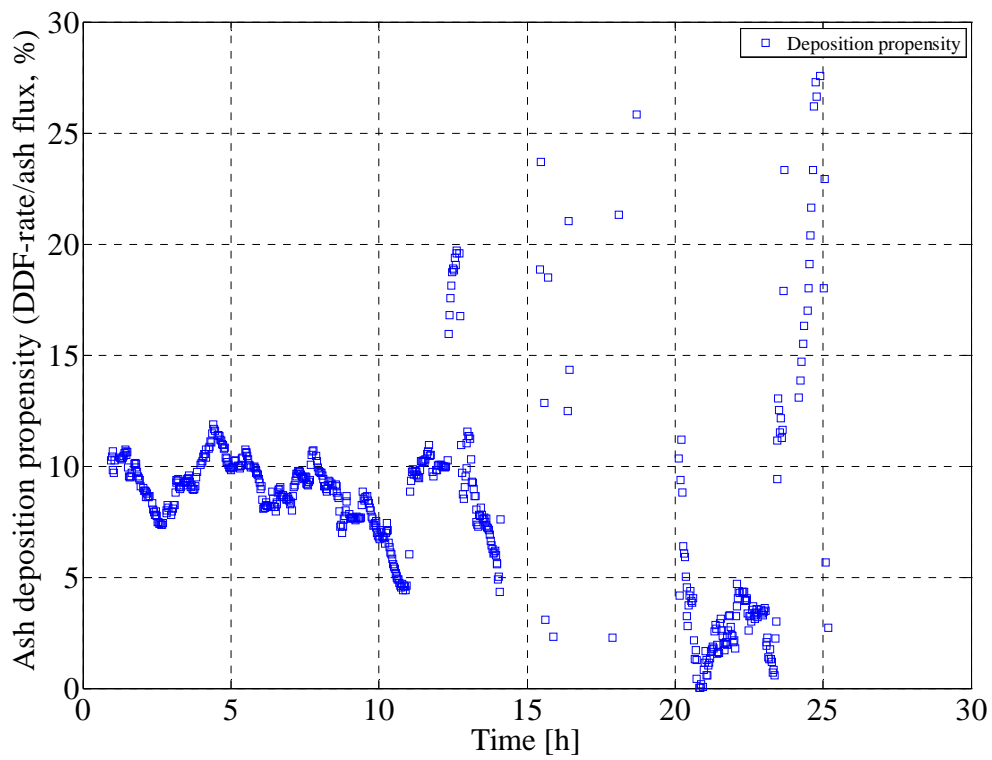
(a)



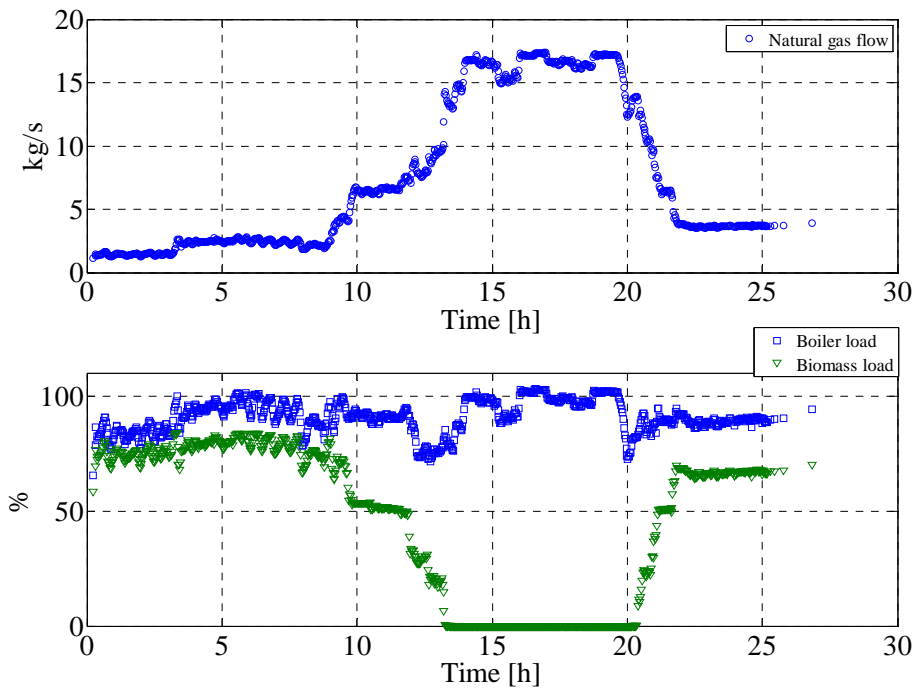
(b)



(c)



(d)



(e)

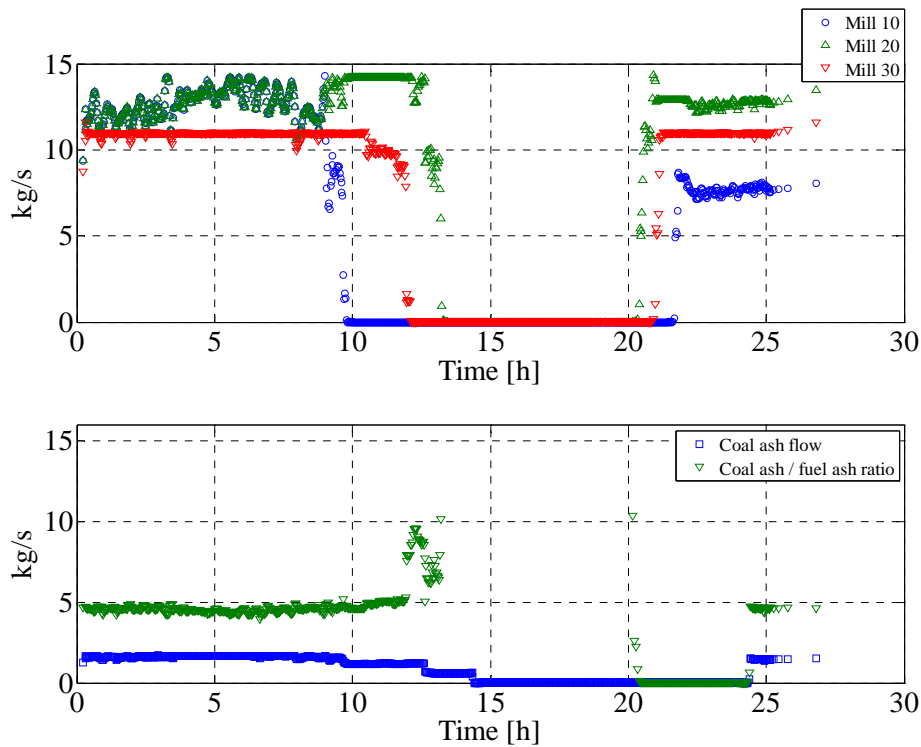
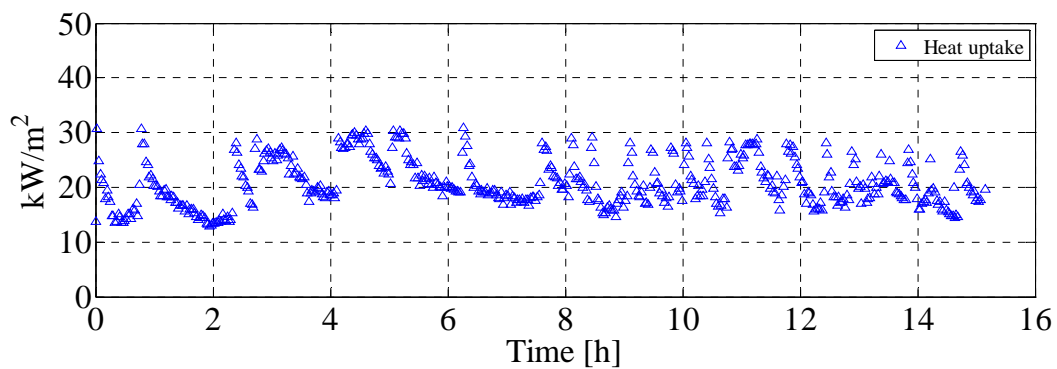
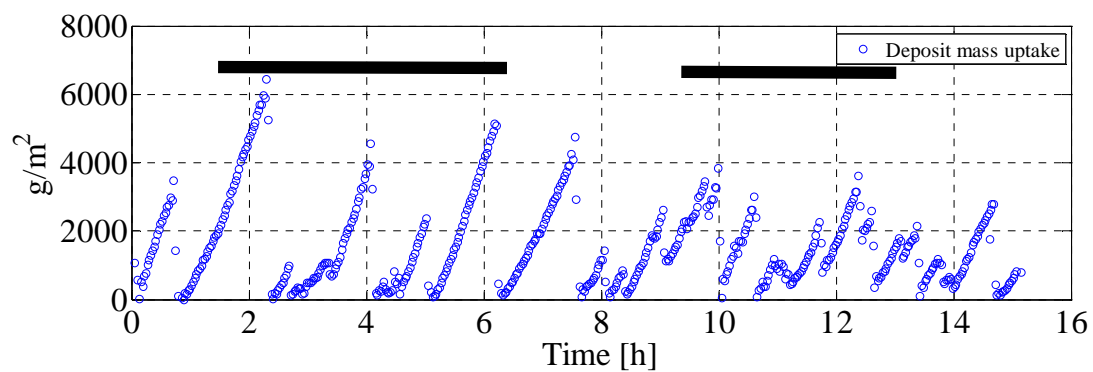
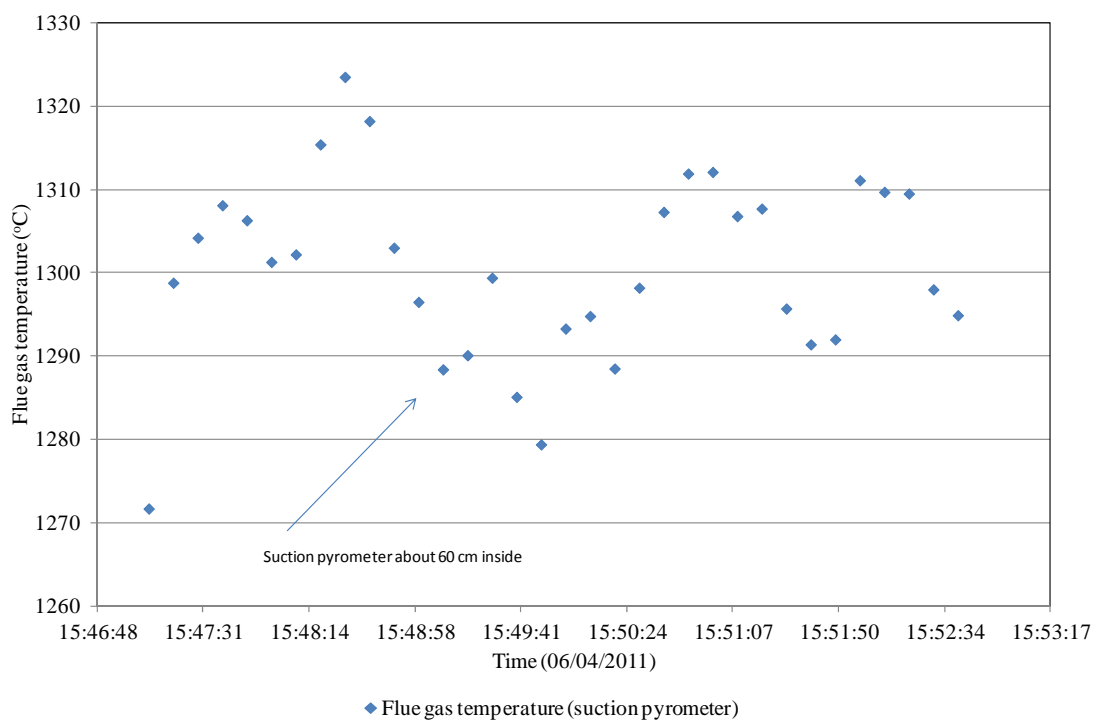


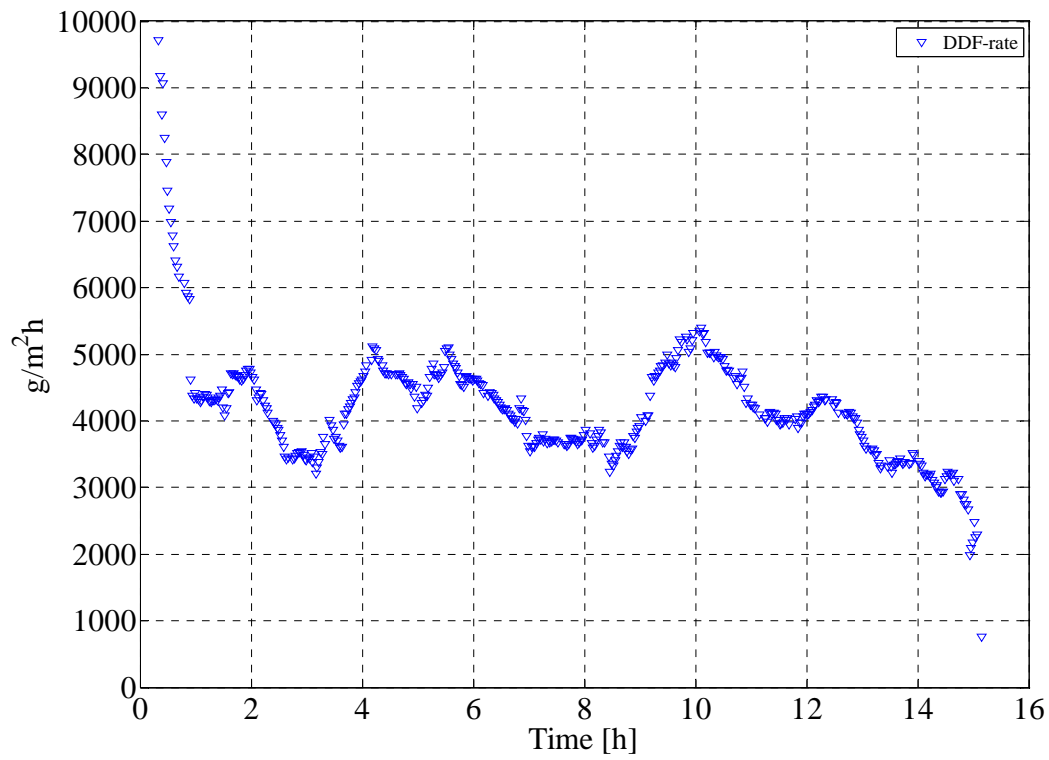
Figure (Appendix C) 1: a) Flue gas temperature, deposit mass uptake signals, sootblowing events (black lines), b) DDF-rate, c) ash deposition propensity, d) natural gas flow rate, biomass load, boiler load, e) fuel flow through each mill, coal ash flow (kg/s), and coal ash to wood ash ratio during test 1 (Chapter 6).

## Appendix C: Full-scale measurements at AVV2

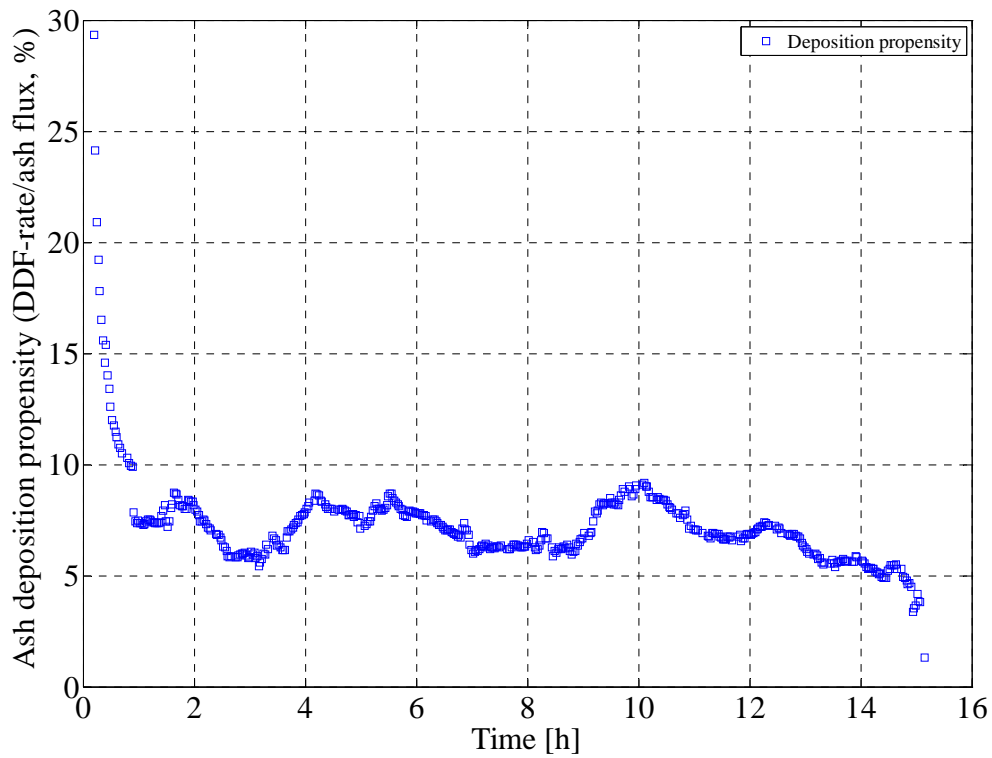
(a)



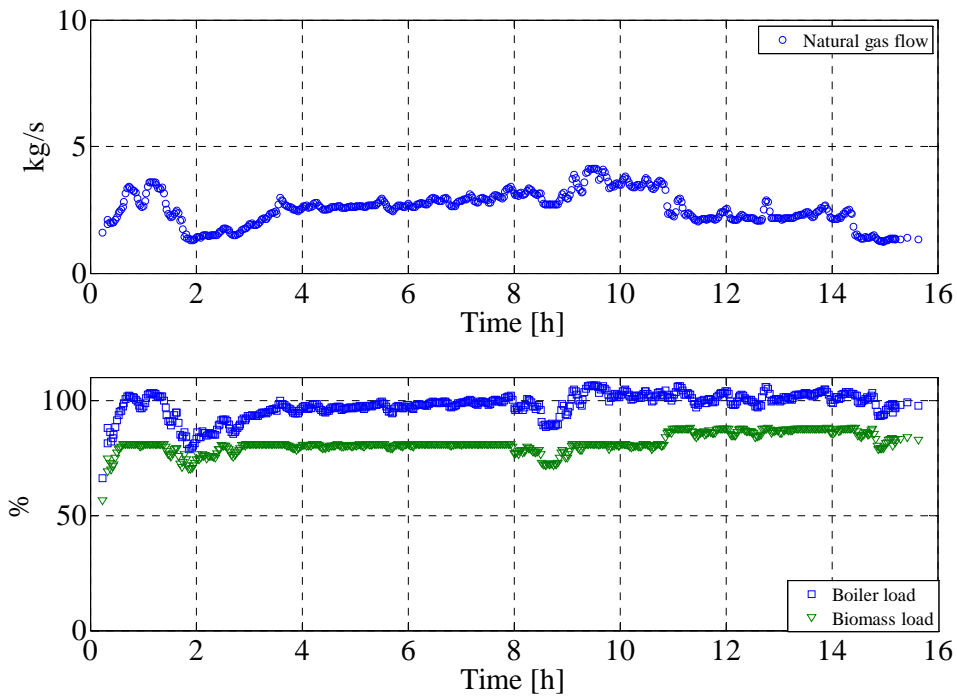
(b)



(c)



(d)



(e)

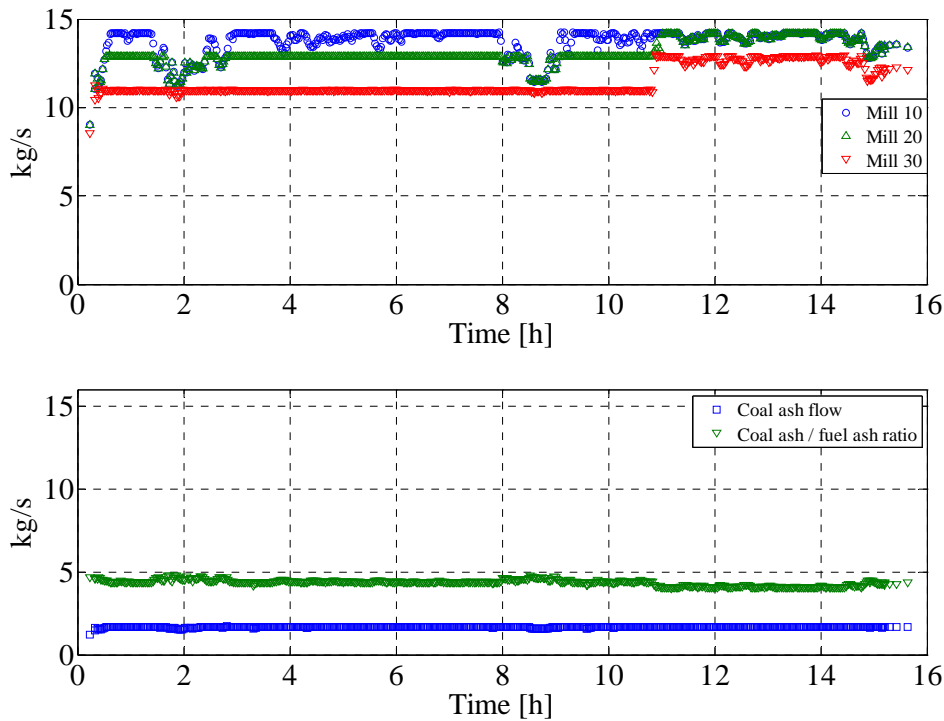
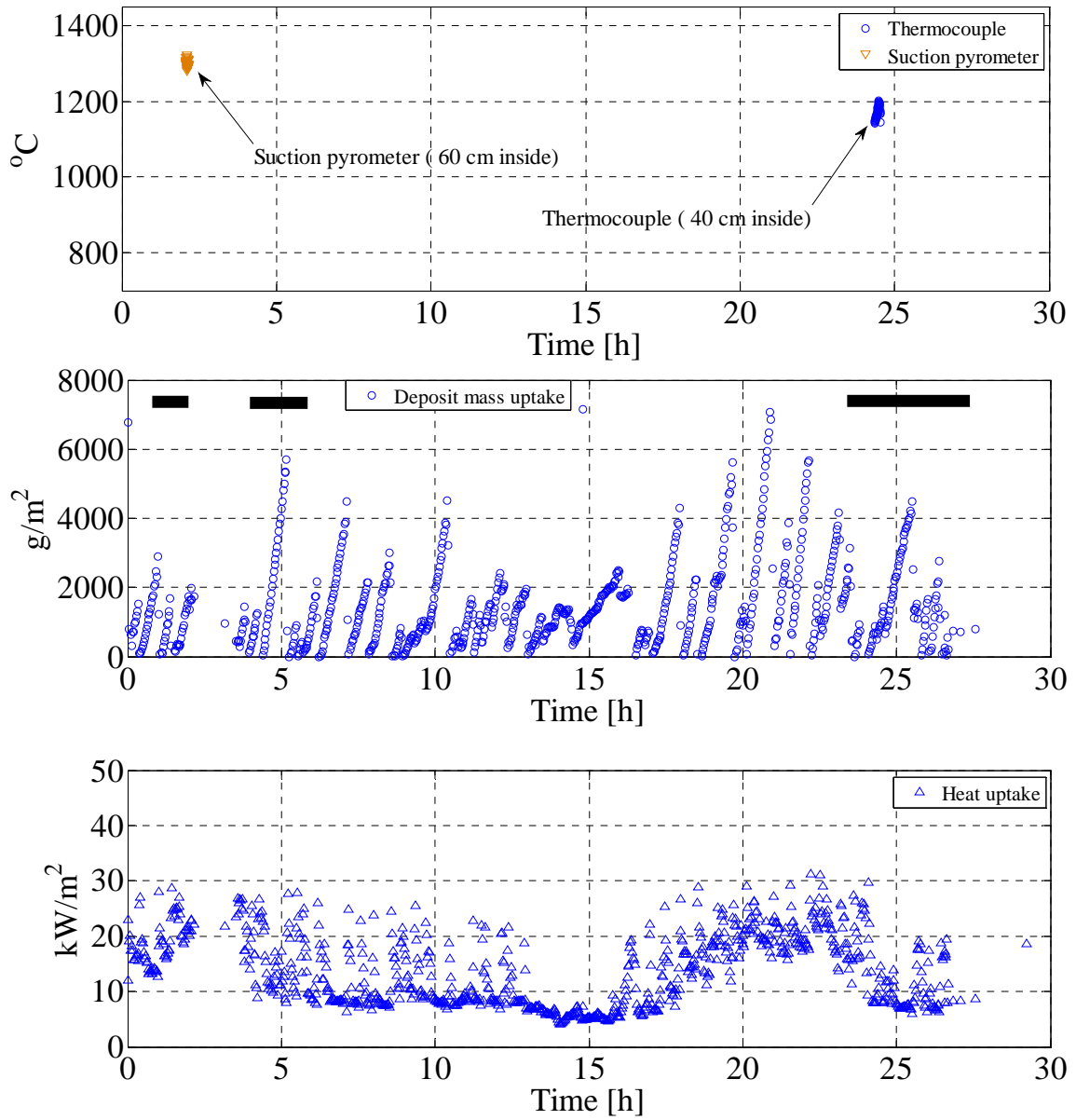


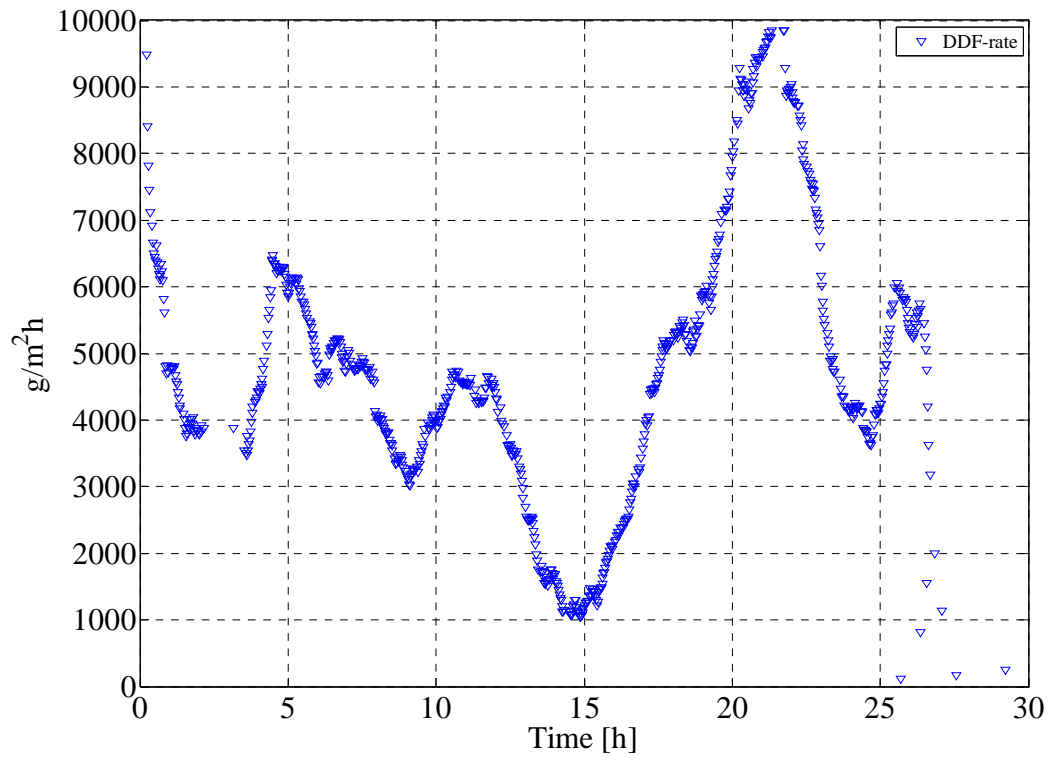
Figure (Appendix C) 2: a) Flue gas temperature, deposit mass uptake signals, sootblowing events (black lines), b) DDF-rate, c) ash deposition propensity, d) natural gas flow rate, biomass load, boiler load, e) fuel flow through each mill, coal ash flow (kg/s), and coal ash to wood ash ratio during test 2 (Chapter 6).

Appendix C: Full-scale measurements at AVV2

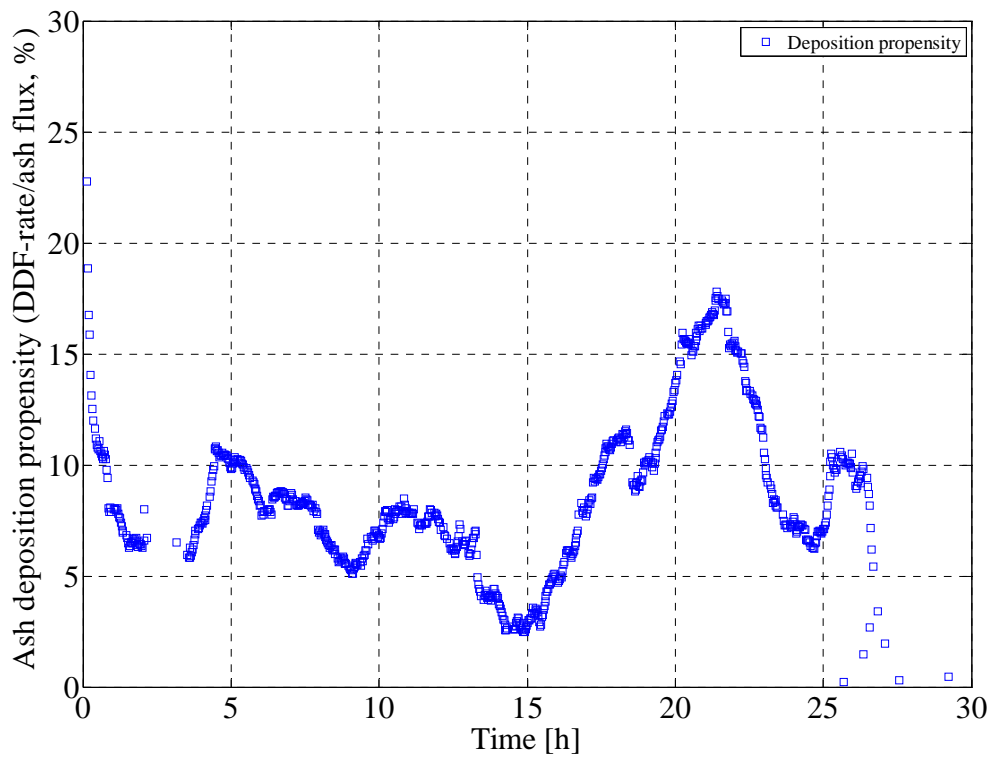
(a)



(b)



(c)





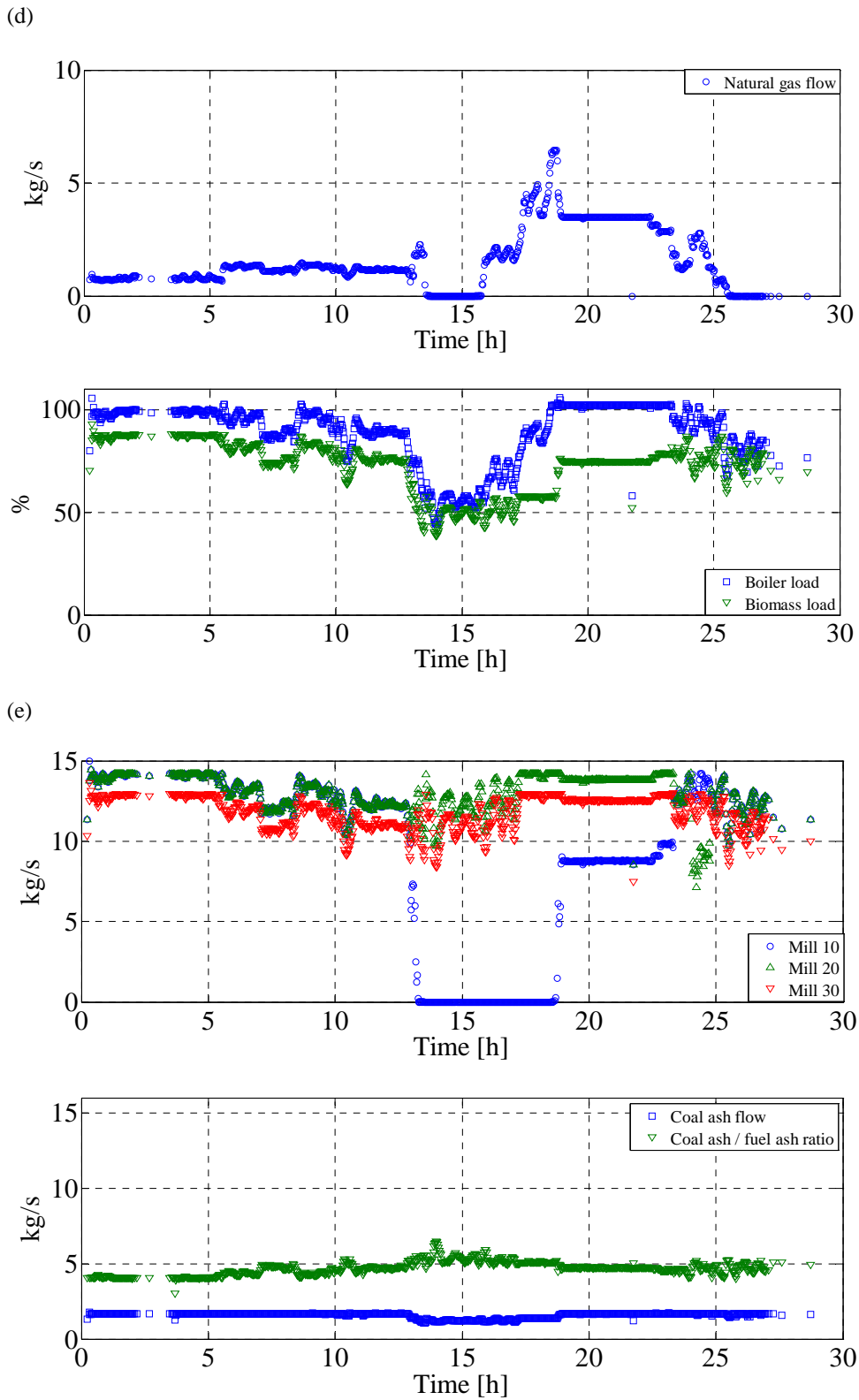
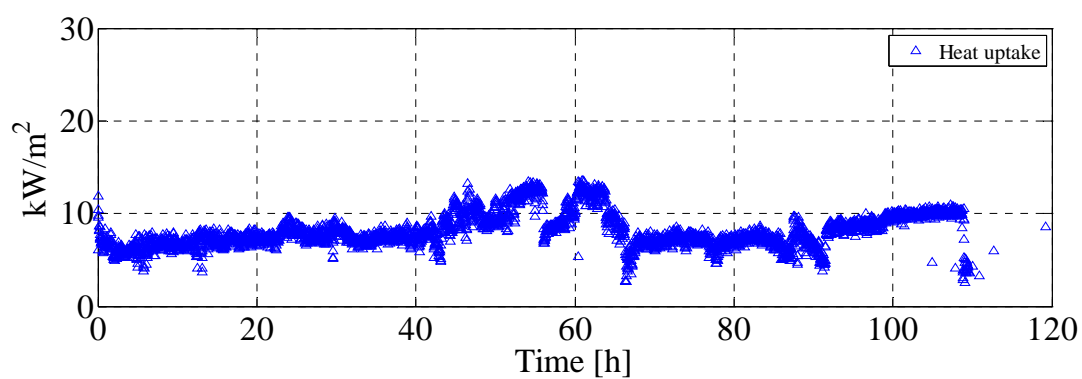
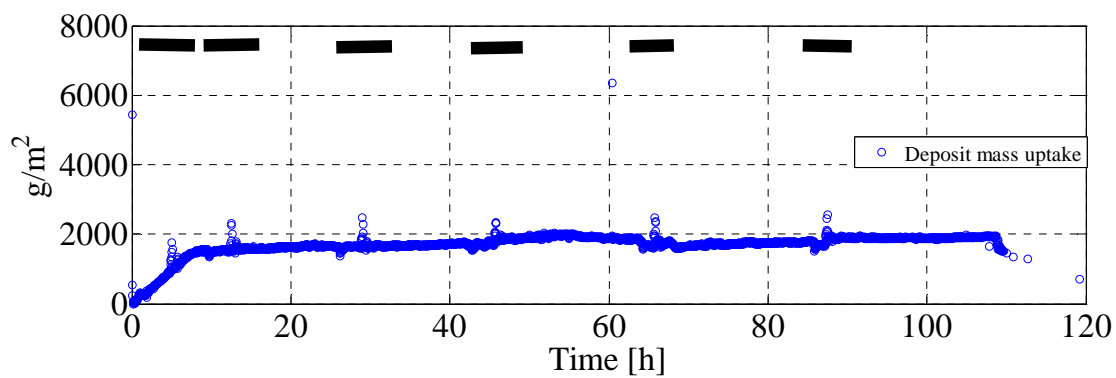
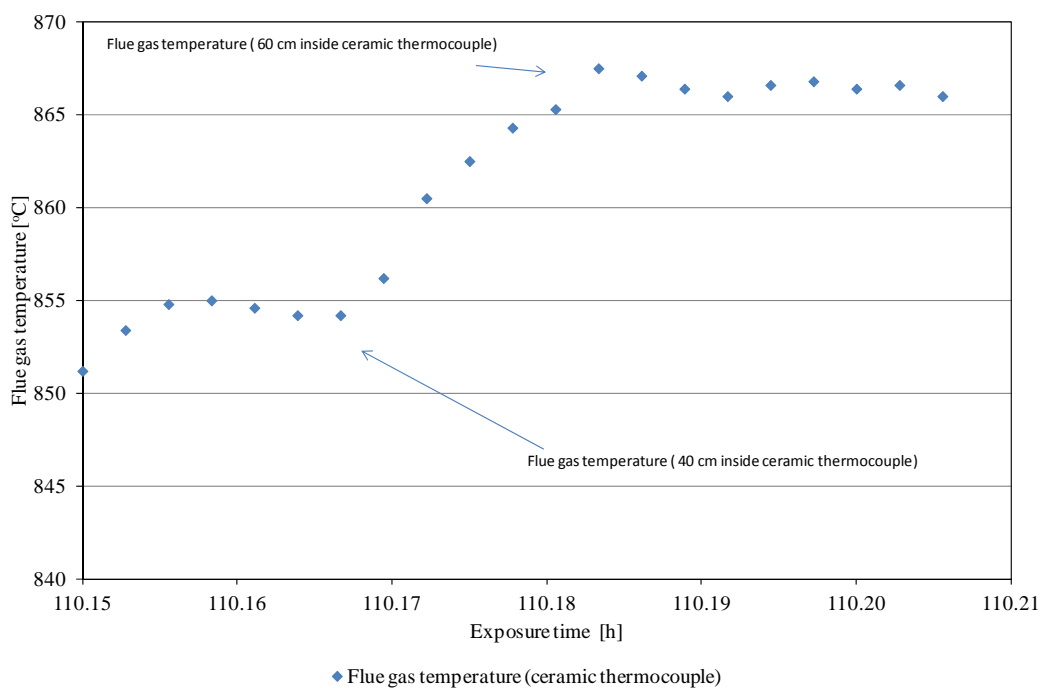


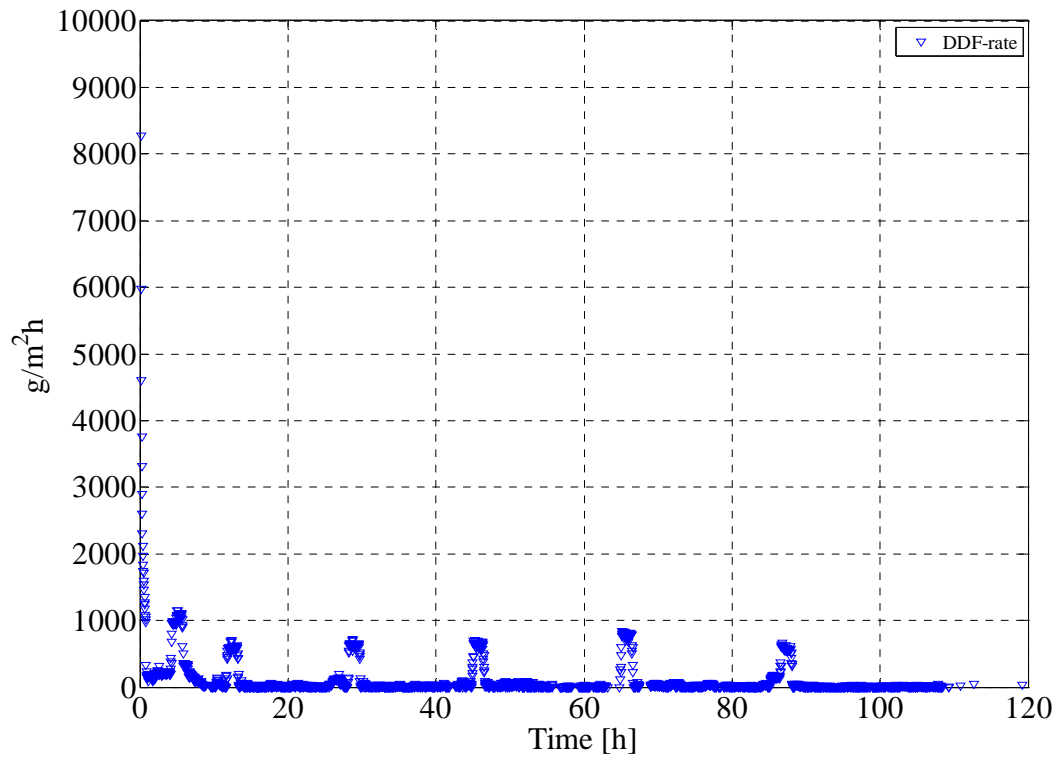
Figure (Appendix C) 3: a) Flue gas temperature, deposit mass uptake signals, sootblowing events (black lines), b) DDF-rate, c) ash deposition propensity, d) natural gas flow rate, biomass load, boiler load, e) fuel flow through each mill, coal ash flow (kg/s), and coal ash to wood ash ratio during test 3 (Chapter 6).

## Appendix C: Full-scale measurements at AVV2

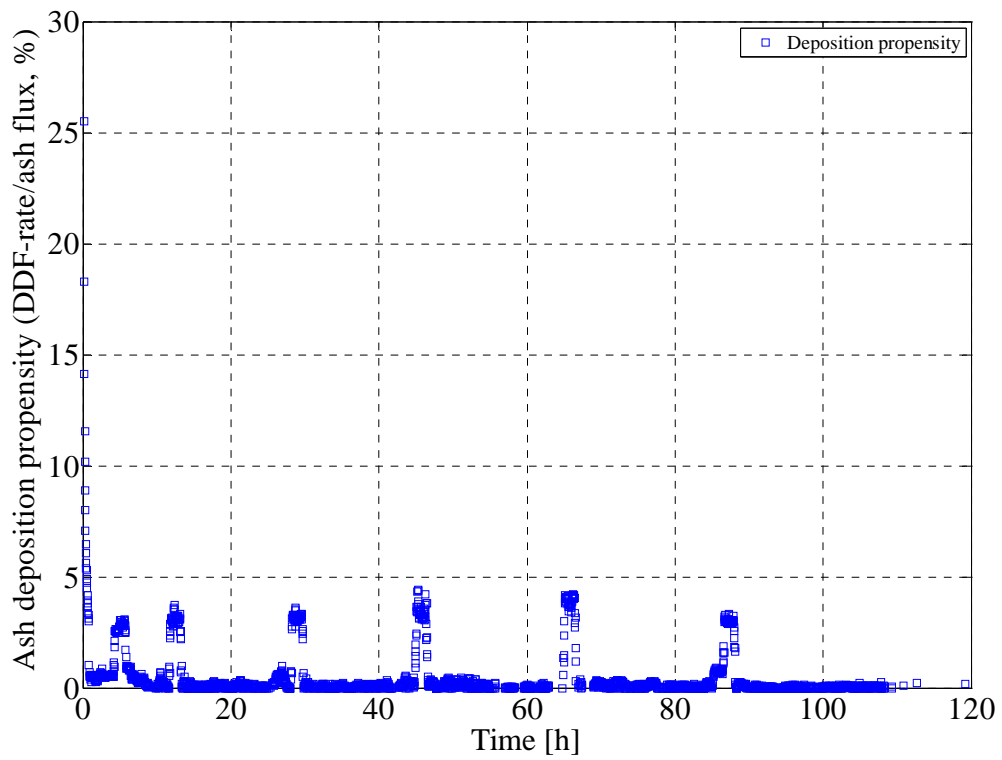
(a)



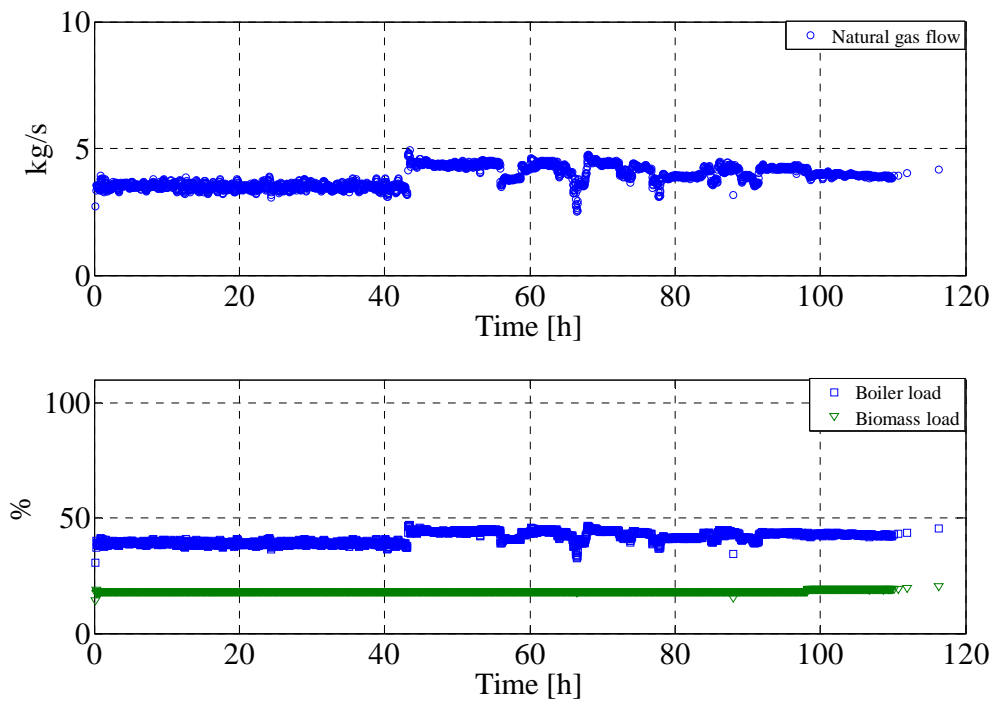
(b)



(c)



(d)



(e)

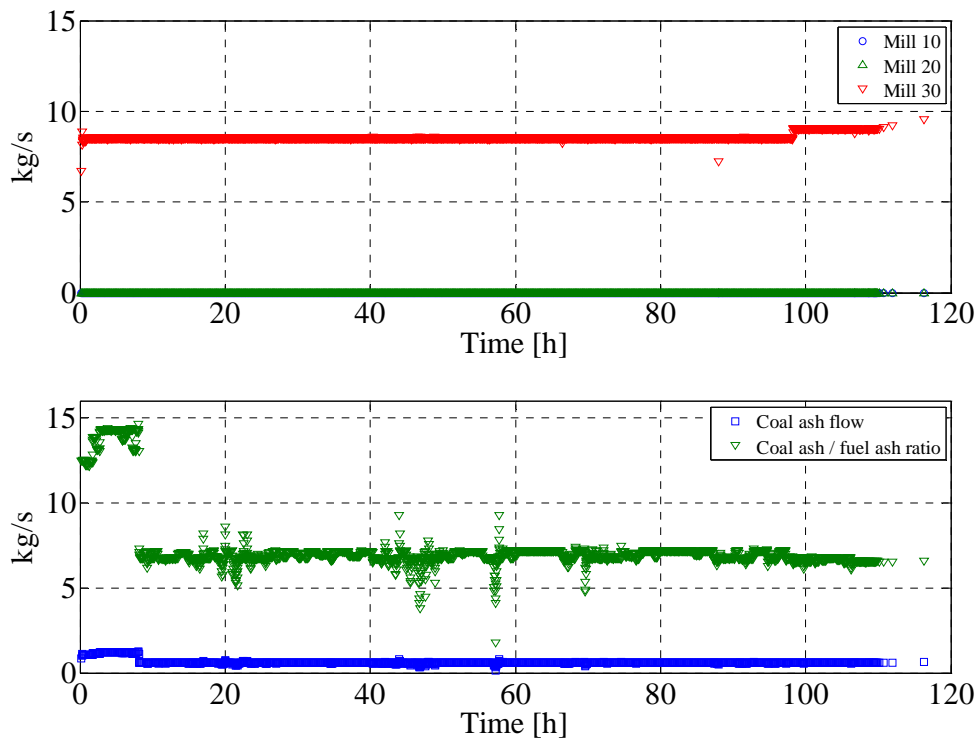
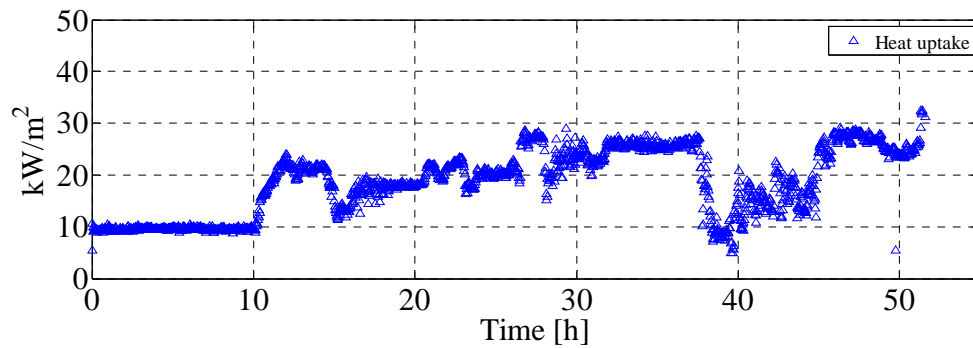
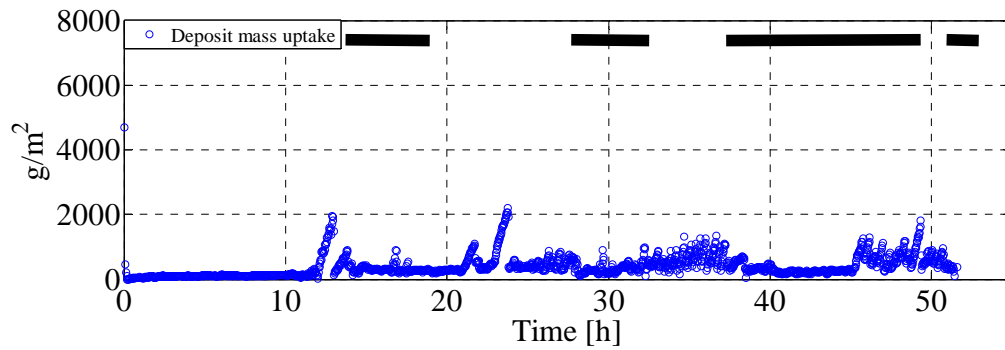
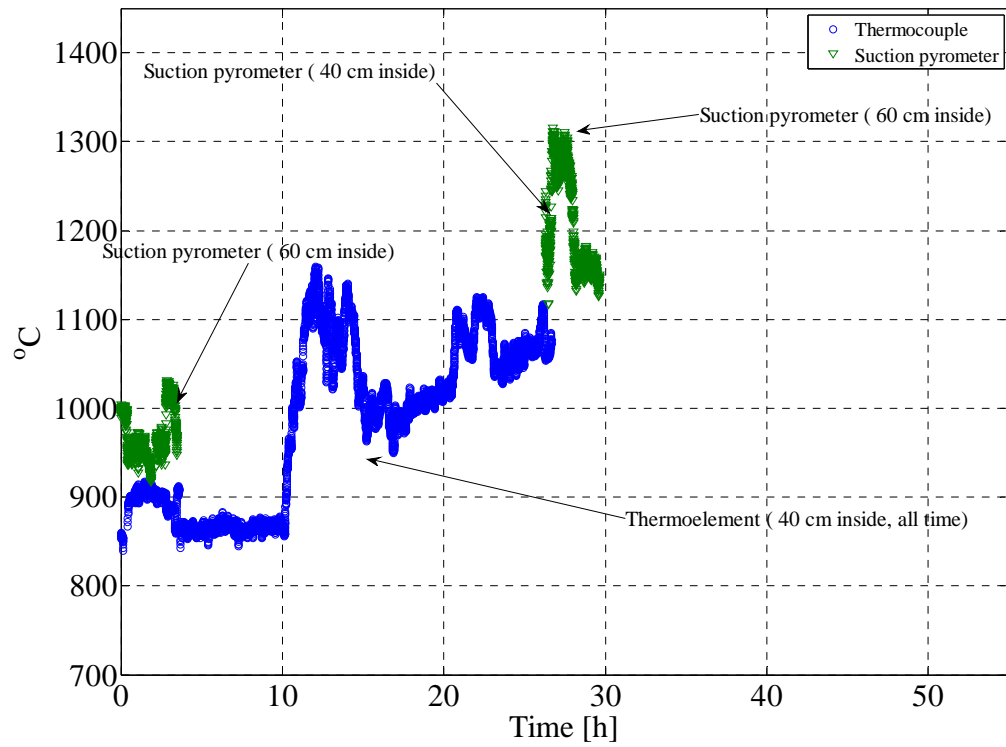


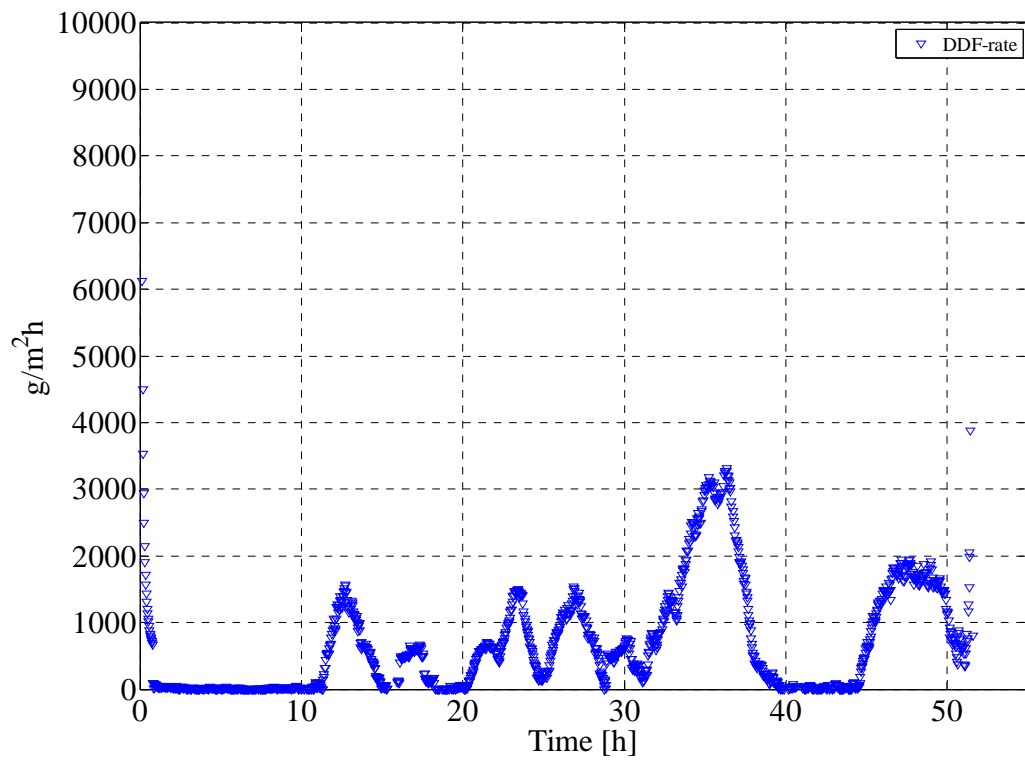
Figure (Appendix C) 4: a) Flue gas temperature, deposit mass uptake signals, sootblowing events (black lines), b) DDF-rate, c) ash deposition propensity, d) natural gas flow rate, biomass load, boiler load, e) fuel flow through each mill, coal ash flow (kg/s), and coal ash to wood ash ratio during test 4 (Chapter 6).

Appendix C: Full-scale measurements at AVV2

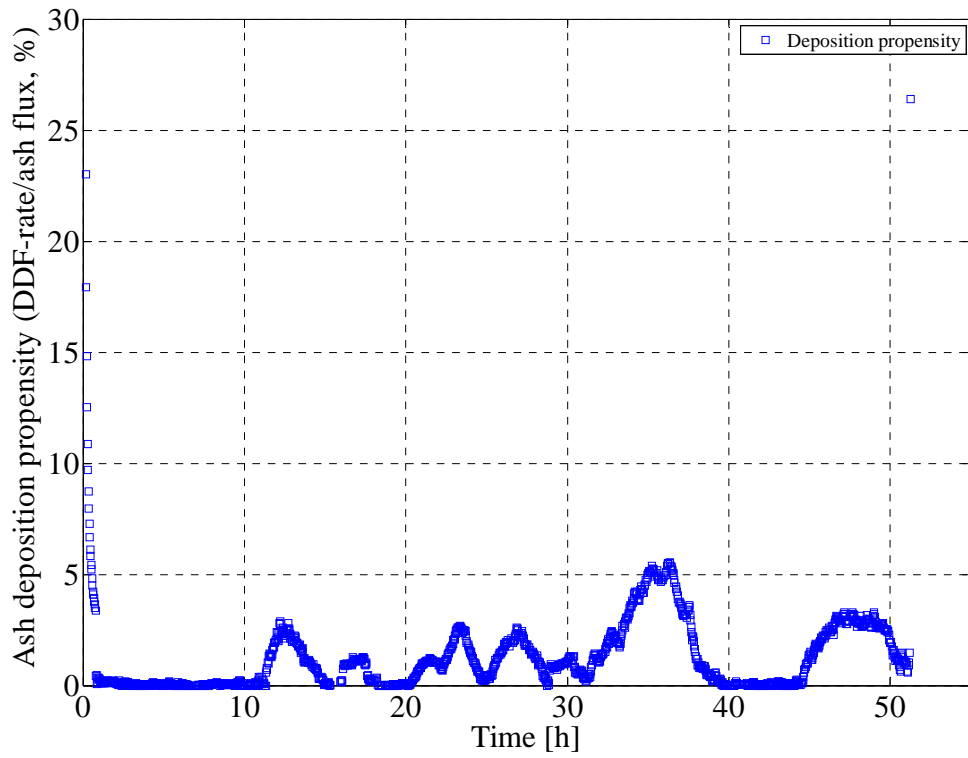
(a)



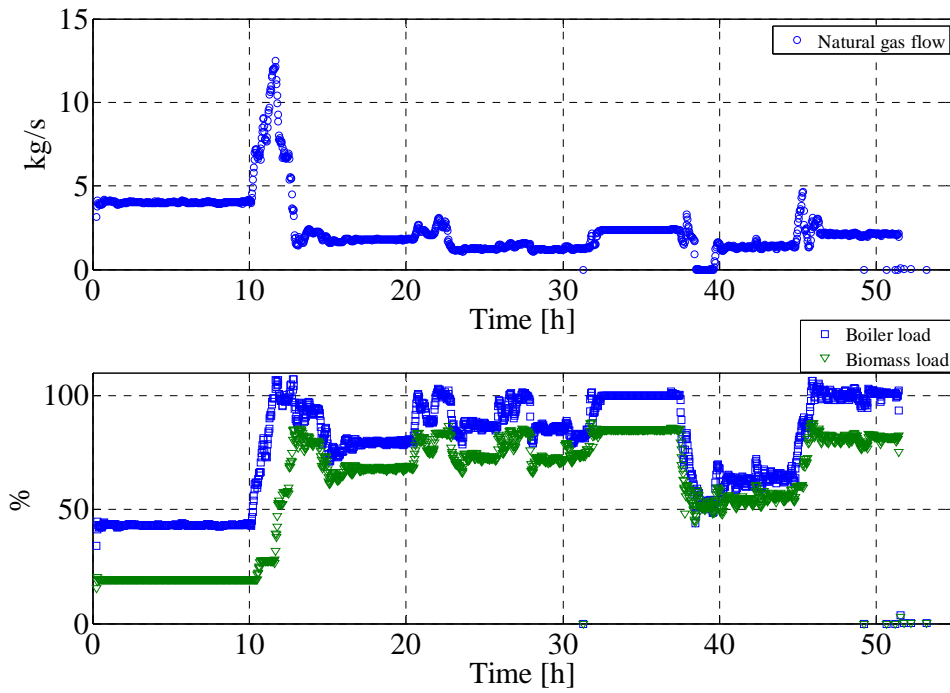
(b)



(c)



(d)



(e)

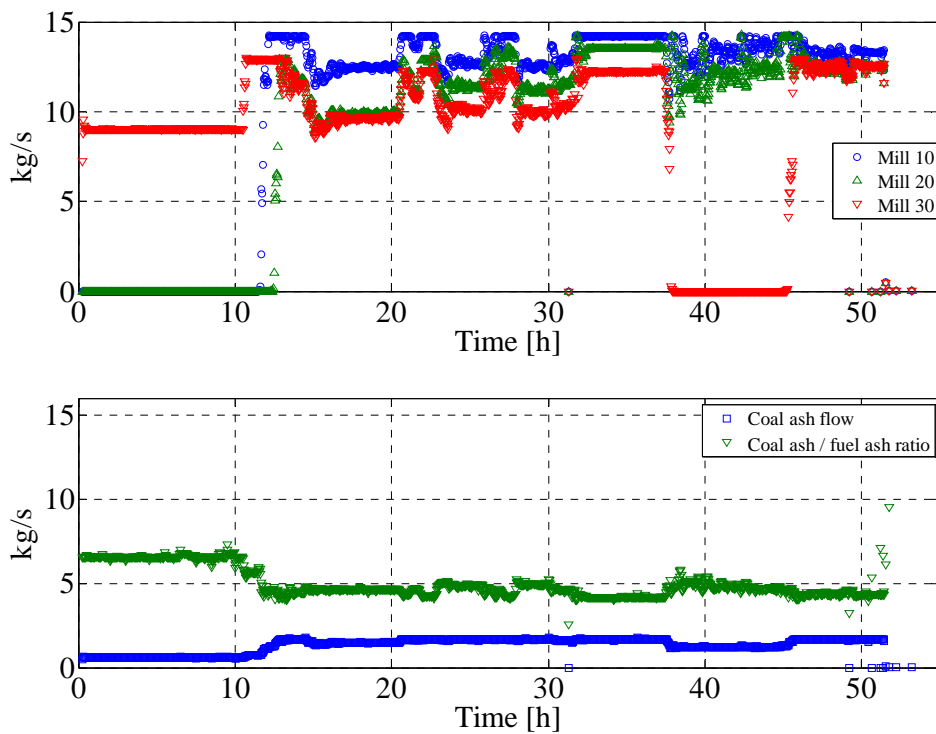
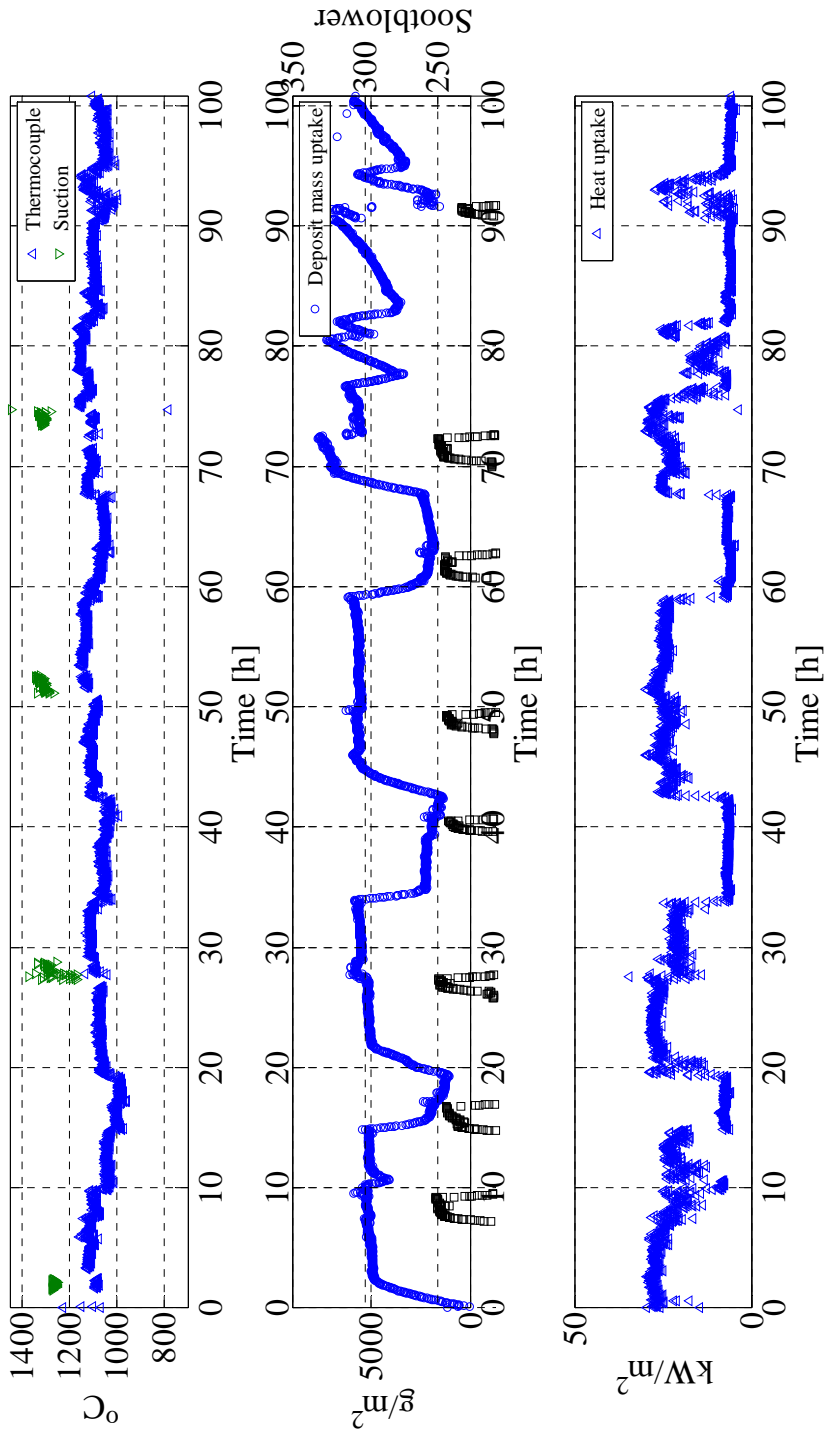


Figure (Appendix C) 5: a) Flue gas temperature, deposit mass uptake signals, sootblowing events (black lines), b) DDF-rate, c) ash deposition propensity, d) natural gas flow rate, biomass load, boiler load, e) fuel flow through each mill, coal ash flow (kg/s), and coal ash to wood ash ratio during test 5 (Chapter 6).

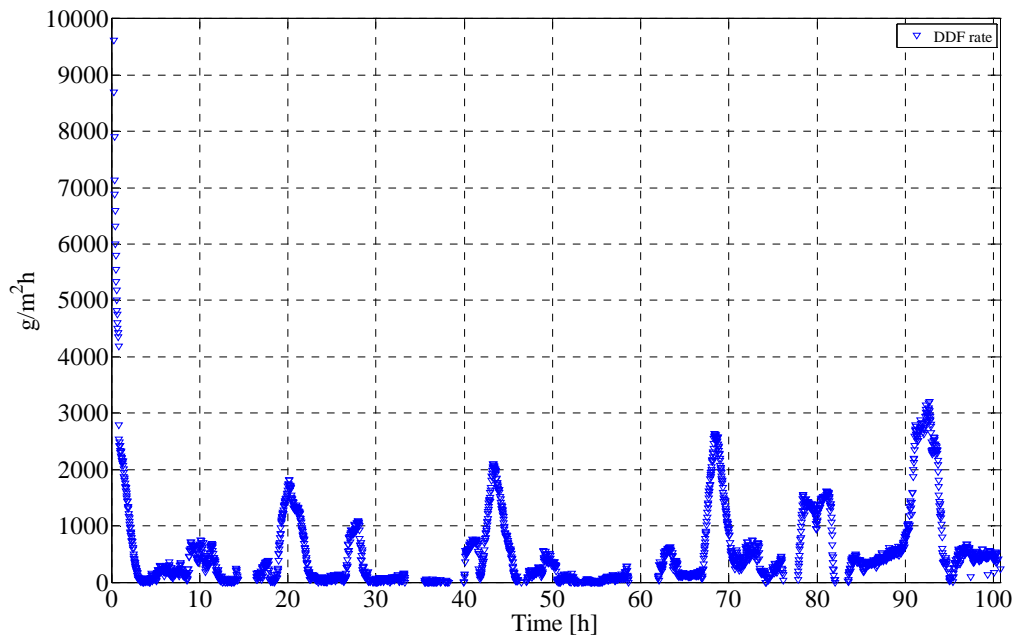
(a)



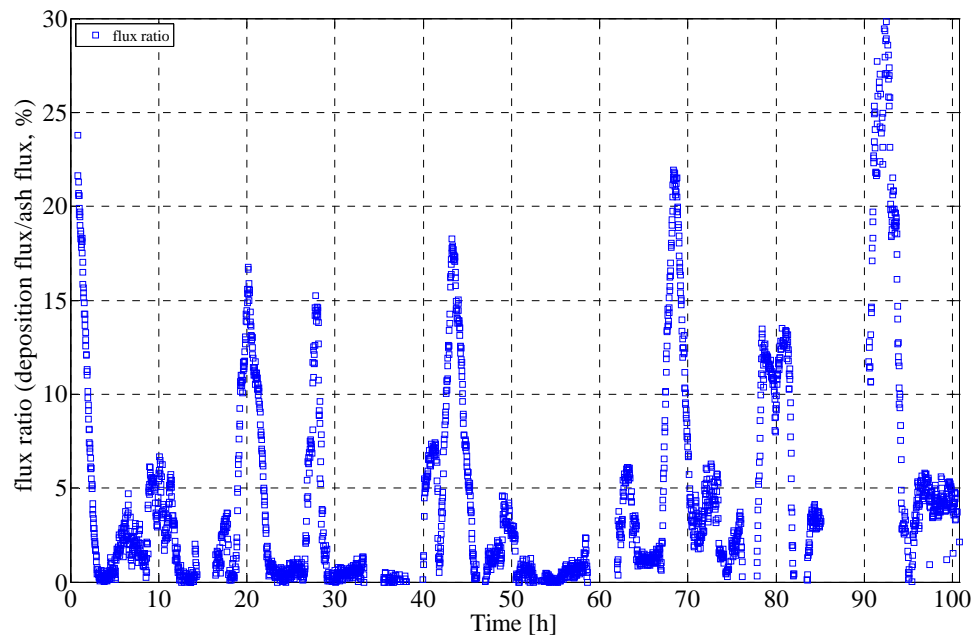


## Appendix C: Full-scale measurements at AVV2

b)



(c)



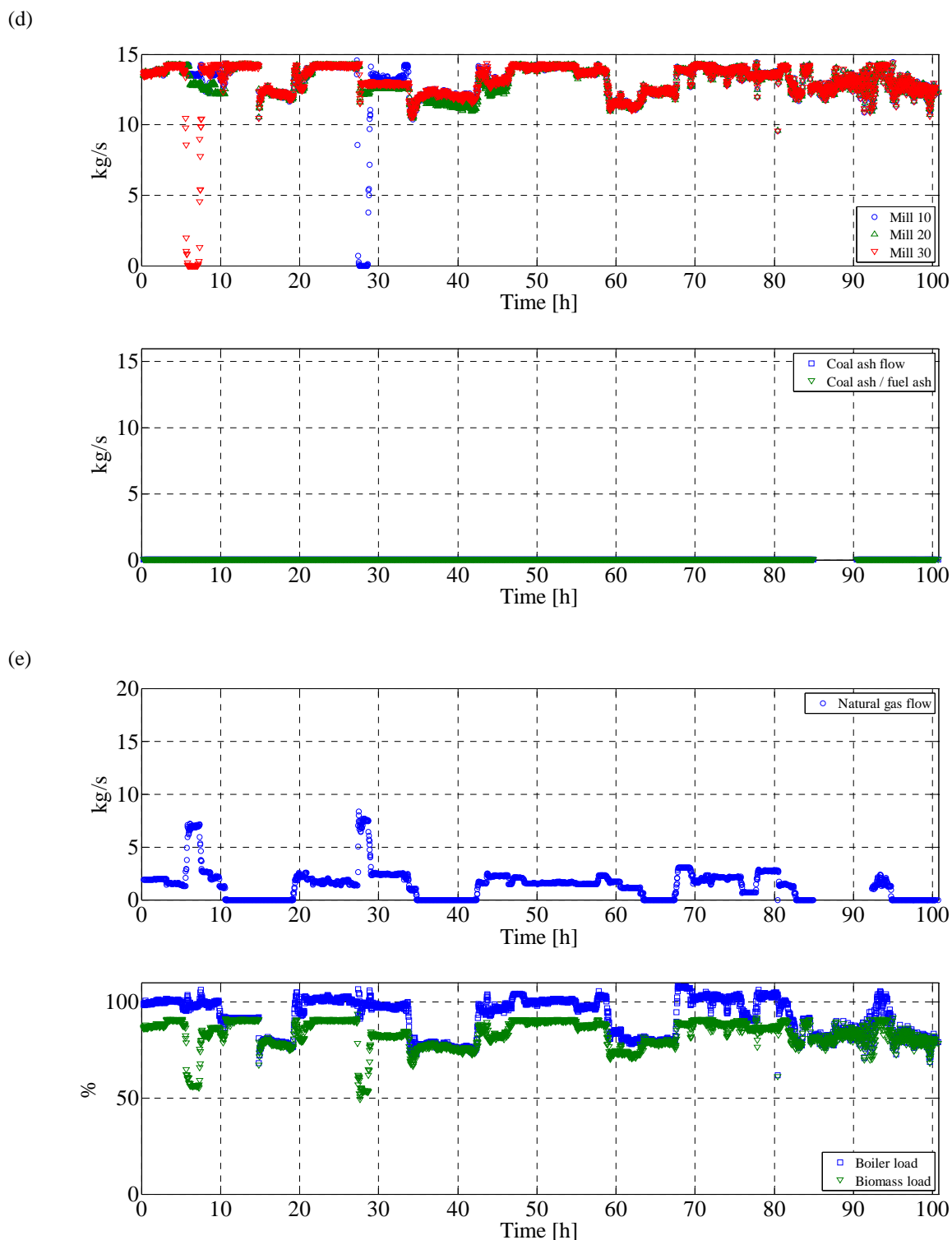
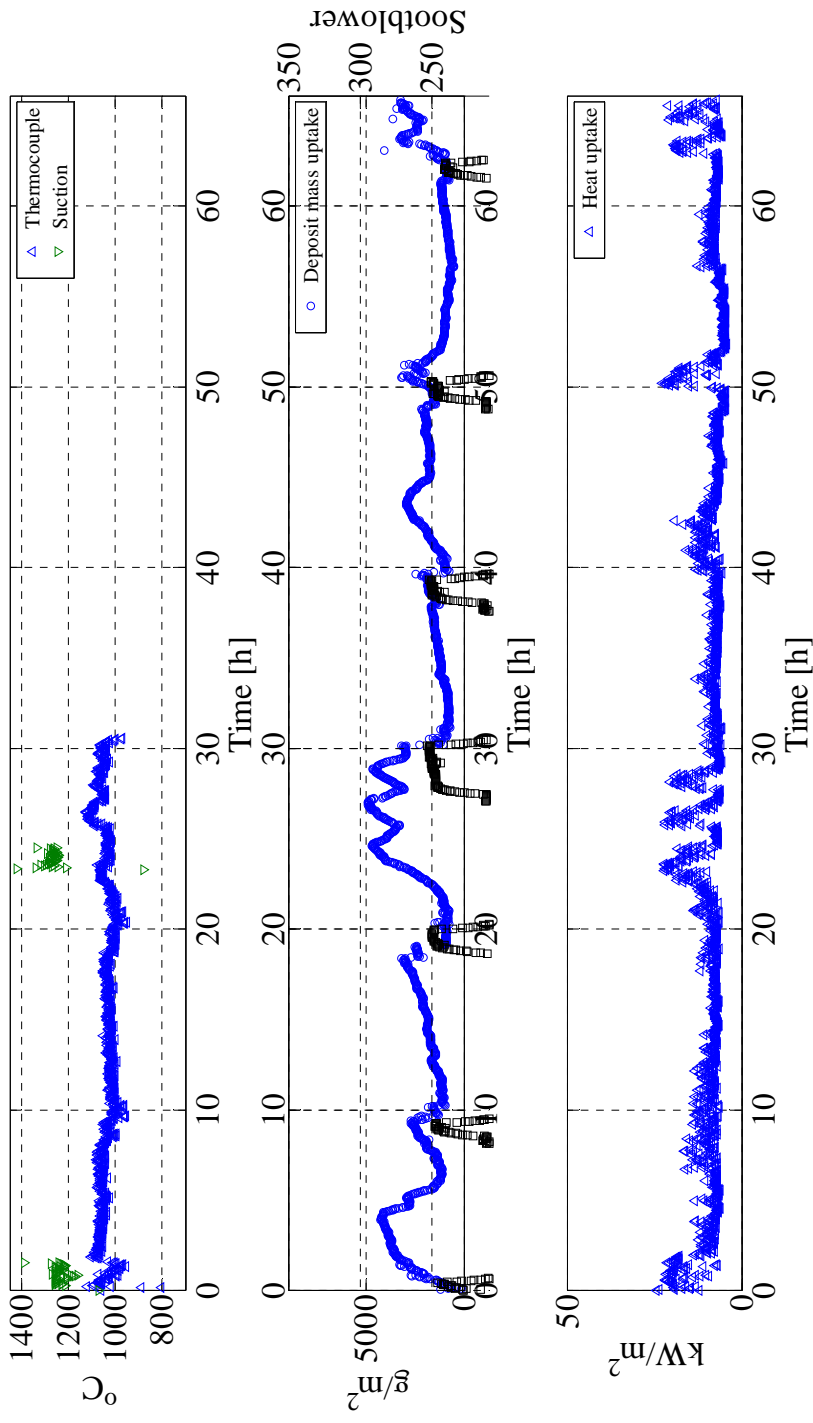


Figure (Appendix C) 6: a) Flue gas temperature, deposit mass uptake signals, sootblowing events, b) DDF-rate, c) ash deposition propensity, d) natural gas flow rate, biomass load, boiler load, e) fuel flow through each mill, coal ash flow (kg/s) , and coal ash to wood ash ratio during test 6 (Chapter 6).

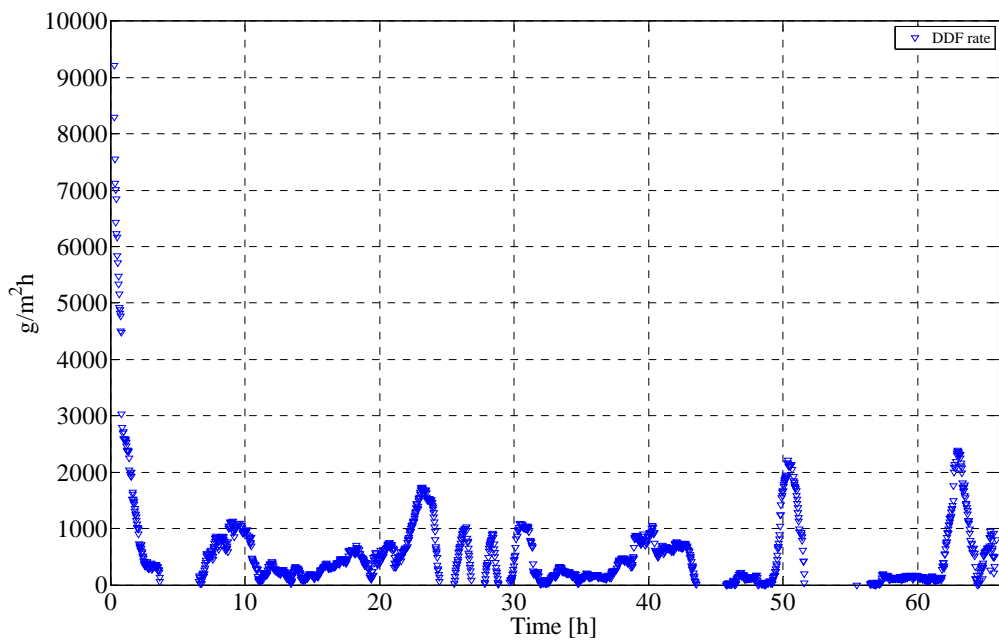
Appendix C: Full-scale measurements at AVV2

(a)

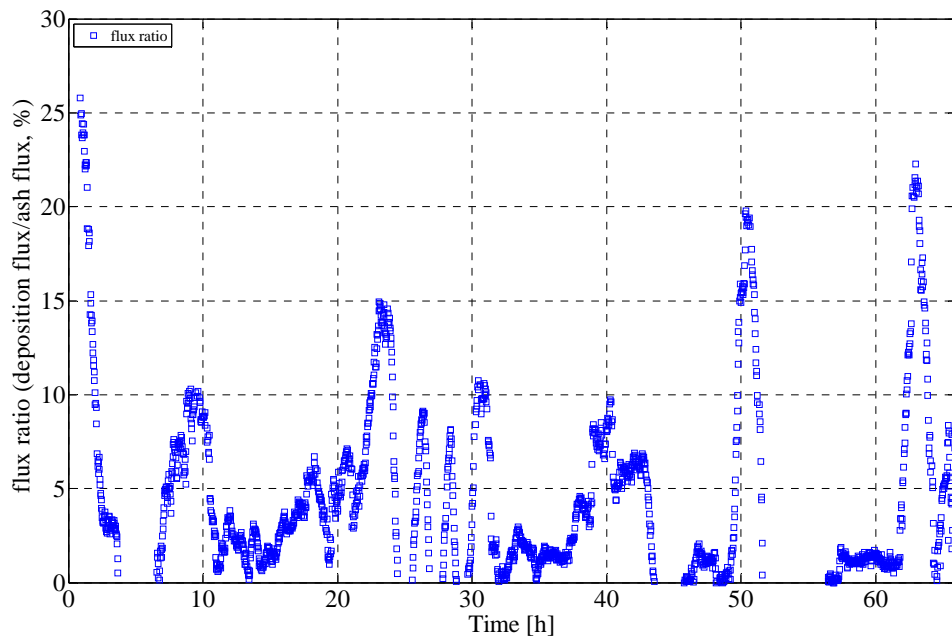


## Appendix C: Full-scale measurements at AVV2

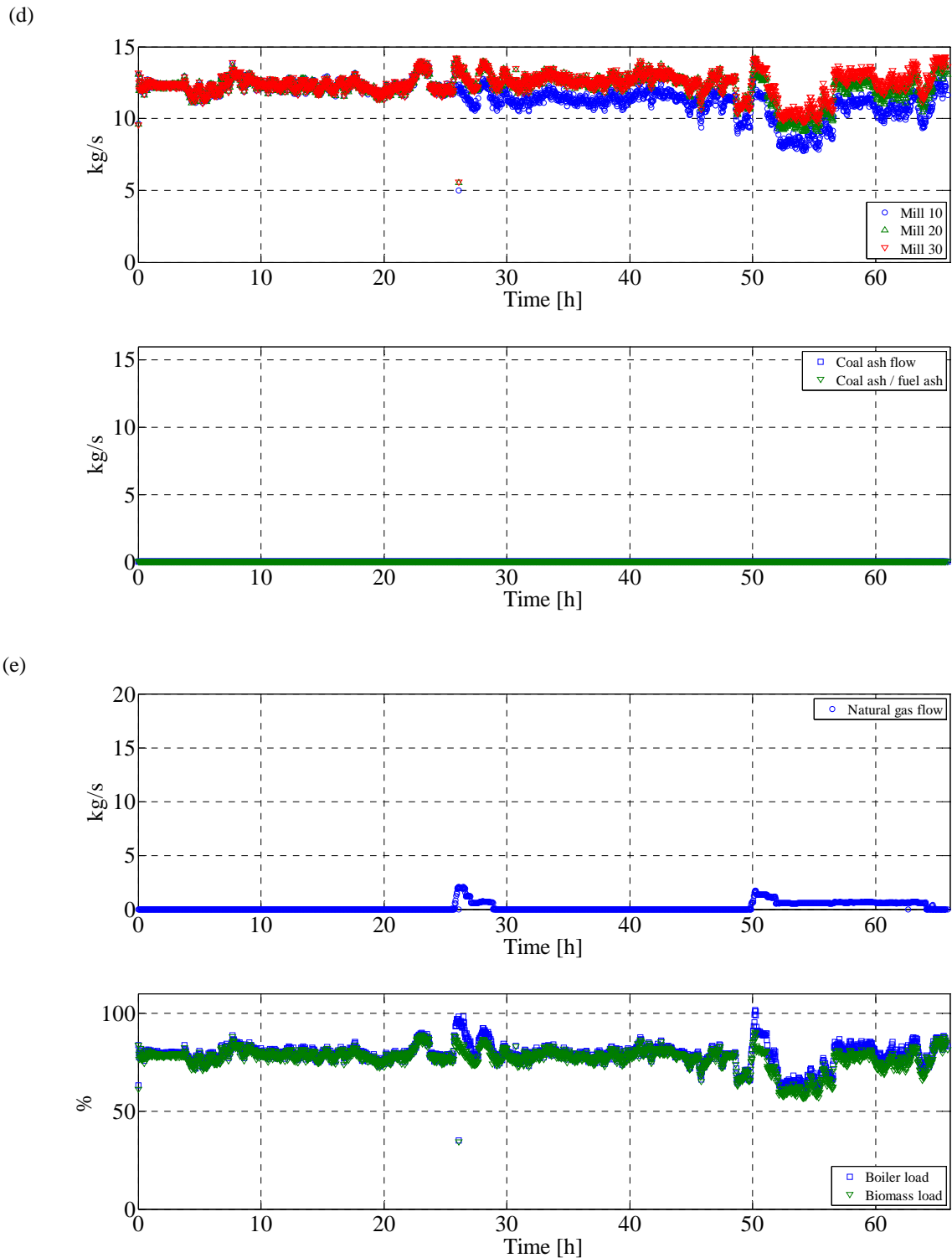
(b)

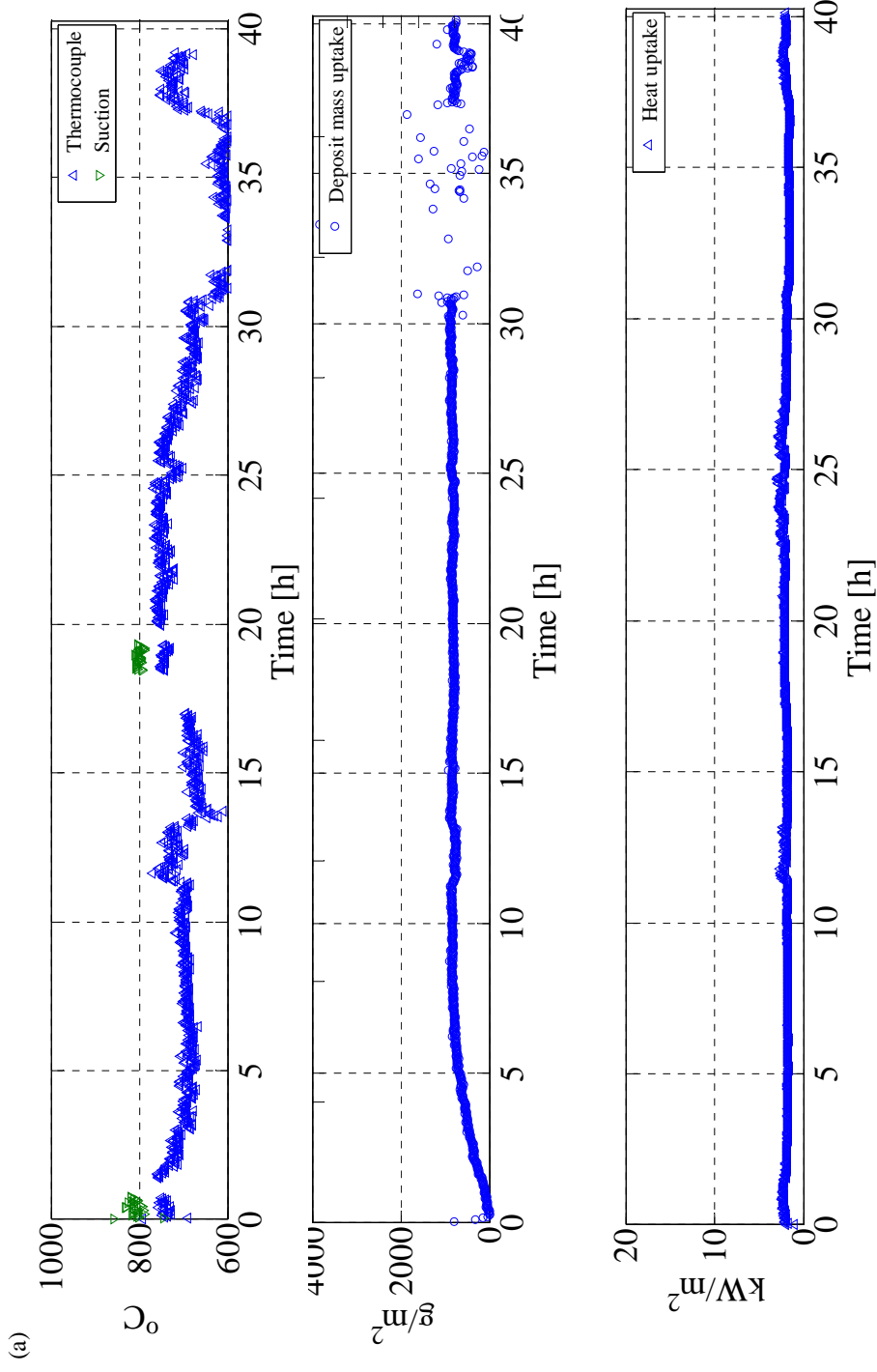


(c)



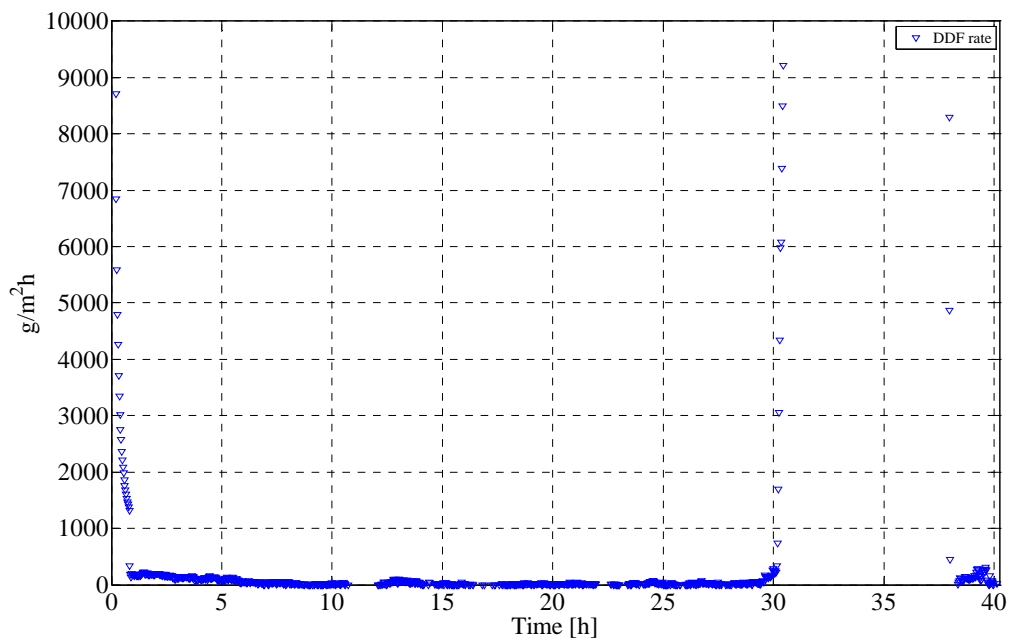
Appendix C: Full-scale measurements at AVV2



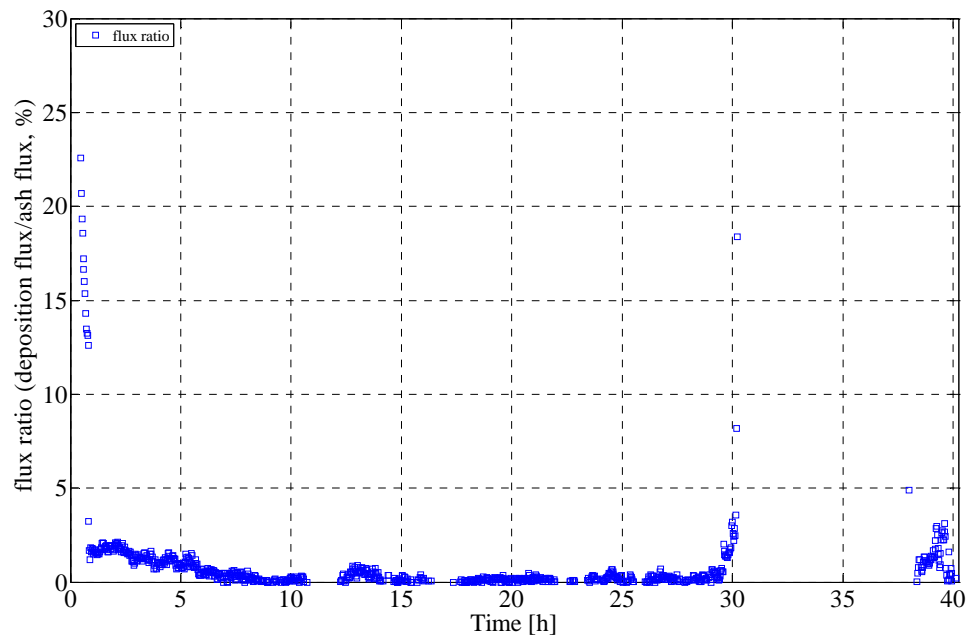


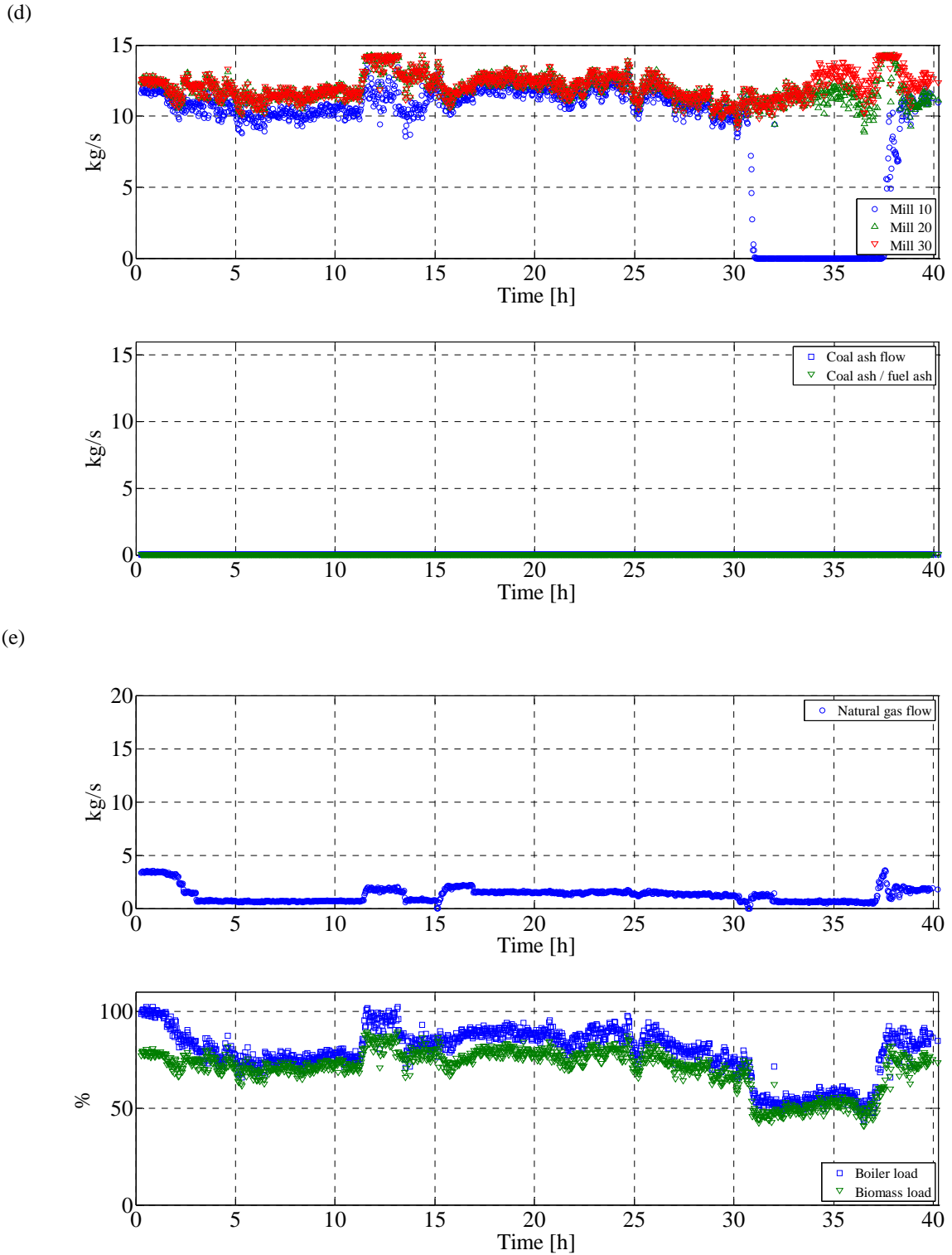
## Appendix C: Full-scale measurements at AVV2

(b)



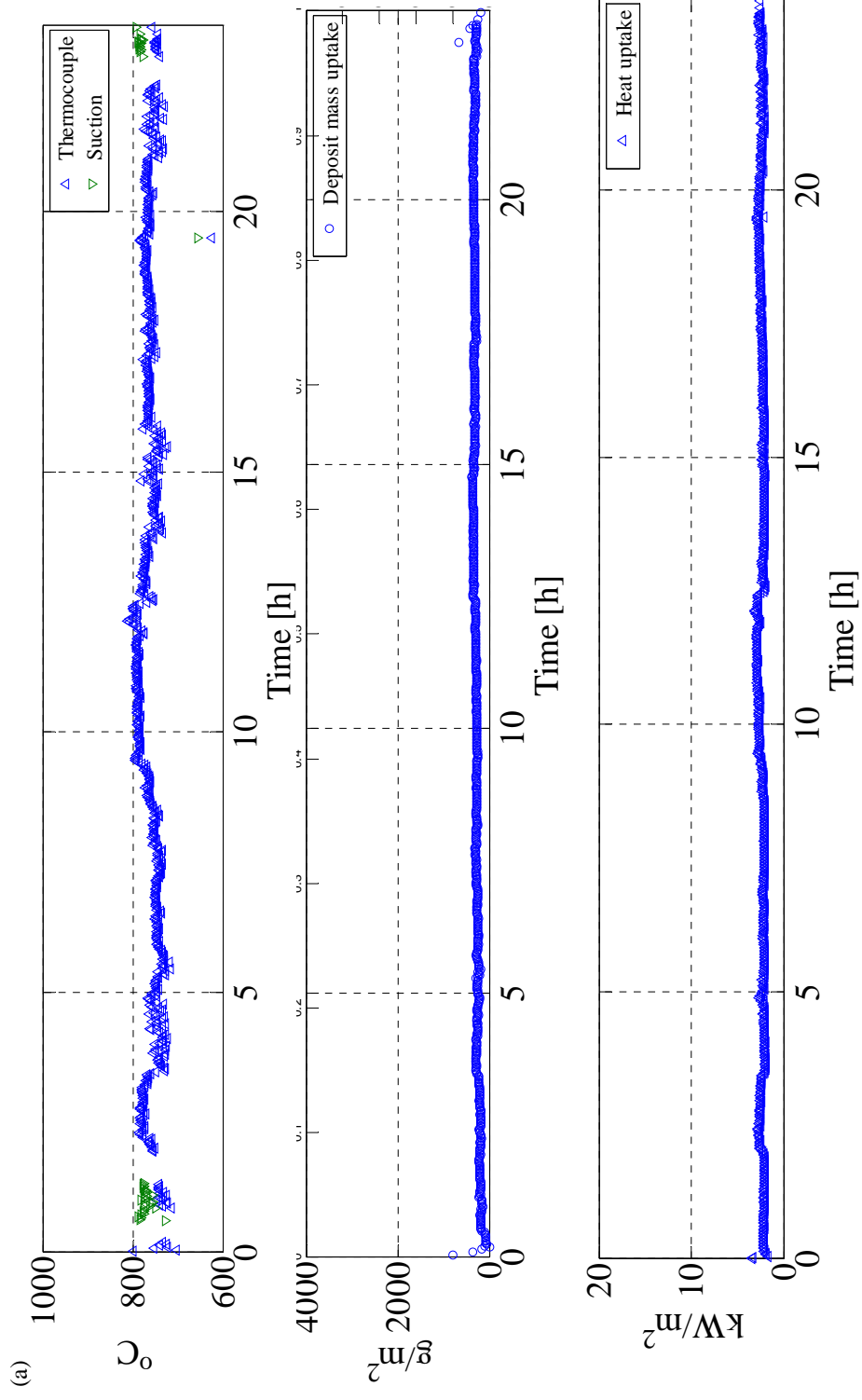
(b)





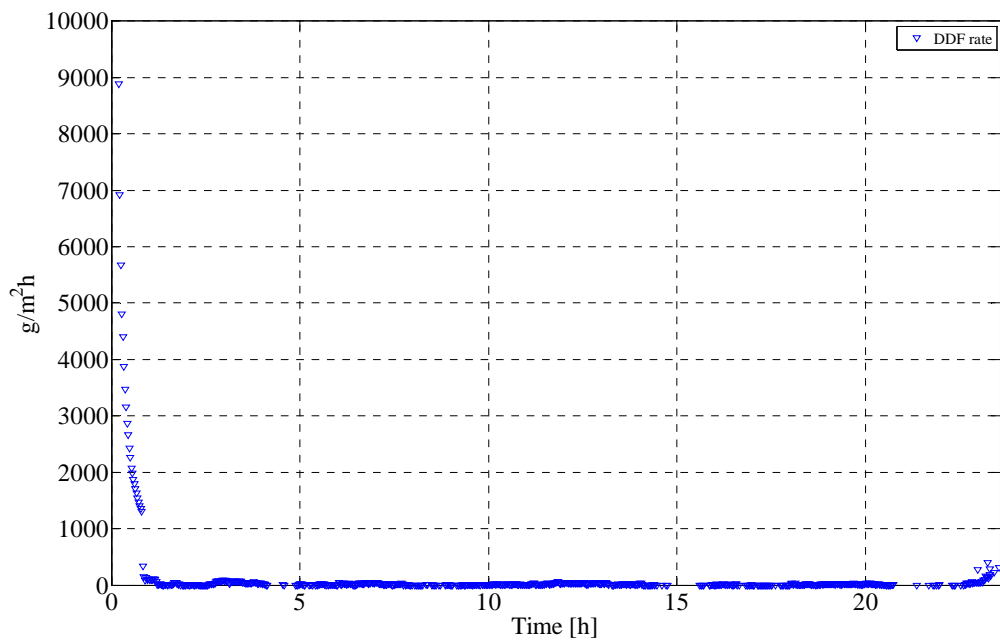


Appendix C: Full-scale measurements at AVV2

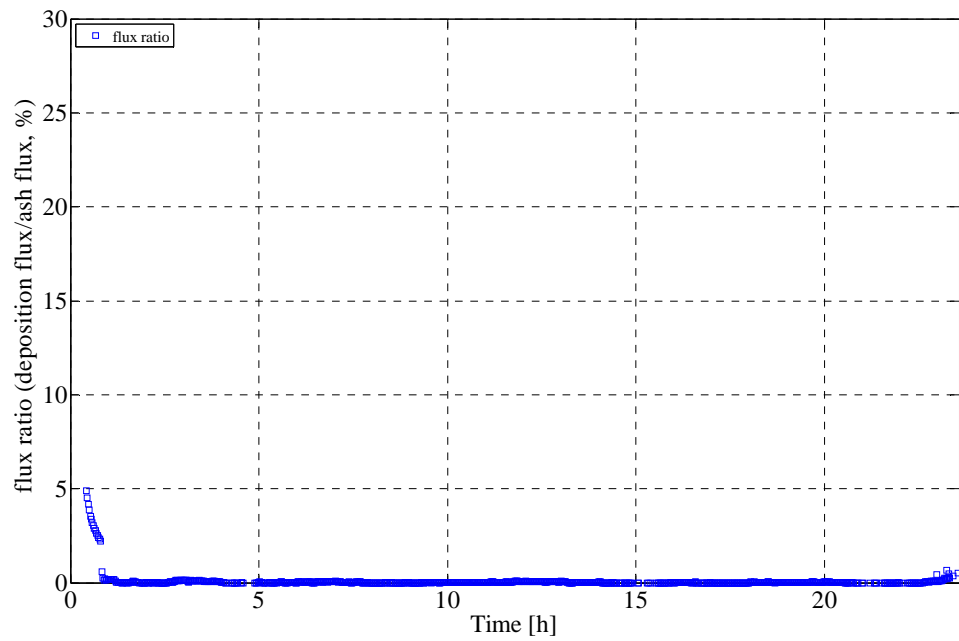


## Appendix C: Full-scale measurements at AVV2

(b)



(c)



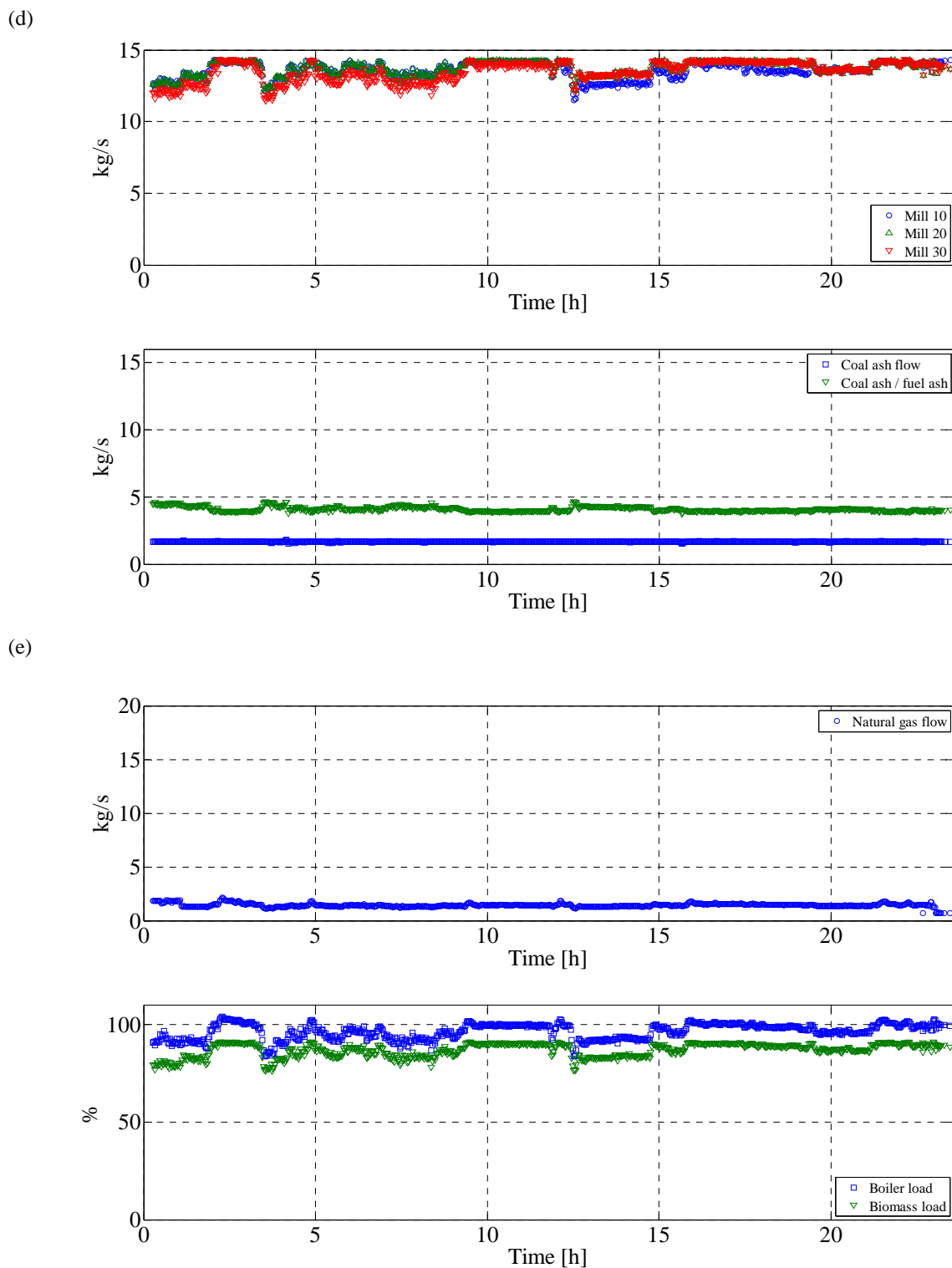
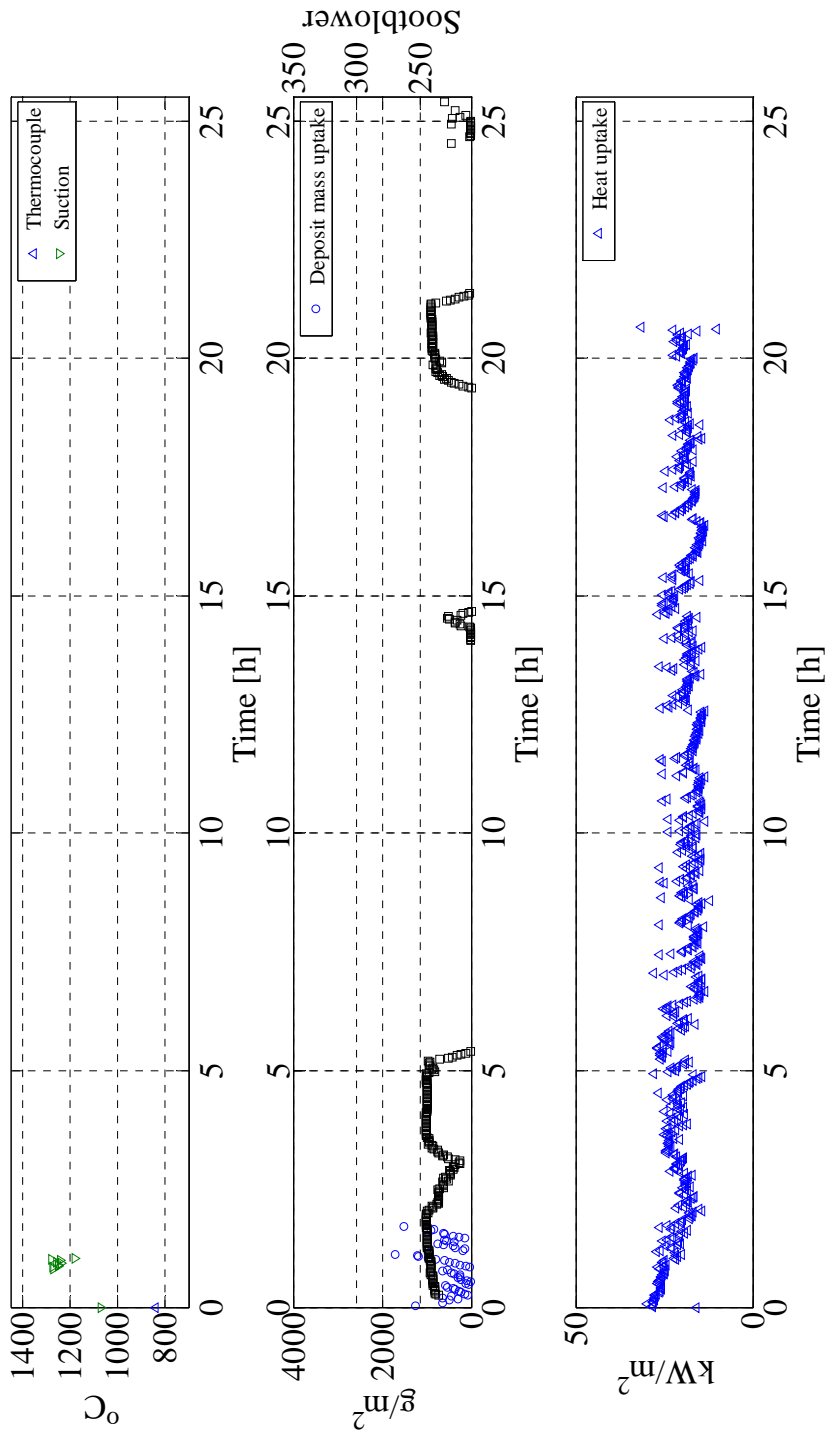


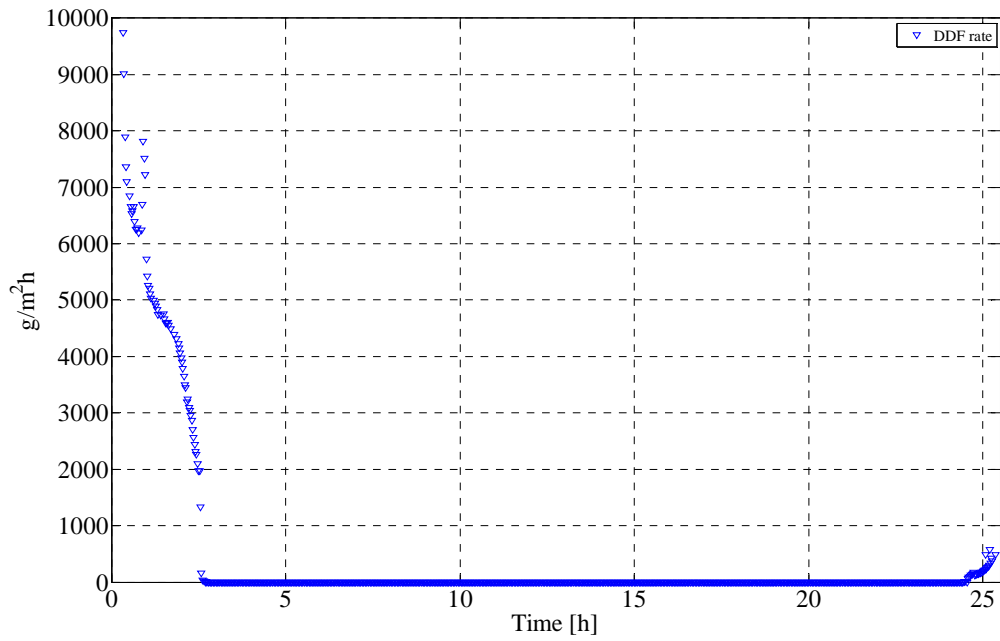
Figure (Appendix C) 9: a) Flue gas temperature, deposit mass uptake signals, sootblowing events, b) DDF-rate, c) ash deposition propensity, d) natural gas flow rate, biomass load, boiler load, e) fuel flow through each mill, coal ash flow (kg/s) , and coal ash to wood ash ratio during test 9 (Chapter 6).

(a)

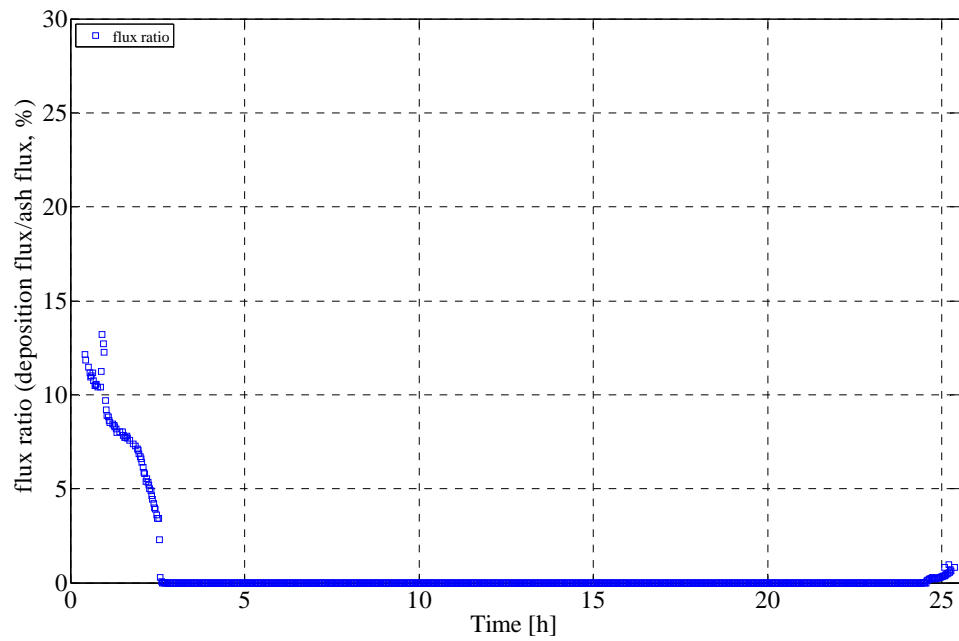


## Appendix C: Full-scale measurements at AVV2

(b)



(c)



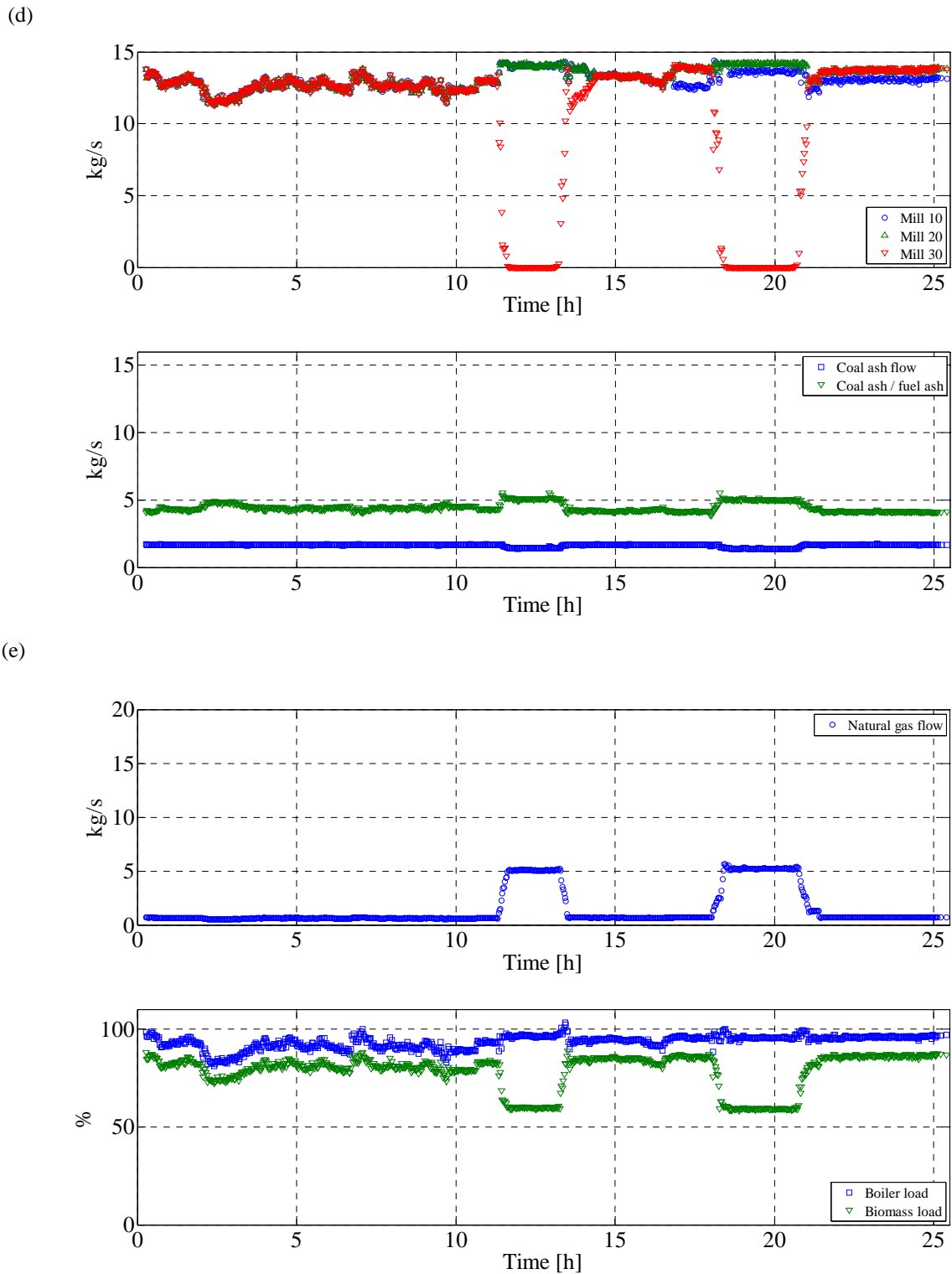
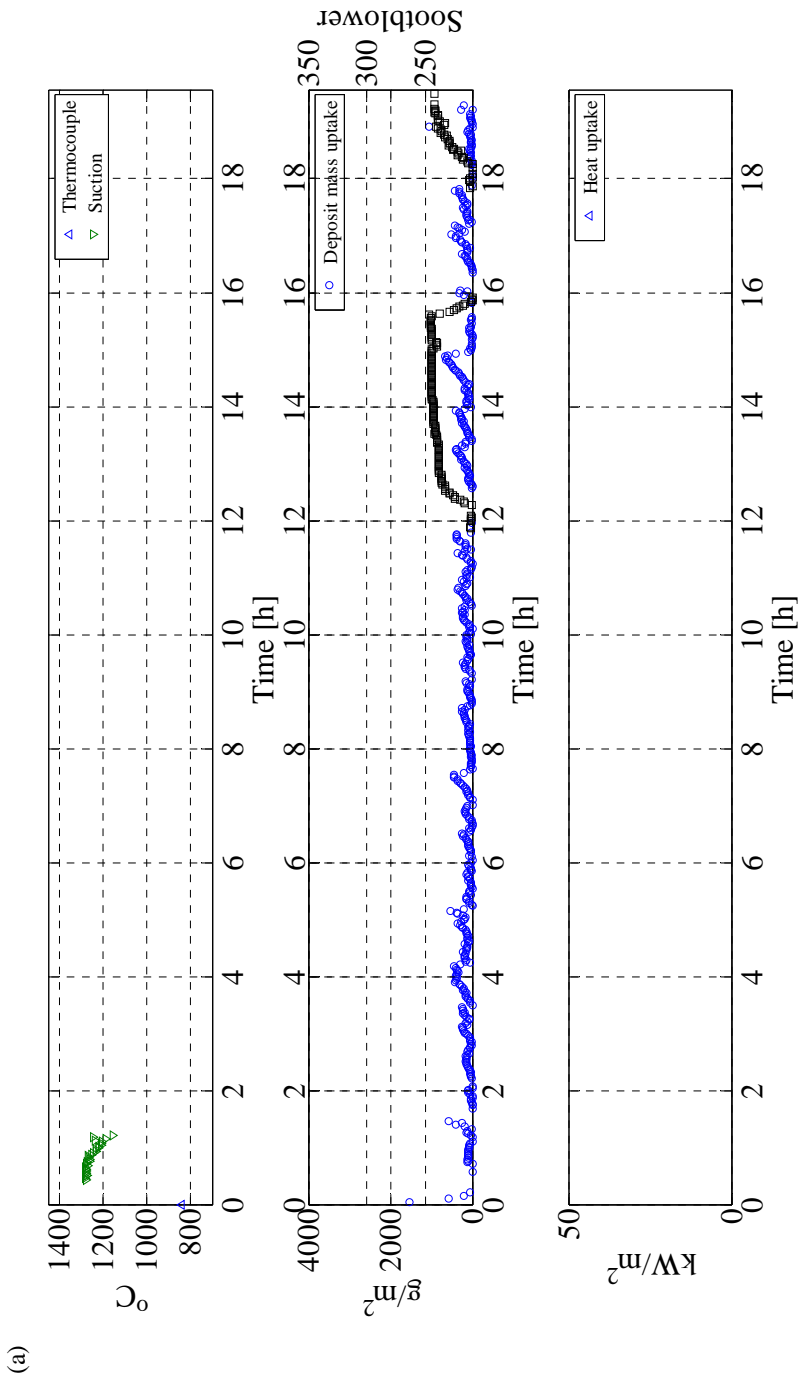


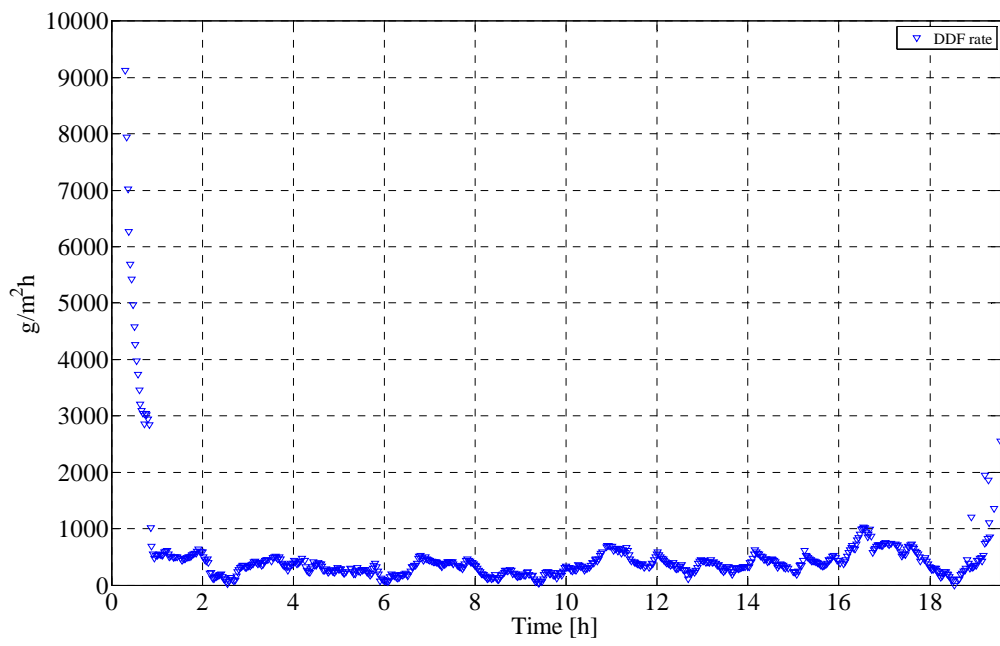
Figure (Appendix C) 10: a) Flue gas temperature, deposit mass uptake signals, sootblowing events, b) DDF-rate, c) ash deposition propensity, d) natural gas flow rate, biomass load, boiler load, e) fuel flow through each mill, coal ash flow (kg/s), and coal ash to wood ash ratio during test 10 (Chapter 6).

Appendix C: Full-scale measurements at AVV2

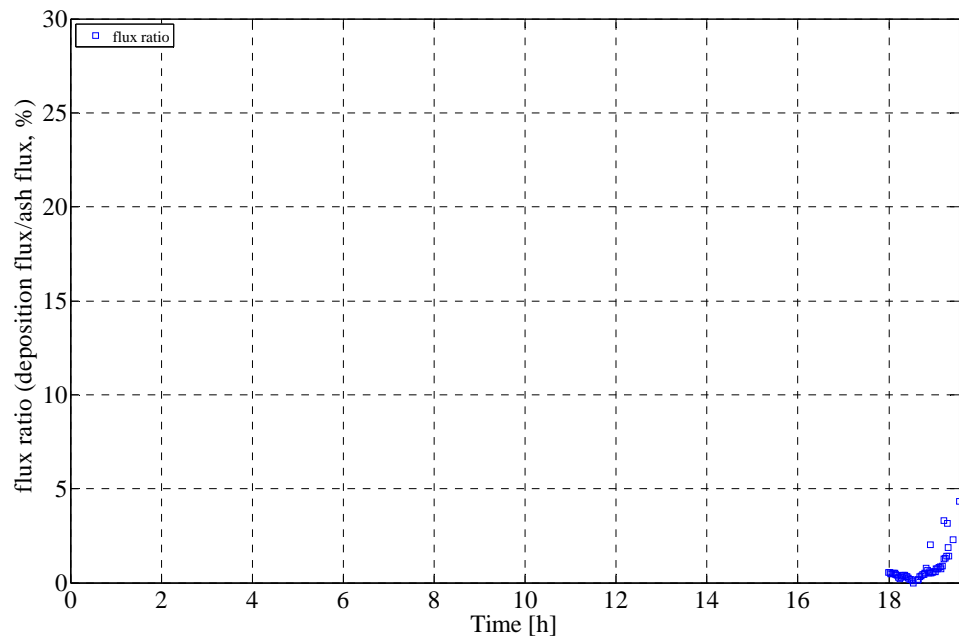


## Appendix C: Full-scale measurements at AVV2

(b)



(c)





## Appendix C: Full-scale measurements at AVV2

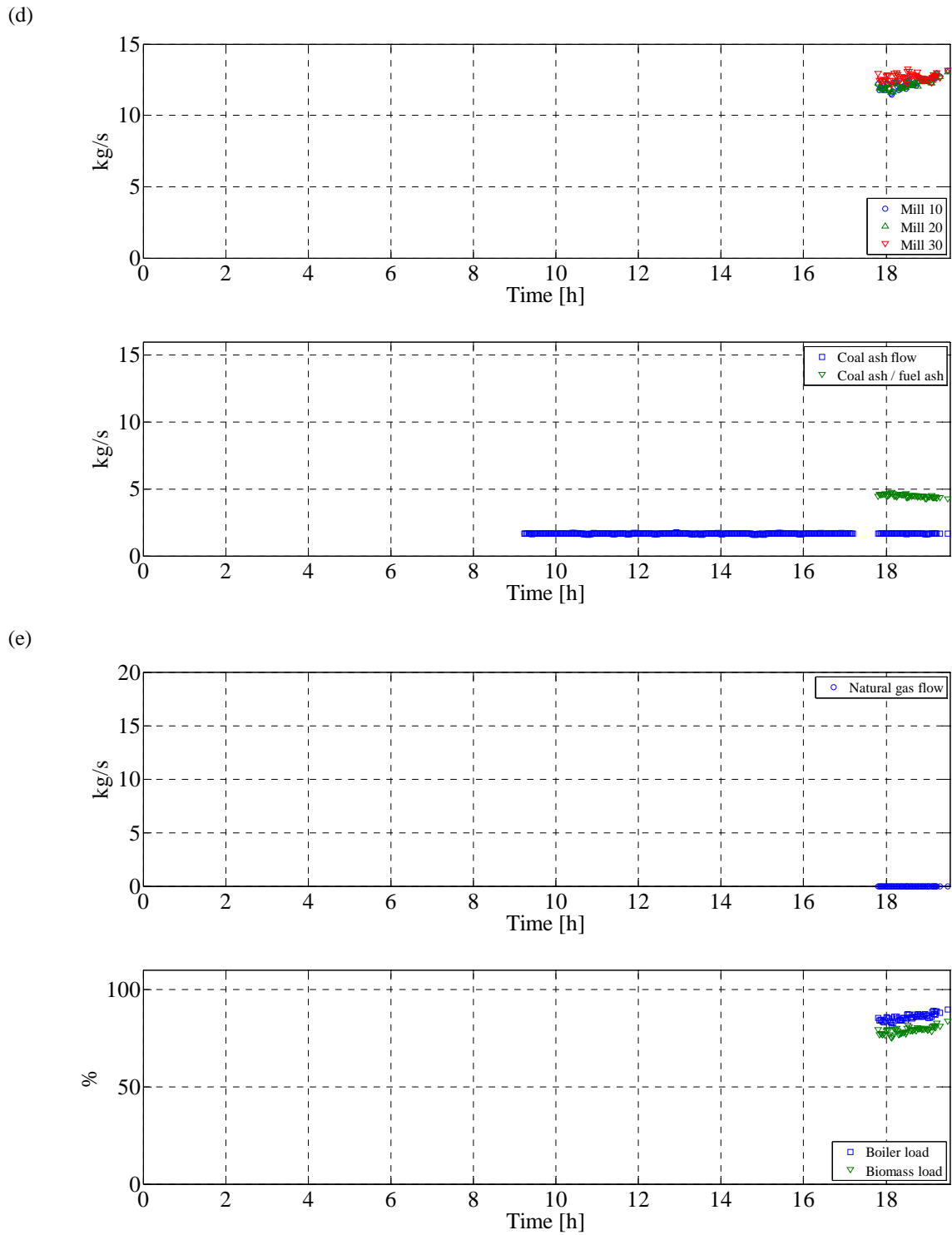
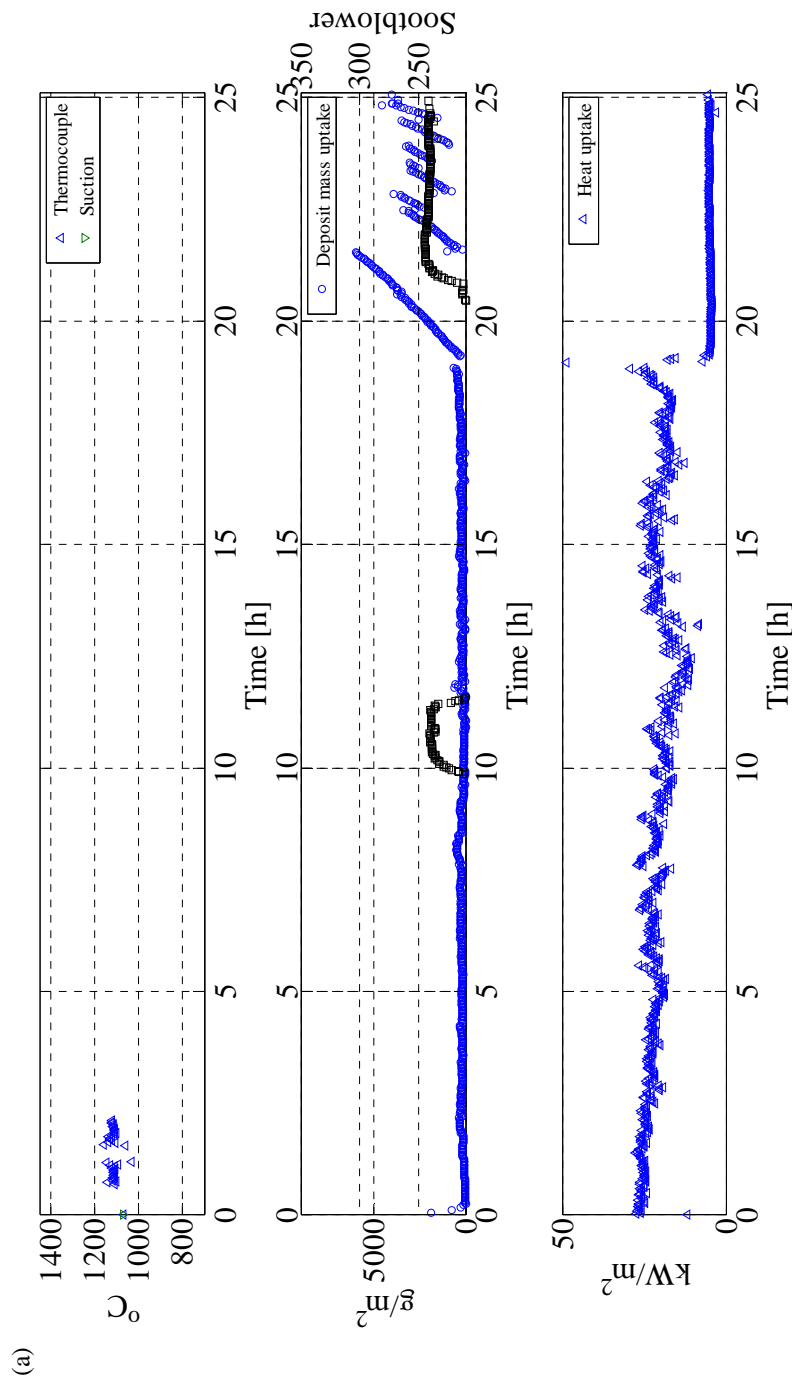


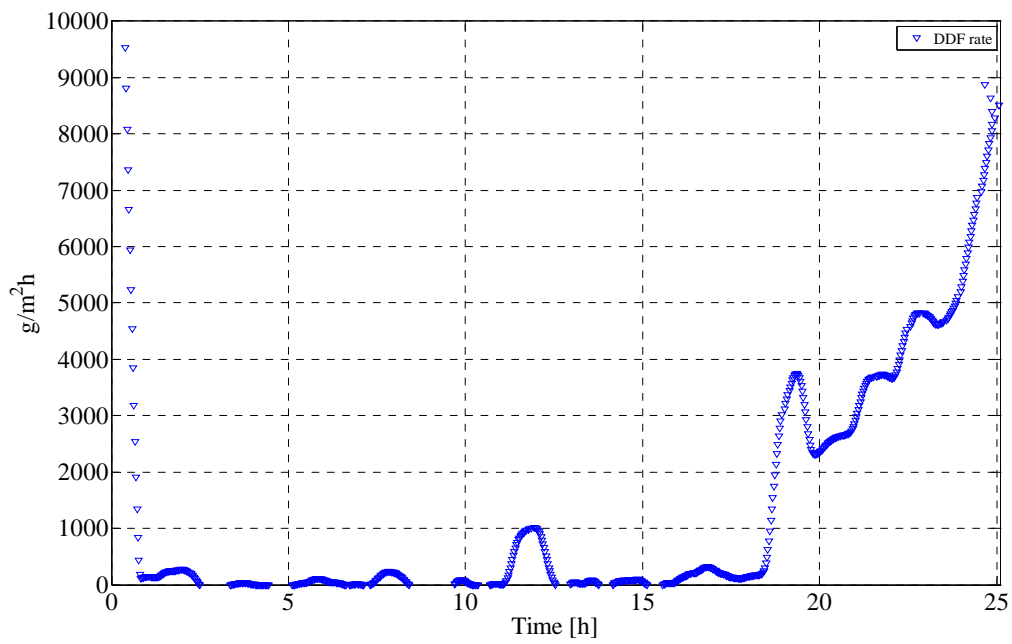
Figure (Appendix C) 11: a) Flue gas temperature, deposit mass uptake signals, sootblowing events, b) DDF-rate, c) ash deposition propensity, d) natural gas flow rate, biomass load, boiler load, e) fuel flow through each mill, coal ash flow (kg/s) , and coal ash to wood ash ratio during test 11 (Chapter 6).

Appendix C: Full-scale measurements at AVV2

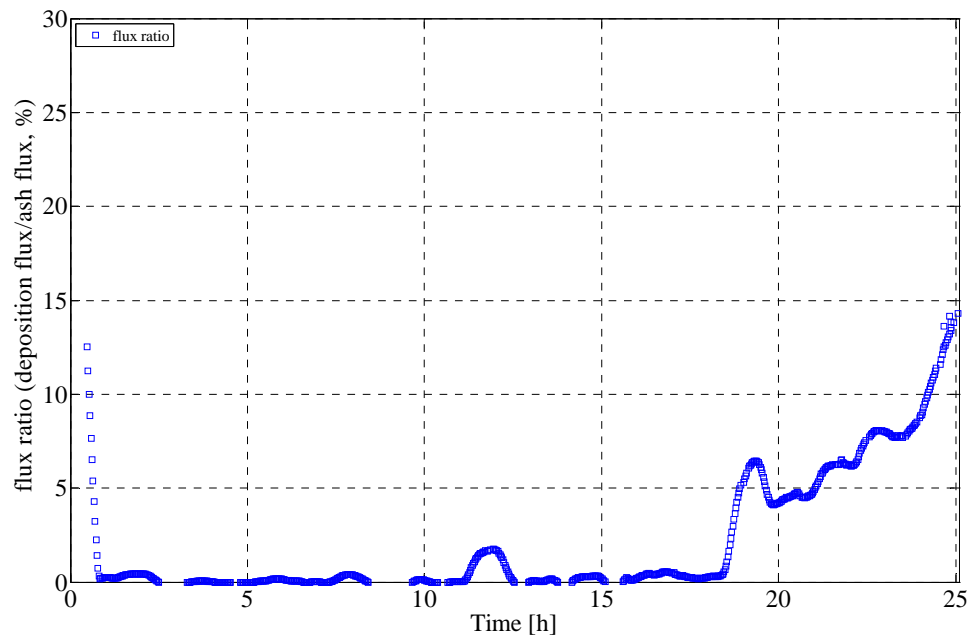


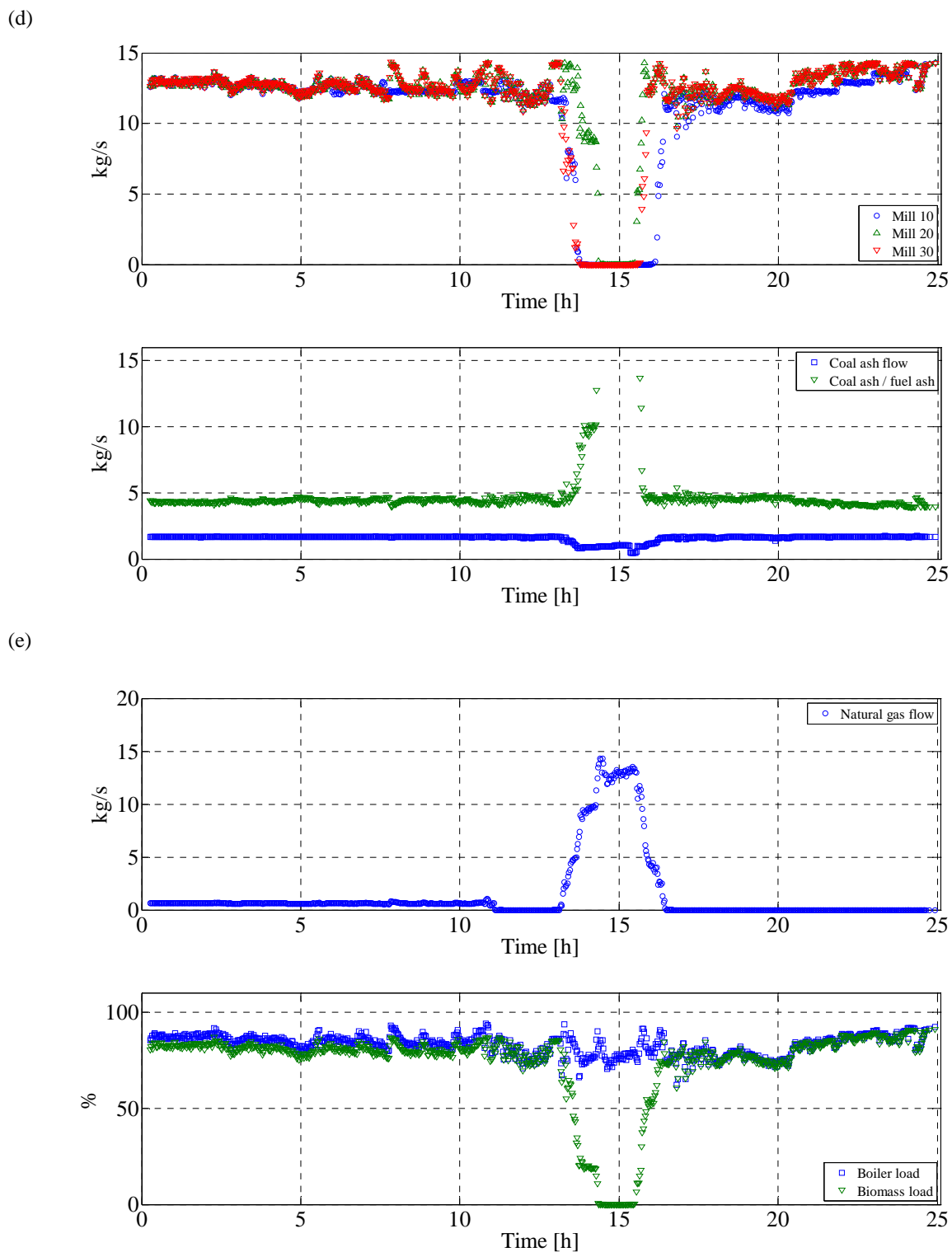
## Appendix C: Full-scale measurements at AVV2

(b)

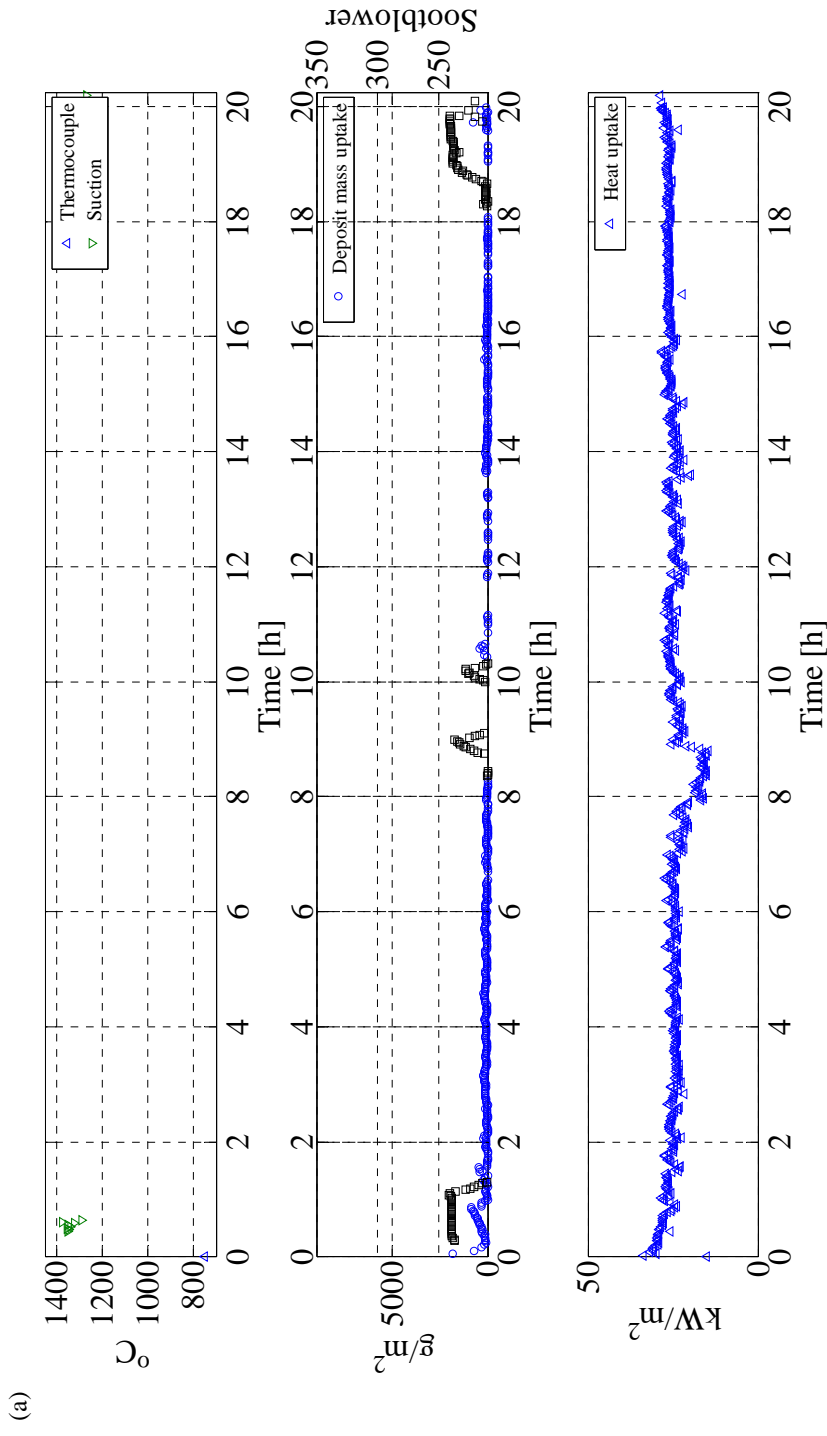


(c)



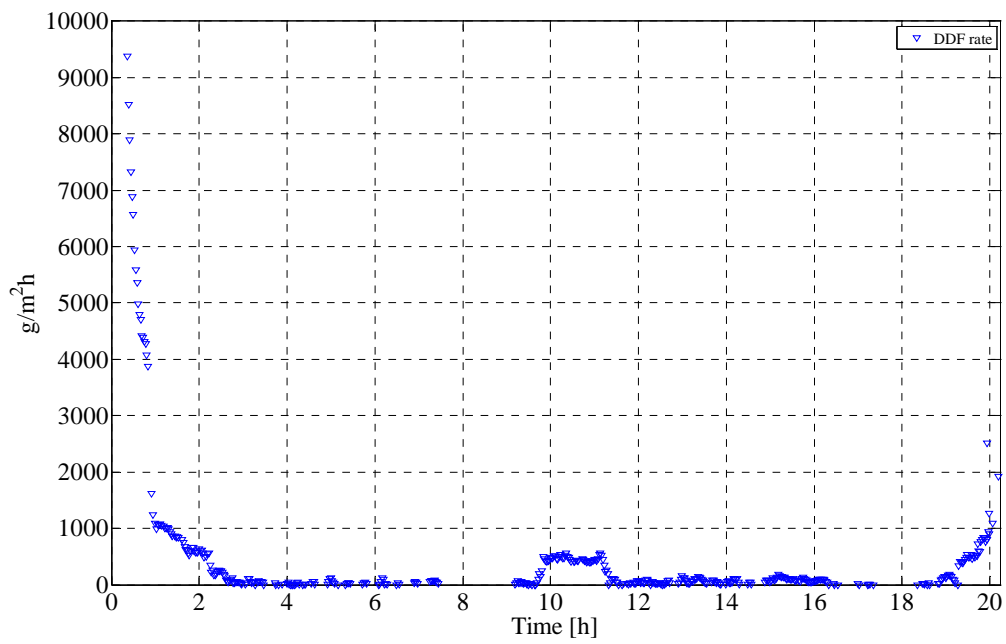


Appendix C: Full-scale measurements at AVV2

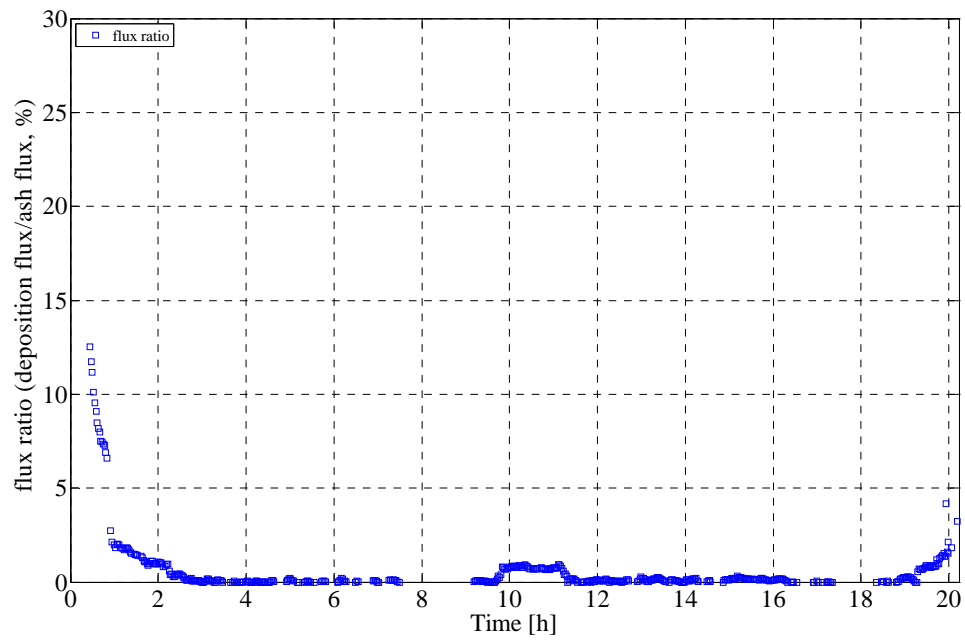


## Appendix C: Full-scale measurements at AVV2

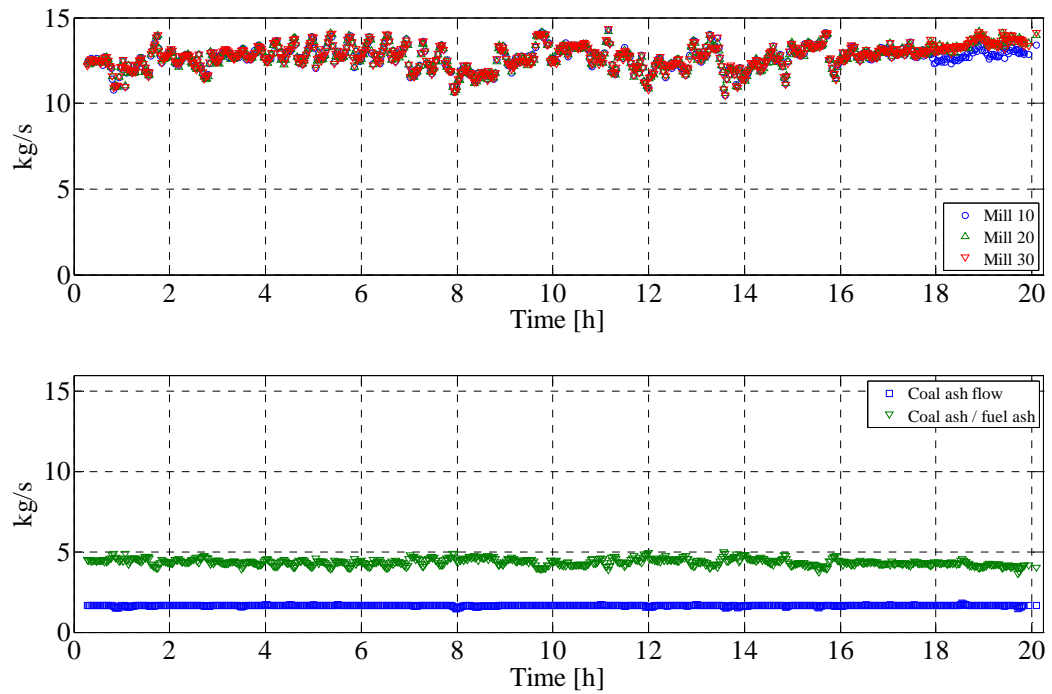
(b)



(c)



(d)



(e)

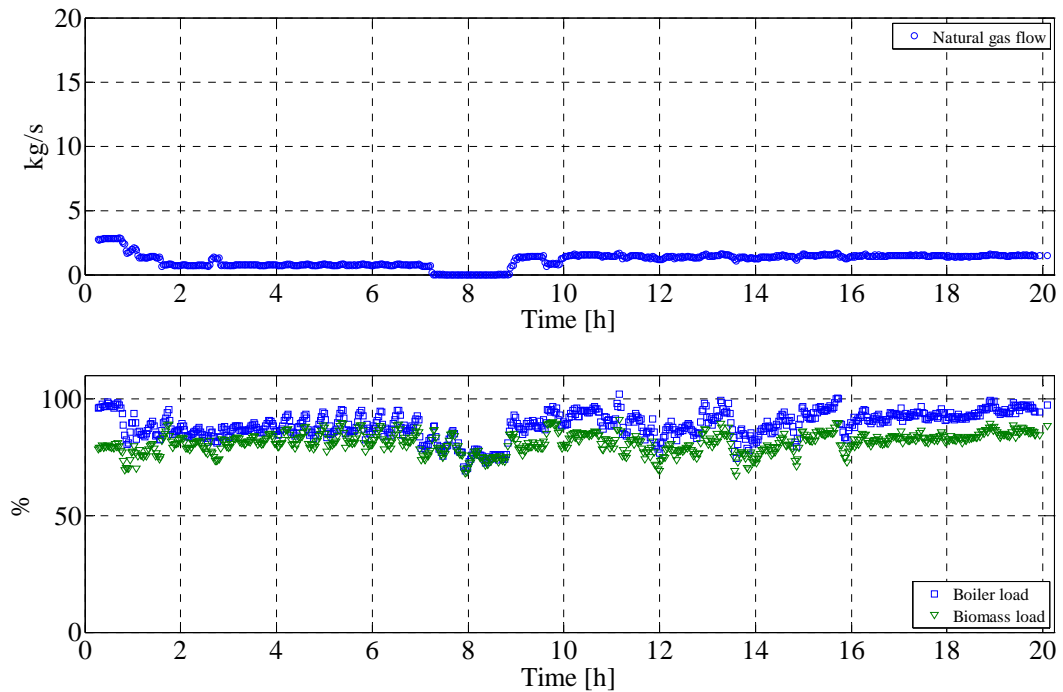


Figure (Appendix C) 13: a) Flue gas temperature, deposit mass uptake signals, sootblowing events, b) DDF-rate, c) ash deposition propensity, d) natural gas flow rate, biomass load, boiler load, e) fuel flow through each mill, coal ash flow (kg/s), and coal ash to wood ash ratio during test 13 (Chapter 6).

